PHYS747: Introduction to Helioseismology

Time: 1:00 pm - 2:20 pm, Monday, Tuesday

Teaching mode: hybrid

Place: GITC, room 1402

Instructor: Alexander Kosovichev

e-mail: alexander.g.kosovichev@njit.edu

Office: Tiernan Hall 482

Office hours: by appointment

Course materials: Canvas

URL: http://sun.stanford.edu/~sasha/PHYS747

NJIT Webex: https://njit.webex.com/join/sasha

Grades: homework (20%), class participation (20%) quizzes (20%), final presentation/project (40%)

Textbooks

1. **M, Stix, The Sun: an Introduction. Second Edition, Springer, 2004.**
2. **C. Aerts, J. Christensen-Dalsgaard, D. W. Kurt, Asteroseismology, Springer, 2010**

Additional sources:

1. **A.G. Kosovichev, Advances in Global and Local Helioseismology: An Introductory Review, Lecture Notes in Physics, Volume 832, 2011**
2. **Extraterrestrial Seismology, V. Tong, R. Garcia (eds), Cambridge Univ. Press, 2015**

Lecture Plan

1. **Sept . 7. Lecture 1. Brief history of helioseismology.**
2. **Sept. 8. Lecture 2. Observations and basic properties of solar oscillations.**
3. **Sept. 13. Lecture 3. Oscillation power spectrum. Excitation by turbulent convection. Line asymmetry and pseudo-modes.**
4. **Sept. 14. Lecture 4. Magnetic effects: sunspot oscillations and acoustic halos.**
5. **Sept. 20. Lecture 5. Helioseismic response to solar flares: sunquakes.**
6. **Sept. 21. Lecture 6. Global helioseismology. Basic equations. I**
7. **Sept. 27. Lecture 7. Global helioseismology. Basic equations. II**
8. **Sept. 28. Lecture 8. JWKB solution; Dispersion relations for p- and g-modes.**
9. **Oct. 4. Lecture 9. Frequencies of p- and g-modes. I. High-degree p-modes**
10. **Oct. 5. Lecture 10. Frequencies of p- and g-modes. II. Low-degree p-modes**
11. **Oct. 11. Lecture 11. Gravity modes.**
12. **Oct. 12. Lecture 12. Surface gravity waves (f-mode).The seismic radius.**

1. **Oct. 18. Lecture 13. Asymptotic ray-path approximation.**
2. **Oct. 19. Lecture 14. Mode-ray duality**
3. **Oct. 25. Lecture 15. Duvall's law. Time-distance relation**
4. **Oct. 26. Lecture 16. Asymptotic sound-speed inversion.**
5. **Nov. 1. Lecture 17. General helioseismic inverse problem. Variational principle; Perturbation theory; Kernel transformations**
6. **Nov. 2. Lecture 18. Solution of inverse problem. Optimally localized averages method.**
7. **Nov. 8. Lecture 19. Inversion results for solar structure**
8. **Nov. 9. Lecture 20. Inversions for solar rotation. Regularized least-squares method.**
9. **Nov. 15. Lecture 21. Local-area helioseismology. Basic principles. Ring-diagram analysis. Time-distance helioseismology; Acoustic holography and imaging.**
10. **Nov. 16. Lecture 22. Solar tomography. Time-distance diagram. Wave travel times. Deep- and surface-focus measurement schemes.**
11. **Nov. 22. Lecture 23. Inversion results of solar acoustic tomography. Diagnostics of supergranulation. Structure and dynamics of sunspots.**
12. **Nov.23. Lecture 24. Large-scale and meridional flows. Solar dynamo.**
13. **Nov. 29-30. Work on student's projects.**
14. **Dec. 6-7. Presentation of student's projects.**

Presentations: Jupyter notebooks, https://jupyter.org/

- Requirements:
  - Present observational facts
  - Explain the basic physical processes
  - Briefly review the current state of research
  - Present project methodology, Python code and results
  - Answer questions
- For each topic I will provide references and initial material.

Topics

1. Doppler-shift modeling and analysis
2. Oscillations power maps – acoustic halo
3. Power spectrum of global oscillations
4. Propagation diagram for solar and stellar models
5. Ray-path theory
6. Line asymmetry modeling
7. Acoustic travel times
8. Time-distance helioseismology
9. Analysis of sunquakes

Brief history of helioseismology

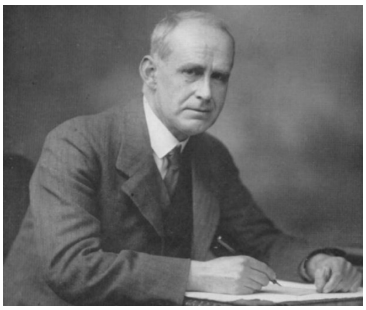

"At first sight it would seem that the deep interior of the sun and stars is less accessible to scientific investigation than any other region of the universe. Our telescopes may probe farther and farther into the depths of space; but how can we ever obtain certain knowledge of that which is hidden behind substantial barriers? *What appliance can pierce through the outer layers of a star and test the conditions within?* "

Sir Arthur Stanley Eddington, *The Internal Constitution of the Stars*, 1926, page 1, line 1.

Discovery of solar oscillations

- 1962: R.Leighton, R.Noyers and G.Simon discovered 5-min oscillations

4. The vertical velocities exhibit a striking repetitive time correlation, with a period $T = 296 \pm 3$ sec. This quasi-sinusoidal motion has been followed for three full periods in the line Ca λ 6103, and is also clearly present in Fe λ 6102, Na λ 5896, and other lines. The energy contained in this oscillatory motion is about 160 J cm^{-2}; the "losses" can apparently be compensated for by the energy transport (2).

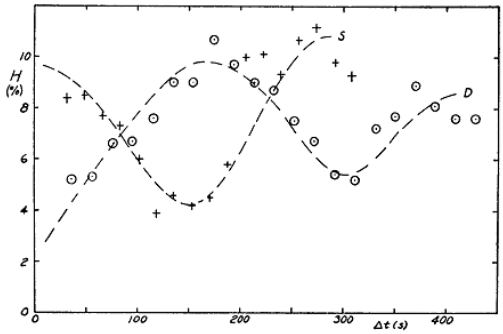

Spectroheliograph

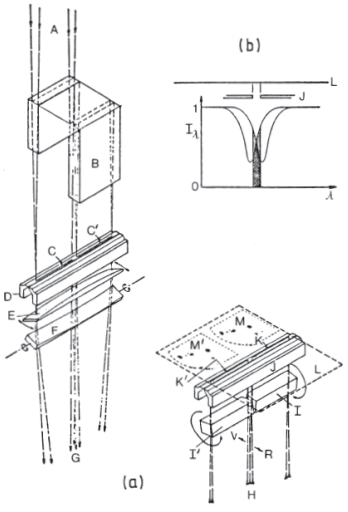

- The spectroheliograph is a solar spectrograph with an exit slit in the spectral plane.
- The solar image is moved across the entrance slit, and simultaneously the photographic plate is moved along behind the exit slit.
- A quarter-wave plate is used as a line shifter, so that two images in red and blue wings were recorder simultaneously.
- The two spectroheliograms which are simultaneously obtained in the two wings of the spectral line are subsequently subtracted photographically.

Discovery of 5-min oscillations

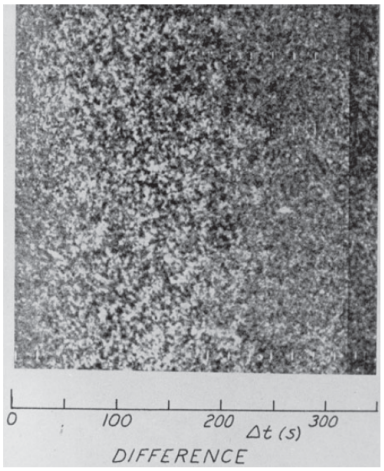

- The result is a “Doppler plate”; its intensity variation has its origin in the local Doppler shift of the line used.
- Two such Doppler plates, obtained by scanning the Sun first in one and immediately afterwards in the opposite direction, are then again subtracted from each other.
- Since each scan takes a few minutes, the resulting “Doppler difference” has a variable time delay Δt between the two constituent Doppler plates: Δt is smallest at the edge where the scanning direction was reversed and increases linearly from there.
- A periodic velocity field on the Sun manifests itself as a periodically changing intensity contrast.

Fig. 5.1. Doppler-difference plate for the Ba II line $\lambda = 455.4$ nm. From Leighton et al. (1962)

Measurement procedure

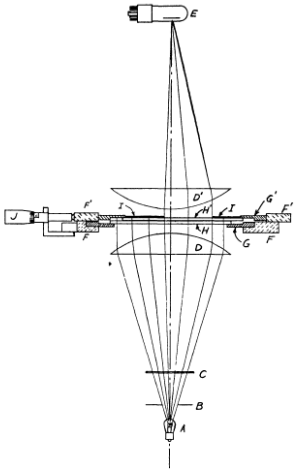

In order to extract reliable statistical information from a Doppler plate without undue amounts of calculation, a device (Fig. 2) was built which carries out the operations involved in evaluating auto-correlation (A-C) and cross-correlation (C-C) functions over a two-dimensional field. The two-dimensional A-C function $C(s, t)$ is defined by

$$C(s,t) \equiv \frac{K}{A}\int\int T(x,y)T(x+s,y+t)\,dA \equiv K\langle T(x,y)T(x+s,y+t)\rangle,$$

where A is the area, $T(x, y)$ is the transmission of the plate at the point (x, y), K is a normalization constant, and the integration area is made sufficiently great that fluctuations due to the boundaries are negligible. To obtain the A-C function over a given area A, two copies of the plate are made, in a right- and left-handed pair, so that they may be placed in register with their emulsions in contact, On one plate, the entire area except for the area of interest is masked off. The plates are fixed to separate frames, which are placed in a holder in such a way that their emulsions are in contact and in register. A motor drive slides one plate slowly past the other. Collimated light is passed through the two plates and is brought to a focus on the photocathode of a photomultiplier tube. When the plates are displaced an amount s in the x-direction and t in the y-direction, relative to each other, the photomultiplier records $C(s, t)$. In practice, t is

Discovery of solar oscillations

- 1962: R.Leighton, R.Noyers and G.Simon discovered 5-min oscillations

4. The vertical velocities exhibit a striking repetitive time correlation, with a period $T = 296 \pm 3$ sec. This quasi-sinusoidal motion has been followed for three full periods in the line Ca λ 6103, and is also clearly present in Fe λ 6102, Na λ 5896, and other lines. The energy contained in this oscillatory motion is about 160 J cm^{-2}; the "losses" can apparently be compensated for by the energy transport (2).

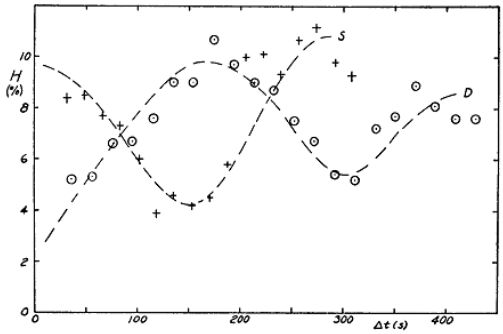

First explanation

- Atmospheric oscillations excited by granular impacts (acting like pistons).

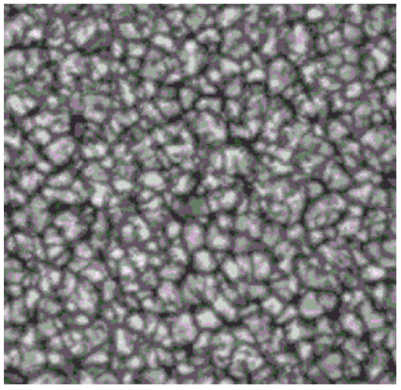

Characteristic frequency of the atmospheric oscillations:

$$\omega = \frac{c}{2H}$$

Where c is the sound speed, H is the pressure scale height

$$H = \frac{\Re \rho T}{\mu g} = \frac{c^2}{\gamma g} \qquad \omega = \frac{\gamma g}{2c}$$

Oscillation period $P = \frac{4\pi c}{\gamma g}$

c=10 km/s=10^6 cm/s, g=2.74x10^4 cm/s^2, γ=5/3: P=275 sec

Discovery of a modal structure

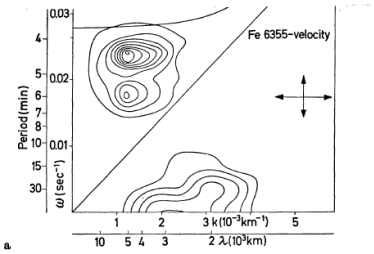

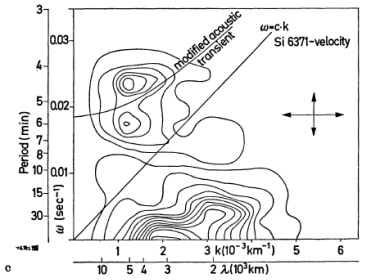

Fig. 3a—d. Observed diagnostic diagrams. Fig. 3a, b, c, and d

- In 1969 Frazier developed computer analysis of Doppler images and calculated first k-omega diagram, where k (or k_h) is the horizontal wavenumber; $\lambda=2\pi/k$ is the horizontal wavelength.
- It showed two oscillating modes.
- This contradicts to the interpretation that the oscillations are atmospheric.
- He suggested that the oscillations are excited below the surface.

- 1970: Roger Ulrich developed a theory of subsurface oscillations and predicted the ridge (modal) structure of 5-min oscillations

The most important finding of this study has been that the 5-minute oscillations are overstable and are capable of supplying the energy lost through radiation in the chromosphere and corona. Also important is the result that the oscillations should be confined to distinct lines on the diagnostic (k_h, ω)-plane. These lines have not yet been found because of poor resolution in k_h and ω. The double peak observed by Frazier

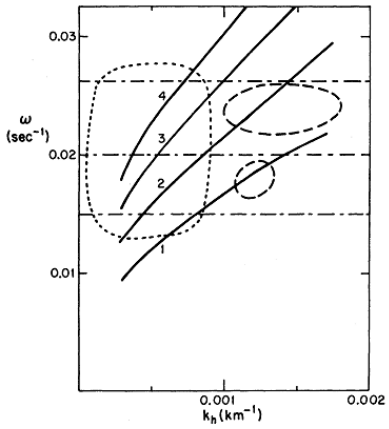

Resonant solar modes: n=1,2,3,4 – number of the nodal point along the radius.

16

Detection of the ridge structure

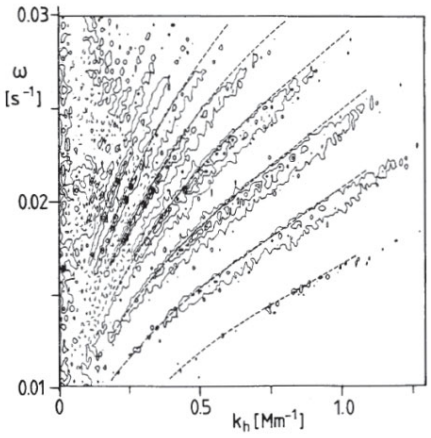

- For the solar oscillations the important fact is that the power is not evenly distributed in the k_h-ω plane, but instead follows certain *ridges*.
- Each of these ridges corresponds to a fixed number of wave nodes in the radial direction.
- The ridges theoretically predicted by Ulrich (1970) were first observed by Deubner (1975) with the Domeless
- Coude Telescope at Capri.
- Figure 5.4 shows an example, where up to 15 ridges can be identified in the *velocity* power spectrum.

Fig. 5.4. Ridges of p and f modes in the k_h, ω-plane (contours of equal power), and eigenfrequencies of a theoretical solar model (*dotted curves*). After Deubner et al. (1979)

Search for global modes: 160-min oscillations

Fig. 2 The best fit for the fluctuations from visual inspection of the records obtained during first 9 d of observations. Each point is the 5-min integrated signal of radial velocity (top). Averaging this gives the sine-like curve shown below.

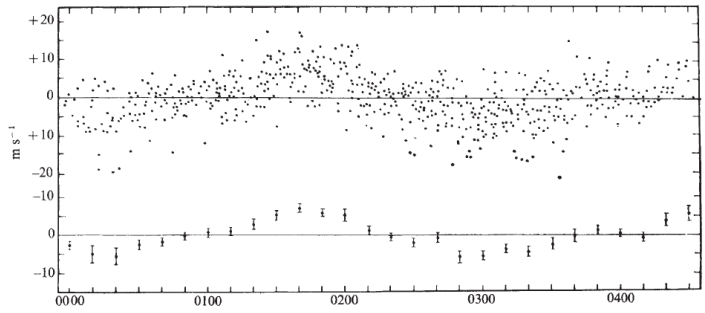

- In 1976, Severny, Kotov and Tsap observed the Doppler-shift difference between the central part of the solar disk and the whole disk and detected global-Sun variations with period of 160.01 min. The result was confirmed by 3 other groups. However, no explanation was found. The period was very close to 1/9 of day.
- This led to suggestions to perform helioseismology observations from space.

Measurements of Line Shift. Doppler Compensator.

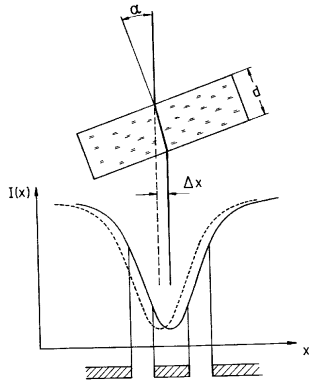

The Doppler compensator is a glass plate which is inclined to balance signals in the line wings recorded by two photomultipliers. It is used in magnetographs. The angle α is proportional to the line shift $\Delta\lambda_D = \lambda v/c$. From this we can determine the line-of-sight velocity v.

Resonance-Scattering Spectrometer.

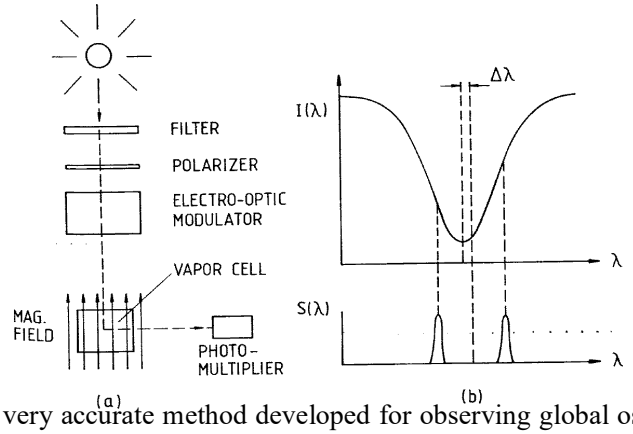

This is a very accurate method developed for observing global oscillations of the Sun in sodium line. The vapor cell with external magnetic field provides signals of the light scattered in two wings, which are measured by a photomultiplier. The difference of these signals is proportional to the Doppler shift.

Resonance-scattering spectrometer- GOLF instrument on SOHO (Global Oscillations at Low Frequencies)

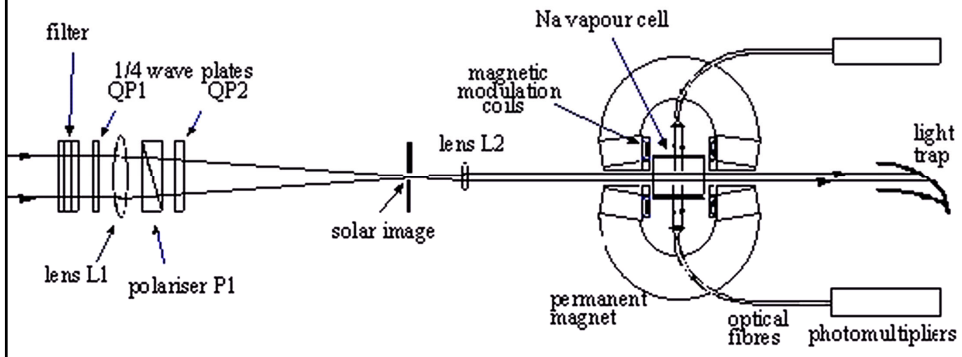

5000 G magnetic field

Discovery of global 5-min oscillations

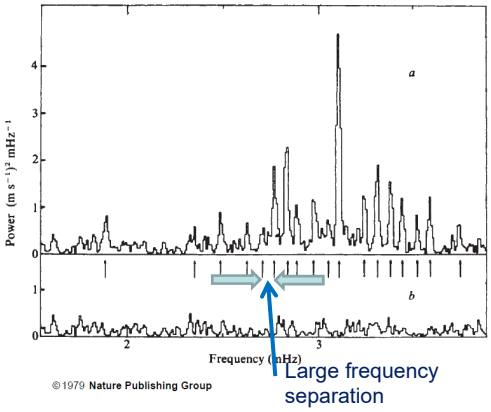

Fig. 5 *a*, Power spectra of two consecutive days of data obtained at Izana on 4 and 5 August 1978. *b*, Power spectra of the same data after subtraction of indicated discrete frequencies.

In 1979 using a new method of resonant spectroscopy Claverie et al observed the Doppler shift of the Sun as a star, and discovered the discrete modal structure of the 5-min oscillations.

The peaks of the global solar oscillation are equidistant in the power spectrum.

It was theoretically predicted by Vandakurov (1968)

Low-degree p-modes

For $l << n$, $r_1 \approx 0$, and we get: $\omega \approx \frac{\pi(n + L/2 + \alpha)}{\int_0^R \frac{dr}{c}}$.

That is the spectrum of low-degree p-modes is approximately equidistant with frequency spacing: $\Delta\nu = \left(4\int_0^R \frac{dr}{c}\right)^{-1}$.

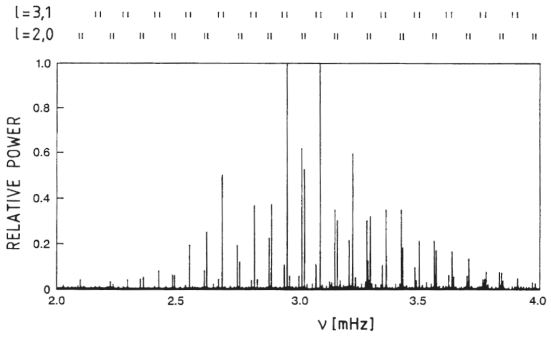

Fig. 5.8. Power spectrum of low-degree solar oscillations. From observations of G. R. Isaak and collaborators, obtained in 1981 over three months at Tenerife and Hawaii. *Top lines*: theoretical identification. From Leibacher et al. (1985)

Maximum amplitude is around 3,300 μHz, or 3.3 mHz. The corresponding oscillation period is 300 seconds or 5 minutes.

Problem of identification of normal modes (1979-1983)

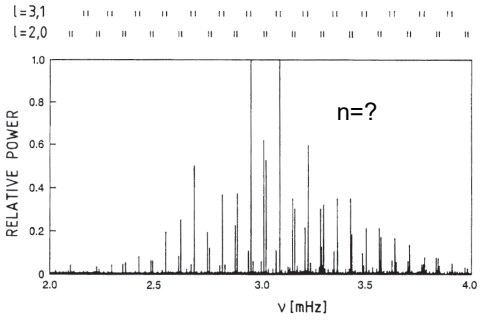

Fig. 5.8. Power spectrum of low-degree solar oscillations. From observations of G. R. Isaak and collaborators, obtained in 1981 over three months at Tenerife and Hawaii. *Top lines*: theoretical identification. From Leibacher et al. (1985)

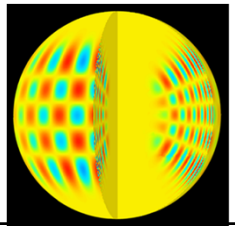

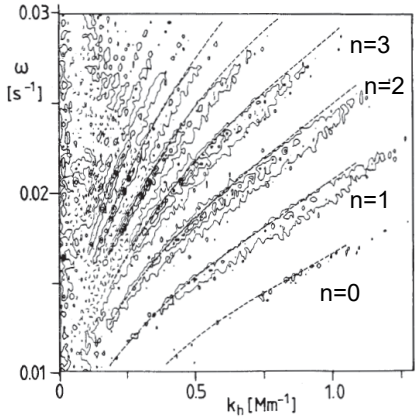

For determining the internal structure of the Sun it is important to identify the observed oscillations as the normal modes with 3 “quantum” numbers: angular degree, l, angular order, m, and radial order, n.

The radial order identifications of low-degree modes

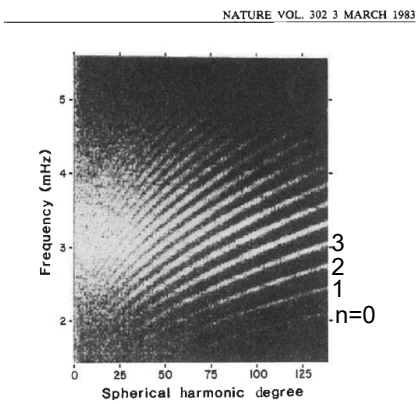

Fig. 2 Spectrum of solar oscillations in the degree range 0–139 and the frequency range 1,416 to 5,583 μHz. The frequency resolution has been degraded to 8 μHz.

- In 1983, using observations made at the South Pole Duvall and Harvey were able to link the high- and low-degree modes, and identified the radial orders in the global oscillation spectrum.
- It turned out that the observed oscillation frequencies closely correspond to the mode frequencies of the standard solar model that predicted high neutrino flux.
- Therefore, helioseismology showed that the solution of the solar neutrino problem is within the particle physics.

- NASA Solar Physics Exploration Seminar (April 10, 1991).
  - Speaker: Douglas Gough

Solar and Heliospheric Observatory (SOHO) makes continuous observations of the Sun since 1996.

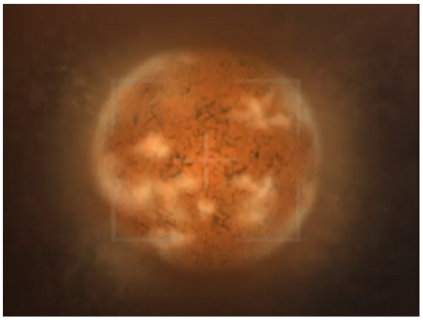

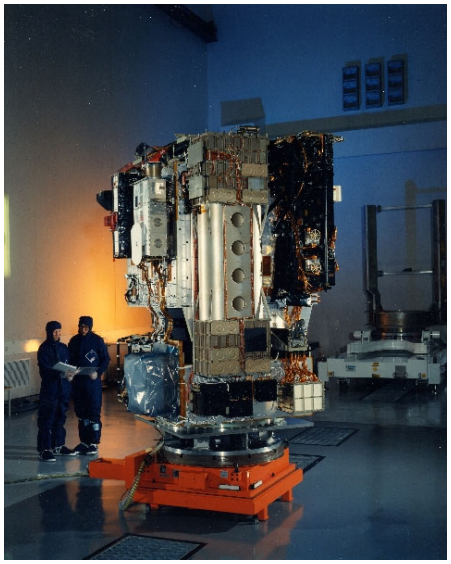

1/21/2022 http://sohowww.nascom.nasa.gov/ 27

Michelson Doppler Imager (MDI)

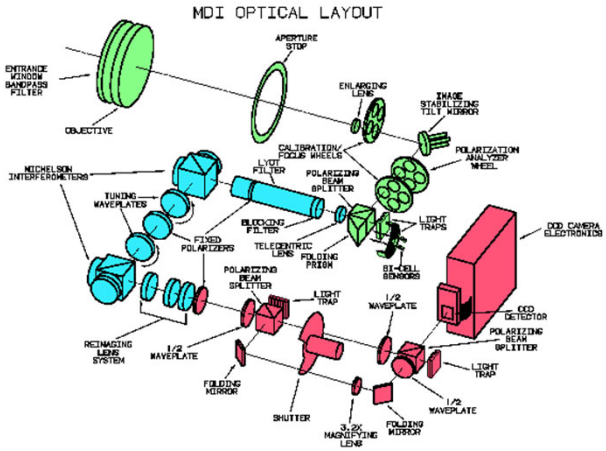

MDI provided Doppler images every minute with resolution 256x256 pixels uninterruptedly, and with resolution 1024x1024 pixels for 2 month a year.

MDI principle

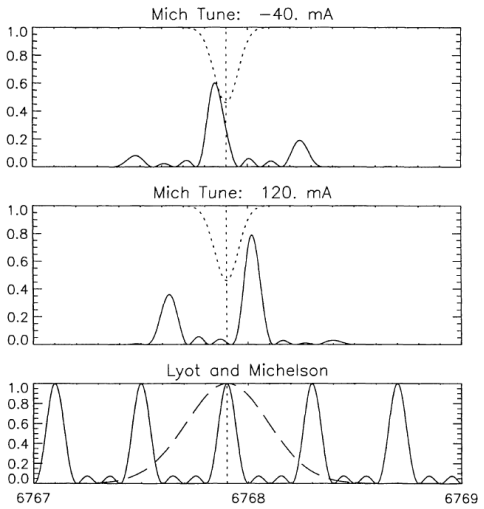

Fig. 7. MDI's principle of operation. The lower panel shows the individual profiles of the Lyot filter (dashed line) and the channel spectrum of both Michelsons in series (solid line). The upper panels illustrate the situation for two of the four nominal Doppler tunings. The solid line represents the resulting instrument transmission profile for the corresponding tuning position with respect to the 6768 Å line profile (dotted line).

The Michelson Doppler Imager (MDI) on SOHO and Helioseismic and Magnetic Imager (HMI) on SDO are examples of the Fourier Transform Spectrometer. MDI measures $I(\lambda)$ at 5 positions across the line (Ni I 6768A) , and HMI measures at 6 positions for Fe I (6173A).

The advantage of these type of measurements is that there is no need for a narrow entrance slit of the spectrometer.

Solar oscillation movie from MDI

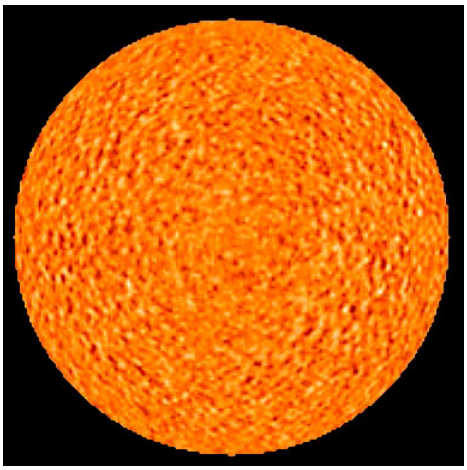

MDI discoveries

http://soi.stanford.edu

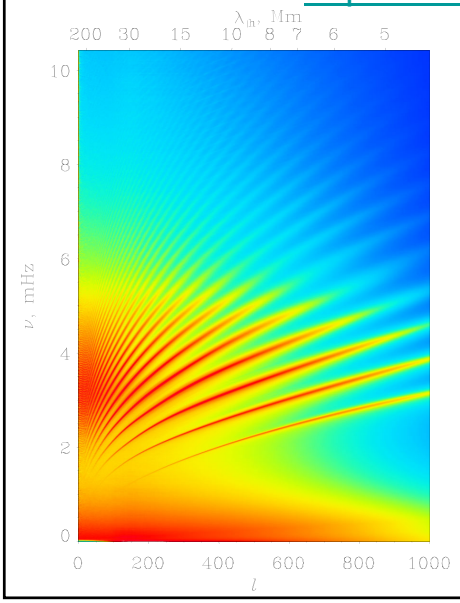

- Differential rotation: near-surface shear layer, tachocline, torsional oscillations
- Subsurface supergranulation and large-scale flows ("Solar Subsurface Weather")
- Structures and flows beneath active regions.
- Sunquakes
- Changes of the meridional circulation with solar cycle
- Far-side imaging

Time-distance helioseismology

A remarkable discovery was made by Tom Duvall in 1993 that the travel times of the solar waves can be measured by using a cross-covariance function of the stochastic wave field:

Integration time

$$\psi(\tau,\Delta)=\int_0^T f(t,r)\,f^*(t+\tau,r+\Delta)\,dt$$

or C(¿;¢)

Time

Distance

Oscillation signal (Doppler velocity, intensity etc) at two points on the Sun's surface

Global helioseismology estimates frequencies of normal modes from oscillation power spectra

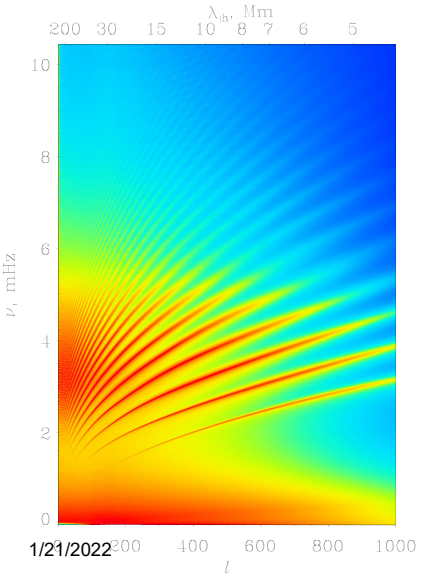

Time-distance helioseismology measures travel time delays and wave phase shifts from cross-covariance:

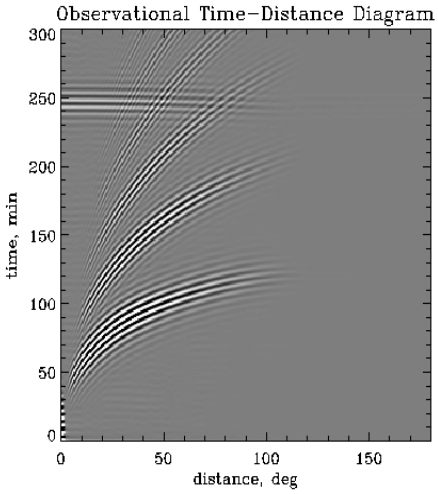

1/21/2022

Time-distance helioseismology

Measures travel times of acoustic or surface gravity waves propagating between different surface points through the interior. The travel times depend on conditions, flow velocity and sound speed along the ray path:

$$\delta\tau = -\int_{\Gamma} \frac{k}{\omega}\frac{\delta c}{c} ds - \int_{\Gamma} \frac{\left(\vec{n}\cdot\vec{U}\right)}{c^2} ds$$

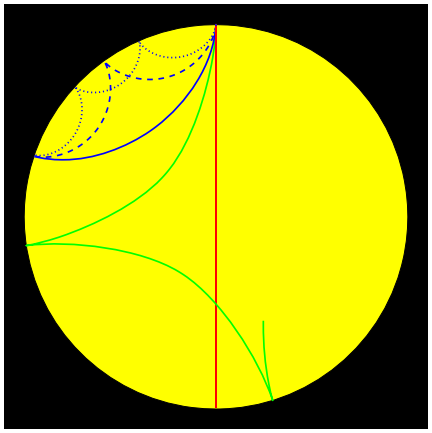

Subsurface image of a sunspot

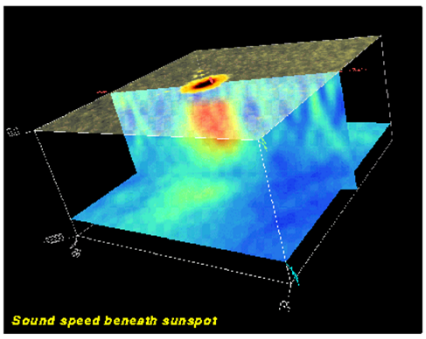

Sunspot data from MDI High Resolution, 18 June 1998

- An image of the sound speed below a sunspot derived from dopplergrams observed with the Michelson Doppler Imager onboard the Solar and Heliospheric Observatory spacecraft using the technique of time-distance helioseismology.
- Three planes are shown, on top the intensity at the surface which shows the sunspot with the dark central umbra surrounded by the somewhat brighter, filamentary penumbra.
- The second plane is a vertical cut from the surface to a depth of 24000 km showing areas of faster sound speed as reddish colors and slower sound speed as bluish colors.
- The sound speed is affected both by the temperature of the gas and the magnetic field, which we know to be strong in the sunspot at the surface. The normal increase of sound speed with depth in the sun has been subtracted so that we are only looking at deviations from the average.
- The third plane (bottom) is a horizontal cut at a depth of 22000 km showing the horizontal variation of sound speed over a region of 150000x150000 km.

Solar Dynamics Observatory
(launched on February 11, 2010)

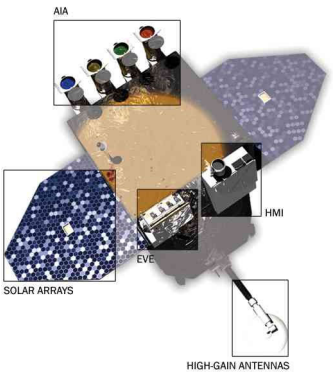

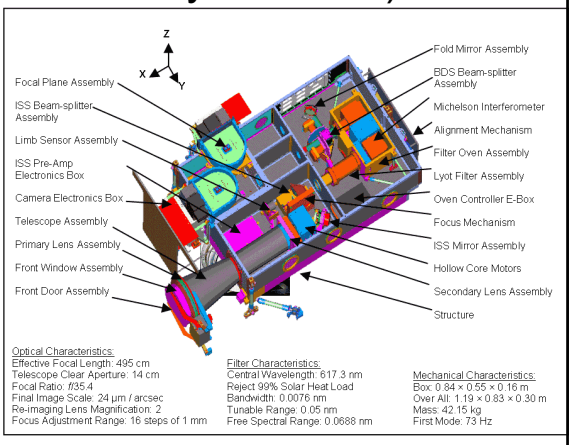

Helioseismic and Magnetic Imager (HMI) provides uninterrupted 4096x4096-pixel Doppler images every 45 sec.

The MDI observation program was terminated on 12 April 2011

HMI principle

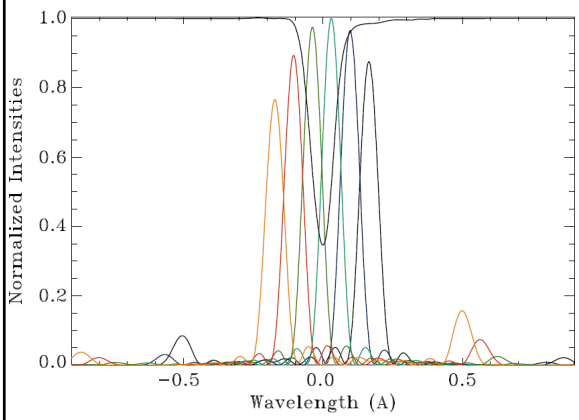

Six tuning positions of the HMI instrument on Solar Dynamics Observatory (SDO) are shown here with respect to the Fe I 6173A solar line at disk center and at rest.

During observations the line profile is shifted due to the surface motions and spacecraft orbital velocity (Doppler effect), and also the line split in magnetic field (Zeeman effect). These line changes are used to measure the Doppler velocity and magnetic field strength.

Solar Dynamics Observatory

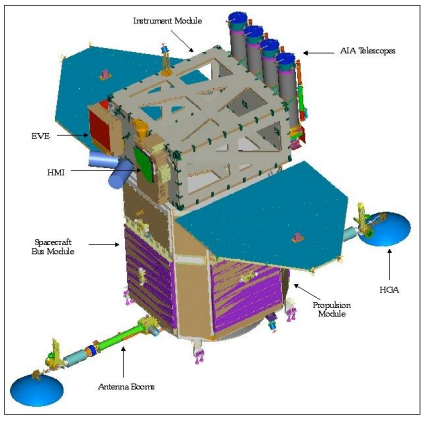

Geostationary orbit for uninterrupted observations of the Sun.

Helioseismic and Magnetic Imager (HMI)
- Full-disk Dopplergrams and magnetograms
Atmospheric Imaging Assembly (AIA)
– Full-disk images of the chromosphere and corona
Extreme Ultraviolet Variability Experiment (EVE)
– EUV solar irradiance

http://hmi.stanford.edu/

Ground-based helioseismology networks: GONG since 1995

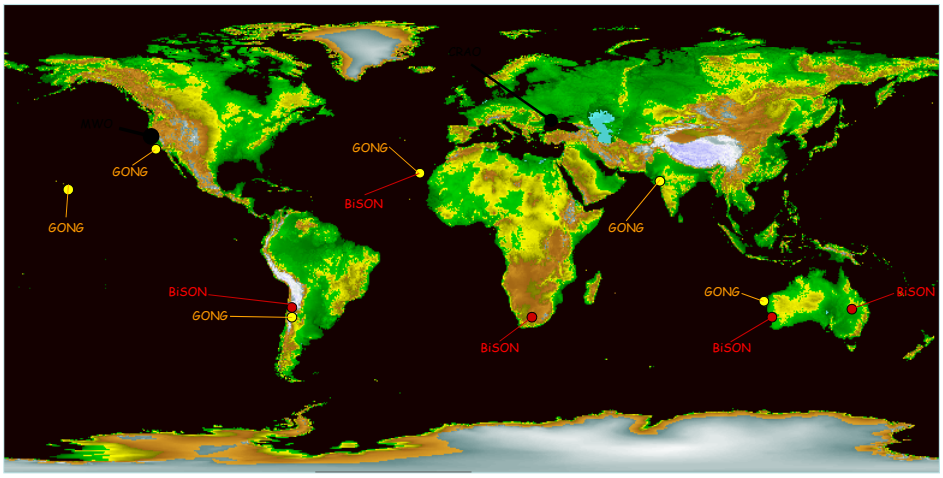

1/21/2022 39

https://gong.nso.edu/

Ground-based helioseismology networks: GONG since 1995

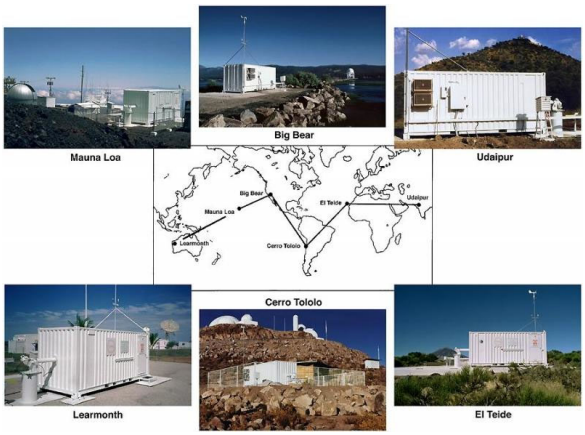

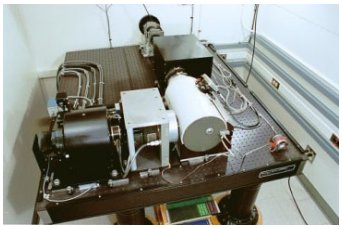

1/21/2022 40

Asteroseismology

Bedding & Kjeldsen (2003)

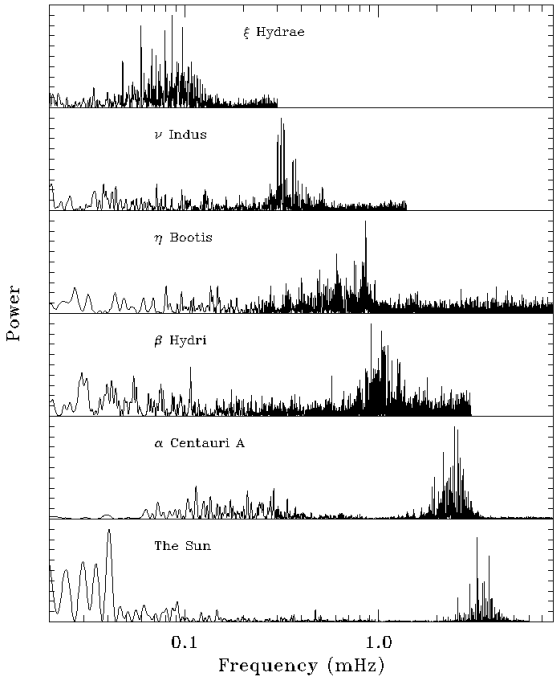

Asteroseismology missions

16 Asteroseismology observations and space missions

Project	Status or Launch	D (in cm)	FOV (in deg × deg)	m_V	Number of stars	Noise (in $ppm^2 \mu Hz^{-1}$)
PRISMA	Phase A	40	1.5 × 1.5	<8	2000	
STARS	Phase A	80	1 × 1	<8	2500	
Eddington	Phase B	120	5 × 5	<11	2000	6
MOST	2003	15	0.4 × 0.4	<6	<6	5.7
CoRoT	2006	25	1 × 1	<7	10	1.7
Kepler	2009	95	10.5 × 10.5	<12	1300	17.6
PLATO	2026	67	47 × 47	<11	85000	4.2
TESS	2018	10	23 × 90	<12	5×10^5	7.6

Stellar oscillations

Solar-type stars

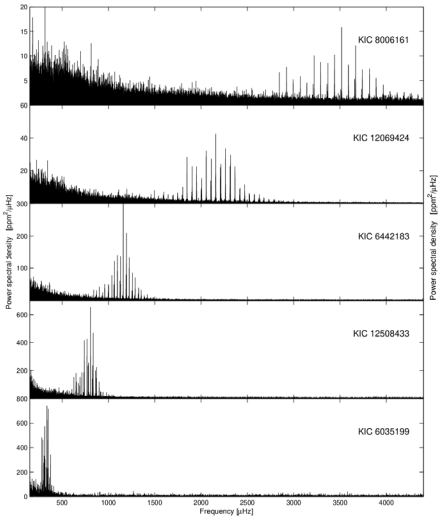

Red giants

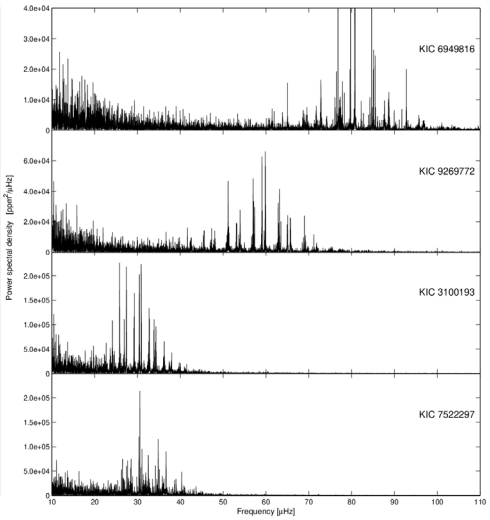

Lecture 2
Observations and basic properties of solar oscillations. Oscillation power spectrum.

(Stix, Chapter 5.1; Kosovichev, p.3-13;
Christensen-Dalsgaard, p. 5-24)

First explanation

- Atmospheric oscillations excited by granular impacts (acting like pistons).

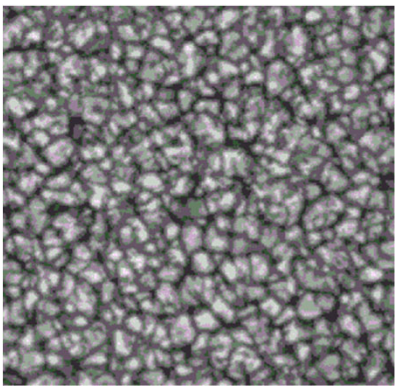

Characteristic frequency of the atmospheric oscillations:

$$\omega = \frac{c}{2H}$$

Where c is the sound speed, H is the pressure scale height

$$H = \frac{\Re \rho T}{\mu g} = \frac{c^2}{\gamma g}$$

$$\omega = \frac{\gamma g}{2c} \qquad P = \frac{4\pi c}{\gamma g}$$

Detection of the ridge structure

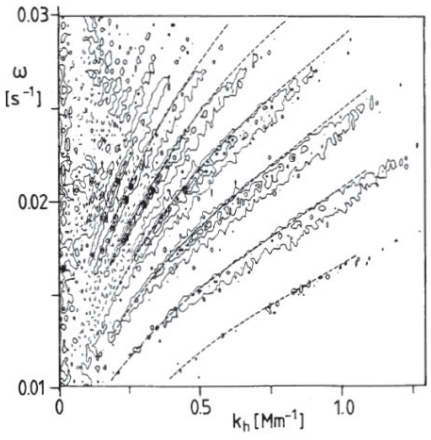

- For the solar oscillations the important fact is that the power is not evenly distributed in the *k*h, *ω*-plane, but instead follows certain *ridges*.
- Each of these ridges corresponds to a fixed number of wave nodes in the radial direction.
- The ridges theoretically predicted by Ulrich (1970) were first observed by Deubner (1975) with the Domeless
- Coude Telescope at Capri.
- Figure 5.4 shows an example, where up to 15 ridges can be identified in the *velocity* power spectrum.

Fig. 5.4. Ridges of p and f modes in the k_h, ω-plane (contours of equal power), and eigenfrequencies of a theoretical solar model (*dotted curves*). After Deubner et al. (1979)

Problem of identification of normal modes

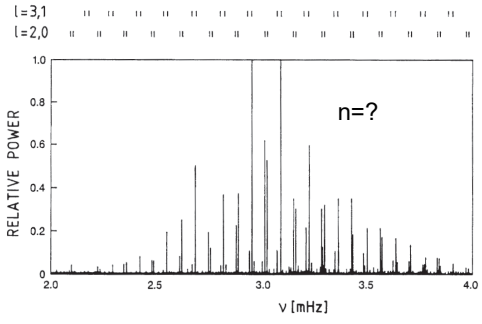

Fig. 5.8. Power spectrum of low-degree solar oscillations. From observations of G. R. Isaak and collaborators, obtained in 1981 over three months at Tenerife and Hawaii. *Top lines*: theoretical identification. From Leibacher et al. (1985)

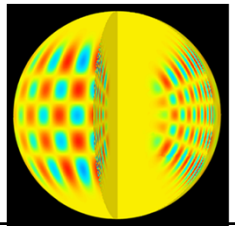

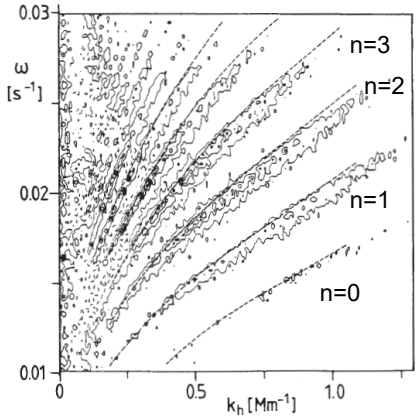

For determining the internal structure of the Sun it is important to identify the observed oscillations as the normal modes with 3 “quantum” numbers: angular degree, l, angular order, m, and radial order, n.

The radial order identifications of low-degree modes

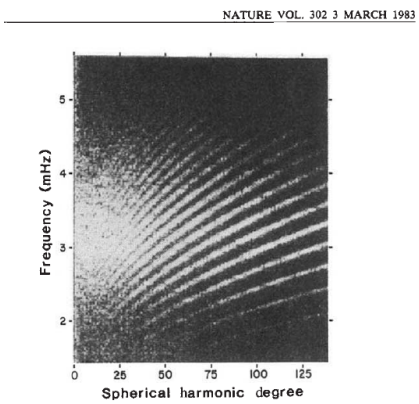

Fig. 2 Spectrum of solar oscillations in the degree range 0–139 and the frequency range 1,416 to 5,583 μHz. The frequency resolution has been degraded to 8 μHz.

- In 1983, using observations made at the South Pole Duvall and Harvey were able to link the high- and low-degree modes, and identified the radial orders in the global oscillation spectrum.
- It turned out that the observed oscillation frequencies closely correspond to the mode frequencies of the standard solar model that predicted high neutrino flux.
- Therefore, helioseismology showed that the solution of the solar neutrino problem is within the particle physics.

Global helioseismology estimates frequencies of normal modes from oscillation power spectra

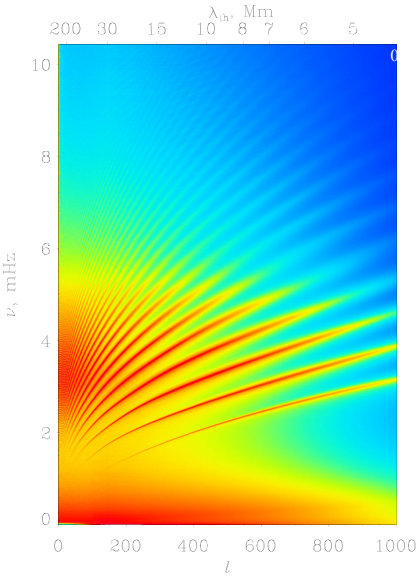

The nature of solar oscillations

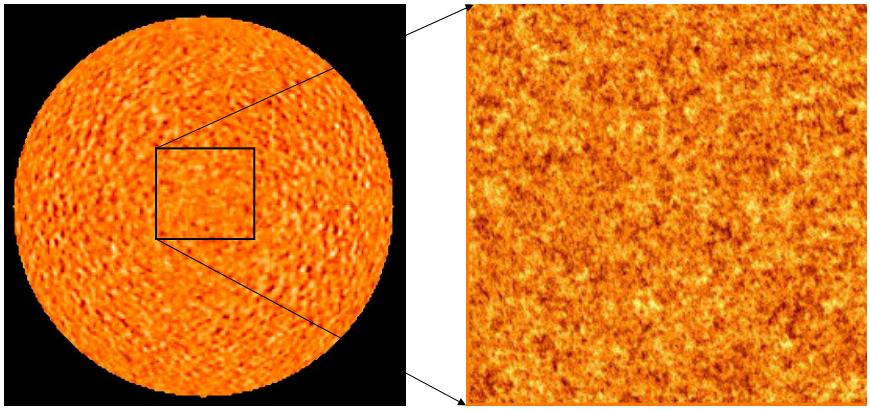

Acoustic and surface gravity waves stochastically excited by turbulent convection in the upper convection zone.

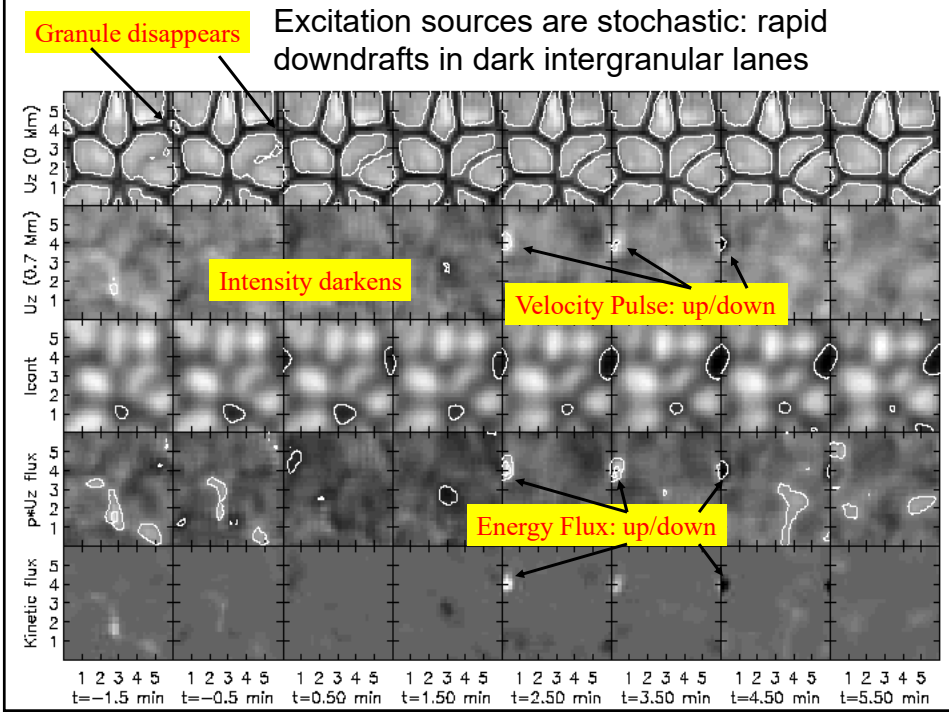

Seismic response to solar flares – “Sunquake”

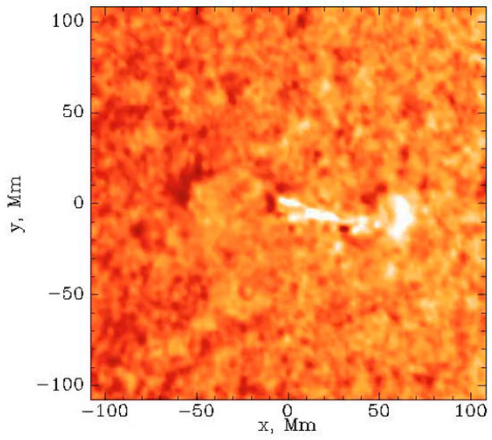

High-energy flare particles heat the solar chromosphere generating a shock propagating downward and hitting the surface.

Enhanced images of the flare ripples on the Sun’s surface

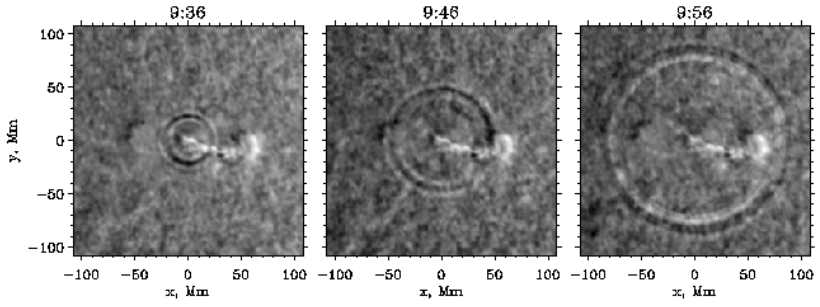

Compare with water ripples

Time-distance diagram of the flare seismic response calculated by averaging the wave front over 360 degrees

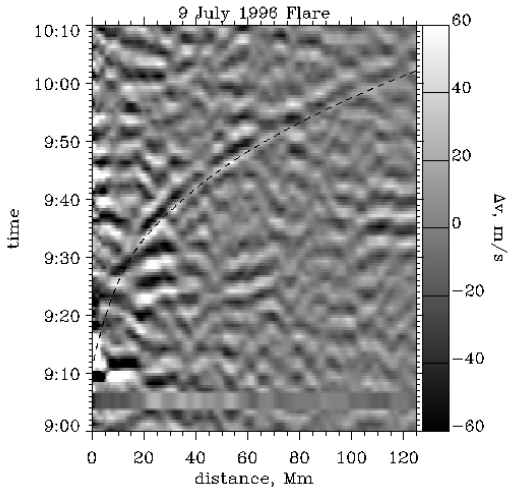

The propagation speed of the seismic wave:

$V=\delta(\text{distance})/\delta(\text{time})$

increases with time from 10 km/s to 100 km/s.

Why?

11

Propagation of acoustic waves on the Sun

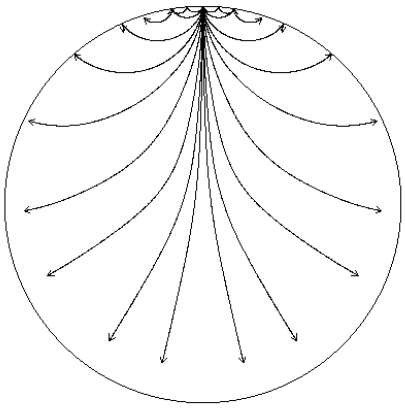

The wave front on the surface accelerates because it is formed by acoustic waves propagating through the solar interior where the sound speed is higher.

12

The basic idea of helioseismology

- To measure travel times τ or resonant frequencies ω, and to determine the internal properties of the Sun, such as the sound speed $c_s(r)$

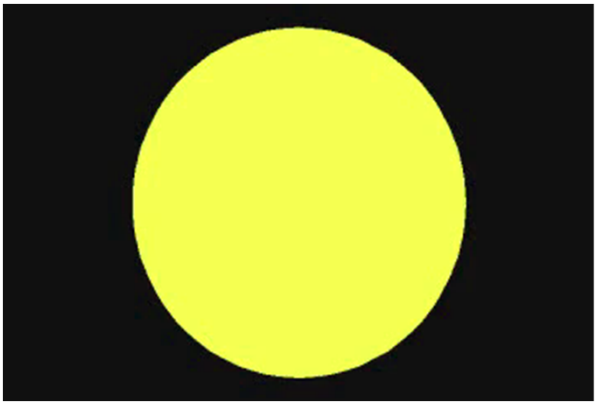

Time-distance helioseismology

- Using the time-distance diagram one can measure the travel time of acoustic waves for various distances, and then infer the sound speed along the wave paths.
- Can we measure the travel times by using the stochastic wave field continuously generated by the turbulent convection?

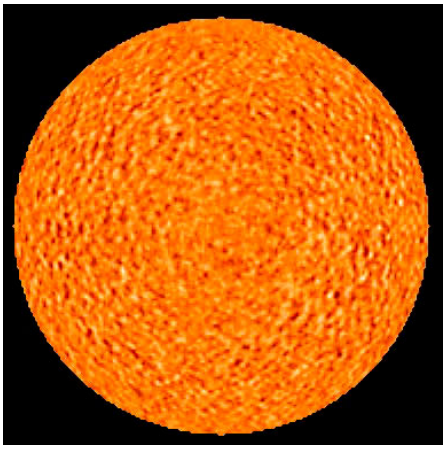

Time-distance helioseismology

A remarkable discovery was made by Tom Duvall in 1993 that the travel times of the solar waves can be measured by using a cross-covariance function of the stochastic wave field:

Integration time

$$\psi(\tau,\Delta) = \int_0^T f(t,r) f^*(t+\tau, r+\Delta) dt$$

or C(¿; ¢)

Time

Distance

Oscillation signal (Doppler velocity, intensity etc) at two points on the Sun's surface

Time-distance helioseismology measures travel time delays and wave phase shifts from cross-covariance:

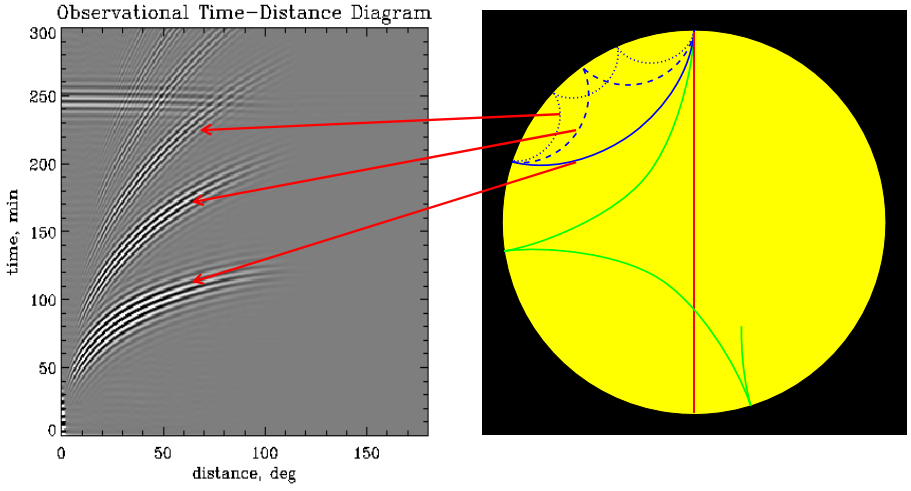

Time-distance helioseismology

Measures travel times of acoustic or surface gravity waves propagating between different surface points through the interior. The travel times depend on conditions, flow velocity and sound speed along the ray path:

$$\delta\tau = -\int_{\Gamma} \frac{k}{\omega}\frac{\delta c}{c} ds - \int_{\Gamma} \frac{\left(\vec{n}\cdot\vec{U}\right)}{c^2} ds$$

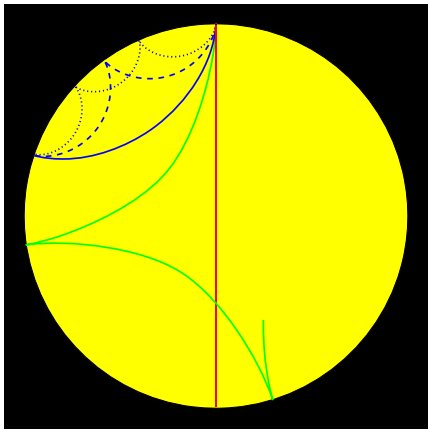

Solar oscillations.

- Observations.
- Theory of p-, g-, and r-modes.
- Excitation mechanisms.
- Oscillations of solar-type stars.

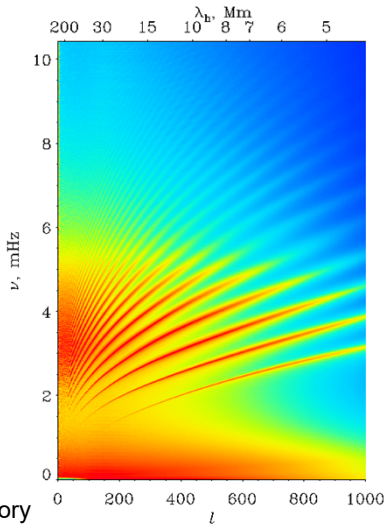

Oscillation power spectrum from Solar and Heliospheric Observatory

Normal Mode of Solar Oscillations –
displacement eigenfunction: $\delta r(r,\theta,\phi)=\xi(r)*Y_{lm}(\theta,\phi)$

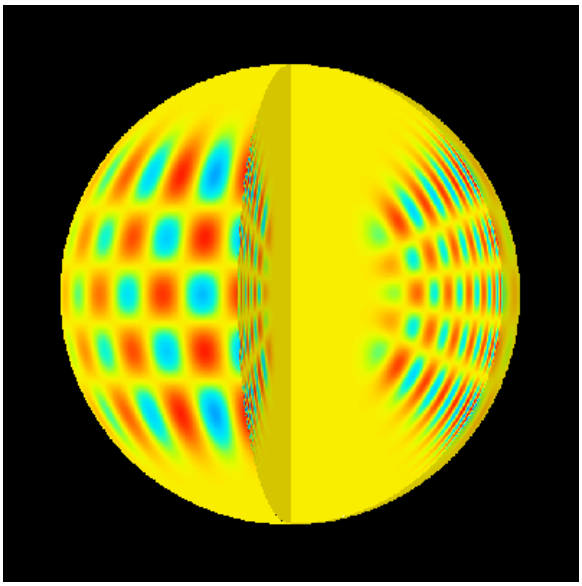

l=20, m=16

The rotation speed of the solar surface is 2km/s.

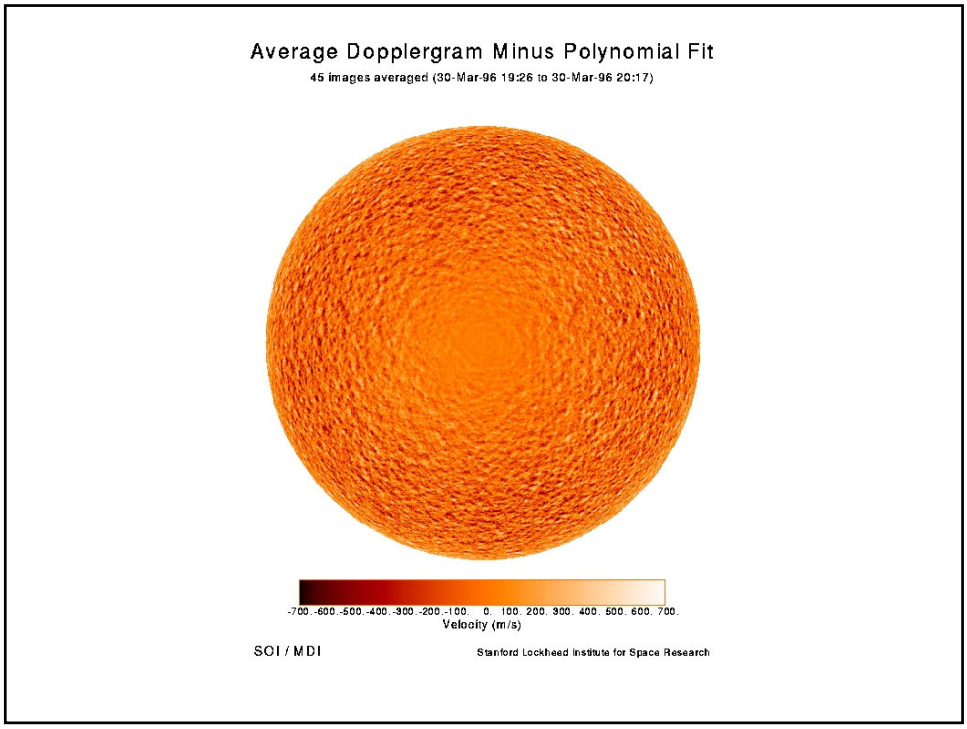

Dopplergram of Solar Oscillations

MDI single Dopplergram minus an average solar velocity image observed over 45 minutes reveals the surface motions associated with sound waves traveling through the Sun's interior. The small scale light and dark regions represent the up and down motions of the hot gas near the Sun's surface. The pattern falls off towards the limb because the acoustic waves are primarily radial.

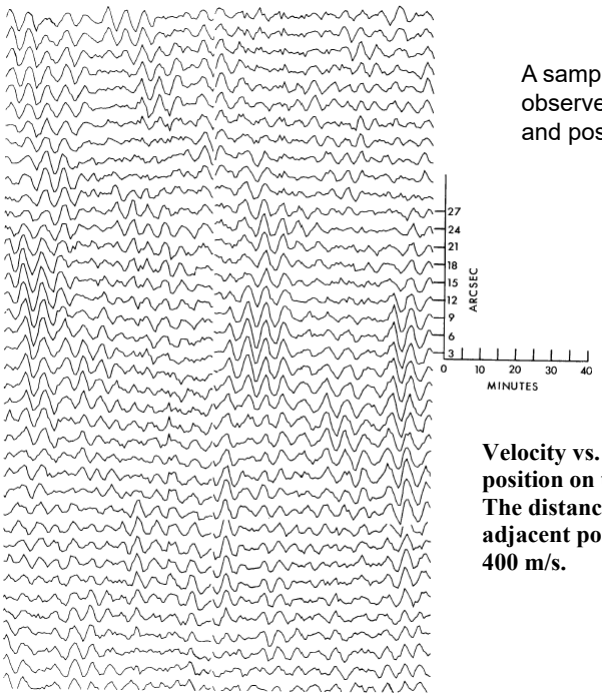

A sample of solar oscillations observed as a function of time and position on the disk

Velocity vs. time (horizontal axis) and position on the solar disk (vertical axis). The distance between the curves for adjacent points is equal to a velocity of 400 m/s.

Power spectrum of solar oscillations

Velocity of oscillations $v(x, y, t)$ can be represented in terms of its Fourier components:

$$a(k_x, k_y, \omega) = \iiint v(x, y, t) e^{i(k_x x + k_y y + \omega t)} dx dy dt,$$

where k_x and k_y are components of the wave vector, ω is the frequency.

The power spectrum is: $P(k_x, k_y, \omega) = a^* a$, where a^* is complex conjugate.

If there is no preference in the direction of the wave propagation then P depends on two variables, the horizontal wavenumber $k_h = \sqrt{k_x^2 + k_y^2}$, and frequency.

Then, we calculate the angular average in the *k*-space:

$$P(k_h, \omega) = \frac{1}{2\pi} \int_0^{2\pi} P(k_{h,} \cos\phi, k_h \sin\phi, \omega) d\phi$$

This is a local power spectrum. It allows us to investigate properties of various regions observed on the solar disk.

Consider example using IDL code: power_spectrum.pro.

3D Power Spectrum

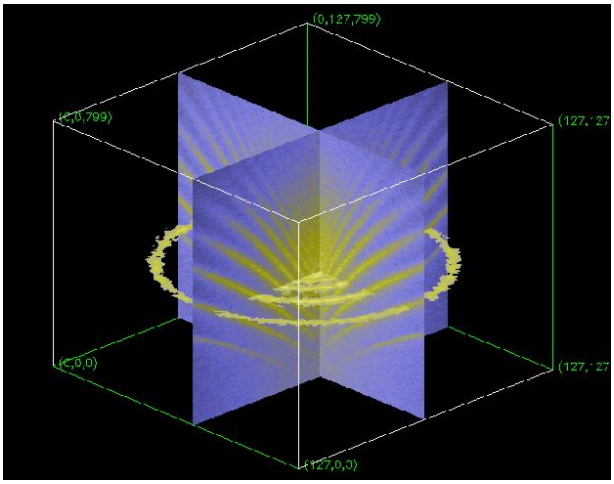

Spherical harmonic transform

For the global oscillations we must use the spherical coordinates (r,θ,ϕ) and expansion in terms of spherical surface harmonics:

$$v(\theta,\phi,t)=\sum_{l=0}^{\infty}\sum_{m=-l}^{l}a_{lm}(t)Y_l^m(\theta,\phi)$$

In the spherical coordinates, θ,ϕ:

$$a(l,m,\omega)=\iiint v(\theta,\phi,t)Y_l^m(\theta,\phi)e^{i\omega t}d\theta d\phi dt,$$

where $Y_l^m(\theta,\phi)=P_l^{|m|}(\theta)e^{im\phi}$ is a spherical harmonic of **the angular degree** l **and angular order** m, $P_l^m(\theta)$ is an associate Legendre function.

Degree l gives the total number of node circles on the sphere; order m is the number nodal circles through the poles.

Single Harmonics

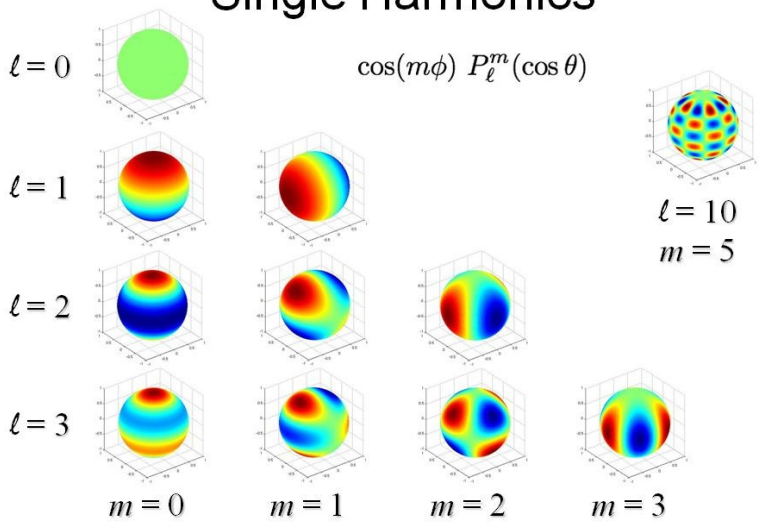

Degree l gives the total number of node circles on the sphere; order m is the number nodal circles through the poles.

Spherical harmonic power spectrum

The coefficients of the spherical harmonic expansion can be found by using the spherical harmonic transform:

$$a(l,m,\omega) = \iiint v(\theta,\phi,t) Y_l^m(\theta,\phi) e^{i\omega t} d\theta d\phi dt,$$

where $Y_l^m(\theta,\phi)$ is a spherical harmonic of **the angular degree** l **and angular order** m.

The power spectrum is:

$$P(l,m,\omega) = a^* a.$$

For a spherically symmetrical star, P depends only on l and ω.
In this case the power spectrum is 'degenerate' with respect of angular order m.

Then we can define the analog of the horizontal wavenumber:

$k_h = \dfrac{\sqrt{l(l+1)}}{R}$, where R is the solar radius.

We will derive this in a future lecture.

Oscillation power spectrum

- The power spectrum represents the oscillation signal in terms of spherical harmonics of **angular degree** l (and the **horizontal wavelength**, $\lambda_h = 2\pi/k_h$), and the oscillation **"cyclic" frequency**, $\nu=\omega/2\pi$.

l is integer number

λ_h is measured in Mm

ν is measured in mHz

ω is measured in rad/sec

(sometimes called angular frequency)

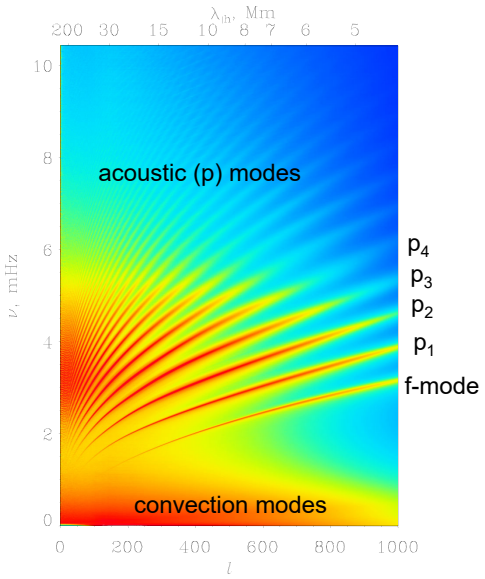

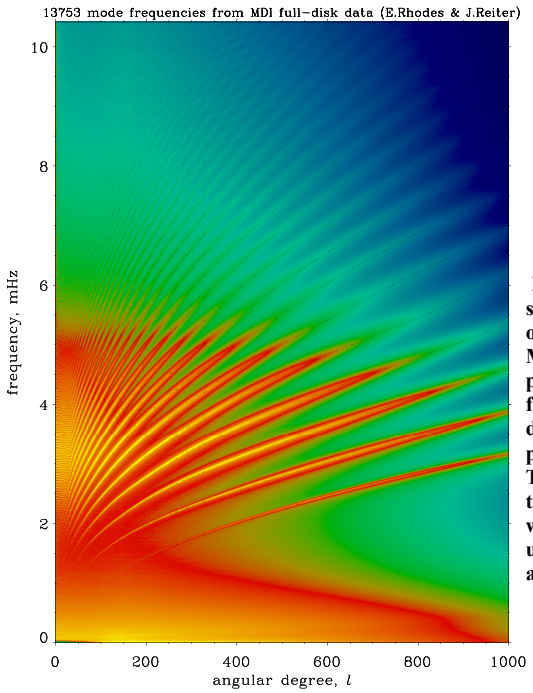

Power spectrum of solar oscillations obtained from the MDI data. Black points are mode frequencies determined from the power spectrum. The lowest ridge is the surface gravity wave (f-mode). The upper ridges are acoustic (p) modes.

Low-Degree (Global) Modes

When the Sun is observed as a star (integrated whole-disk Doppler-shift measurements) the power spectrum consists only of low-degree p-modes of $l = 0, 1, 2$ and 3.

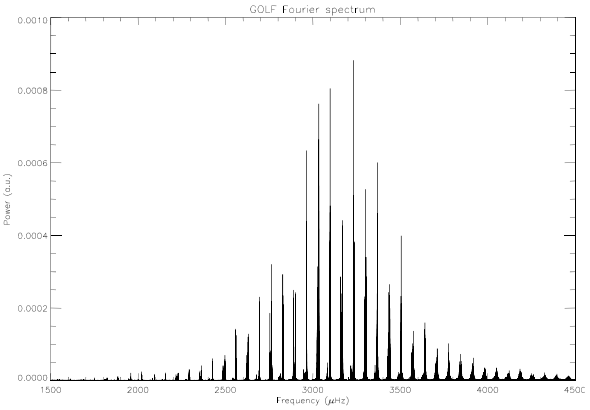

The distance between main peaks in the power spectrum is about 68 μHz. The corresponding time: $1/(68 \cdot 10^{-6}) = 245$ min is the travel time for acoustic waves propagate through the center of the Sun to the far side and come back. The low-degree mode provide information about physical conditions of the solar core.

This figure is a Fourier spectrum of the longest continuous GOLF time series (805 days). GOLF is an instrument on SOHO that measures the oscillations in the line-of-sight velocity of the solar photosphere from the whole Sun. These oscillations appear at precise frequencies, visible as sharp peaks in this spectrum, mainly around 3mHz, corresponding to periods about 5min.

Lecture 3

Basic questions of helioseismology
Oscillation power spectrum.

(Stix, Chapter 5.1.2-5.1.4; Kosovichev, p.11-17; Christensen-Dalsgaard, p. 5-24)

Basic questions of helioseismology

1. What are the chemical composition and thermodynamic conditions inside the Sun?
2. How fast is the internal rotation of the Sun?
3. Is there meridional circulation inside the Sun?
4. What is the structure of solar convections?
5. What is the source of solar magnetic fields?
6. How are the magnetic active regions and sunspots formed?
7. What is the cause of the instability of magnetic fields and mass eruptions?
8. How can we predict the periods of high solar activity?

Internal structure

- Convective instability.
- Convective energy transfer.
- Non-standard solar models.
- Solar neutrinos, neutrino transitions, MSW effect.

- Variations of the sound speed detected by helioseismology

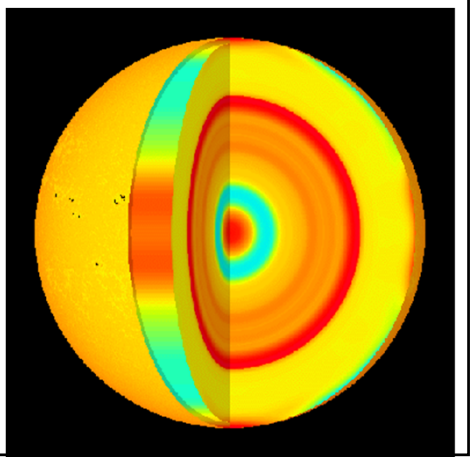

Global Helioseismology

- Variational principle
- Perturbation theory.
- Inversions, sound speed and rotation inferences.

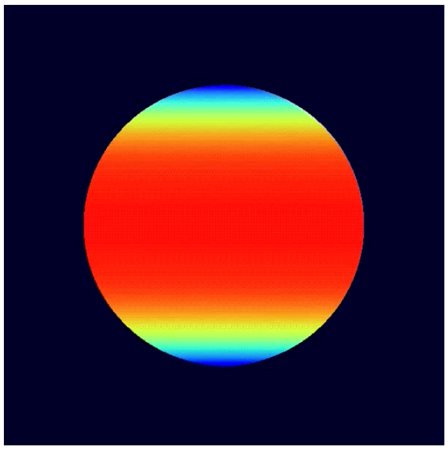

Local Helioseismology

- Local-area helioseismology
- Ring-diagrams
- Acoustic imaging
- Time-distance tomography.

Subsurface structure of sunspot

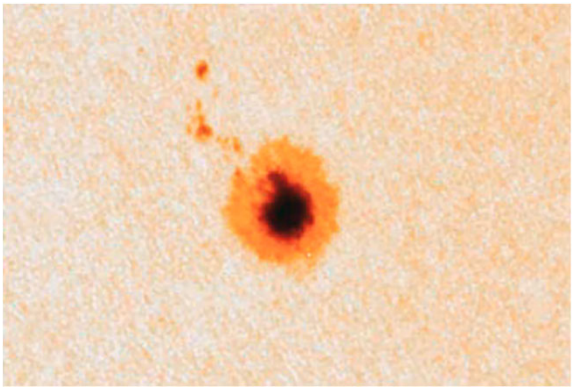

Subsurface structure and dynamics.

- Far-side imaging.
- Meridional circulation.
- Emerging magnetic flux.
- Active region dynamics.

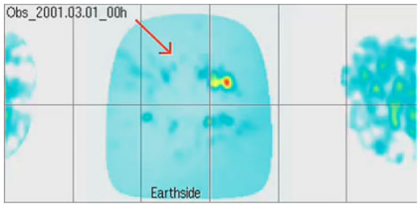

Illustration of far-side imaging of active regions

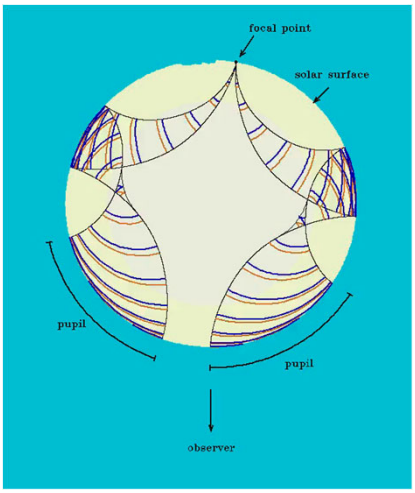

Convection.

- Granulation, supergranulation, giant cells.
- Near-Surface Shear Layer.
- Rotational and magnetic effects.
- Numerical simulations.

3D numerical simulations of solar granulation

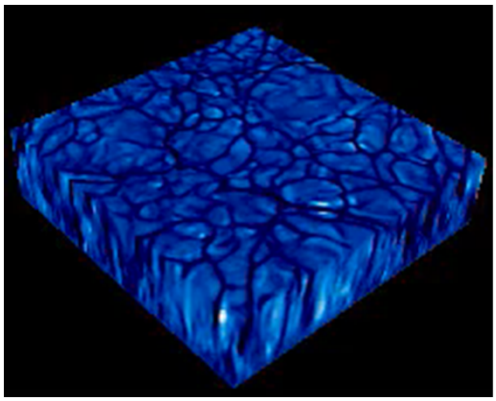

Differential rotation.

.

- Oblateness, quadrupole moment, test of the general relativity.
- Models of differential rotation.
- Rotation of solar-type stars.

Rotation rate inside the Sun determined by helioseismology

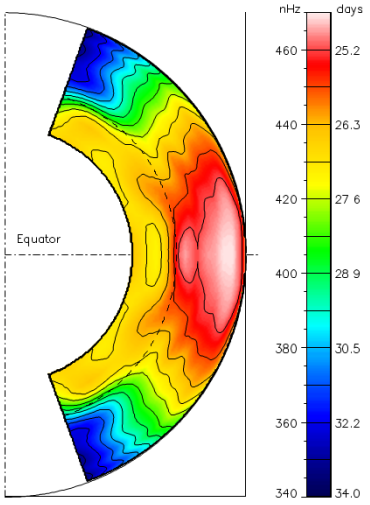

Dynamo theory.

- Mean-field electrodynamics.
- Alpha- and Omega-effects.
- Dynamo models.
- 3D MHD simulations.

Animation of the solar dynamo

Zonal acceleration reveals patterns of dynamo waves

Measurements of the zonal acceleration revealed zones of deceleration, caused by internal magnetic fields (blue areas in the movie).

The flow deceleration originates at the base of the solar convection zone, 200 Mm beneath the solar surface, at about 60 degrees latitude.

This is the primary seat of the solar dynamo.

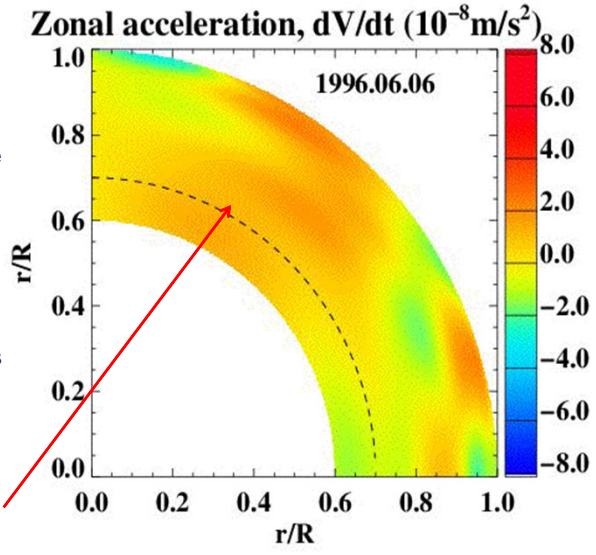

Sunquakes

- Energetic particles.
- Thin- and thick-target models, chromosphe evaporation, heat conduction.
- Radiative and MHD shocks.

Sunquakes – helioseismic waves excited by solar flares

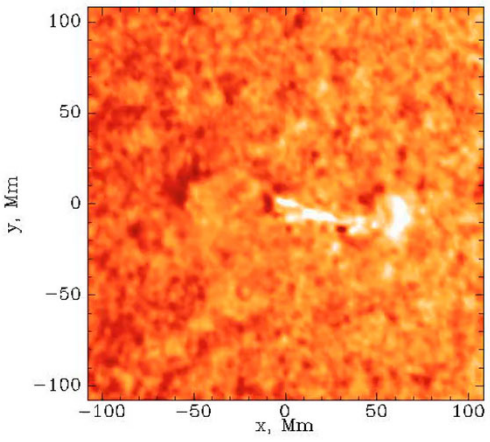

Power spectrum of solar oscillations

Velocity of oscillations $v(x, y, t)$ can be represented in terms of its Fourier components:

$$a(k_x, k_y, \omega) = \iiint v(x, y, t) e^{i(k_x x + k_y y + \omega t)} dx dy dt,$$

where k_x and k_y are components of the wave vector, ω is the frequency.

The power spectrum is: $P(k_x, k_y, \omega) = a^* a$, where a^* is complex conjugate.

If there is no preference in the direction of the wave propagation then P depends on two variables, the horizontal wavenumber $k_h = \sqrt{k_x^2 + k_y^2}$, and frequency.

Then, we calculate the angular average in the *k*-space:

$$P(k_h, \omega) = \frac{1}{2\pi} \int_0^{2\pi} P(k_h \cos\phi, k_h \sin\phi, \omega) d\phi$$

This is a local power spectrum. It allows us to investigate properties of various regions observed on the solar disk.

Consider example using IDL codepower_spectrum.pro.

3D Power Spectrum

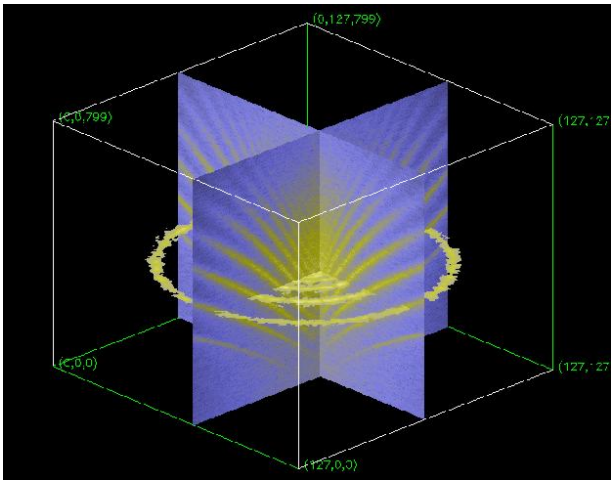

Spherical harmonics

For the global oscillations we must use the spherical coordinates (r, [illegible])
and expansion in terms of spherical surface harmonics:

$$v(\theta,\phi,t)=\sum_{l=0}^{\infty}\sum_{m=-l}^{l}a_{lm}(t)Y_l^m(\theta,\phi)$$

In the spherical coordinates, θ,ϕ:

$$a(l,m,\omega)=\iiint v(\theta,\phi,t)Y_l^m(\theta,\phi)e^{i\omega t}\sin(\theta)d\theta d\phi dt,$$

where $Y_l^m(\theta,\phi)=P_l^{|m|}(\theta)e^{im\phi}$ is a spherical harmonic of **the angular degree** l **and angular order** m, $P_l^m(\theta)$ is an associate Legendre function.

Degree l gives the total number of node circles on the sphere; order m is the number nodal circles through the poles; m=*-l,-l+1,…,l-1, l* that is (2l+1) m-values on m for given l.

Spherical harmonics

The coefficients of the spherical harmonic expansion can be found by using the spherical harmonic transform:

$$a(l,m,\omega) = \iiint v(\theta,\phi,t) Y_l^m(\theta,\phi) e^{i\omega t} \sin(\theta) d\theta d\phi dt,$$

where $Y_l^m(\theta,\phi)$ is a spherical harmonic of **the angular degree** l **and angular order** m.

The power spectrum is:

$$P(l,m,\omega) = a^* a.$$

For a spherically symmetrical star, P depends only on l and ω.
In this case the power spectrum is 'degenerate' with respect of angular order m.

Then we can define the analog of the horizontal wavenumber:

$k_h = \frac{\sqrt{l(l+1)}}{R}$, where R is the solar radius.

We will derive this in a future lecture.

Oscillation power spectrum

- The power spectrum represents the oscillation signal in terms of spherical harmonics of **angular degree** l (and the **horizontal wavelength**, $\lambda_h = 2\pi/k_h$), and the oscillation **"cyclic" frequency**, $\nu = \omega/2\pi$.

l is integer number
λ_h is measured in Mm
ν is measured in mHz
ω is measured in rad/sec
(sometimes called angular frequency)

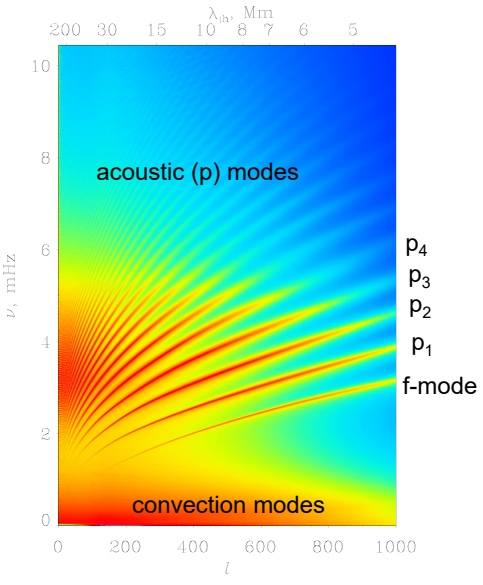

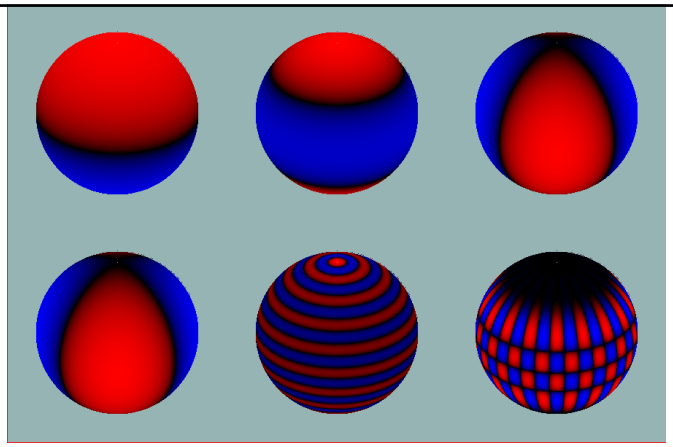

Cyclic frequency $\nu = \frac{\omega}{2\pi}$ is often used as frequency variable.

Because only a hemisphere of the Sun is observed in the power spectrum for a given mode of target l, m beside peaks corresponding to this mode peaks of other modes appear (so-called 'mode leaks'). The spherical harmonics are not orthogonal on a hemisphere.

Mode leakage matrix

For the global oscillations we must use the spherical coordinates $(r, \square\boxtimes)$ and expansion in terms of spherical surface harmonics:

$$v(\theta,\phi,t) = \sum_{l'=0}^{\infty} \sum_{m'=-l'}^{l'} a_{l'm'}(t) Y_{l'}^{m'}(\theta,\phi)$$

The coefficients can found by applying spherical harmonic transform:

$$a_{lm}(t) = \iint_{\Omega} v(\theta,\phi,t) Y_l^m(\theta,\phi) \sin\theta d\theta d\phi,$$

where the integral is calculated over the whole sphere. In this case because the spherical functions are orthogonal the integral will give the exact coefficients, because

$$\iint_{\Omega} Y_{l'}^{m'}(\theta,\phi) Y_l^m(\theta,\phi) \sin\theta d\theta d\phi = \delta_{ll'}\delta_{mm'}$$

However, the oscillations are observed only in one hemisphere the orthogonally is not satisfied, and the spherical harmonic transform gives a combination of the a-coefficients:

$$a_{lm}(t) = \sum_{l'=0}^{\infty} \sum_{m'=-l'}^{l'} S_{l'l}^{m'm} a_{l'm'}(t),$$

where $S_{l'l}^{m'm} = \iint_{hemisphere} Y_{l'}^{m'}(\theta,\phi) Y_l^m(\theta,\phi) \sin\theta d\theta d\phi$ is the "mode leakage matrix"

The mode leakage complicates the analysis of the observed spectra.

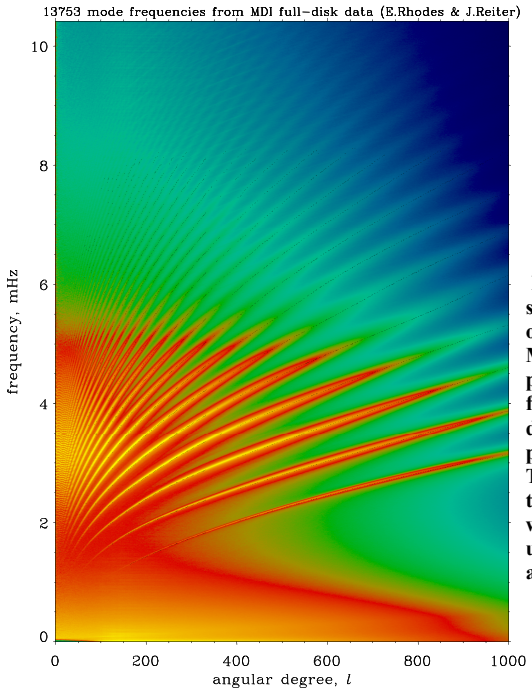

Power spectrum of solar oscillations obtained from the MDI data. Black points are mode frequencies determined from the power spectrum. The lowest ridge is the surface gravity wave (f-mode). The upper ridges are acoustic (p) modes.

Low-Degree (Global) Modes

When the Sun is observed as a star (integrated whole-disk Doppler-shift measurements) the power spectrum consists only of low-degree p-modes of $l = 0, 1, 2$ and 3.

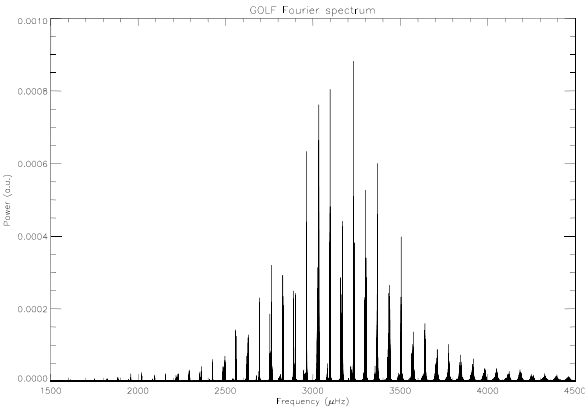

The distance between main peaks in the power spectrum is about 68 μHz. The corresponding time: $1/(68 \cdot 10^{-6}) = 245$ min is the travel time for acoustic waves propagate through the center of the Sun to the far side and come back. The low-degree mode provide information about physical conditions of the solar core.

This figure is a Fourier spectrum of the longest continuous GOLF time series (805 days). GOLF is an instrument on SOHO that measures the oscillations in the line-of-sight velocity of the solar photosphere from the whole Sun. These oscillations appear at precise frequencies, visible as sharp peaks in this spectrum, mainly around 3mHz, corresponding to periods about 5min.

Asteroseismology

Bedding & Kjeldsen (2003)

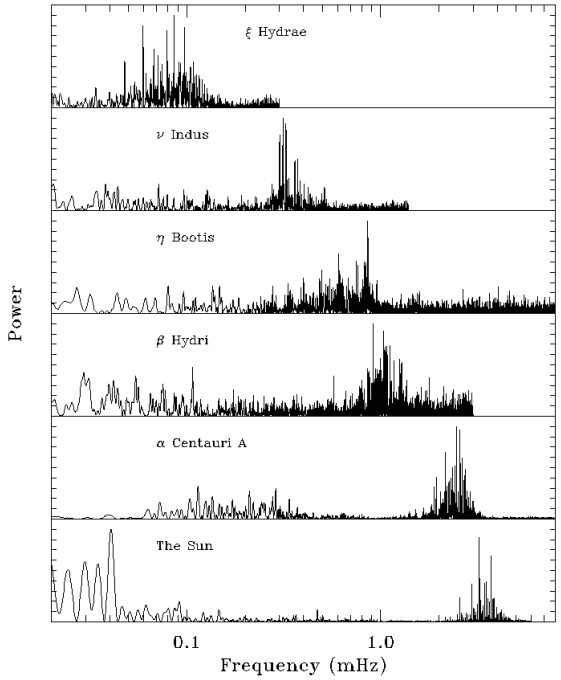

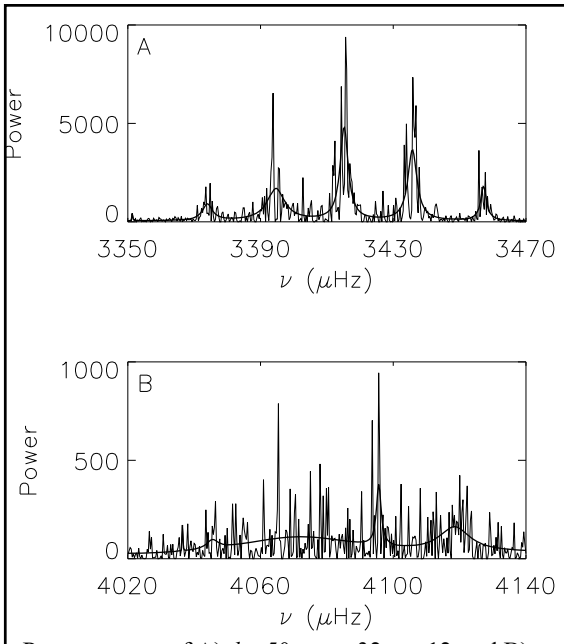

Power spectra of A) $l = 50, m = -32, n = 12$ and B) $l = 50, m = 0, n = 16$.

Excitation of Solar Oscillations

Solar oscillations are randomly excited by turbulent convection. The random excitation function appears as multiplicative noise in the power spectra. This represents the most serious problem for measuring mode frequencies. This figure shows examples of good and poor fits of an oscillation model to the power spectra.

Elements of signal processing

Forward and inverse Fourier transform

$$\tilde{x}(\omega) = \int_{-\infty}^{\infty} x(t) e^{-i\omega t} dt \qquad \omega = 2\pi f$$

$$x(t) = \frac{1}{2\pi} \int_{-\infty}^{\infty} \tilde{x}(\omega) e^{i\omega t} d\omega \qquad e^{i\omega t} = \cos\ \omega t + i \sin\ \omega t$$

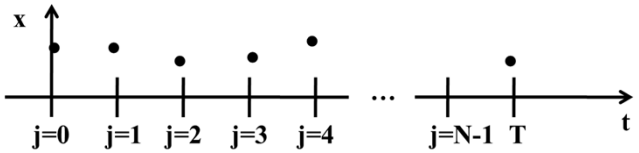

Sample rate, f_s: $f_s = 1/\Delta t$

Duration T, number of samples N, Nyquist frequency:

$$f_s T = N; \qquad f_{Nyquist} = f_s / 2$$

Time index j:

$$t_j = j\Delta t; \qquad j = 0, 1, 2, \ldots N-1;$$

Frequency resolution:

$$\Delta f = 1/T$$

Frequency index k:

$$f_k = k/T; \qquad f_k T = k; \qquad k = 0, 1, 2, \ldots N-1$$

G. Mendel, LIGO-G1200759

Discrete Fourier Transform (DFT)

$$\tilde{x}_k = \sum_{j=0}^{N-1} x_j e^{-2\pi i j k/N} \qquad x_j = \frac{1}{N} \sum_{k=0}^{N-1} \tilde{x}_k e^{2\pi i j k/N}$$

The DFT is of order N^2 operations.
The Fast Fourier Transform (FFT) is a fast way of doing the DFT, of order $N \log_2 N$.

DFT Aliasing

$$f \to -f; \qquad \tilde{x}_{-k} = \tilde{x}_k^*$$

$$f \to f \pm m f_s; \qquad \tilde{x}_{k \pm mN} = \tilde{x}_k; \qquad \tilde{x}_{N-k} = \tilde{x}_k^*$$

$$Useful \quad Band: \qquad [0, f_{Nyquist}] \to k = [0, N/2]$$

Power outside this band is aliased into this band. Thus need to filter data before digitizing, or when changing f_s, to prevent aliasing of unwanted power into this band.

Parseval's Theorem

$$\sum_{j=0}^{N-1}\left|x_j\right|^2 = \frac{1}{N}\sum_{k=0}^{N-1}\left|\tilde{x}_k\right|^2 \qquad \sum_{j=0}^{N-1} x_j y_j = \frac{1}{N}\sum_{k=0}^{N-1}\tilde{x}_k\tilde{y}_k^*$$

Correlation Theorem

$$c_{j'} = \sum_{j=0}^{N-1} x_j y_{j+j'} \qquad \tilde{c}_k = \tilde{x}_k\tilde{y}_k^*$$

Convolution Theorem

$$C_{j'} = \sum_{j=0}^{N-1} x_j y_{j'-j} \qquad \tilde{C}_k = \tilde{x}_k\tilde{y}_k$$

One-sided Power Spectral Density (PSD) Estimation

$$P_k = \frac{2\left\langle\left|\tilde{x}_k\right|^2\right\rangle\Delta t^2}{T} \equiv \frac{2\left\langle\left|\tilde{x}_k\right|^2\right\rangle\Delta t}{N} \equiv \frac{2\left\langle\left|\tilde{x}_k\right|^2\right\rangle}{Nf_S}$$

The absolute square of a Fourier Transform gives what we call "power". A one-sided PSD is defined for positive frequencies (the factor of 2 counts the power from negative frequencies). The angle brackets, < >, indicate "average value". Without the angle brackets, the above is called a periodogram. Thus, the PSD estimate is found by averaging periodograms. The other factors normalize the PSD so that the area under the PDS curves gives the RMS^2 of the time domain data.

Power Spectral Density of Gaussian White Noise

$$\langle n_j \rangle = 0; \qquad \left\langle |n_j|^2 \right\rangle = \frac{1}{N}\sum_{j=0}^{N-1} |n_j|^2 = \sigma^2$$

$$\left\langle |\tilde{n}_k|^2 \right\rangle = \frac{1}{N}\sum_{k=0}^{N-1} |\tilde{n}_k|^2 = \sum_{j=0}^{N-1} |n_j|^2 = N\sigma^2$$

$$P_k = \frac{2\left\langle |\tilde{n}_k|^2 \right\rangle \Delta t^2}{T} = \frac{2N\sigma^2\Delta t^2}{T} = 2\sigma^2\Delta t = \frac{2\sigma^2}{f_s}$$

$$\sum_{k=0}^{N/2} P_k \Delta f = \sum_{k=0}^{N/2} \frac{2\sigma^2}{f_s}\frac{1}{T} = \frac{N}{2}\frac{2\sigma^2}{N} = \sigma^2 \rightarrow Area = RMS^2$$

For Gaussian white noise, the square root of the area under the PSD gives the RMS of time domain data.

Amplitude and Phase of a spectral line

$$x_j = A\cos(2\pi f t_j + \varphi_0) = A\frac{e^{2\pi i f t_j + i\varphi_0} + e^{-2\pi i f t_j - i\varphi_0}}{2}$$

$$fT = k; \qquad \tilde{x}_k = \frac{AN}{2}e^{i\varphi_0}$$

If the product of f and T is an integer k, we call say this frequency is "bin centered".

For a sinusoidal signal with a "bin centered" frequency, all the power lies in one bin.

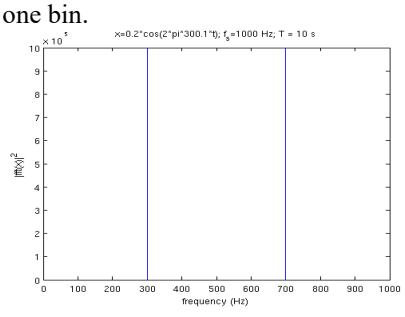

For a signal with a non- bin-centered frequency, power leaks out into the neighboring bins.

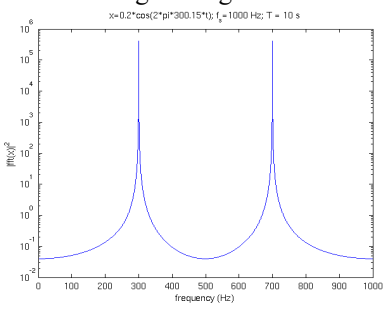

PSD Statistics

$\tilde{n} = x + iy$ **Gaussian noise with 2 degrees of freedom:**

$$|\tilde{n}|^2 = x^2 + y^2; \qquad if < x >=< y >= 0; < x^2 >=< y^2 >= 1$$

$$\mathrm{P}(x,y)dxdy = \frac{1}{\sqrt{2\pi}} e^{-x^2/2} \frac{1}{\sqrt{2\pi}} e^{-y^2/2} dxdy$$

$$r = \sqrt{x^2 + y^2}; \phi = \tan^{-1}(y/x); dxdy \rightarrow rdrd\phi$$

Rayleigh Distribution:

$$\mathrm{P}(r,\phi)drd\phi = \frac{1}{2\pi} re^{-r^2/2} drd\phi; \qquad \mathrm{P}(r)dr = re^{-r^2/2}dr$$

Chi-squared for 2 degrees of freedom:

$$\rho = r^2; \frac{1}{2}d\rho = rdr; \qquad \mathrm{P}(\rho)d\rho = \frac{1}{2} e^{-\rho/2} d\rho$$

Histograms of Real and Imaginary Parts of DFT

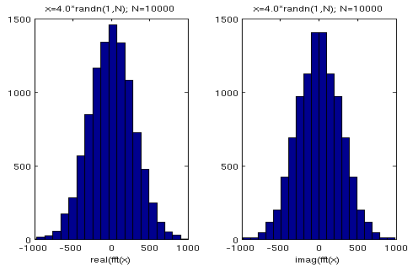

Rayleigh Distribution

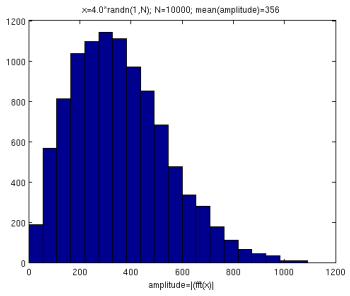

Histogram DFT Power – a chi-squared distribution for 2 degrees of freedom.

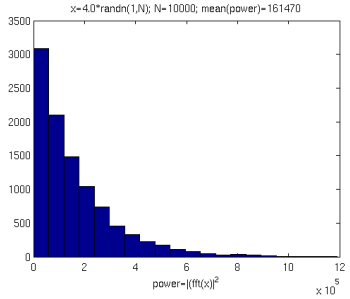

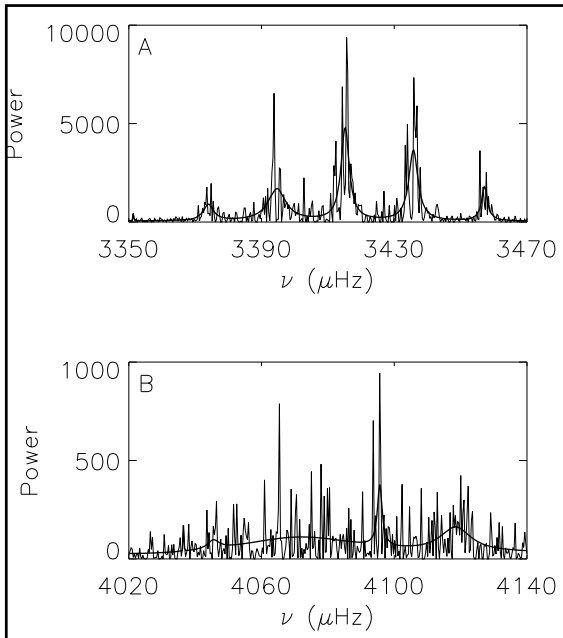

Power spectra of A) $l = 50, m = -32, n = 12$ and B) $l = 50, m = 0, n = 16$.

Excitation of Solar Oscillations

Solar oscillations are randomly excited by turbulent convection. The random excitation function appears as multiplicative noise in the power spectra. This represents the most serious problem for measuring mode frequencies. This figure shows examples of good and poor fits of an oscillation model to the power spectra.

Modeling the oscillation power spectrum

Consider a harmonic oscillator with damping driven by a random forcing function: $\frac{d^2x}{dt^2} - \gamma\frac{dx}{dt} + \omega_0^2 x = f(f)$

Solution: $x(t) = \int_{-\infty}^{\infty} h(t')f(t-t')dt'$

where $h(t)$ is the impulsive response function for $f(t) = \delta(t)$.

Using the convolution theorem, the Fourier transform of the solution: $\tilde{x}(\omega) = \tilde{h}\tilde{f}$

We find Fourier transform of the response function

$-\omega^2\tilde{h} - i\gamma\omega\tilde{h} + \omega_0^2\tilde{h} = 1 \qquad \tilde{h} = \frac{1}{\omega_0^2 - \omega^2 - i\gamma\omega} \qquad |\tilde{h}|^2 = \frac{1}{(\omega_0^2 - \omega^2)^2 + \gamma^2\omega^2}$

If $\gamma \ll \omega \qquad |\tilde{h}|^2 \approx \frac{1}{(2\omega_0)^2}\frac{1}{(\omega_0 - \omega)^2 + (\gamma/2)^2}$

Lorentzian line profile: $\Gamma(\omega) = \frac{A}{1 + \left(\frac{\omega - \omega_0}{\gamma/2}\right)^2}$

Sample spectrum and true spectrum

We compute the power spectrum of a finite realization of $x(t)$ of length T - a sample spectrum $C_x^T(\omega)$.

At frequencies separated by $1/T$, the values of $C_x^T(\omega)$ are independent and distributed as chi-squared with two degrees of freedom.

We can define the spectrum of $x(t)$ as:

$$\Gamma_x(t) = \lim_{T\to\infty} E[C_x^T(\omega)]$$

where E is the expectation operator, an average over many independent realizations.

For a white noise, this is just a constant. As for the white noise, the ratio (at a given frequency) of the sample spectrum divided by the true spectrum is distributed as chi-squared with two degrees of freedom.

Maximum likelihood

The probability density of the sample spectrum C_i at a given frequency ω_i is:

$$p(C_i) = \frac{1}{\Gamma_i}\exp(-C_i/\Gamma_i)$$

The maximum likelihood technique is used to estimate the model parameters of a spectral line. It consists of maximizing the joint probability function:

$$P = \prod_i p(C_i) = \exp-[(\ln\Gamma_i + C_i/\Gamma_i)]$$

where C_i is the sample spectrum,

$$\Gamma_i = \frac{A}{1+\left(\frac{\omega_i-\omega_0}{\gamma/2}\right)^2} + r$$

is the Lorentzian profile plus background noise. This equivalent to minimizing

$$M[A,\omega_0,\gamma,r] = -\sum_i[(\ln\Gamma_i + C_i/\Gamma_i)]$$

Example: analysis of global-Sun oscillations from GOLF

- GOLF (Global Oscillations at Low Frequencies) observes the Sun-as-a-star from SOHO spacecraft.
- Calculate the power spectrum using the GOLF data from April 11, 1996 to 2018 (22 years with 95% duty cycle).
- The data are available in the class webpage: http://sun.stanford.edu/~sasha/PHYS747

Resonance-Scattering Spectrometer.

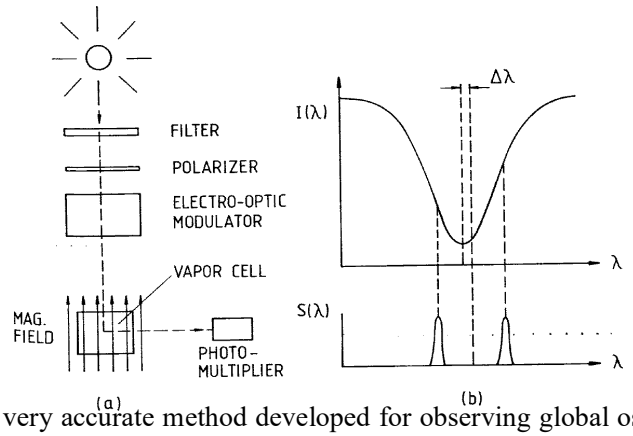

This is a very accurate method developed for observing global oscillations of the Sun in sodium line. The vapor cell with external magnetic field provides signals of the light scattered in two wings, which are measured by a photomultiplier. The difference of these signals is proportional to the Doppler shift.

Resonance-scattering spectrometer- GOLF instrument on SOHO (Global Oscillations at Low Frequencies)

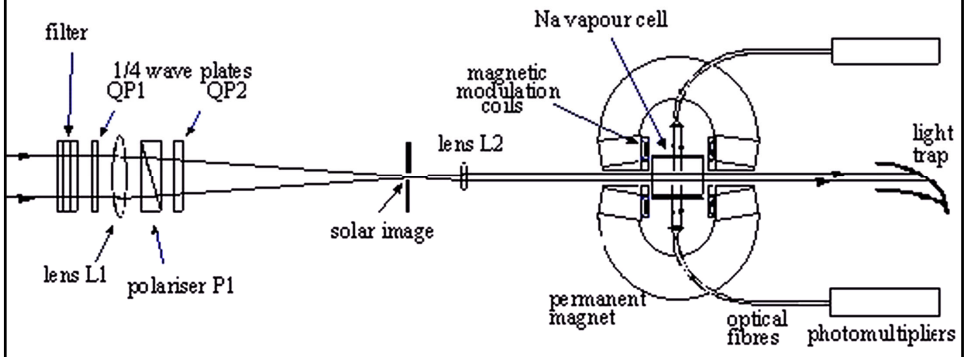

5000 G magnetic field

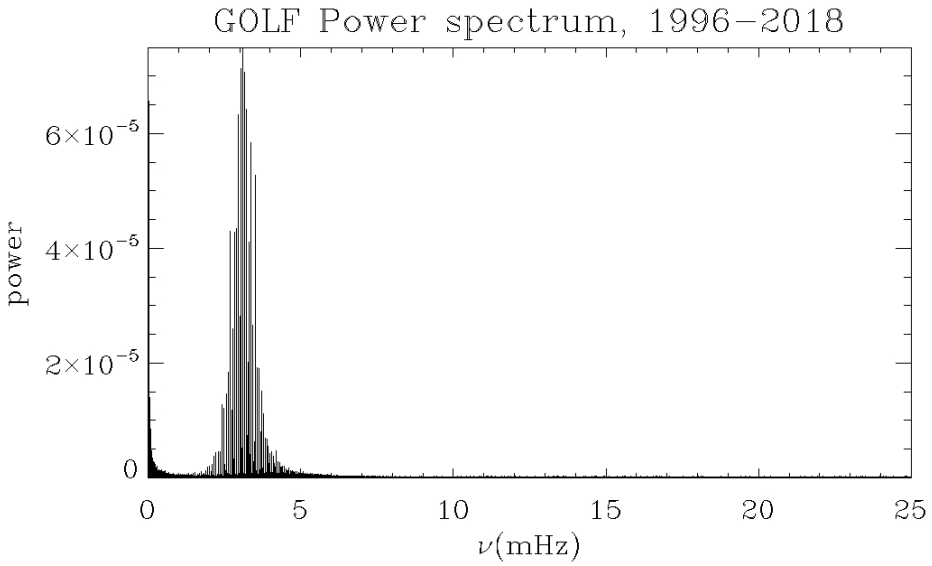

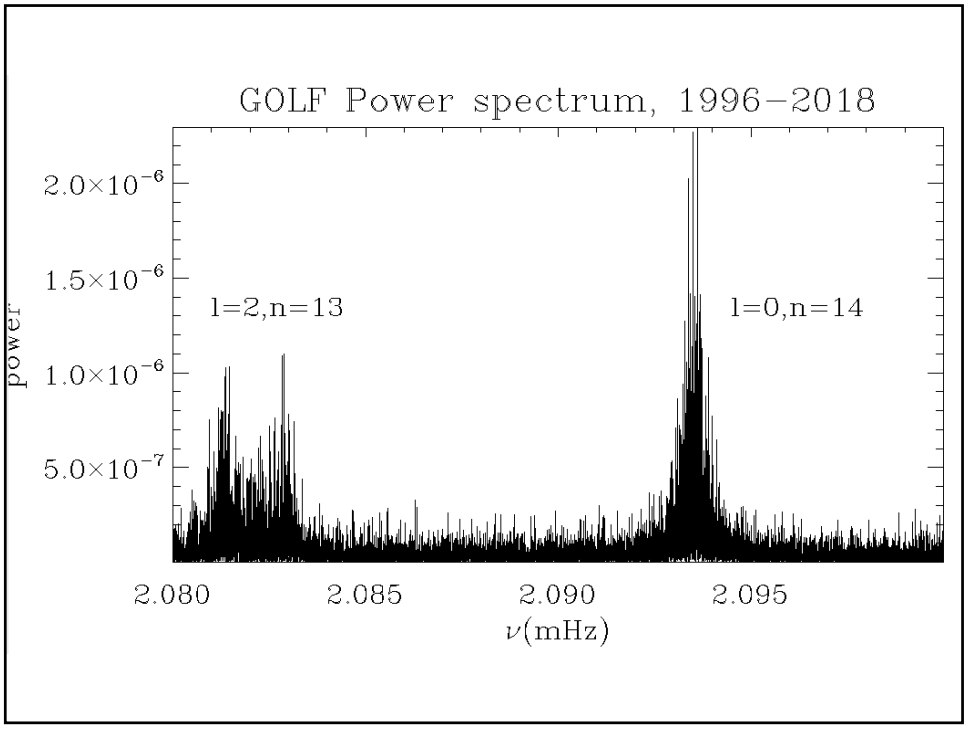
GOLF Power spectrum, 1996−2018
2.0×10⁻⁶
1.5×10⁻⁶
1.0×10⁻⁶
5.0×10⁻⁷
power
l=2,n=13
l=0,n=14
2.080
2.085
2.090
2.095
ν(mHz)

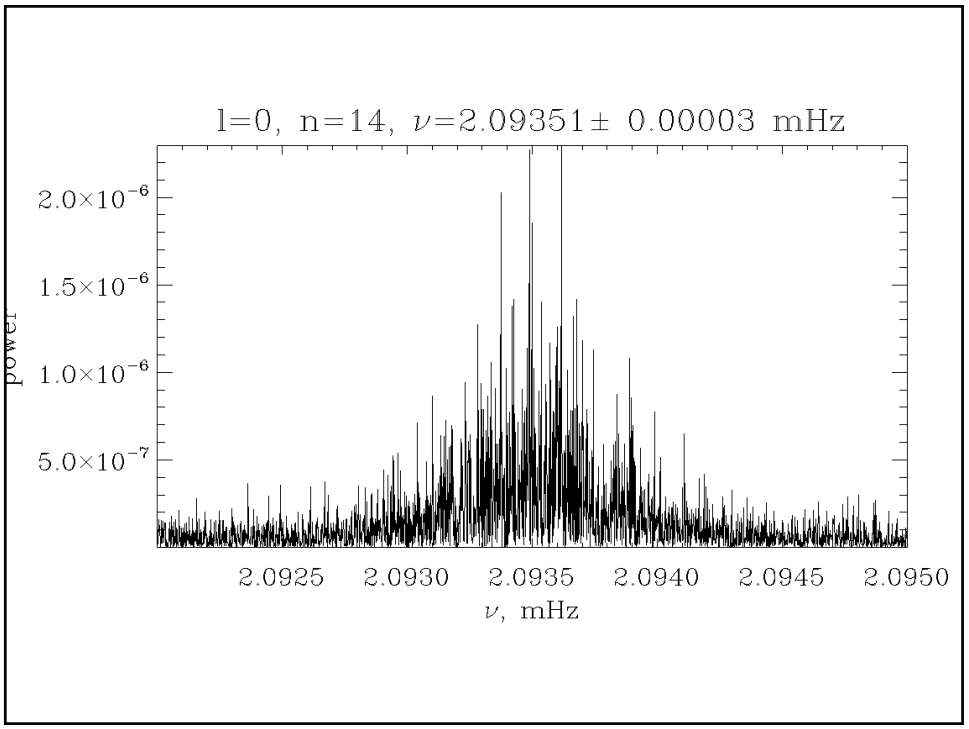
l=0, n=14, ν=2.09351± 0.00003 mHz
2.0×10⁻⁶
1.5×10⁻⁶
1.0×10⁻⁶
5.0×10⁻⁷
power
2.0925
2.0930
2.0935
2.0940
2.0945
2.0950
ν, mHz

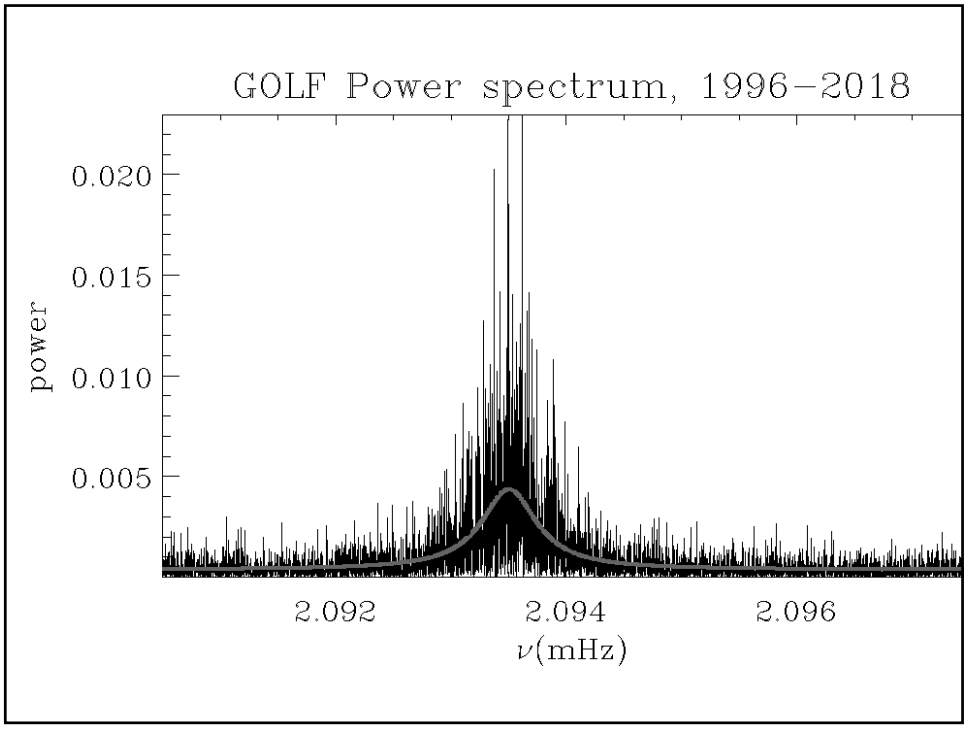
GOLF Power spectrum, 1996−2018
power
0.020
0.015
0.010
0.005
2.092
2.094
2.096
ν(mHz)

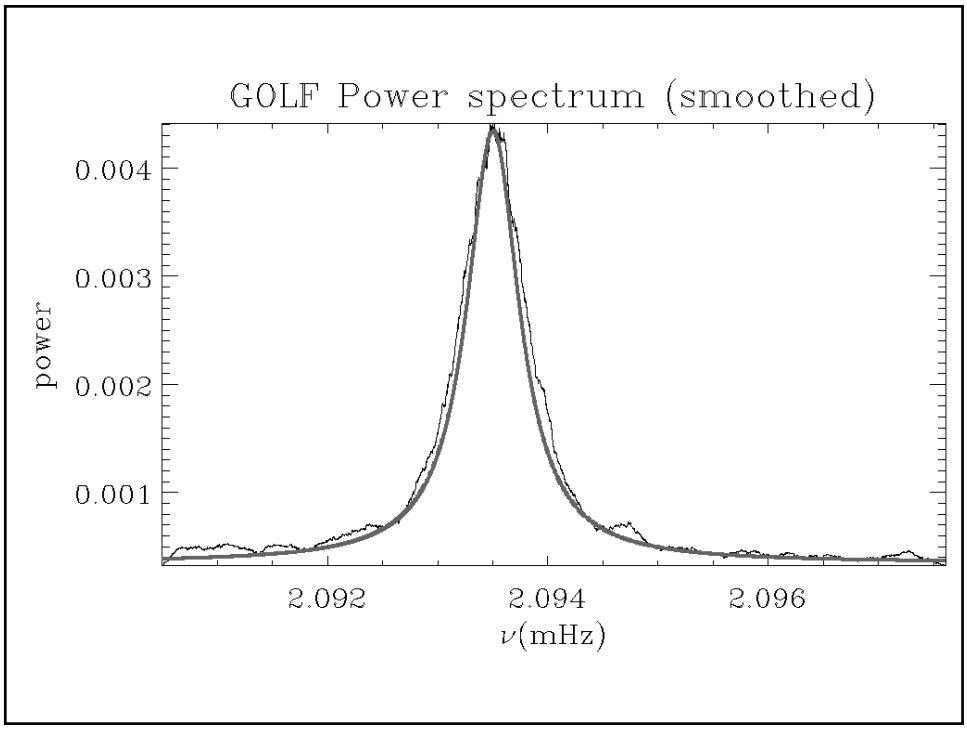
GOLF Power spectrum (smoothed)
power
0.004
0.003
0.002
0.001
2.092
2.094
2.096
ν(mHz)

Rotational frequency splitting

The modes with $m \neq 0$ represent azimuthally propagating waves. The modes with $m > 0$ propagate in the direction of solar rotation and, thus, have higher frequencies in the inertial frame than the modes $m < 0$ which propagate in opposite direction. As a result the modes with fixed n and l are split in frequency: $\Delta\nu_{nlm} = \nu_{nlm} - \nu_{nl0}$. Thus, the internal rotation is inferred from splitting of normal mode frequencies with respect to the azimuthal order, m .

$$\vec{\xi} \propto e^{i\omega t} Y_l^m(\theta,\phi) = a_{lm} \cdot P_l^m(\theta) e^{im\phi + i\omega t}$$

- displacement of the solar surface in solar modes

$\nu = \omega / 2\pi$

- ν is cyclic frequency, measured in Hz
- The oscillation period is 1/ν (in sec, min, etc).

ω is the angular frequency, measured in rad/s

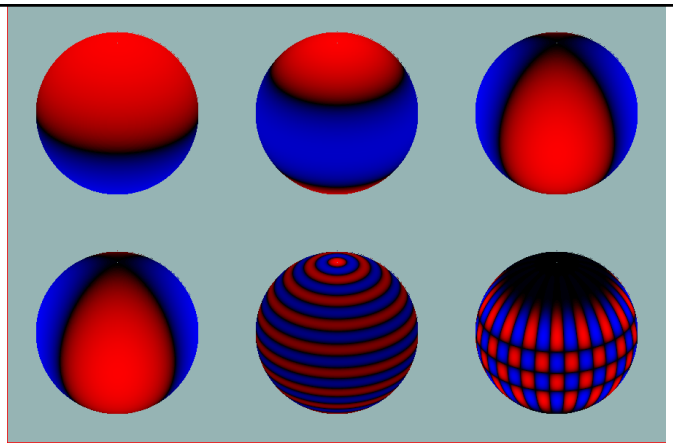

Cyclic frequency $\nu = \frac{\omega}{2\pi}$ is often used as frequency variable.

Because only a hemisphere of the Sun is observed in the power spectrum for a given mode of target l, m beside peaks corresponding to this mode peaks of other modes appear (so-called 'mode leaks'). The spherical harmonics are not orthogonal on a hemisphere.

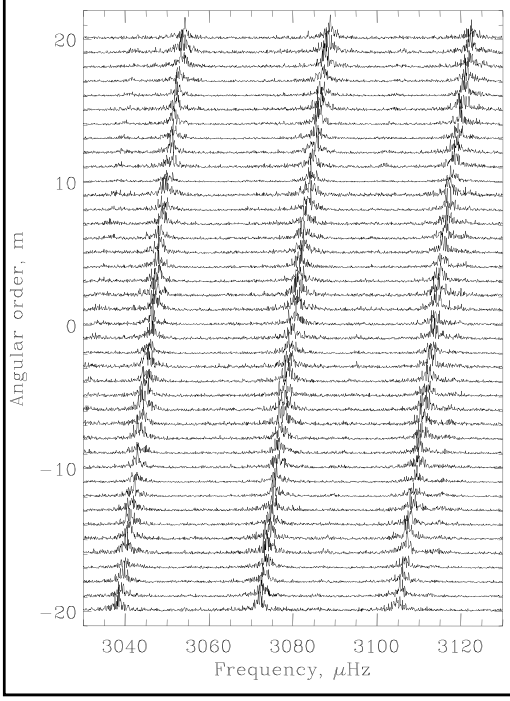

Illustration of the frequency shift due to the solar rotation

Typical power spectra of solar oscillation data from the MDI instrument on SOHO. Each horizontal curve shows three lines of the power spectrum for different azimuthal order m with radial order $n = 15$ and angular degree $l = 19, 20$, and 21 (from left to right). The slope of the modal lines is due to the rotational frequency shift: prograde modes with positive m have higher frequencies than retrograde modes with negative m.

Line Asymmetry and Pseudo-modes

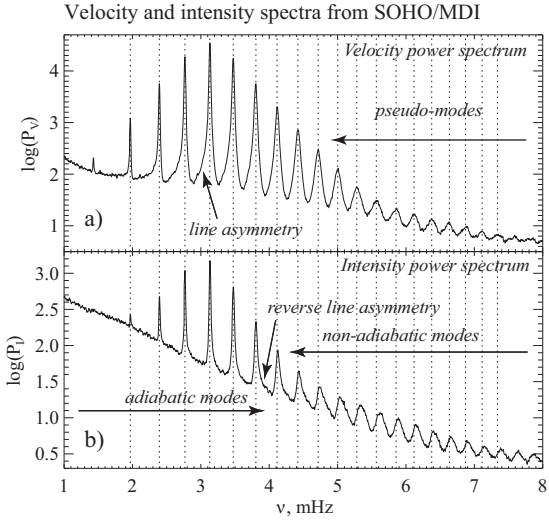

Power spectra of $l = 200$ modes obtained from SOHO/MDI observations of
a Doppler velocity,
b continuum intensity.

Acoustic waves with frequencies below the cut-off frequency are completely reflected by the surface layers because of the steep density gradient. These waves are trapped in the interior, and their frequencies are determined by the resonant conditions, which depend on the solar structure. But the waves with frequencies above the cut-off frequency escape into the solar atmosphere.

Above this frequency the power spectrum peaks correspond to so-called "pseudo-modes"

Line Asymmetry and Pseudo-modes

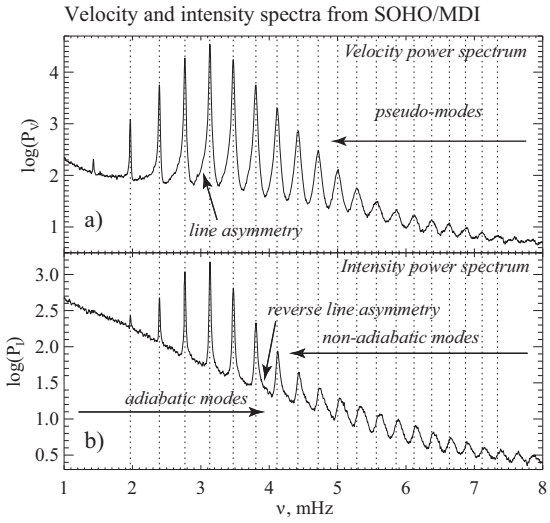

Power spectra of $l = 200$ modes obtained from SOHO/MDI observations of
a Doppler velocity,
b continuum intensity.

The line asymmetry is apparent, particularly, at low frequencies. In the velocity spectrum, there is more power in the low-frequency wings than in the high-frequency wings of the spectral lines. In the intensity spectrum, the distribution of power is reversed.

The asymmetry is the strongest for the f-mode and low-frequency p-mode peaks. At higher frequencies the peaks become more symmetrical, and extend well above the acoustic cut-off frequency: $\omega_c \sim 5–5.5$ mHz.

Lecture 4

Excitation of solar oscillations.
Line asymmetry and pseudo-modes.

(Stix, Chapters 5.1 and 5.4; Kosovichev, p.13-17)

Projects

- Power spectrum: Ivan Oparin
- Global modes from GOLF: Sheldon Fereira
- Oscillation model, line asymmetry: Bryce Cannon
- Power maps, acoustic halo: Bhairavi Apte
- Time-distance helioseismology: Sadaf Iqbal Ansari
- Observational sensitivity of solar/stellar oscillations. Leakage matrix:
- Ray paths, travel times:
- Propagation diagram for solar and stellar models:
- Analysis of sunquakes:

Solar oscillations are stochastically excited by turbulent convection

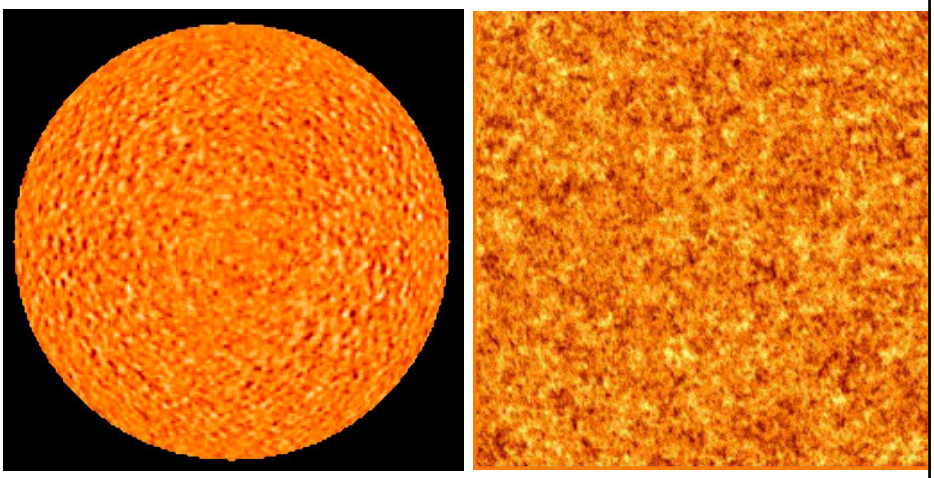

Power spectrum of solar oscillations

Velocity of oscillations $v(x, y, t)$ can be represented in terms of its Fourier components:

$$a(k_x, k_y, \omega) = \iiint v(x, y, t) e^{i(k_x x + k_y y + \omega t)} dx dy dt,$$

where k_x and k_y are components of the wave vector, ω is the frequency.

The power spectrum is: $P(k_x, k_y, \omega) = a^* a$, where a^* is complex conjugate.

If there is no preference in the direction of the wave propagation then P depends on two variables, the horizontal wavenumber $k_h = \sqrt{k_x^2 + k_y^2}$, and frequency.

Then, we calculate the angular average in the *k*-space:

$$P(k_h, \omega) = \frac{1}{2\pi} \int_0^{2\pi} P(k_{h,} \cos\phi, k_h \sin\phi, \omega) d\phi$$

This is a local power spectrum. It allows us to investigate properties of various regions observed on the solar disk.

Consider example using IDL codepower_spectrum.pro.

3D Power Spectrum

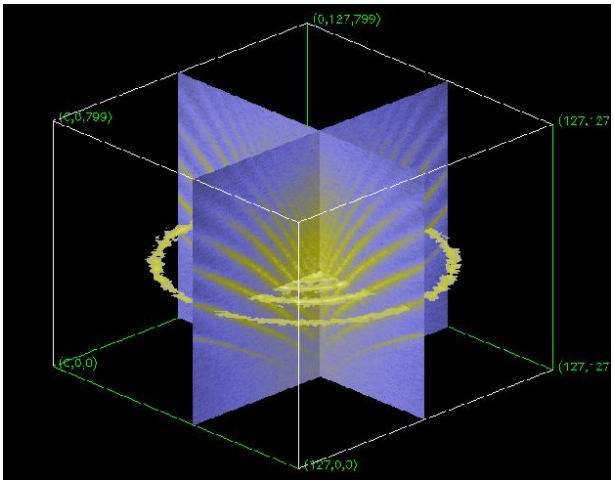

Spherical harmonics

For the global oscillations we must use the spherical coordinates (r, [illegible])
and expansion in terms of spherical surface harmonics:

$$v(\theta,\phi,t)=\sum_{l=0}^{\infty}\sum_{m=-l}^{l}a_{lm}(t)Y_l^m(\theta,\phi)$$

In the spherical coordinates, θ,ϕ:

$$a(l,m,\omega)=\iiint v(\theta,\phi,t)Y_l^m(\theta,\phi)e^{i\omega t}\sin(\theta)d\theta d\phi dt,$$

where $Y_l^m(\theta,\phi)=P_l^{|m|}(\theta)e^{im\phi}$ is a spherical harmonic of **the angular degree** l **and angular order** m, $P_l^m(\theta)$ is an associate Legendre function.

Degree l gives the total number of node circles on the sphere; order m is the number nodal circles through the poles; m=*-1,-l+1,…,l-1, l* that is (2l+1) m-values on m for given l.

Spherical harmonics

The coefficients of the spherical harmonic expansion can be found by using the spherical harmonic transform:

$$a(l,m,\omega) = \iiint v(\theta,\phi,t) Y_l^m(\theta,\phi) e^{i\omega t} \sin(\theta) d\theta d\phi dt,$$

where $Y_l^m(\theta,\phi)$ is a spherical harmonic of **the angular degree** l **and angular order** m.

The power spectrum is:

$$P(l,m,\omega) = a^* a.$$

For a spherically symmetrical star, P depends only on l and ω.
In this case the power spectrum is 'degenerate' with respect of angular order m.

Then we can define the analog of the horizontal wavenumber:

$k_h = \frac{\sqrt{l(l+1)}}{R}$, where R is the solar radius.

We will derive this in a future lecture.

Oscillation power spectrum

- The power spectrum represents the oscillation signal in terms of spherical harmonics of **angular degree** l (and the **horizontal wavelength**, $\lambda_h = 2\pi/k_h$), and the oscillation **"cyclic" frequency**, $\nu = \omega/2\pi$.

l is integer number
λ_h is measured in Mm
ν is measured in mHz
ω is measured in rad/sec
(sometimes called angular frequency)

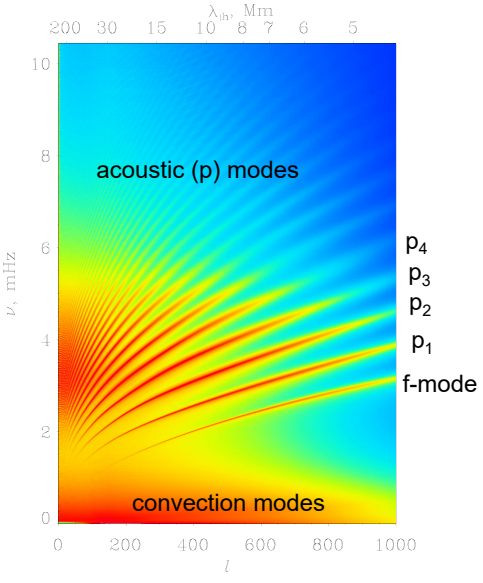

Rotational frequency splitting

The modes with $m \neq 0$ represent azimuthally propagating waves. The modes with $m > 0$ propagate in the direction of solar rotation and, thus, have higher frequencies in the inertial frame than the modes $m < 0$ which propagate in opposite direction. As a result the modes with fixed n and l are split in frequency: $\Delta\nu_{nlm} = \nu_{nlm} - \nu_{nl0}$. Thus, the internal rotation is inferred from splitting of normal mode frequencies with respect to the azimuthal order, m .

$$\vec{\xi} \propto e^{i\omega t} Y_l^m(\theta,\phi) = a_{lm} \cdot P_l^m(\theta) e^{im\phi + i\omega t}$$

- displacement of the solar surface in solar modes

$\nu = \omega / 2\pi$

- ν is cyclic frequency, measured in Hz
- The oscillation period is 1/ν (in sec, min, etc).

ω is the angular frequency, measured in rad/s

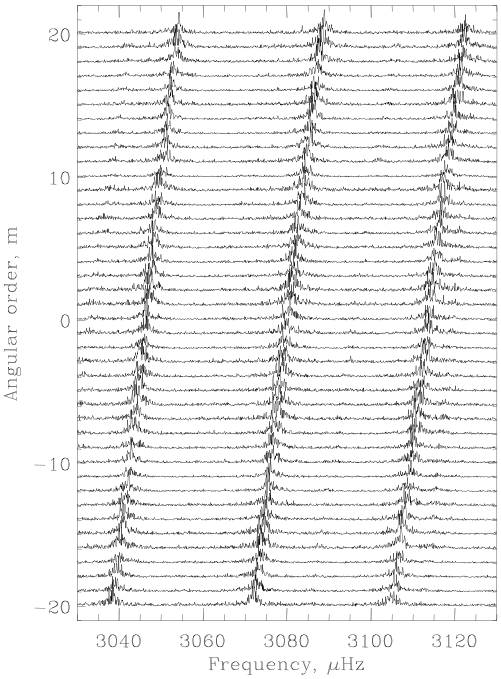

Illustration of the frequency shift due to the solar rotation

Typical power spectra of solar oscillation data from the MDI instrument on SOHO. Each horizontal curve shows three lines of the power spectrum for different azimuthal order m with radial order $n = 15$ and angular degree $l = 19, 20$, and 21 (from left to right). The slope of the modal lines is due to the rotational frequency shift: prograde modes with positive m have higher frequencies than retrograde modes with negative m .

Line Asymmetry and Pseudo-modes

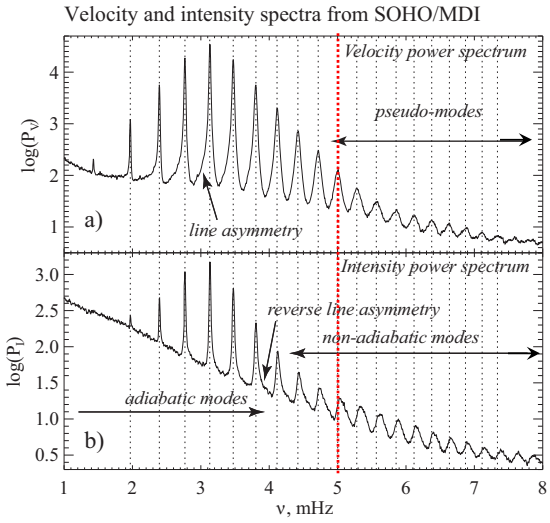

Power spectra of $l = 200$ modes obtained from SOHO/MDI observations of
a Doppler velocity,
b continuum intensity.

Acoustic waves with frequencies below the cut-off frequency are completely reflected by the surface layers because of the steep density gradient. These waves are trapped in the interior, and their frequencies are determined by the resonant conditions, which depend on the solar structure. But the waves with frequencies above the cut-off frequency escape into the solar atmosphere.

Above this frequency the power spectrum peaks correspond to so-called “pseudo-modes”

Line Asymmetry and Pseudo-modes

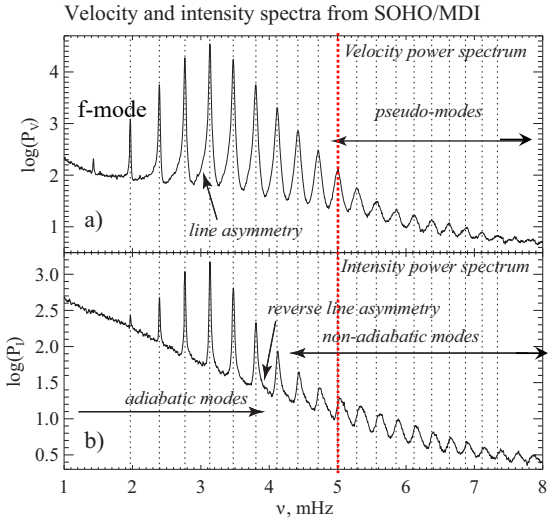

Power spectra of $l = 200$ modes obtained from SOHO/MDI observations of
a Doppler velocity,
b continuum intensity.

The line asymmetry is apparent, particularly, at low frequencies. In the velocity spectrum, there is more power in the low-frequency wings than in the high-frequency wings of the spectral lines. In the intensity spectrum, the distribution of power is reversed.

The asymmetry is the strongest for the f-mode and low-frequency p-mode peaks. At higher frequencies the peaks become more symmetrical, and extend well above the acoustic cut-off frequency: $\nu_c \sim 5$ mHz.

Physical interpretation

- Hydrodynamic equations
- Waves in the solar atmosphere: interpretation of acoustic cut-off frequency
- Excitation of solar oscillations: interpretation of modes, pseudo-modes and line asymmetry

Hydrodynamic Equations

Basic assumptions:

1. linearity: $\vec{v}/c_s << 1$
2. adiabaticity: $dS/dt = 0$
3. spherical symmetry of the background
4. magnetic forces and Reynolds stresses are negligible

The basic equations are conservations of mass, momentum, energy and Newton's gravity law.

1. Conservation of mass (continuity equation):

The rate of mass change in a fluid element of volume V is equal to the mass flux through the surface of this element (of area A):

$$\frac{\partial}{\partial t}\int_V \rho dV = -\int_A \rho\vec{v}d\vec{a} = -\int_V \nabla(\rho\vec{v})dV.$$

divergence

Then,

$$\frac{\partial\rho}{\partial t} + \nabla(\rho\vec{v}) = 0,$$

or

$$\frac{d\rho}{dt} + \rho\nabla\vec{v} = 0.$$

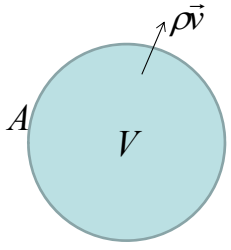

2. Momentum equation (conservation of momentum of a fluid element): $\rho \frac{d\vec{v}}{dt} = -\nabla P + \rho \vec{g},$

where P is pressure, $\vec{g}$ is the gravity acceleration.

Also, $\frac{d\vec{v}}{dt} = \frac{\partial \vec{v}}{\partial t} + (\vec{v} \cdot \nabla)\vec{v}$. This is the 'material' derivative.

e.g. $v_x \frac{\partial v_x}{\partial x} + v_y \frac{\partial v_x}{\partial y} + v_z \frac{\partial v_x}{\partial z}$ for v_x component

3. Adiabaticity equation (conservation of energy) for a fluid element:

$$\frac{d}{dt}\left(\frac{P}{\rho^\gamma}\right) = 0, \qquad \text{or} \qquad \frac{dP}{dt} = c^2 \frac{d\rho}{dt},$$

where $c^2 = \gamma P/\rho$ is the adiabatic sound speed. Finally,

$$\frac{\partial P}{\partial t} + (\vec{v} \cdot \nabla)P = c^2 \left(\frac{\partial \rho}{\partial t} + (\vec{v} \cdot \nabla)\rho\right).$$

Waves in the solar atmosphere: initial state

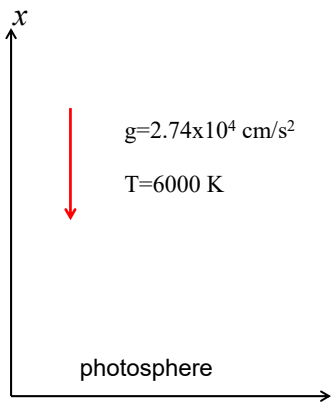

Initial (hydrostatic) state:

$$\frac{\partial P_0}{\partial x} = -g\rho_0$$

Equation of state defines pressure in terms of temperature, density and molecular weight:

$$P = \frac{R\rho T}{\mu},$$

where μ is the molecular weight.

For non-ionized hydrogen gas $\mu = 1$, for fully ionized hydrogen gas $\mu = 0.5$. Because of ionization the number of particles increases by 2 (ions+electrons). R is the gas constant.

Then, $P_0(x) = P(0)e^{-\frac{x}{H}}$ where $H = \frac{RT}{g\mu}$ is the pressure scale height.

Waves in the solar atmosphere: initial equations

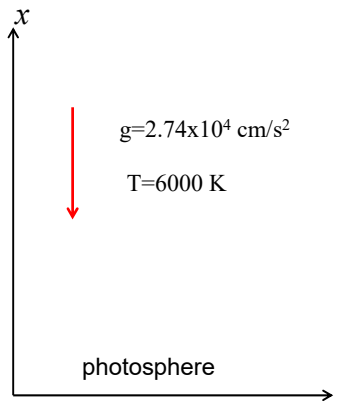

Continuity (mass conservation) equation:

$$\frac{\partial \rho}{\partial t} + \frac{\partial \rho v}{\partial x} = 0.$$

Momentum equation:

$$\rho \frac{dv}{dt} = -\frac{\partial P}{\partial x} - g\rho.$$

Velocity v can be expressed in terms of displacement ξ of fluid elements: $v = \frac{d\xi}{dt}$

Adiabaticity equation:

$$\frac{\partial P}{\partial t} + v\frac{\partial P}{\partial x} - c^2\left(\frac{\partial \rho}{\partial t} + v\frac{\partial \rho}{\partial x}\right) = 0,$$

where $c^2 = \frac{\gamma P}{\rho}$ in the squared adiabatic sound speed.

Waves in the solar atmosphere: linearized equations for small perturbations

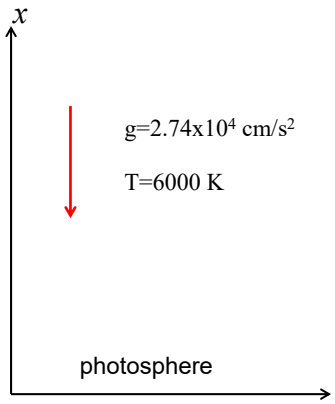

Consider small perturbations:

$$\rho = \rho_0 + \rho_1, \quad P = P_0 + P_1,$$

$$v = v_0 + v_1, \quad v_0 = 0, \quad v_1 = \frac{\partial \xi}{\partial t}$$

Continuity (mass conservation) equation:

$$\frac{\partial \rho_1}{\partial t} + \frac{\partial \rho_0 v_1}{\partial x} = 0.$$

Momentum equation:

$$\rho_0 \frac{\partial v_1}{\partial t} = -\frac{\partial P_1}{\partial x} - g\rho_1.$$

Adiabaticity equation:

$$\frac{\partial P_1}{\partial t} + v_1\frac{\partial P_0}{\partial x} - c^2\left(\frac{\partial \rho_1}{\partial t} + v_1\frac{\partial \rho_0}{\partial x}\right) = 0.$$

Waves in the solar atmosphere: dispersion relation

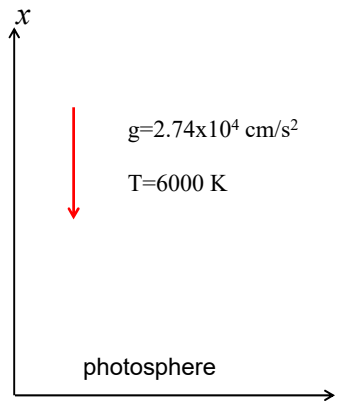

Eliminating ρ_1, P_1, v_1 we find that displacement ξ satisfies the second-order PDE:

$$\frac{\partial^2 \xi}{\partial t^2} = c^2 \frac{\partial^2 \xi}{\partial x^2} - \gamma g \frac{\partial \xi}{\partial x},$$

using the substitution $u = \xi \exp(\alpha x)$ we eliminate the first-order term:

$$\frac{\partial^2 u}{\partial t^2} = c^2 \frac{\partial^2 u}{\partial x^2} - \omega_c^2 u,$$

where $\omega_c = \frac{\gamma g}{2c}$ is the acoustic cut-off frequency.

For the dispersion relation we seek the solution in terms of Fourier harmonics: $u \propto \exp(-i\omega t + ikx)$:

$$-\omega^2 u = -c^2 k^2 u - \omega_c^2 u$$

$$\boxed{\omega^2 = c^2 k^2 + \omega_c^2}$$

The frequencies of plane-parallel acoustic waves traveling in the atmosphere are higher than the acoustic cut-off frequency.

Waves in the solar atmosphere: calculation of the acoustic cut-off frequency

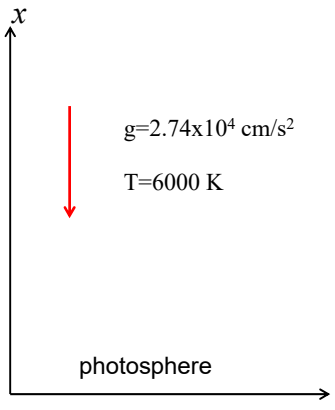

$\omega_c = \frac{\gamma g}{2c}$ is the acoustic cut-off frequency.

We assume that the Sun's material is ideal gas with $\gamma = 5/3$ and molecular weight μ.

The solar composition by mass is: 73% of H, 25% of He, and 2% of heavy elements (C, O, Fe, Ni,…): X=0.73, Y=0.25, Z=0.02.

When temperature is high (in the solar interior or corona) the gas is fully ionized, and:

$$\mu = \frac{1}{2X + \frac{3}{4}Y + \frac{1}{2}Z} \approx 0.6$$

For non-ionized (or weakly ionized) gas (in the photosphere and chromosphere):

$$\mu = \frac{1}{X + \frac{1}{4}Y + \frac{1}{16}Z} \approx 1.25$$

Equation of state for solar composition

The pressure in the solar interior can be described by the ideal gas law: $P = nkT$,

where k is the Boltzman constant and n is the particle density.

$$n = n_H + n_{He} + n_Z + n_e,$$

where n_Z is the particle density of atom heavier than helium.

The particle density can be expressed in terms of fractional mass abundances of hydrogen, X, helium, Y, and heavier elements, Z, such as

$$X + Y + Z = 1.$$

Then, $$n_H = \frac{\rho X}{M}, \quad n_{He} = \frac{\rho Y}{4M}, \quad n_Z = \frac{\rho Z}{AM}$$

where M is the proton mass, A is a mean mass of the heavy elements (typically, $A \simeq 16$).

For fully ionized plasma (in the deep interior of the Sun or the corona):

$$n_e = n_H + 2n_{He} + \frac{1}{2} A n_Z$$

Then

$$n = 2n_H + 3n_{He} + (1 + \frac{1}{2} A) n_Z = \frac{\rho}{M}\left(2X + \frac{3}{4}Y + \frac{1 + A/2}{A} Z\right)$$

or $$n \approx \frac{\rho}{M}\left(2X + \frac{3}{4}Y + \frac{1}{2}Z\right).$$

Finally, $$P = nkT = \frac{k}{m}\rho T\left(2X + \frac{3}{4}Y + \frac{1}{2}Z\right) = \frac{R\rho T}{\mu},$$

where μ is the mean molecular weight: $\mu = \dfrac{1}{2X + \frac{3}{4}Y + \frac{1}{2}Z}$.

For pure hydrogen plasma, X=1, Y=Z=0: μ=0.5.

For weakly ionized plasma (in the photosphere and chromosphere):

$$n_e \approx 0$$

Then $n = n_H + n_{He} + n_Z = \frac{\rho}{M}\left(X + \frac{1}{4}Y + \frac{1}{A}Z \right)$

or $n \approx \frac{\rho}{M}\left(X + \frac{1}{4}Y + \frac{1}{16}Z \right).$

Finally, $P = nkT = \frac{k}{m}\rho T\left(X + \frac{1}{4}Y + \frac{1}{16}Z \right) = \frac{R\rho T}{\mu},$

where μ is the mean molecular weight:

$$\mu = \frac{1}{X + \frac{1}{4}Y + \frac{1}{16}Z}.$$

Waves in the solar atmosphere: calculation of the acoustic cut-off frequency

$\omega_c = \frac{\gamma g}{2c}$ is the acoustic cut-off frequency.

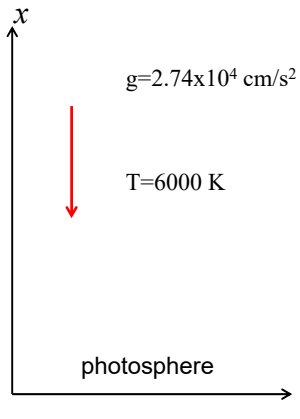

In the photosphere: $\gamma = 5/3, \quad \mu = 1.25$

$$c = \sqrt{\frac{\gamma P}{\rho}}, \quad P = \frac{R\rho T}{\mu},$$

$$c = \sqrt{\frac{\gamma RT}{\mu}} \approx 8.1 \times 10^5 \text{ cm/s} \approx 8 \text{ km/s}.$$

$$\nu_c = \omega_c / 2\pi = \frac{\gamma g}{4\pi c} \approx 4.5 \times 10^{-3} Hz = 4.5 \text{ mHz}$$

The corresponding period $1/\nu_c$ = 3.6 min.

Waves in the solar atmosphere: measurements of the acoustic cut-off frequency

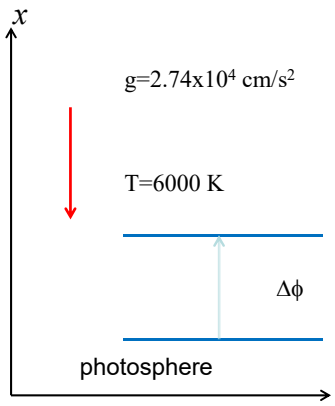

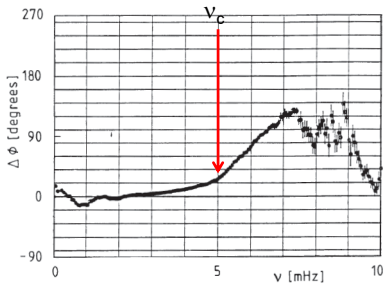

Fig. 5.3. Phase difference, Δφ, of oscillations measured in two lines originating deep (Fe I, λ = 593.0 nm) and high (Na I, λ = 589.6 nm) in the solar atmosphere, as a function of frequency. After Staiger (1987)

Excitation of solar oscillations

- The primary source is turbulent convection. The basic idea is that parcels of gas moving back and forth during their convective motion provide perturbations that lead to acoustic waves. However, the precise mechanism is still not known. Numerical simulations provide interesting examples.
- Formally we may describe such an oscillator by an equation of type of the atmospheric wave equation except that the right-hand side is not zero, but a given (stochastic) function of frequency, the *forcing* function.

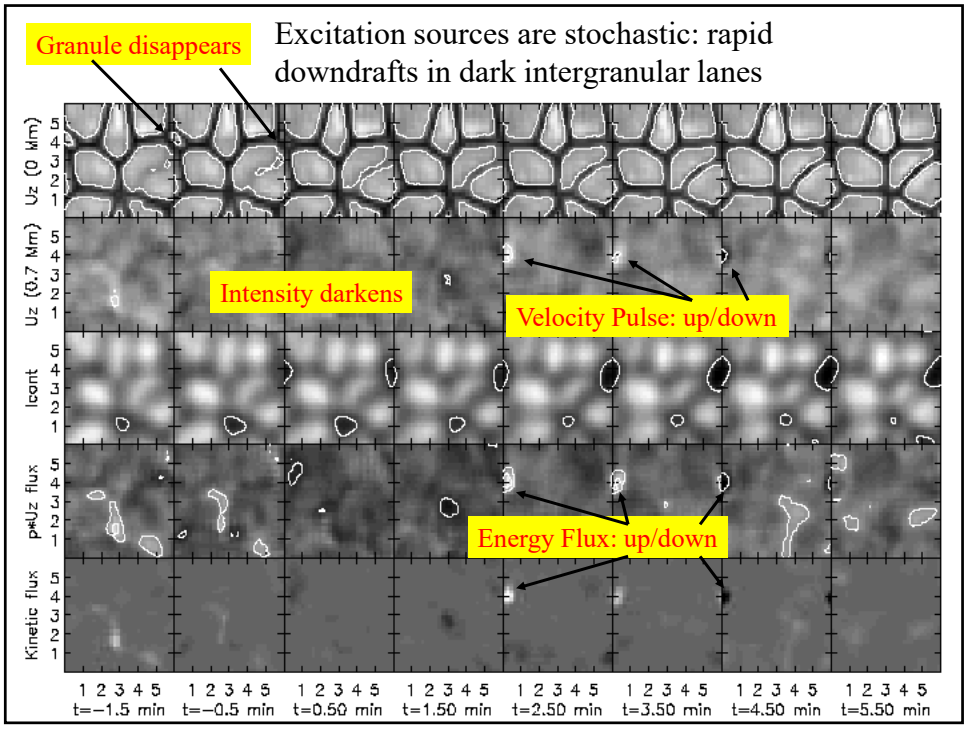

Excitation of solar oscillations

- Kumar and Lu (1991) proposed a simple model where the forcing is concentrated to a single surface, at $r = r_s$. Although the excitation is not stochastic in this model, the model illustrates some principle aspects of the solar oscillations.
- Consider the wave equation with a forcing function:

$$\frac{\partial^2 u}{\partial t^2} = c^2 \frac{\partial^2 u}{\partial x^2} - \omega_c^2 u + f(x,t)$$

and seek a solution in the form of Fourier harmonics:

$$u(x,t) = \int \tilde{u}(x,\omega) e^{-i\omega t} dt$$

Then, for $\tilde{u}(x,\omega)$ we obtain: $-\omega^2 \tilde{u} = c^2 \frac{d^2 \tilde{u}}{dx^2} - \omega_c^2 \tilde{u} + \tilde{f}(x,\omega)$

or $$\frac{d^2 \tilde{u}}{dx^2} - \frac{\omega_c^2 - \omega^2}{c^2} \tilde{u} = -\frac{1}{c^2} \tilde{f}(x,\omega)$$

We consider a solution for a localized source function in the form of a delta-function: $\delta(r - r_s)$ at all frequencies.

Simple analytical model of solar oscillations: excitation by a localized source located beneath the surface

- "Potential well model"

$$\frac{d^2u}{dr^2}+\frac{\omega^2-\omega_c^2}{c^2}u=f(r)$$

$$f(r)=\delta(r-r_S)$$

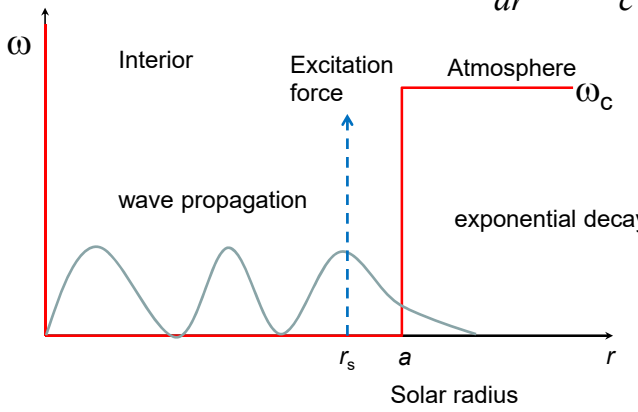

Calculate the Green's function.

Simple analytical model of solar oscillations

- "Potential well model"

$$\frac{d^2u}{dr^2}+\frac{\omega^2-\omega_c^2}{c^2}u=\delta(r-r_s)$$

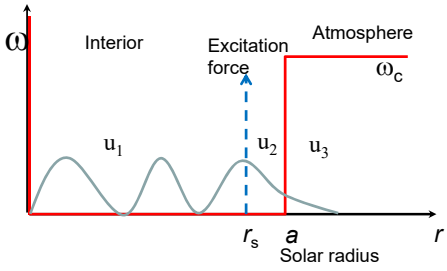

Consider general solutions in 3 regions: $0<r<r_s$, $r_s<r<a$, and $r>a$, and match the solutions and their first derivatives at $r=r_s$ and $r=a$, e.g.

$$u_1\big|_{r_s}=u_2\big|_{r_s}$$

Because of the δ-function the first derivate du/dr is discontinuous at $r=r_s$. Indeed, integrating the equation over a small region around r_s we find:

$$\int_{r_s-\epsilon}^{r_s+\epsilon}\frac{d^2u}{du^2}dr+\frac{\omega^2-\omega_c^2}{c^2}\int_{r_s-\epsilon}^{r_s+\epsilon}udr=\int_{r_s-\epsilon}^{r_s+\epsilon}\delta(r-r_s)dr$$

For $\varepsilon\to 0$ we obtain: $\frac{du_1}{dr}\Big|_{r_s}-\frac{du_2}{dr}\Big|_{r_s}=1$

Simple analytical model of solar oscillations

- "Potential well model"

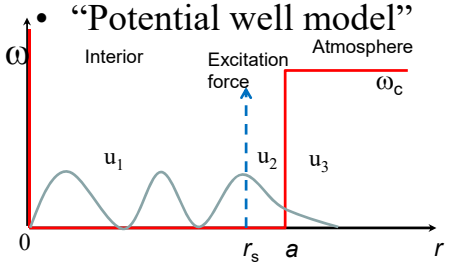

$$\frac{d^2u}{dr^2}+\frac{\omega^2-\omega_c^2}{c^2}u=\delta(r-r_s)$$

The general solutions in the three regions are:

$u_1(x) = C_1 \sin\left(\frac{\omega}{c}r\right) \equiv C_1 \sin(\alpha r),$

where $\alpha = \omega/c.$

$u_2(x) = C_2 \sin(\alpha r) + C_3 \cos(\alpha r)$

$u_3(x) = C_4 \exp\left(-\frac{\sqrt{\omega_c^2-\omega^2}}{c}(r-a)\right) \equiv C_4 \exp(-\beta(r-a)),$

where $\beta = \sqrt{\omega_c^2-\omega^2}/c$

Simple analytical model of solar oscillations

- "Potential well model"

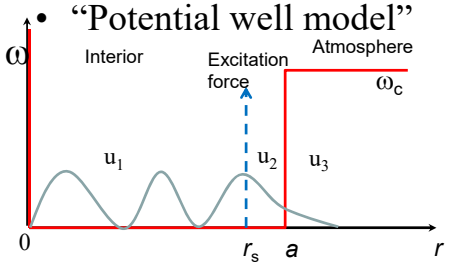

$$\frac{d^2u}{dr^2}+\frac{\omega^2-\omega_c^2}{c^2}u=\delta(r-r_s)$$

Matching u and du/dr at $r = r_s$:

$C_1 \sin(\alpha r_s) - C_2 \sin(\alpha r_s) - C_3 \cos(\alpha r_s) = 0$

$\alpha(C_1 \cos(\alpha r_s) - C_2 \cos \alpha r_s + C_3 \sin(\alpha r_s)) = 1$

we find: $C_3 = \sin(\alpha r_s)/\alpha.$

Matching u and du/dr at $r = a$:

$C_2 \sin(\alpha a) + C_3 \cos(\alpha a) = C_4$

$\alpha(C_2 \cos(\alpha a) - C_3 \sin(\alpha a)) = -\beta C_4$

we find: $C_3 = C_4\left(\cos(\alpha a) + \frac{\beta \sin(\alpha a)}{\alpha}\right).$

The solution at the surface point $r = a$ is:

$$u(a,\omega) = C_4 = \frac{\sin(\alpha r_s)}{\alpha \cos(\alpha a) + \beta \sin(\alpha a)}$$

Simple analytical model of solar oscillations

- "Potential well model"

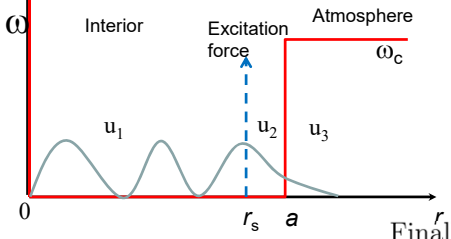

$$\frac{d^2u}{dr^2}+\frac{\omega^2-\omega_c^2}{c^2}u=\delta(r-r_s)$$

Finally,

$$u(a,\omega)=\frac{c\sin\left(\frac{\omega r_s}{c}\right)}{\omega\cos\left(\frac{\omega a}{c}\right)+\sqrt{\omega_c^2-\omega^2}\sin\left(\frac{\omega a}{c}\right)}$$

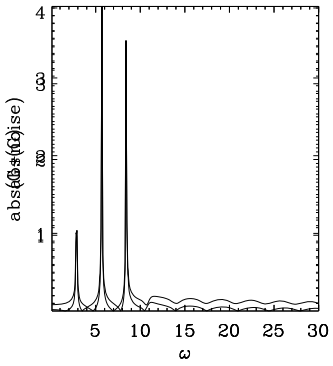

Asymmetrical line profile (Nigam & Kosovichev, 1998):

$$\Gamma=A\frac{(1+Bx)^2+B^2}{1+x^2}+r$$

where $x=2(\nu-\nu_0)/\gamma$,

$\nu=\omega/2\pi$ is the cyclic frequency,

B is the parameter of asymmetry

Power spectrum for the model

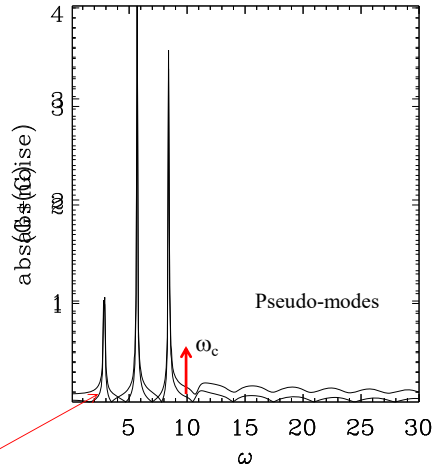

Line asymmetry

Pseudo-modes are caused by the interference of waves coming directly from the source and after the reflection in the interior. This is so-called "source resonance".

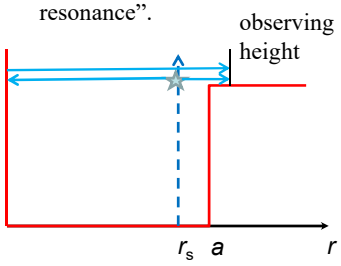

Reversal of the line asymmetry is caused by correlated noise

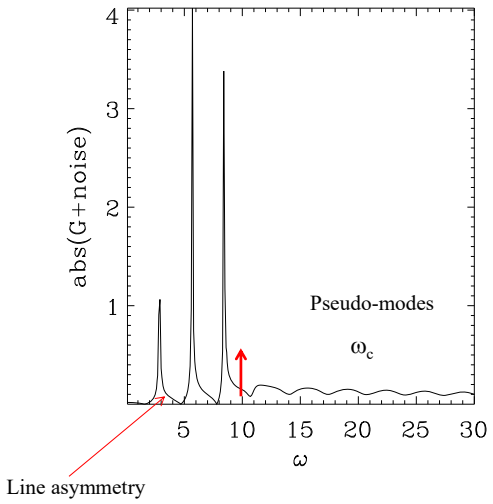

The correlated noise is added to oscillation signal and uncorrelated noise is added to the oscillation power, so that the observed power spectrum has two types of noise:

$$P_{obs}(\omega) = |u(\omega) + N_{corr}(\omega)|^2 + N_{uncorr}(\omega)$$

Correlated noise means that in the observed oscillation signal in additions to wave signal there is a component that comes directly from the source. When the solar oscillations are observed in intensity the correlated noise may be caused by changes of brightness of granules during the wave excitation events.

Measurement of the acoustic cut-off frequency

- The acoustic cut-off frequency can be determined from a sharp decrease of the mode peaks in the power spectra (marking a transition from modes to pseudo-modes).
- From a change in the peak separation. Example, measurements from stellar oscillation spectra (Jimenez et al, 2015).

Measurement of the acoustic cut-off frequency (Jimenez et al. 2015)

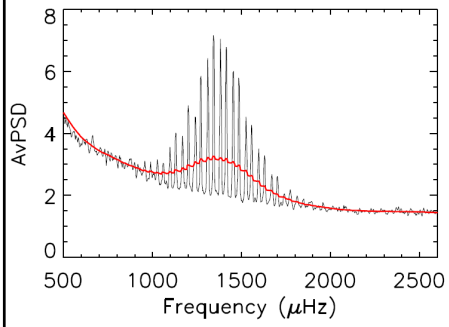

Fig. 1. Top panel: smoothed averaged power spectral density of four-day subseries of KIC 11244118. The red line is the severe smoothing used to normalize the spectrum.

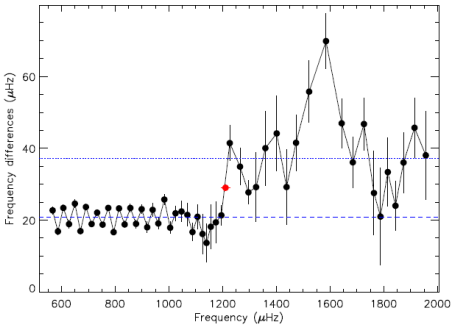

Fig. 5. Consecutive frequency differences of KIC 3424541. The blue dashed and dotted lines are the weighted mean value of the frequency differences in the p-mode ($20.75 \pm 0.20\,\mu$Hz) and pseudo-mode regions ($37.31 \pm 1.58\,\mu$Hz), respectively. The red symbol represents the estimated cut-off frequency, $\nu_{\rm cut} = 1210.67 \pm 15.70\,\mu$Hz.

Oscillation power spectrum

The ridges of the k-omega diagram are extended above the acoustic cut-off frequency because of the pseudo-modes caused by interference of waves excited by sources located just beneath the solar surface.

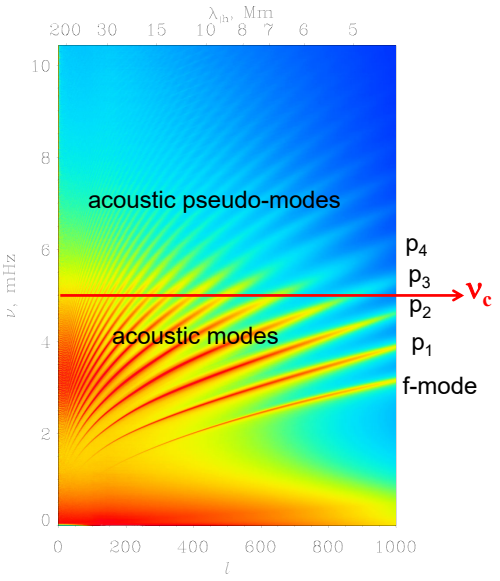

Homework and quiz

- Download problem set #1 from: http://sun.stanford.edu/~sasha/PHYS747/Homework
- Due date: Oct.4
- Quiz #1: Monday, Sept.20
  - Topics: properties of solar oscillations (period, amplitude, ridge structure); observations of solar oscillations (Nyquist frequency); excitation mechanisms; acoustic cut-off frequency.

Lecture 5

Oscillation power maps.
Magnetic field effects.
Numerical simulations of solar oscillations.

Projects

- Power spectrum: Ivan Oparin
- Global modes from GOLF: Sheldon Fereira
- Oscillation model, line asymmetry: Bryce Cannon
- Power maps, acoustic halo: Bhairavi Apte
- Time-distance helioseismology:
- Ray paths, travel times: Sadaf Iqbal Ansari
- Propagation diagram for solar and stellar models: Ying Wang
- Analysis of sunquakes: Youra Shin
- Asteroseismic analysis: John Stefan
- Observational sensitivity of solar/stellar oscillations. Leakage matrix:
- Asymptotic sound-speed inversion:

Recap of L1-4

Solar oscillations are stochastically excited by turbulent convection

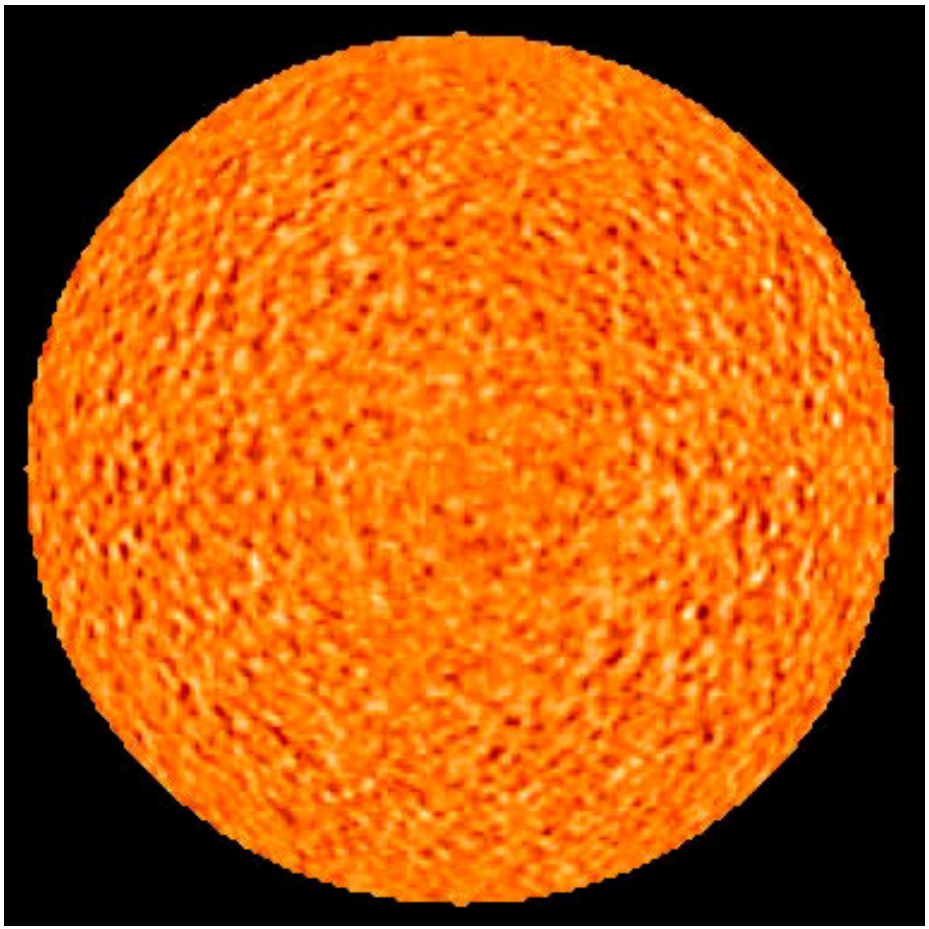

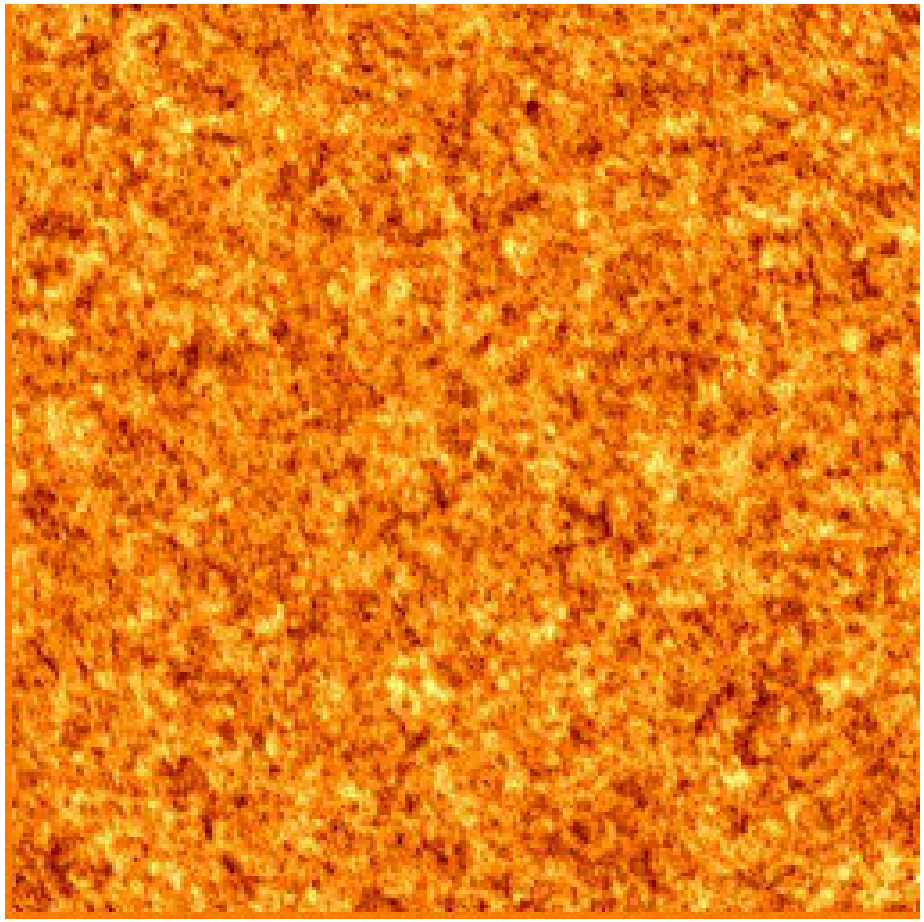

Characteristic oscillation period: 5 min, amplitude ~300 m/s

Power spectrum of solar oscillations

Velocity of oscillations $v(x, y, t)$ can be represented in terms of its Fourier components:

$$a(k_x, k_y, \omega) = \iiint v(x, y, t) e^{i(k_x x + k_y y + \omega t)} dx dy dt,$$

where k_x and k_y are components of the wave vector, ω is the frequency.

The power spectrum is: $P(k_x, k_y, \omega) = a^* a,$ where a^* is complex conjugate.

If there is no preference in the direction of the wave propagation then P depends on two variables, the horizontal wavenumber $k_h = \sqrt{k_x^2 + k_y^2}$, and frequency.

Then, we calculate the angular average in the *k*-space:

$$P(k_h, \omega) = \frac{1}{2\pi} \int_0^{2\pi} P(k_{h,} \cos\phi, k_h \sin\phi, \omega) d\phi$$

This is a local power spectrum. It allows us to investigate properties of various regions observed on the solar disk.

Consider example using IDL codepower_spectrum.pro.

3D Power Spectrum

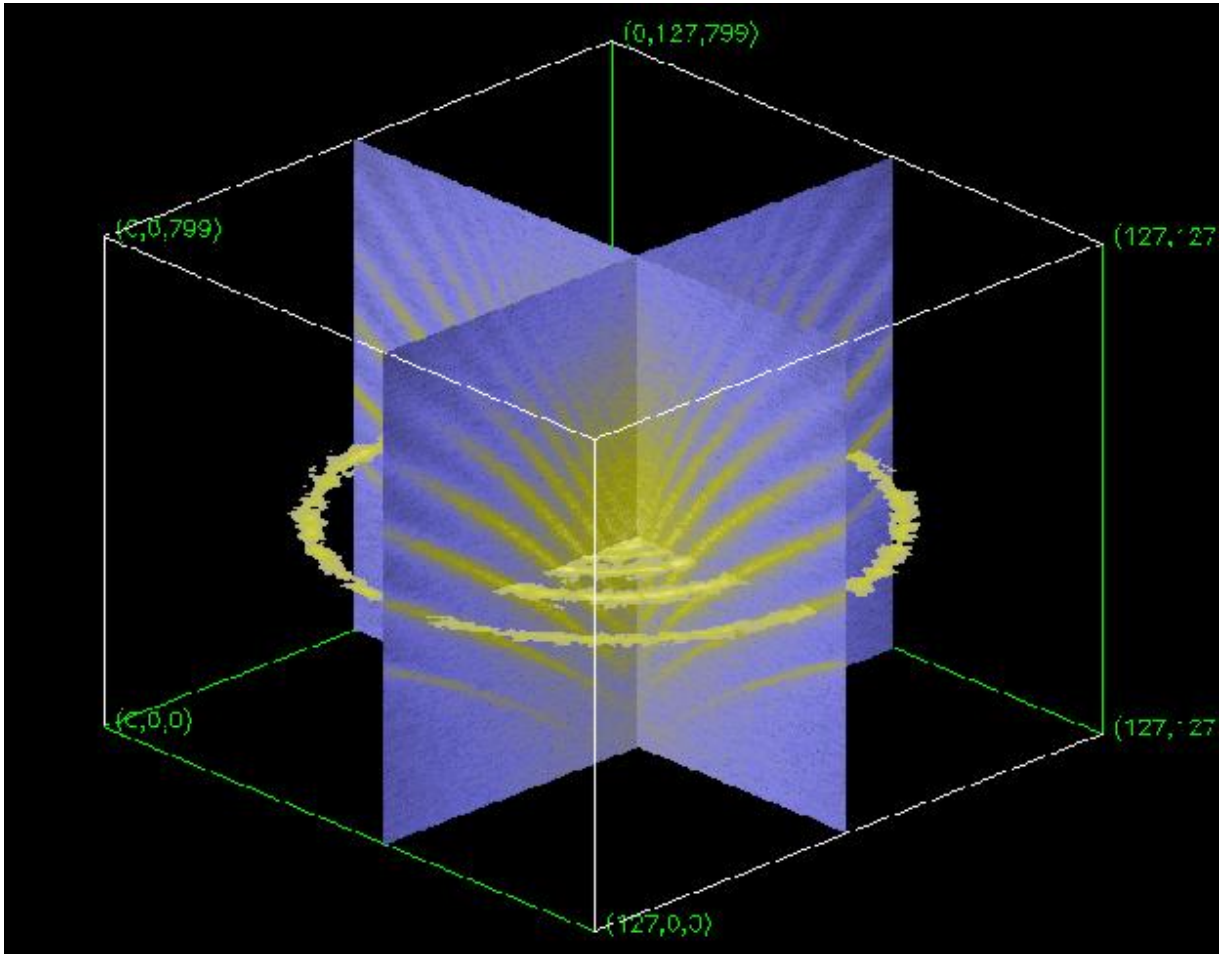

Spherical harmonics

For the global oscillations we must use the spherical coordinates (r,□□)
and expansion in terms of spherical surface harmonics:

$$v(\theta,\phi,t)=\sum_{l=0}^{\infty}\sum_{m=-l}^{l}a_{lm}(t)Y_l^m(\theta,\phi)$$

In the spherical coordinates, θ,ϕ:

$$a(l,m,\omega)=\iiint v(\theta,\phi,t)Y_l^m(\theta,\phi)e^{i\omega t}\sin(\theta)d\theta d\phi dt,$$

where $Y_l^m(\theta,\phi)=P_l^{|m|}(\theta)e^{im\phi}$ is a spherical harmonic of **the angular degree** l **and angular order** m, $P_l^m(\theta)$ is an associate Legendre function.

Degree l gives the total number of node circles on the sphere; order m is the number nodal circles through the poles; m=*-1,-l+1,...,l-1, l* that is (2l+1) m-values on m for given l.

Spherical harmonics

The coefficients of the spherical harmonic expansion can be found by using the spherical harmonic transform:

$$a(l,m,\omega) = \iiint v(\theta,\phi,t) Y_l^m(\theta,\phi) e^{i\omega t} \sin(\theta) d\theta d\phi dt,$$

where $Y_l^m(\theta,\phi)$ is a spherical harmonic of **the angular degree** l **and angular order** m.

The power spectrum is:

$$P(l,m,\omega) = a^* a.$$

For a spherically symmetrical star, P depends only on l and ω.
In this case the power spectrum is 'degenerate' with respect of angular order m.

Then we can define the analog of the horizontal wavenumber:

$k_h = \dfrac{\sqrt{l(l+1)}}{R}$, where R is the solar radius.

We will derive this in a future lecture.

Oscillation power spectrum

- The power spectrum represents the oscillation signal in terms of spherical harmonics of **angular degree** l (and the **horizontal wavelength**, $\lambda_h = 2\pi/k_h$), and the oscillation **"cyclic" frequency**, $\nu=\omega/2\pi$.

l is integer number

λ_h is measured in Mm

ν is measured in mHz

ω is measured in rad/sec

(sometimes called angular frequency)

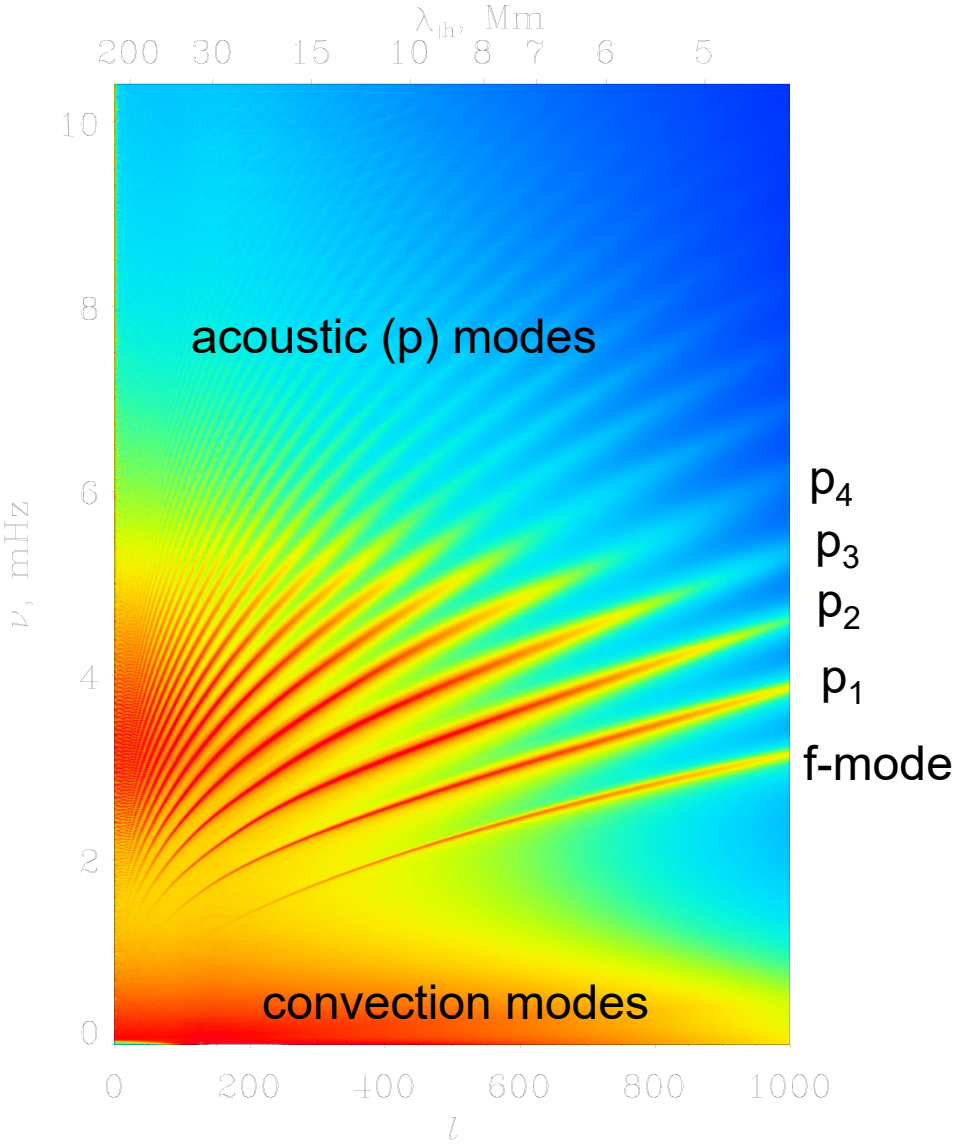

The basic idea of helioseismology

- To measure travel times τ or resonant frequencies ω, and to determine the internal properties of the Sun, such as the sound speed $c_s(r)$

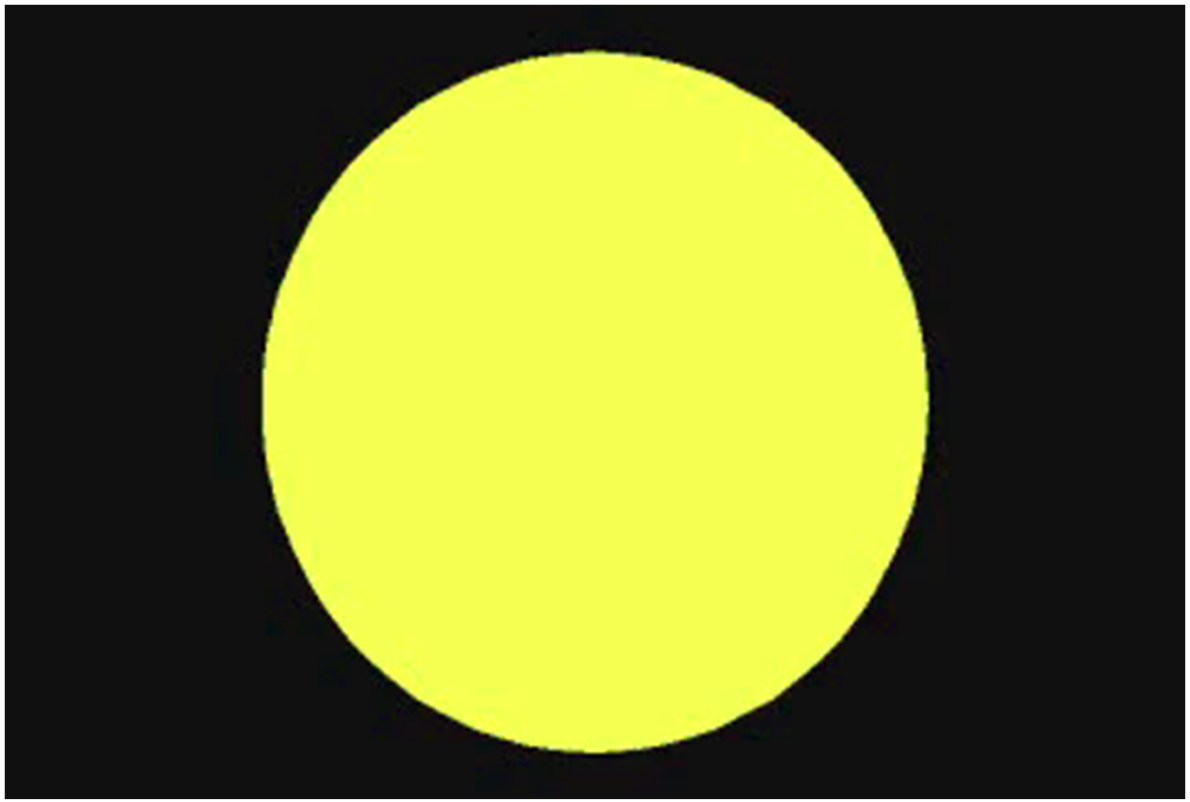

Normal Mode of Solar Oscillations –
displacement eigenfunction: $\delta r(r,\theta,\phi)=\xi(r)*Y_{lm}(\theta,\phi)$

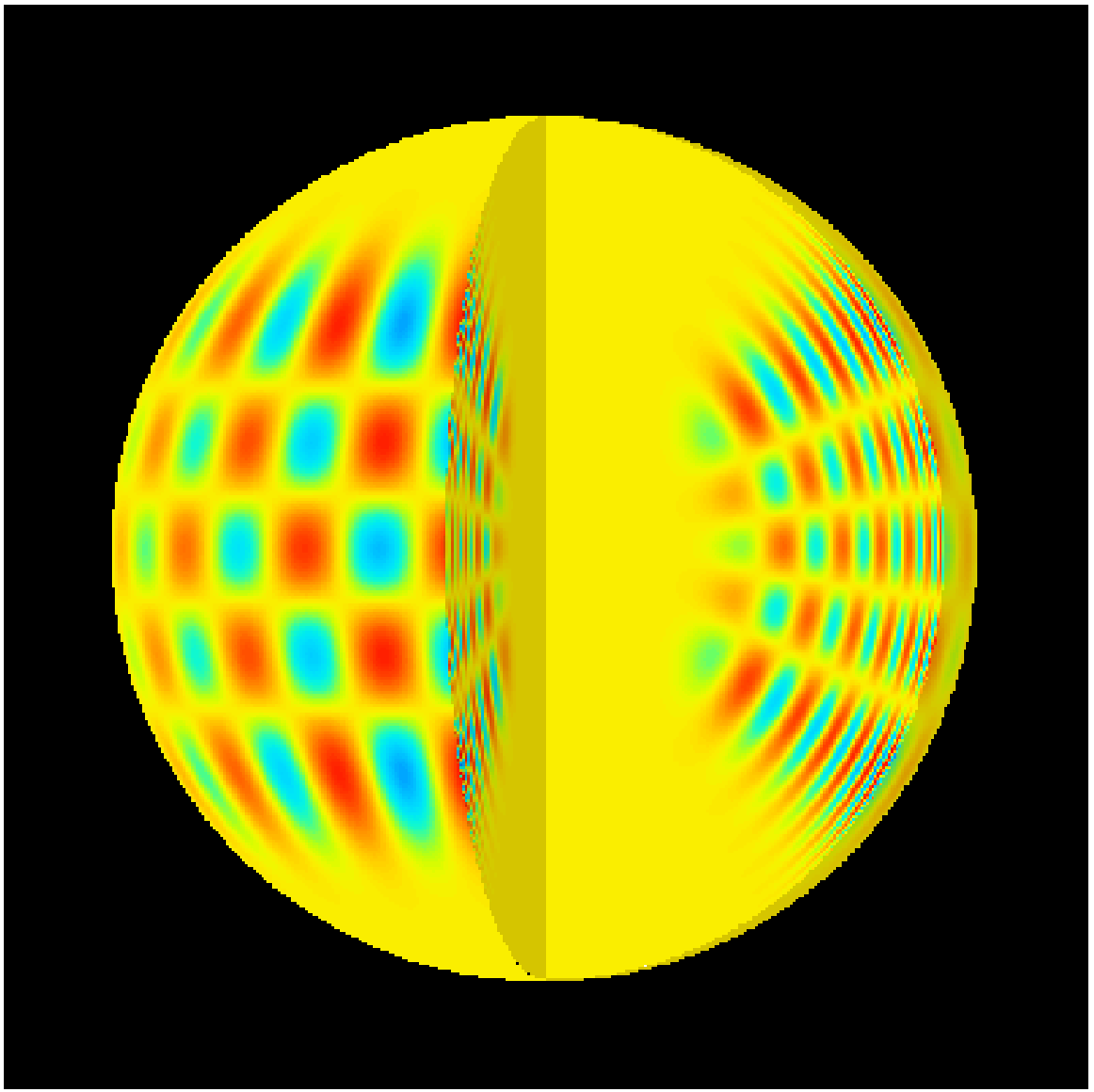

l=20, m=16

Low-Degree (Global) Modes

When the Sun is observed as a star (integrated whole-disk Doppler-shift measurements) the power spectrum consists only of low-degree p-modes of $l = 0, 1, 2$ and 3.

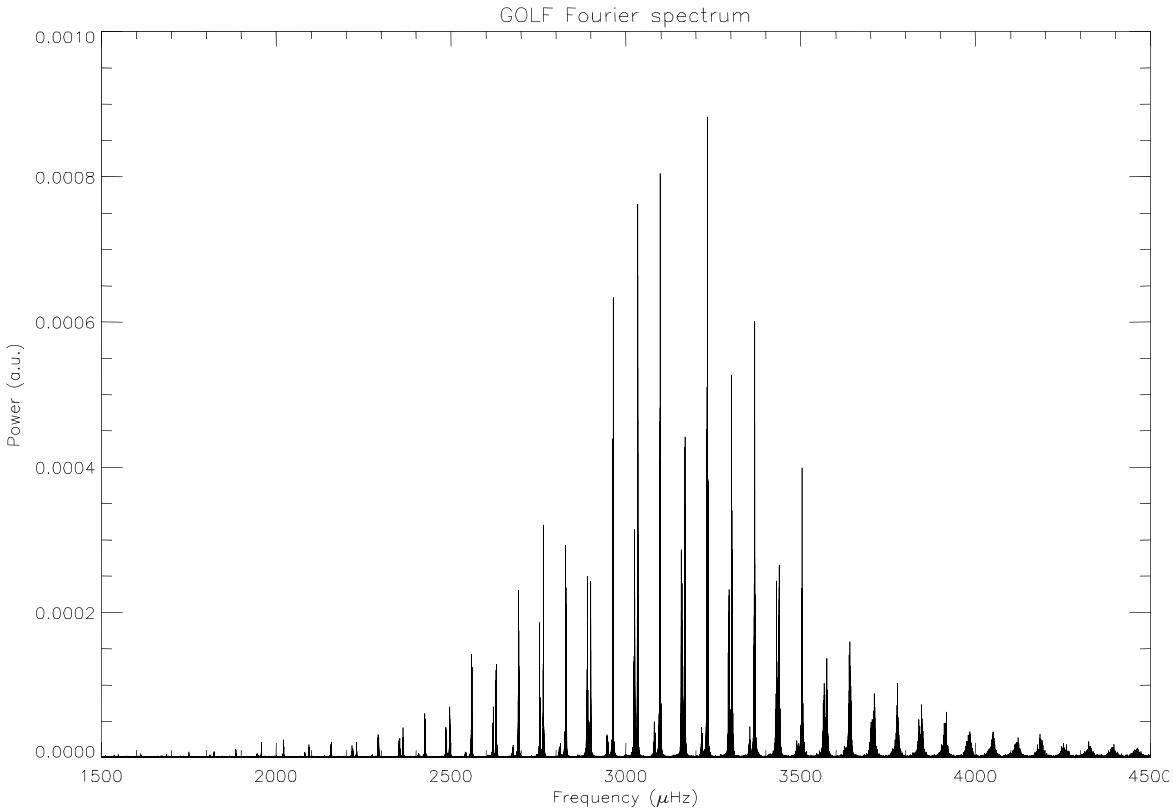

The distance between main peaks in the power spectrum is about 68 μHz. The corresponding time: $1/(68 \cdot 10^{-6}) = 245$ min is the travel time for acoustic waves propagate through the center of the Sun to the far side and come back. The low-degree mode provide information about physical conditions of the solar core.

This figure is a Fourier spectrum of the longest continuous GOLF time series (805 days). GOLF is an instrument on SOHO that measures the oscillations in the line-of-sight velocity of the solar photosphere from the whole Sun. These oscillations appear at precise frequencies, visible as sharp peaks in this spectrum, mainly around 3mHz, corresponding to periods about 5min.

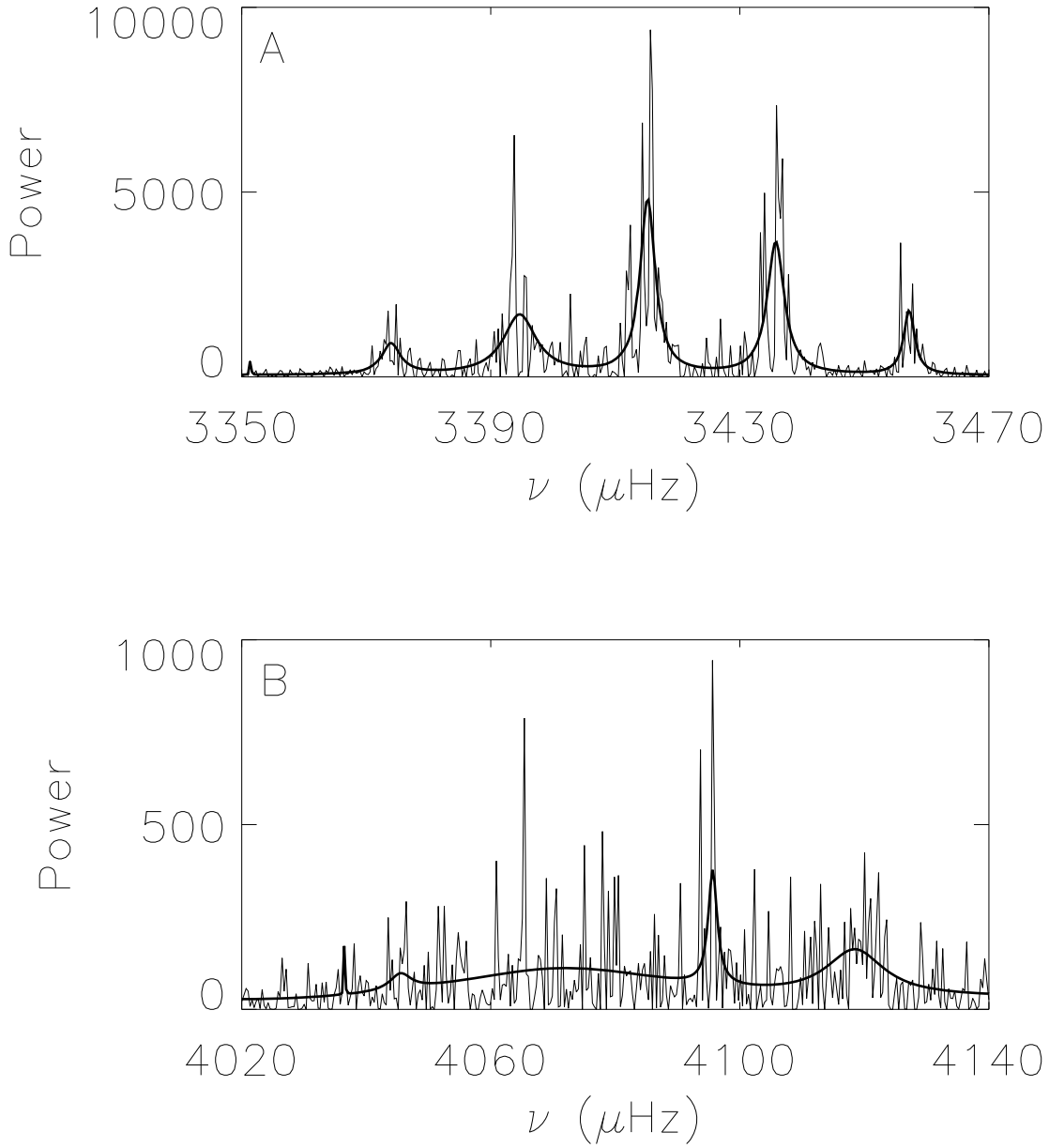

Power spectra of A) $l = 50, m = -32, n = 12$ and B) $l = 50, m = 0, n = 16$.

Excitation of Solar Oscillations

Solar oscillations are randomly excited by turbulent convection. The random excitation function appears as multiplicative noise in the power spectra. This represents the most serious problem for measuring mode frequencies. This figure shows examples of good and poor fits of an oscillation model to the power spectra.

Elements of signal processing

Forward and inverse Fourier transform

$$\tilde{x}(\omega) = \int_{-\infty}^{\infty} x(t) e^{-i\omega t} dt$$

$$x(t) = \frac{1}{2\pi} \int_{-\infty}^{\infty} \tilde{x}(\omega) e^{i\omega t} d\omega$$

$$\omega = 2\pi f$$

$$e^{i\omega t} = \cos \omega t + i \sin \omega t$$

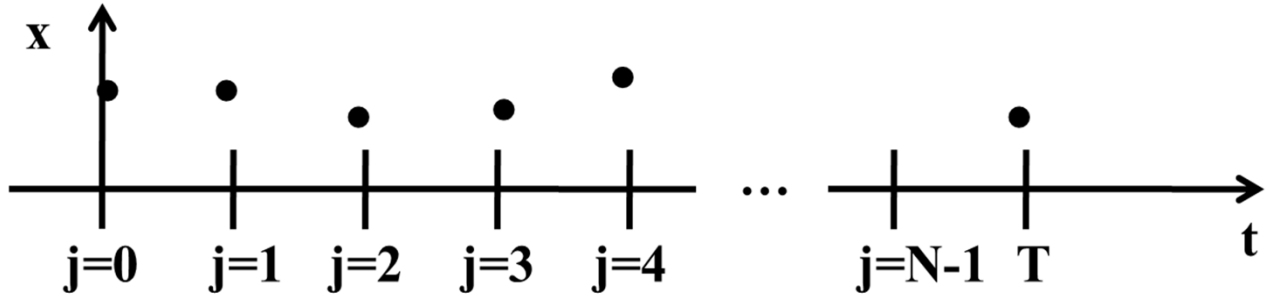

Sample rate, f_s: $f_s = 1 / \Delta t$

Duration T, number of samples N, Nyquist frequency:

$$f_s T = N; \qquad f_{Nyquist} = f_s / 2$$

Time index j:

$$t_j = j\Delta t; \qquad j = 0, 1, 2, \ldots N-1;$$

Frequency resolution:

$$\Delta f = 1 / T$$

Frequency index k:

$$f_k = k / T; \qquad f_k T = k; \qquad k = 0, 1, 2, \ldots N-1$$

Line Asymmetry and Pseudo-modes

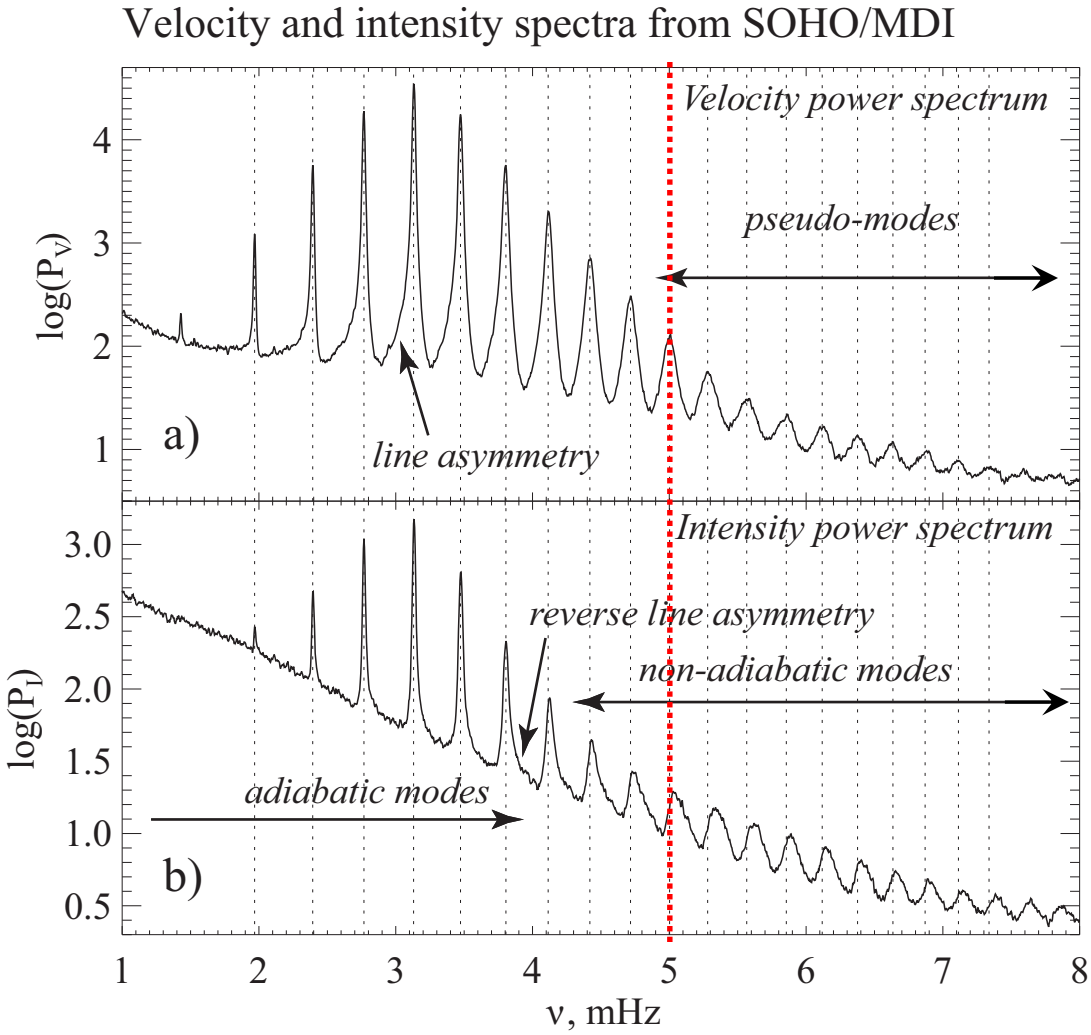

Power spectra of l = 200 modes obtained from SOHO/MDI observations of
a Doppler velocity,
b continuum intensity.

Acoustic waves with frequencies below the cut-off frequency are completely reflected by the surface layers because of the steep density gradient. These waves are trapped in the interior, and their frequencies are determined by the resonant conditions, which depend on the solar structure. But the waves with frequencies above the cut-off frequency escape into the solar atmosphere.

Above this frequency the power spectrum peaks correspond to so-called “pseudo-modes”

Waves in the solar atmosphere: dispersion relation

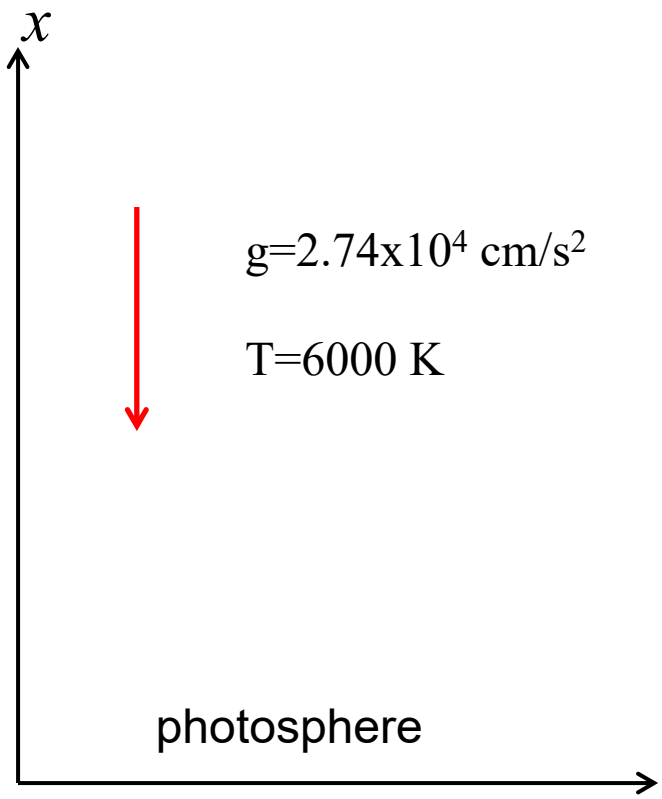

Eliminating ρ_1, P_1, v_1 we find that displacement ξ satisfies the second-order PDE:

$$\frac{\partial^2 \xi}{\partial t^2} = c^2 \frac{\partial^2 \xi}{\partial x^2} - \gamma g \frac{\partial \xi}{\partial x},$$

using the substitution $u = \xi \exp(\alpha x)$ we eliminate the first-order term:

$$\frac{\partial^2 u}{\partial t^2} = c^2 \frac{\partial^2 u}{\partial x^2} - \omega_c^2 u,$$

where $\omega_c = \frac{\gamma g}{2c}$ is the acoustic cut-off frequency.

For the dispersion relation we seek the solution in terms of Fourier harmonics: $u \propto \exp(-i\omega t + ikx)$:

$$-\omega^2 u = -c^2 k^2 u - \omega_c^2 u$$

$$\boxed{\omega^2 = c^2 k^2 + \omega_c^2}$$

The frequencies of plane-parallel acoustic waves traveling in the atmosphere are higher than the acoustic cut-off frequency.

Waves in the solar atmosphere: calculation of the acoustic cut-off frequency

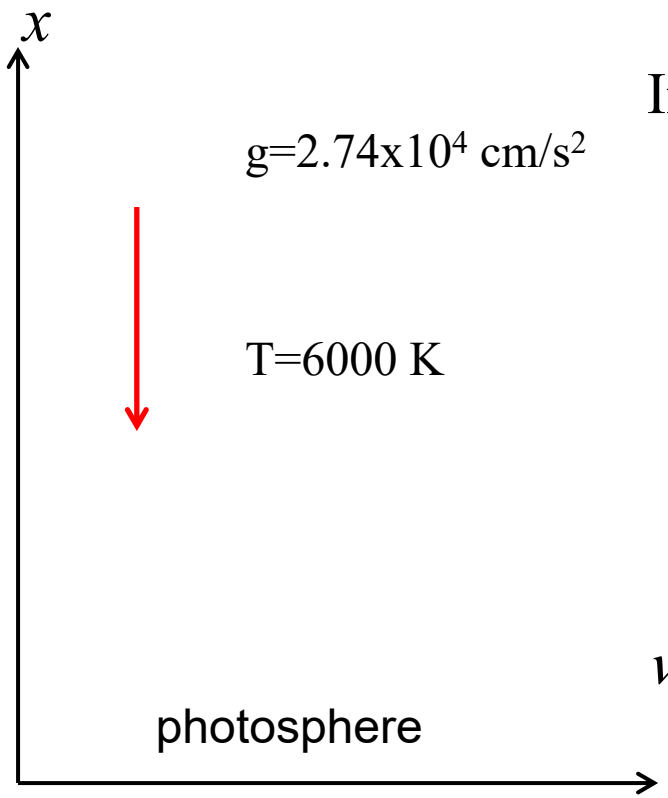

$\omega_c = \dfrac{\gamma g}{2c}$ is the acoustic cut-off frequency.

In the photosphere: $\gamma = 5/3$, μ=1.25

$$c = \sqrt{\frac{\gamma P}{\rho}}, \quad P = \frac{R\rho T}{\mu},$$

$$c = \sqrt{\frac{\gamma RT}{\mu}} \approx 8.1\times 10^5 \text{ cm/s} \approx 8 \text{ km/s}.$$

$$\nu_c = \omega_c / 2\pi = \frac{\gamma g}{4\pi c} \approx 4.5\times 10^{-3} Hz = 4.5 \text{ mHz}.$$

The corresponding period $1/\nu_c$ = 3.6 min.

Simple analytical model of solar oscillations

- "Potential well model"

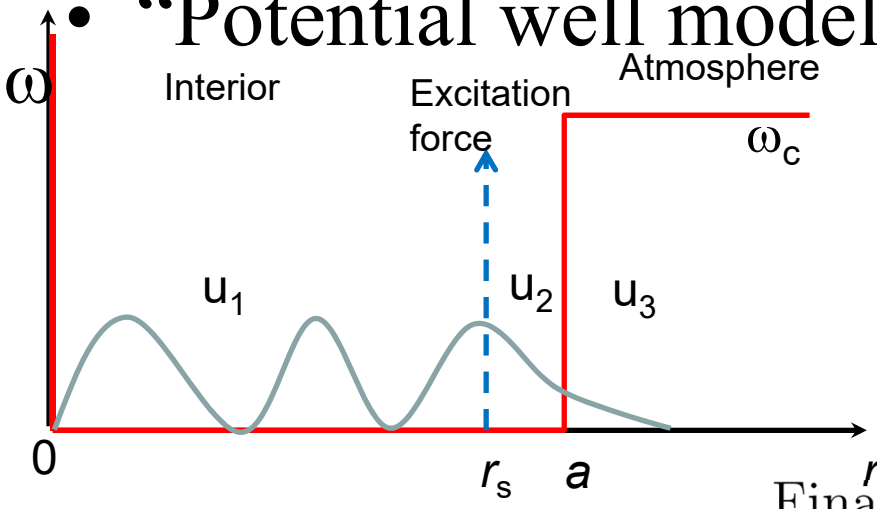

$$\frac{d^2u}{dr^2}+\frac{\omega^2-\omega_c^2}{c^2}u=\delta(r-r_s)$$

Finally,

$$u(a,\omega)=\frac{c\sin\left(\frac{\omega r_s}{c}\right)}{\omega\cos\left(\frac{\omega a}{c}\right)+\sqrt{\omega_c^2-\omega^2}\sin\left(\frac{\omega a}{c}\right)}$$

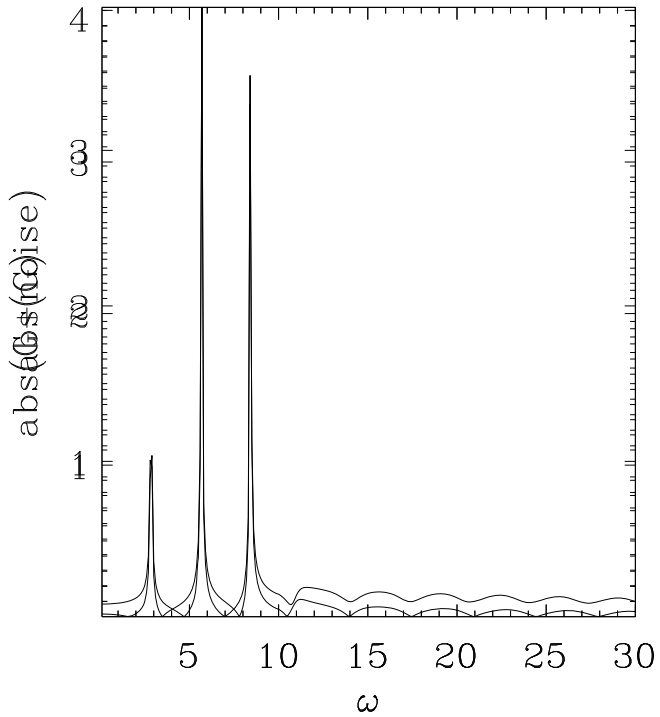

Asymmetrical line profile (Nigam & Kosovichev, 1998):

$$\Gamma=A\frac{(1+Bx)^2+B^2}{1+x^2}+r$$

where $x=2(\nu-\nu_0)/\gamma$,

$\nu=\omega/2\pi$ is the cyclic frequency,

B is the parameter of asymmetry

Power spectrum for the model

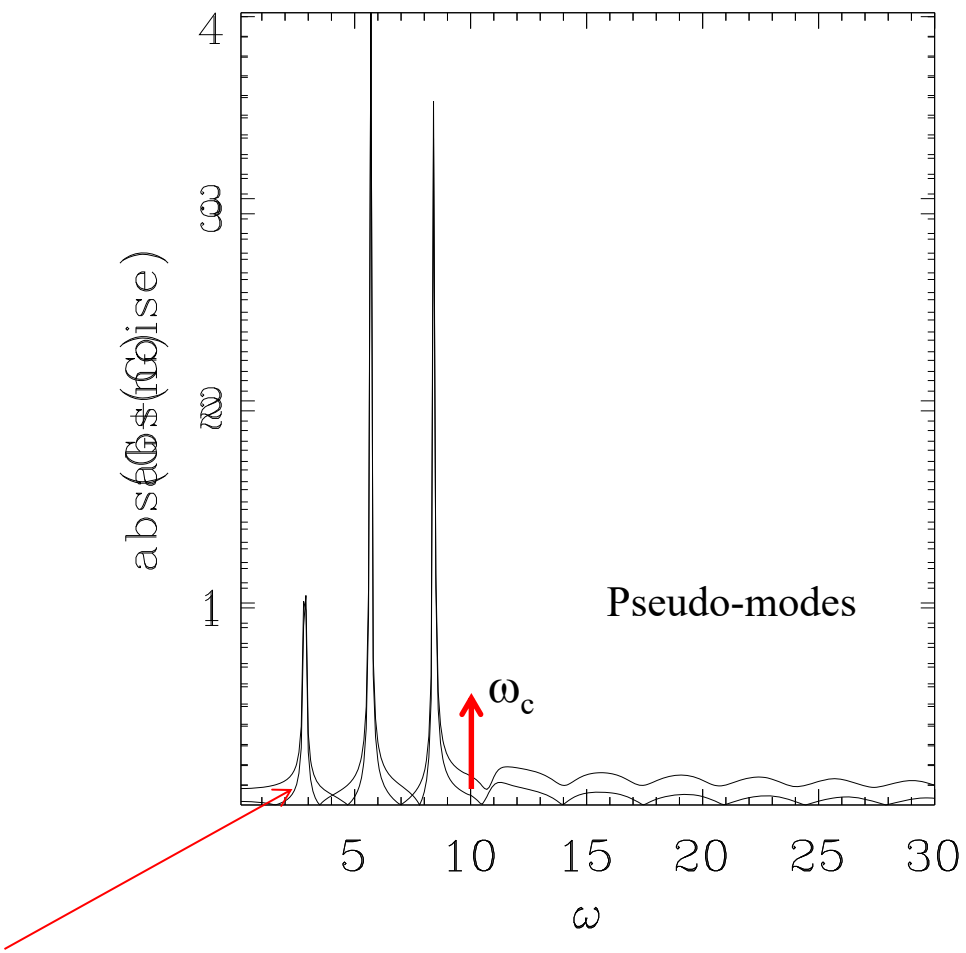

Pseudo-modes are caused by the interference of waves coming directly from the source and after the reflection in the interior.

This is so-called “source resonance”.

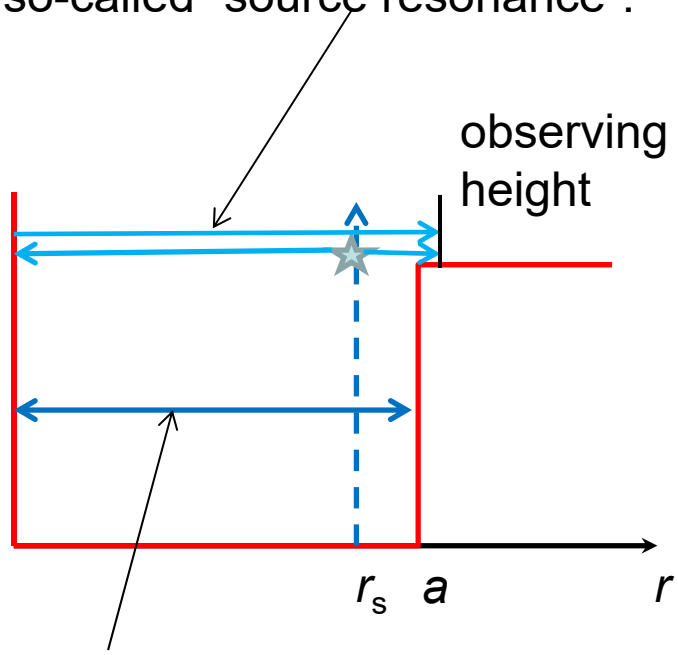

Reversal of the line asymmetry is caused by correlated noise

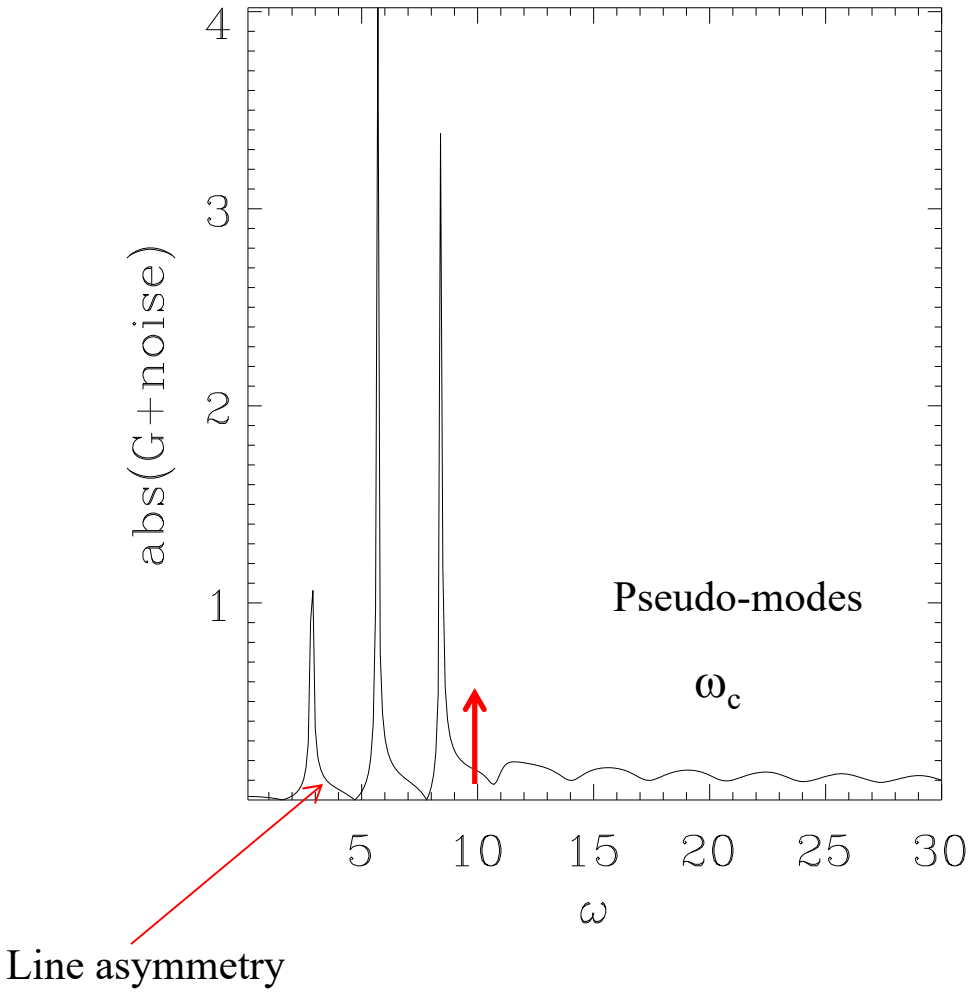

The correlated noise is added to oscillation signal and uncorrelated noise is added to the oscillation power, so that the observed power spectrum has two types of noise:

$$P_{obs}(\omega) = | u(\omega) + N_{corr}(\omega) |^2 + N_{uncorr}(\omega)$$

Correlated noise means that in the observed oscillation signal in additions to wave signal there is a component that comes directly from the source. When the solar oscillations are observed in intensity the correlated noise may be caused by changes of brightness of granules during the wave excitation events.

http://sun.stanford.edu/~sasha/PHYS747/Projects/Simple_oscillation_model

Oscillation power maps.
Effects of magnetic field.

Oscillation power maps

Magnetic field effects are displayed in the oscillation power maps. These are calculated by performing Fourier transform for each pixel, and averaging in different frequency intervals.

$$a(x,y,\omega) = \int_0^T v(x,y,t) e^{i\omega t} dt$$

$$P(x,y,\omega) = a^* a$$

http://sun.stanford.edu/~sasha/PHYS747/Projects/Power_Maps/

Oscillation power maps for HMI data of 09/06/16

http://sun.stanford.edu/~sasha/PHYS747/Projects/Power_Maps/

2-4 mHz

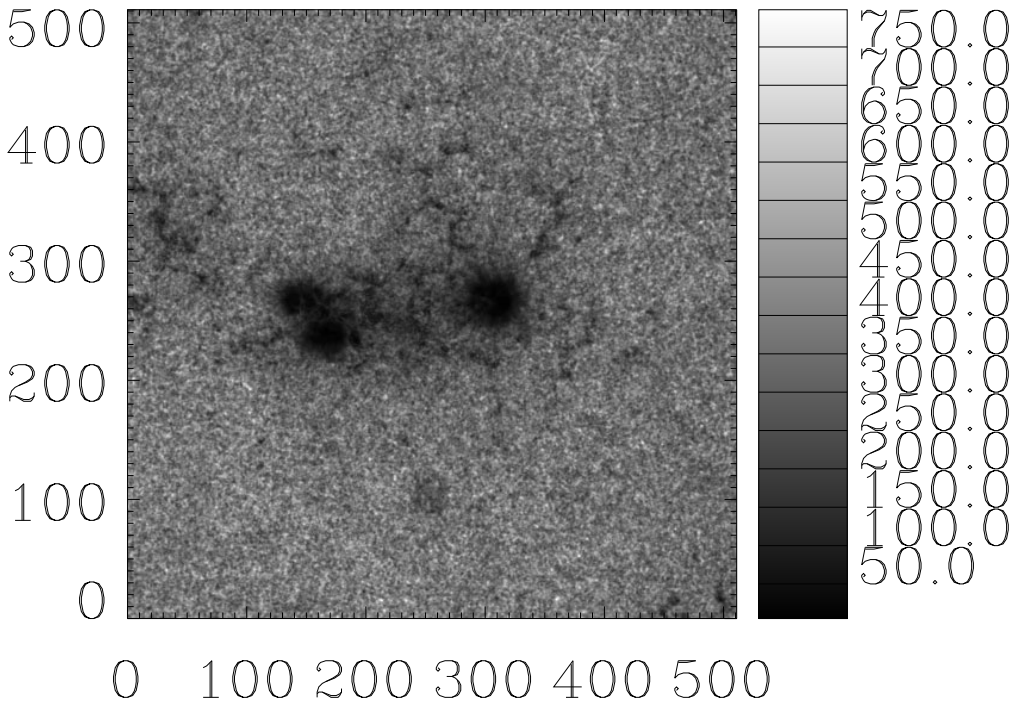

6-8 mHz

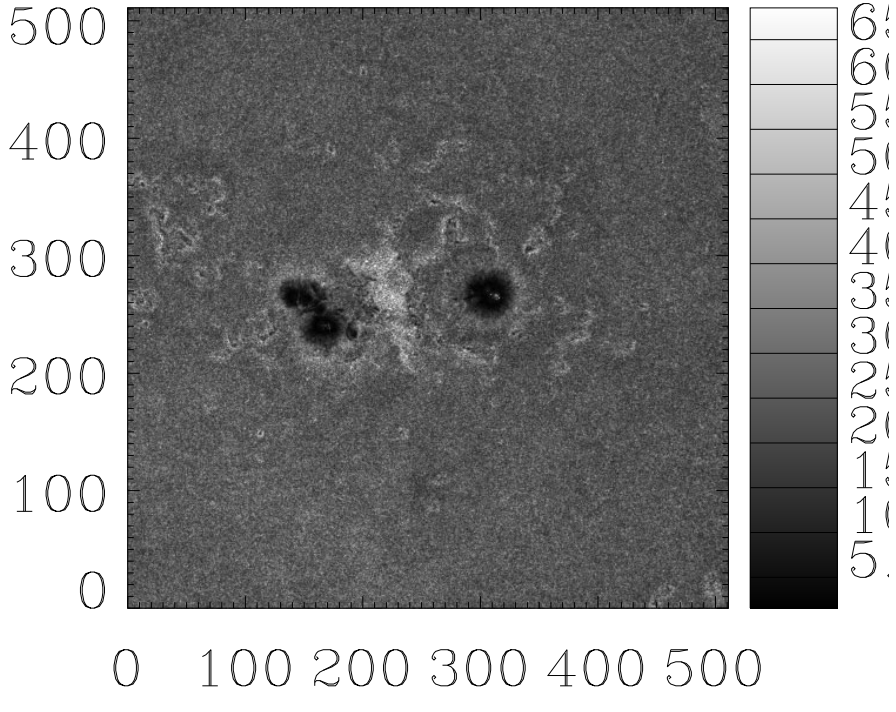

Using power maps to detect emerging active regions

Power suppression in the oscillation power maps appears prior emergence of active regions on the solar surface.

Example: AR 10488: in the frequency range 3-4 mHz the power in the AR area was reduced 200 min prior the AR appearance ; outside the AR area the signal remained constant.

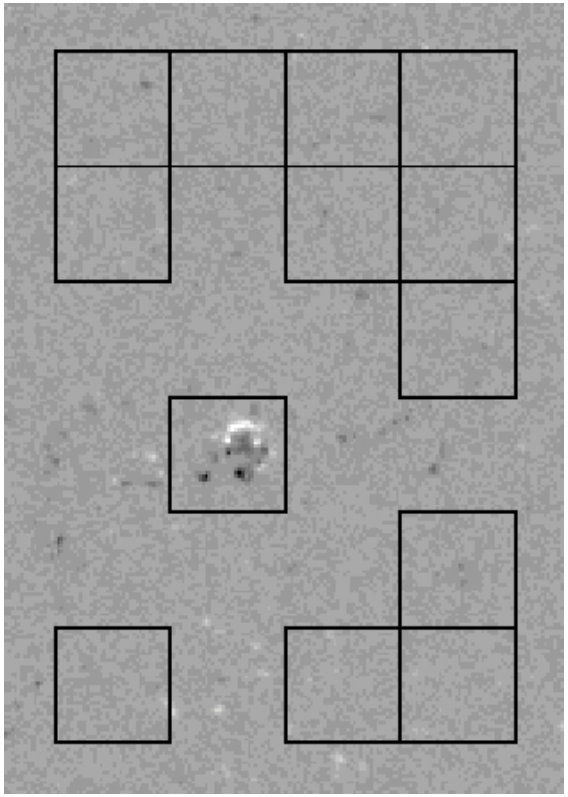

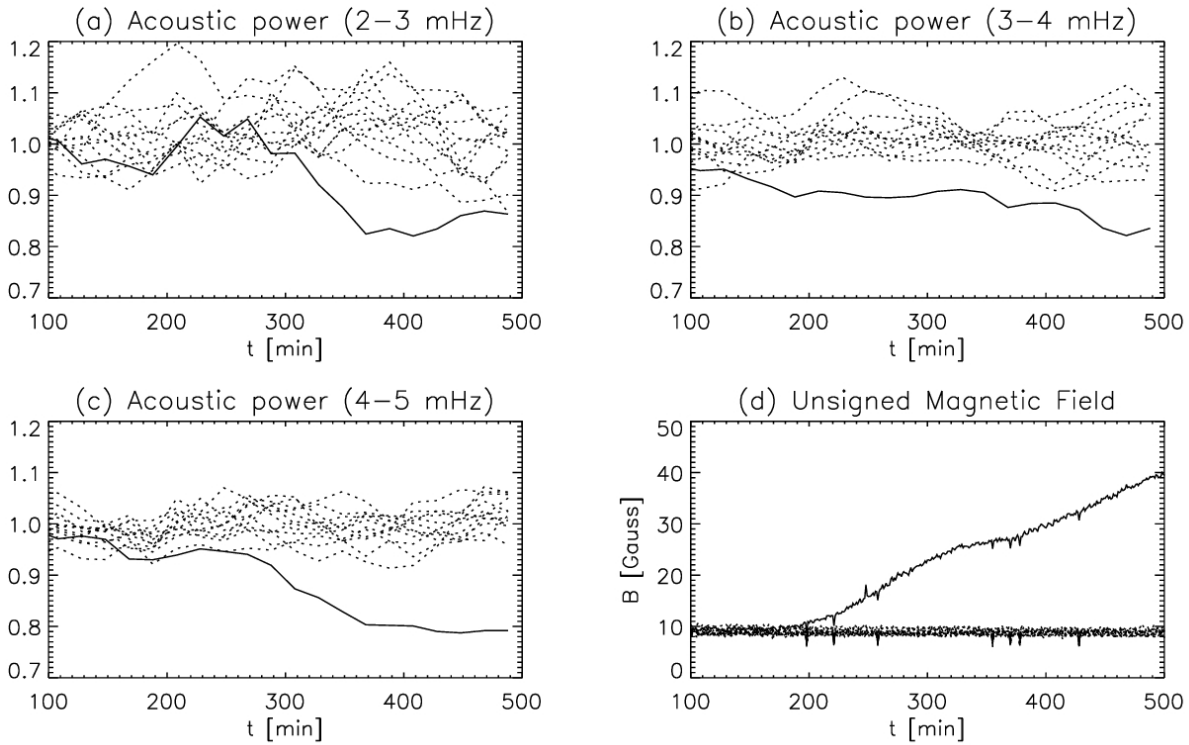

Hartlep, T. et al. 2011 Solar Physics, Volume 268, Issue 2, pp.321-327

Magnetic field effects are revealed in oscillation power maps

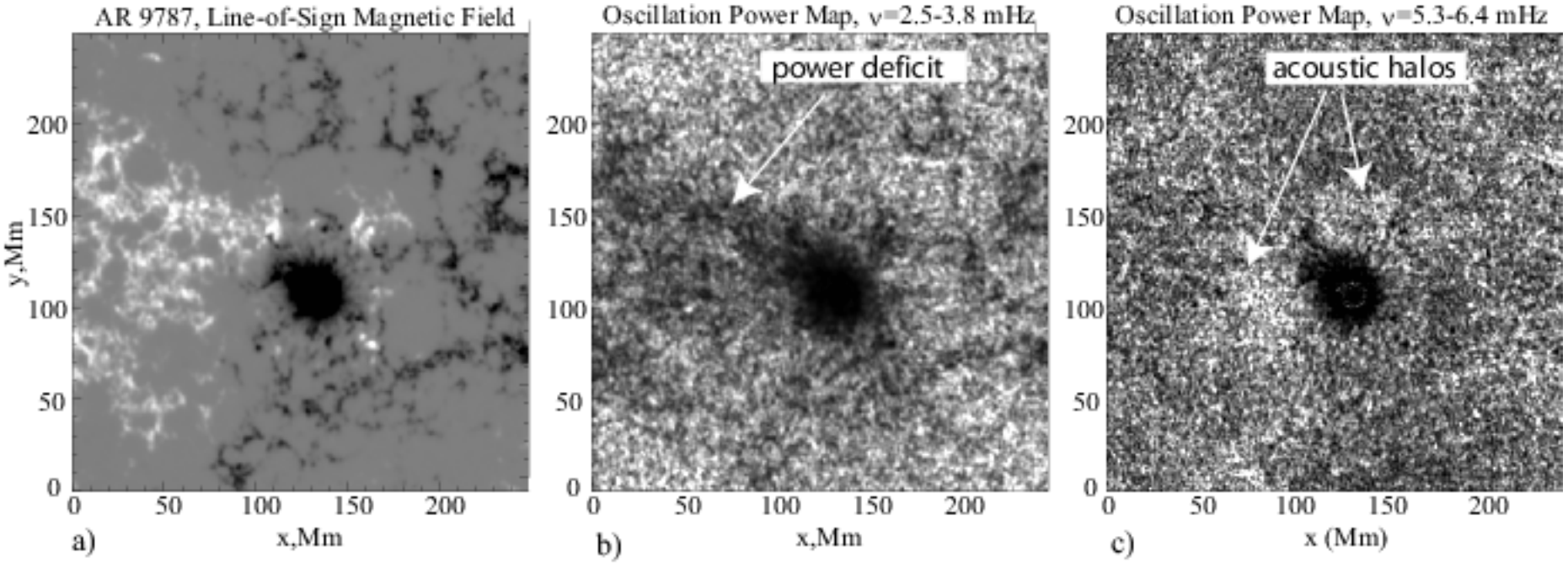

Numerical simulations of solar convection and oscillations.

3D radiative MHD simulations

- The mathematical model is based on first-physics principles
- It takes into account all essential physical processes:
  - Conservation laws
  - Maxwell equations
  - Radiative energy transport
  - Real-gas equation of state
- Models sub-grid scale turbulent dissipation

Numerical Model: Basic equations

The equations we solved are the grid-cell average conservation of mass:

$$\frac{\partial \rho}{\partial t} + \left(\rho u_i\right)_{,i} = 0$$

Conservation of momentum:

$$\frac{\partial \rho u_i}{\partial t} + \left(\rho u_i u_j + P_{ij}\right)_{,j} = -\rho \phi_{,i}$$

Conservation of energy:

$$\frac{\partial E}{\partial t} + \left(\begin{array}{l} E u_i + P_{ij} u_j - \kappa T_{,i} + \\ + \left(\frac{c}{4\pi}\right)^2 \frac{1}{\sigma}\left(B_{i,j} - B_{j,i}\right) B_j + F_i^{\mathrm{rad}} \end{array} \right)_{,i} = 0$$

with

$$P_{ij} = \left(p + \frac{2}{3}\mu u_{k,k} + \frac{1}{8\pi} B_k B_k \right)\delta_{ij} - \mu\left(u_{i,j} + u_{j,i}\right) - \frac{1}{4\pi} B_i B_j$$

Conservation of magnetic flux:

$$\frac{\partial B_i}{\partial t} + \left(u_j B_i - u_i B_j - \frac{c^2}{4\pi\sigma}\left(B_{i,j} - B_{j,i}\right) \right)_{,j} = 0$$

p(ρ,e)

ρ denotes the average mass density,

u_i, the Favre-averaged velocity

"SolarBox" code: Basic characteristics of the code

- ✓ 3D rectangular geometry
- ✓ Fully conservative compressible
- ✓ Fully coupled radiation solver:
  - LTE using 4 opacity-distribution-function bins
  - Ray-tracing transport by Feautrier method
  - 14 ray (2 vertical, 4 horizontal, 8 slanted) angular quadrature
- ✓ Non-ideal (tabular) EOS
- ✓ 4th order Padé spatial derivatives
- ✓ 4th order Runge-Kutta in time
- ✓ LES-Eddy Simulation options (turbulence models):
  - Compressible Smagorinsky model
  - Compressible Dynamics Smagorinsky model (Germano et a., 1991; Moin et al, 1991)
  - MHD subgrid models (Balarac et al., 2010)
- ✓ MPI parallelization (plane and pencil versions)

Strategy of simulations

"quiet Sun"

uniform vertical weak (0-1200 G) magnetic field

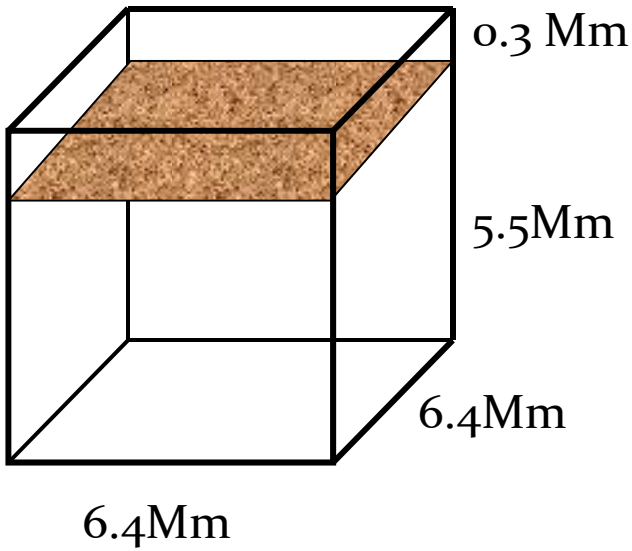

Resolution:

1. 128^3 (50^2 x 43 km)
2. 256^3 (25^2 x 21.7 km)
3. 512^3 (12.5^2 x 11 km)

Magnetic field effects are explained by changes in the excitation and interaction of acoustic waves with magnetic field

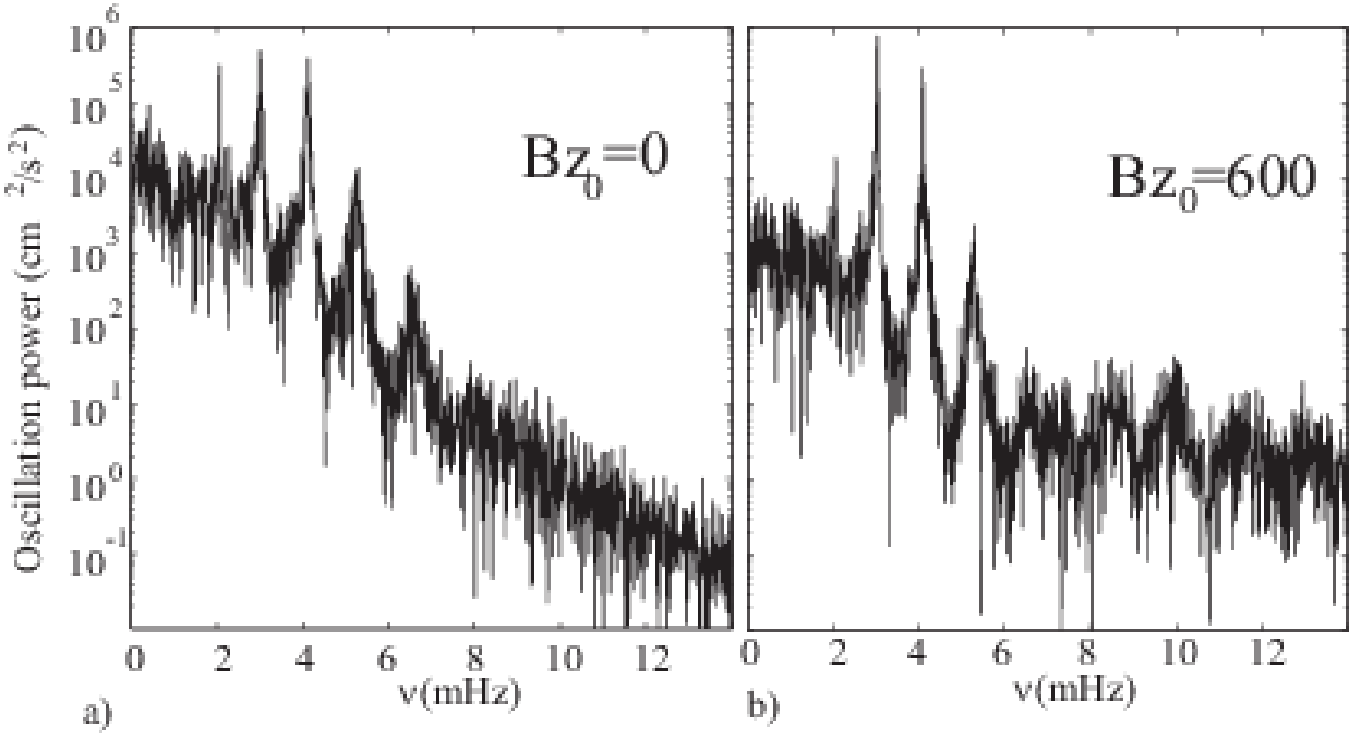

The appearance of acoustic halo can be explained by changes in the dynamics of granulations. In magnetic field granules becomes smaller and faster and therefore excite high-frequency waves (Jacoutot et al, 2008)

Magnetic field effects are explained by changes in the excitation (granulation properties) and interaction of acoustic waves with magnetic field

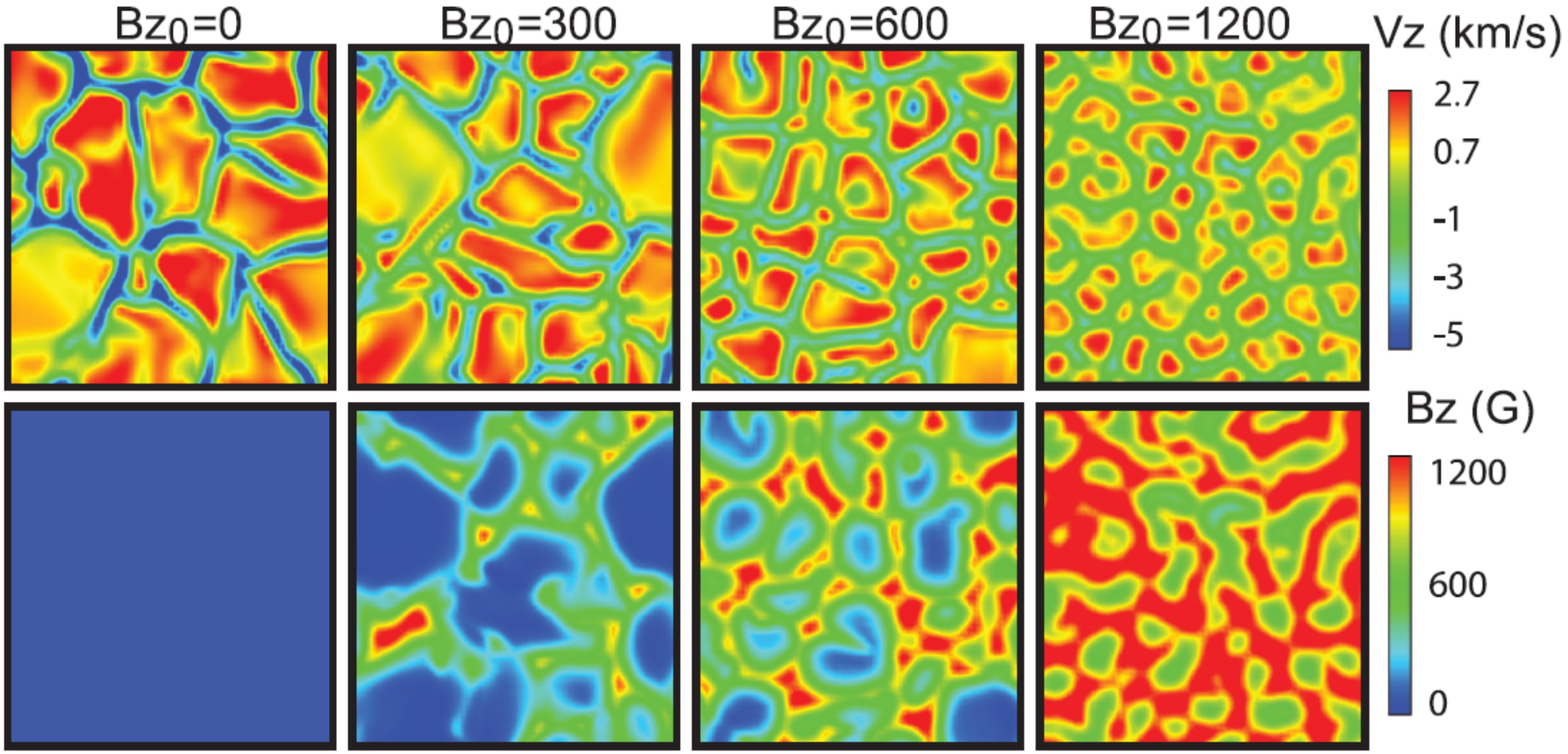

FIG. 1.—Vertical velocity, Vz, and vertical magnetic field, Bz, distributions at the visible surface for different initial vertical magnetic fields, Bz_0.

Magnetic field effects are explained by changes in the excitation and interaction of acoustic waves with magnetic field

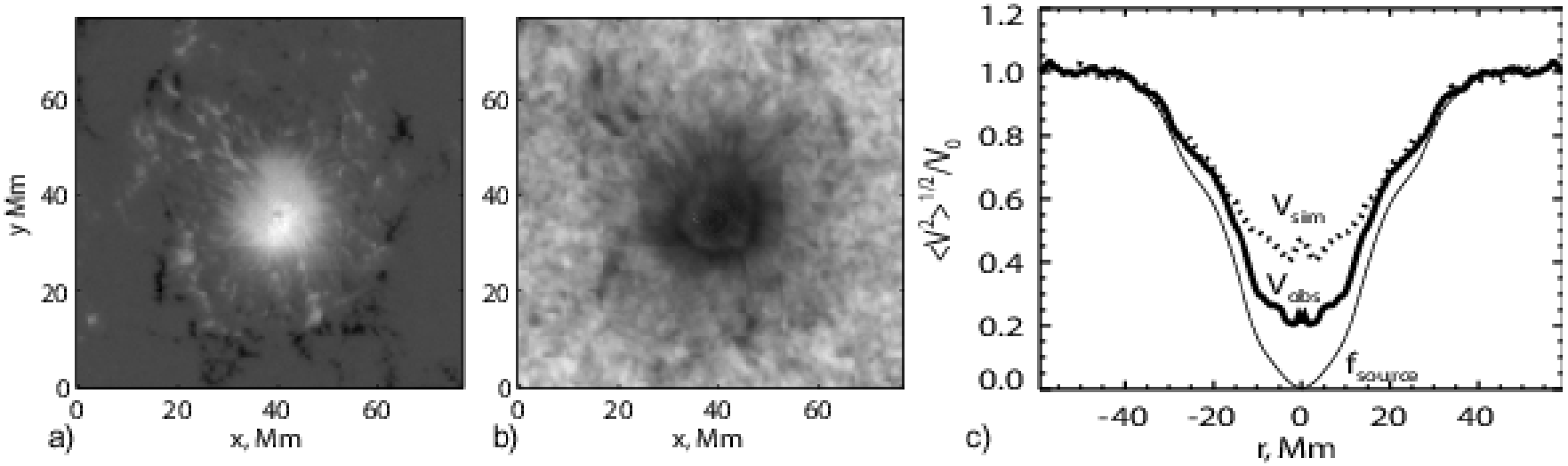

Numerical simulations show that the power reduction in sunspots can be explained by suppression of acoustic sources.

“Quiet Sun” simulations

Temperature

Density

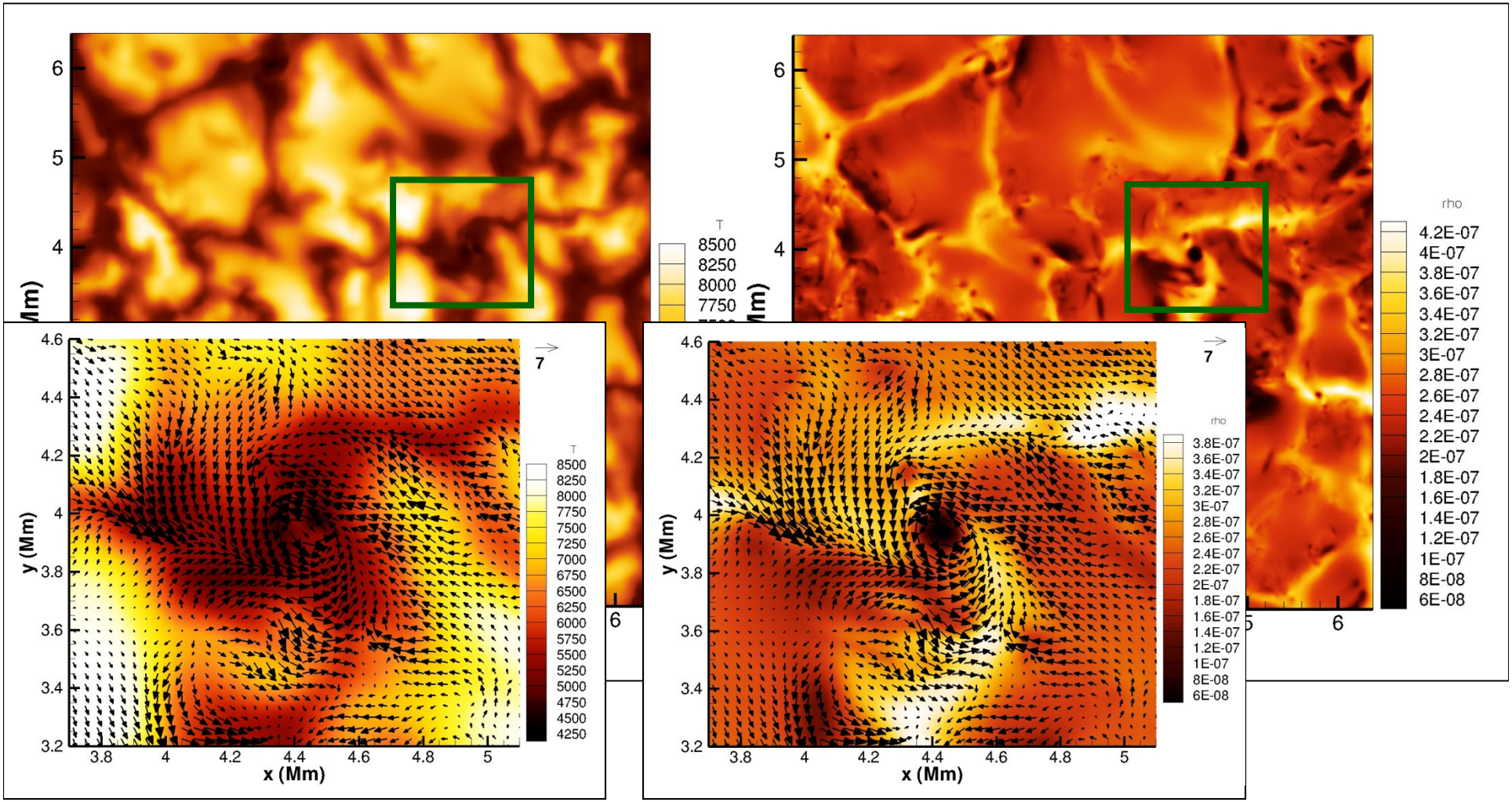

noMHD, 6.4^2x5.5Mm box, 512^2x503, 12.5km

Simulations of solar convection –Stokes I 4505.5A

(Kitiashvili et al, 2011)

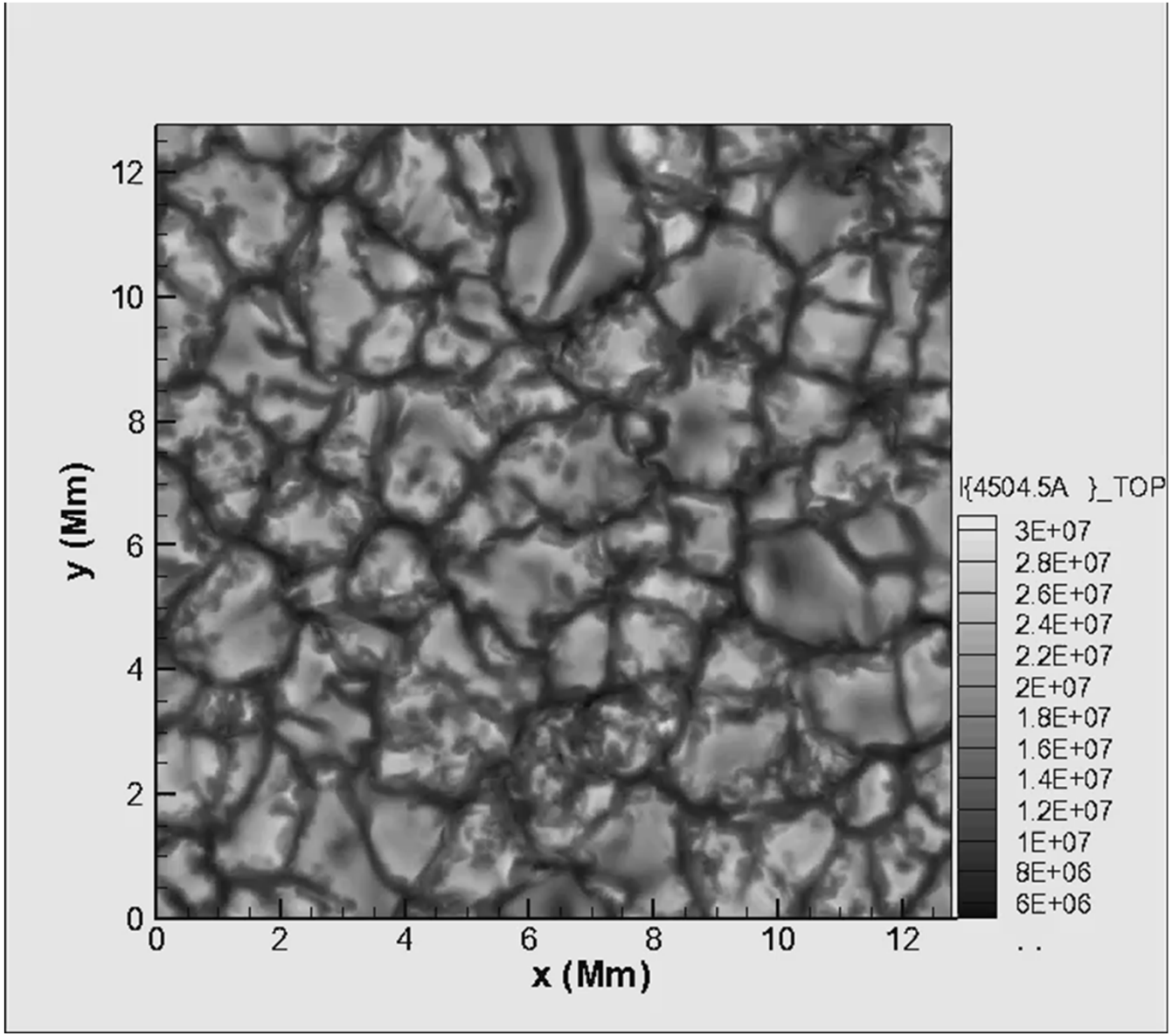

Simulations of solar convection –Stokes I 4505.5A: the line blue wing (Kitiashvili et al, 2011)

View at 60 degrees from the disk center reveals oscillations flowing on top of the granulation

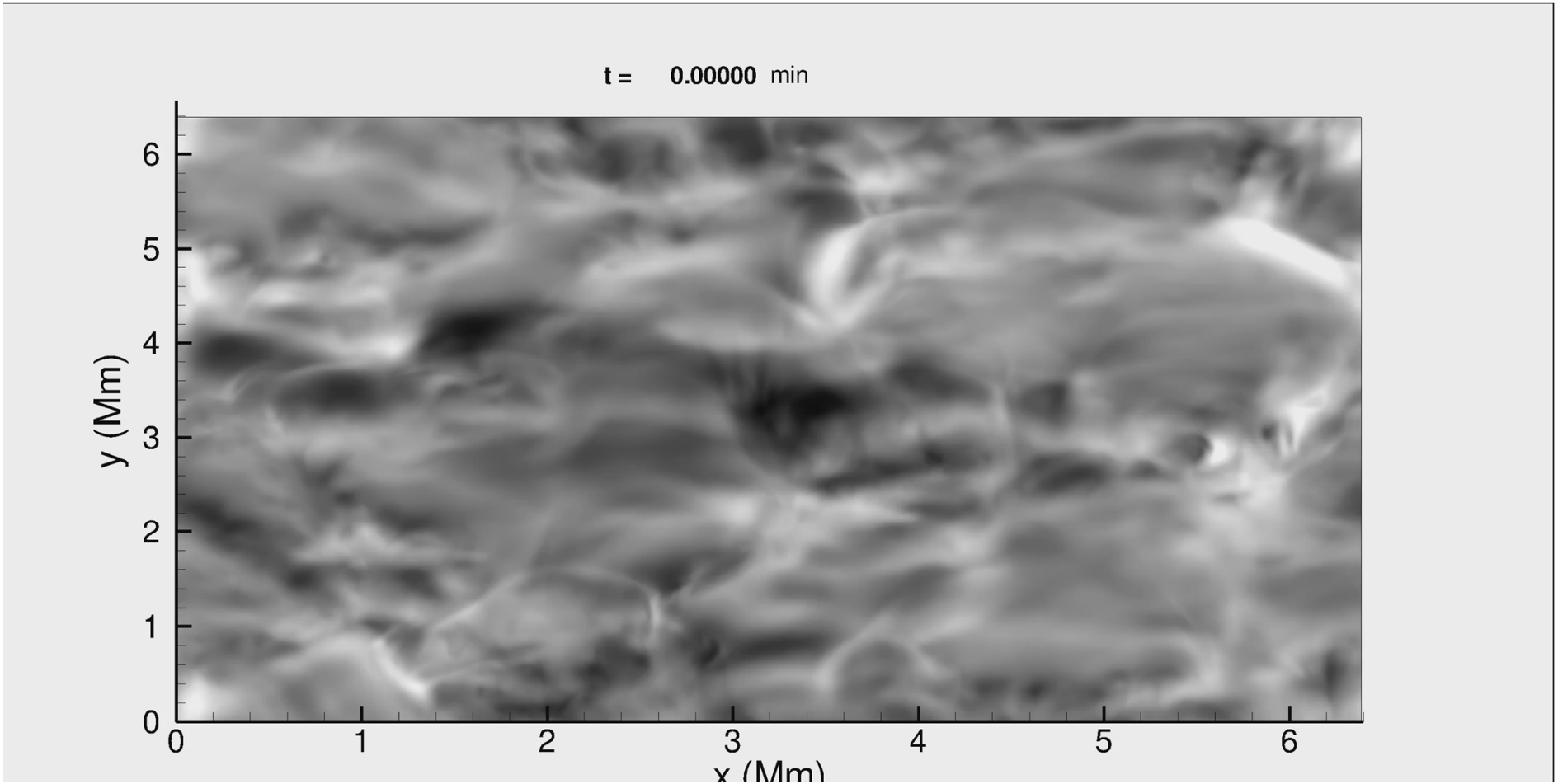

Observations of solar convection from Hinode spacecraft in the photosphere (left – blue continuum) and chromosphere (right – CaII H line)

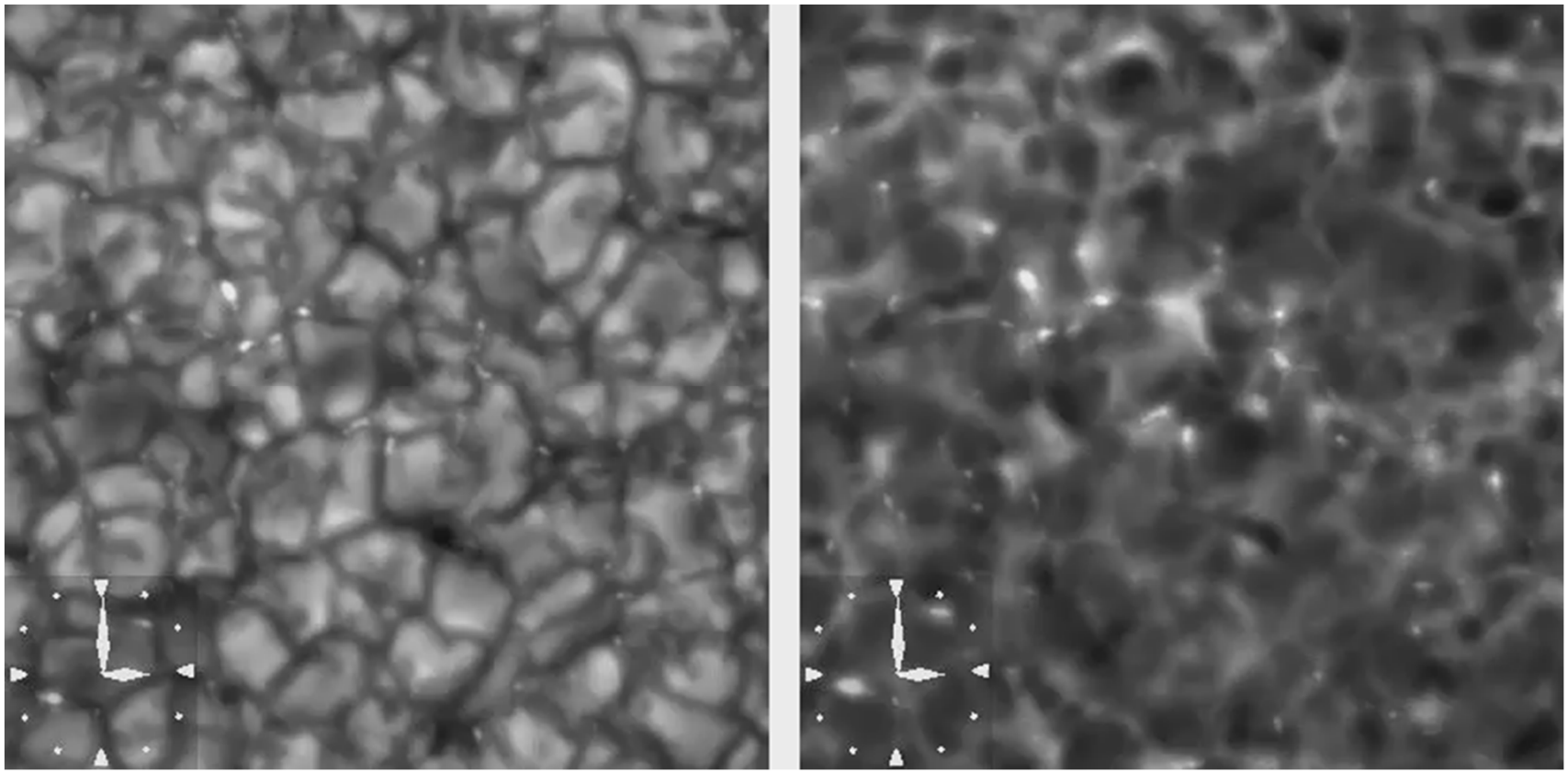

Observations of the individual acoustic events using oscillation power maps

Goode et al., 1992

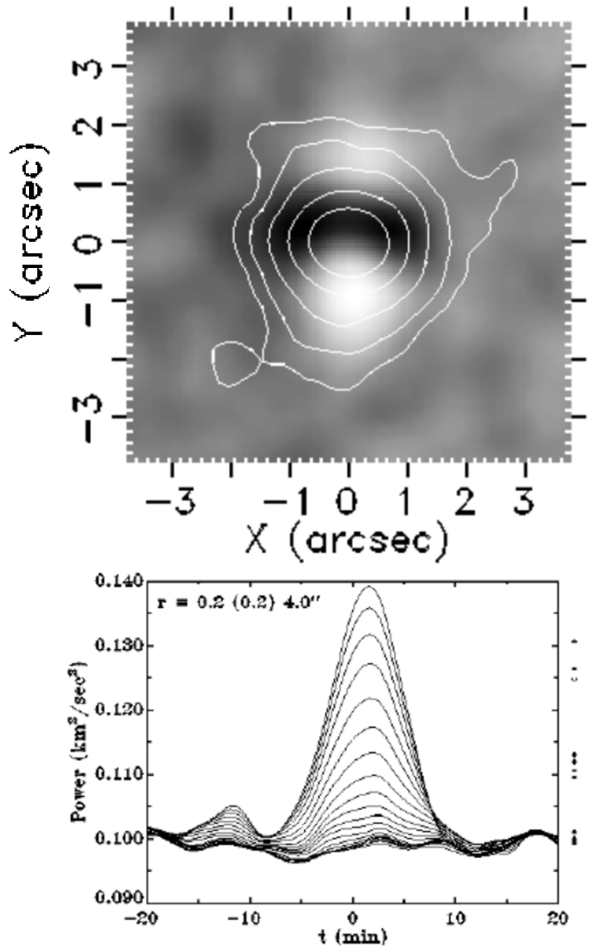

The average excess power (v^2) in the neighborhood of more than 2000 seismic events (Goode et al, 1998)

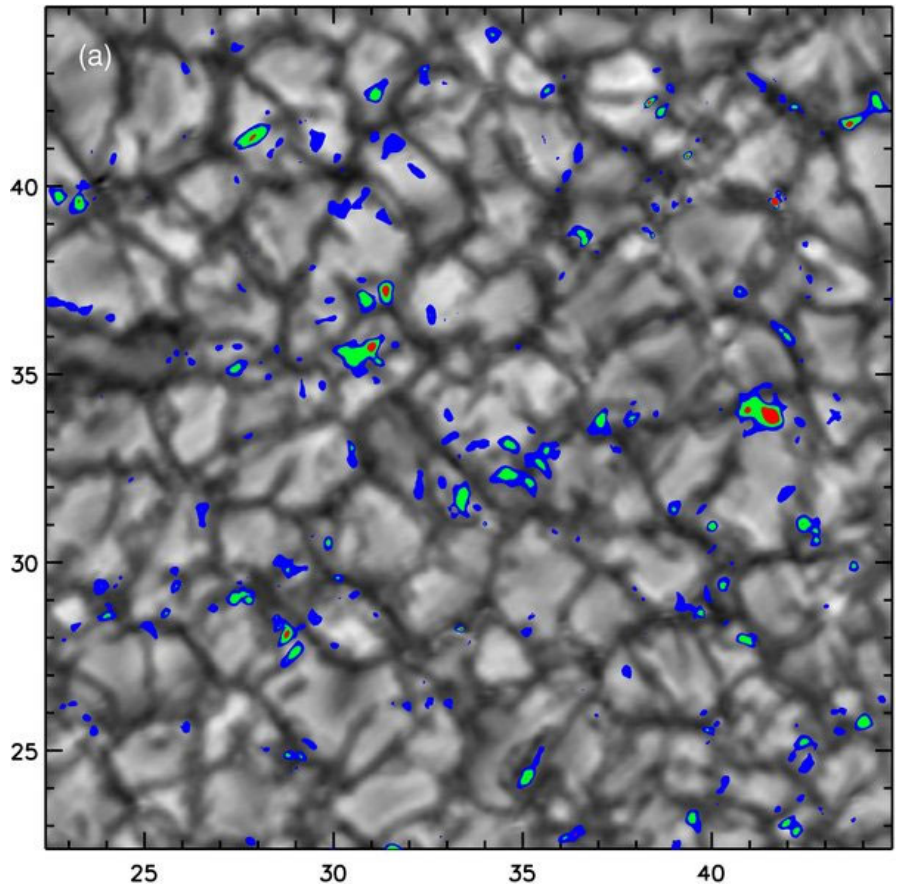

Intensity continuum of the averaged acoustic power. Blue, green and red colors correspond to 12, 20 and 32% of the maximum power (Bello González et al., 2010).

Observations of the vortical structures in photosphere (molecular G-band)

(Bonet et. al, 2008)

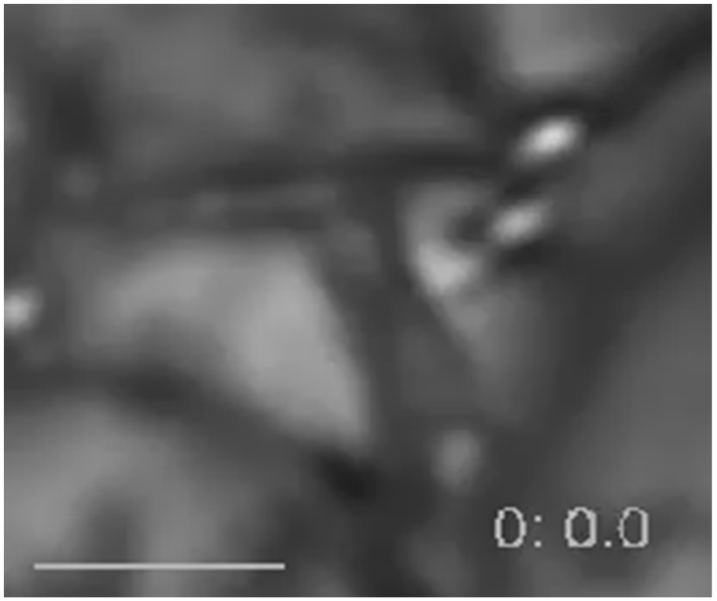

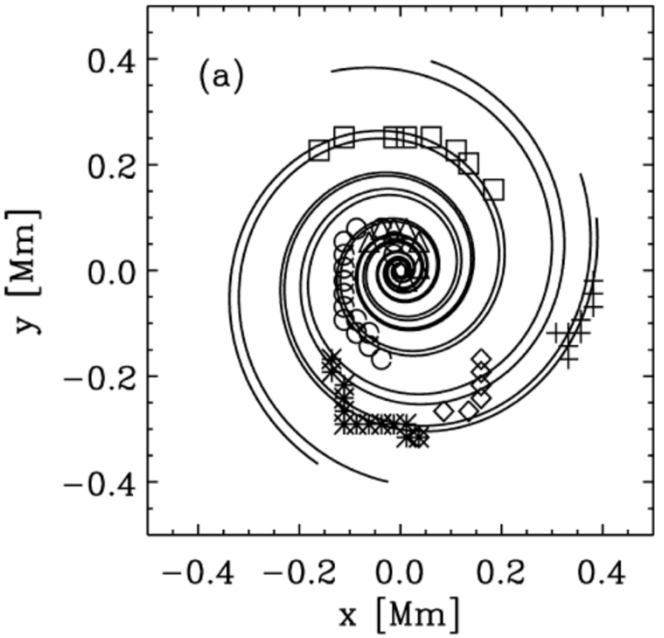

The vortex flows are created at the downdrafts where the plasma returns to the solar interior after cooling down. It was detected because some magnetic bright points follow logarithmic spiral in their way to be engulfed by a downdraft.
The G-band often shows bright points swirling around intergranular points where several dark lanes converge. These motions are reminiscent of the bathtub vortex flows predicted by numerical simulations of convection, and which are driven by the granulation downdrafts.

Vortex tubes in the solar convection

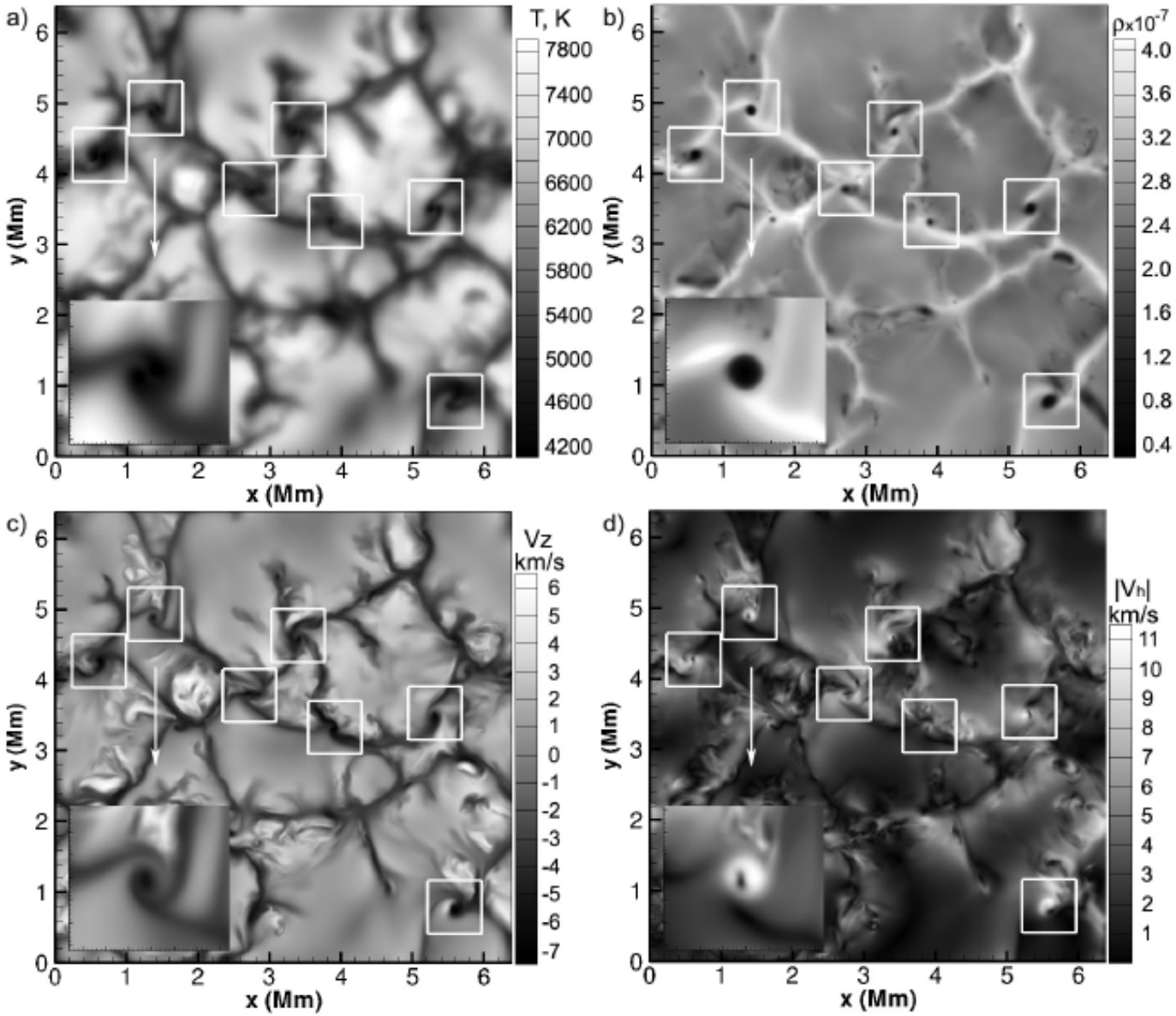

Vortex tubes dynamics: images of vertical vorticity, curl(V)

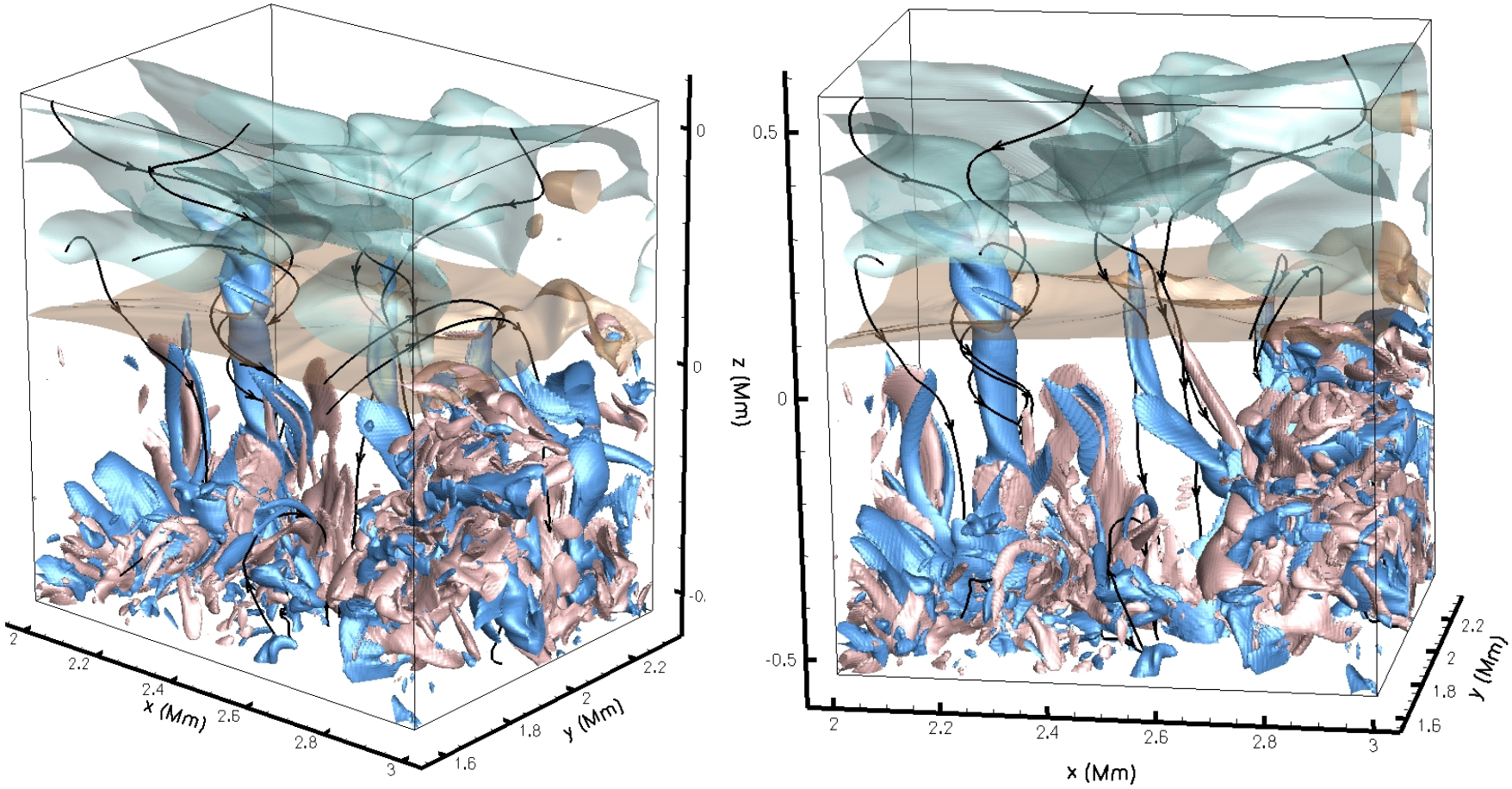

Excitation of individual acoustic waves

Density

Vertical velocity

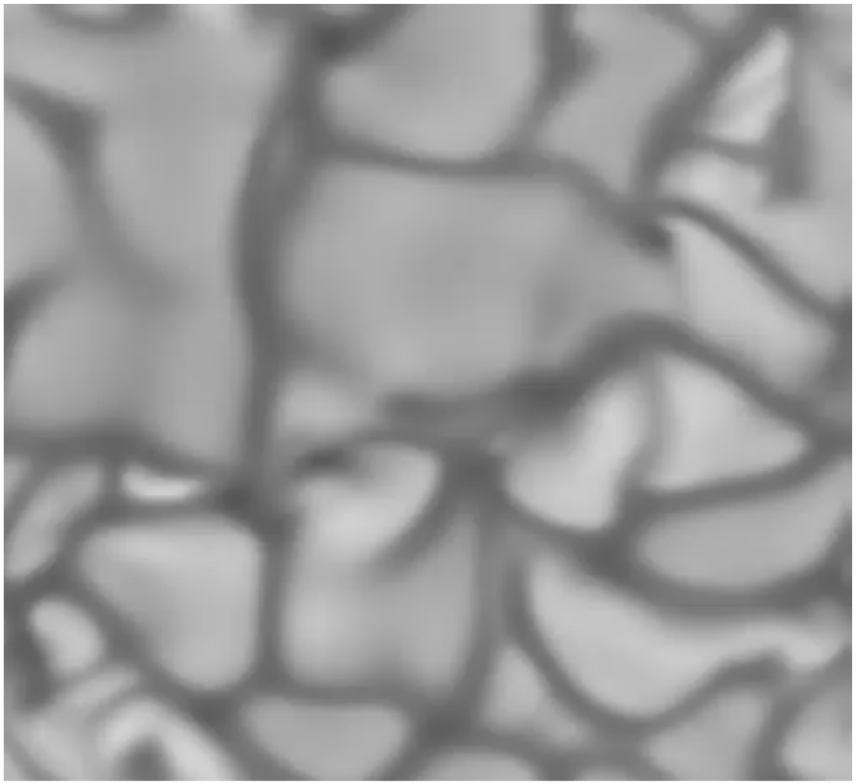

Excitation of individual acoustic waves when two vortex tubes with opposite vorticity collide and partially annihilate.

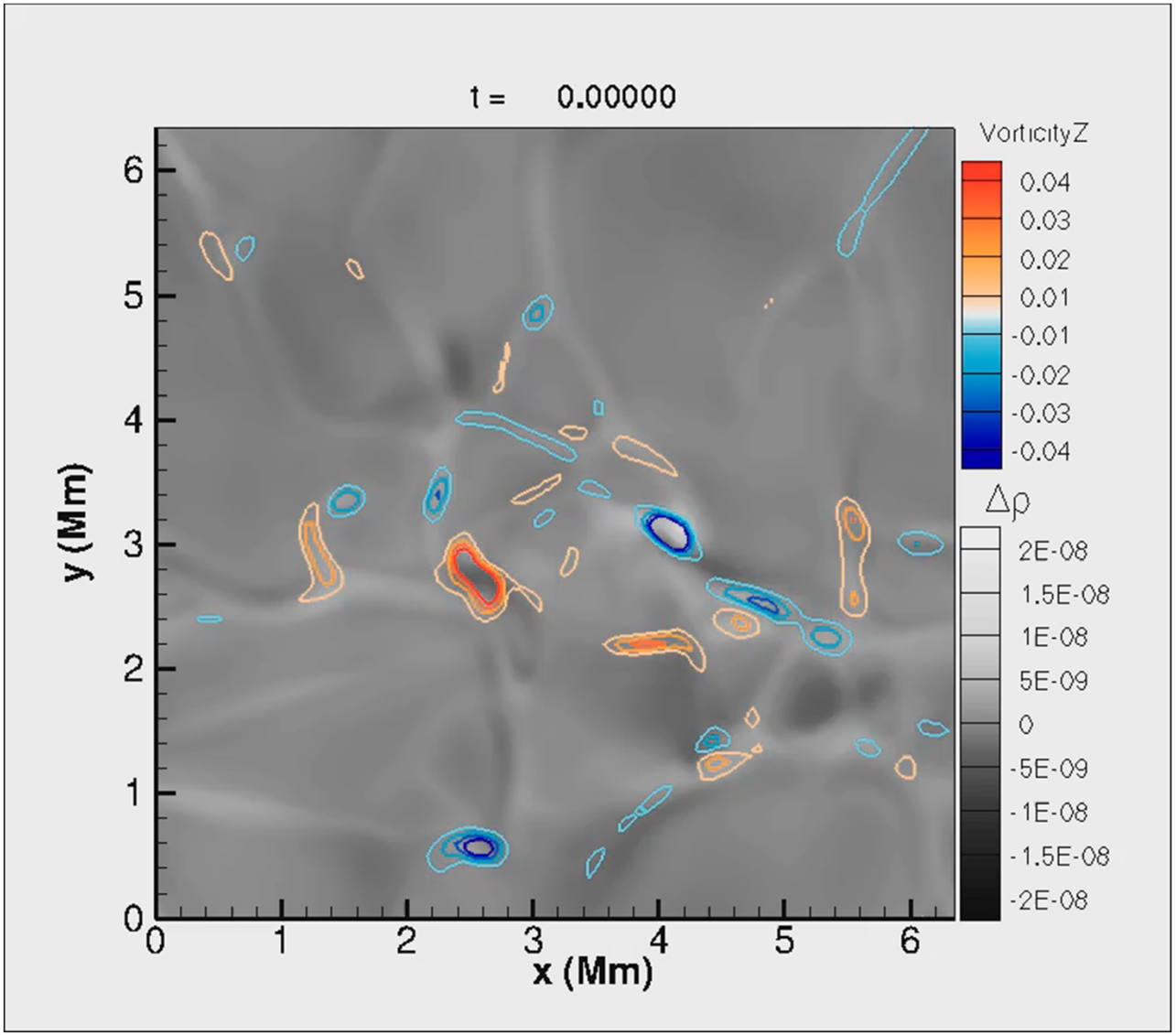

Excitation of individual acoustic waves due the vortex annihilation

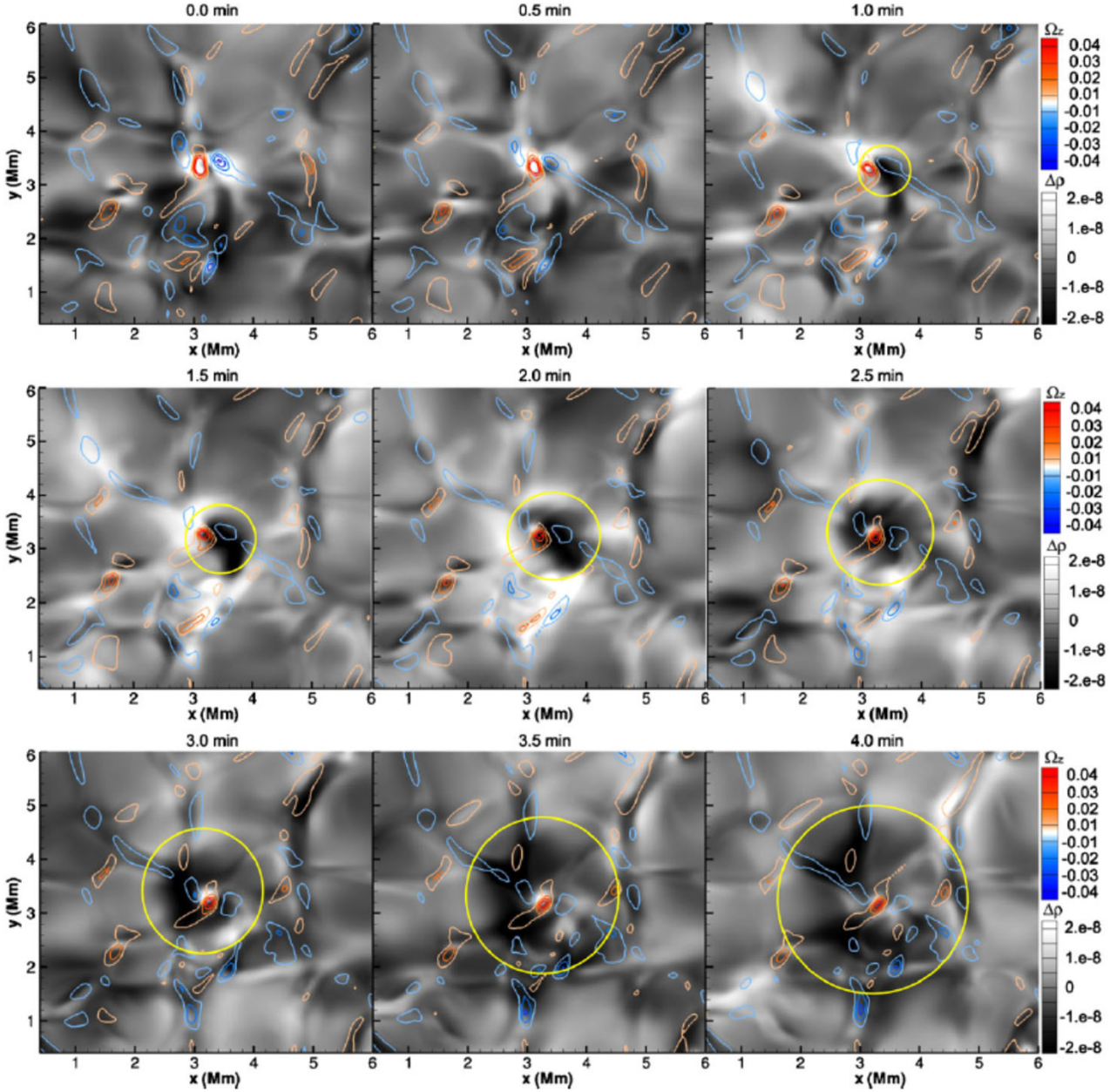

Examples of waves propagation

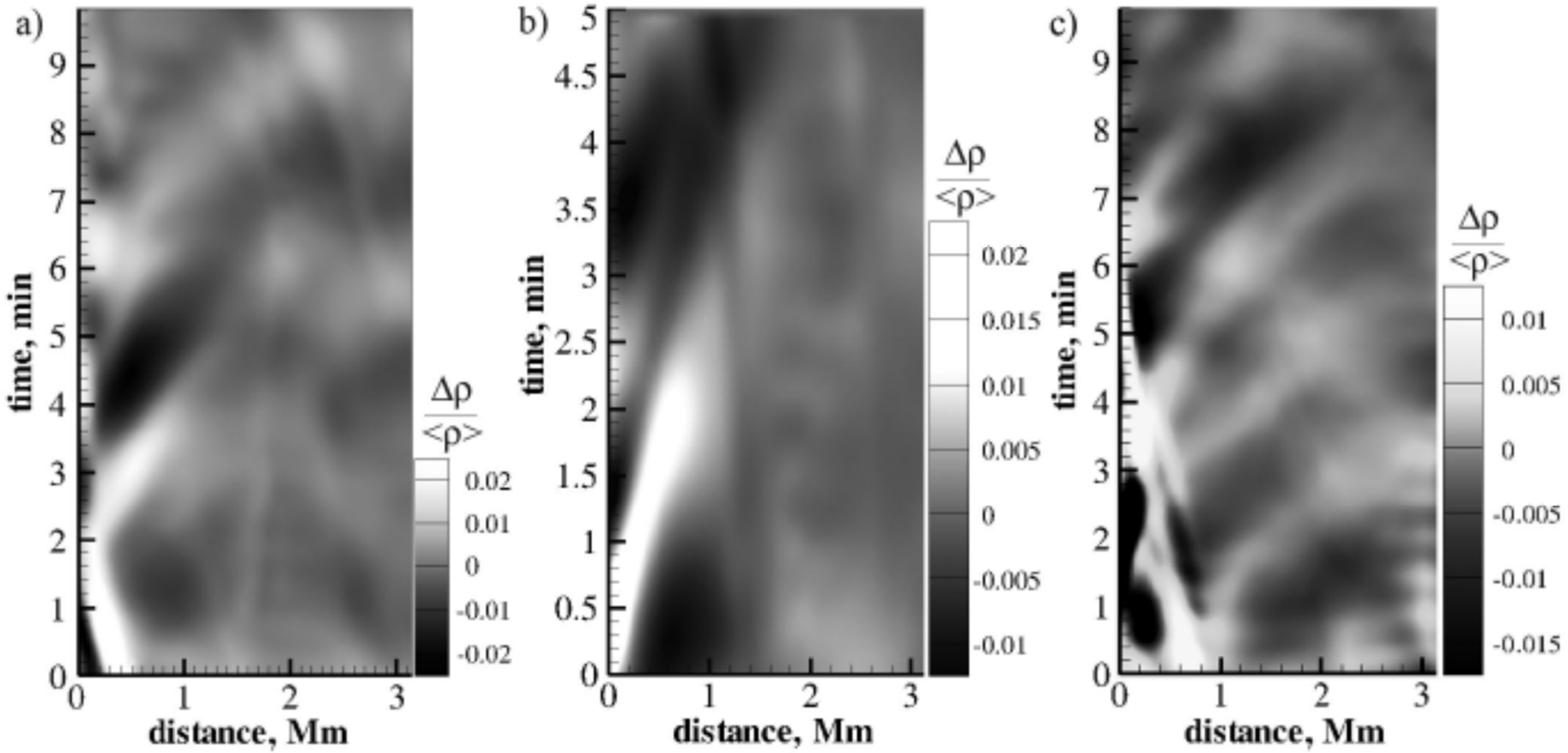

Time-distance diagrams of the normalized density fluctuations show inclined ridges, corresponding to acoustic waves. The slope of the ridges corresponds to a mean speed of 7 – 14 km/s.

Process of annihilation of vortex tubes

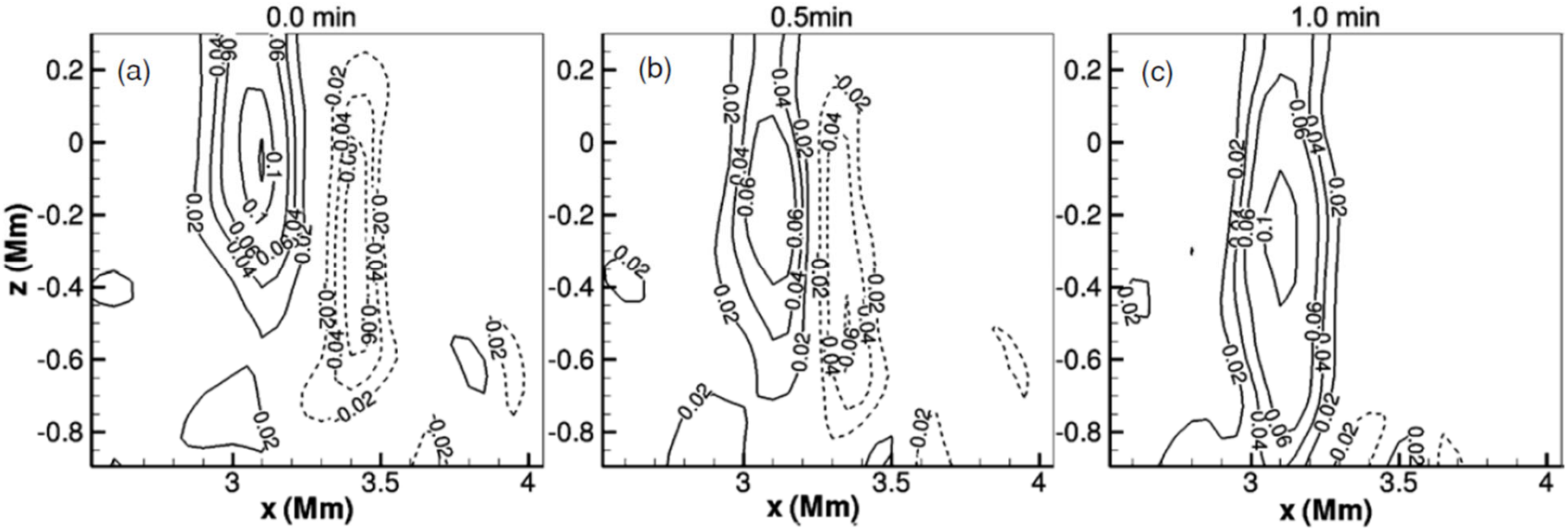

Subsurface interaction of the vortices shown in at different stages: initial structure of the vortices, closing-up stage, and after partial annihilation. Solid and dashed isolines show the magnitude of the positive and negative vertical vorticity (s^{-1}).

Wave propagation in subsurface layers

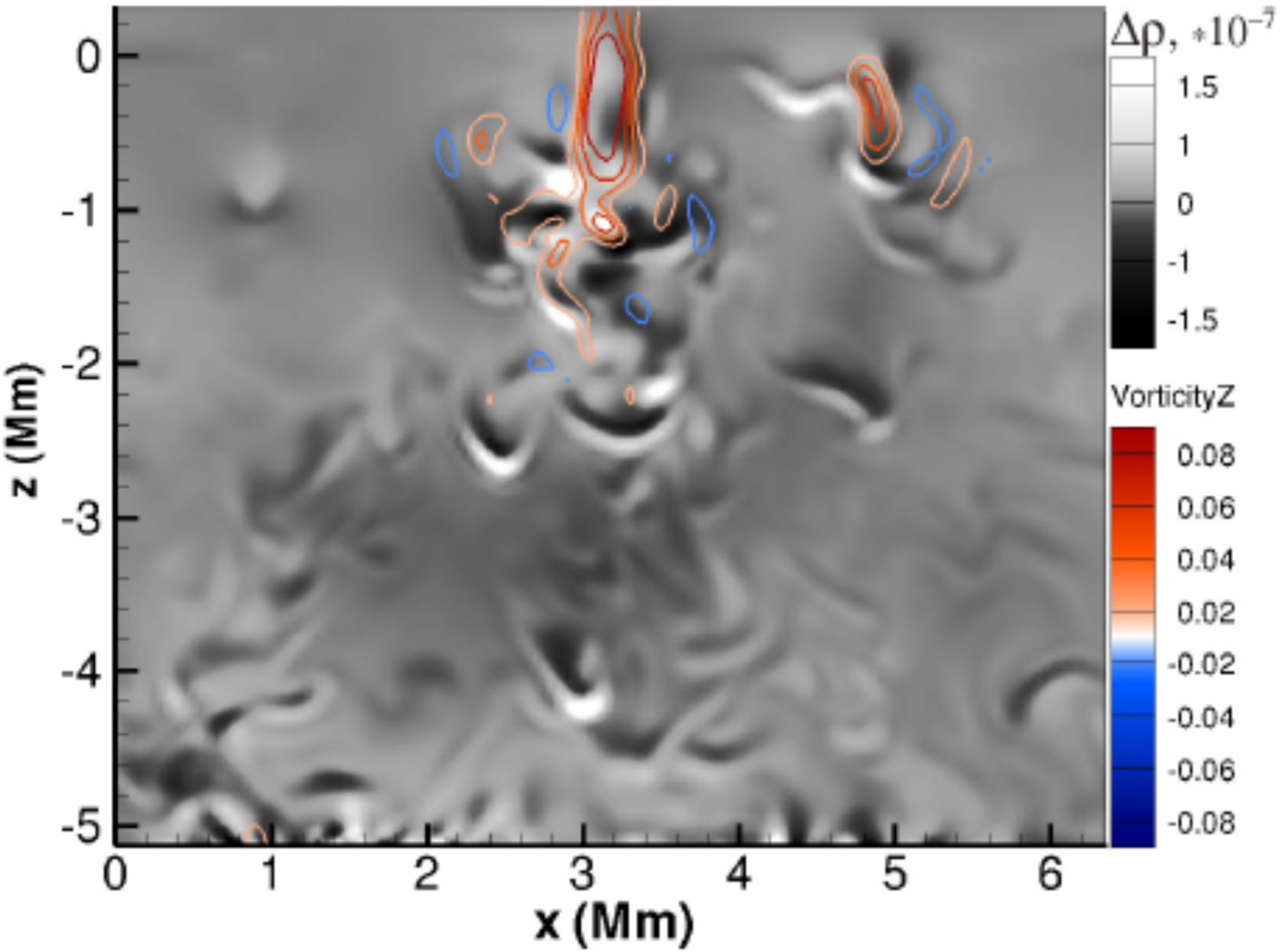

Numerical simulation reveal the subsurface structure of the oscillation modes

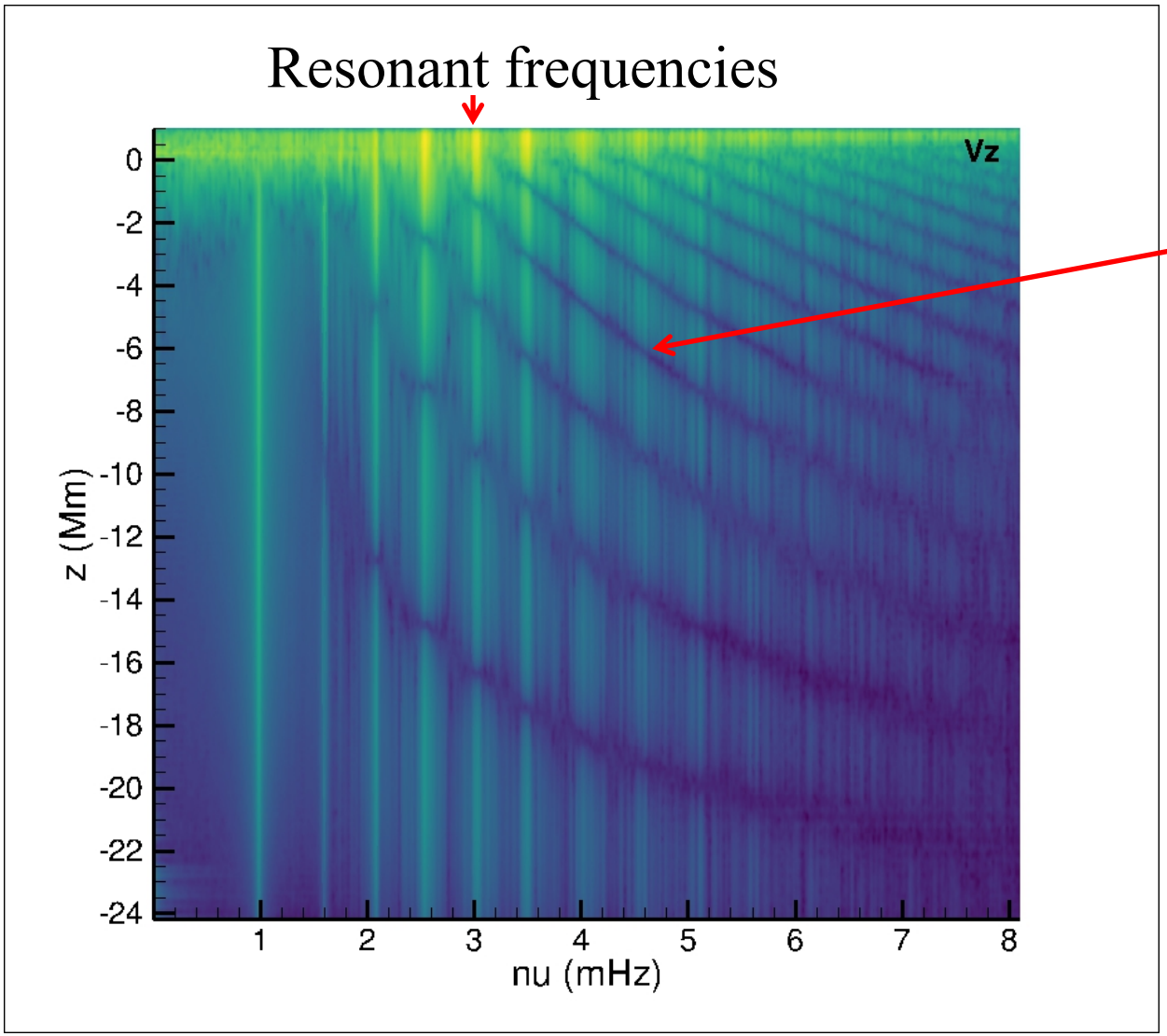

QUIZ #1 - Canvas

Lecture 6

Sunquakes

Propagation of acoustic waves excited by impulsive localized source

The wave front on the surface accelerates because it is formed by acoustic waves propagating through the solar interior where the sound speed is higher.

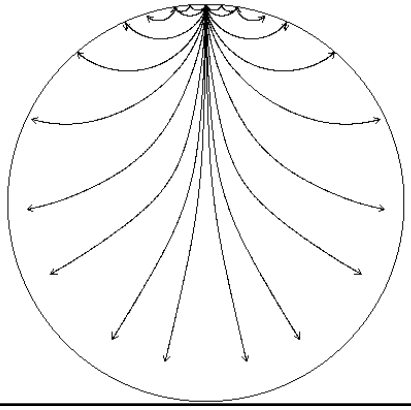

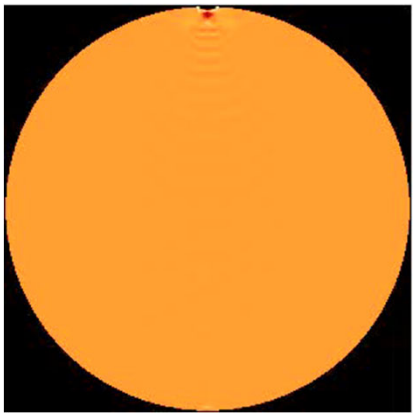

The ray paths are perpendicular to the wave fronts.

Seismic response to solar flares (sunquakes)

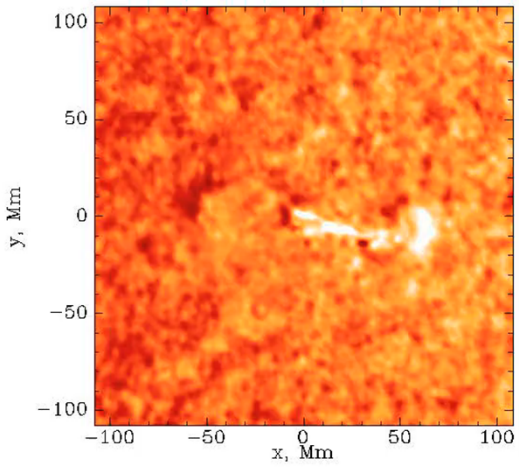

High-energy flare particles heat the solar chromosphere generating a shock propagating downward and hitting the surface.

Time-distance diagram of the flare seismic response calculated by averaging the wave front over 360 degrees

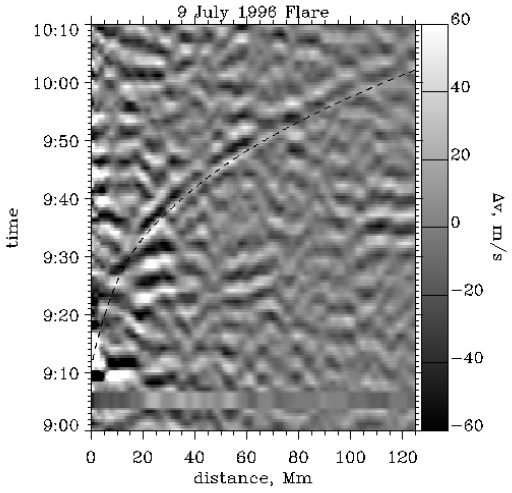

The propagation speed of the seismic wave:

$V=\delta(\text{distance})/\delta(\text{time})$

increases with time from 10 km/s to 100 km/s because the sound speed increases with depth.

Example of sunquake

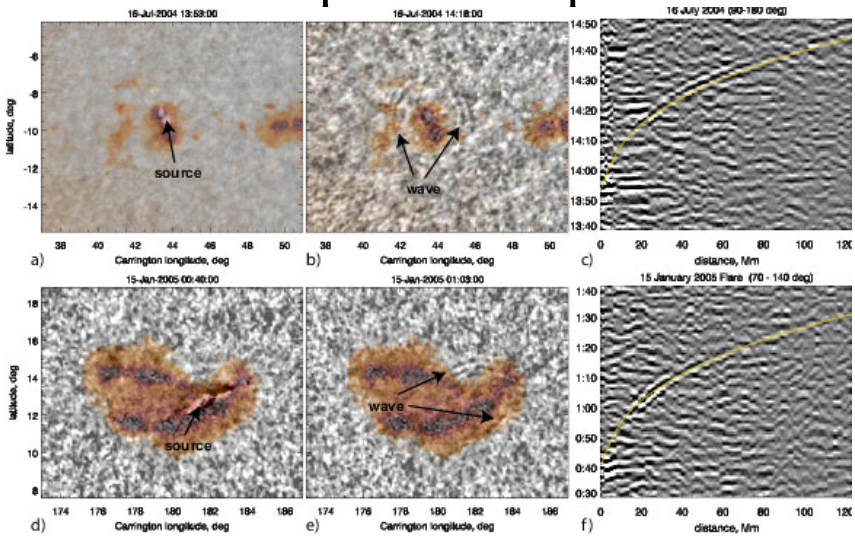

Energy transport in solar flares: thick-target model

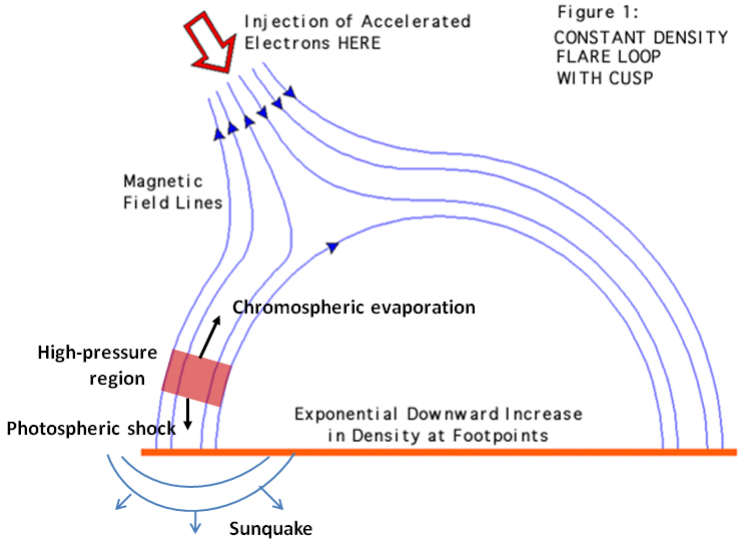

Standard model of solar flares (Sturrock, Shibata et)

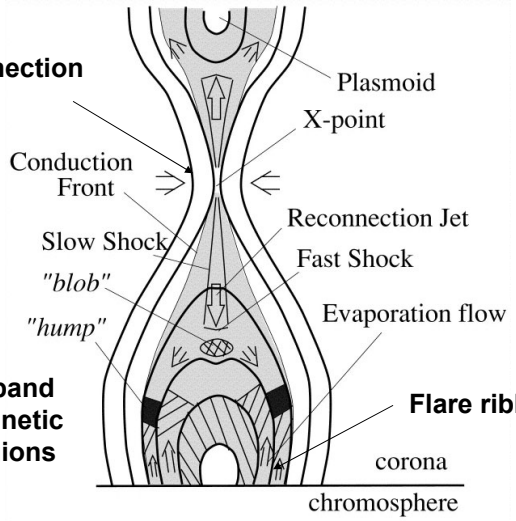

Sunquake of January 15, 2005, X1.2 flare

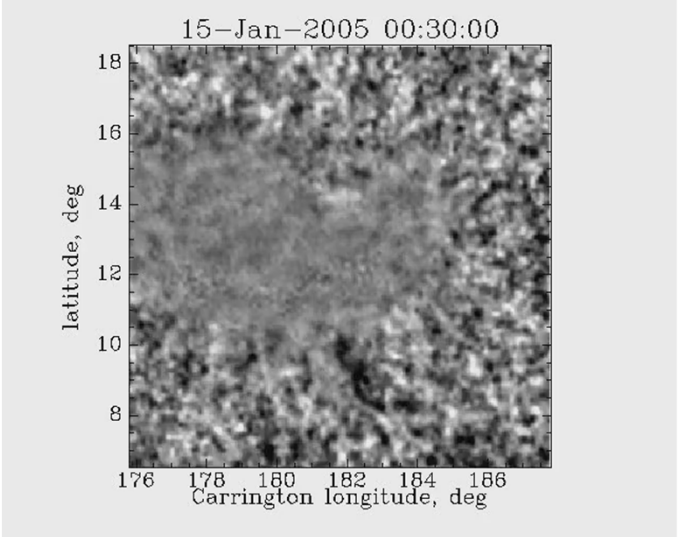

January 15, 2005, X1.2 flare: Magnetogram, soft and hard X-ray images

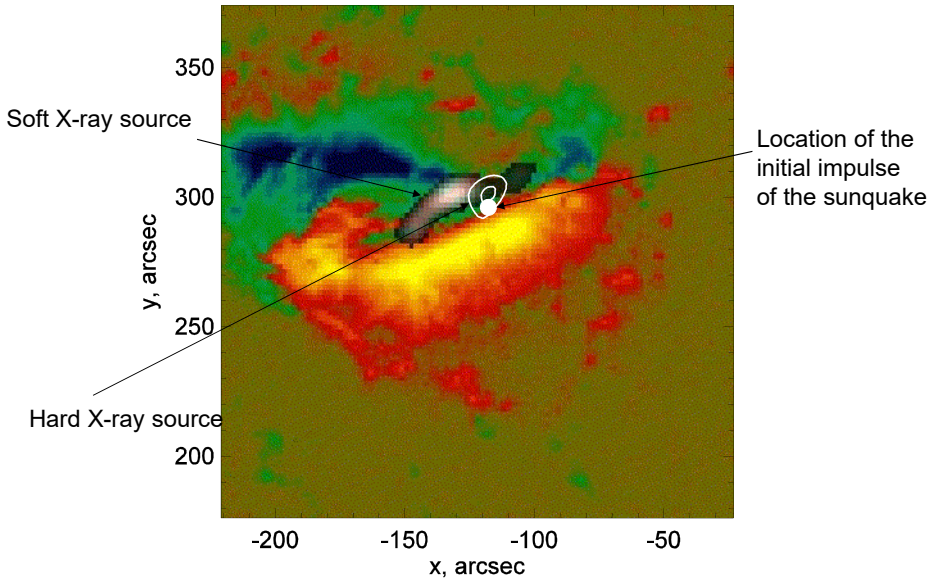

January 15, 2005, X1.2 flare: Dopplergram and hard X-ray image

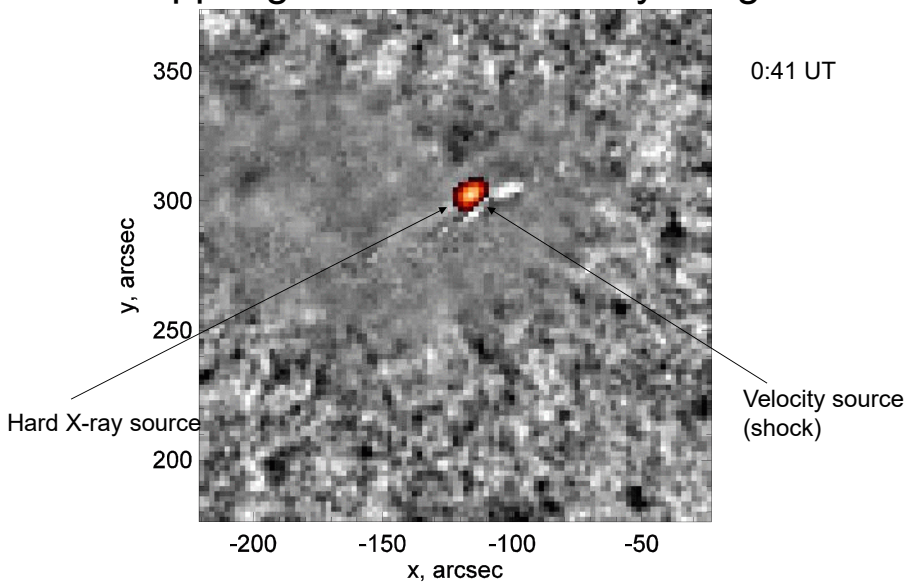

January 15, 2005, X1.2 flare: Doppler and hard X-ray sources

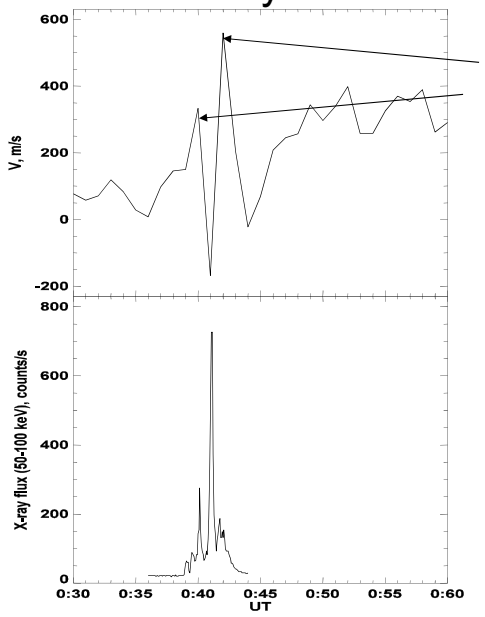

Two shocks generated by two beams of high-energy electrons

Sequence of flare events

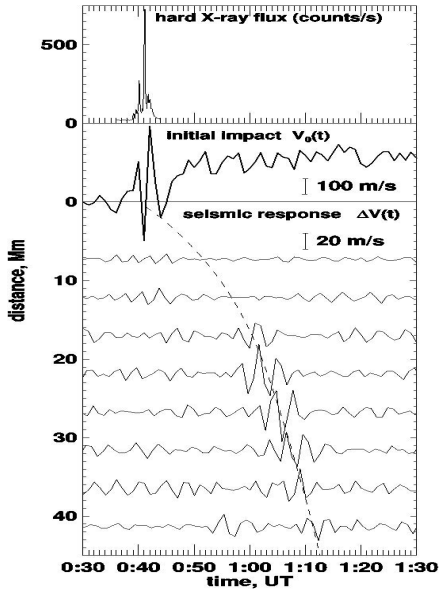

Anisotropy of sunquake waves

- The sunquake waves are anisotropic and propagate mostly in the direction of the expanding flare ribbons because they are excited of moving sources associated with series of pressure or momentum impulses caused by energetic particles.

X17 flare October 28, 2003

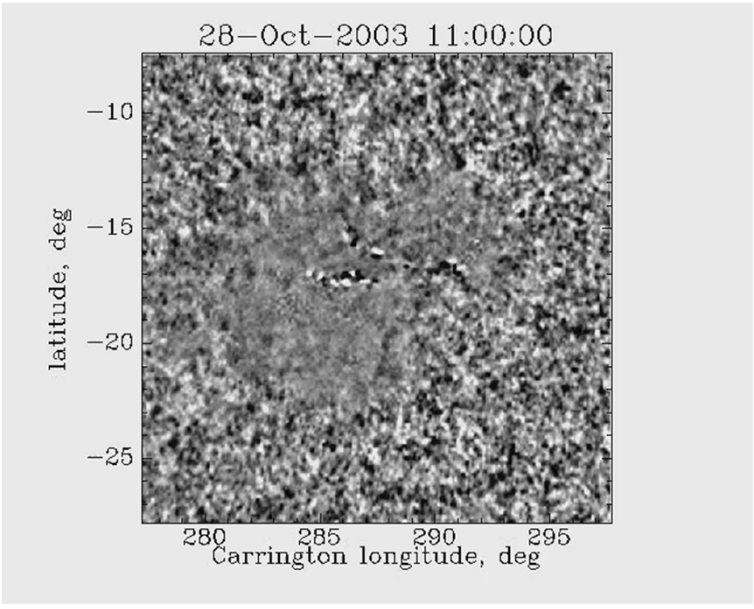

X17 flare October 28, 2003

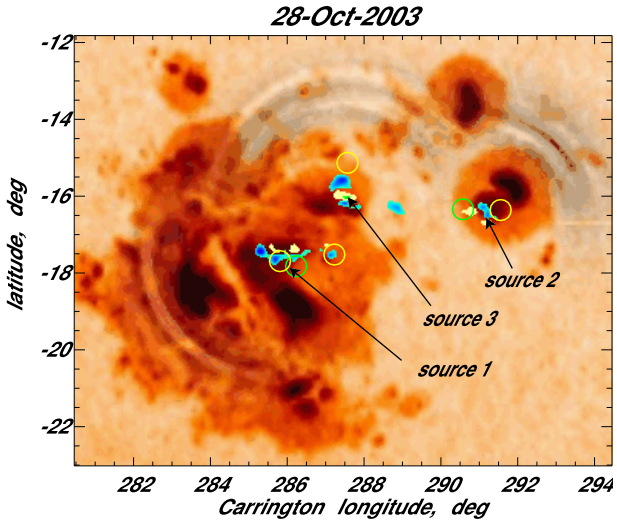

Model of sunquakes with moving source: wave interference effect

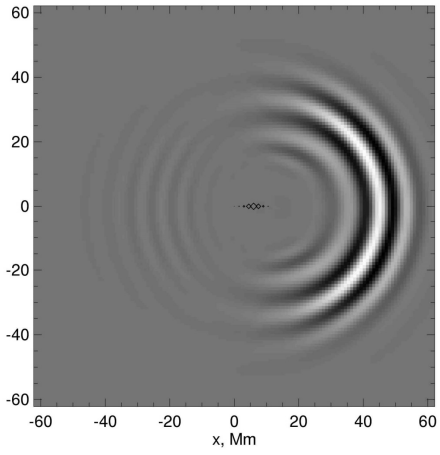

Great sunquakes of solar cycle 23

- July 23, 2002, X5.6
- October 28, 2003, X17 – three events
- October 29, 2003, X10
- July 16, 2004, X3.6
- January 15, 2005, X1.2 – last sunquake of Cycle 23

- No sunquake of comparable magnitude was observed between 1996 and 2002.

Sunspot counts and X-flares during the last three solar cycles.

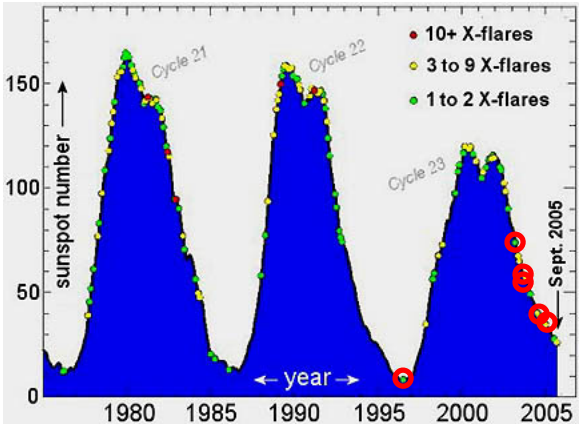

Graphic courtesy David Hathaway, NASA/NSSTC.

Primary questions

1. How frequent are sunquakes? What types of flares produce sunquakes?
2. Can the hydrodynamic flare models explain sunquakes?
3. What kind of flare perturbations can cause sunquakes?

References

Sharykin, I. N. & Kosovichev, A. G. (2020), 'Sunquakes of Solar Cycle 24', *Astrophys.J.* **895**(1), 76.

Stefan, J. T. & Kosovichev, A. G. (2020), 'Estimation of Key Sunquake Parameters through Hydrodynamic Modeling and Cross-correlation Analysis', *Astrophys.J.* **895**(1), 65.

Sadykov, V. M.; Kosovichev, A. G.; Kitiashvili, I. N. & Kerr, G. S. (2020), 'Response of SDO/HMI Observables to Heating of the Solar Atmosphere by Precipitating High-energy Electrons', *Astrophys.J.* **893**(1), 24.

19

1. Statistical analysis of sunquakes of Solar Cycle 24

Catalog of Sunquakes of Solar Cycle 24
is obtained from analysis of HMI Dopplergrams of all flares of the X-ray class greater than M1.0
The catalog is available at http://sun.njit.edu

Start time (UT)	GOES class	AR NOAA	Location (arcsec)	Movie method	Holography method	TD method	$\|H_+\|^2$, 10^{26} ergs	S_{max}, 10^{17} cm^2	df/dt(1-8A), 10^{-7} Watt m^{-2} s^{-1}
13.02.2011 17:28	M6.6	11158	211	-	?	-	3.0	4.4	5.8
14.02.2011 17:20	M2.2	11158	278	-	?	-	3.4	2.9	3.8
15.02.2011 01:44	X2.2	11158	319	+	+	+	10.6	9.6	10.5
18.02.2011 09:55	M6.6	11158	809	+	+	+	12.4	9.0	12.2

- 94 flares among 507 flares of the X-ray class greater than M1.0 were seismically active.
- There are many solar flares of moderate class with strong sunquakes, while in some powerful X-class flares, helioseismic waves were not observed or were weak.
- During Solar Cycle 24, there were several active regions characterized by the most efficient generation of sunquakes.

20

Sunquakes of Solar Cycle 24

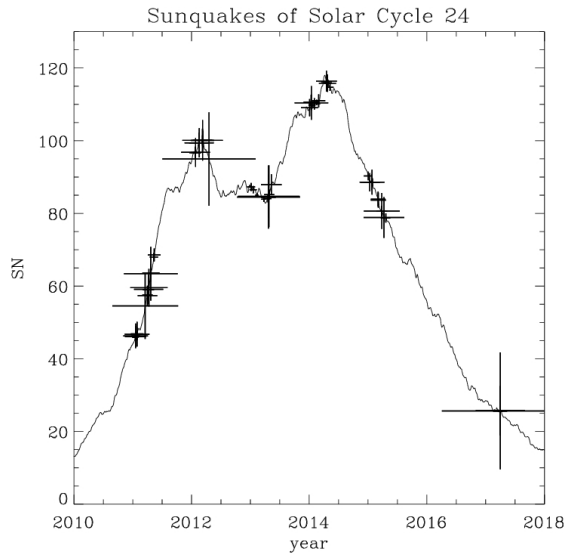

Sunquakes are associated with strong photospheric perturbations observed by HMI in Doppler velocity and magnetic field data

One of the powerful sunquake of Cycle 24 was observed during X1.8 flare on 23 October 2012

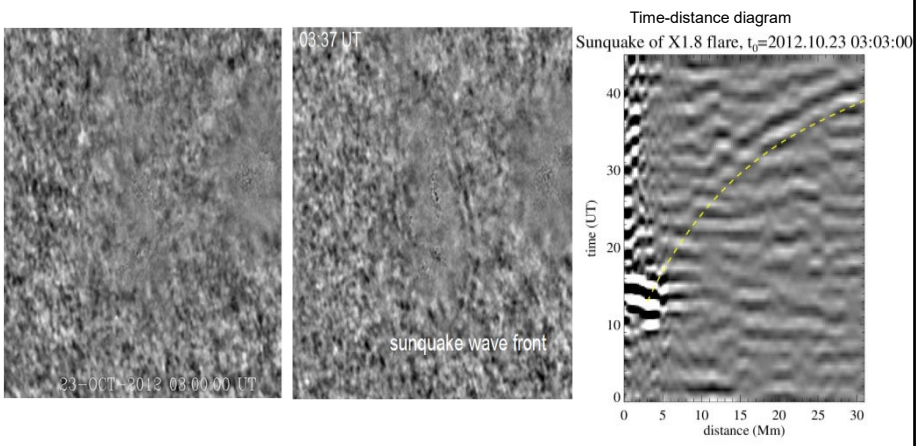

Most powerful sunquake of Cycle 24 was observed during X9.3 flare on 6 September 2017

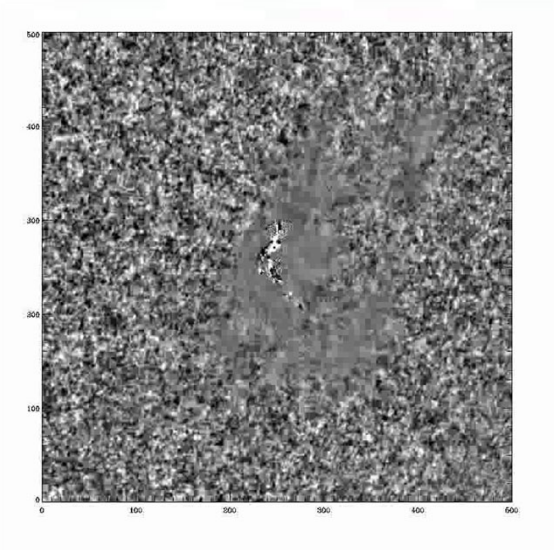

Sunquake energy correlates with impulsiveness of the energy release

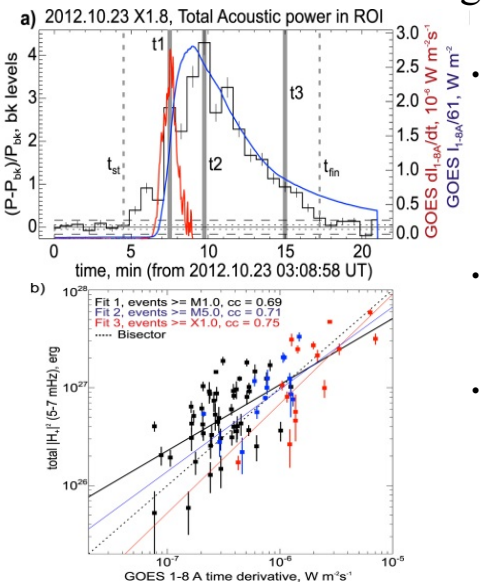

- The sunquake total energy correlates with the maximum value of the soft X-ray time derivative better than with the X-ray class (contrary to what one could expect from the "big-flare syndrome" idea). The impulsiveness of the energy release plays an important role.
- The flares producing sunquakes are more impulsive (shorter flare times and higher heating rate) compared to the flares without sunquakes.
- The most evident difference between distributions of the seismic and nonseismic flares appears in terms of the maximum values of the flare-energy release rate.

24

2. Can hydrodynamic (RADYN) flare models explain the photospheric perturbations and sunquakes?

- SDO/HMI camera obtains filtergrams in six wavelength positions across Fe 6173Å line in two polarizations (LCP&RCP) during approximately 45 s
- The flare hydrodynamic model (RADYN) models are used to synthesize Fe 6173Å line Stokes components using the radiative transfer RH1.5 code, and apply HMI LOS pipeline algorithm to model observables (line depth and continuum, Doppler shift, magnetic field)

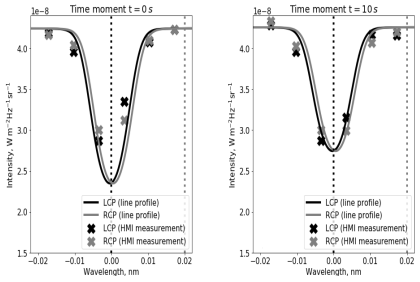

Illustration of the synthesized Fe 6173Å line profiles and corresponding synthesized HMI measurements for 0 s and 10 s snapshots of the RADYN model val3c_d4_1.0e12_t20s_20keV augmented with 100 G background magnetic field

25

The photospheric perturbations in the RADYN models are too weak to explain the variations observed by HMI

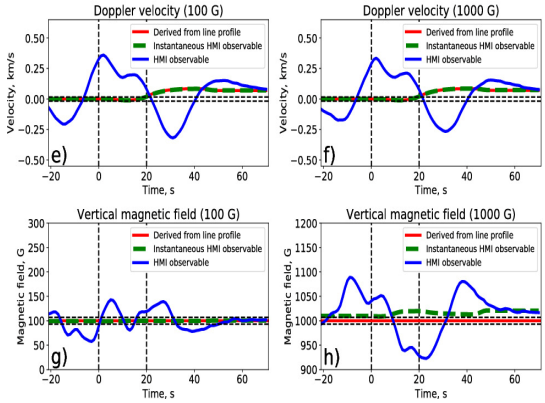

Simulated SDO/HMI observables for RADYN model: F=10^{12} erg/cm^2/s, E_{cutoff}=25 keV, t=20s, delta=3. for the vertical uniform 100 G and 1000 G.

The 1D radiative hydrodynamic flare models augmented with the uniform vertical magnetic field setup do not explain the strong magnetic field transients, sharp changes of the LOS velocities, and continuum enhancements observed during solar flares by the HMI instrument.

26

3. What kind of flare perturbations can cause sunquakes?

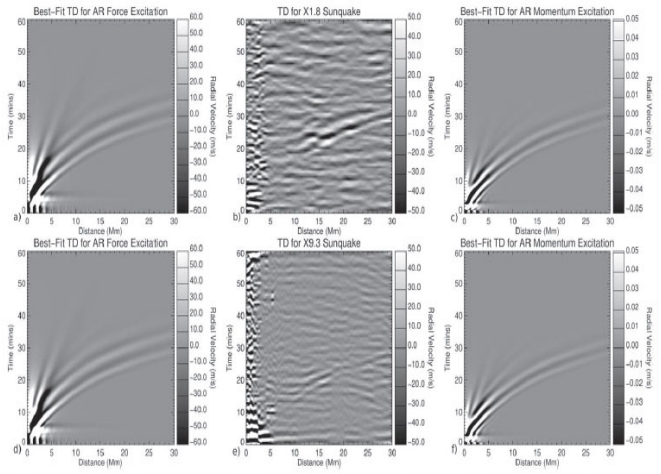

Figure 5. Time–distance diagrams of: (a) the best-fit force case for the sunquake of the X1.8 flare; (b) the sunquake produced by the X1.8 flare; (c) the best-fit momentum case for the sunquake of the X1.8 flare; (d) the best-fit force case for the sunquake of the X9.3 flare; (e) the sunquake produced by the X9.3 flare; (f) the best-fit momentum case of the X9.3 flare. Darker pixels correspond to more negative velocities, lighter pixels correspond to more positive velocities.

- We developed 3D models of the helioseismic and atmospheric response to localized impulsive perturbations in the solar atmosphere.
- We explored two possible excitation mechanisms of sunquakes in the context of the electron beam hypothesis: an instantaneous transfer of momentum and a gradual applied force due to flare eruption.
- We modeled the sunquake excitation and compare with observed sunquake events using a cross-correlation analysis.

27

Best fit model parameters show that both the force maximum and the momentum impact are within 2 min of the observed photospheric perturbations. The sunquake sources are located in the low photosphere, but the uncertainty in the source location is rather large.

John Stefan, Estimation of Key Sunquake Parameters through Hydrodynamic Modeling and Cross-correlation Analysis, 2020, ApJ, 895,65

Momentum Case				
Flare	T_{shift} (s)	Height (km)	Amp. (g cm s^{-1})	Energy (ergs)
X1.8	-45	-104	3.31*e*23	1.39*e*30
X9.3	+112.5	-33	1.54*e*23	3.74*e*29
X3.3	+67.5	+386	2.83*e*22	6.57*e*28
X1.0	+78.75	-86	9.48*e*23	1.21*e*31
M1.1	+135	-203	7.34*e*23	5.19*e*30

Force Case				
Flare	T_{shift} (s)	Height (km)	Amp. (dyn cm^{-3})	Energy (ergs)
X1.8	-157.5	-203	1.01*e*−1	5.58*e*28
X9.3	-33.75	-203	2.29*e*−1	1.27*e*29
X3.3	+157.5	+255	1.30*e*−2	1.32*e*28
X1.0	-157.5	+155	5.34*e*−2	4.73*e*28
M1.1	-78.5	-203	2.59*e*−1	1.44*e*29

Positive T_{shift} means a delay of the maximum forcing in the model relative to the initial photospheric perturbation, observed by HMI.

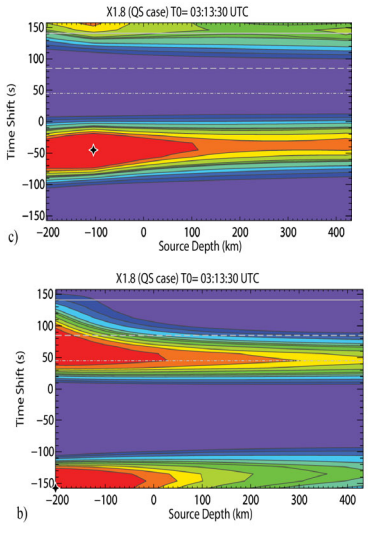

Lecture 7

Solar Oscillation Theory

(Stix, Chapter 5.1.2-5.1.4; Kosovichev, p.11-17;
Christensen-Dalsgaard, p. 5-24)

Projects

- Power spectrum: Ivan Oparin
- Global modes from GOLF: Sheldon Fereira
- Oscillation model, line asymmetry: Bryce Cannon
- Power maps, acoustic halo: Bhairavi Apte
- Ray paths, travel times: Sadaf Iqbal Ansari
- Propagation diagram for solar and stellar models: Ying Wang
- Analysis of sunquakes: Youra Shin
- Asteroseismic analysis: John Stefan
- Asymptotic sound-speed inversion: Yunpeng Gao

- October 11: Tutorial on Python and Jupyter notebook in class – Dr. Andrey Stejko

Solar oscillation theory

1. Oscillations are small-amplitude perturbations to the Sun's hydrodynamic structure
2. The oscillations are described by the 3D linearized hydrodynamics equations and mathematically represent an eigenvalue problem for a system of linear PDEs in the spherical coordinates.
3. The eigenvalues correspond to resonant oscillations frequencies and the eigenfunctions describe the structure of the resonant modes (standing waves).
4. The background model (the distribution of density, pressure, temperature with the radius) is obtained from the stellar evolution theory applied to the Sun.
5. We assume that the structure of the Sun is spherically symmetrical. This will allow us to apply a method of separation of variables, and separate the angular and radial components of the eigenfunctions.
6. We find that the angular component is described by the spherical harmonics.
7. The radial structure of the eigenfunctions is described by a system of ODEs.
8. Thus, the oscillation theory is reduced to solving an eigenvalue problem for a system of ODEs. This is similar to finding the energy spectrum in quantum mechanics.
9. We perform quantitative and qualitative analysis of the oscillation equations and, similarly to quantum mechanics, we apply the asymptotic JWKB theory to obtain analytical eigenvalues.

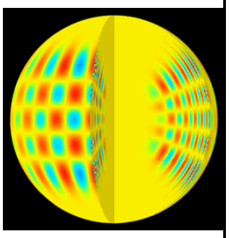

Equations of Stellar Structure

1. Hydrostatic Equations

Basic assumptions:

1. hydrostatic equilibrium: gravity force = pressure gradient;
2. thermal balance: energy generation rate = luminosity.

Consider a thin spherical shell of radius r, thickness dr, mass dm, and density ρ. The mass equation is:

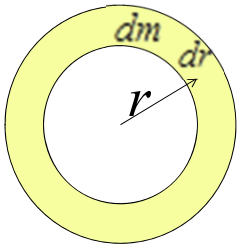

$$dm = 4\pi\rho r^2 dr$$

$$\frac{dm}{dr} = 4\pi\rho r^2.$$

The balance between the pressure and gravity forces is:

$$4\pi r^2 dP = -\frac{Gmdm}{r^2} = -Gm\frac{4\pi\rho r^2 dr}{r^2},$$

or

$$\frac{dP}{dr} = -\frac{Gm\rho}{r^2}.$$

Energy transfer and balance equations

The total energy flux, $L = 4\pi r^2 F$, integrated over a sphere of radius r:

$$L = -\frac{16\pi acT^3}{3\kappa\rho}\frac{dT}{dr}.$$

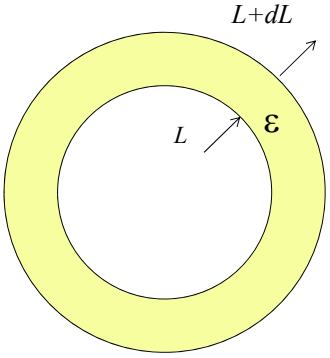

If ε is the energy release per unit mass then the energy flux change in a shell *dr* is:

$$dL = \varepsilon\rho 4\pi r^2 dr$$

$$\frac{dL}{dr} = 4\pi\rho r^2\varepsilon$$

This is the equation for conservation of energy (energy balance).

Equations of the stellar structure

$$\frac{dm}{dr} = 4\pi\rho r^2 \quad (1)$$

$$\frac{dP}{dr} = -\frac{Gm\rho}{r^2} \quad (2)$$

$$\frac{dL}{dr} = 4\pi\rho r^2\varepsilon \quad (3)$$

$$\frac{dT}{dr} = -\frac{\kappa\rho}{16\pi r^2 acT^3}L \equiv -F \quad (4)$$

$$P = \frac{\Re\rho T}{\mu} \quad (5)$$

$$\mu = \frac{1}{2X + \frac{3}{4}Y + \frac{1}{2}Z} \quad (6)$$

$$\varepsilon = \varepsilon_0 X^2\rho T^4 \quad (7)$$

$$\kappa = \kappa_0(X+1)Z\rho T^{-3.5} \quad (8)$$

Kramer's opacity law

These equations describe the structure of stellar radiative zones. In the convection zone Eq.(4) is replaced by an equation of convective energy transport, e.g. mixing length theory.

A numerical code for solving these equations is available in the book: C.J. Hansen, S.D. Kawaler, *Stellar Interiors. Physical Principles, Structure and Evolution,* Springer, 1995.

Abundances of the elements in the pp-chain are determined from the balance equation, e.g. for hydrogen abundance, $X \equiv X_1$:

$$\rho \frac{dX}{dt} = \rho^2(-3\lambda_{11}X^2 + 2\lambda_{33}X_3^2 - \lambda_{34}X_3X_4),$$

where X_3 is the abundance (mass fraction) of ^{3}He, $X_4 \equiv Y$ is the ^{4}He abundance

pp	$\rightarrow$	$^2H + e^+ + \nu_e$	
$^2H + p$	$\rightarrow$	$^3He + \gamma$	
$^3He + {}^3He$	$\rightarrow$	$^4He + 2p$	85%
$^3He + {}^4He$	$\rightarrow$	$^7Be + \gamma$	15%
$e^- + {}^7Be$	$\rightarrow$	$^7Li + \nu_e$	
$^7Li + p$	$\rightarrow$	$2\,^4He$	
$p + {}^7Be$	$\rightarrow$	$^8B + \gamma$	0.02%
^8B	$\rightarrow$	$^8Be^* + e^+ + \nu_e$	
$^8Be^*$	$\rightarrow$	$2\,^4He$	

Estimates from the balance equations

Balancing the main terms in the nuclear reaction equations we obtain relations among various elements.

ppI:

$$\rho^2 X_1^2 T^4 \propto \rho^2 X_3^2 T^{16}$$

$$X_3 \propto X_1 T^{-6}$$

Standard solar model

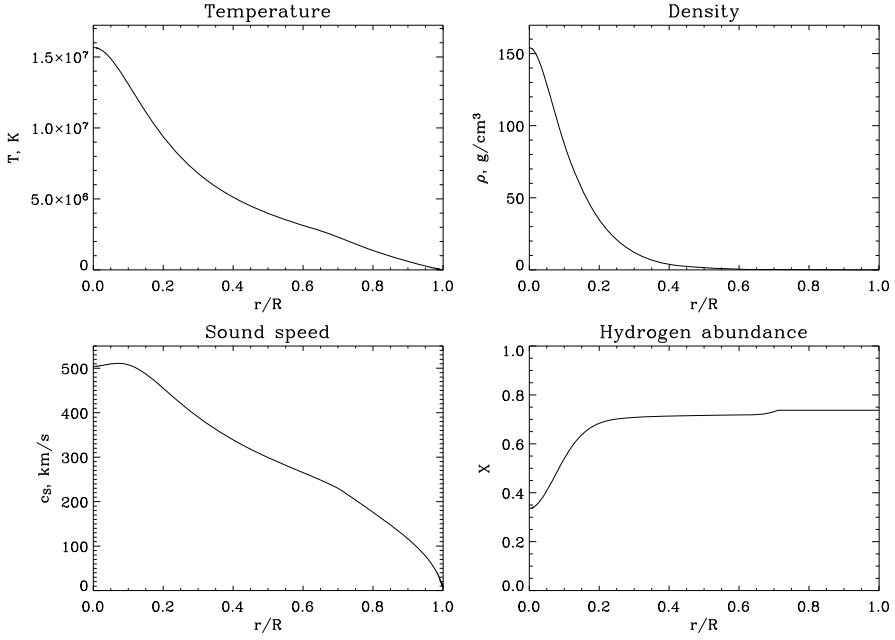

Standard solar model

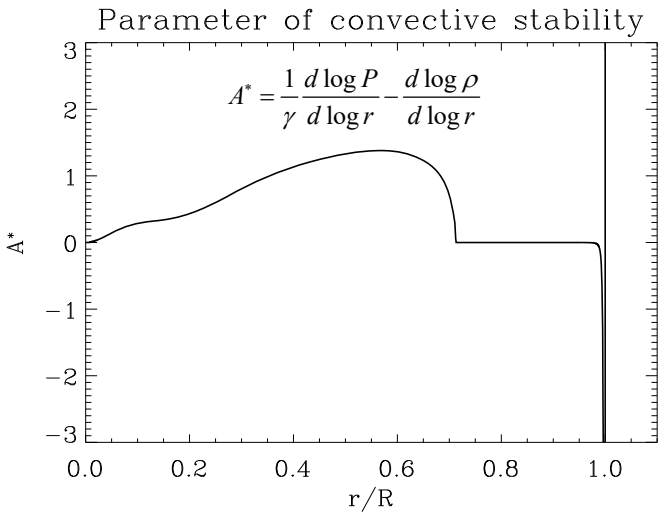

Entropy density of ideal gas

$S = c_V \log(P/\rho^\gamma)$

$$N^2 = \frac{g}{r}\left(\frac{1}{\gamma}\frac{d\log P}{d\log r} - \frac{d\log \rho}{d\log r}\right) \equiv \frac{g}{r}A^*$$

Brunt–Väisälä frequency or buoyancy frequency

Basic Equations

Basic assumptions:

1. linearity: $\vec{v}/c_s << 1$
2. adiabaticity: $dS/dt = 0$
3. spherical symmetry of the background
4. magnetic forces and Reynolds stresses are negligible

The basic equations are conservations of mass, momentum, energy and Newton's gravity law.

1. Conservation of mass (continuity equation):

The rate of mass change in a fluid element of volume V is equal to the mass flux through the surface of this element (of area A):

$$\frac{\partial}{\partial t}\int_V \rho dV = -\int_A \rho\vec{v}d\vec{a} = -\int_V \nabla(\rho\vec{v})dV.$$

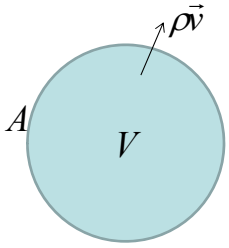

divergence

Then,

$$\frac{\partial\rho}{\partial t} + \nabla(\rho\vec{v}) = 0,$$

or

$$\frac{d\rho}{dt} + \rho\nabla\vec{v} = 0.$$

where $\frac{d\rho}{dt} = \frac{\partial\rho}{\partial t} + (\vec{v}\cdot\nabla)\rho$ is the 'material' derivative

2. Momentum equation (conservation of momentum of a fluid element): $\rho \frac{d\vec{v}}{dt} = -\nabla P + \rho \vec{g},$

where P is pressure, $\vec{g}$ is the gravity acceleration, which can be expressed in terms of gravitational potential Φ: $\vec{g} = \nabla \Phi$.

Also, $\frac{d\vec{v}}{dt} = \frac{\partial \vec{v}}{\partial t} + (\vec{v} \cdot \nabla)\vec{v}$. This is the 'material' derivative.

e.g. $v_x \frac{\partial v_x}{\partial x} + v_y \frac{\partial v_x}{\partial y} + v_z \frac{\partial v_x}{\partial z}$ for v_x component

3. Adiabaticity equation (conservation of energy) for a fluid element:

$$\frac{d}{dt}\left(\frac{P}{\rho^\gamma}\right) = 0, \qquad \text{or} \qquad \frac{dP}{dt} = c^2 \frac{d\rho}{dt},$$

where $c^2 = \gamma P/\rho$ is the adiabatic sound speed.

4. Poisson equation: $\nabla^2 \Phi = 4\pi G \rho.$

Plan to solve the solar oscillation equations

1. Linearize - consider small-amplitude oscillations.
2. Neglect the perturbations of the gravitational potential (Cowling approximation).
3. Write the linearized equations in the spherical coordinates: *r, θ, ϕ.*
4. Consider harmonic (periodic) oscillations
5. Separate the radial and angular coordinates.
6. Show that the angular dependence can be represented by spherical harmonics.
7. Derive equations for the radial dependence, representing the eigenvalue problem for the normal modes
8. Solve the eigenvalue problem in the asymptotic (short wave-length) JWKB approximation.
9. Investigate properties of p- and g-modes

1. Linearization

Consider small perturbations of a stationary spherically symmetrical star in the hydrostatic equilibrium:

$$v_0 = 0,\ \rho = \rho_0(r),\ P = P_0(r).$$

If $\vec{\xi}(t)$ is a vector of displacement of a fluid element then velocity of this element:

$$\vec{v} = \frac{d\vec{\xi}}{dt} \approx \frac{\partial \vec{\xi}}{\partial t}.$$

Perturbations of scalar variables ρ, P, Φ are two types: **Eulerian, at a fixed position** $\vec{r}$:

$$\rho(\vec{r},t) = \rho_0(r) + \rho'(\vec{r},t),$$

and **Lagrangian perturbation in moving elements**:

$$\rho(\vec{r} + \vec{\xi}) = \rho_0(r) + \delta\rho(\vec{r},t).$$

The Eulerian and Lagrangian perturbations are related to each other:

$$\delta\rho = \rho' + (\vec{\xi} \cdot \nabla\rho_0) = \rho' + (\vec{\xi} \cdot \vec{e}_r)\frac{d\rho_0}{dr} = \rho' + \xi_r \frac{d\rho_0}{dr},$$

where $\vec{e}_r$ is a radial unit vector. In our case, the density gradient is radial.

Then, the linearized equations are:

$$\rho' + \nabla(\rho_0 \vec{\xi}) = 0,$$ the continuity (mass conservation) equation

$$\rho_0 \frac{\partial^2 \vec{\xi}}{\partial t^2} = -\nabla P' - g_0 \vec{e}_r \rho' + \rho_0 \nabla\Phi',$$ the momentum equation

$$P' + \xi_r \frac{dP_0}{dr} = c_0^2(\rho' + \xi_r \frac{d\rho_0}{dr}),$$ the adibaticity (energy) equation, or

$\delta P = c_0^2 \delta\rho$ for the Largangian perturbations of pressure and density.

$$\nabla^2\Phi' = 4\pi G\rho'.$$ the equation for the gravitational potential

2. Cowling approximation: $\Phi' = 0.$

3. Consider the linearized equations in the spherical coordinates r,θ,ϕ:

$$\vec{\xi} = \xi_r \vec{e}_r + \xi_\theta \vec{e}_\theta + \xi_\phi \vec{e}_\phi \equiv \xi_r \vec{e}_r + \vec{\xi}_h,$$

where $\vec{\xi}_h = \xi_\theta \vec{e}_\theta + \xi_\phi \vec{e}_\phi$ is the horizontal component of displacement.

$$\nabla \vec{\xi} \equiv \mathrm{div}\,\xi = \frac{1}{r^2}\frac{\partial}{\partial r}(r^2 \xi_r) + \frac{1}{r\sin\theta}\frac{\partial}{\partial \theta}(\sin\theta \xi_\theta) + \frac{1}{r\sin\theta}\frac{\partial \xi_\phi}{\partial \phi} =$$

$$= \frac{1}{r^2}\frac{\partial}{\partial r}(r^2 \xi_r) + \frac{1}{r}\nabla_h \vec{\xi}_h.$$

4. Consider periodic perturbations with frequency ω:

$$\vec{\xi} \propto e^{i\omega t} Y_l^m(\theta,\phi) = C P_l^m(\theta) e^{im\phi + i\omega t}$$

$\nu = \omega / 2\pi$, where ν is the cyclic frequency (measured in Hz), and ω is the angular frequency (measure in rad/s).

Then, in the Cowling approximation, we get (leaving out subscript 0 for unperturbed variables):

$$\rho' + \frac{1}{r^2}\frac{\partial}{\partial r}(r^2 \rho \xi_r) + \frac{\rho}{r}\nabla_h \vec{\xi}_h = 0, \quad \text{the continuity equation}$$

$$-\omega^2 \rho \xi_r = -\frac{\partial P'}{\partial r} + g\rho', \quad \text{the radial component of the momentum equation}$$

$$-\omega^2 \rho \vec{\xi}_h = -\frac{1}{r}\nabla_h P', \quad \text{the horizontal component of the momentum equation}$$

$$\rho' = \frac{1}{c^2}P' + \frac{\rho N^2}{g}\xi_r, \quad \text{the adiabatic equation}$$

where $N^2 = g\left(\frac{1}{\gamma P}\frac{dP}{dr} - \frac{1}{\rho}\frac{d\rho}{dr}\right)$ is the Brunt-Vaisala frequency.

Boundary conditions:

$\xi_r(r=0) = 0$, - displacement at the Sun's center is zero,
(or a regularity condition for $l = 1$).

$\delta P(r = R) = 0$, - Lagrangian pressure perturbation at the solar surface is zero.
(this is equivalent to absence of external forces).

Also, we assume that the solution is regular at the poles $\theta = 0, \pi$.

5. Consider the separation of radial and angular variables in the form:

$$\rho'(r,\theta,\phi) = \rho'(r)\cdot f(\theta,\phi),$$
$$P'(r,\theta,\phi) = P'(r)\cdot f(\theta,\phi),$$
$$\xi_r(r,\theta,\phi) = \xi_r(r)\cdot f(\theta,\phi),$$
$$\vec{\xi}_h(r,\theta,\phi) = \xi_h(r)\nabla_h f(\theta,\phi).$$

Then, the continuity equation is:

$$\left[\rho' + \frac{1}{r^2}\frac{\partial}{\partial r}(r^2\rho\xi_r)\right] f(\theta,\phi) + \frac{\rho}{r}\xi_h\nabla_h^2 f = 0.$$

The variables are separated if

$$\nabla_h^2 f = \alpha f,$$

where α is a constant.
This equation has non-zero solutions regular at the poles, $\theta = 0, \pi$ only when

$$\alpha = -l(l+1),$$

where l is an integer.

6. The non-zero solution of equation $\nabla_h^2 f + l(l+1)f = 0$ represents the spherical harmonics:

$$f(\theta,\phi) = Y_l^m(\theta,\phi) = CP_l^m(\theta)e^{im\phi},$$

where $P_l^m(\theta)$ is the Legendre function.

7. Derive equations for the radial dependence, representing the eigenvalue problem for the normal modes

After the separation of variables the continuity equation for the radial dependence $\rho'(r)$ is

$$\rho' + \frac{1}{r^2}\frac{\partial}{\partial r}\left(r^2\rho\xi_r\right) - \frac{l(l+1)}{r}\rho\xi_h = 0.$$

Compare with the original equation: $\rho' + \nabla(\rho_0\vec{\xi}) = 0,$

and with this equation in the spherical coordinates:

$$\rho' + \frac{1}{r^2}\frac{\partial}{\partial r}(r^2\rho\xi_r) + \frac{\rho}{r}\nabla_h\vec{\xi}_h = 0,$$

Transform this equation in terms of 2 variables: ξ_r and P'
- radial displacement and Eulerian pressure perturbation.

The horizontal component of displacement ξ_h can be determined from the horizontal component of the momentum equation:

$$-\omega^2 \rho \xi_h(r) = -\frac{1}{r} P'(r), \quad \text{or} \quad \xi_h = \frac{1}{\omega^2 \rho r} P'.$$

Substituting this into the continuity equation $\rho' + \frac{1}{r^2}\frac{\partial}{\partial r}\left(r^2 \rho \xi_r\right) - \frac{l(l+1)}{r}\rho \xi_h = 0.$

we obtain: $$\rho \frac{d\xi_r}{dr} + \xi_h \frac{d\rho}{dr} + \frac{2}{r}\rho \xi_r + \frac{P'}{c^2} + \frac{\rho N^2}{g}\xi_r - \frac{L^2}{r^2 \omega^2 \rho} P' = 0,$$

where we define $L^2 = l(l+1)$ (note the similarity to quantum mechanics).

Using the hydrostatic equation for the background (unperturbed) state

$$\frac{dP}{dr} = -g\rho,$$

finally get: $$\frac{d\xi_r}{dr} + \frac{2}{r}\xi_r - \frac{g}{c^2}\xi_r + \left(1 - \frac{L^2 c^2}{r^2 \omega^2}\right)\frac{P'}{\rho c^2} = 0,$$

or $$\frac{d\xi_r}{dr} + \frac{2}{r}\xi_r - \frac{g}{c^2}\xi_r + \left(1 - \frac{S_l^2}{\omega^2}\right)\frac{P'}{\rho c^2} = 0,$$

where $S_l^2 = \frac{L^2 c^2}{r^2}$ is **the Lamb frequency,** $L^2=l(l+1)$, $c^2(r)=\gamma P/\rho$ is the squared sound speed, $g(r)=Gm(r)/r^2$ is the gravity acceleration at radius r.

Similarly, the momentum equation is:

$$\frac{dP'}{dr} + \frac{g}{c^2} P' + (N^2 - \omega^2)\rho \xi_r = 0,$$

where N^2 is the Brunt-Vaisala frequency.

The bottom boundary condition (r=0): $\xi_r = 0,$ (or a regularity condition).

The top boundary condition (r=R): $\delta P = P' + \frac{dP}{dr}\xi_r = 0,$

or using the hydrostatic equation: $P' - g\rho\xi_r = 0.$

From the horizontal component of the momentum equation:

$$P' = \omega^2 \rho r \xi_h,$$

Then from the upper boundary condition: $\frac{\xi_h}{\xi_r} = \frac{g}{\omega^2 r},$

that is the ratio of the horizontal and radial components of displacement is inverse proportional to squared frequency. However, this relation does not hold in observations, presumably, because of the external force caused by the solar atmosphere.

7. The derived equations with the boundary conditions constitute an eigenvalue problem for solar oscillation modes

$$\frac{d\xi_r}{dr}+\frac{2}{r}\xi_r-\frac{g}{c^2}\xi_r+\left(1-\frac{S_l^2}{\omega^2}\right)\frac{P'}{\rho c^2}=0,$$

$$\frac{dP'}{dr}+\frac{g}{c^2}P'+(N^2-\omega^2)\rho\xi_r=0.$$

Properties of oscillations depend on the signs of these coefficients in brackets.

$S_l^2=\dfrac{L^2c^2}{r^2}$ is the Lamb frequency.

$N^2=g\left(\dfrac{1}{\gamma P}\dfrac{dP}{dr}-\dfrac{1}{\rho}\dfrac{d\rho}{dr}\right)$ is Brunt–Väisälä frequency.

The bottom boundary condition (r=0): $\xi_r=0..$

The top boundary condition (r=R): $\delta P=P'+\dfrac{dP}{dr}\xi_r=0$

Reduction to a 2-nd order equation – qualitative analysis of solar oscillation modes

The reduction can be done via a transformation of variables to eliminate the first derivatives. However, this is cumbersome (see lectures of Douglas Gough, "Linear Adiabatic Stellar Pulsations" Ch.5)

It is most convenient to express the second-order equation in terms of the Lagrangian pressure perturbation, δP.

By a transformation of variables: $\delta P=\rho^{1/2}\cdot\Psi$, the oscillation equations for ξ and P' can be reduced to:

$$\frac{d^2\Psi}{dr^2}+K^2\Psi=0$$

$$K^2=\frac{\omega^2-\omega_c^2}{c^2}-\frac{L^2}{r^2}\left(1-\frac{N^2}{\omega^2}\right)$$

where c is the sound speed, $L^2=l(l+1)$

$\omega_c^2=\dfrac{c^2}{4H^2}\left(1-2\dfrac{dH}{dr}\right)$ is the acoustic cut-off frequency,

$H=\left|\dfrac{d\log\rho}{dr}\right|^{-1}$ is the density scale height,

$N^2=g\left(\dfrac{1}{\gamma}\dfrac{d\log P}{dr}-\dfrac{d\log\rho}{dr}\right)$ is square of the Brunt-Väisälä buoyancy frequency.

Propagation of :high-frequency oscillations: acoustic waves

$$K^2 = \frac{\omega^2 - \omega_c^2}{c^2} - \frac{L^2}{r^2}\left(1 - \frac{N^2}{\omega^2}\right)$$

Consider high-frequency oscillations: $\omega^2 \gg N^2$.

The acoustic cut-off frequency is significant only near the surface (like in the potential well model). In the interior, $\omega \gg \omega_c$.

Therefore, the propagation condition for high-frequecy oscillation (acoustic waves) is:

$$K^2 \approx \frac{\omega^2}{c^2} - \frac{L^2}{r^2} > 0$$

At the reflection point $K^2 = 0$.

From this equation, we can find the wave propagation depth for oscillation of frequency ω and angular degree l (called ***the radius of the inner turning point*** r_t):

$$\omega = \frac{Lc(r_t)}{r_t}$$

Propagation of low frequency waves: internal gravity waves

$$\frac{d^2\Psi}{dr^2} + K^2\Psi = 0$$

$$K^2 = \frac{\omega^2 - \omega_c^2}{c^2} - \frac{L^2}{r^2}\left(1 - \frac{N^2}{\omega^2}\right)$$

For the low-frequency oscillations: $\omega^2 < N^2$.

Consider the wave propagation condition: $K^2 > 0$.

The parameters, $c^2(r)$, $\omega_c^2(r)$, and $N^2(r)$ are calculated from a theoretical (standard) solar model.

therefore, the propagation condition is:

$$K^2 \approx -\frac{L^2}{r^2}\left(1 - \frac{N^2}{\omega^2}\right) > 0 \;\Rightarrow\; \omega < N$$

Propagation diagram: ω_c

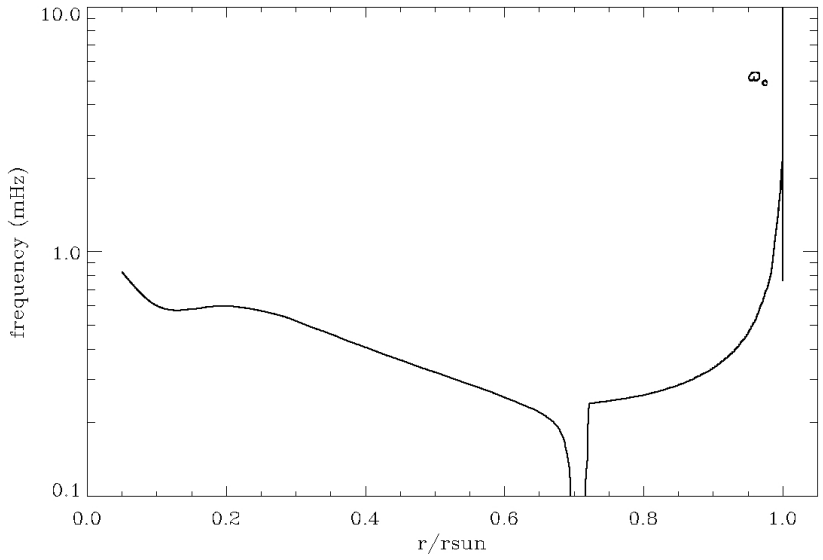

http://sun.stanford.edu/~sasha/PHYS747/Projects/Propagation_Diagram/

Propagation diagram: ω_c S_l

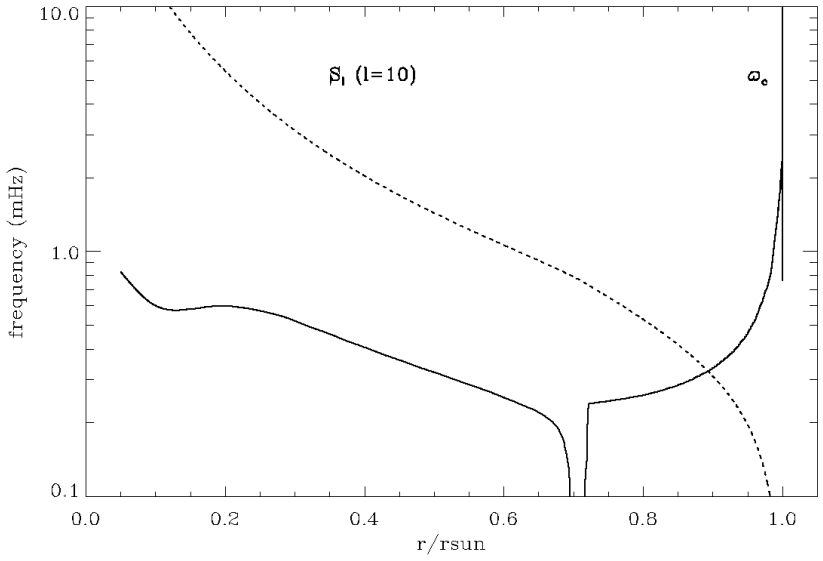

http://sun.stanford.edu/~sasha/PHYS747/Projects/Propagation_Diagram/

Propagation diagram: ω_c S_l,N^2

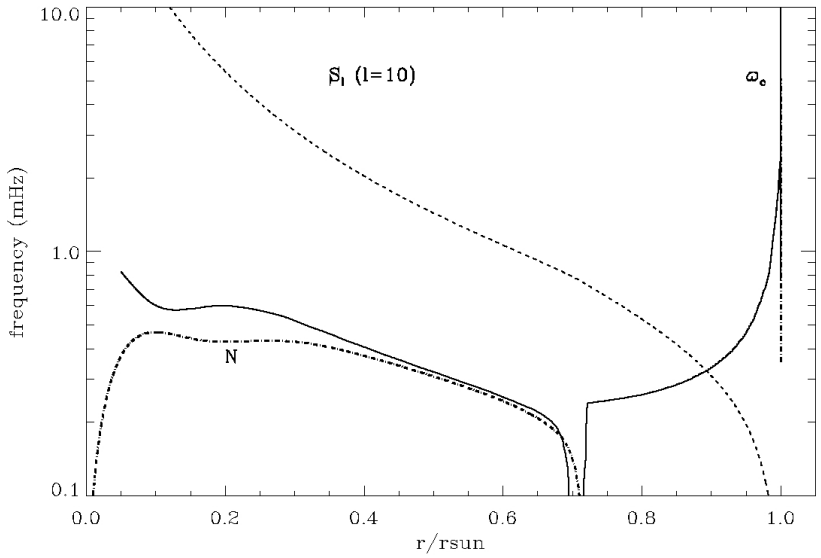

http://sun.stanford.edu/~sasha/PHYS747/Projects/Propagation_Diagram/

Propagation diagram: ω_c S_l,N^2

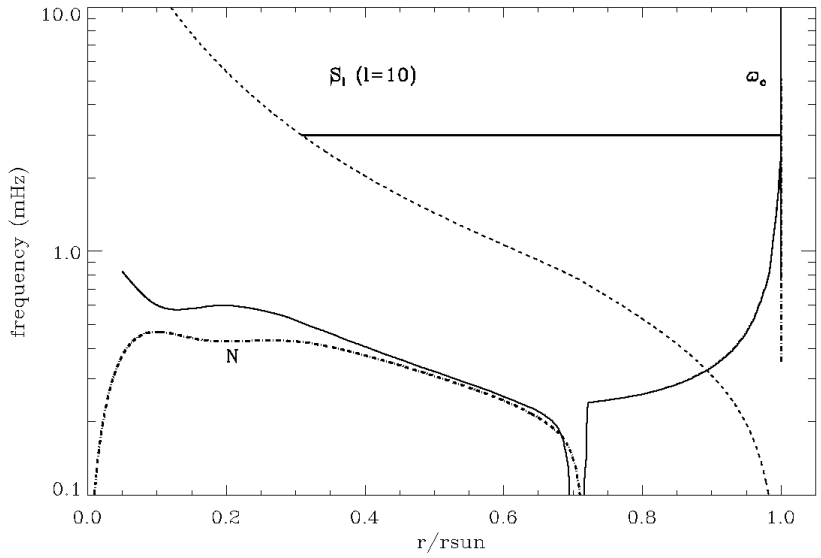

http://sun.stanford.edu/~sasha/PHYS747/Projects/Propagation_Diagram/

Propagation diagram: ω_c S_l,N^2

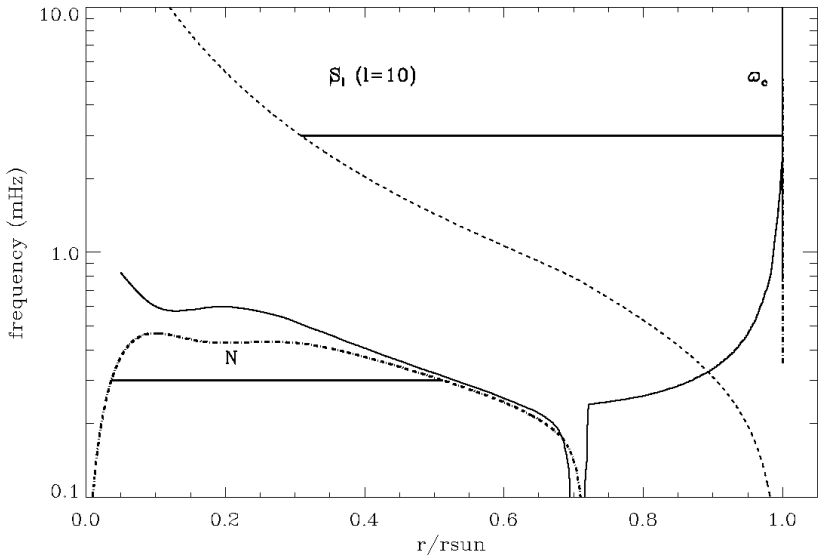

http://sun.stanford.edu/~sasha/PHYS747/Projects/Propagation_Diagram/

Propagation diagram

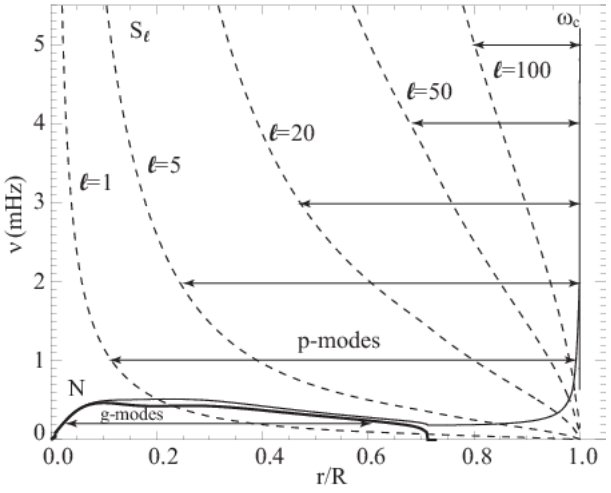

Low angular degree modes (low-l modes) may be mixed modes, which behave like acoustic modes in the envelope and like gravity modes in the deep interior.

Propagation diagram of solar oscillations

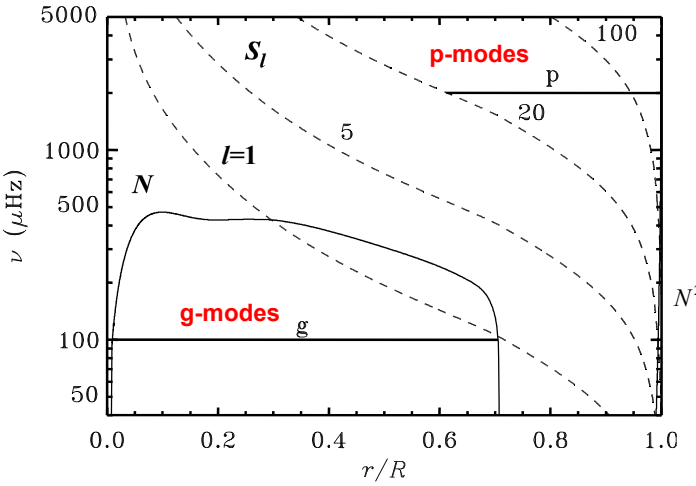

$$S_l^2 = \frac{L^2 c^2}{r^2}$$

the Lamb frequency.

$$N^2 = g\left(\frac{1}{\gamma P}\frac{dP}{dr} - \frac{1}{\rho}\frac{d\rho}{dr}\right)$$

Brunt–Väisälä frequency

Buoyancy (Brunt-Vaisala) frequency N, and Lamb frequency S_l for $l = 1, 5, 20$ and 100 vs. fractional radius r/R for a standard solar model. The horizontal lines indicate the trapping regions for a g mode with frequency $\nu = 100\mu$ Hz, and for a p mode of degree $l = 20$ and $\nu = 2000\mu$ Hz.

Theoretical *l*-ν diagram is obtained by solving the eigenvalue problem numerically

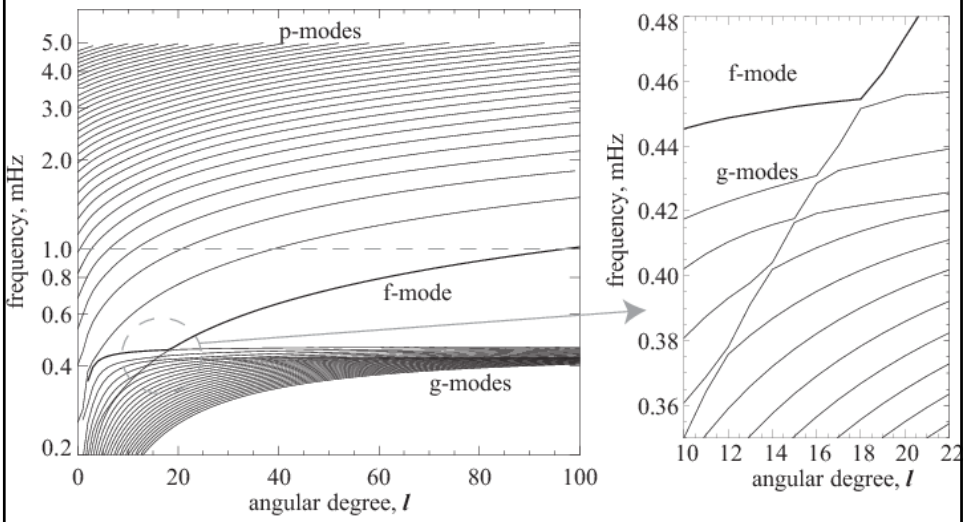

Spatial structure of p- and g-modes

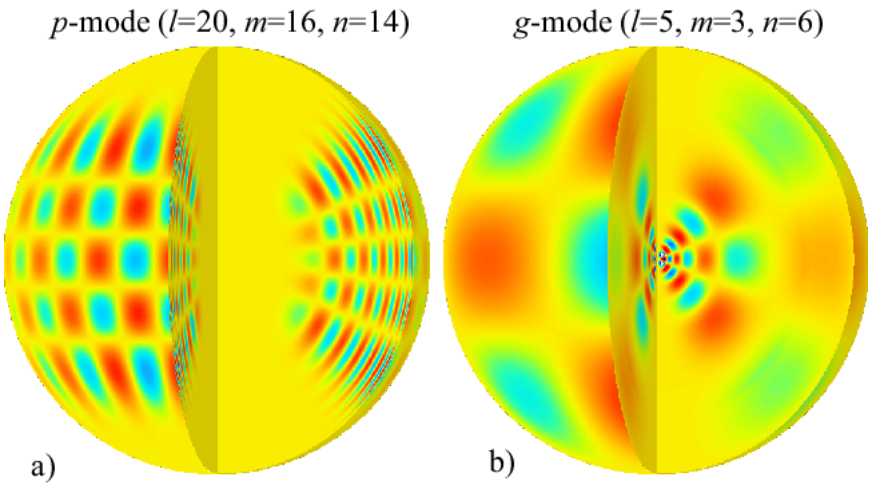

P-mode ray paths

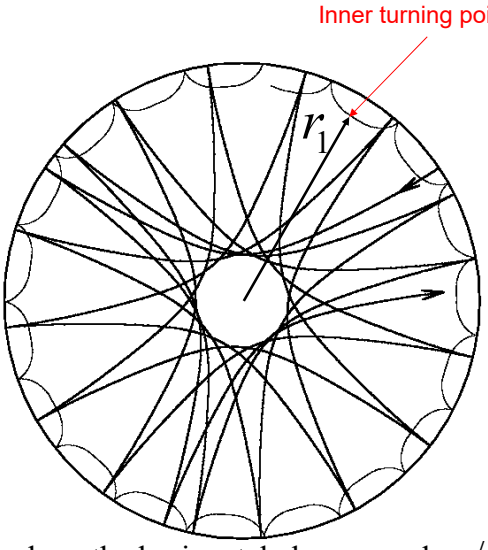

$$k_r^2 = \frac{\omega^2 - \omega_c^2}{c^2} - \frac{S_l^2}{c^2}$$

- The waves propagate where $k_r^2>0$.
- The waves are evanescent where $k_r^2<0$
- The wave turning points are located where $k_r^2=0$.
- Because $\omega_c = c/2H$ has a sharp peak near the surface the upper turning point (r_2) is where $\omega = \omega_c$

The lower turning point (r_1) is where $\omega = S_l = (L/r)c = k_h c$ where the horizontal phase speed $\omega / k_h = c$ is equal to the sound speed.

John's sunquake movie illustrate the wave behavior at the inner turning points:
wave fronts are perpendicular to the ray paths

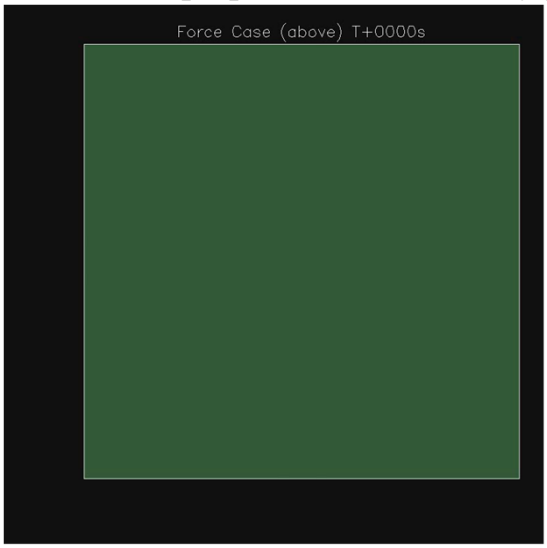

g-mode ray paths

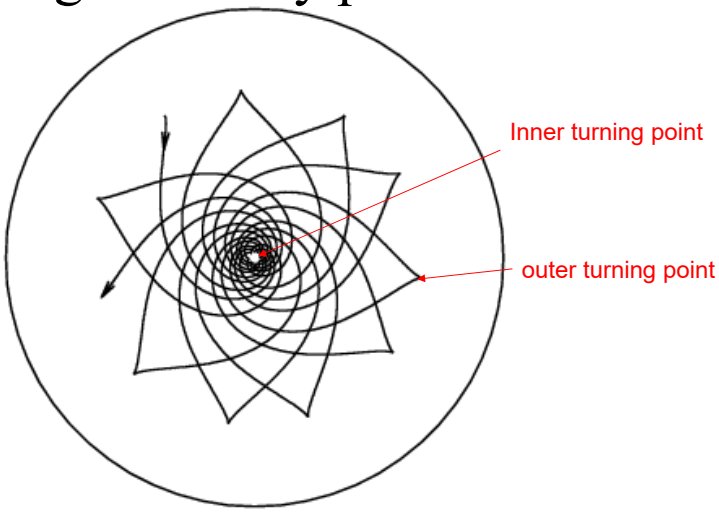

g-modes propagate only in the radiative zone which is convectively stable $N^2 > 0$

Lecture 8

Solar oscillation theory
JWKB (Jeffreys-Wentzel–Kramers–Brillouin) Solution

(Stix, Chapter 5.2; Kosovichev, p.29-34;
Christensen-Dalsgaard, Chapters 5.2, 7)

Plan to solve the solar oscillation equations

1. Linearize - consider small-amplitude oscillations.
2. Neglect the perturbations of the gravitational potential (Cowling approximation).
3. Write the linearized equations in the spherical coordinates: r, θ, ϕ.
4. Consider harmonic (periodic) oscillations
5. Separate the radial and angular coordinates.
6. Show that the angular dependence can be represented by spherical harmonics.
7. Derive equations for the radial dependence, representing the eigenvalue problem for the normal modes
8. Solve the eigenvalue problem in the asymptotic (short wave-length) JWKB approximation.
9. Investigate properties of p- and g-modes

7. The derived equations with the boundary conditions constitute an eigenvalue problem for solar oscillation modes

$$\frac{d\xi_r}{dr}+\frac{2}{r}\xi_r-\frac{g}{c^2}\xi_r+\left(1-\frac{S_l^2}{\omega^2}\right)\frac{P'}{\rho c^2}=0,$$

$$\frac{dP'}{dr}+\frac{g}{c^2}P'+(N^2-\omega^2)\rho\xi_r=0.$$

Properties of oscillations depend on the signs of these coefficients in brackets.

$S_l^2=\dfrac{L^2c^2}{r^2}$ is the Lamb frequency.

$N^2=g\left(\dfrac{1}{\gamma P}\dfrac{dP}{dr}-\dfrac{1}{\rho}\dfrac{d\rho}{dr}\right)$ is the Brunt-Vaisala frequency.

The lower boundary condition: $\xi_r=0,$ (or a regularity condition).

The upper boundary condition: $\delta P=P'+\dfrac{dP}{dr}\xi_r=0,$

Reduction to a 2-nd order equation – qualitative analysis of solar oscillation modes

The reduction can be done via a transformation of variables to eliminate the first derivatives. However, this is cumbersome (see lectures of Douglas Gough, "Linear Adiabatic Stellar Pulsations" Ch.5)

It is most convenient to express the second-order equation in terms of the Lagrangian pressure perturbation, δP.

By a transformation of variables: $\delta P=\rho^{1/2}\cdot\Psi$, the oscillation equations for ξ and P' can be reduced to:

$$\frac{d^2\Psi}{dr^2}+K^2\Psi=0$$

$$K^2=\frac{\omega^2-\omega_c^2}{c^2}-\frac{L^2}{r^2}\left(1-\frac{N^2}{\omega^2}\right)$$

where c is the sound speed, $L^2=l(l+1)$

$\omega_c^2=\dfrac{c^2}{4H^2}\left(1-2\dfrac{dH}{dr}\right)$ is the acoustic cut-off frequency,

$H=\left|\dfrac{d\log\rho}{dr}\right|^{-1}$ is the density scale height,

$N^2=g\left(\dfrac{1}{\gamma}\dfrac{d\log P}{dr}-\dfrac{d\log\rho}{dr}\right)$ is square of the Brunt-Väisälä buoyancy frequency.

Propagation of acoustic waves: high-frequency oscillations

The acoustic cut-off frequency is significant only near the surface (like in the potential well model). In the interior, $\omega \gg \omega_c$.

Therefore, the propagation condition for acoustic waves is:

$$K^2 \approx \frac{\omega^2}{c^2} - \frac{L^2}{r^2} > 0$$

At the reflection point $K^2 = 0$.
From this equation, we can find the wave propagation depth for oscillation of frequency ω and angular degree l (called ***the radius of the inner turning point*** r_t):

$$\omega = \frac{Lc(r_t)}{r_t}$$

Propagation of internal gravity waves – low frequency waves

$$\frac{d^2\Psi}{dr^2} + K^2\Psi = 0$$

$$K^2 = \frac{\omega^2 - \omega_c^2}{c^2} - \frac{L^2}{r^2}\left(1 - \frac{N^2}{\omega^2}\right)$$

Consider the wave propagation condition: $K^2 > 0$.
The parameters, $c^2(r)$, $\omega_c^2(r)$, and $N^2(r)$ are calculated from a theoretical (standard) solar model.
For the low-frequency oscillations: $\omega^2 < N^2$,
therefore, the propagation condition is:

$$K^2 \approx -\frac{L^2}{r^2}\left(1 - \frac{N^2}{\omega^2}\right) > 0 \;\Rightarrow\; \omega < N$$

Propagation diagram of solar oscillations

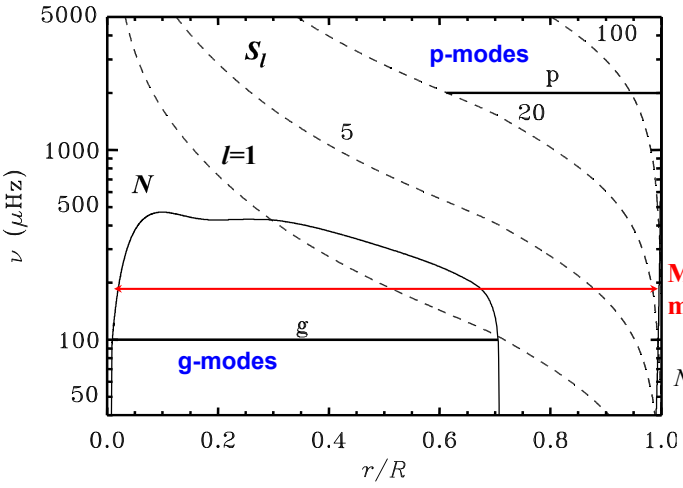

Mixed modes

$$S_l^2 = \frac{L^2 c^2}{r^2}$$

the Lamb frequency.

$$N^2 = g\left(\frac{1}{\gamma P}\frac{dP}{dr} - \frac{1}{\rho}\frac{d\rho}{dr}\right)$$

the Brunt-Vaisala frequency.

Buoyancy (Brunt-Vaisala) frequency N, and Lamb frequency S_l for $l = 1, 5, 20$ and 100 vs. fractional radius r/R for a standard solar model. The horizontal lines indicate the trapping regions for a g mode with frequency $\nu = 100\mu$ Hz, and for a p mode of degree $l = 20$ and $\nu = 2000\mu$ Hz.

Propagation diagram

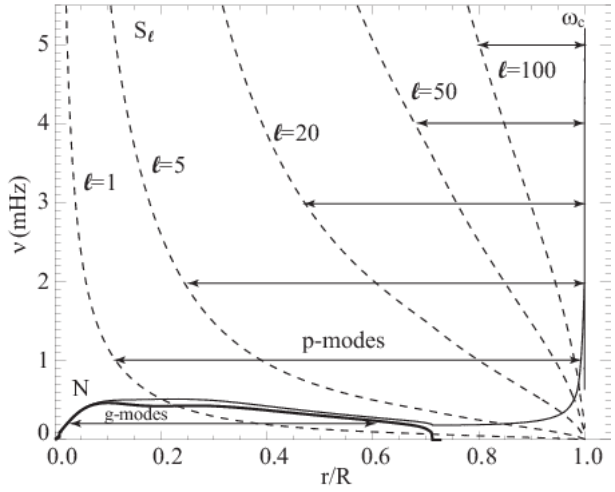

http://sun.stanford.edu/~sasha/PHYS747/Propagation_Diagram/

Asymptotic Theory. JWKB (Jeffreys-Wentzel–Kramers–Brillouin) Solution

General idea of the JWKB approximation

Consider a second-order oscillation equation in a uniform medium without gravity: c=const, $\omega_c = 0$, $N = 0$.

$$\frac{d^2\Psi}{dr^2} + K^2\Psi = 0, \qquad \text{where } K^2 = \frac{\omega^2}{c^2}$$

For a one-dimensional potential well of the length R with infinite walls, the boundary conditions are: $\Psi = 0$ at $r = 0$ and $r = R$.
We seeks the solution in the form:

$$\Psi(r) = Ae^{\pm ikr}$$

Then, the solution satisfying the boundary conditions is:

$$\Psi(r) = A\sin(kr)$$

where $kR = \pi n$, n is an integer number.

Thus, we obtain the oscillation spectrum (eigenvalues):

$$\omega_n = \pi nc / R.$$

Then, we consider the wave equation with the coefficients varying with r:

$$\frac{d^2\Psi}{dr^2} + K^2(r)\Psi = 0$$

$$K^2(r) = \frac{\omega^2 - \omega_c^2}{c^2} - \frac{L^2}{r^2}\left(1 - \frac{N^2}{\omega^2}\right).$$

If $K(r)$ is a slowly varying function of r we can seek the solution in the form:

$$\Psi(r) = Ae^{iu(r)}$$

where $u(r)$ is a slowly varying function.We find $u(r)$ by substituting this form in the wave equation:

$$\frac{d\Psi}{dr} = i\frac{du}{dr}Ae^{iu(r)}$$

$$\frac{d^2\Psi}{dr^2} = i\frac{d^2u}{dr^2}Ae^{iu(r)} - \left(\frac{du}{dr}\right)^2 Ae^{iu(r)}$$

Because $u(r)$ is a slowly varying function, in the first approximation we neglect the first term in this expression. Substituting in the wave equation, we obtain:

$$-\left(\frac{du}{dr}\right)^2 Ae^{iu(r)} + K(r)^2 Ae^{iu(r)} = 0$$

$$\left(\frac{du}{dr}\right)^2 = K^2 \qquad \rightarrow \qquad \frac{du}{dr} = \pm K \quad \rightarrow \quad u(r) = \pm\int kdr$$

$$\Psi(r) = Ae^{\pm i\int kdr}$$

The eigenvalues are determined by matching the boundary conditions:

$$\int_{cavity} kdr = \pi(n + \alpha)$$

where α is a phase shift due to imperfectly reflecting boundary conditions.

The JWKB approximation is valid if $\left|\frac{1}{K}\frac{dK}{dr}\right| \ll 1$.

It can be improved considering A as a function of r.

JWKB solution

$$\xi_r(r) = A\rho^{-1/2} e^{\pm i\int k_r dr}$$

where $k(r)^2 = \dfrac{\omega^2 - \omega_c^2}{c^2} - \dfrac{L^2}{r^2}\left(1 - \dfrac{N^2}{\omega^2}\right)$

The wave propagation region is determined from $k(r) > 0$.

The resonant condition is:

$$\int_{r_1}^{r_2} k_r dr = \pi(n + \alpha)$$

$$\int_{r_1}^{r_2} \sqrt{\frac{\omega^2 - \omega_c^2}{c^2} - \frac{L^2}{r^2}\left(1 - \frac{N^2}{\omega^2}\right)}\, dr = \pi(n + \alpha)$$

8. JWKB (Jeffreys-Wentzel–Kramers–Brillouin) Solution (short-wavelength asymptotic approximation – similar to quantum mechanics)

We assume that only density $\rho(r)$ varies significantly among the solar properties in the oscillation equations, and seek for an oscillatory solution in the JWKB form:

$$\xi_r = A\rho^{-1/2} e^{i\int k_r dr},$$

$$P' = B\rho^{1/2} e^{i\int k_r dr},$$

where the radial wavenumber k_r is a slowly varying function of r.

Then,

$$\frac{d\xi_r}{dr} = A\rho^{-1/2}\left(ik_r + \frac{1}{2H}\right) e^{i\int k_r dr},$$

$$\frac{dP'}{dr} = B\rho^{1/2}\left(ik_r - \frac{1}{2H}\right) e^{i\int k_r dr},$$

where $H = -\left(\dfrac{d\log\rho}{dr}\right)^{-1}$ **is the density scale height**.

From the oscillation equations we get a linear system:

$$\left(ik_r + \frac{1}{2H}\right)A - \frac{g}{c^2}A + \frac{1}{c^2}\left(1 - \frac{S_l^2}{\omega^2}\right)B = 0,$$

$$\left(ik_r - \frac{1}{2H}\right)B + \frac{g}{c^2}B + (N^2 - \omega^2)A = 0.$$

The determinant of this system is equal zero when

$$k_r^2 = \frac{\omega^2 - \omega_c^2}{c^2} + \frac{S_l^2}{c^2\omega^2}\left(N^2 - \omega^2\right)$$

where $\omega_c = \frac{c}{2H}$ is the **acoustic cut-off frequency**

We use the relation: $N^2 = g\left(\frac{1}{\gamma P}\frac{dP}{dr} - \frac{1}{\rho}\frac{d\rho}{dr}\right) \equiv g/H - g^2/c^2$.

The solar waves propagate in the regions where $k_r^2 > 0$.

If $k_r^2 < 0$, the waves exponentially decay ('evanescent').

Properties of Solar Oscillation Modes

Equation $$k_r^2 = \frac{\omega^2 - \omega_c^2}{c^2} + \frac{S_l^2}{c^2\omega^2}\left(N^2 - \omega^2\right)$$

represents a **dispersion relation of solar waves**.

It relates frequency ω with radial wavenumber k_r and angular order l.

Consider two simple cases:

1: the high-frequency case. If $\omega^2 >> N^2$ then

$$k_r^2 = \frac{\omega^2 - \omega_c^2}{c^2} - \frac{S_l^2}{c^2}$$

or $$\omega^2 = \omega_c^2 + k_r^2c^2 + k_h^2c^2,$$

where $k_h = S_l / c \equiv \frac{L}{r} \equiv \frac{\sqrt{l(l+1)}}{r}$ is **the horizontal wave number**.

Then, $k^2 = k_r^2 + k_h^2$ is the squared total wavenumber.

Finally, $\omega^2 = \omega_c^2 + k^2c^2$, where $\omega_c = \frac{c}{2H}$ is the acoustic cut-off frequency.

This is **the dispersion relation for acoustic (p) modes**; **ω_c is the acoustic cutoff frequency. Physically, the waves with frequencies below the acoustic cutoff frequency cannot propagate. Their wavelength becomes shorter than the density scale height. For the Sun $\nu_c \equiv \omega_c / 2\pi \approx 5$ *mHz*. (c~10 km/s, H~150km).**

$$k_r^2 = \frac{\omega^2 - \omega_c^2}{c^2} + \frac{S_l^2}{c^2\omega^2}\left(N^2 - \omega^2\right)$$

2: consider the low-frequency case when $\omega^2 << S_l^2$

then $k_r^2 = \frac{S_l^2}{c^2\omega^2}(N^2 - \omega^2)$ (remember $S_l = ck_h = cL/r$)

Then, $\omega^2 = \frac{k_h^2 N^2}{k^2} \equiv N^2 \cos^2\theta$, where $k^2 = k_r^2 + k_h^2$

where θ is the angle between wavevector k and the horizontal direction.

This is a dispersion relation for internal gravity (g). modes. They propagate mostly horizontally.

Normal modes of solar oscillations

The frequencies of normal modes are determined for the Borh quantization rule (resonant condition): $\int_{r_1}^{r_2} k_r dr = \pi(n + \alpha),$

where r_1 and r_2 are the radii of the turning points where k_r=0, n is a radial order -integer number, and α is a phase shift which depends on properties of the reflecting boundaries.

$$k_r^2 = \frac{\omega^2 - \omega_c^2}{c^2} + \frac{S_l^2}{c^2\omega^2}\left(N^2 - \omega^2\right)$$

c(r) is the sound speed

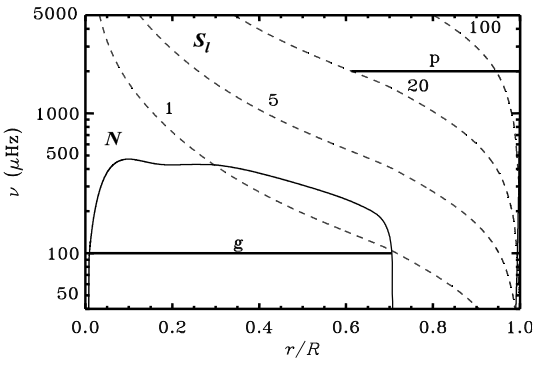

$\omega_c = \frac{c}{2H}$ is the acoustic cut-off frequency; it has very sharp increase at r/R=1

$H = \left(\frac{d\log\rho}{dr}\right)^{-1},$

$S_l^2 = \frac{L^2c^2}{r^2}$ $L^2 = l(l+1)$

$N^2 = g/H - g^2/c^2$

P-mode ray paths

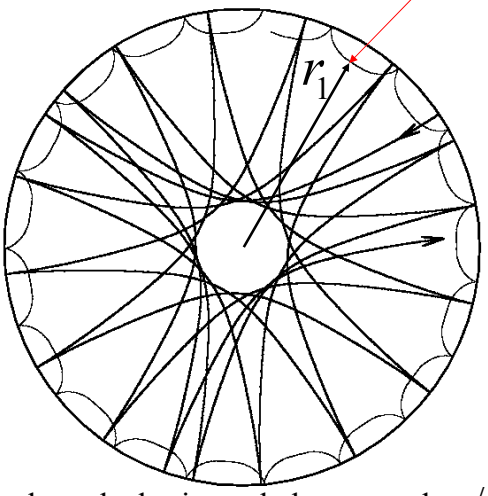

$$k_r^2 = \frac{\omega^2 - \omega_c^2}{c^2} - \frac{S_l^2}{c^2}$$

- The waves propagate where $k_r^2>0$.
- The waves are evanescent where $k_r^2<0$
- The wave turning points are located where $k_r^2=0$.
- Because $\omega_c = c/2H$ has a sharp peak near the surface the upper turning point (r_2) is where $\omega = \omega_c$

The lower turning point (r_1) is where $\omega = S_l = (L/r)c = k_h c$ where the horizontal phase speed $\omega / k_h = c$ is equal to the sound speed.

g-mode ray paths

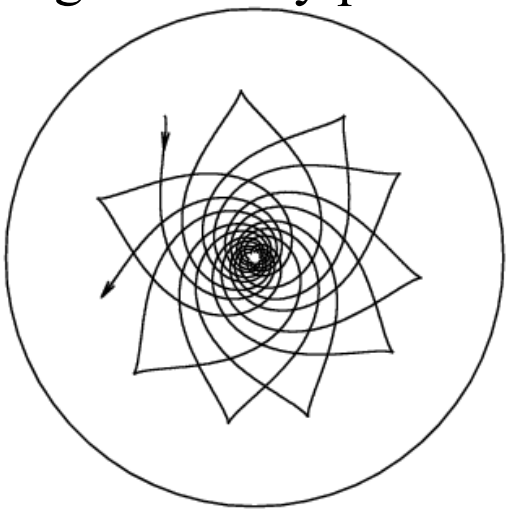

g-modes propagate only in the radiative zone which is convectively stable $N^2 > 0$

Calculation of normal mode frequencies in the JWKB Approximation

Estimate frequencies of normal modes for these 2 cases.

1. **p-modes:**

propagating region: $k_r^2 > 0$

turning points $k_r^2 = 0$: $\omega^2 = \omega_c^2 + \frac{L^2 c^2}{r^2}$.

For the lower turning point in the interior: $\omega_c << \omega$.

Then, $\omega \approx \frac{Lc}{r}$, or $\frac{c(r_1)}{r_1} = \frac{\omega}{L}$ is the equation for the lower turning point.

The upper turning point: $\omega_c(r_2) \approx \omega$. Since $\omega_c(r)$ is a steep function of r near the surface, $r_2 \approx R$.

Then, the resonant condition for p-modes is: $$\int_{r_1}^{R} \sqrt{\frac{\omega^2}{c^2} - \frac{L^2}{r^2}}\, dr = \pi(n + \alpha)$$

Abel integral equation.

Frequencies of low-degree p-modes

For $l << n$, $r_1 \approx 0$, and we obtain: $\omega \approx \frac{\pi(n + L/2 + \alpha)}{\int_0^R \frac{dr}{c}}$.

That is the spectrum of low-degree p-modes is approximately equidistant with frequency spacing: $\Delta\nu = \left(4\int_0^R \frac{dr}{c}\right)^{-1}$.

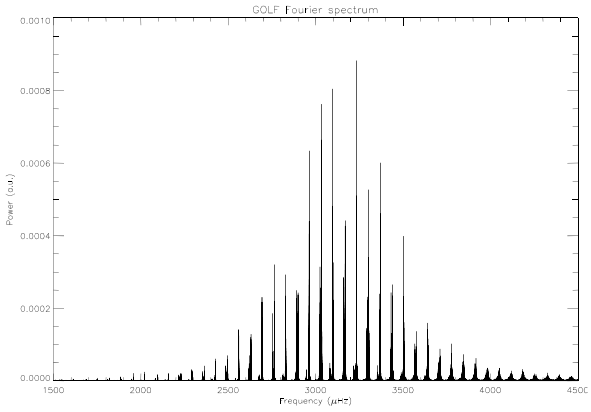

Maximum amplitude is around 3,300 μHz, or 3.3 mHz. The corresponding oscillation period is 300 seconds or 5 minutes.

Frequencies of the internal gravity modes (g-modes):

The turning points are determined from equation: $N(r) = \omega.$

In the propagation region, $k_r > 0$, far from the turning points ($N >> \omega$):

$$k_r \approx \frac{LN}{r\omega}.$$

Then, from the resonant condition:

$$\int_{r_1}^{r_2} \frac{L}{\omega} N \frac{dr}{r} = \pi(n+\alpha).$$

we find:
$$\omega \approx \frac{L\int_{r_1}^{r_2} N \frac{dr}{r}}{\pi(n+\alpha)}.$$

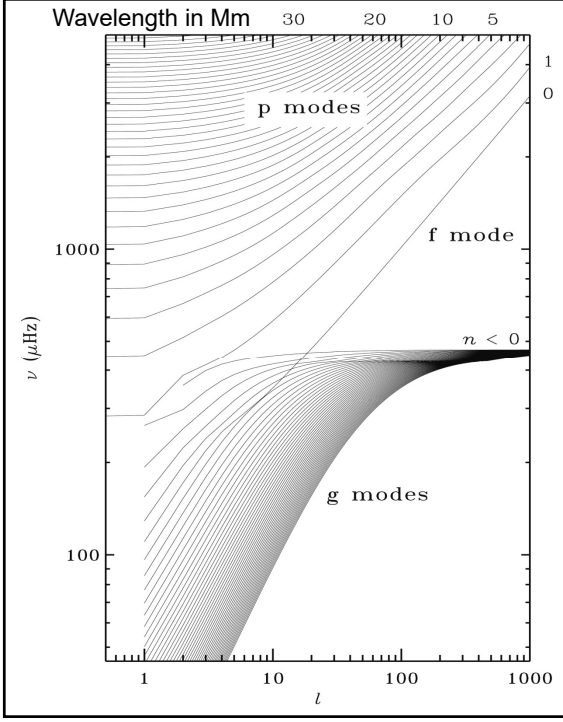

Spectrum of the normal oscillation modes of the Sun calculated by solving the oscillation equations numerically for a standard solar model.

Note the 'avoided crossing effect' for f and g-modes.

Surface gravity mode (f-mode)

These wave propagate at the surface boundary where Lagrangian pressure perturbation $\delta P \sim 0$.

Consider the oscillation equations in terms of δP by making use of the relation between Eulerian and Lagrangian variables: $P' = \delta P + g\rho\xi_r$.

$$\frac{d\xi_r}{dr} - \frac{L^2 g}{\omega^2 r^2}\xi_r + \left(1 - \frac{L^2 c^2}{\omega^2 r^2}\right)\frac{\delta P}{\rho c^2} = 0,$$

$$\frac{d\delta P}{dr} + \frac{L^2 g}{\omega^2 r^2}\delta P - \frac{g\rho f}{r}\xi_r = 0,$$

where $f \approx \frac{\omega^2 r}{g} - \frac{L^2 g}{\omega^2 r}$.

These equations have a peculiar solution: $\delta P = 0, \ f = 0.$

For this solution: $\omega^2 = \frac{Lg}{R} = k_h g$

-dispersion relation for f-mode.

The eigenfunction equation: $\frac{d\xi_r}{dr} - \frac{L}{r}\xi_r = 0$

has a solution $\xi_r \propto e^{k_h (r-R)}$ exponentially decaying with depth.

Theoretical *l*-ν diagram: numerical solution of the oscillation equations

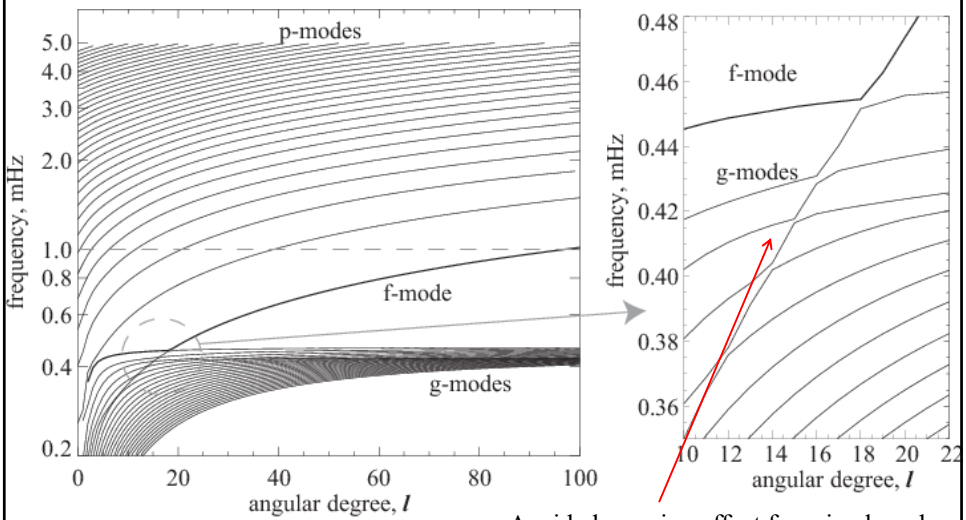

Avoided crossing effect for mixed modes

Lecture 9

Properties of acoustic waves and p- modes; low degree modes

(Stix, Chapter 5.2; Kosovichev, p.29-34;
Christensen-Dalsgaard, Chapters 5.2, 7)

Plan to solve the solar oscillation equations

1. Linearize - consider small-amplitude oscillations.
2. Neglect the perturbations of the gravitational potential (Cowling approximation).
3. Write the linearized equations in the spherical coordinates: r, θ, ϕ.
4. Consider harmonic (periodic) oscillations
5. Separate the radial and angular coordinates.
6. Show that the angular dependence can be represented by spherical harmonics.
7. Derive equations for the radial dependence, representing the eigenvalue problem for the normal modes
8. Solve the eigenvalue problem in the asymptotic (short wave-length) JWKB approximation.
9. Investigate properties of p-modes
10. Properties of g-modes

Overview of the Asymptotic Theory. JWKB (Jeffreys-Wentzel–Kramers–Brillouin) Solution

General idea of the JWKB approximation

Consider a second-order oscillation equation in a uniform medium without gravity: c=const, $\omega_c = 0$, $N = 0$.

$$\frac{d^2\Psi}{dr^2} + K^2\Psi = 0, \qquad \text{where } K^2 = \frac{\omega^2}{c^2}$$

For a one-dimensional potential well of the length R with infinite walls, the boundary conditions are: $\Psi = 0$ at $r = 0$ and $r = R$.
We seeks the solution in the form:

$$\Psi(r) = Ae^{\pm ikr}$$

Then, the solution satisfying the boundary conditions is:

$$\Psi(r) = A\sin(kr)$$

where $kR = \pi n$, n is an integer number.
Thus, we obtain the oscillation spectrum (eigenvalues):

$$\omega_n = \pi nc / R.$$

Then, we consider the wave equation with the coefficients varying with r:

$$\frac{d^2\Psi}{dr^2} + K^2(r)\Psi = 0$$

$$K^2(r) = \frac{\omega^2 - \omega_c^2}{c^2} - \frac{L^2}{r^2}\left(1 - \frac{N^2}{\omega^2}\right).$$

If $K(r)$ is a slowly varying function of r we can seek the solution in the form:

$$\Psi(r) = Ae^{iu(r)}$$

where $u(r)$ is a slowly varying function.We find $u(r)$ by substituting this form in the wave equation:

$$\frac{d\Psi}{dr} = i\frac{du}{dr}Ae^{iu(r)}$$

$$\frac{d^2\Psi}{dr^2} = i\frac{d^2u}{dr^2}Ae^{iu(r)} - \left(\frac{du}{dr}\right)^2 Ae^{iu(r)}$$

Because $u(r)$ is a slowly varying function, in the first approximation we neglect the first term in this expression. Substituting in the wave equation, we obtain:

$$-\left(\frac{du}{dr}\right)^2 Ae^{iu(r)} + K(r)^2 Ae^{iu(r)} = 0$$

$$\left(\frac{du}{dr}\right)^2 = K^2 \qquad \rightarrow \qquad \frac{du}{dr} = \pm K \quad \rightarrow \quad u(r) = \pm\int kdr$$

$$\Psi(r) = Ae^{\pm i\int kdr}$$

The eigenvalues are determined by matching the boundary conditions:

$$\int_{cavity} kdr = \pi(n + \alpha)$$

where α is a phase shift due to imperfectly reflecting boundary conditions.

The JWKB approximation is valid if $\left|\frac{1}{K}\frac{dK}{dr}\right| \ll 1$.

It can be improved considering A as a function of r.

JWKB solution

$$\xi_r(r) = A\rho^{-1/2} e^{\pm i\int k_r dr}$$

where $k(r)^2 = \dfrac{\omega^2 - \omega_c^2}{c^2} - \dfrac{L^2}{r^2}\left(1 - \dfrac{N^2}{\omega^2}\right)$

The wave propagation region is determined from $k(r) > 0$.

The resonant condition is:

$$\int_{r_1}^{r_2} k_r dr = \pi(n + \alpha)$$

$$\int_{r_1}^{r_2} \sqrt{\frac{\omega^2 - \omega_c^2}{c^2} - \frac{L^2}{r^2}\left(1 - \frac{N^2}{\omega^2}\right)}\, dr = \pi(n + \alpha)$$

Normal modes of solar oscillations

The frequencies of normal modes are determined for the Borh quantization rule (resonant condition): $\int_{r_1}^{r_2} k_r dr = \pi(n + \alpha),$

where r_1 and r_2 are the radii of the turning points where k_r=0, n is a radial order -integer number, and α is a phase shift which depends on properties of the reflecting boundaries.

$$k_r^2 = \frac{\omega^2 - \omega_c^2}{c^2} + \frac{S_l^2}{c^2\omega^2}\left(N^2 - \omega^2\right)$$

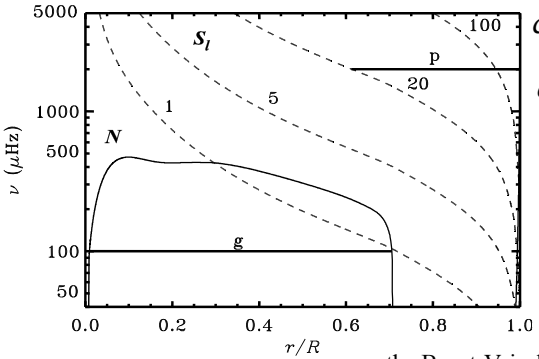

$c^2 = \gamma P / \rho$ - the squared sound speed

$\omega_c = \dfrac{c}{2H}$ - the acoustic cut-off frequency; it has very sharp increase at r/R=1

$H = -\left(\dfrac{d\log\rho}{dr}\right)^{-1}$, - the density scale height

$S_l^2 = \dfrac{L^2 c^2}{r^2}$ - the Lamb frequency

$L^2 = l(l+1)$

$N^2 = g/H - g^2/c^2$ - the Brunt-Vaisala frequency after substituting H and the hydrostatic equation $dP/dr = -g\rho$

Propagation diagram of solar oscillations

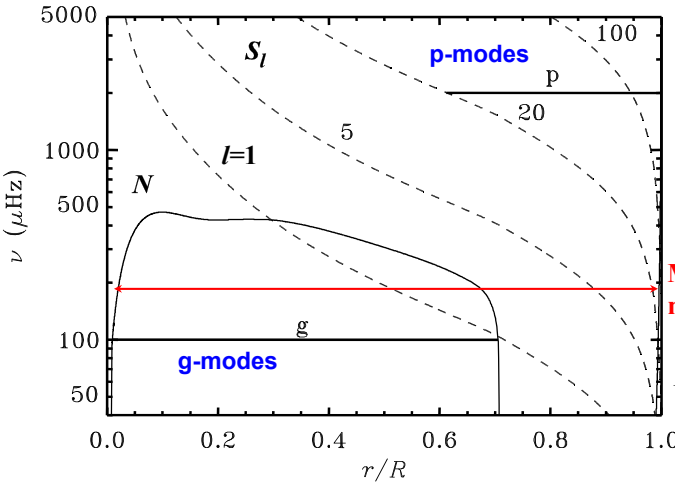

$$S_l^2 = \frac{L^2 c^2}{r^2}$$

the Lamb frequency.

$$N^2 = g\left(\frac{1}{\gamma P}\frac{dP}{dr} - \frac{1}{\rho}\frac{d\rho}{dr}\right)$$

the Brunt-Vaisala frequency.

Buoyancy (Brunt-Vaisala) frequency N, and Lamb frequency S_l for $l = 1, 5, 20$ and 100 vs. fractional radius r/R for a standard solar model. The horizontal lines indicate the trapping regions for a g mode with frequency $\nu = 100\mu$ Hz, and for a p mode of degree $l = 20$ and $\nu = 2000\mu$ Hz.

Spatial structure of p- and g-modes is obtained by multiplying the radial eigenfunctions by the corresponding spherical harmonics

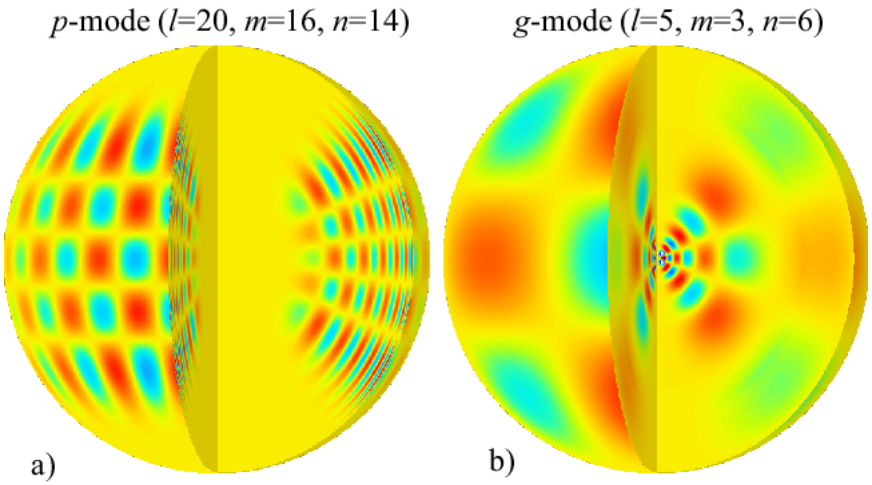

Properties of Solar Oscillation Modes

Equation $$k_r^2 = \frac{\omega^2 - \omega_c^2}{c^2} + \frac{S_l^2}{c^2\omega^2}\left(N^2 - \omega^2\right)$$

represents a **dispersion relation of solar waves**.

It relates frequency ω with radial wavenumber k_r and angular order l.

Consider two cases:

1: **the high-frequency case.**

If $\omega^2 >> N^2$ then $$k_r^2 = \frac{\omega^2 - \omega_c^2}{c^2} - \frac{S_l^2}{c^2}$$

or $$\omega^2 = \omega_c^2 + k_r^2 c^2 + k_h^2 c^2,$$

where $k_h = S_l / c \equiv \frac{L}{r} \equiv \frac{\sqrt{l(l+1)}}{r}$ is **the horizontal wave number**.

Then, $k^2 = k_r^2 + k_h^2$ is the squared total wavenumber.

Finally, $\omega^2 = \omega_c^2 + k^2 c^2$, where $\omega_c = \frac{c}{2H}$ is the acoustic cut-off frequency.

This is **the dispersion relation for acoustic (p) modes**; **ω_c is the acoustic cutoff frequency. Physically, the waves with frequencies below the acoustic cutoff frequency cannot propagate. Their wavelength becomes shorter than the density scale height. For the Sun $\nu_c \equiv \omega_c / 2\pi \approx 5$ *mHz*. (c~10 km/s, H~150km).**

$$k_r^2 = \frac{\omega^2 - \omega_c^2}{c^2} + \frac{S_l^2}{c^2\omega^2}\left(N^2 - \omega^2\right)$$

2: consider the low-frequency case when $\omega^2 << S_l^2$

then $k_r^2 = \frac{S_l^2}{c^2\omega^2}(N^2 - \omega^2)$ (remember $S_l = ck_h = cL / r$)

Then, $$\omega^2 = \frac{k_h^2 N^2}{k^2} \equiv N^2 \cos^2\theta, \text{ where } k^2 = k_r^2 + k_h^2$$

where θ is the angle between wavevector k and the horizontal direction.

This is a dispersion relation for internal gravity (g). modes. They propagate mostly horizontally.

Calculation of normal mode frequencies

Estimate frequencies of normal modes for these 2 cases.

1. **p-modes:**

propagating region: $k_r^2 > 0$

turning points $k_r^2 = 0$: $\omega^2 = \omega_c^2 + \frac{L^2 c^2}{r^2}$.

For the lower turning point in the interior: $\omega_c << \omega$.

Then, $\omega \approx \frac{Lc}{r}$, or $\frac{c(r_1)}{r_1} = \frac{\omega}{L}$ is the equation for the lower turning point.

The upper turning point: $\omega_c(r_2) \approx \omega$. Since $\omega_c(r)$ is a steep function of r near the surface, $r_2 \approx R$.

Then, the resonant condition for p-modes is: $\int_{r_1}^{R} \sqrt{\frac{\omega^2}{c^2} - \frac{L^2}{r^2}}\, dr = \pi(n + \alpha)$

Abel integral equation.

Waves in the solar atmosphere: initial state

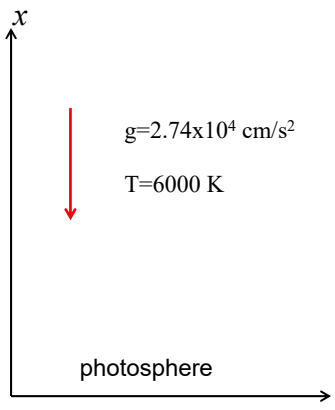

Initial (hydrostatic) state:

$$\frac{\partial P_0}{\partial x} = -g\rho_0$$

Equation of state defines pressure in terms of temperature, density and molecular weight:

$$P = \frac{R\rho T}{\mu},$$

where μ is the molecular weight.

For non-ionized hydrogen gas $\mu = 1$, for fully ionized hydrogen gas $\mu = 0.5$. Because of ionization the number of particles increases by 2 (ions+electrons). R is the gas constant.

Then, $P_0(x) = P(0)e^{-\frac{x}{H}}$ where $H = \frac{RT}{g\mu}$ is the pressure scale height.

Waves in the solar atmosphere: initial equations

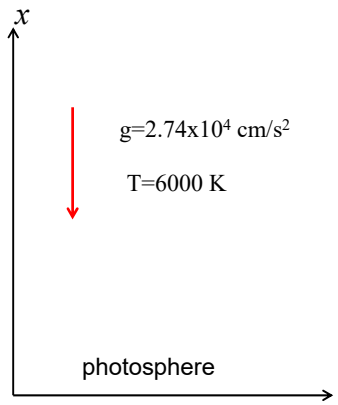

Continuity (mass conservation) equation:

$$\frac{\partial \rho}{\partial t} + \frac{\partial \rho v}{\partial x} = 0.$$

Momentum equation:

$$\rho \frac{dv}{dt} = -\frac{\partial P}{\partial x} - g\rho.$$

Velocity v can be expressed in terms of displacement ξ of fluid elements: $v = \frac{d\xi}{dt}$

Adiabaticity equation:

$$\frac{\partial P}{\partial t} + v\frac{\partial P}{\partial x} - c^2\left(\frac{\partial \rho}{\partial t} + v\frac{\partial \rho}{\partial x}\right) = 0,$$

where $c^2 = \frac{\gamma P}{\rho}$ in the squared adiabatic sound speed.

Waves in the solar atmosphere: linearized equations for small perturbations

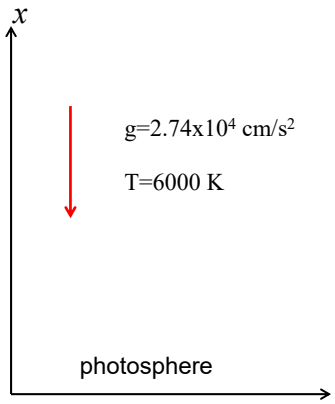

Consider small perturbations:

$$\rho = \rho_0 + \rho_1, \quad P = P_0 + P_1,$$

$$v = v_0 + v_1, \quad v_0 = 0, \quad v_1 = \frac{\partial \xi}{\partial t}$$

Continuity (mass conservation) equation:

$$\frac{\partial \rho_1}{\partial t} + \frac{\partial \rho_0 v_1}{\partial x} = 0.$$

Momentum equation:

$$\rho_0 \frac{\partial v_1}{\partial t} = -\frac{\partial P_1}{\partial x} - g\rho_1.$$

Adiabaticity equation:

$$\frac{\partial P_1}{\partial t} + v_1\frac{\partial P_0}{\partial x} - c^2\left(\frac{\partial \rho_1}{\partial t} + v_1\frac{\partial \rho_0}{\partial x}\right) = 0.$$

Acoustic waves in the solar atmosphere

The linearized system of 1D hydrodynamic equations describing vertical propagation of acoustic waves in a stationary isothermal atmosphere can be reduced to a single PDE in terms of the vertical displacement ξ of a mass element. The velocity of the element is $v_1 = \frac{d\xi}{dt}$. The linearized equations of the conservation of mass, momentum and entropy are:

$$\frac{\partial \rho_1}{\partial t} + \rho_0 \frac{\partial v_1}{\partial x} = 0$$

$$\rho_0 \frac{\partial v_1}{\partial t} = -\frac{\partial P_1}{\partial x} - g\rho_1$$

$$\frac{\partial P_1}{\partial t} + v_1 \frac{\partial P_0}{\partial x} - c^2 \left(\frac{\partial \rho_1}{\partial t} + v_1 \frac{\partial \rho_0}{\partial x} \right) = 0.$$

where $\rho_0(x)$ and $P_0(x)$ are the equilibrium distributions of the density and pressure, defined by the hydrostatic equation: $\frac{\partial P_0}{\partial x} = -g\rho_0$, where g is the gravity acceleration; $c^2 = \gamma P_0 / \rho_0$ is the sound speed which is constant because the atmosphere is isothermal, γ is the adiabatic exponent. From these two equations, we obtain:

$$\frac{\partial \rho_0}{\partial x} = \frac{\gamma}{c^2} \frac{\partial P_0}{\partial x} = -\frac{\gamma g}{c^2} \rho_0$$

Substituting $v_1 = \frac{d\xi}{dt}$ and the hydrostatic equations in the linearized equations, we obtain:

$$\rho_1 + \rho_0 \frac{\partial \xi}{\partial x} = 0$$

$$\rho_0 \frac{\partial^2 \xi}{\partial t^2} = -\frac{\partial P_1}{\partial x} - g\rho_1$$

$$P_1 = c^2 \rho_1 + g\rho_0 \xi$$

Substituting ρ_1 and P_1 in the second equation, we obtain:

$$\frac{\partial^2 \xi}{\partial t^2} = c^2 \frac{\partial^2 \xi}{\partial x^2} - \gamma g \frac{\partial \xi}{\partial x}$$

Waves in the solar atmosphere: dispersion relation

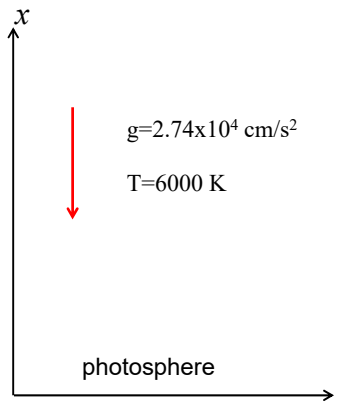

Eliminating ρ_1, P_1, v_1 we find that displacement ξ satisfies the second-order PDE:

$$\frac{\partial^2 \xi}{\partial t^2} = c^2 \frac{\partial^2 \xi}{\partial x^2} - \gamma g \frac{\partial \xi}{\partial x},$$

using the substitution $u = \xi \exp(\alpha x)$ we eliminate the first-order term:

$$\frac{\partial^2 u}{\partial t^2} = c^2 \frac{\partial^2 u}{\partial x^2} - \omega_c^2 u,$$

where $\omega_c = \frac{\gamma g}{2c}$ is the acoustic cut-off frequency.

For the dispersion relation we seek the solution in terms of Fourier harmonics: $u \propto \exp(-i\omega t + ikx)$:

$$-\omega^2 u = -c^2 k^2 u - \omega_c^2 u$$

$$\boxed{\omega^2 = c^2 k^2 + \omega_c^2}$$

The frequencies of plane-parallel acoustic waves traveling in the atmosphere are higher than the acoustic cut-off frequency.

Problem 1.5. (extra credit). Consider acoustic waves in the solar atmosphere excited by an impulsive force:

• show that the solution of Eq.1 for acoustic wave excited by an impulsive delta-function force described by the initial conditions:

$$\xi|_{t=0} = 0, \quad \frac{\partial \xi}{\partial t}|_{t=0} = \delta(x),$$

is written in terms of the Bessel function, J_0:

$$\xi(x,t) = \begin{cases} 0, & \text{if } t < x/c \\ \frac{1}{2}\exp\left(\frac{\gamma g x}{2c^2}\right) J_0\left(\frac{\gamma g}{2c}\sqrt{t^2 - \frac{x^2}{c^2}}\right), & \text{if } t \geq x/c \end{cases}$$

• plot $\xi(t)$ for several values of x, and $\xi(x)$ for several t for parameters corresponding to the solar atmosphere, and explain the solutions from the physics point of view[1].

• show that the frequency of oscillations behind the wave front approaches the acoustic cut-off frequency.

[1] Hint. For explanation calculate the phase and group velocities using the dispersion relation (Eq.2).

Propagation of acoustic wave in the atmosphere

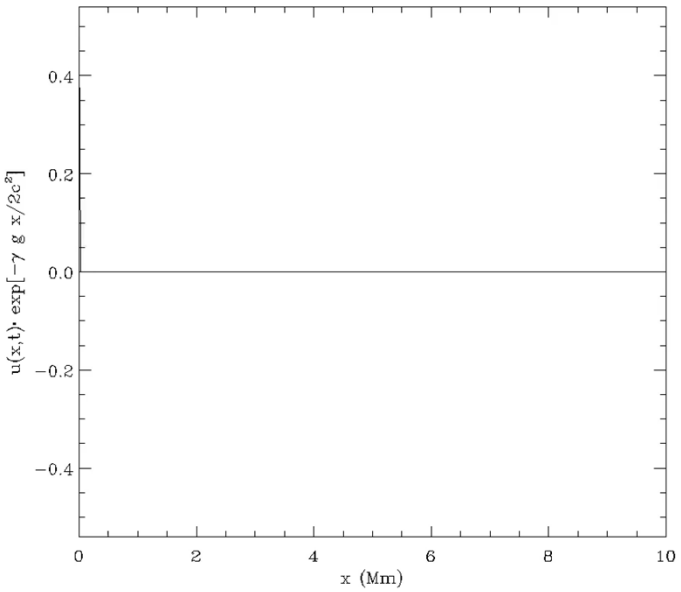

Time-distance diagram of atmospheric waves

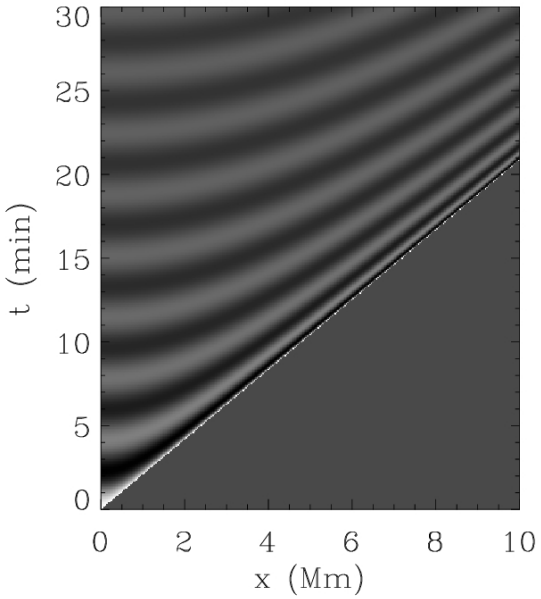

c=8 km/s
$g=2.74 \times 10^4$ cm/s^2
$\gamma=5/3$

Physical interpretation of acoustic cut-off frequency

The acoustic waves propagate only when their frequency is higher than the acoustic cut-off frequency:

$$\omega_c = \frac{c}{2H}$$

where H is the density scale height:

$$H = -\left(\frac{d\log\rho}{dr}\right)^{-1}$$

Consider a high-frequency acoustic wave with frequency ω and wavenumber k. In this case, from the wave dispersion relation we have:

$$k = \frac{\omega}{c}$$

The corresponding wavelength is:

$$\lambda = \frac{2\pi}{\omega}c$$

When $\omega > \omega_c$:

$$\lambda < \lambda_c = \frac{2\pi c}{\omega_c} = 4\pi H$$

This means that the acoustic waves propagate if their wavelength is substantially shorter than the density scale height. For the waves with shorter wavelength, the background density and pressure substantially decrease on the scale of a wavelength, so that the wave compression becomes insufficient for building the pressure restoring force and maintaining the wave propagation.

Phase and group velocities

Consider the acoustic wave dispersion relation:

$$\omega^2 = \omega_c^2 + k^2c^2$$

The phase velocity:

$$v_{ph} = \frac{\omega}{k} = \frac{\sqrt{\omega_c^2 + k^2c^2}}{k}$$

Substituting $k = \frac{\sqrt{\omega^2 - \omega_c^2}}{c}$ we obtain:

$$v_{ph} = \frac{\omega c}{\sqrt{\omega^2 - \omega_c^2}}$$

We find that if $\omega \gg \omega_c$ then $v_{ph} = c$, and if $\omega \to \omega_c$ then $v_{ph} \to \infty$.

The wave group velocity:

$$v_{gr} = \frac{\partial\omega}{\partial k} = \frac{k}{\omega}\frac{\partial\omega^2}{\partial k^2} = \frac{k}{\omega}c^2 = \frac{c^2}{v_{ph}}$$

$$v_{gr} = \frac{\sqrt{\omega^2 - \omega_c^2}}{\omega}c$$

We find that if $\omega \gg \omega_c$ then $v_{gr} = c$, if $\omega \to \omega_c$ then $v_{gr} \to 0$.

Interpretation of the lower turning point of acoustic waves in the Sun

The dispersion relation for acoustic (p) modes is:

$$k_r^2 = \frac{\omega^2 - \omega_c^2}{c^2} - \frac{S_l^2}{c^2}$$

where $S_l = \frac{Lc}{r}$, $L^2 = l(l+1)$.

$$\omega^2 = \omega_c^2 + k_r^2 c^2 + S_l^2$$

In terms of the horizontal wavenumber:

$$k_h = \frac{S_l}{c} = \frac{L}{r} = \frac{\sqrt{l(l+1)}}{r}$$

the dispersion relation:

$$\omega^2 = \omega_c^2 + k_r^2 c^2 + k_h^2 c^2 = \omega_c^2 + k^2 c^2$$

where $k^2 = k_r^2 + k_h^2$ is the total wavenumber.

At the lower turning point of acoustic modes $\omega_c \ll \omega$, and the dispersion relation is: $\omega^2 \approx k_r^2 c^2 + S_l^2$. The wave propagates where $k_r > 0$, and the lower turning point is where $k_r = 0$, that is $\omega = S_l$. The horizontal component of the phase velocity at this point:

$$v_{ph}^h = \frac{\omega}{k_h} = \frac{S_l}{k_h} = c(r)$$

At the lower turning point, the horizontal phase speed is equal to the local sound speed.

Low-degree p-modes (l=0,1,2, and 3)

For $l << n$, $r_1 \approx 0$, and we get: $\omega \approx \frac{\pi(n + L/2 + \alpha)}{\int_0^R \frac{dr}{c}}$.

That is the spectrum of low-degree p-modes is approximately equidistant with frequency spacing: $\Delta\nu = \left(4\int_0^R \frac{dr}{c}\right)^{-1}$. $\nu_{nl} \approx \Delta\nu(2n + l + 1/2 + 2\alpha) \approx \Delta\nu(2n + l + 3/2)$

Large frequency separation: $\Delta\nu$=68 μHz

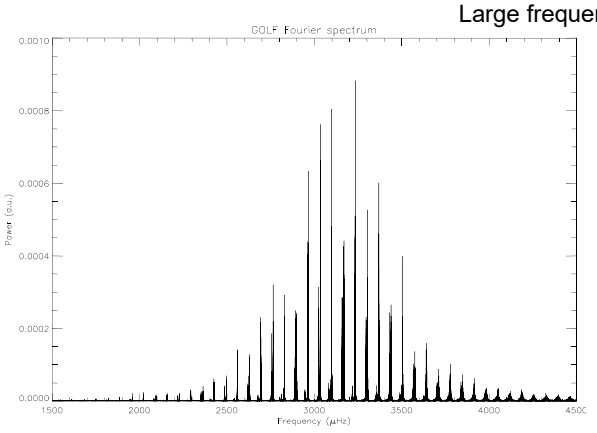

$$\delta\nu_{nl} = \nu_{nl} - \nu_{n-1,l+2} \approx$$

$$\approx -(4l+6)\frac{\Delta_{nl}}{2\pi^2 \nu_{nl}} \int_0^{R_\odot} \frac{dc}{dr}\frac{dr}{r}$$

Small frequency separation : $\delta\nu$=9μHz

Solar -modes from 1979 days of the GOLF experiment, B. Gelly - M. Lazrek- G. Grec - A. Ayad - F. X. Schmider- C. Renaud - D. Salabert - E. Fossat· A&A 394, 285-297 (2002)

Low-degree p-modes

Consider acoustic modes (p-modes) of low angular degree $\ell = 0,1,2,$ and 3. These oscillations modes are observed in oscillations of the Sun as a star, and often called global oscillation modes.

We start from the JWKB equation for the p-mode frequencies.

$$\int_{r_1}^{R} k_r dr = \pi(n+\alpha)$$

where r_1 is the radius of the lower turning point of the oscillation modes, which is determined from the equation: $k_r = 0$, or

$$\frac{\omega^2}{c(r_1)^2} = \frac{L^2}{r_1^2}$$

. For the low-degree modes, the turning point is located close to the solar center, so that $r_1 / R \ll 1$. Assuming that the sound speed is constant near the center of the Sun: $c(r_1) \approx c_0$, where c_0 is the sound speed at the solar center. Therefore, $r_1 \approx \frac{Lc_0}{\omega}$.

In this case, we can calculate the p-mode frequencies by transforming the JWKB integral

$$\int_{r_1}^{R} \sqrt{\frac{\omega^2}{c^2} - k_h^2}\, dr = \omega \int_{r_1}^{R} \sqrt{1 - \frac{L^2 c^2}{\omega^2 r^2}}\, \frac{dr}{c} = \omega I_1$$

in the following way:

$$I_1 = \int_{r_1}^{R} \frac{dr}{c} - \int_{r_1}^{R} \frac{dr}{c} + \int_{r_1}^{R} \sqrt{1 - \frac{L^2 c^2}{\omega^2 r^2}}\, \frac{dr}{c} =$$

$$= \int_0^R \frac{dr}{c} - \int_0^{r_1} \frac{dr}{c} - \int_{r_1}^{R} \left[1 - \sqrt{1 - \frac{L^2 c^2}{\omega^2 r^2}} \right] \frac{dr}{c}$$

We estimate the second integral as:

$$\int_0^{r_1} \frac{dr}{c} \approx \frac{r_1}{c_0} \approx \frac{L}{\omega}$$

The integrand of the third integral is substantially different from zero only in the vicinity of the turning point, where we assume $c(r) \approx c_0$. Substituting r with $x = r / r_1$ and $Lc / \omega = r_1$, we obtain:

$$\int_{r_1}^{R} \left[1 - \sqrt{1 - \frac{L^2 c^2}{\omega^2 r^2}} \right] \frac{dr}{c} \approx \int_{r_1}^{R} \left[1 - \sqrt{1 - \frac{r_1^2}{r^2}} \right] \frac{dr}{c_0} \approx$$

$$\approx \frac{r_1}{c} \int_1^{\infty} \left[1 - \sqrt{1 - \frac{1}{x^2}} \right] dx = \frac{r_1}{c_0} \frac{1}{2} (\pi - 2) = \frac{L}{\omega} \left(\frac{\pi}{2} - 1 \right)$$

where, in the upper limit, we replaced R / r_1 with infinity.
Thus,

$$I_1 \approx \int_0^R \frac{dr}{c} - \frac{L}{\omega} - \frac{L}{\omega} \left(\frac{\pi}{2} - 1 \right) = \int_0^R \frac{dr}{c} - \frac{L}{\omega} \frac{\pi}{2}$$

Then, from the equation for p-mode frequencies,

$$\omega I_1 = \pi (n + \alpha)$$

we find:

$$\omega \int_0^R \frac{dr}{c} \approx \pi \left(n + \frac{L}{2} + \alpha \right)$$

Approximating

$$\frac{L}{2} = \frac{\sqrt{l(l+1)}}{2} \approx \frac{l + 1/2}{2}$$

the frequencies ω_{nl} of the oscillation modes of angular degree l and radial order n are:

$$\omega_{nl} \approx \frac{\pi (n + l/2 + 1/4 + \alpha)}{\int_0^R \frac{dr}{c}}.$$

The corresponding cyclic frequencies:

$$\nu_{nl} = \frac{\omega_{nl}}{2\pi} = \frac{n + l/2 + 1/4 + \alpha}{2\int_0^R \frac{dr}{c}} = \Delta\nu(2n + l + 1/2 + \alpha)$$

where

$$\Delta\nu = \frac{1}{4\int_0^R \frac{dr}{c}} \equiv 1/T,$$

is equal to the inverse time for the acoustic waves travel through the center of the Sun to the antipodal point on the far side of the Sun and come back to the front side.

This equation shows that in the low-degree p-mode frequencies are approximately equidistant, and separated by $\Delta\nu$, which is called 'the large frequency separation'. For the Sun, $\Delta\nu \approx 68\ \mu$Hz.

It also shows that in the first order: $\nu_{nl} \approx \nu_{n-1,l+2}$. In the next order of approximation this frequencies are separated by:

$$\nu_{nl} = \nu_{nl} - \nu_{n-1,l+2} \approx -(4l+6)\frac{\Delta\nu}{2\pi^2\nu_{nl}}\int_0^R \frac{dc}{dr}\frac{dr}{r} \approx 9\ \mu\text{Hz}$$

which is called 'the small frequency separation', which primarily depends on the gradient of the sound speed in the central regions of the Sun.

The large and small frequency separations are among the primary tools of asteroseismology.

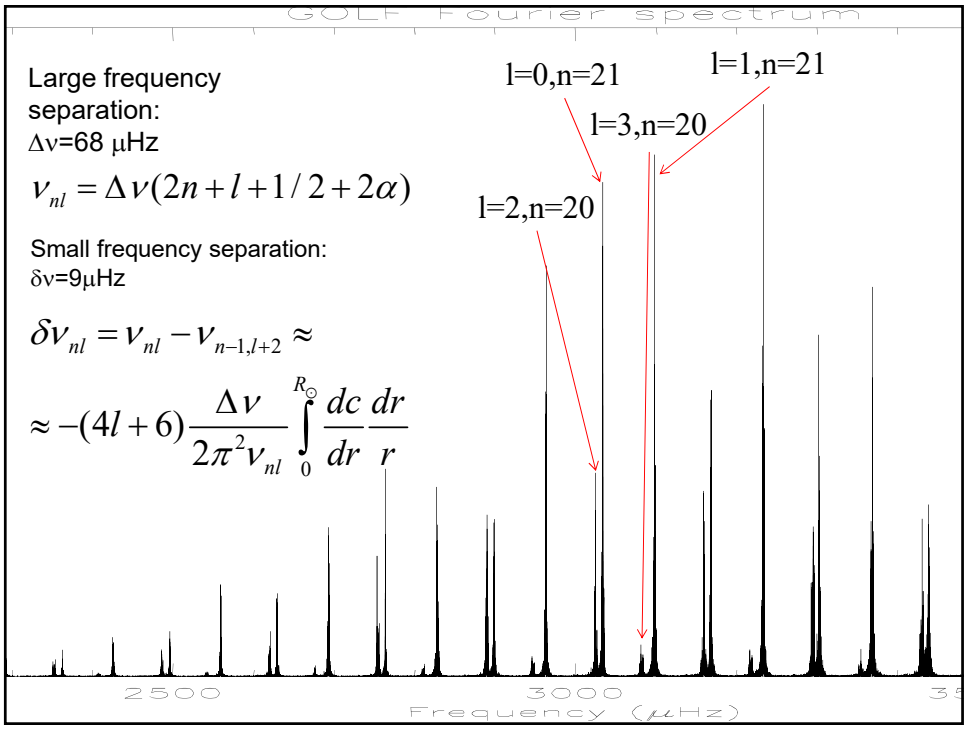

Frequency table for *l*=0, 1, 2, and 3 with associated error bars. Frequencies listed in here are the average of determinations over 16-month data span. Above 4400 μHz, and *l*=0 and 2 cannot be separated clearly.

n	ℓ_0	σ_0	ℓ_1	σ_1	ℓ_2	σ_2	ℓ_3	σ_3
16							2541.55	± 0.07
17			2559.20	± 0.04	2619.64	± 0.04	2676.22	± 0.06
18	2629.72	± 0.04	2693.38	± 0.04	2754.39	± 0.04	2811.48	± 0.06
19	2764.17	± 0.04	2828.15	± 0.04	2889.57	± 0.04	2947.00	± 0.05
20	2899.05	± 0.04	2963.29	± 0.04	3024.71	± 0.05	3082.24	± 0.06
21	3033.77	± 0.03	3098.14	± 0.05	3159.84	± 0.04	3217.84	± 0.06
22	3168.65	± 0.04	3233.10	± 0.04	3295.06	± 0.05	3353.54	± 0.10
23	3303.39	± 0.04	3368.48	± 0.06	3430.75	± 0.09	3489.51	± 0.09
24	3439.02	± 0.05	3503.89	± 0.07	3566.68	± 0.12	3625.99	± 0.20
25	3574.68	± 0.09	3640.22	± 0.08	3702.84	± 0.14	3763.11	± 0.32
26	3710.75	± 0.12	3776.40	± 0.11	3839.11	± 0.21	3900.44	± 0.48
27	3846.79	± 0.17	3913.03	± 0.13	3976.41	± 0.26	4037.02	± 0.60
28	3984.45	± 0.22	4049.91	± 0.16	4114.13	± 0.29	4174.46	± 0.96
29	4121.30	± 0.34	4187.18	± 0.20	4249.90	± 0.33	4312.98	± 1.04
30	4259.77	± 0.34	4325.71	± 0.25	4389.30	± 0.37	4454.11	± 1.83
31	4397.43	± 0.60	4462.00	± 0.39	4525.71	± 0.65[1]		
32	4534.65	± 0.70[1]	4599.03	± 0.33	4663.86	± 0.65[1]		
33	4675.52	± 0.95[1]	4737.61	± 0.40	4806.45	± 1.70[1]		
34	4808.60	± 3.96[1]	4875.75	± 0.59	4944.88	± 0.81[1]		
35	4955.59	± 2.31[1]	5016.82	± 0.82				
36	5086.18	± 0.98[1]	5157.08	± 1.10				
37	5230.68	± 1.23[1]	5308.08	± 2.22				
38	5371.29	± 2.59[1]	5452.50	± 3.66				

Asteroseismology

Bedding & Kjeldsen (2003)

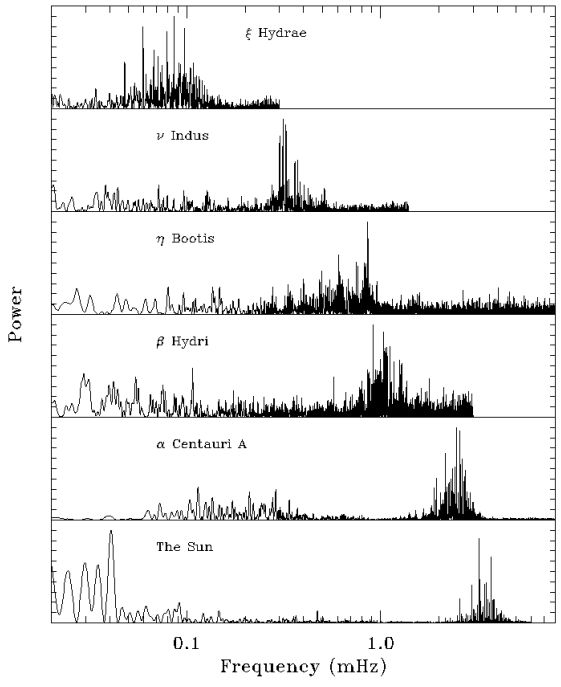

Asteroseismic calibration of stellar masses and ages

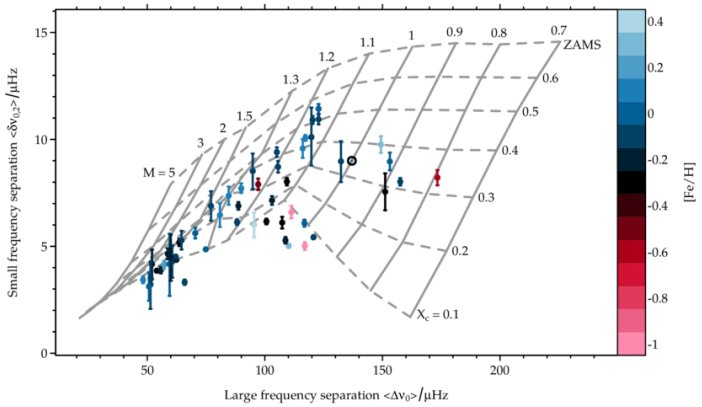

Small frequency separations against large frequency separations with [Fe/H] abundance indicated by color for 52 main-sequence Kepler LEGACY stars overplotted on top of evolutionary models varied in mass and core hydrogen abundance.

(Bellinger et al 2017)

Lecture 10

Properties of high-degree p- and f-modes

(Stix, Chapter 5.2; Kosovichev, p.29-34;
Christensen-Dalsgaard, Chapters 5.2, 7)

The nature of solar oscillations

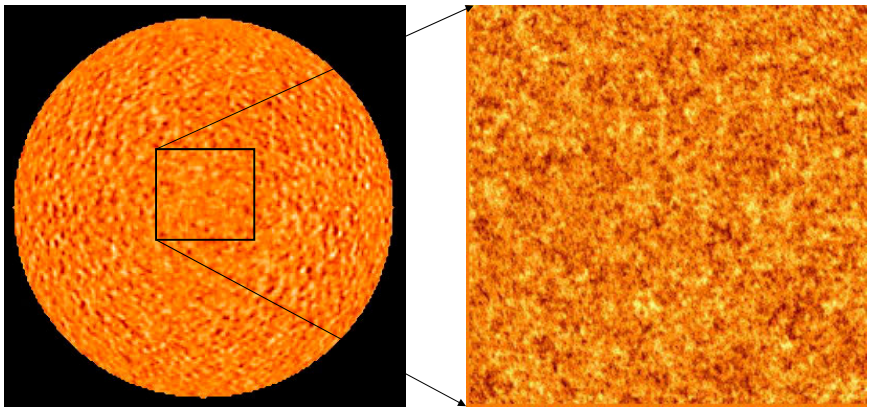

Acoustic and surface gravity waves stochastically excited by turbulent convection in the upper convection zone.

Spherical harmonic transform

For the global oscillations we must use the spherical coordinates $(r,\square\!\!\square)$ and expansion in terms of spherical surface harmonics:

$$v(\theta,\phi,t)=\sum_{l=0}^{\infty}\sum_{m=-l}^{l}a_{lm}(t)Y_l^m(\theta,\phi)$$

In the spherical coordinates, θ,ϕ:

$$a(l,m,\omega)=\iiint v(\theta,\phi,t)Y_l^m(\theta,\phi)e^{i\omega t}d\theta d\phi dt,$$

where $Y_l^m(\theta,\phi)=P_l^{|m|}(\theta)e^{im\phi}$ is a spherical harmonic of **the angular degree** l **and angular order** m, $P_l^m(\theta)$ is an associate Legendre function.

Degree l gives the total number of node circles on the sphere; order m is the number nodal circles through the poles.

Spherical harmonic power spectrum

The coefficients of the spherical harmonic expansion can be found by using the spherical harmonic transform:

$$a(l,m,\omega)=\iiint v(\theta,\phi,t)Y_l^m(\theta,\phi)e^{i\omega t}d\theta d\phi dt,$$

where $Y_l^m(\theta,\phi)$ is a spherical harmonic of **the angular degree** l **and angular order** m.

The power spectrum is:

$$P(l,m,\omega)=a^*a.$$

For a spherically symmetrical star, P depends only on l and ω.
In this case the power spectrum is 'degenerate' with respect of angular order m.

Then we can define the analog of the horizontal wavenumber:

$k_h=\dfrac{\sqrt{l(l+1)}}{R}$, where R is the solar radius.

Oscillation power spectrum

- The power spectrum represents the oscillation signal in terms of spherical harmonics of **angular degree** l (and the **horizontal wavelength**, $\lambda_h = 2\pi/k_h$), and the oscillation **"cyclic" frequency**, $\nu=\omega/2\pi$.

  l is integer number

  λ_h is measured in Mm

  ν is measured in mHz

  ω is measured in rad/sec

  (sometimes called angular frequency)

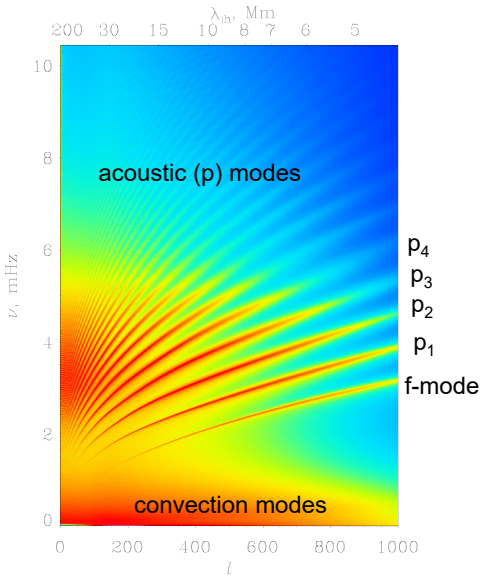

Low-degree p-modes (l=0,1,2, and 3)

For $l << n$, $r_1 \approx 0$, and we get: $\omega \approx \dfrac{\pi(n + L/2 + \alpha)}{\int_0^R \frac{dr}{c}}$.

That is the spectrum of low-degree p-modes is approximately equidistant with frequency spacing: $\Delta\nu = \left(4\int_0^R \frac{dr}{c}\right)^{-1}$. $\nu_{nl} \approx \Delta\nu(2n + l + \frac{1}{2} + 2\alpha) \approx \Delta\nu(2n + l + \frac{3}{2})$

Large frequency separation: $\Delta\nu$=68 μHz

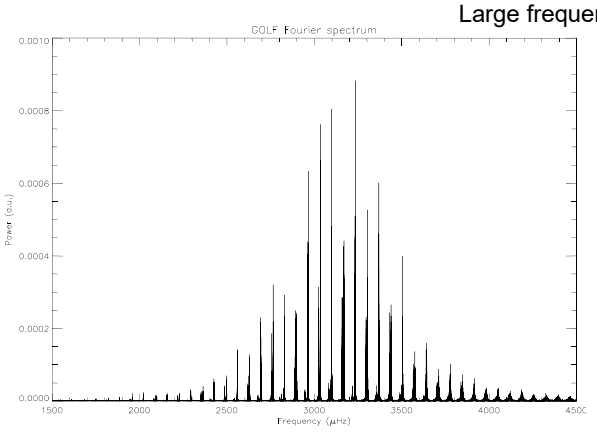

$$\delta\nu_{nl} = \nu_{nl} - \nu_{n-1,l+2} \approx$$

$$\approx -(4l + 6)\frac{\Delta_{nl}}{2\pi^2\nu_{nl}} \int_0^{R_\odot} \frac{dc}{dr}\frac{dr}{r}$$

Small frequency separation : $\delta\nu$=9μHz

Solar -modes from 1979 days of the GOLF experiment, B. Gelly - M. Lazrek- G. Grec - A. Ayad - F. X. Schmider- C. Renaud - D. Salabert - E. Fossat· A&A 394, 285-297 (2002)

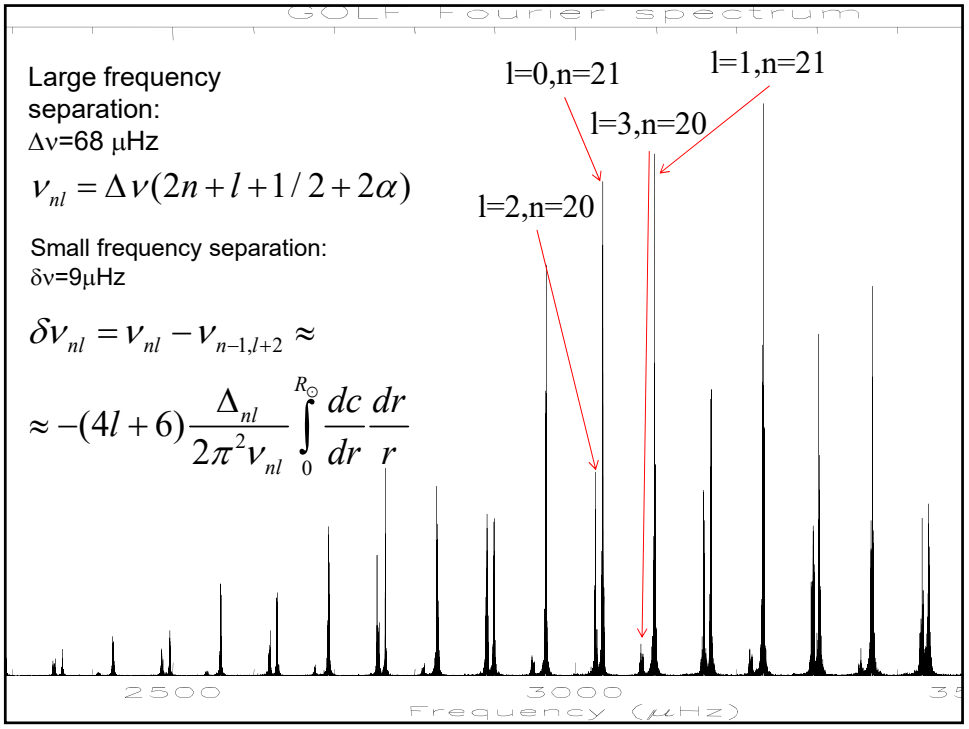

Theoretical *l*-ν diagram: numerical solution of the oscillation equations

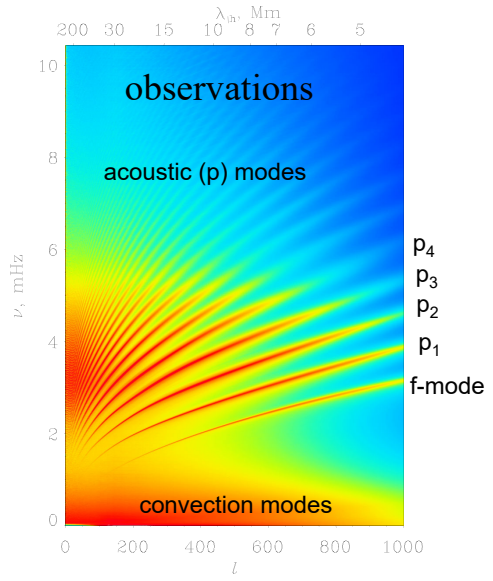

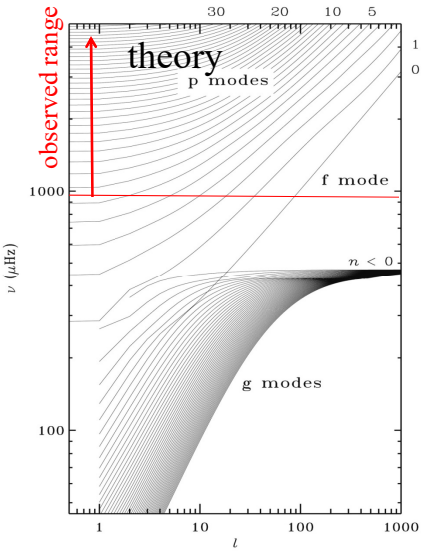

Normal modes of solar oscillations

The frequencies of normal modes are determined for the Borh quantization rule (resonant condition): $\int_{r_1}^{r_2} k_r dr = \pi(n+\alpha),$

where r_1 and r_2 are the radii of the turning points where k_r=0, n is a radial order -integer number, and α is a phase shift which depends on properties of the reflecting boundaries.

$$k_r^2 = \frac{\omega^2 - \omega_c^2}{c^2} + \frac{S_l^2}{c^2\omega^2}\left(N^2 - \omega^2\right)$$

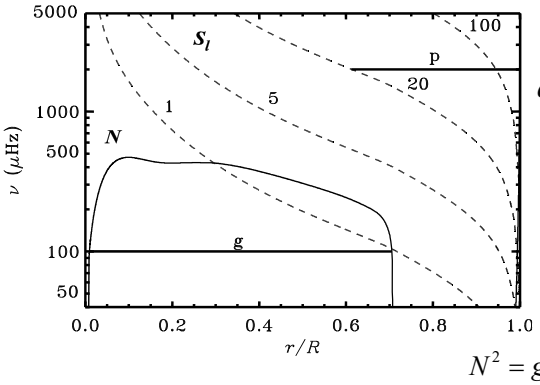

$c(r)$ is the sound speed

$\omega_c = \frac{c}{2H}$ is the acoustic cut-off frequency; it has very sharp increase at r/R=1

$$H = \left(\frac{d\log\rho}{dr}\right)^{-1},$$

$$S_l^2 = \frac{L^2c^2}{r^2} \qquad L^2 = l(l+1)$$

$$N^2 = g\left(\frac{1}{\gamma P}\frac{dP}{dr} - \frac{1}{\rho}\frac{d\rho}{dr}\right) \equiv g/H - g^2/c^2$$

Properties of Solar Oscillation Modes. I

Equation $$k_r^2 = \frac{\omega^2 - \omega_c^2}{c^2} + \frac{S_l^2}{c^2\omega^2}\left(N^2 - \omega^2\right)$$

represents **dispersion relation of solar oscillations**.

It relates frequency ω with radial wavenumber k_r and angular order l.

Consider two cases:

1: p-modes (acoustic modes): the high-frequency case. If $\omega^2 >> N^2$ then

$$k_r^2 = \frac{\omega^2 - \omega_c^2}{c^2} - \frac{S_l^2}{c^2}$$

or $$\omega^2 = \omega_c^2 + k_r^2c^2 + k_h^2c^2,$$

where $k_h = S_l/c \equiv \frac{L}{r} \equiv \frac{\sqrt{l(l+1)}}{r}$ is **the horizontal wave number**.

Then, $k^2 = k_r^2 + k_h^2$ is the squared total wavenumber.

Finally, $\omega^2 = \omega_c^2 + k^2c^2$, where $\omega_c = \frac{c}{2H}$ is the acoustic cut-off frequency.

This is **the dispersion relation for acoustic (p) modes**; ω_c **is the acoustic cutoff frequency. Physically, the waves with frequencies below the acoustic cutoff frequency cannot propagate. Their wavelength becomes shorter than the density scale height. For the Sun** $\nu_c \equiv \omega_c/2\pi \approx 5$ *mHz*. **(c~10 km/s, H~150km).**

Calculation of p-mode frequencies

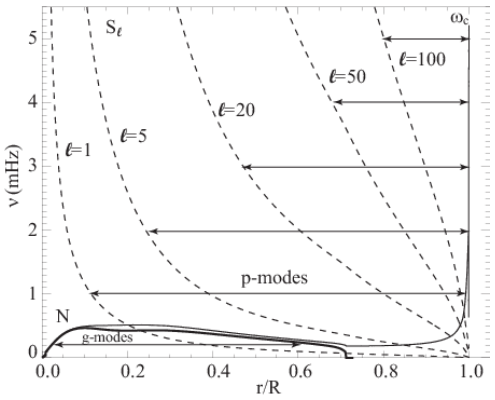

Wave propagation region: $k_r^2 > 0$

Turning points are determined from equation $k_r^2 = 0$:

$$\omega^2 = \omega_c^2 + \frac{L^2 c^2}{r^2}.$$

For the lower turning point in the interior: $\omega_c << \omega$.

Then, $\omega \approx \frac{Lc}{r}$, or $\frac{c(r_1)}{r_1} = \frac{\omega}{L}$ is the equation for the lower turning point.

The upper turning point: $\omega_c(r_2) \approx \omega$. Since $\omega_c(r)$ is a steep function of r near the surface, $r_2 \approx R$.

Then, the resonant condition for p-modes is: $\int_{r_1}^{R} \sqrt{\frac{\omega^2}{c^2} - \frac{L^2}{r^2}}\, dr = \pi(n + \alpha)$

High-degree modes (l >>1)

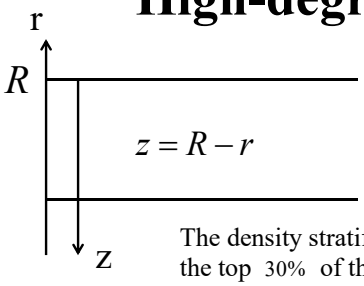

The wave propagation region is a shallow subsurface layer.
We consider it as a plane-parallel layer of depth z.

The density stratification in the convection zone that occupies the top 30% of the Sun's interior is almost adiabatic:

$$P(z) = A\rho(z)^\gamma$$

where A is a constant.

Using the equation for hydrostatic equilibrium: $\frac{dP}{dz} = g\rho$ we obtain:

$$\rho^{\gamma-1}\frac{d\rho}{dz} = \frac{g\rho}{A\gamma}$$

$$\rho(z)^{\gamma-1} = \frac{gz}{A}\frac{(\gamma-1)}{\gamma} \quad \Rightarrow \quad \rho(z) = \left(\frac{gz}{A}\frac{(\gamma-1)}{\gamma}\right)^{1/(\gamma-1)}$$

Then, temperature $T(z) = \frac{\mu P}{R_G \rho} = \frac{\mu A}{R_G}\rho^{\gamma-1} = \frac{\mu(\gamma-1)g}{R_G\gamma}z$,

where R_G is the gas constant.

The sound speed: $c^2 = \frac{\gamma R_G T}{\mu} = (\gamma - 1) g z$.

Calculation of mode frequencies ($z = R - r$):

$$-\int_{z_1}^{0} k_r dz = \pi (n + \alpha)$$

where $k_r^2 = \frac{\omega^2}{c^2} - k_h^2$ and $k_h \approx \frac{l(l+1)}{R^2}$.

Find the depth of the lower turning point ($k_r^2 = 0$):

$$z_1 = \frac{\omega^2 R^2}{(\gamma - 1) g l (l+1)}.$$

Calculate the integral:

$$-\int_{z_1}^{0} \sqrt{\frac{\omega^2}{(\gamma-1)gz} - \frac{l(l+1)}{R^2}}\, dz = \frac{\pi \omega^2 R}{2(\gamma-1)g\sqrt{l(l+1)}} = \pi(n+\alpha)$$

Then, the frequencies of high-degree modes ($l \gg 1$) are:

$$\omega_{ln}^2 = \frac{2(\gamma-1)g}{R}\sqrt{l(l+1)}(n+\alpha) = 2(\gamma-1)g k_h (n+\alpha)$$

This explains the parabolic shape of the p-mode ridges in the power spectrum ($l - \nu$ diagram):

$$\omega_{nl}^2 \propto l \quad \text{or} \quad \omega_{nl} \propto l^{1/2}$$

Power spectra of $l = 200$ modes obtained from SOHO/MDI observations of **a)** Doppler velocity, **b)** continuum intensity.

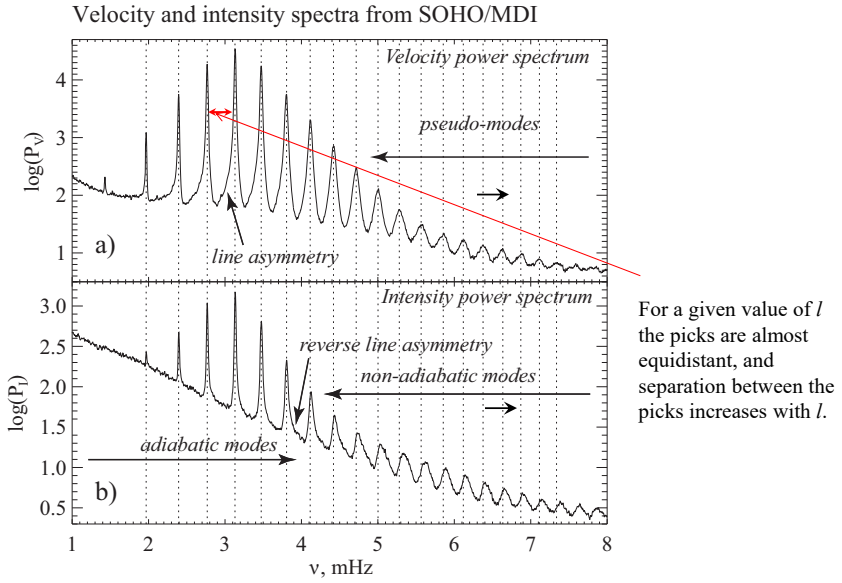

For a given value of l the picks are almost equidistant, and separation between the picks increases with l.

Surface gravity waves (f-mode)

At the visible surface of the Sun (the photosphere), the density drops so fast that the photosphere can be considered as a free surface of the Sun, without a substantial external force. This means that the Lagrangian pressure variations on the surface: $\delta P = 0$.

The oscillations associated with the free surface are called 'surface gravity waves', and the corresponding normal oscillation modes are called f-mode (or 'fundamental mode'). The surface gravity waves are similar to ocean waves. The frequencies and the penetration depth of these waves depend on the horizontal wavenumber.

To describe the surface gravity waves, we consider the general oscillation equations in the Cowling approximation:

$$\frac{d\xi_r}{dr} + \frac{2}{r} - \frac{g}{c^2}\xi_r + \left(1 - \frac{L^2c^2}{r^2\omega^2}\right)\frac{P'}{\rho c^2} = 0$$

$$\frac{dP'}{dr} + \frac{g}{c^2}P' + \left(N^2 - \omega^2\right)\rho\xi_r = 0$$

and replace the Eilerian pressure variations P', with the Lagrangian variations, δP:

$$\delta P = P' + \xi_r \frac{dP}{dr} = P' - \xi_r \rho g$$

Near the surface, $r \sim R$, $g \sim$ const.

Substituting $P' = \delta P + \rho g \xi_r$,

$$\frac{d\xi_r}{dr} + \frac{2}{r}\xi_r - \frac{g}{c^2}\xi_r + \left(1 - \frac{L^2c^2}{r^2\omega^2}\right)\frac{\delta P + \rho g \xi_r}{\rho c^2} = 0$$

Neglecting the sphericity term $\frac{2}{r}\xi_r$ we obtain:

$$\frac{d\xi_r}{dr} - \frac{L^2 g}{r^2\omega^2}\xi_r + \left(1 - \frac{L^2c^2}{r^2\omega^2}\right)\frac{\delta P}{\rho c^2} = 0$$

Substituting P', $N^2 = g\left(\frac{1}{\gamma P}\frac{dP}{dr} - \frac{1}{\rho}\frac{d\rho}{dr}\right)$ and $\frac{dP}{dr} = -g\rho$, in the second equation:

$$\frac{dP'}{dr} + \frac{g}{c^2}P' + \left(N^2 - \omega^2\right)\rho\xi_r = 0$$

we obtain:

$$\frac{d\delta P}{dr} + g\xi_r\frac{d\rho}{dr} + g\rho\frac{d\xi_r}{dr} + \frac{g}{c^2}\delta P + \frac{g^2\rho}{c^2}\xi_r + g\frac{\rho}{\gamma P}\frac{dP}{dr}\xi_r - g\xi_r\frac{d\rho}{dr} - \omega^2\rho\xi_r = 0$$

After substitution of $\frac{d\xi_r}{dr}$ from the first equation:

$$\frac{d\delta P}{dr} + g\rho\frac{L^2 g}{r^2\omega^2}\xi_r - g\rho\left(1 - \frac{L^2c^2}{r^2\omega^2}\right)\frac{\delta P}{\rho c^2} + \frac{g}{c^2}\delta P - \omega^2\rho\xi_r = 0$$

Finally, we obtain the oscillation equations in terms of δP and ξ_r:

$$\frac{d\delta P}{dr}+\frac{L^2 g}{\omega^2 r^2}\delta P-\frac{g\rho}{r}\left(\frac{\omega^2 r}{g}-\frac{L^2 g}{\omega^2 r}\right)\xi_r=0$$

$$\frac{d\xi_r}{dr}-\frac{L^2 g}{r^2\omega^2}\xi_r+\left(1-\frac{L^2 c^2}{r^2\omega^2}\right)\frac{\delta P}{\rho c^2}=0$$

This system has a solution: $\delta P=0$ and $\xi_r\neq 0$, at the surface $r=R$ if

$$\frac{\omega^2 R}{g}-\frac{L^2 g}{\omega^2 R}=0$$

Thus, we find the f-mode frequencies:

$$\omega_l^2=\frac{Lg}{R}=k_h\cdot g=\frac{\sqrt{l(l+1)}g}{R}$$

. This is a dispersion relation for the surface gravity waves (f-modes) traveling at the solar surface.

The f-mode eigenfunctions can be found from the equation for ξ_r at $r\sim R$:

$$\frac{d\xi_r}{dr}-\frac{L^2 g}{R^2\omega^2}\xi_r=0$$

or

$$\frac{d\xi_r}{dr}-\frac{L}{R^2}\xi_r=0$$

The solution is:

$$\xi_r\propto e^{-\frac{L}{R}(R-r)}$$

The eigenfunctions exponentially decay with the depth. The characteristic penetration depth is: R/L (equal to the horizontal wavelength).

For high values of the angular spherical harmonic degree l, the f-modes are concentrated near the surface.

However, for low l they penetrate in the deep interior where they interact with the internal gravity waves, and their properties are calculated numerically.

Theoretical *l*-ν diagram: numerical solution of the oscillation equations

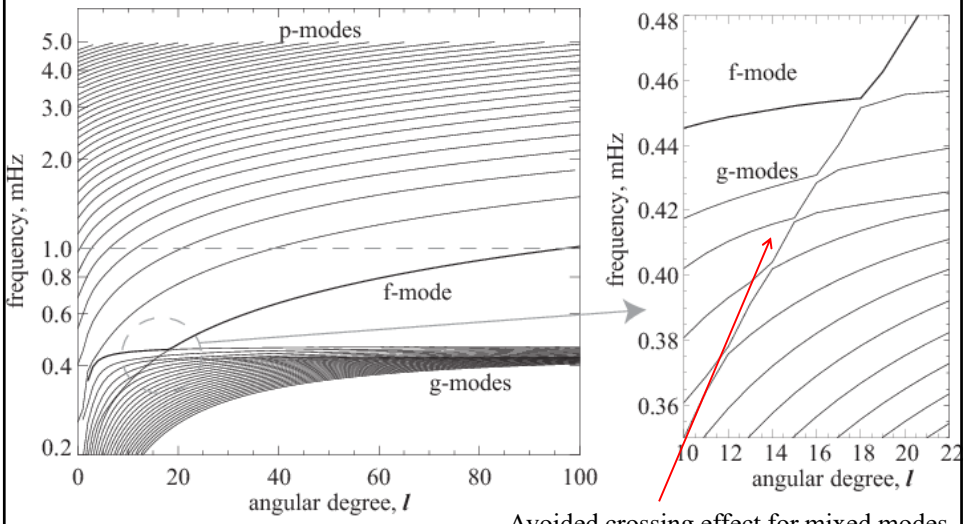

Avoided crossing effect for mixed modes

Seismic radius

The f-mode frequencies can be expressed in terms of the solar mass and radius:

$$\omega_l^2 = \sqrt{l(l+1)}\,\frac{g}{R} = \frac{Lg}{R}$$

where g is the gravity acceleration on the surface of the Sun:

$$g = \frac{GM}{R^2}$$

thus

$$\omega_l^2 = \frac{LGM}{R^3}$$

The value of GM is known with very high precision from interplanetary spacecraft orbits. The f-mode frequencies are determined from helioseismic measurements by fitting the f-mode lines in the oscillation power spectra for various values of angular degree l. Then, we can calculate the solar radius radius as:

$$R = \left(\frac{LGM}{\omega_l^2}\right)^{1/3}$$

ot in term of the cyclic frequencies $\nu_l = \omega_l / 2\pi$:

$$R = \left(\frac{LGM}{4\pi^2 \nu_l^2}\right)^{1/3}$$

Thus, the measurements of the f-mode frequencies allow us to estimate the solar radius, called 'the seismic solar radius'.

There is no sharp solar surface. The standard measurements of the solar radius are based on determining the locations of the inflection point in the solar brightness profile, which depends on the radiation bandwidth and the structure of the atmosphere.

The seismic radius provides the radius of the sharp density decrease at the surface. It can be directly compared with the solar models.

It turned out that the solar radius was overestimated by about 300 km. The deviations of the seismic radius from the model can be calculated from the perturbation equations:

$$\frac{\delta R}{R} = -<\frac{2}{3}\frac{\delta \nu_l}{\nu_l}>$$

This relation is also use to estimate the variations of the seismic radius during the solar activity cycles. However, evolving magnetic fields also affect the f-mode and their effects have to be taken into account.

Because the f-mode penetration depth depends on the mode angular degree, the f-mode measurements can be used for measuring the displacement of subsurface layers of Sun.

Measurements of the seismic radius relative to the standard solar model

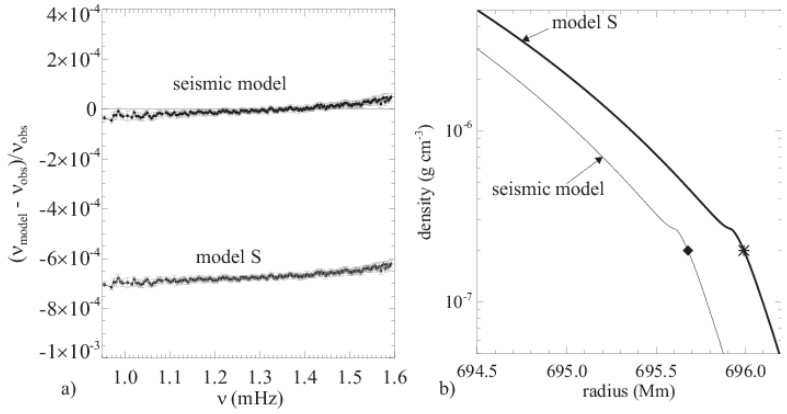

$$\frac{\Delta R}{R} = -\frac{2}{3}\frac{\Delta \nu}{\nu} \approx 4.4\times 10^{-4}$$

This means that the seismic radius is approximately equal to 695.68 Mm, which is about 0.3 Mm less than the standard radius, 695.99 Mm, used for calibrating the model calculation.

Cyclic Changes of the Sun's Seismic Radius

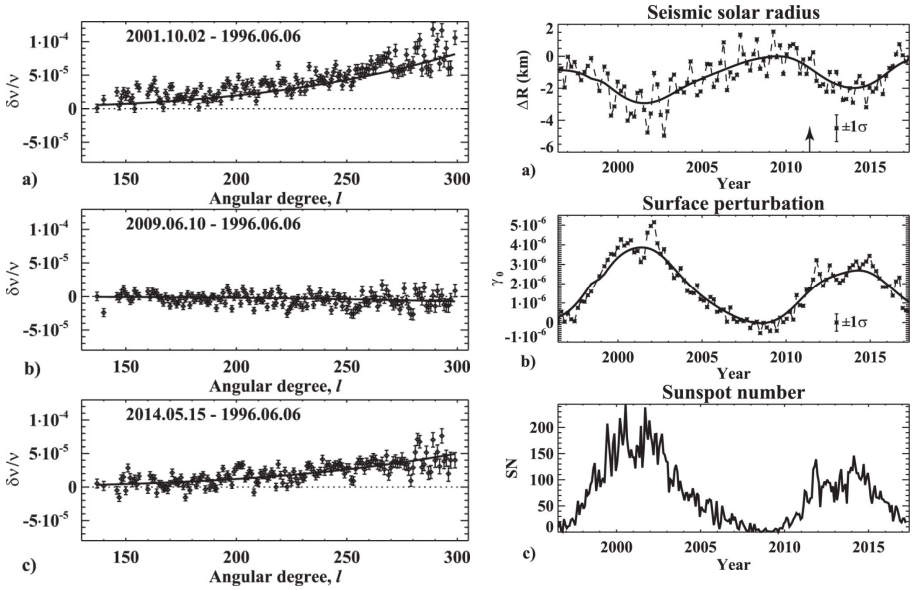

(Kosovichev & Rozelot, 2018)

Variations of the seismic radius at different depths: inversion of the f-mode frequencies

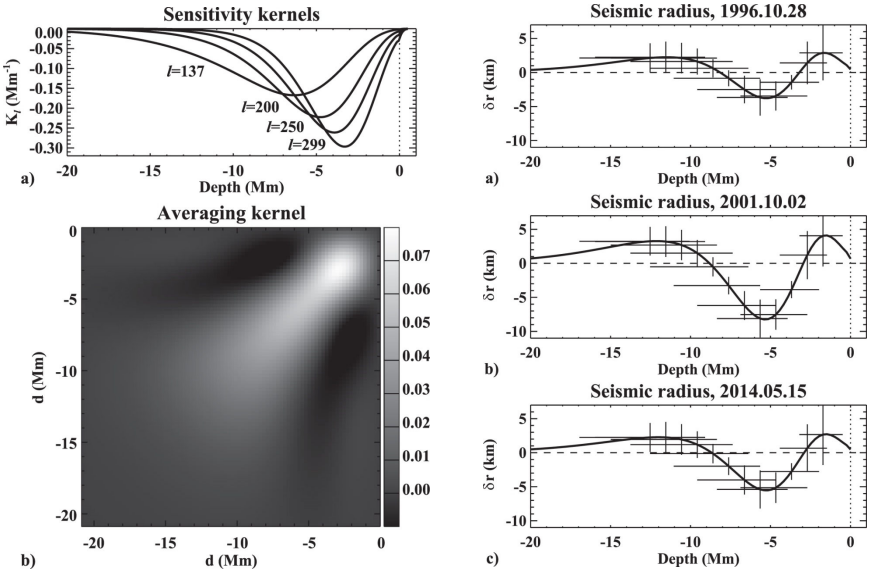

Variations of the seismic radius with time and depth

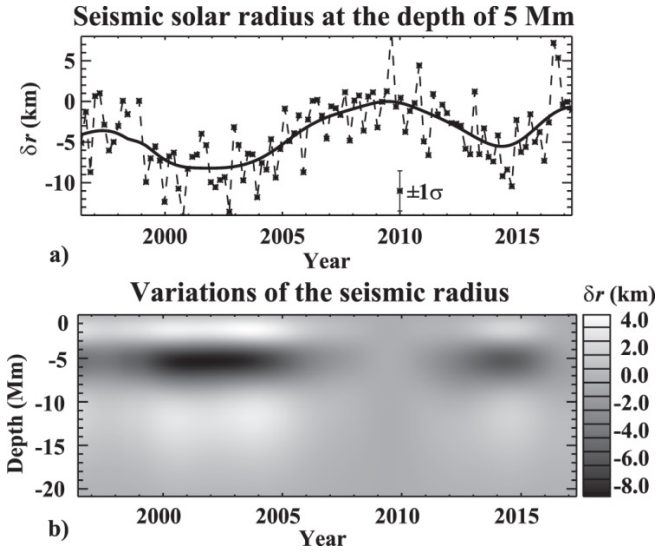

Lecture 11

Internal gravity waves and g-modes

Overview of the Asymptotic Theory.
JWKB (Jeffreys-Wentzel–Kramers–Brillouin) Solution

General idea of the JWKB approximation

Consider a second-order oscillation equation in a uniform medium without gravity: c=const, $\omega_c = 0$, $N = 0$.

$$\frac{d^2\Psi}{dr^2} + K^2\Psi = 0, \qquad \text{where } K^2 = \frac{\omega^2}{c^2}$$

For a one-dimensional potential well of the length R with infinite walls, the boundary conditions are: $\Psi = 0$ at $r = 0$ and $r = R$.
We seeks the solution in the form:

$$\Psi(r) = Ae^{\pm ikr}$$

Then, the solution satisfying the boundary conditions is:

$$\Psi(r) = A\sin(kr)$$

where $kR = \pi n$, n is an integer number.
Thus, we obtain the oscillation spectrum (eigenvalues):

$$\omega_n = \pi nc / R.$$

Then, we consider the wave equation with the coefficients varying with r:

$$\frac{d^2\Psi}{dr^2} + K^2(r)\Psi = 0$$

$$K^2(r) = \frac{\omega^2 - \omega_c^2}{c^2} - \frac{L^2}{r^2}\left(1 - \frac{N^2}{\omega^2}\right).$$

If $K(r)$ is a slowly varying function of r we can seek the solution in the form:

$$\Psi(r) = Ae^{iu(r)}$$

where $u(r)$ is a slowly varying function.We find $u(r)$ by substituting this form in the wave equation:

$$\frac{d\Psi}{dr} = i\frac{du}{dr}Ae^{iu(r)}$$

$$\frac{d^2\Psi}{dr^2} = i\frac{d^2u}{dr^2}Ae^{iu(r)} - \left(\frac{du}{dr}\right)^2 Ae^{iu(r)}$$

Because $u(r)$ is a slowly varying function, in the first approximation we neglect the first term in this expression. Substituting in the wave equation, we obtain:

$$-\left(\frac{du}{dr}\right)^2 Ae^{iu(r)} + K(r)^2 Ae^{iu(r)} = 0$$

$$\left(\frac{du}{dr}\right)^2 = K^2 \qquad \rightarrow \qquad \frac{du}{dr} = \pm K \quad \rightarrow \quad u(r) = \pm\int kdr$$

$$\Psi(r) = Ae^{\pm i\int kdr}$$

The eigenvalues are determined by matching the boundary conditions:

$$\int_{cavity} kdr = \pi(n+\alpha)$$

where α is a phase shift due to imperfectly reflecting boundary conditions.

The JWKB approximation is valid if $\left|\frac{1}{K}\frac{dK}{dr}\right| \ll 1$.

It can be improved considering A as a function of r.

JWKB solution

$$\xi_r(r) = A\rho^{-1/2}e^{\pm i\int k_r dr}$$

where $k(r)^2 = \frac{\omega^2 - \omega_c^2}{c^2} - \frac{L^2}{r^2}\left(1 - \frac{N^2}{\omega^2}\right)$

The wave propagation region is determined from $k(r) > 0$.

The resonant condition is:

$$\int_{r_1}^{r_2} k_r dr = \pi(n+\alpha)$$

$$\int_{r_1}^{r_2} \sqrt{\frac{\omega^2 - \omega_c^2}{c^2} - \frac{L^2}{r^2}\left(1 - \frac{N^2}{\omega^2}\right)}\, dr = \pi(n+\alpha)$$

Normal modes of solar oscillations

The frequencies of normal modes are determined for the Borh quantization rule (resonant condition): $\int_{r_1}^{r_2} k_r dr = \pi(n+\alpha),$

where r_1 and r_2 are the radii of the turning points where k_r=0, n is a radial order -integer number, and α is a phase shift which depends on properties of the reflecting boundaries.

$$k_r^2 = \frac{\omega^2 - \omega_c^2}{c^2} + \frac{S_l^2}{c^2\omega^2}\left(N^2 - \omega^2\right)$$

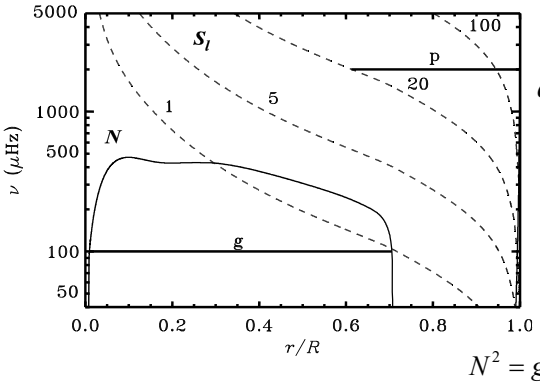

c(r) is the sound speed

$\omega_c = \frac{c}{2H}$ is the acoustic cut-off frequency; it has very sharp increase at r/R=1

$$H = \left(\frac{d\log\rho}{dr}\right)^{-1},$$

$$S_l^2 = \frac{L^2c^2}{r^2} \qquad L^2 = l(l+1)$$

$$N^2 = g\left(\frac{1}{\gamma P}\frac{dP}{dr} - \frac{1}{\rho}\frac{d\rho}{dr}\right) \equiv g/H - g^2/c^2$$

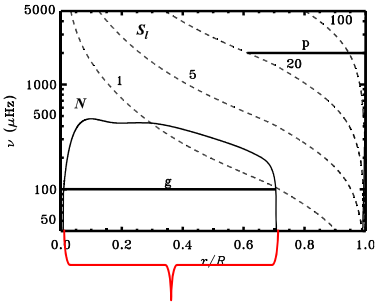

g-mode cavity

Internal gravity waves (g-modes)

The acoustic (p) waves propagate in the region where their frequency is greater than the Lamb and acoustic cutoff frequencies: $\omega > S_l$ and $\omega > \omega_c$.

where $S_l = \frac{Lc}{r} = \frac{\sqrt{l(l+1)}c}{r}$.

Consider low-frequency waves: $\omega \ll S_l$.

In this case, the second term in the dispersion equation is dominant:

$$k_r^2 \simeq \frac{S_l^2}{c^2\omega^2}\left(N^2 - \omega^2\right) = \frac{l(l+1)}{r^2\omega^2}\left(N^2 - \omega^2\right)$$

The propagation region region, $k_r^2 > 0$ is where $\omega < N$.

The wave turning points, $k_r^2 = 0$, are determined from the equation: $N(r_{1,2}) = \omega$.

Thus, the resonant condition is:

$$\frac{\sqrt{l(l+1)}}{\omega}\int_{r_1}^{r_2}\sqrt{N^2-\omega^2}\,\frac{dr}{r} = \pi(n+\alpha)$$

Assuming that far from the turning points, $\omega \ll N^2$, we obtain the resonant mode frequencies:

$$\omega_{nl} = \frac{\sqrt{l(l+1}}{\pi(n+\alpha)} \int_{r_1}^{r_2} N \frac{dr}{r}$$

These resonant modes are called internal gravity modes, or g-modes. They are driven by the buoyancy force. The g-mode are non-radial, $l \geq 1$.

The periods of the g-modes:

$$P_{nl} = \frac{2\pi}{\omega_{nl}} = \frac{\pi(n+\alpha)}{\sqrt{l(l+1)} \int_{r_1}^{r_2} N \frac{dr}{r}}$$

for a given l are equidistant in terms of the radial order, n. This property is often used for searching of g-modes in the noisy power spectra of solar oscillations, by performing a Fourier transform and searching for a signal corresponding to the period separation, or applying a 'comb' filter.

The frequency separation decreases for higher n values as $\Delta\omega \sim \frac{1}{n^2}$, forming a dense spectrum.

Theoretical *l*-ν diagram: numerical solution of the oscillation equations

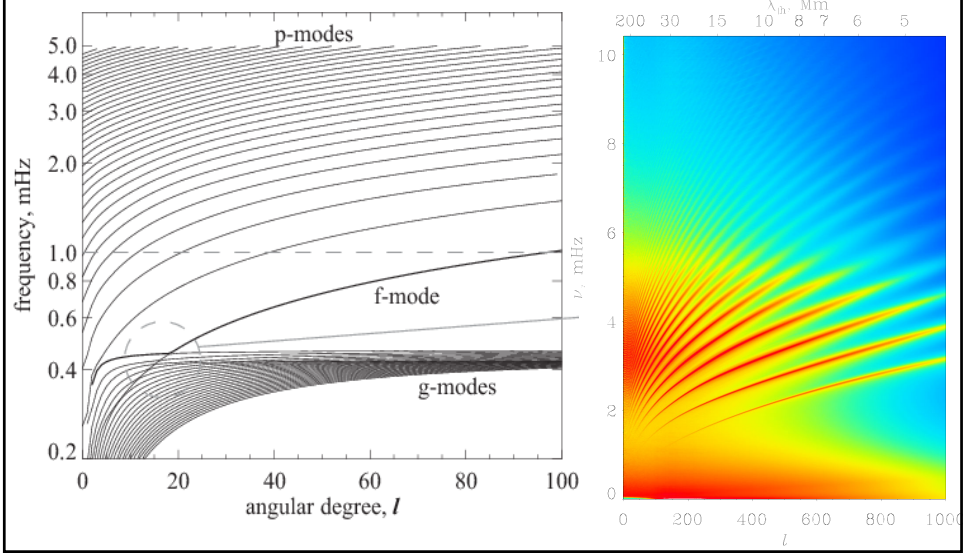

Theoretical *l*-ν diagram: numerical solution of the oscillation equations

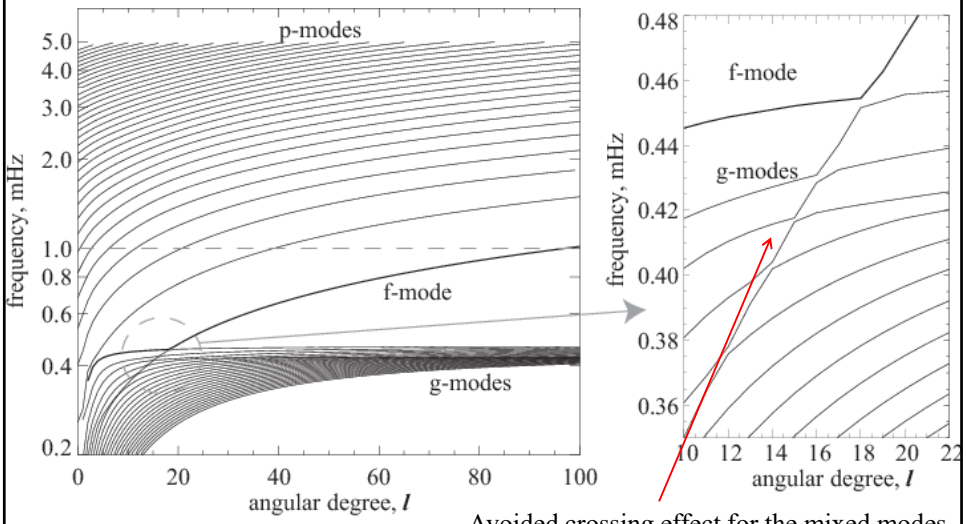

Avoided crossing effect for the mixed modes

Periods of solar oscillations

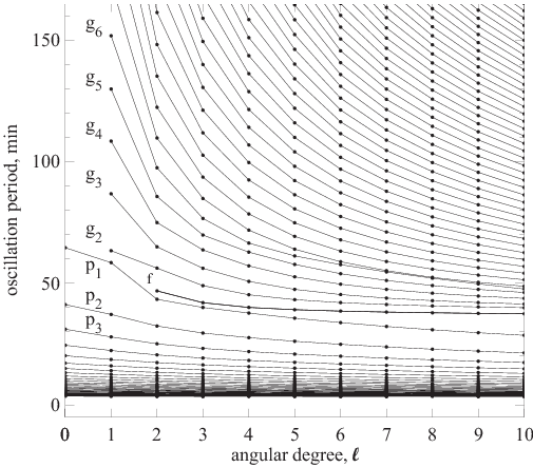

g-mode periods:

$$P_{nl} = \frac{2\pi}{\omega} = \frac{\pi(n+\alpha)}{L\int_{r_1}^{r_2} N\frac{dr}{r}}$$

$$P_{n+1,l} - P_{nl} = const$$

Spatial structure of p- and g-modes is obtained by multiplying the radial eigenfunctions by the corresponding spherical harmonics

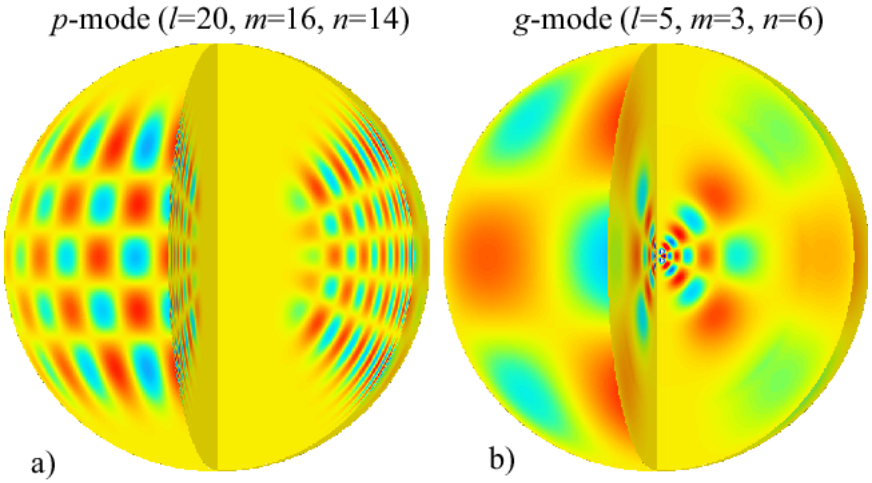

g-mode ray paths

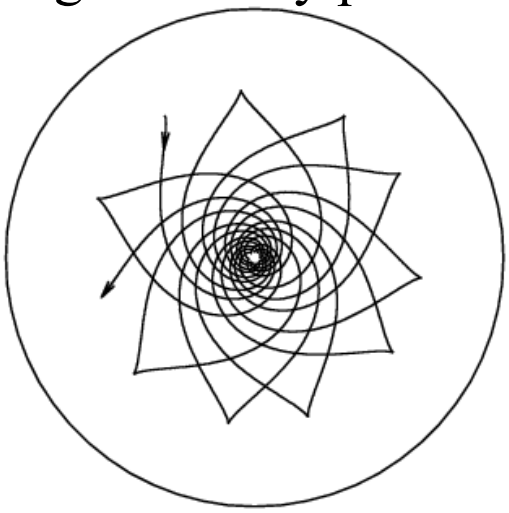

g-modes propagate only in the radiative zone which is convectively stable $N^2 > 0$

Simple description of internal gravity waves

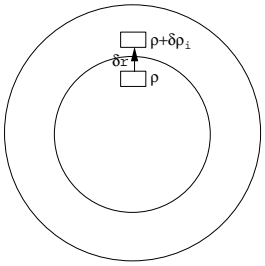

Consider a displacement, δr, of a small fluid element along the radius. If the density inside the displaced element, $\rho + \delta\rho_i$ is smaller the density of surrounding plasma, $\rho + \delta\rho$, then the element will continue moving up under the buoyancy force. Therefore, the condition of the convective instability is:

$$\Delta\rho \equiv \delta\rho_i - \delta\rho < 0.$$

Physical conditions inside the element obey the adiabatic law because the characteristic time for heat exchange is much longer than the dynamic time. Then,

$$\delta\rho_i = \left(\frac{d\rho}{dr}\right)_{\text{ad}} \delta r = \frac{\rho}{\gamma P}\left(\frac{dP}{dr}\right)\delta r,$$

where γ is the adiabatic exponent.

The density variation in the surrounding plasma is: $\delta\rho = \dfrac{d\rho}{dr}\delta\rho.$

Finally, the instability condition is: $A^* \equiv \dfrac{1}{\gamma}\dfrac{d\log P}{d\log r} - \dfrac{d\log\rho}{d\log r} < 0.$

Parameter A^* is called the Ledoux parameter of convective stability.

If $A^* > 0$ then the fluid element will move downward and start oscillating.

Oscillations of a fluid element

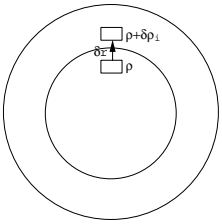

The momentum equation of a fluid element moving under the buoyancy force, $F_{buoyancy} = g(\delta\rho - \delta\rho_i)$ is:

$$\rho\frac{d^2\delta r}{dt^2} = \rho(\delta\rho - \delta\rho_i) = g\left(\frac{d\rho}{dr} - \frac{\rho}{\gamma P}\frac{dP}{dr}\right)\delta\rho = -N^2\rho\delta r$$

where δr is displacement of a fluid element from its equilibrium state,

$N^2 = g\left(\dfrac{1}{\gamma P}\dfrac{dP}{dr} - \dfrac{d\rho}{dr}\right)$ is the Brunt-Vaisala frequency.

The equation of motion is: $\dfrac{d^2\delta r}{dt^2} + N^2\delta r = 0$

For $N^2 > 0$, the general solution is:

$$\delta r = A\sin(Nt) + B\cos(Nt)$$

- the fluid elements oscillate with frequency N, representing the internal gravity oscillations.

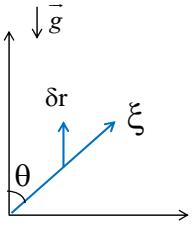

If $N^2 < 0$, then $\delta r \sim e^{\pm|N|t}$. This solution contains an exponentially growing perturbations, representing the convective instability.

If the fluid displacement ξ is not vertical, then the vertical component of the displacement is $\delta r = \xi\cos(\theta)$, where θ is the angle between the displacement vector and the vertical.

In this case, the equation of motion is:

$$\frac{d^2\xi}{dt^2} + N^2\cos^2\theta\cdot\xi = 0$$

and the oscillation frequency is $\omega = N\cos\theta$.

Propagation of internal gravity waves

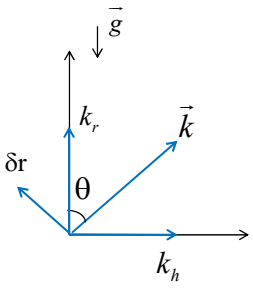

To analyze wave properties, we calculate the phase and group velocities from the dispersion relation:

$$k_r^2 = \frac{S_l^2}{c^2\omega^2}\left(N^2 - \omega^2\right)$$

Substituting $S_l^2 = \frac{L^2c^2}{r^2} = k_h^2c^2$

where $k_h = L/r$ is the horizontal wavenumber defined in the previous lecture, we obtain:

$$k_r^2 = \frac{k_h^2}{\omega^2}\left(N^2 - \omega^2\right) = \frac{k_h^2}{\omega^2}N^2 - k_h^2.$$

We find

$$\omega^2 = \frac{k_h^2N^2}{k_h^2 + k_r^2} = \frac{k_h^2N^2}{k^2}$$

$$\omega = \pm N\frac{k_h}{k}$$

where k is the total wavenumber, $k^2 = k_h^2 + k_r^2$.

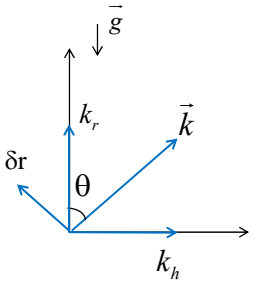

If θ is the angle between the wave vector $\vec{k} = (k_h, k_r)$ and the horizontal direction, then $k_h/k = \cos\theta$, and

$$\omega^2 = N^2\cos^2\theta$$

If $\theta = 0$, that is $k = k_h$, and the waves travel horizontally, $\omega^2 = N^2$.

The wave phase velocity is:

$$\vec{v}_{ph} = \frac{\omega}{k}\frac{\omega}{k^2}\vec{k}$$

or in terms of the horizontal and vertical components:

$$\vec{v}_{ph} = \left(\frac{\omega k_h}{k^2}, \frac{\omega k_r}{k^2}\right) = \left(\frac{Nk_h^2}{k^3}, \frac{Nk_rk_h}{k^3}\right).$$

The group velocity:

$$\vec{v}_{gr} = \frac{\partial\omega}{\partial\vec{k}} = \left(\frac{N}{k}\left(1 - \frac{k_h^2}{k^2}\right), -\frac{N}{k}\frac{k_hk_r}{k^2}\right) = \left(\frac{Nk_r^2}{k^3}, -\frac{Nk_hk_r}{k^3}\right)$$

Note that the vertical component of the group velocity has the opposite sign to the vertical component of the wavevector, k_r.

We find that $\vec{v}_{ph}\cdot\vec{v}_{gr} = 0$, that is $\vec{v}_{gr} \perp \vec{v}_{ph}$. This means that the wave energy is transported perpendicular to the wave propagation.

Calculating the amplitudes of the group and phase velocities, we find:

$$v_{gr}^2 = \frac{N^2}{k^2}\left(\frac{k_h^2}{k^4} + \frac{N^2}{k^2}\frac{k_h^2 k_r^2}{k^4}\right) = \frac{N^2}{k^4}k_r^2$$

$$|v_{gr}| = \frac{Nk_r}{k^2} = \frac{N}{k}\sin\theta$$

Similarly, $|v_{ph}| = \frac{N}{k}\cos\theta$

Consider propagation of a wave front from an impulsive source.
The radius of the wave front expands with the group velocity:

$$r = v_{gr}t = \frac{N}{k}\sin\theta t = N\frac{\lambda t}{2\pi}\sin\theta,$$

where $\lambda = 2\pi / k$ is the wavelength.

Laboratory experiments are performed in a stratified salt solution with a constant Brunt-Vaisala frequency N. A horizontal cylinder vertically oscillating with frequency ω generates a wave pattern with constant phases at angle $\cos^{-1}(\omega / N)$ to the vertical, resembling the St.Andrew's Cross pattern.

Internal gravity waves experiment

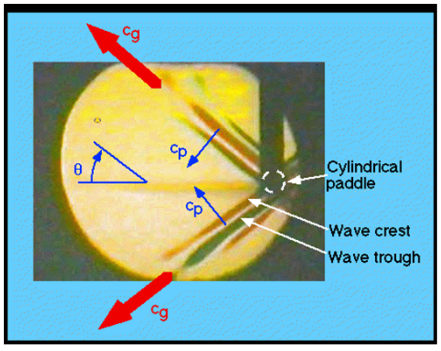

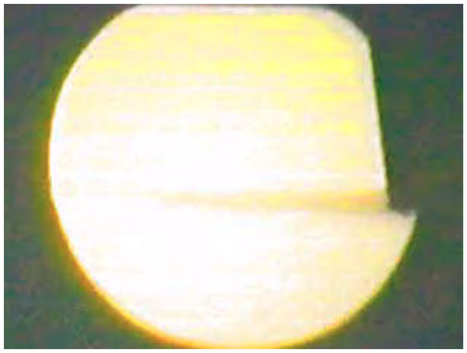

A tank about 30 cm deep is filled with a salt stratification of buoyancy period 2π/N of about 6 seconds. A solid cylinder of a few cm diameter runs across the tank at mid depth, in the right of the field of view (see diagram). This cylinder is oscillated horizontally (to the left and right in the diagram) at frequency less than N, generating internal waves. The flow is visualized with a schlieren system that shows regions of positive isopycnal (constant density) slope in red, and negative isopycnal slope in green. Slopes close to zero show as yellow. The movie is in time lapse, so that the waves appear to have higher than real frequency. The movie starts from rest, and after the paddle motion begins, the wave field starts to fill the tank outwards from the paddle. In the movie clip, wave energy appears to travel at an angle from the horizontal, and the wave crests sweep at right angles to this direction.

http://www.phys.ocean.dal.ca/programs/doubdiff/demos/IW1-Lowfrequency.html

Internal gravity waves excited by oscillating source

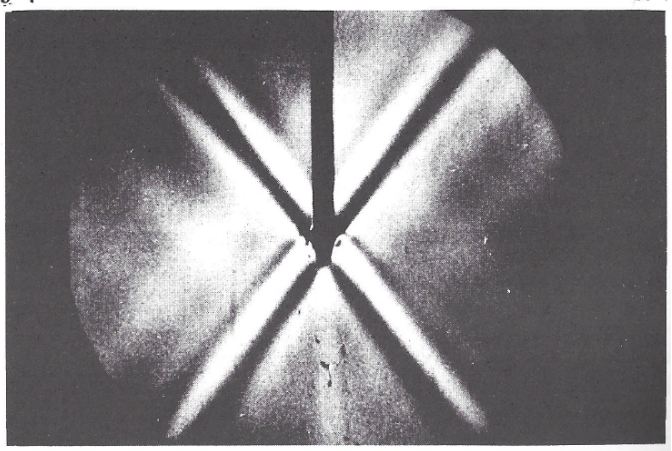

Figure 76. Schlieren picture of waves generated in stratified fluid of uniform Väisälä–Brunt frequency N by oscillation of a horizontal cylinder at frequency $0.70N$. Note that surfaces of constant phase stretch out radially from the source. [*Photograph by D. H. Mowbray.*]

Lighthill, James, 1978. (Chapters 3 and 4.) Waves in fluids. Cambridge University Press.

Internal gravity waves excited by impulsive source

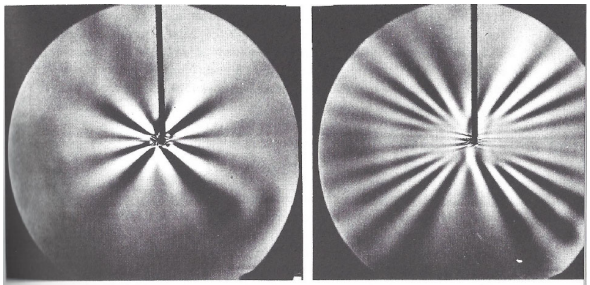

(*a*) Figure 77. Schlieren picture of waves generated by a brief horizontal displacement of a circular cylinder (*a*) after 10 seconds, (*b*) after 25 seconds. Note that the angle between crests decreases with time and is greatest, at any one time, for crests nearest to the vertical. [*Photograph by T. N. Stevenson.*] (*b*)

A localized source of finite duration generates waves of various wavelength and frequencies. The wave frequencies obey the dispersion relation: $\omega = N\cos\theta$, so that the waves with different frequencies travel in different directions. The waves of wavelength λ travel to the distance proportional to the wavelength: $(N\lambda t/2\pi)\sin\theta$. The waves with frequency ω traveling in direction θ become spread out in wavelength. The waves with shorter wavelength travel slower. The neighboring wave crests are separated by the wavelength λ. Therefore, over time, the distance between the crests decreases.

Numerical model of internal gravity waves excited by impulsive source

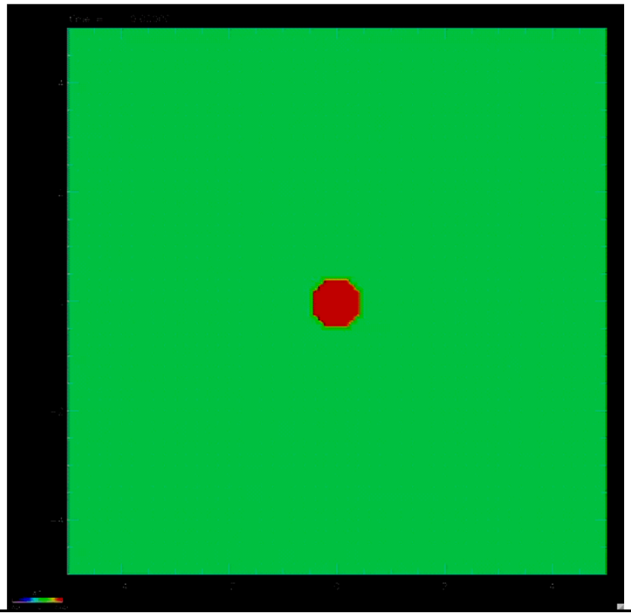

http://web.khu.ac.kr/~magara/page17/page5/page5.html

Detection of g-modes on the Sun

The g-mode can be excited by the turbulent convection, like the p-modes. Theoretical calculations show that, the expected surface amplitude is less than 1 mm/s. The g-mode has not been reliably detected. The upper observational limits are greater than 1 mm/s. The main difficulty in the g-mode detection is the high background convective noise.

Theoretical prediction of the mode amplitude

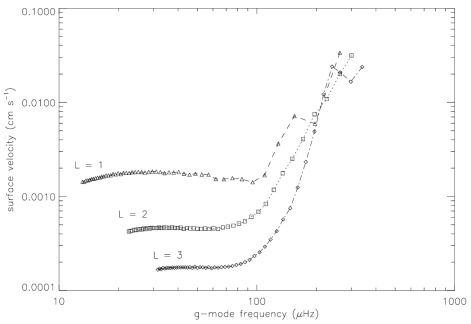

Kumar et al, (1996)

Observational limit

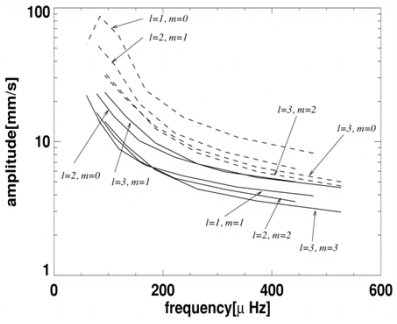

(Wachter et al, 2002)

Numerical simulations of excitation of modes by convection at the bottom of a stellar convection zone

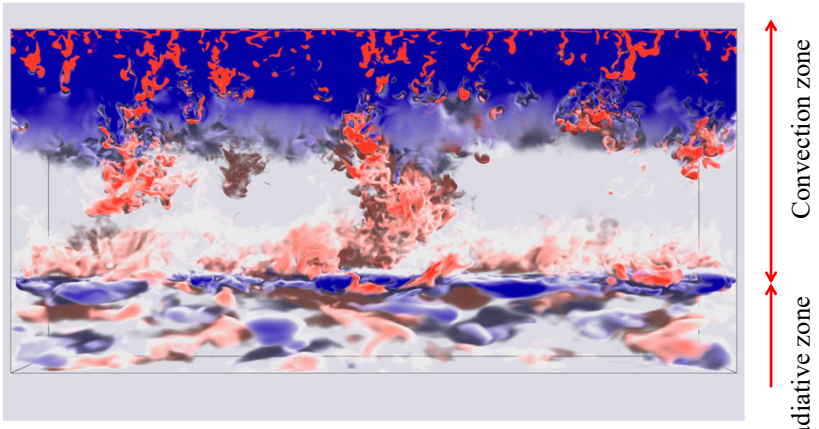

The video shows volume rendering of density fluctuations in 3D simulations of the convection zone in a solar-type star with 1.47 solar masses. Fast flickering in the upper part is caused by acoustic (p) modes. Slow variations in the lower part are caused by the internal gravity waves (g-modes) traveling in the radiative zone where N>0.

Lecture 12
Asymptotic raypath approximation

(Stix, Chapter 5.2; Kosovichev, p.31-36, 41-44;
Christensen-Dalsgaard, Chapters 5.2, 7)

Projects

- *Power spectrum: Ivan Oparin
- *Global modes from GOLF: Sheldon Fereira
- *Oscillation model, line asymmetry: Bryce Cannon
- *Power maps, acoustic halo: Bhairavi Apte
- *Propagation diagram for solar and stellar models: Ying Wang
- Ray paths, travel times: Sadaf Iqbal Ansari -today
- Asymptotic sound-speed inversion: Yunpeng Gao -tomorrow
- Analysis of sunquakes: Youra Shin
- Asteroseismic analysis: John Stefan
- November 29-30: Work on the Python and Jupyter notebooks in class – Dr. Andrey Stejko

The solar oscillation theory

1. Linearize - consider small-amplitude oscillations.
2. Neglect the perturbations of the gravitational potential (Cowling approximation).
3. Write the linearized equations in the spherical coordinates: r, θ, ϕ.
4. Consider harmonic (periodic) oscillations
5. Separate the radial and angular coordinates.
6. Show that the angular dependence can be represented by spherical harmonics.
7. Derive equations for the radial dependence, representing the eigenvalue problem for the normal modes
8. Solve the eigenvalue problem in the asymptotic (short wave-length) JWKB approximation.
9. Investigate properties of p-modes
10. Properties of g- and f-modes

Solar oscillation spectrum obtained from the HMI instrument on Solar Dynamics Observatory.

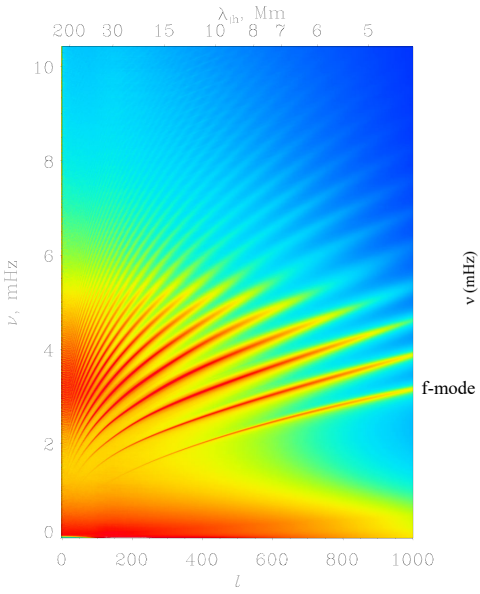

Spectrum of normal modes calculated for a standard solar model. Note the 'avoided crossing effect' for f and g-modes.

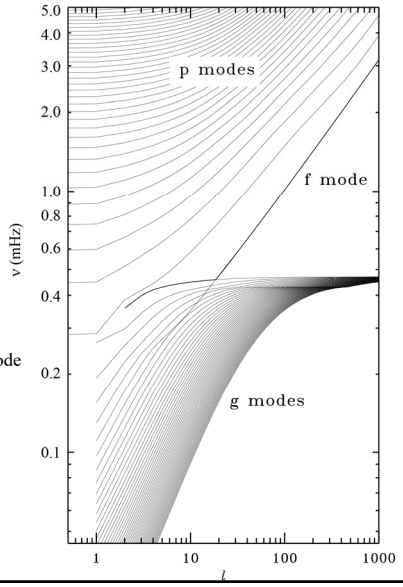

Spatial structure of p- and g-modes is obtained by multiplying the radial eigenfunctions by the corresponding spherical harmonics

p-mode (*l*=20, *m*=16, *n*=14) *g*-mode (*l*=5, *m*=3, *n*=6)

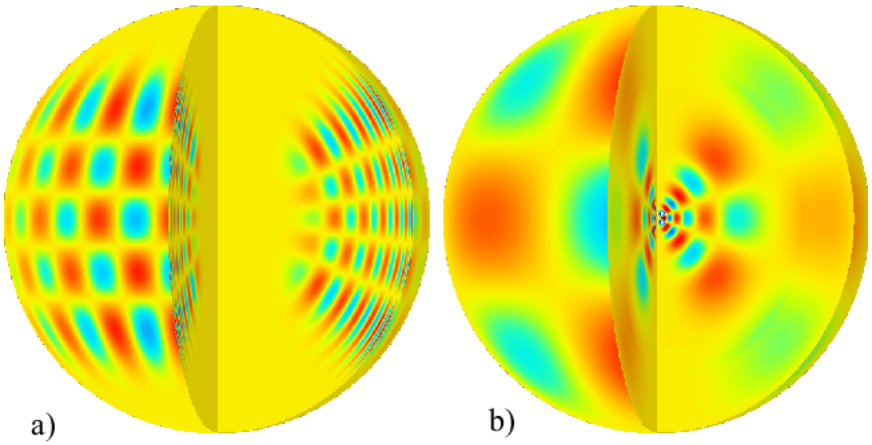

a) b)

Calculation of p-mode frequencies

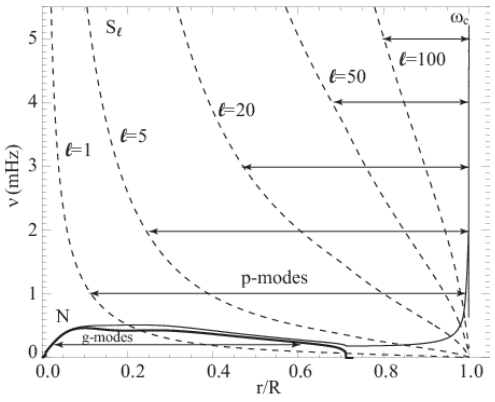

Wave propagation region: $k_r^2 > 0$

Turning points are determined from equation $k_r^2 = 0$:

$$\omega^2 = \omega_c^2 + \frac{L^2 c^2}{r^2}.$$

For the lower turning point in the interior: $\omega_c << \omega$.

Then, $\omega \approx \frac{Lc}{r}$, or $\frac{c(r_1)}{r_1} = \frac{\omega}{L}$ is the equation for the lower turning point.

The upper turning point: $\omega_c(r_2) \approx \omega$. Since $\omega_c(r)$ is a steep function of r near the surface, $r_2 \approx R$.

Then, the resonant condition for p-modes is: $\int_{r_1}^{R} \sqrt{\frac{\omega^2}{c^2} - \frac{L^2}{r^2}}\, dr = \pi(n + \alpha)$

Properties of Solar Oscillation Modes. I

Equation $$k_r^2 = \frac{\omega^2 - \omega_c^2}{c^2} + \frac{S_l^2}{c^2\omega^2}\left(N^2 - \omega^2\right)$$

represents **dispersion relation of solar oscillations**.

It relates frequency ω with radial wavenumber k_r and angular order l.

Consider two cases:

1: p-modes (acoustic modes): the high-frequency case. If $\omega^2 >> N^2$ then

$$k_r^2 = \frac{\omega^2 - \omega_c^2}{c^2} - \frac{S_l^2}{c^2}$$

or $$\omega^2 = \omega_c^2 + k_r^2 c^2 + k_h^2 c^2,$$

where $k_h = S_l / c \equiv \frac{L}{r} \equiv \frac{\sqrt{l(l+1)}}{r}$ is **the horizontal wave number**.

Then, $k^2 = k_r^2 + k_h^2$ is the squared total wavenumber.

Finally, $\omega^2 = \omega_c^2 + k^2 c^2$, where $\omega_c = \frac{c}{2H}$ is the acoustic cut-off frequency.

This is **the dispersion relation for acoustic (p) modes**; ω_c **is the acoustic cutoff frequency. Physically, the waves with frequencies below the acoustic cutoff frequency cannot propagate. Their wavelength becomes shorter than the density scale height. For the Sun** $\nu_c \equiv \omega_c / 2\pi \approx 5\ mHz$. **(c~10 km/s, H~150km).**

Frequencies of g-modes:

The turning points are determined from equation: $N(r) = \omega.$

In the propagation region, $k_r > 0$, far from the turning points ($N >> \omega$):

$$k_r \approx \frac{LN}{r\omega}.$$

Then, from the resonant condition:

$$\int_{r_1}^{r_2} \frac{L}{\omega} N \frac{dr}{r} = \pi(n + \alpha).$$

we find: $$\omega \approx \frac{L\int_{r_1}^{r_2} N \frac{dr}{r}}{\pi(n+\alpha)}.$$

Surface gravity waves (f-mode)

These wave propagate at the surface boundary where Lagrangian pressure perturbation $\delta P \sim 0$.

Consider the oscillation equations in terms of δP by making use of the relation between Eulerian and Lagrangian variables: $P' = \delta P + g\rho\xi_r$.

$$\frac{d\xi_r}{dr} - \frac{L^2 g}{\omega^2 r^2}\xi_r + \left(1 - \frac{L^2 c^2}{\omega^2 r^2}\right)\frac{\delta P}{\rho c^2} = 0,$$

$$\frac{d\delta P}{dr} + \frac{L^2 g}{\omega^2 r^2}\delta P - \frac{g\rho f}{r}\xi_r = 0,$$

where $f \approx \frac{\omega^2 r}{g} - \frac{L^2 g}{\omega^2 r}$.

These equations have a peculiar solution: $\delta P = 0,\ f = 0.$

For this solution: $\omega^2 = \frac{Lg}{R} = k_h g$

-dispersion relation for f-mode.

The eigenfunction equation: $\frac{d\xi_r}{dr} - \frac{L}{r}\xi_r = 0$

has a solution $\xi_r \propto e^{k_h (r-R)}$ exponentially decaying with depth.

Asymptotic raypath approximation

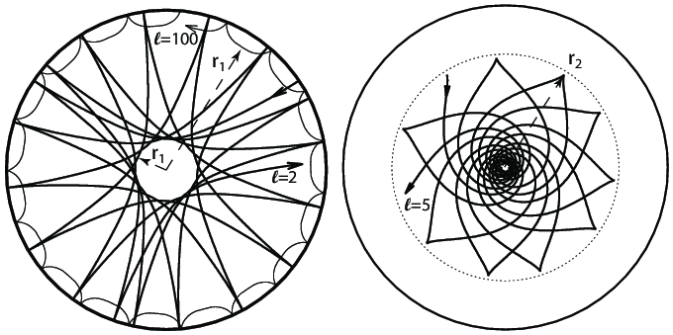

Ray paths for:
a) two solar p-modes of angular degree $l = 2$, frequency $\nu = 1429.4\ \mu$ Hz (thick curve), and $l = 100$, $\nu = 3357.5\ \mu$ Hz (thin curve);

b) g-mode of $l = 5$, $\nu = 192.6\ \mu$ Hz (the dotted curve indicates the base of the convection zone). The lower turning points, r_1 of the p-modes are shown by arrows. The upper turning points of these modes are close to the surface and not shown. For the g-mode, the upper turning point, r_2, is shown by arrow. The inner turning point is close to the center and not shown.

P-mode ray paths

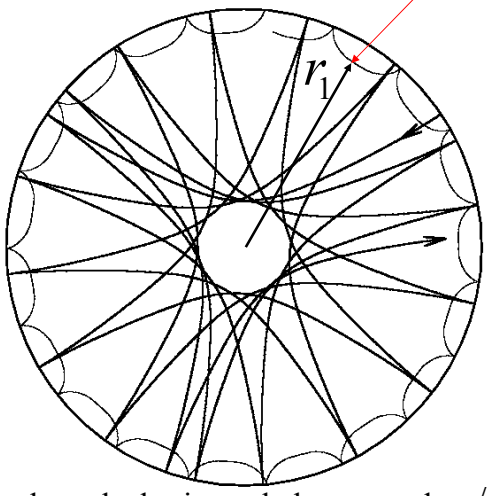

$$k_r^2 = \frac{\omega^2 - \omega_c^2}{c^2} - \frac{S_l^2}{c^2}$$

- The waves propagate where $k_r^2>0$.
- The waves are evanescent where $k_r^2<0$
- The wave turning points are located where $k_r^2=0$.
- Because $\omega_c = c / 2H$ has a sharp peak near the surface the upper turning point (r_2) is where $\omega = \omega_c$

The lower turning point (r_1) is where $\omega = S_l = (L / r)c = k_h c$ where the horizontal phase speed $\omega / k_h = c$ is equal to the sound speed.

John's sunquake movie illustrate the wave behavior at the inner turning points:
wave fronts are perpendicular to the ray paths

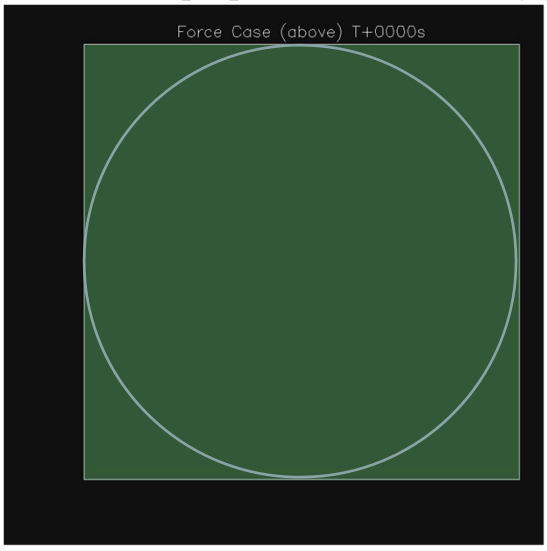

Theory of the raypath approximation

The asymptotic approximation provides an important representation of solar oscillations in terms of the ray theory. Consider the wave path equation in the ray approximation:

$$\frac{\partial \vec{r}}{\partial t} = \frac{\partial \omega}{\partial \vec{k}}.$$

Then, the radial and angular components of this equation are:

$$\frac{dr}{dt} = \frac{\partial \omega}{\partial k_r}, \qquad r\frac{d\theta}{dt} = \frac{\partial \omega}{\partial k_h}.$$

1. **Consider p-modes.**

Using the dispersion relation for acoustic (p) modes: $\omega^2 = c^2(k_r^2 + k_h^2)$,
in which we neglected the ω_c term. (It can be neglected everywhere except near the upper turning point, R), we get equation for the acoustic ray path is given by the ratio of equations:

$$r\frac{d\theta}{dr} = \left(\frac{\partial \omega}{\partial k_h}\right) / \left(\frac{\partial \omega}{\partial k_r}\right) = \frac{k_h}{k_r},$$

or

$$r\frac{d\theta}{dr} = \frac{k_h}{k_r} = \frac{L/r}{\sqrt{\omega^2/c^2 - L^2/r^2}}.$$

For any given values of ω and l, and initial coordinates, r and θ, this equation gives trajectories of ray paths of p-modes inside the Sun.

Acoustic travel time

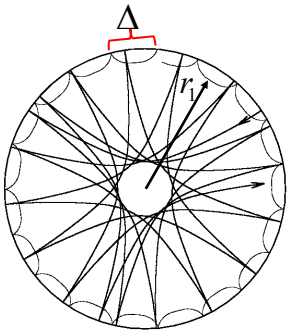

The distance, Δ, between the surface points for one skip can be calculated as the integral:

$$\Delta = 2\int_{r_1}^{R} d\theta = 2\int_{r_1}^{R} \frac{L/r}{\sqrt{\omega^2/c^2 - L^2/r^2}}\,dr \equiv 2\int_{r_1}^{R} \frac{c/r}{\sqrt{\omega^2/L^2 - c^2/r^2}}\,dr.$$

The corresponding travel time is calculated by integrating equation: $\frac{dr}{dt} = \frac{\partial \omega}{\partial k_r}$: $dt = \frac{dr}{c\left(1 - k_h^2 c^2/\omega^2\right)^{1/2}}$.

$$\tau = 2\int_{r_1}^{R} dt = \int_{r_1}^{R} \frac{dr}{c\left(1 - k_h^2 c^2/\omega^2\right)^{1/2}} \equiv \int_{r_1}^{R} \frac{dr}{c\left(1 - L^2 c^2/r^2\omega^2\right)^{1/2}}.$$

These equations give a *time-distance* relation, $\tau - \Delta$, for acoustic waves traveling between two surface points through the solar interior. The ray representation of the solar modes and the time-distance relation provided a motivation for developing *time-distance helioseismology*

Calculation of p-mode ray paths:
1) Isolate the singularity at r_1

Use the sound-speed profile, c(r), from the standard solar model to calculate the integral:

$$\Delta\theta = \int_{r_1}^{R} \frac{Lc}{r\omega} \frac{1}{\sqrt{1-\frac{L^2c^2}{\omega^2 r^2}}} \frac{dr}{r}$$

Integrand is singular (division by zero) at the lower turning point, $r = r_1$, where $\frac{Lc(r_1)}{\omega r_1} = 1$.

We divide the integration interval in two parts: 1) $[r_1, r_1+x]$, 2) $[r_1+x, R]$, where x is small compared to r_1:

$$\Delta\theta = \int_{r_1}^{r_1+x} \frac{Lc}{r\omega} \frac{1}{\sqrt{1-\frac{L^2c^2}{\omega^2 r^2}}} \frac{dr}{r} + \int_{r_1+x}^{R} \frac{Lc}{r\omega} \frac{1}{\sqrt{1-\frac{L^2c^2}{\omega^2 r^2}}} \frac{dr}{r} = \delta\theta + \Delta\theta'$$

Calculation of p-mode ray paths:
2) Use Taylor expansion in the vicinity of r_1

To calculate integral $\delta\theta$ use the Taylor expansion in the vicinity of r_1:

$$\delta\theta = \int_{r_1}^{r_1+x} \frac{Lc}{r\omega} \frac{1}{\sqrt{1-\frac{L^2c^2}{\omega^2 r^2}}} \frac{dr}{r}$$

The first term of the integrand: $\frac{Lc(r_1)}{\omega r_1} = 1$.

Expand the denumerator:

$$1-\frac{L^2c^2}{\omega^2 r^2} = 1 - \frac{L^2 c_1^2 \left(1 + \left(\frac{d\log c^2}{d\log r}\right)_{r_1} \frac{x}{r_1}\right)}{\omega^2 r_1^2 \left(1+2\frac{x}{r_1}\right)} = \left(2 - \left(\frac{d\log c^2}{d\log r}\right)_{r_1}\right)\frac{x}{r_1} \equiv \alpha \frac{x}{r_1}$$

Calculation of p-mode ray paths:

3) Outside singularity use numerical integration

Substitute the expansion in $\delta\theta$:

$$\delta\theta = \int_0^x \frac{1}{\sqrt{\alpha \frac{x}{r_1}}} \frac{dx}{r_1} = \frac{1}{\sqrt{\alpha r_1}} \int_0^x \frac{dx}{\sqrt{x}} = 2\sqrt{\frac{x}{\alpha r_1}}$$

Define x, calculate $\delta\theta$, and evaluate integral θ' numerically.

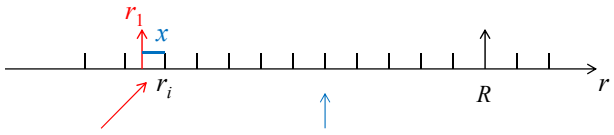

$$\Delta\theta = \int_{r_1}^{r_1+x} \frac{Lc}{r\omega} \frac{1}{\sqrt{1-\frac{L^2c^2}{\omega^2 r^2}}} \frac{dr}{r} + \int_{r_1+x}^{R} \frac{Lc}{r\omega} \frac{1}{\sqrt{1-\frac{L^2c^2}{\omega^2 r^2}}} \frac{dr}{r} = \delta\theta + \Delta\theta'$$

Ray paths of g-modes

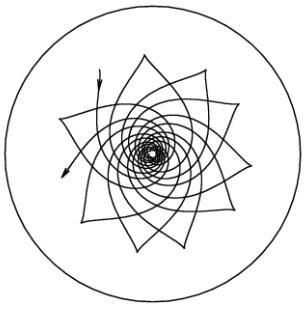

For the g-modes, the dispersion relation is:

$$\omega^2 = \frac{k_h^2 N^2}{k_r^2 + k_h^2}.$$

Then, the corresponding ray path equation:

$$r\frac{d\theta}{dr} = -\frac{k_r}{k_h} = -\sqrt{\frac{N^2}{\omega^2} - 1}.$$

Note that the g-mode travels mostly in the central region.

Therefore, the frequencies of g-modes are mostly sensitive to the central conditions (the energy-generating core).

Duvall's law (asymptotic p-mode relation)

Consider the p-mode dispersion relation:

$$\int_{r_1}^{R} k_r dr = \pi(n+\alpha)$$

$$\int_{r_1}^{R} \left(\frac{\omega^2}{c^2} - \frac{L^2}{r^2} \right)^{1/2} dr = \pi(n+\alpha)$$

Dividing left and right-hand sides by ω we get:

$$\int_{r_1}^{R} \left(\frac{r^2}{c^2} - \frac{L^2}{\omega^2} \right)^{1/2} \frac{dr}{r} = \frac{\pi(n+\alpha)}{\omega}$$

Radius r_1 (or r_t) of the lower turning point depends only on ratio L/ω. Hence, the left-hand side is a function of L/ω:

$$\Psi\left(\frac{L}{\omega} \right) = \frac{\pi(n+\alpha)}{\omega}$$

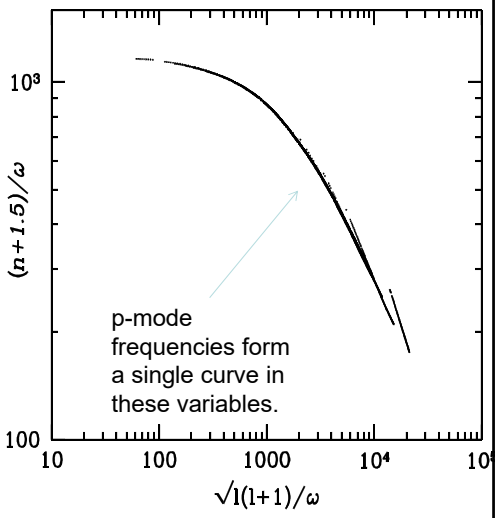

where $L = \sqrt{l(l+1)}$ $\alpha \approx 1.5$

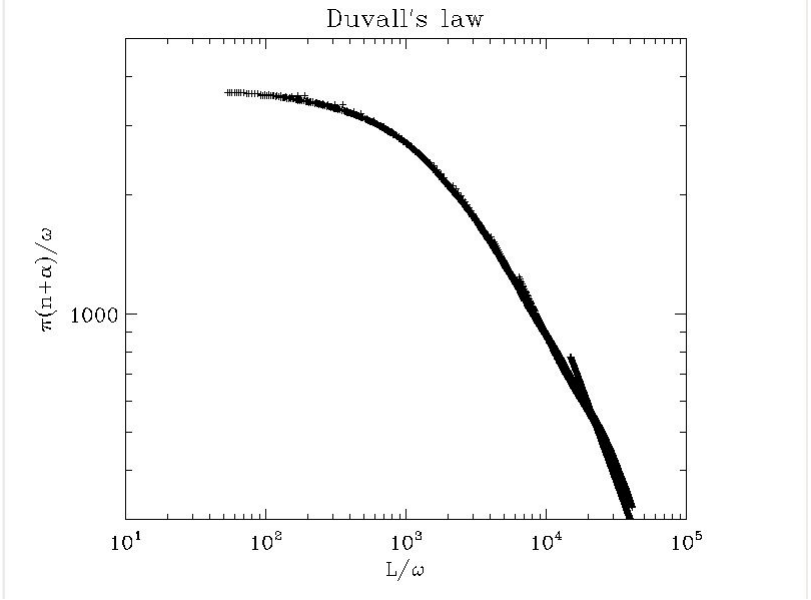

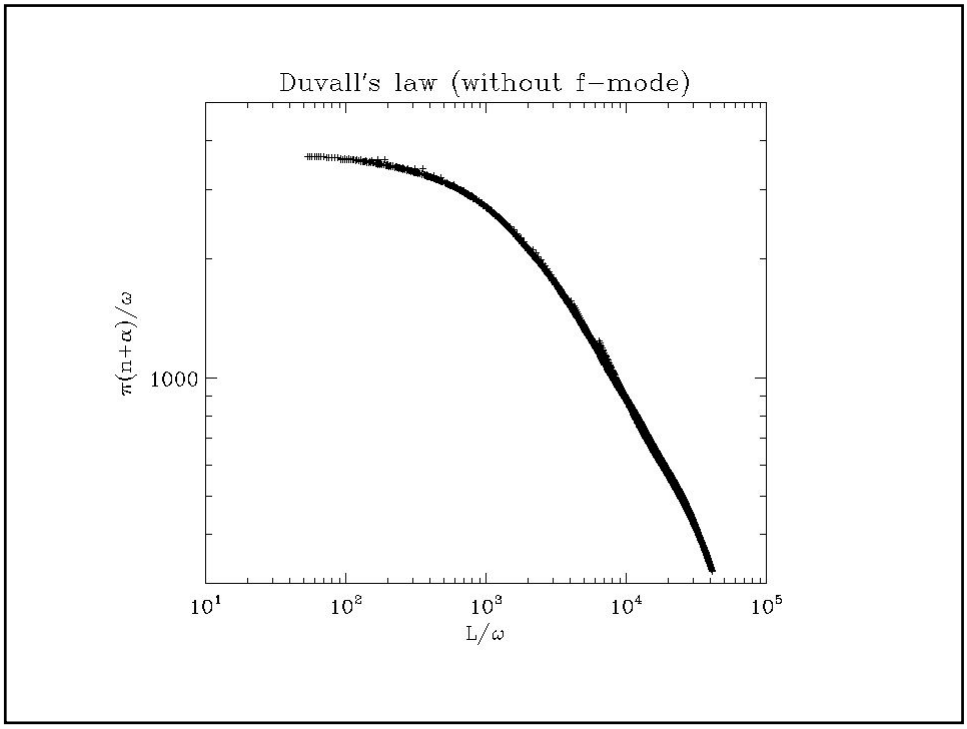
Duvall's law (without f−mode)
π(n+α)/ω
1000
10¹
10²
10³
10⁴
10⁵
L/ω

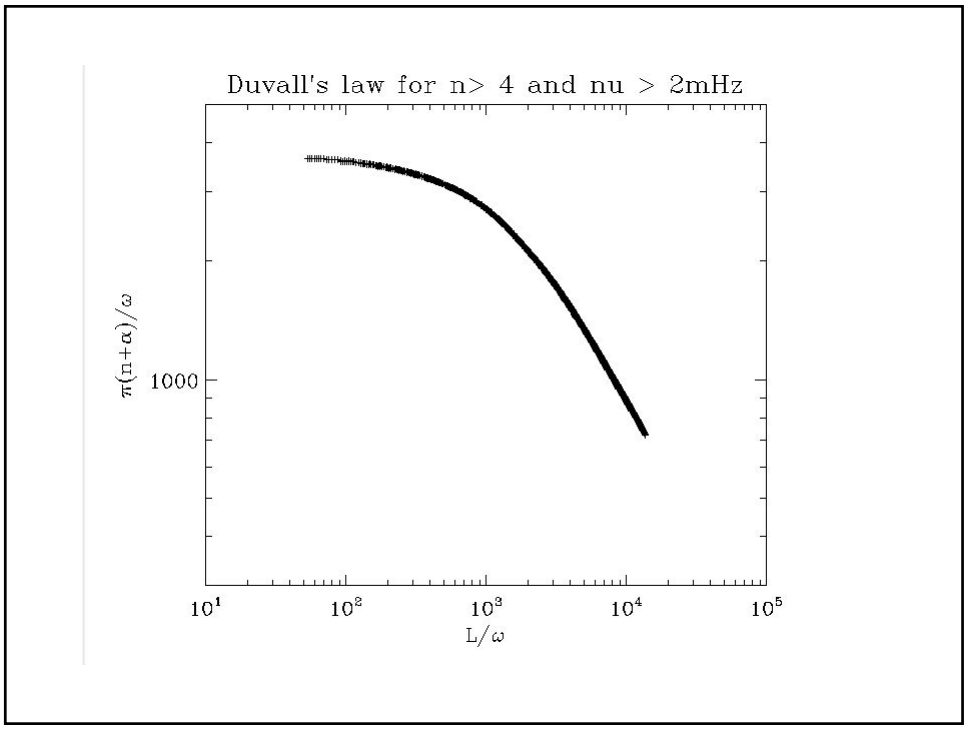
Duvall's law for n> 4 and nu > 2mHz
π(n+α)/ω
1000
10¹
10²
10³
10⁴
10⁵
L/ω

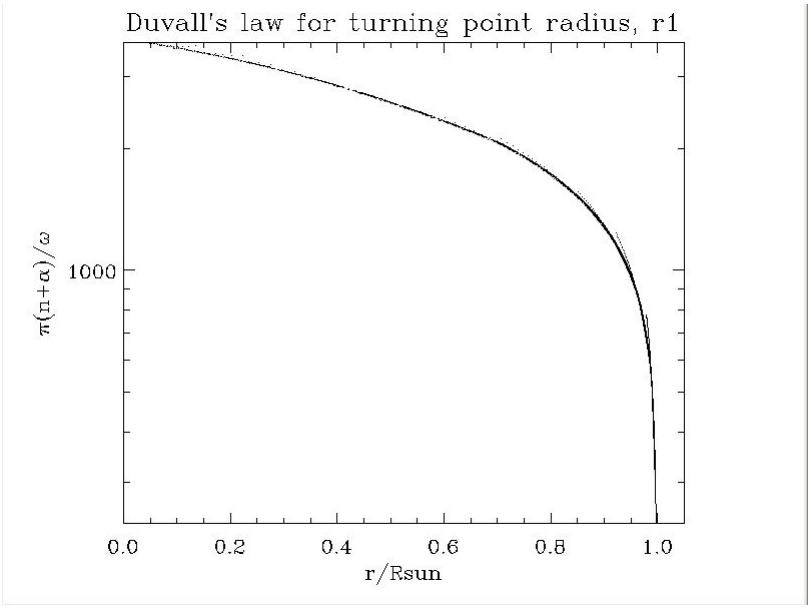
Duvall's law for turning point radius, r1
$\pi(n+\alpha)/\omega$
1000
0.0
0.2
0.4
0.6
0.8
1.0
r/Rsun

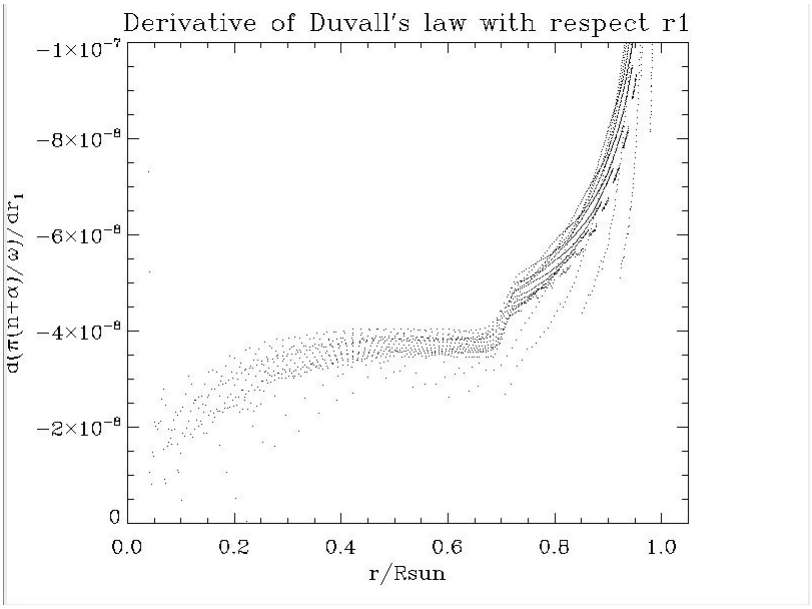
Derivative of Duvall's law with respect r1
$d(\pi(n+\alpha)/\omega)/dr_1$
-1×10^{-7}
-8×10^{-8}
-6×10^{-8}
-4×10^{-8}
-2×10^{-8}
0
0.0
0.2
0.4
0.6
0.8
1.0
r/Rsun

Determination of the sound-speed profile from Duvall's law

The asymptotic relation for the p-mode frequencies in the form of the Duvall's law:

$$\int_{r_1}^{R} \sqrt{1-\frac{L^2c^2}{\omega^2 r^2}}\,\frac{dr}{c} = \frac{\pi(n+\alpha)}{\omega}$$

allows us to determine the sound-speed profile inside the Sun. It was the first determination of the Sun's internal structure to test the stellar evolution theory.

Substitute new variables: $x = \frac{r^2}{c^2}$ and $y = \frac{L^2}{\omega^2}$, and consider the right-hand side as a function of y:

$$\int_y^X \sqrt{1-\frac{y}{x}}\,\frac{r}{c}\,d\ln r = \frac{\pi(n+\alpha)}{\omega} \equiv F(y),$$

where X is the value of x at the solar surface: $X = \frac{R^2}{c(R)^2}$.

This equation can be rewritten as:

$$\int_y^X \sqrt{x-y}\,\frac{d\ln r}{dx}\,dx = F(y)$$

The parameter y and function $F(y)$ are known from observation. Our task is to find r as a function of x by solving this integral equation. Once we know $r(x)$ we can reconstruct the sound-speed, c, as a function of radius r.

First, we differentiate this equation with respect to y:

$$\frac{1}{2}\int_y^X \frac{1}{\sqrt{x-y}}\,\frac{d\ln r}{dx}\,dx = -\frac{dF}{dy}$$

By introducing $f(x) = \frac{d\ln r}{dx}$ and $\Phi(y) = -2\frac{dF}{dy}$, we write it in the form of the Abel integral equation:

$$\int_y^X \frac{f(x)}{\sqrt{x-y}}\,dx = \Phi(y)$$

To solve this equation, we multiply both sides by $\frac{1}{\sqrt{y-u}}$ and integrate over y from u to X:

$$\int_u^X \left[\int_y^X \frac{f(x)}{\sqrt{x-y}}\,dx\right]\frac{dy}{\sqrt{y-u}} = \int_u^X \frac{\Phi(y)}{\sqrt{y-u}}\,dy$$

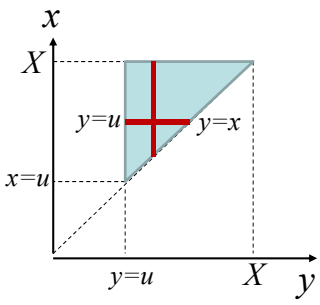

In the left-hand side, we change the order of integration – first, integrate over y and then over x:

$$\int_u^X \left[\int_y^X \frac{f(x)}{\sqrt{x-y}}dx\right]\frac{dy}{\sqrt{y-u}} = \int_u^X f(x)\left[\int_{y=u}^{y=x}\frac{dy}{\sqrt{x-y}\sqrt{y-u}}\right]dx$$

This transformation is easy to understand by plotting the integration region in the $x-y$ diagram.

The integration region covers the gray triangle. Before the transformation, the integration over x was along the vertical lines, and then horizontally over y.

After the transformation, the inner integration is along the horizontal lines from $y=u$ to $y=x$.

This integral is calculated analytically:

$$\int_u^y \frac{dy}{\sqrt{(x-y)(y-u)}} = \pi$$

Thus,

$$\pi\int_y^X f(x)dx = \int_u^X \frac{\Phi(y)}{\sqrt{y-u}}dy$$

Substituting back $f(x)=\frac{d\ln r}{dx}$ and $\Phi(y)=-2\frac{dF}{dy}$ we get:

$$\pi\int_u^X \frac{d\ln r}{dx}dx = -2\int_u^X \frac{dF/dy}{\sqrt{y-u}}dy$$

Integrating the left-hand side:

$$\pi[\ln R - \ln r(u)] = -2\int_u^X \frac{dF/dy}{\sqrt{y-u}}dy$$

where R is the solar radius. Replacing independent variable u with x:

$$\ln\left(\frac{r}{R}\right) = \frac{2}{\pi}\int_x^X \frac{dF/dy}{\sqrt{y-x}}dy$$

The solution is often represented in terms of variables w and a defined in terms of x and y as:

$y=\frac{L^2}{\omega^2}=w^2$ and $x=\frac{r^2}{c^2}=a^2$:

$$\ln\frac{r(a)}{R} = \frac{2}{\pi}\int_a^A \frac{dF/dw}{\sqrt{w^2-a^2}}dw$$

where $a=r/c$, $w=L/\omega$ and $A=R/c(R)$. The integral is calculated by approximating $F(w)\equiv F(L/\omega)=\frac{\pi(n+\alpha)}{\omega}$ by a smooth function of w, differentiating with respect to w and calculating the integral numerically, taking into the singularity at the lower limit. The singularity is of the type of $1/\sqrt{x}$ and the integral is calculated analytically in the vicinity of the singular point . This type of integrals are called the Abel integral equation. It gives the relationship between r and $a=r/c$, from which $c(r)$ can be calculated by interpolation.

Taking into account the Brunt-Vaisala frequency and the surface phase shift

An application of short-wave asymptotic theory to the non-radial adiabatic oscillation equation yields, in the first-order approximation, the dispersion relation which includes the Brunt-Vaisala frequency N:

$$\frac{\pi(n+\alpha)}{\omega}=\int_{r_t}^{R}\left(\frac{r^2}{c^2}-\frac{L^2}{\omega^2}\right)^{1/2}\left(1-\frac{N^2}{\omega^2}\right)^{1/2}\frac{dr}{r}$$

where N is the buoyancy frequency and r_t 1s radius of the turning point of the mode, $\left(r_t/c(r_t)=L/\omega\right)$. In general, the phase shift α, which depends on the wave reflection at the solar surface, is a function of frequency: $\alpha=\alpha(\omega)$.

In this case, the Duvall's law depends not only on the parameter $y=L/\omega$ but also on the frequency, ω:

$$\frac{\pi(n+\alpha)}{\omega}=F_1(y,\omega)$$

For high-frequency p modes $\omega^2\gg N^2$, and therefore, by using the Taylor expansion, the dispersion equation can be rewritten as:

$$\frac{\pi(n+\alpha)}{\omega}=\int_{r_t}^{R}\left(\frac{r^2}{c^2}-y^2\right)^{1/2}\frac{dr}{r}-\frac{1}{2\omega^2}\int_{r_t}^{R}N^2\left(\frac{r^2}{c^2}-y^2\right)^{1/2}\frac{dr}{r}$$

or $f(y,\omega)=F(y)-\frac{1}{\omega^2}\Psi(y)-\beta(\omega)$ where $f(y,\omega)=\frac{\pi n}{\omega}$

$$F(y)=\int_{r_t}^{R}\left(\frac{r^2}{c^2}-y^2\right)^{1/2}\frac{dr}{r}$$

$$\Psi(y)=\frac{1}{2}\int_{r_t}^{R}N^2\left(\frac{r^2}{c^2}-y^2\right)^{1/2}\frac{dr}{r}$$

$$\beta(\omega)=\frac{\pi\alpha}{\omega}$$

All terms on the RHS of the equation for $f(y,\omega)$ have different functional dependencies on y and ω, and therefore derivatives of F,Ψ and β can be determined separately.

By differentiating equation: $f(y,\omega) = F(y) - \frac{1}{\omega^2}\Psi(y) - \beta(\omega)$

$$\frac{dF}{dy} = \frac{\partial f}{\partial y} + \frac{\omega}{2}\frac{\partial^2 f}{\partial \omega \partial y}$$

$$\frac{d\Psi}{dy} = \frac{\omega^3}{2}\frac{\partial^2 f}{\partial \omega \partial y}$$

$$\frac{d\beta}{d\omega} = -\frac{\partial f}{\partial \omega} + \frac{2}{\omega^3}\Psi(y)$$

The application of the natural parameters of the asymptotic theory (n/ω) and (L/ω) simplifies the calculations of the derivatives. We obtain an improved estimate of the derivative $\frac{dF}{dy}$ which is needed for determining the sound-speed profile.

A numerically stable method of evaluating the partial derivatives of the function $f(y,\omega)$ is provided by least-squares fitting of a bicubic spline to the observational data. The method employs products of B-splines to represent the bicubic splines. The positions of the B-spline knots are used to control the smoothing process, which is dependent on observational errors.

Result of the asymptotic inversion

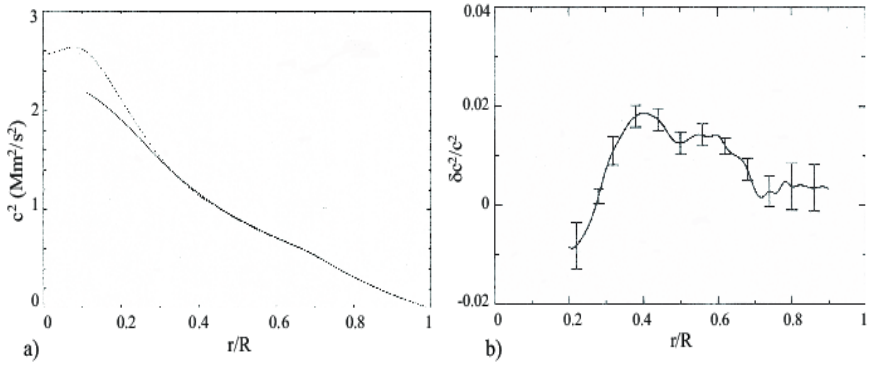

a) Result of the asymptotic sound inversion (solid curve) for the p-mode frequencies. It confirmed the standard solar model (model 1) (dots). The large discrepancy in the central region is due inaccuracy of the data and the asymptotic approximation. b) The relative difference in the squared sound speed between the asymptotic inversions of the observed and theoretical frequencies.

Lecture 13
Mode-ray duality.
3D ray paths

(Stix, p.202-203; Chapter 5.3.2; Kosovichev, p.34-41;
Christensen-Dalsgaard, Chapter 7.7)

HW1 presentations (Oct. 25+ quiz)

- 1.1 (a) Bryce
- 1.1 (b-d) Youra
- 1.2 (a) John
- 1.2 (b) Sadaf Iqbal
- 1.3 (a-c) Yunpeng
- 1.3 (d-f) Bhairavi
- 1.4 Ying
- 1.5 Ivan

Asymptotic raypath approximation

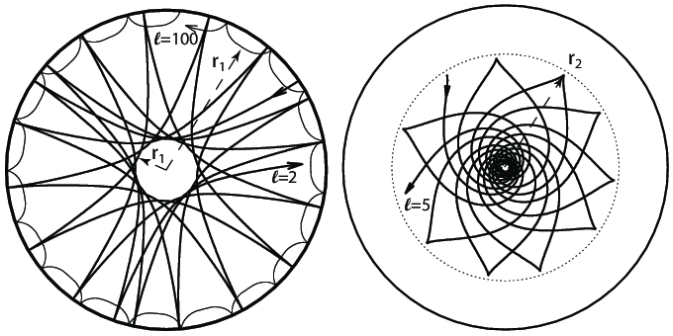

Ray paths for:
a) two solar p-modes of angular degree $l = 2$, frequency $\nu = 1429.4\ \mu$ Hz (thick curve), and $l = 100$, $\nu = 3357.5\ \mu$ Hz (thin curve);

b) g-mode of $l = 5$, $\nu = 192.6\ \mu$ Hz (the dotted curve indicates the base of the convection zone). The lower turning points, r_1 of the p-modes are shown by arrows. The upper turning points of these modes are close to the surface and not shown. For the g-mode, the upper turning point, r_2, is shown by arrow. The inner turning point is close to the center and not shown.

Theory of the raypath approximation

The asymptotic approximation provides an important representation of solar oscillations in terms of the ray theory. Consider the wave path equation in the ray approximation:

$$\frac{\partial \vec{r}}{\partial t} = \frac{\partial \omega}{\partial \vec{k}}.$$

Then, the radial and angular components of this equation are:

$$\frac{dr}{dt} = \frac{\partial \omega}{\partial k_r}, \qquad r\frac{d\theta}{dt} = \frac{\partial \omega}{\partial k_h}.$$

1. **Consider p-modes.**

Using the dispersion relation for acoustic (p) modes: $\omega^2 = c^2(k_r^2 + k_h^2)$,
in which we neglected the ω_c term. (It can be neglected everywhere except near the upper turning point, R), we get equation for the acoustic ray path is given by the ratio of equations:

$$r\frac{d\theta}{dr} = \left(\frac{\partial \omega}{\partial k_h}\right) / \left(\frac{\partial \omega}{\partial k_r}\right) = \frac{k_h}{k_r},$$

or

$$r\frac{d\theta}{dr} = \frac{k_h}{k_r} = \frac{L/r}{\sqrt{\omega^2/c^2 - L^2/r^2}}.$$

For any given values of ω and l, and initial coordinates, r and θ, this equation gives trajectories of ray paths of p-modes inside the Sun.

Calculation of p-mode ray paths:
1) Isolate the singularity at r_1

Use the sound-speed profile, c(r), from the standard solar model to calculate the integral:

$$\Delta\theta = \int_{r_1}^{R} \frac{Lc}{r\omega} \frac{1}{\sqrt{1-\frac{L^2c^2}{\omega^2 r^2}}} \frac{dr}{r}$$

Integrand is singular (division by zero) at the lower turning point, $r = r_1$, where $\frac{Lc(r_1)}{\omega r_1} = 1$.

We divide the integration interval in two parts: 1) $[r_1, r_1+x]$, 2) $[r_1+x, R]$, where x is small compared to r_1:

$$\Delta\theta = \int_{r_1}^{r_1+x} \frac{Lc}{r\omega} \frac{1}{\sqrt{1-\frac{L^2c^2}{\omega^2 r^2}}} \frac{dr}{r} + \int_{r_1+x}^{R} \frac{Lc}{r\omega} \frac{1}{\sqrt{1-\frac{L^2c^2}{\omega^2 r^2}}} \frac{dr}{r} = \delta\theta + \Delta\theta'$$

Calculation of p-mode ray paths:
2) Use Taylor expansion in the vicinity of r_1

To calculate integral $\delta\theta$ use the Taylor expansion in the vicinity of r_1:

$$\delta\theta = \int_{r_1}^{r_1+x} \frac{Lc}{r\omega} \frac{1}{\sqrt{1-\frac{L^2c^2}{\omega^2 r^2}}} \frac{dr}{r}$$

The first term of the integrand: $\frac{Lc(r_1)}{\omega r_1} = 1$.

Expand the denumerator:

$$1-\frac{L^2c^2}{\omega^2 r^2} = 1 - \frac{L^2 c_1^2 \left(1 + \left(\frac{d\log c^2}{d\log r}\right)_{r_1} \frac{x}{r_1}\right)}{\omega^2 r_1^2 \left(1+2\frac{x}{r_1}\right)} = \left(2 - \left(\frac{d\log c^2}{d\log r}\right)_{r_1}\right)\frac{x}{r_1} \equiv \alpha \frac{x}{r_1}$$

Calculation of p-mode ray paths:

3) Outside singularity use numerical integration

Substitute the expansion in $\delta\theta$:

$$\delta\theta = \int_0^x \frac{1}{\sqrt{\alpha \frac{x}{r_1}}} \frac{dx}{r_1} = \frac{1}{\sqrt{\alpha r_1}} \int_0^x \frac{dx}{\sqrt{x}} = 2\sqrt{\frac{x}{\alpha r_1}}$$

Define x, calculate $\delta\theta$, and evaluate integral θ' numerically.

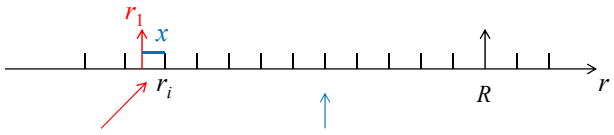

$$\Delta\theta = \int_{r_1}^{r_1+x} \frac{Lc}{r\omega} \frac{1}{\sqrt{1-\frac{L^2c^2}{\omega^2 r^2}}} \frac{dr}{r} + \int_{r_1+x}^{R} \frac{Lc}{r\omega} \frac{1}{\sqrt{1-\frac{L^2c^2}{\omega^2 r^2}}} \frac{dr}{r} = \delta\theta + \Delta\theta'$$

Ray paths of g-modes

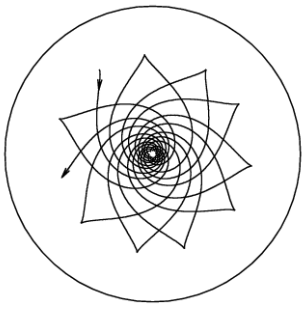

For the g-modes, the dispersion relation is:

$$\omega^2 = \frac{k_h^2 N^2}{k_r^2 + k_h^2}.$$

Then, the corresponding ray path equation:

$$r\frac{d\theta}{dr} = -\frac{k_r}{k_h} = -\sqrt{\frac{N^2}{\omega^2} - 1}.$$

Note that the g-mode travels mostly in the central region.

Therefore, the frequencies of g-modes are mostly sensitive to the central conditions (the energy-generating core).

Solar oscillation spectrum obtained from the HMI instrument on Solar Dynamics Observatory.

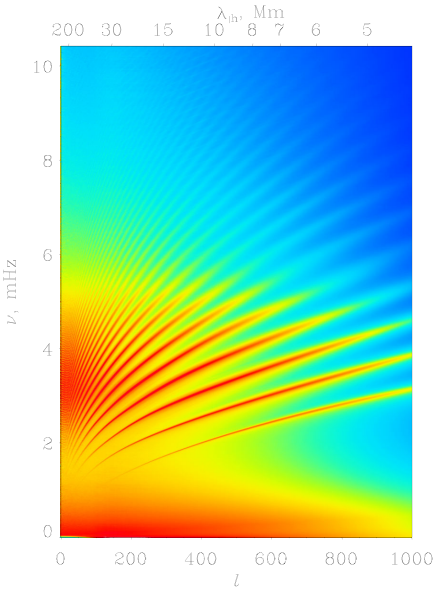

Spectrum of normal modes calculated for a standard solar model. Note the 'avoided crossing effect' for f and g-modes.

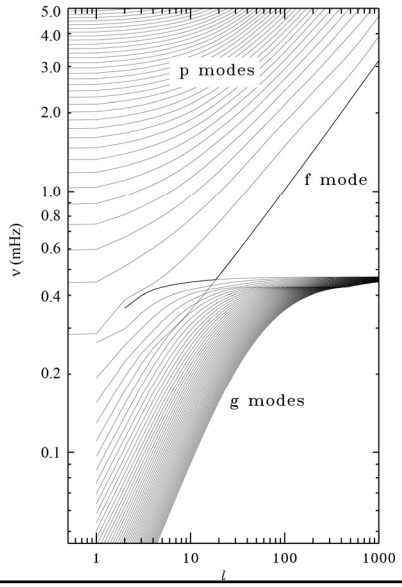

Spatial structure of p- and g-modes is obtained by multiplying the radial eigenfunctions by the corresponding spherical harmonics

p-mode (*l*=20, *m*=16, *n*=14)

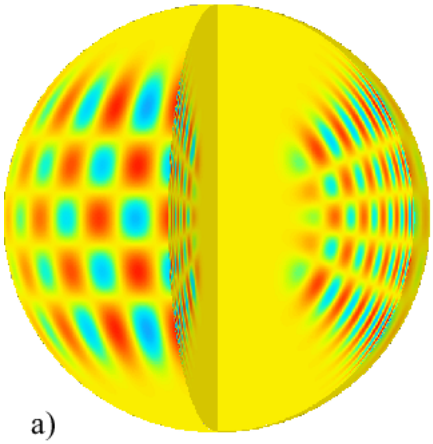

a)

g-mode (*l*=5, *m*=3, *n*=6)

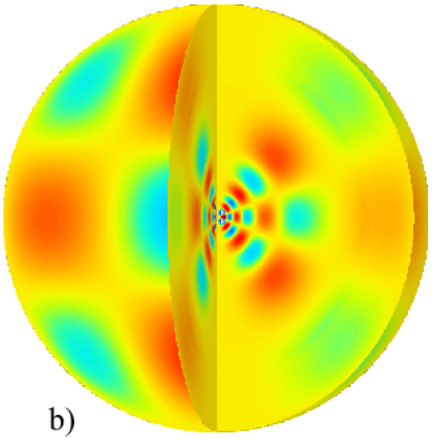

b)

Compare the p-mode eigenfunction and raypaths

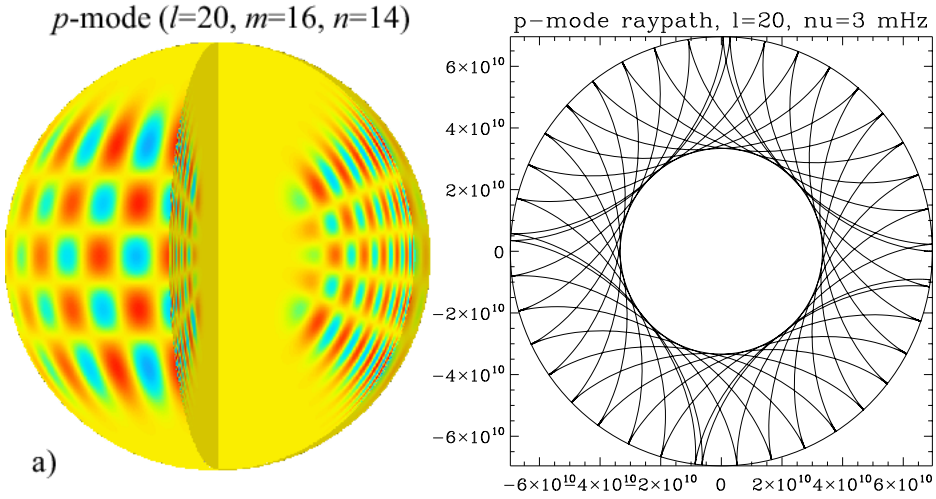

Compare the p-mode eigenfunction and raypaths

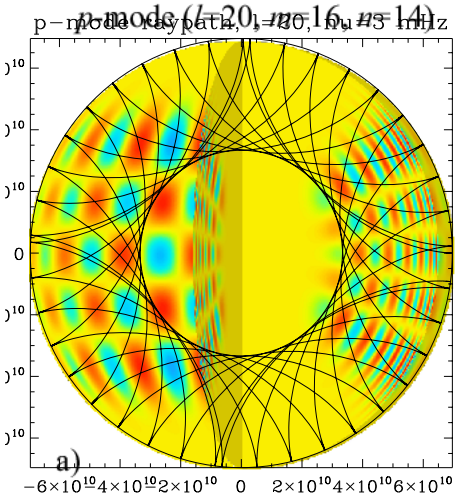

Mode-ray duality

Oscillations of the Sun are described in terms of the 'normal modes' which represent standing resonant waves in side the Sun. The resonant cavity is the region where wave of specific nature propagate. The physical nature of oscillations and waves depends on the restoring force. We considered oscillations of three types: 1) acoustic waves (p-modes) are associated with fluctuations of gas pressure; 2) buoyancy force in the Sun's radiative zone causes internal gravity waves (g-modes); 3) surface gravity waves (f-modes) traveling on the solar surface and driven by the surface gravity.

The oscillation modes are described in terms of eigenfunctions of a system of linearized hydrodynamic equations, which can be written in an operator form: $L\vec{\xi} = \omega^2 \vec{\xi}$

where L is a differential operator, $\vec{\xi}(r,\theta,\phi)e^{i\omega t}$ describes oscillatory displacements of fluid elements in the spherical coordinates. We showed that this equation has non-zero solution (eigenfunctions) in the form:

$$\vec{\xi}_{nlm}(r,\theta,\phi) = \xi_r \vec{e}_r + \vec{\xi}_h$$

where n is the radial order, l is the angular degree, m is the angular order,

$$\xi_r(r,\theta,\phi) = \xi_{r,nl}(r) \cdot Y_l^m(\theta,\phi)$$

$$\vec{\xi}_h(r,\theta,\phi) = \xi_\theta \vec{e}_\theta + \xi_\phi \vec{e}_\phi = \xi_{h,nl}(r) \nabla_h Y_l^m(\theta,\phi)$$

1. Linearization

Consider small perturbations of a stationary spherically symmetrical star in the hydrostatic equilibrium:

$$v_0 = 0,\ \rho = \rho_0(r),\ P = P_0(r).$$

If $\vec{\xi}(t)$ is a vector of displacement of a fluid element then velocity of this element:

$$\vec{v} = \frac{d\vec{\xi}}{dt} \approx \frac{\partial \vec{\xi}}{\partial t}.$$

Perturbations of scalar variables ρ, P, Φ are two types: **Eulerian, at a fixed position** $\vec{r}$:

$$\rho(\vec{r},t) = \rho_0(r) + \rho'(\vec{r},t),$$

and **Lagrangian perturbation in moving elements**:

$$\rho(\vec{r} + \vec{\xi}) = \rho_0(r) + \delta\rho(\vec{r},t).$$

The Eulerian and Lagrangian perturbations are related to each other:

$$\delta\rho = \rho' + (\vec{\xi} \cdot \nabla\rho_0) = \rho' + (\vec{\xi} \cdot \vec{e}_r)\frac{d\rho_0}{dr} = \rho' + \xi_r \frac{d\rho_0}{dr},$$

where $\vec{e}_r$ is a radial unit vector. In our case, the density gradient is radial.

1. Linearization

Consider small perturbations of a stationary spherically symmetrical star in the hydrostatic equilibrium:

$$v_0 = 0,\ \rho = \rho_0(r),\ P = P_0(r).$$

If $\vec{\xi}(t)$ is a vector of displacement of a fluid element then velocity of this element:

$$\vec{v} = \frac{d\vec{\xi}}{dt} \approx \frac{\partial \vec{\xi}}{\partial t}.$$

Perturbations of scalar variables ρ, P, Φ are two types: **Eulerian, at a fixed position** $\vec{r}$:

$$\rho(\vec{r},t) = \rho_0(r) + \rho'(\vec{r},t),$$

and **Lagrangian perturbation in moving elements**:

$$\rho(\vec{r} + \vec{\xi}) = \rho_0(r) + \delta\rho(\vec{r},t).$$

The Eulerian and Lagrangian perturbations are related to each other:

$$\delta\rho = \rho' + (\vec{\xi} \cdot \nabla\rho_0) = \rho' + (\vec{\xi} \cdot \vec{e}_r)\frac{d\rho_0}{dr} = \rho' + \xi_r \frac{d\rho_0}{dr},$$

where $\vec{e}_r$ is a radial unit vector. In our case, the density gradient is radial.

Then, the linearized equations are:

$$\rho' + \nabla(\rho_0\vec{\xi}) = 0,$$ the continuity (mass conservation) equation

$$\rho_0 \frac{\partial^2 \vec{\xi}}{\partial t^2} = -\nabla P' - g_0 \vec{e}_r \rho' + \rho_0 \nabla\Phi',$$ the momentum equation

$$P' + \xi_r \frac{dP_0}{dr} = c_0^2(\rho' + \xi_r \frac{d\rho_0}{dr}),$$ the adibaticity (energy) equation, or

$\delta P = c_0^2 \delta\rho$ for the Largangian perturbations of pressure and density.

$$\nabla^2\Phi' = 4\pi G\rho'.$$ the equation for the gravitational potential

2. Cowling approximation: $\Phi' = 0.$

3. Consider the linearized equations in the spherical coordinates r,θ,ϕ:

$$\vec{\xi} = \xi_r \vec{e}_r + \xi_\theta \vec{e}_\theta + \xi_\phi \vec{e}_\phi \equiv \xi_r \vec{e}_r + \vec{\xi}_h,$$

where $\vec{\xi}_h = \xi_\theta \vec{e}_\theta + \xi_\phi \vec{e}_\phi$ is the horizontal component of displacement.

$$\nabla \vec{\xi} \equiv \mathrm{div}\,\xi = \frac{1}{r^2}\frac{\partial}{\partial r}(r^2 \xi_r) + \frac{1}{r\sin\theta}\frac{\partial}{\partial \theta}(\sin\theta \xi_\theta) + \frac{1}{r\sin\theta}\frac{\partial \xi_\phi}{\partial \phi} =$$

$$= \frac{1}{r^2}\frac{\partial}{\partial r}(r^2 \xi_r) + \frac{1}{r}\nabla_h \vec{\xi}_h.$$

4. Consider periodic perturbations with frequency ω:

$$\vec{\xi} \propto e^{i\omega t} Y_l^m(\theta,\phi) = C P_l^m(\theta) e^{im\phi + i\omega t}$$

$\nu = \omega / 2\pi$, where ν is the cyclic frequency (measured in Hz), and ω is the angular frequency (measure in rad/s).

Then, in the Cowling approximation, we get (leaving out subscript 0 for unperturbed variables):

$$\rho' + \frac{1}{r^2}\frac{\partial}{\partial r}(r^2 \rho \xi_r) + \frac{\rho}{r}\nabla_h \vec{\xi}_h = 0, \quad \text{the continuity equation}$$

$$-\omega^2 \rho \xi_r = -\frac{\partial P'}{\partial r} + g\rho', \quad \text{the radial component of the momentum equation}$$

$$-\omega^2 \rho \vec{\xi}_h = -\frac{1}{r}\nabla_h P', \quad \text{the horizontal component of the momentum equation}$$

$$\rho' = \frac{1}{c^2}P' + \frac{\rho N^2}{g}\xi_r, \quad \text{the adiabatic equation}$$

where $N^2 = g\left(\frac{1}{\gamma P}\frac{dP}{dr} - \frac{1}{\rho}\frac{d\rho}{dr}\right)$ is the Brunt-Vaisala frequency.

Boundary conditions:

$\xi_r(r=0) = 0$, - displacement at the Sun's center is zero,
(or a regularity condition for $l = 1$).

$\delta P(r = R) = 0$, - Lagrangian pressure perturbation at the solar surface is zero.
(this is equivalent to absence of external forces).

Also, we assume that the solution is regular at the poles $\theta = 0, \pi$.

5. Consider the separation of radial and angular variables in the form:

$$\rho'(r,\theta,\phi) = \rho'(r)\cdot f(\theta,\phi),$$
$$P'(r,\theta,\phi) = P'(r)\cdot f(\theta,\phi),$$
$$\xi_r(r,\theta,\phi) = \xi_r(r)\cdot f(\theta,\phi),$$
$$\vec{\xi}_h(r,\theta,\phi) = \xi_h(r)\nabla_h f(\theta,\phi).$$

Then, the continuity equation is:

$$\left[\rho' + \frac{1}{r^2}\frac{\partial}{\partial r}(r^2\rho\xi_r)\right] f(\theta,\phi) + \frac{\rho}{r}\xi_h\nabla_h^2 f = 0.$$

The variables are separated if

$$\nabla_h^2 f = \alpha f,$$

where α is a constant.
This equation has non-zero solutions regular at the poles, $\theta = 0, \pi$ only when

$$\alpha = -l(l+1),$$

where l is an integer.

6. The non-zero solution of equation $\nabla_h^2 f + l(l+1)f = 0$ represents the spherical harmonics:

$$f(\theta,\phi) = Y_l^m(\theta,\phi) = CP_l^m(\theta)e^{im\phi},$$

where $P_l^m(\theta)$ is the Legendre function.

7. Derive equations for the radial dependence, representing the eigenvalue problem for the normal modes

After the separation of variables the continuity equation for the radial dependence $\rho'(r)$ is

$$\rho' + \frac{1}{r^2}\frac{\partial}{\partial r}\left(r^2\rho\xi_r\right) - \frac{l(l+1)}{r}\rho\xi_h = 0.$$

Compare with the original equation: $\rho' + \nabla(\rho_0\vec{\xi}) = 0,$

and with this equation in the spherical coordinates:

$$\rho' + \frac{1}{r^2}\frac{\partial}{\partial r}(r^2\rho\xi_r) + \frac{\rho}{r}\nabla_h\vec{\xi}_h = 0,$$

Transform this equation in terms of 2 variables: ξ_r and P'
- radial displacement and Eulerian pressure perturbation.

The horizontal component of displacement ξ_h can be determined from the horizontal component of the momentum equation:

$$-\omega^2 \rho \xi_h(r) = -\frac{1}{r} P'(r), \quad \text{or} \quad \xi_h = \frac{1}{\omega^2 \rho r} P'.$$

Substituting this into the continuity equation $\rho' + \frac{1}{r^2}\frac{\partial}{\partial r}\left(r^2 \rho \xi_r\right) - \frac{l(l+1)}{r}\rho \xi_h = 0.$

we obtain: $$\rho \frac{d\xi_r}{dr} + \xi_h \frac{d\rho}{dr} + \frac{2}{r}\rho \xi_r + \frac{P'}{c^2} + \frac{\rho N^2}{g}\xi_r - \frac{L^2}{r^2 \omega^2 \rho} P' = 0,$$

where we define $L^2 = l(l+1)$ (note the similarity to quantum mechanics).

Using the hydrostatic equation for the background (unperturbed) state

$$\frac{dP}{dr} = -g\rho,$$

finally get: $$\frac{d\xi_r}{dr} + \frac{2}{r}\xi_r - \frac{g}{c^2}\xi_r + \left(1 - \frac{L^2 c^2}{r^2 \omega^2}\right)\frac{P'}{\rho c^2} = 0,$$

or $$\frac{d\xi_r}{dr} + \frac{2}{r}\xi_r - \frac{g}{c^2}\xi_r + \left(1 - \frac{S_l^2}{\omega^2}\right)\frac{P'}{\rho c^2} = 0,$$

where $S_l^2 = \frac{L^2 c^2}{r^2}$ is **the Lamb frequency,** $L^2=l(l+1)$, $c^2(r)=\gamma P/\rho$ is the squared sound speed, $g(r)=Gm(r)/r^2$ is the gravity acceleration at radius r.

Similarly, the momentum equation is:

$$\frac{dP'}{dr} + \frac{g}{c^2} P' + (N^2 - \omega^2)\rho \xi_r = 0,$$

where N^2 is the Brunt-Vaisala frequency.

The bottom boundary condition (r=0): $\xi_r = 0,$ (or a regularity condition).

The top boundary condition (r=R): $\delta P = P' + \frac{dP}{dr}\xi_r = 0,$

or using the hydrostatic equation: $P' - g\rho\xi_r = 0.$

From the horizontal component of the momentum equation:

$$P' = \omega^2 \rho r \xi_h,$$

Then from the upper boundary condition: $\frac{\xi_h}{\xi_r} = \frac{g}{\omega^2 r},$

that is the ratio of the horizontal and radial components of displacement is inverse proportional to squared frequency. However, this relation does not hold in observations, presumably, because of the external force caused by the solar atmosphere.

7. The derived equations with the boundary conditions constitute an eigenvalue problem for solar oscillation modes

$$\frac{d\xi_r}{dr}+\frac{2}{r}\xi_r-\frac{g}{c^2}\xi_r+\left(1-\frac{S_l^2}{\omega^2}\right)\frac{P'}{\rho c^2}=0,$$

$$\frac{dP'}{dr}+\frac{g}{c^2}P'+(N^2-\omega^2)\rho\xi_r=0.$$

Properties of oscillations depend on the signs of these coefficients in brackets.

$S_l^2=\dfrac{L^2c^2}{r^2}$ is the Lamb frequency.

$N^2=g\left(\dfrac{1}{\gamma P}\dfrac{dP}{dr}-\dfrac{1}{\rho}\dfrac{d\rho}{dr}\right)$ is Brunt–Väisälä frequency.

The bottom boundary condition (r=0): $\xi_r=0$..

The top boundary condition (r=R): $\delta P=P'+\dfrac{dP}{dr}\xi_r=0$

Using the JWKB (asymptotic short-wavelength approximation) theory for the radial eigenfunctions $\xi_r(r)$ and $P'(r)$, we found the solution in the form:

$$\xi_r(r)\propto e^{i\int k_r dr}$$

where the radial wave vector, k_r is determined from the wave dispersion relation:

$$k_r^2=\frac{\omega^2-\omega_c^2}{c^2}-k_h^2$$

The horizontal wave vector, k_h, can be expressed in terms of the spherical harmonic degree, l: $k_h=\dfrac{L}{r}$, $L^2=l(l+1)$.

The wave propagation region (the resonant cavity) is where $k_r^2>0$, and the resonant oscillation frequencies are determined from the quantization rule:

$$\int_{r_1}^{r_2}k_r dr=\pi(n+\alpha).$$

Using the wave dispersion relation and the ray theory, we described the propagation of wave fronts in terms of acoustic rays. The acoustic rays are calculated from the wave group velocity. They are perpendicular to the traveling acoustic wave fronts. The solar oscillations can be described in terms of the resonant (normal) modes, and in terms of the acoustic rays trapped in the propagation regions inside the Sun. These two descriptions can be considered as the mode-ray duality.

JWKB solution for the angular eigenfunctions

We have found that the angular structure of the oscillation modes is described by the spherical harmonics, $Y_{lm}(\theta,\phi)$, which are solutions of:

$$\nabla_h^2 Y_l^m + l(l+1)Y_l^m = 0$$

where ∇_h^2 is the angular part of the Laplacian operator in the spherical coordinates.

$$\frac{1}{\sin\theta}\frac{\partial}{\partial\theta}\left(\sin\theta\frac{\partial Y_l^m}{\partial\theta}\right)+\frac{1}{\sin^2\theta}\frac{\partial^2 Y_l^m}{\partial\phi^2}+l(l+1)Y_l^m=0$$

The spherical harmonics are represented in terms of the associated Legendre functions:

$$Y_l^m(\theta,\phi)=\frac{1}{\sqrt{2\pi}}P_l^m(\cos\theta)e^{im\phi}$$

Substituting this equation and defining variable $x=\cos\theta$ ($dx=\sin\theta d\theta$) we get an equation for $P_l^m(x)$:

$$\frac{d}{dx}\left[(1-x^2)\frac{dP_l^m}{dx}\right]+\left[l(l+1)-\frac{m^2}{1-x^2}\right]P_l^m=0$$

Substituting: $g(x)=\sqrt{1-x^2}P_l^m(x)$, we obtain:

$$(1-x^2)\frac{d^2g}{dx^2}+\left[L^2-\frac{m^2-1}{1-x^2}\right]g=0$$

Thus, we get a second-order 'wave-like' equation for function $g(x)$:

$$\frac{d^2g}{dx^2}+\frac{1}{1-x^2}\left[L^2-\frac{m^2-1}{1-x^2}\right]g=0$$

Using the analogy with the wave equation, we define the longitudinal wave vector k_θ as:

$$k_\theta^2=\frac{1}{1-x^2}\left[L^2-\frac{m^2-1}{1-x^2}\right]$$

or substituting $x=\cos\theta$ for $l,m\gg1$: $k_\theta^2=\frac{1}{\sin^2\theta}\left[L^2-\frac{m^2}{\sin^2\theta}\right]$

The solution of $\frac{d^2g}{dx^2}+k_\theta^2 g=0$ is oscillatory when $k_\theta^2>0$,

that is when $\sin^2\theta>\frac{m^2}{L^2}$, or $|\sin\theta|>\frac{m}{L}$.

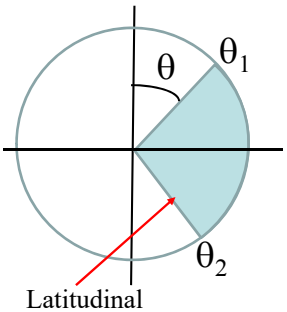

Latitudinal propagation region

This defines the propagation region with the turning points:

$|\sin\theta_{1,2}|=\frac{m}{L}$; $\theta_1=\arcsin\frac{m}{L}$ and $\theta_2=\pi-\theta_1$.

For $m=0$ (zonal spherical harmonics) the resonant cavity is extended from the pole to pole.

For $m=l$ (sectoral harmonics), the resonant cavity is near the equatorial regions.

Three types of spherical harmonics

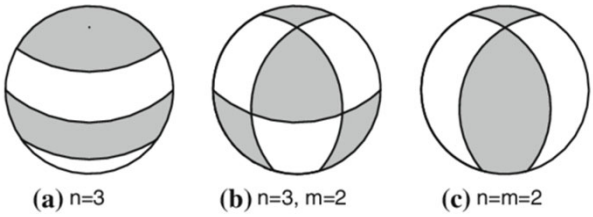

Spherical harmonics: a) zonal, b) tesseral, c) sectoral

Example of latitudinal eigenfunction

p-mode (*l*=20, *m*=16, *n*=14)

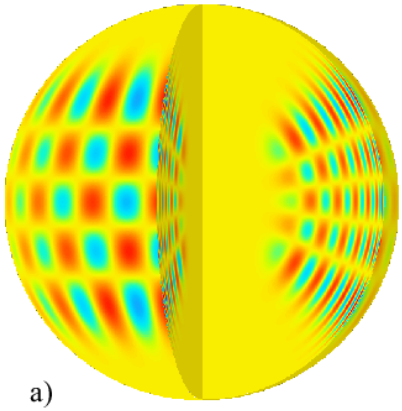

a)

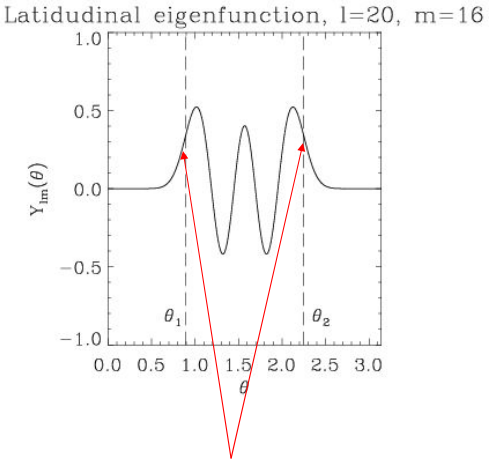

turning points

3D propagation region

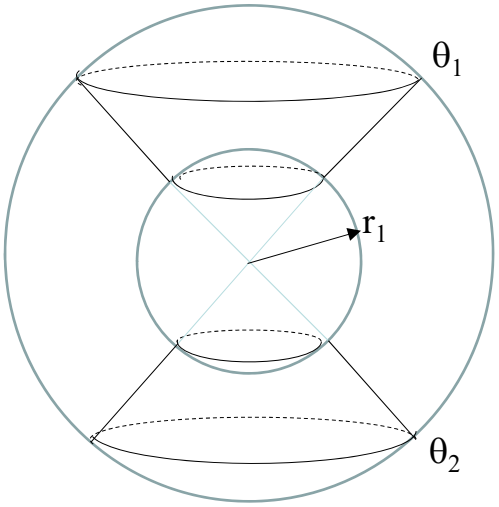

$$\theta_1 = \arcsin\frac{m}{L}$$

$$\frac{c(r_1)}{r_1} = \frac{\omega}{L}$$

$$\theta_2 = \pi - \theta_1$$

3D propagation region

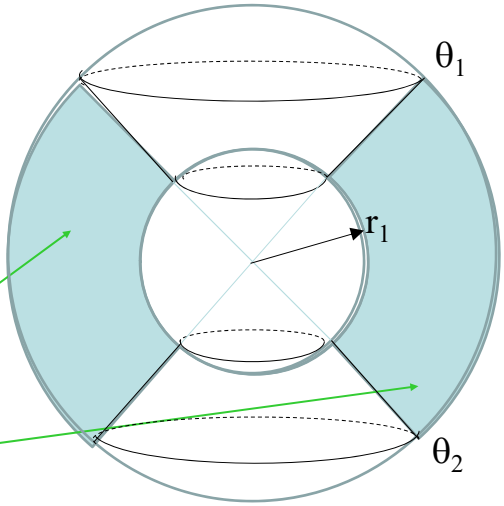

Propagation region

$$\theta_1 = \arcsin\frac{m}{L}$$

$$\frac{c(r_1)}{r_1} = \frac{\omega}{L}$$

$$\theta_2 = \pi - \theta_1$$

3D raypaths

We considered the ray paths for p- and g-mode in a two-dimensional plane defined by the radial and horizontal wave vectors, k_r and k_h. Now, we consider the p-mode ray paths in the 3D Sun. The ray paths correspond to the coordinates of the wave front defined by the wave group velocity, which can be determined by integrating the Hamilton equation:

$$\frac{\partial \vec{r}}{\partial t} = \frac{\partial \omega}{\partial \vec{k}}$$

In the spherical coordinates (r, θ, ϕ), the horizontal wave number: $k_h^2 = k_\theta^2 + k_\varphi{}^2$, and the relation between ω and $\vec{k}$ is given by the dispersion relation:

$$\omega^2 = \omega_c^2 + c^2 k^2 = \omega_c^2 + c^2 (k_r^2 + k_\theta^2 + k_\phi^2)$$

In terms of the spherical harmonic angular degree l and angular degree m: $k_h^2 = \frac{L^2}{r^2}$, $k_\theta^2 = \frac{1}{r}\left[L^2 - \frac{m^2}{\sin^2\theta} \right]$ and $k_\phi = \frac{m}{r \sin\theta}$.

Thus, the time evolution of the wavefront in these coordinates is given by:

$$\frac{\partial r}{\partial t} = \frac{\partial \omega}{\partial k_r} = \frac{c^2}{\omega} k_r = \pm \frac{c^2}{\omega} \sqrt{\frac{\omega^2}{c^2} - \frac{L^2}{r^2}}$$

$$r \frac{\partial \theta}{\partial t} = \frac{\partial \omega}{\partial k_\theta} = \frac{c^2}{\omega} k_\theta = \pm \frac{c^2}{\omega} \sqrt{\frac{L^2}{r^2} - \frac{m^2}{r^2 \sin^2\theta}}$$

$$r \sin\theta \frac{\partial \phi}{\partial t} = \frac{\partial \omega}{\partial k_\phi} = \frac{c^2}{\omega} k_\phi = \frac{c^2}{\omega} \frac{m}{r \sin\theta}$$

The $\pm$ signs in the first two equation determine the direction of wave propagation between the inner turning point and the surface, and between the hemispheres. The wave propagation in the azimuthal (ϕ) direction depends on the m sign.

The relationship between the angles ϕ and θ along the ray path can be determined analytically by solving the equation:

$$\sin\theta\frac{d\phi}{d\theta}=\frac{k_\phi}{k_\theta}=\frac{1}{\sqrt{\frac{L^2}{m^2}\sin^2\theta-1}}$$

$$\phi=\int\frac{d\theta}{\sin\theta\sqrt{\frac{L^2}{m^2}\sin^2\theta-1}}=-\arcsin\left[\frac{\cot\theta}{\sqrt{L^2/m^2-1}}\right]+C$$

$$\sqrt{\frac{L^2}{m^2}-1}=\sqrt{1-\frac{m^2}{L^2}}\frac{L}{m}=\frac{\cos\theta_1}{\sin\theta_1}=\cot\theta_1$$

where we used the turning point equation: $\sin\theta_1=m/L$. Thus, we find:

$$\sin(\phi+C)=\frac{\cot\theta}{\cot\theta_1}$$

This is the great circle equation (the intersection of the sphere and a plane that passes through the center point of the sphere).

3D propagation region

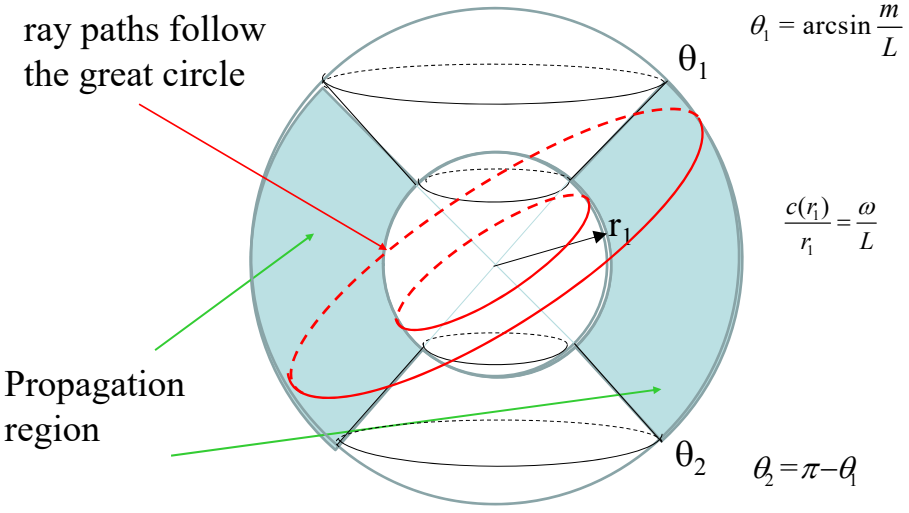

$$\theta_1=\arcsin\frac{m}{L}$$

$$\frac{c(r_1)}{r_1}=\frac{\omega}{L}$$

$$\theta_2=\pi-\theta_1$$

3D propagation region

ray paths follow the great circle

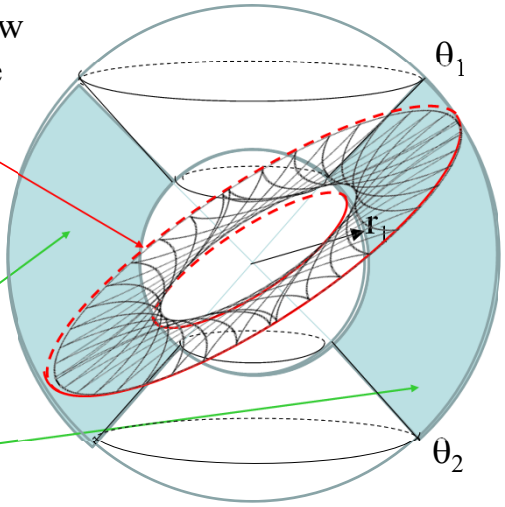

$\theta_1 = \arcsin\frac{m}{L}$

$\frac{c(r_1)}{r_1} = \frac{\omega}{L}$

Propagation region

$\theta_2 = \pi - \theta_1$

These equations are reduced to a system of ODE:

$$\frac{dr}{dt} = \pm\sqrt{1-\frac{L^2c^2}{r^2\omega^2}}$$

$$\frac{d\theta}{dt} = \pm\frac{c^2L}{r^2\omega}\sqrt{1-\frac{m^2}{L^2\sin^2\theta}}$$

$$\frac{d\phi}{dt} = \frac{c^2m}{\omega r^2\sin^2\theta}$$

For numerical integration it is convenient to introduce variables:

$a = \frac{c}{r}$, $b = \frac{cL}{r\omega}$, and $d = \frac{m}{L\sin\theta}$:

$$\frac{dr}{dt} = \pm\sqrt{1-b^2}$$

$$\frac{d\theta}{dt} = \pm ab\sqrt{1-d^2}$$

$$\frac{d\phi}{dt} = \frac{abd}{\sin\theta}$$

For the initial condition, we can choose at the surface equator: $r(t=0)=R$, $\theta(t=0)=\pi/2$, $\phi(t=0)=0$. During the integration, we change the sign at the turning points, r_1 and R, in the first equation, and at θ_1 and θ_2 in the second equation.

The integration results show that the ray paths gradually fill in the 3D region defined by the radial and latitudinal turning points, corresponding the 3D structure of the mode eigenfunctions.

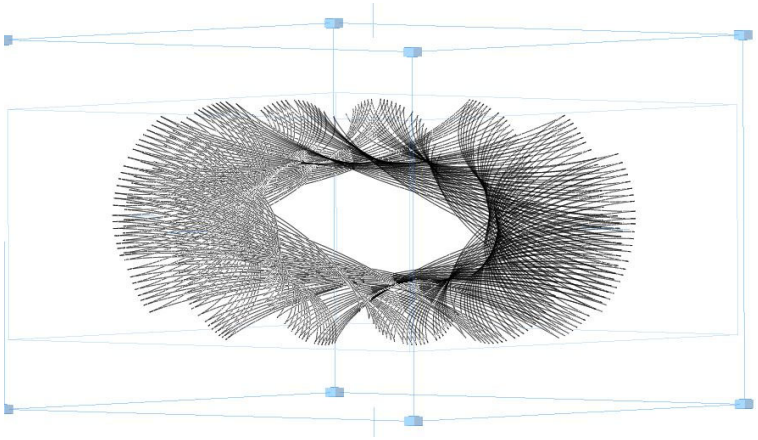

3D ray paths of the oscillation mode: l=20, m=16, n=14

Top view

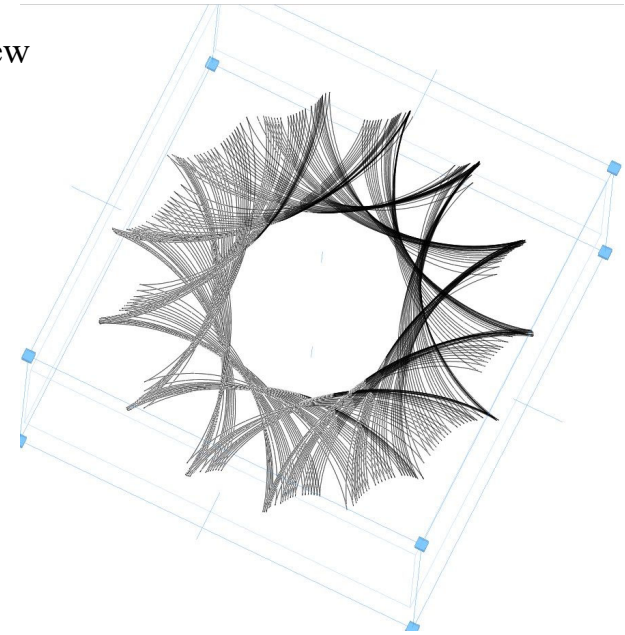

3D ray paths of the oscillation mode: l=20, m=16, n=14

EBK quantization

- The Einstein–Brillouin–Keller method (EBK) is a semiclassical method (named after Albert Einstein, Léon Brillouin, and Joseph B. Keller) used to compute eigenvalues in quantum-mechanical systems. EBK quantization is an improvement from Bohr-Sommerfeld quantization which did not consider the caustic phase jumps at classical turning points.
- It can be applied to 3D systems, for which the number of the quantization rules is equal to the number of the space dimensions.
- (see Course materials:

Gough_Linear_Adiabatic_Stellar_Pulsations.pdf)

Lecture 14
Differential asymptotic inversion. Effects of solar asphericity, rotation and magnetic field

(Stix, Chapter 5.3.1; Kosovichev, p.34-41, 44-48; Christensen-Dalsgaard, Chapters 5.5)

Solar oscillation spectrum obtained from the HMI instrument on Solar Dynamics Observatory.

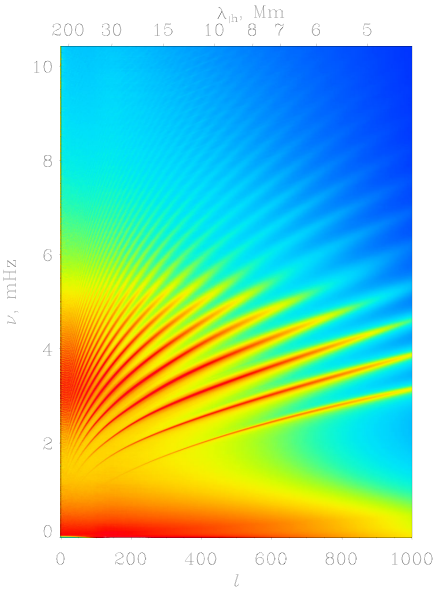

Spectrum of normal modes calculated for a standard solar model. Note the 'avoided crossing effect' for f and g-modes.

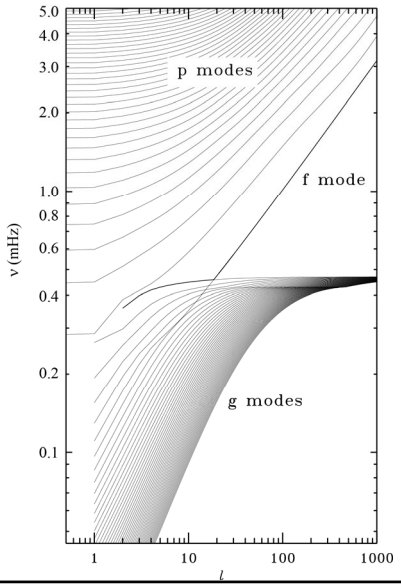

Asymptotic raypath approximation

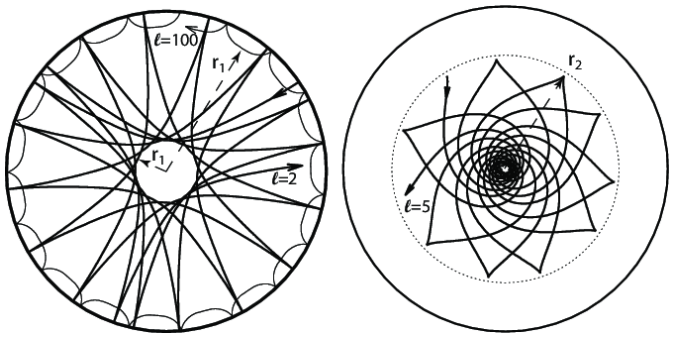

Ray paths for:
a) two solar p-modes of angular degree $l = 2$, frequency $\nu = 1429.4$ μHz (thick curve), and $l = 100$, $\nu = 3357.5$ μHz (thin curve);

b) g-mode of $l = 5$, $\nu = 192.6$ μHz (the dotted curve indicates the base of the convection zone). The lower turning points, r_1 of the p-modes are shown by arrows. The upper turning points of these modes are close to the surface and not shown. For the g-mode, the upper turning point, r_2, is shown by arrow. The inner turning point is close to the center and not shown.

Duvall's law (asymptotic p-mode relation)

Consider the p-mode dispersion relation:

$$\int_{r_1}^{R} k_r dr = \pi(n+\alpha)$$

$$\int_{r_1}^{R} \left(\frac{\omega^2}{c^2} - \frac{L^2}{r^2} \right)^{1/2} dr = \pi(n+\alpha)$$

Dividing left and right-hand sides by ω we get:

$$\int_{r_1}^{R} \left(\frac{r^2}{c^2} - \frac{L^2}{\omega^2} \right)^{1/2} \frac{dr}{r} = \frac{\pi(n+\alpha)}{\omega}$$

Radius r_1 (or r_t) of the lower turning point depends only on ratio L/ω. Hence, the left-hand side is a function of L/ω:

$$F\left(\frac{L}{\omega}\right) = \frac{\pi(n+\alpha)}{\omega}$$

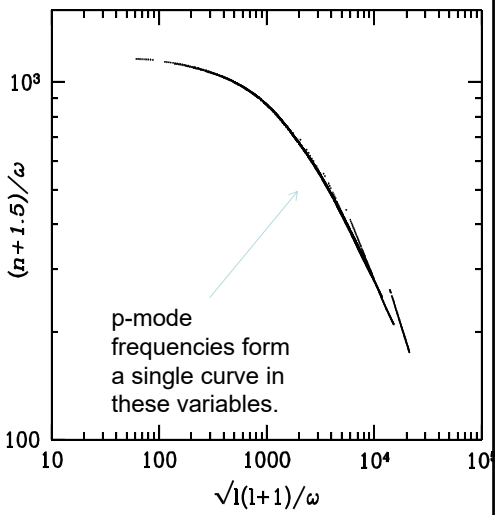

where $L = \sqrt{l(l+1)}$ $\alpha \approx 1.5$

Acoustic travel time

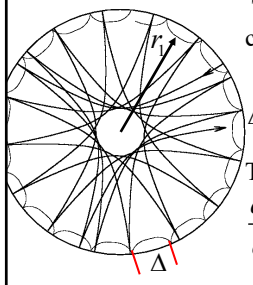

The distance, Δ, between the surface points for one skip can be calculated as the integral:

$$\Delta = 2\int_{r_1}^{R} d\theta = 2\int_{r_1}^{R} \frac{L/r}{\sqrt{\omega^2/c^2 - L^2/r^2}}\,dr \equiv 2\int_{r_1}^{R} \frac{c/r}{\sqrt{\omega^2/L^2 - c^2/r^2}}\,dr.$$

The corresponding travel time is calculated by integrating equation:

$$\frac{dr}{dt} = \frac{\partial\omega}{\partial k_r}: \qquad dt = \frac{dr}{c\left(1 - k_h^2 c^2/\omega^2\right)^{1/2}}.$$

$$\tau = 2\int_{r_1}^{R} dt = 2\int_{r_1}^{R} \frac{dr}{c\left(1 - k_h^2 c^2/\omega^2\right)^{1/2}} \equiv 2\int_{r_1}^{R} \frac{dr}{c\left(1 - L^2 c^2/r^2\omega^2\right)^{1/2}}$$

These equations give a *time-distance* relation, $\tau - \Delta$, for acoustic waves traveling between two surface points through the solar interior. The ray representation of the solar modes and the time-distance relation provided a motivation for developing *time-distance helioseismology*

Differential asymptotic sound-speed inversion. 1

To find corrections to the standard solar model we consider small perturbations to the sound speed profile and oscillation frequencies, and linearize the dispersion relation by using the first-order Taylor expansion:

$$\int_{r_1}^{R} \left[\frac{(\omega+\Delta\omega)^2}{(c+\Delta c)^2} - \frac{L^2}{r^2}\right]^{1/2} dr = \pi(n+\alpha+\Delta\alpha).$$

$$\int_{r_1}^{R} \frac{\omega^2}{c^2} \frac{\left(\frac{\Delta\omega}{\omega} - \frac{\Delta c}{c}\right)dr}{\left(\frac{\omega^2}{c^2} - \frac{L^2}{r^2}\right)^{1/2}} = \pi\Delta\alpha$$

$$\frac{\Delta\omega}{\omega}\int_{r_1}^{R} \frac{dr}{c\left(1 - \frac{L^2c^2}{r^2\omega^2}\right)^{1/2}} = \int_{r_1}^{R} \frac{\Delta c}{c} \frac{dr}{c\left(1 - \frac{L^2c^2}{r^2\omega^2}\right)^{1/2}} + \frac{\pi\Delta\alpha}{\omega}.$$

$T(L/\omega)$ $\qquad$ $\Phi(L/\omega)$ $\qquad$ $\beta(\omega)$

r_1 is a function of L/ω.

Differential asymptotic sound-speed inversion. 2

The p-mode travel time is calculated by using the ray-path theory.
It corresponds to the half-skip time: T=τ/2, and is a function of L/ω.
Therefore, the observed frequency difference can be represented in the form:

$$\frac{\Delta\omega}{\omega}T = \Phi\left(\frac{L}{\omega}\right) + \beta(\omega)$$

$$\Phi\left(\frac{L}{\omega}\right) = \int_{r_1}^{R} \frac{\Delta c}{c} \frac{dr}{c\left(1 - \frac{L^2c^2}{r^2\omega^2}\right)^{1/2}}$$

Once the function Φ(L/ω) is determined from the observed frequency difference we can find Δc/c as a function of radius by solving the integral equation. This equation is reduced to the Abel integral equation, and has an analytical solution.

Functions Φ(L/w) and β(ω) are determined by fitting (Δω/ω)T which depends on both L/ω and ω.

Differential asymptotic sound-speed inversion. 3

$$\Phi\left(\frac{L}{\omega}\right) = \int_{r_1}^{R} \frac{\Delta c}{c} \frac{dr}{c\left(1 - \frac{L^2c^2}{r^2\omega^2}\right)^{1/2}},$$

Here c(r) is the sound-speed profile of the standard solar model, and *ω(l,n)* are the p-mode frequencies calculated for the standard solar model. This equation can be reduced to the standard Abel integral equation by making a substitution of variables. The new variables are:

$x = \frac{\omega^2}{L^2}$ and $y = \frac{c^2}{r^2}$, where x is a measured quantity, y is unknown function

x can be considered as a continuous function according to the Duvall's law

$$F(x) = \int_0^x \frac{f(y)dy}{\sqrt{x-y}}, \quad \text{where} \quad F(x) = \Phi(x)\frac{1}{\sqrt{x}},$$

$$f(y) = \frac{\Delta c}{c} \frac{1}{2y^{3/2}\left(1 - \frac{d\log c}{d\log r}\right)}.$$

Solution of the Abel integral equation

$$F(x) = \int_0^x \frac{f(y)dy}{\sqrt{x-y}},$$

To solve for $f(y)$ we multiply both sides of this equation by $dx/\sqrt{z-x}$ and integrate with respect to x from 0 to z:

$$\int_0^z \frac{F(x)dx}{\sqrt{z-x}} = \int_0^z \frac{dx}{\sqrt{z-x}} \int_0^x \frac{f(y)dy}{\sqrt{x-y}} == \int_0^z f(y)dy \int_y^z \frac{dx}{\sqrt{(z-x)(x-y)}}.$$

Here we changed the order of integration.

Note that $$\int_y^z \frac{dx}{\sqrt{(z-x)(x-y)}} = \pi,$$

then $$\int_0^z \frac{F(x)dx}{\sqrt{z-x}} = \pi \int_0^z f(y)dy.$$

Differentiating with respect to z, and replacing z with y we obtain the final solution:

$$f(y) = \frac{1}{\pi}\frac{d}{dy}\int_0^y \frac{F(x)dx}{\sqrt{y-x}}.$$

Asymptotic sound-speed inversion. 4

The asymptotic inversion is performed in 3 steps:

1) Find $\Phi\left(\frac{L}{\omega}\right)$ and $\beta(\omega)$ by fitting $\frac{\Delta\omega}{\omega}T = \Phi\left(\frac{L}{\omega}\right) + \beta(\omega)$

2) Solve $F(x) = \int_0^x \frac{f(y)dy}{\sqrt{x-y}}$, where $F(x) = \Phi(x)\frac{1}{\sqrt{x}}$, $x = \frac{\omega^2}{L^2}$

$$f(y) = \frac{1}{\pi}\frac{d}{dy}\int_0^y \frac{F(x)dx}{\sqrt{y-x}}.$$

3) Calculate $\frac{\Delta c}{c} = 2f(y)y^{3/2}\left(1 - \frac{d\log c}{d\log r}\right)$ where $y = \frac{c^2}{r^2}$,

$c(r)$ is the sound speed from the standard model.

Finally, we find the difference in the sound speed between the Sun and the model.

Abel integral equation and fractional calculus

Consider the Abel integral equation in the operator form:

$$F(x) = \frac{1}{\sqrt{\pi}} \int_0^x \frac{f(y)dy}{\sqrt{x-y}} = A \cdot f(y),$$

where A is the integrating operator with the weighting function $1/\sqrt{x-y}$. By applying operator A to the Abel equation we obtain:

$$A \cdot F(x) = \int_0^z f(y)dy.$$

Hence,

$$A^2 \cdot f(y) = \int_0^z f(y)dy.$$

This means that operator A^2 is integral, and A can be interpreted as half-integral.

Therefore, the solution of the Abel equation is a half-derivative:

$$f(y) = A^{-1} \cdot F(z)|_{z=y} \equiv D^{1/2} F.$$

Example: $D^{1/2} x = \frac{2}{\sqrt{\pi}} x^{1/2}$. Roughly, $\frac{\Delta c}{c} \propto D^{1/2}\left(\frac{\Delta \omega}{\omega}\right)$.

Test of the differential inversion technique

For small deviations of the solar structure from a solar model this technique is substantially more accurate than the original (non-linear) asymptotic inversion.

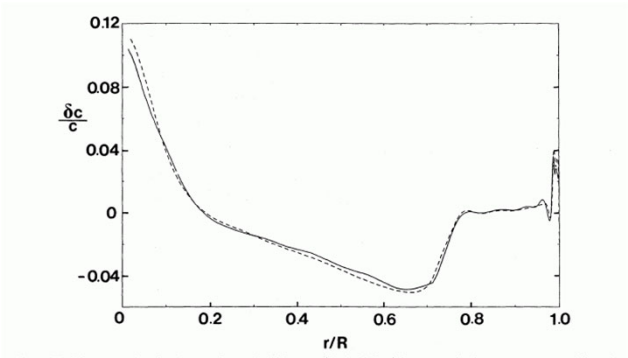

Figure 7. The exact fractional sound-speed difference (dashed line) between the homogeneous model and Model 1, as a fraction of the sound speed of the latter, and the estimate (solid line) inferred using a 28 w-, 20 ω-spline knot fit and the mode set defined at the beginning of Section 5. The functions are plotted against fractional radius r/R.

(Christensen-Dalsgaard et al 1989)

Illustration of asymptotic sound-speed inversion

Codes:

1) Time-distance diagram for p-modes (travel_time.pro)
2) Frequency difference, determination of functions $\Phi(L/\omega)$ and $\beta(\omega)$ (frequency_difference.pro)

Input data:

1. SOHO/MDI frequency measurements of Johann Reiter
2. Standard solar model (Christensen-Dalsgaard et al)

Observed p- and f-mode frequencies

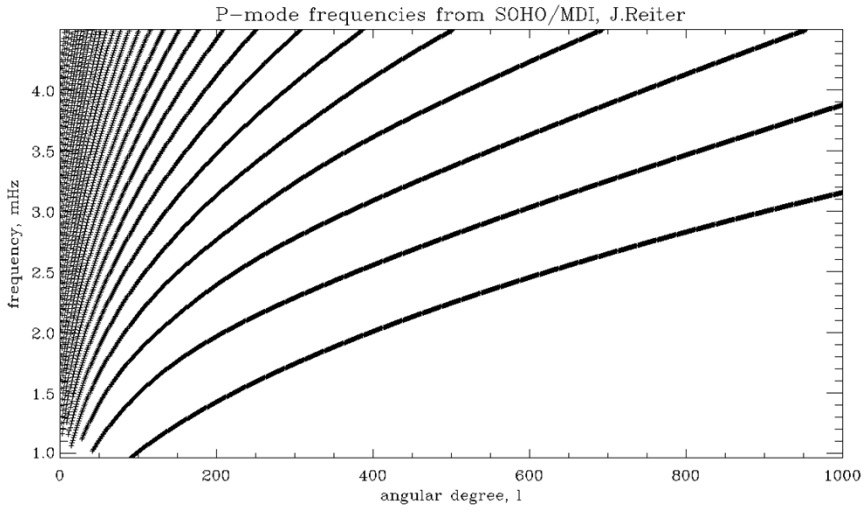

Difference between observed and model frequencies vs l/ν

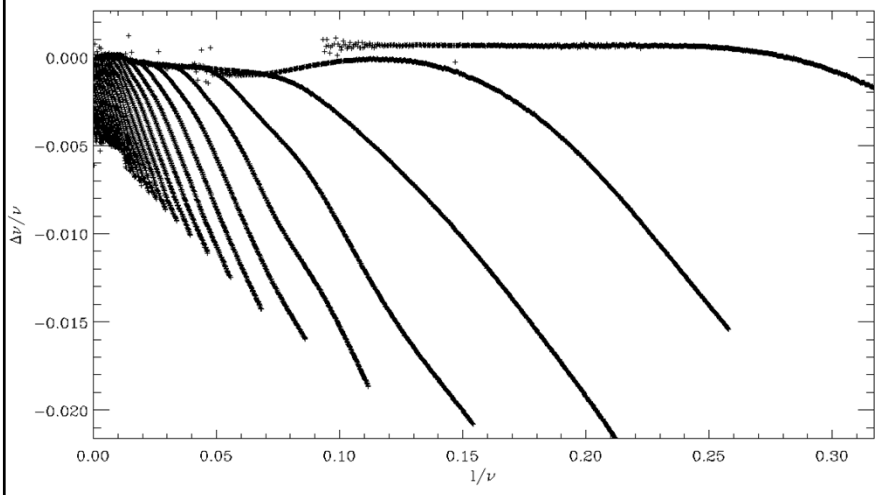

Difference between observed and model frequencies vs ν

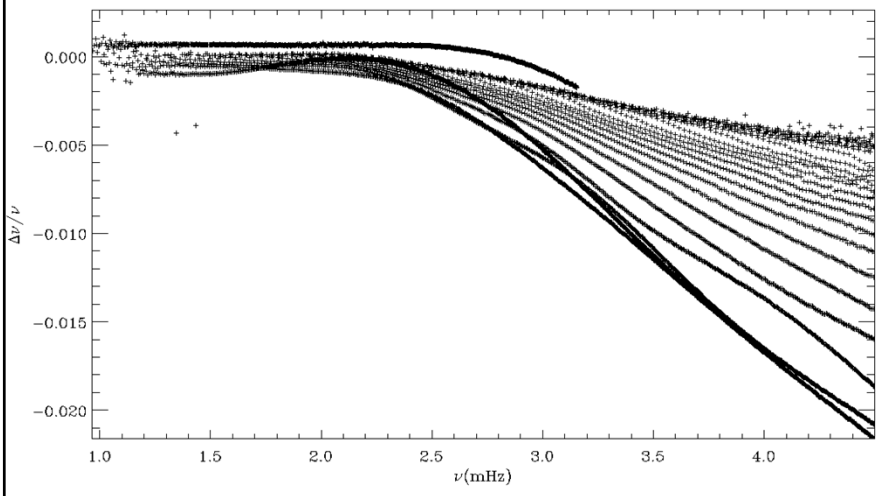

Difference between observed and model frequencies vs l/ν for $\nu < 2$ mHz

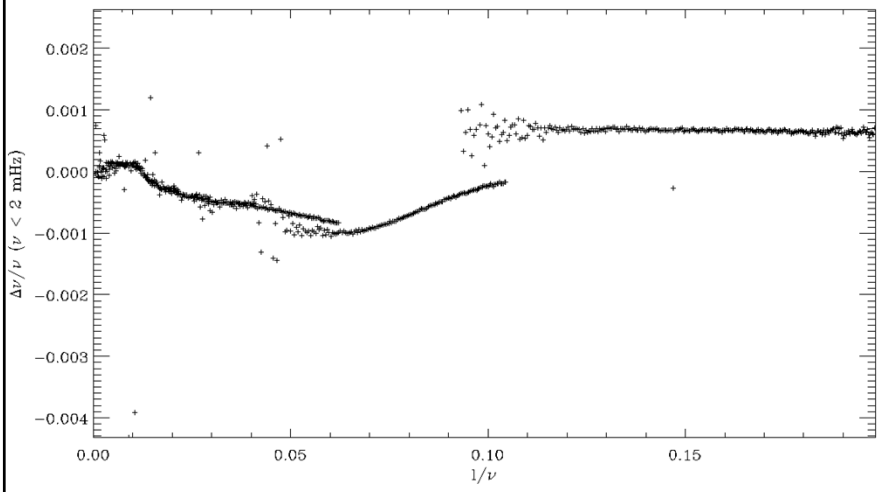

Difference between observed and model frequencies vs r_1 for $\nu < 2$ mHz

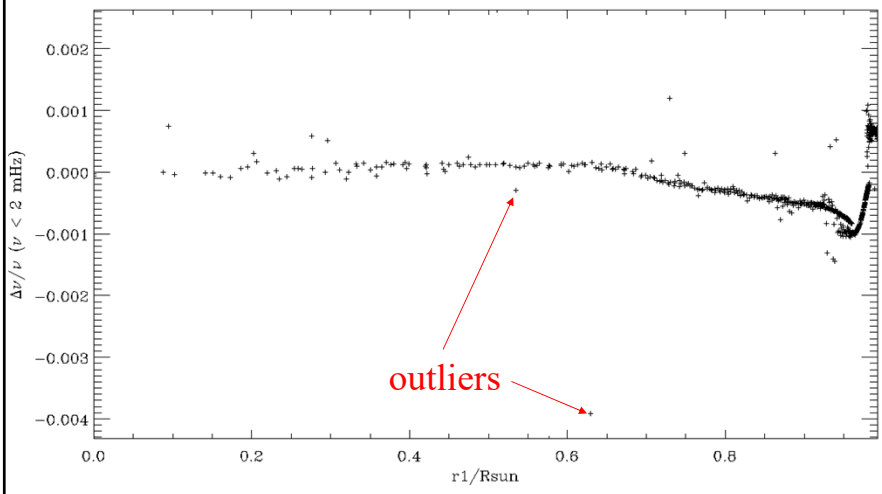

Difference between observed and model frequencies vs r_1 for $\nu < 2$ mHz

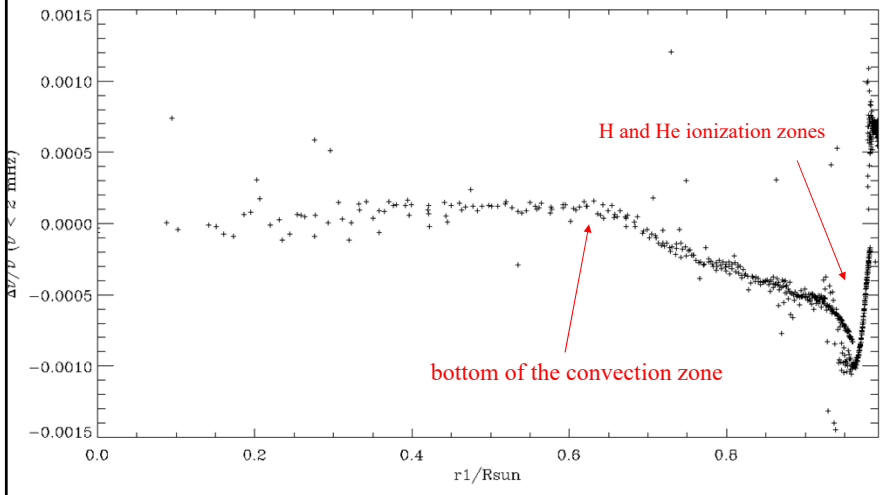

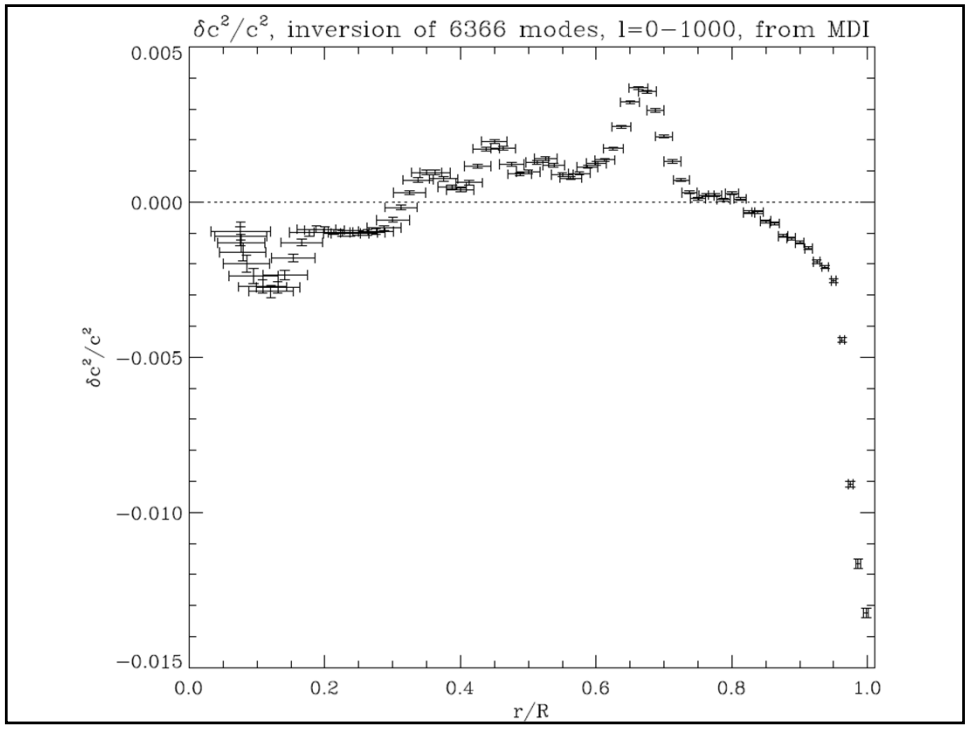

Effects solar asphericity

For a spherically symmetrical solar structure, when the sound speed is a function of radius, $c = c(r)$, the p-mode frequencies are determined from the Bohr quantization rule:

$$\int_{r_1}^{R} k_r dr = \pi(n+\alpha)$$

where $k_r = \sqrt{\frac{\omega^2}{c^2} - \frac{L^2}{r^2}}$, and $L^2 = l(l+1)$. The RHS of this equation can be considered as averaging of the radial wave vector, k_r, within the wave propagation region, $[r_1, R]$.

If the sound-speed variations are not spherically symmetric, e.g. due internal flows and magnetic fields, $c = c(r,\theta,\phi)$, then we have to use the EBK quantization rule, and average the wave vector over the 3D wavepath great circle:

$$\frac{1}{2\pi}\int_0^{2\pi}\int_{r_1}^{R} k_r dr d\phi' = \pi(n+\alpha)$$

where ϕ' is the polar angle along the great circle.

3D propagation region

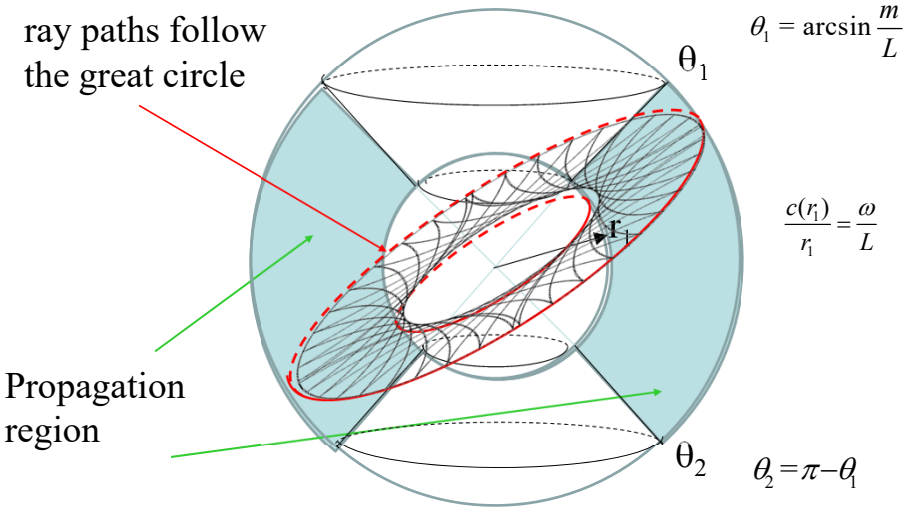

3D raypaths

We considered the ray paths for p- and g-mode in a two-dimensional plane defined by the radial and horizontal wave vectors, k_r and k_h. Now, we consider the p-mode ray paths in the 3D Sun. The ray paths correspond to the coordinates of the wave front defined by the wave group velocity, which can be determined by integrating the Hamilton equation:

$$\frac{\partial \vec{r}}{\partial t} = \frac{\partial \omega}{\partial \vec{k}}$$

In the spherical coordinates (r, θ, ϕ), the horizontal wave number: $k_h^2 = k_\theta^2 + k_\varphi{}^2$, and the relation between ω and $\vec{k}$ is given by the dispersion relation:

$$\omega^2 = \omega_c^2 + c^2 k^2 = \omega_c^2 + c^2 (k_r^2 + k_\theta^2 + k_\phi^2)$$

In terms of the spherical harmonic angular degree l and angular degree m: $k_h^2 = \frac{L^2}{r^2}$, $k_\theta^2 = \frac{1}{r}\left[L^2 - \frac{m^2}{\sin^2\theta} \right]$ and $k_\phi = \frac{m}{r \sin\theta}$.

Thus, the time evolution of the wavefront in these coordinates is given by:

$$\frac{\partial r}{\partial t} = \frac{\partial \omega}{\partial k_r} = \frac{c^2}{\omega} k_r = \pm \frac{c^2}{\omega} \sqrt{\frac{\omega^2}{c^2} - \frac{L^2}{r^2}}$$

$$r \frac{\partial \theta}{\partial t} = \frac{\partial \omega}{\partial k_\theta} = \frac{c^2}{\omega} k_\theta = \pm \frac{c^2}{\omega} \sqrt{\frac{L^2}{r^2} - \frac{m^2}{r^2 \sin^2\theta}}$$

$$r \sin\theta \frac{\partial \phi}{\partial t} = \frac{\partial \omega}{\partial k_\phi} = \frac{c^2}{\omega} k_\phi = \frac{c^2}{\omega} \frac{m}{r \sin\theta}$$

The $\pm$ signs in the first two equation determine the direction of wave propagation between the inner turning point and the surface, and between the hemispheres. The wave propagation in the azimuthal (ϕ) direction depends on the m sign.

The relationship between the angles ϕ and θ along the ray path can be determined analytically by solving the equation:

$$\sin\theta\frac{d\phi}{d\theta}=\frac{k_\phi}{k_\theta}=\frac{1}{\sqrt{\frac{L^2}{m^2}\sin^2\theta-1}}$$

$$\phi=\int\frac{d\theta}{\sin\theta\sqrt{\frac{L^2}{m^2}\sin^2\theta-1}}=-\arcsin\left[\frac{\cot\theta}{\sqrt{L^2/m^2-1}}\right]+C$$

$$\sqrt{\frac{L^2}{m^2}-1}=\sqrt{1-\frac{m^2}{L^2}}\frac{L}{m}=\frac{\cos\theta_1}{\sin\theta_1}=\cot\theta_1$$

where we used the turning point equation: $\sin\theta_1=m/L$. Thus, we find:

$$\sin(\phi+C)=\frac{\cot\theta}{\cot\theta_1}$$

This is the great circle equation (the intersection of the sphere and a plane that passes through the center point of the sphere).

The integration results show that the ray paths gradually fill in the 3D region defined by the radial and latitudinal turning points, corresponding the 3D structure of the mode eigenfunctions.

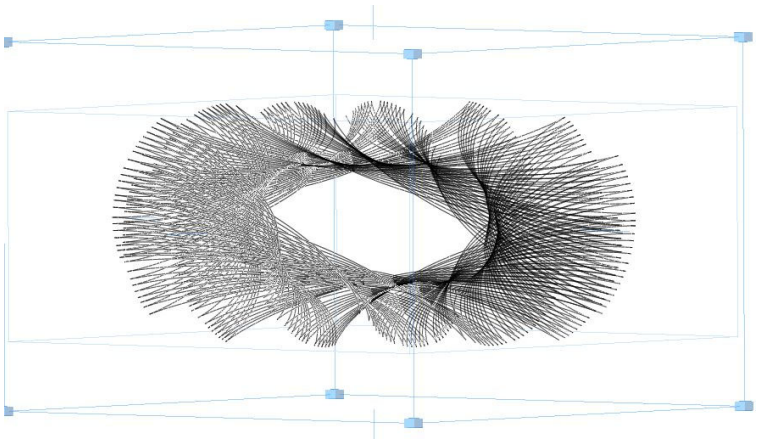

3D ray paths of the oscillation mode: l=20, m=16, n=14

Top view

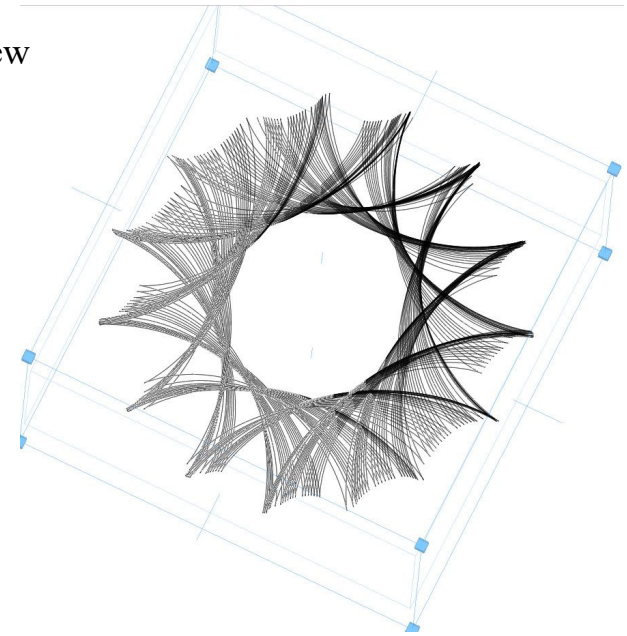

3D ray paths of the oscillation mode: l=20, m=16, n=14

If the sound-speed variations are not spherically symmetric, e.g. due internal flows and magnetic fields, $c = c(r,\theta,\phi)$, then we have to use the EBK quantization rule, and average the wave vector over the 3D wavepath great circle:

$$\frac{1}{2\pi}\int_0^{2\pi}\int_{r_1}^{R} k_r dr d\phi' = \pi(n+\alpha)$$

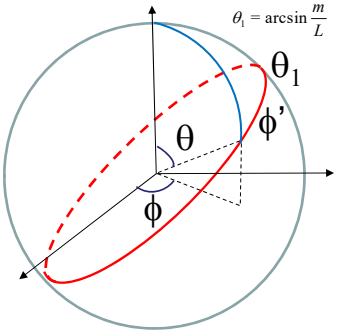

The 3D ray tracing shows that each of the wavepath great circles, filling in the 3D propagation region, is inclined relative to the polar axis by the angle, θ_1. This angle represents the co-latitude of the angular turning point, and depends on the mode angular degree, l, and order, m: $\theta_1 = \arcsin(m/L)$.

Thus, the angle ϕ' can be determined as the distance from the angular turning point with coordinates $(\theta_1, \pi/2)$ and a point on the great circle with coordinates (θ,ϕ) in the coordinate system shown in the figure.

This angle is determined from the spherical triangle equation:

$$\cos\phi' = \cos\theta_1\cos\theta + \sin\theta_1\sin\theta\cos(\pi/2-\phi)$$

$$\cos\phi' = \cos\theta_1\cos\theta + \sin\theta_1\sin\theta\sin(\phi)$$

Then, substituting the great circle equation:

$\sin\phi = \dfrac{\cot\theta}{\cot\theta_1}$, we get: $\cos\phi' = \dfrac{\cos\theta}{\cos\theta_1}$.

Differentiating this equation, we find $d\phi'$ as a function of colatitude θ: $\sin\phi' d\phi' = -\dfrac{\sin\theta}{\cos\theta_1} d\theta$.

$$d\phi' = -\frac{\sin\theta}{\cos\theta_1}\frac{1}{\sqrt{1-\cos^2\theta/\cos^2\theta_1}}d\theta = -\frac{\sin\theta d\theta}{\sqrt{\cos^2\theta_1-\cos^2\theta}} = \frac{d\mu}{\sqrt{M^2-\mu^2}},$$

where $\mu = \cos\theta$, and $M^2 = \cos^2\theta_1 = 1-\sin^2\theta_1 = 1-\dfrac{m^2}{L^2}$.

Substituting in the 3D quantization equation:

$$\frac{1}{\pi}\int_0^{\pi} d\phi' \int_{r_1}^{R} k_r dr = \frac{1}{\pi}\int_{-M}^{M} \frac{d\mu}{\sqrt{M^2-\mu^2}} \int_{r_1}^{R} k_r dr = \pi(n+\alpha)$$

or

$$\frac{2}{\pi}\int_0^{M} \frac{d\mu}{\sqrt{M^2-\mu^2}} \int_{r_1}^{R} \sqrt{\frac{\omega_{nml}^2}{c^2(r,\mu)} - \frac{L^2}{r^2}}\, dr = \pi(n+\alpha)$$

In this case, the oscillation frequencies depend on all three quantum numbers: radial order n, angular degree l, and angular degree m.

Because all the ray paths sample the sound speed over the whole range of longitude ϕ, only the azimuthally averaged 2D sound-speed component $c(r,\theta)$ or $c(r,\mu)$ can be determined from the oscillation frequencies. However, this is valid only when the deviations from the sphericity are small.

Repeating the linearization procedure for the case of small deviations $\Delta c(r,\mu)$ from a spherically symmetrical solar model, we obtain the equation for the 2D differential asymptotic inversion:

$$\frac{\Delta\omega_{nlm}}{\omega_{0,nl}} = \frac{2}{\pi T}\int_0^{M} d\mu \int_{r_1}^{R} \frac{\Delta c(r,\mu)/c}{\sqrt{M^2-\mu^2}\sqrt{1-L^2c^2/\omega_{0,nl}^2 r^2}} \frac{dr}{c}$$

where $\Delta\omega_{nlm} = \omega_{nlm} - \omega_{0,nl}$ is the difference between the observed frequencies ω_{nlm} and model frequencies $\omega_{0,nl}$.

The model frequencies are calculated for a spherically symmetric solar model and do not depend on m. The latitudinal dependence of the sound speed (solar asphericity) lifts the frequency degeneracy with respect to m.

This equation represents a 2D Abel integral equation, and can be solved similarly to the 1D equation.

Effects of rotation

Solar rotation and other plasma flows inside the Sun cause Doppler shift of the wave frequencies. The dispersion relation for the acoustic waves becomes:

$$(\omega - \vec{k}\vec{v})^2 = \omega_c^2 + k^2 c^2$$

where $\vec{k}$ is the wave vector, and $\vec{v}$ is the plasma velocity.

Because of the acoustic ray paths travel in the great circles, they sample the radial and latitudinal components of velocity twice in the opposite directions. Thus, the contribution of these components to the quantization integral is canceled in the first approximation, and the mode frequencies depend only on the azimuthal component, v_ϕ:

$$(\omega - k_\phi v_\phi)^2 = \omega_c^2 + k^2 c^2$$

where $k_\phi = \dfrac{m}{r\sin\theta}$. Representing v_ϕ in terms of the angular velocity, $\Omega(r,\theta)$:

$$v_\phi = r\sin\theta\,\Omega(r,\theta),$$

we get:

$$(\omega - m\Omega)^2 = \omega_c^2 + k^2 c^2$$

The EBK quantization equation takes form:

$$\frac{2}{\pi}\int_0^M \frac{d\mu}{\sqrt{M^2-\mu^2}}\int_{r_1}^R \sqrt{\frac{(\omega_{nlm}-m\Omega)^2}{c^2} - \frac{L^2}{r^2}}\,dr = \pi(n+\alpha)$$

Assuming that $m\Omega/\omega_{nlm} \ll 1$ and that the background solar structure is spherically symmetric, we represent ω_{nlm} in terms of the frequency deviations from the model frequencies: $\Delta\omega_{nlm} = \omega_{nlm} - \omega_{0,nl}$.

$$\frac{2}{\pi}\int_0^M \frac{d\mu}{\sqrt{M^2-\mu^2}}\int_{r_1}^R \sqrt{\frac{(\omega_{0,nl}+\Delta\omega_{nlm}-m\Omega)^2}{c^2} - \frac{L^2}{r^2}}\,dr = \pi(n+\alpha)$$

Performing the first-order Taylor expansion and subtracting the quantization rule for the background state, we get:

$$\frac{2}{\pi}\int_0^M \frac{d\mu}{\sqrt{M^2-\mu^2}}\int_{r_1}^R \frac{\omega^2}{c^2}\frac{\left[\dfrac{\Delta\omega_{nlm}}{\omega} - \dfrac{m\Omega}{\omega}\right]}{\sqrt{\dfrac{\omega^2}{c^2} - \dfrac{L^2}{r^2}}}\,dr = 0$$

where for simplicity we drop subscript for the model frequencies: $\omega = \omega_{0,nl}$.

Thus, we obtain:

$$\Delta\omega_{nlm} = \frac{2}{\pi T}\int_0^M \int_{r_1}^R \frac{m\Omega(r,\mu)drd\mu}{c\sqrt{M^2-\mu^2}\sqrt{1-L^2c^2/r^2\omega^2}}$$

where $T = \int_{r_1}^R \frac{dr}{c\sqrt{1-L^2c^2/r^2\omega^2}}$ is the "half-skip" travel time of acoustic waves.

The solar rotation causes 'rotational frequency splitting' proportional to the mode angular degree m.

The physical interpretation is that the modes with positive m travel in the same direction as the solar rotation and thus have higher frequencies then the modes with negative m traveling in the opposite direction.

Recall that that the oscillation modes are represented in terms of the spherical harmonics: $\xi_r(r,\theta,\phi,t) \propto P_l^m(\theta)\exp(im\phi - i\omega t)$, and thus, in the form of azimuthal traveling waves

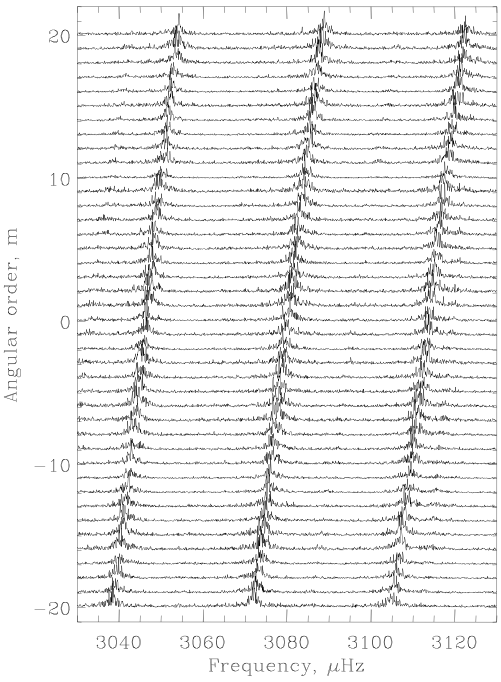

Illustration of the frequency shift due to the solar rotation

Typical power spectra of solar oscillation data from the MDI instrument on SOHO. Each horizontal curve shows three lines of the power spectrum for different azimuthal order m with radial order $n = 15$ and angular degree $l = 19, 20$, and 21 (from left to right). The slope of the modal lines is due to the rotational frequency shift: prograde modes with positive m have higher frequencies than retrograde modes with negative m.

Frequency splitting, l=150

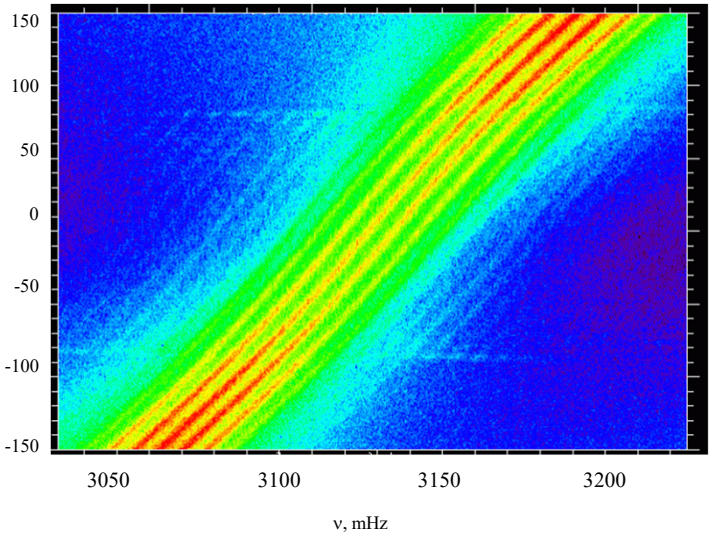

(F. Hill)

By comparing the effect of the sound-speed asphericity and rotation:

$$\frac{\Delta\omega_{nlm}}{\omega} = \frac{2}{\pi T}\int_0^M \int_{r_1}^R \frac{\left[\Delta c(r,\mu)/c\right] dr d\mu}{c\sqrt{M^2-\mu^2}\sqrt{1-L^2c^2/\omega^2 r^2}}$$

$$\Delta\omega_{nlm} = \frac{2}{\pi T}\int_0^M \int_{r_1}^R \frac{m\Omega(r,\mu) dr d\mu}{c\sqrt{M^2-\mu^2}\sqrt{1-L^2c^2/r^2\omega^2}}$$

where $M = \sqrt{1-m^2/L^2}$

We notice that the frequency splitting due to the sound-speed asphericity is an even function of m and an odd function of m due the rotation.

This difference allows us to separate effects of the solar asphericity and rotation in the observational data.

The a-coefficients

The observational data are often represented as an expansion in terms of the Legendre polynomials:

$$\Delta\omega_{nlm} = L\sum_{k=1}^{N} a_k^{nl} P_k\left(\frac{m}{L}\right)$$

For a more accurate (non-asymptotic) representation, the expansion is performed in terms of Clebsch-Gordon coefficients, which will be considered later.

In this representation, the 'even' a-coefficients represent effects of the solar asphericity, and the 'odd' a-coefficients represent the internal solar rotation and its variations with latitude (zonal flows). In addition, the representations in the form of the a-coefficients allows us to replace the 2D inversions of $\Delta\omega_{nlm}$ with a series of 1D inversions of the a-coefficients.

Specifically, representing the sound-speed perturbation in terms of the Legendre polynomials:

$$\frac{\Delta c}{c}(r,\mu) = \sum_{j=1}^{J} A_{2j}(r) P_{2j}(\mu)$$

where $\mu = \cos\theta$.

Substituting this representation of $\frac{\Delta c}{c}(r,\mu)$ in the equation for $\Delta\omega_{nlm}/\omega$, we obtain:

$$\frac{\Delta\omega_{nlm}}{\omega} = \sum_{j=1}^{J} \frac{1}{T}\int_{r_1}^{R} \frac{A_{2j}(r)dr}{\sqrt{1-L^2c^2/r^2\omega^2}} \left(\frac{2}{\pi}\int_0^M \frac{P_{2j}(\mu)}{\sqrt{M^2-\mu^2}} d\mu\right)$$

The second integral is calculated analytically:

$$\frac{2}{\pi}\int_0^M \frac{P_{2j}(\mu)}{\sqrt{M^2-\mu^2}} d\mu = (-1)^j P_{2j}(0) P_{2j}(m/L)$$

Thus, both the observational data and the angular integral of the sound-speed asphericity are represented in terms of the series of Legendre polynomial $P_{2j}(m/L)$.

We obtain a series of the Abel integral equations for the radial functions of the asphericity, $A_{2j}(r)$:

$$\frac{1}{T}\int_{r_1}^{R} \frac{A_{2j}(r)dr}{\sqrt{1-L^2c^2/\omega^2r^2}} = (-1)^j \frac{La_{2j}^{ln}}{P_{2j}(0)}.$$

These equations establish a relationship between the even a-coefficients and the solar asphericity expressed in terms of the Legendre polynomials.

A similar type of solution can be obtained for the angular velocity $\Omega(r,\mu)$. In this case, it is convenient to use the expansion in terms of associate Legendre functions:

$$\Omega(r,\mu)=\sum_{j=0}^{J}\Omega_{2j+1}(r)\frac{P_{2j+!}^{1}(\cos\theta)}{\sin\theta}$$

Substituting in:

$$\Delta\omega_{nlm}=\frac{2}{\pi T}\int_0^M\int_{r_1}^R\frac{m\Omega(r,\mu)drd\mu}{c\sqrt{M^2-\mu^2}\sqrt{1-L^2c^2/r^2\omega^2}}$$

we obtain:

$$\Delta\omega_{nlm}=\sum_{j=0}^{J}\frac{1}{T}\int_{r_1}^R\frac{\Omega_{2j+1}(r)dr}{c\sqrt{1-L^2c^2/r^2\omega^2}}\left(\frac{2m}{\pi}\int_0^M\frac{P_{2j+1}^{1}d\mu}{\sqrt{1-\mu^2}\sqrt{M^2-\mu^2}}\right)$$

The second integral is calculated analytically:

$$\frac{2m}{\pi}\int_0^M\frac{P_{2j+1}^{1}d\mu}{\sqrt{1-\mu^2}\sqrt{M^2-\mu^2}}=-\frac{\pi}{2}(2j+1)P_{2j}(0)\frac{L}{m}P_{2j+1}\left(\frac{m}{L}\right)$$

Both the observational data and the angular integral of the solar rotation are expressed in terms of the odd Legendre polynomial of m/L.

Thus, we obtain a series of the 1D Abel integral equations for the radial functions of the solar rotation expansion:

$$\frac{1}{T}\int_{r_1}^R\frac{\Omega_{2j+1}(r)dr/c}{\sqrt{1-\dfrac{L^2r^2}{r^2\omega_{0,nl}^2}}}=-\frac{a_{2j+1}^{nl}}{(2j+1)P_{2j}(0)}$$

In the asymptotic JWKB/EBK approximation, the a-coefficients are the functions of the ratio L/ω or the lower turning point radius, r_1. This helps to identify 'outliers' in the observational data.

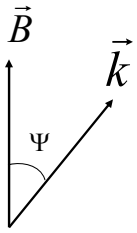

Effects of magnetic field

In the presence of magnetic field, acoustic waves become fast-magnetoacoustic waves with the dispersion relation:

$$\omega^2 = k^2c^2 + k^2V_A^2\sin^2\Psi$$

where $V_A = B/\sqrt{4\pi\rho}$ is the Alfven speed, Ψ is teh angle between the wave vector, $\vec{k}$ and magnetic field $\vec{B}$.

Assuming $V_A \ll c$ and applying the same procedure as for the sound-speed perturbations, we obtain:

$$\frac{\Delta\omega_{nlm}}{\omega} = \frac{2}{\pi T}\int_0^M d\mu \int_{r_1}^R \frac{\left(V_A^2/2c^2\right)\sin^2\Psi}{\sqrt{M^2-\mu^2}\sqrt{1-L^2c^2/\omega^2r^2}}\frac{dr}{c}$$

$$\frac{V_A^2}{2c^2}\sin^2\Psi = \frac{V_1^2}{2c^2}(1-\cos^2\Psi) = \left[1-\frac{(\vec{k}\cdot\vec{B})}{(k^2B^2)}\right] = \frac{1}{8\pi\rho c^2k^2}\left[k^2B^2-(\vec{k}\cdot\vec{B})\right] =$$

$$= \frac{1}{8\pi c^2k^2}[B_r^2(k^2-k_r^2)+B_\theta^2(k^2-k_\theta^2)+B_\phi^2(k^2-k_\phi^2)] \equiv \frac{1}{8\pi c^2k^2}\left[b_r+b_\theta+b_\phi\right]$$

Substituteing the wave vector $k^2 = \frac{\omega^2}{c^2}$ and its components:

$$k_r^2 = \frac{\omega^2}{c^2}-\frac{L^2}{c^2}, \quad k_\theta^2 = \frac{L^2}{c^2}-\frac{m^2}{r^2\sin^2\theta}, \quad k_\phi^2 = \frac{m^2}{r^2\sin^2\theta}$$

and using the definitions: $\mu = \cos\theta$ and $M^2 = 1-\frac{m^2}{L^2}$,

we calculate:

$$b_r = B_r^2\left(k^2-\frac{\omega^2}{c^2}+\frac{L^2}{r^2}\right) = B_r^2k^2\frac{L^2c^2}{r^2c^2}$$

$$b_\theta = B_\theta^2\left(\frac{\omega^2}{c^2}-\frac{L^2}{r^2}+\frac{m^2}{r^2\sin^2\theta}\right) = B_\theta^2k^2\left[1-\frac{L^2c^2}{\omega^2r^2}\left(\frac{M^2-\mu^2}{1-\mu^2}\right)\right]$$

$$b_\phi = B_\phi^2k^2\left(1-\frac{c^2}{\omega^2}\frac{m^2}{r^2\sin^2\theta}\right) = B_\phi^2k^2\left[1-\frac{L^2c^2}{r^2\omega^2}\left(\frac{1-M^2}{1-\mu^2}\right)\right]$$

Putting it all together:

$$\frac{\Delta\omega_{nlm}}{\omega}=\frac{2}{\pi T}\int_0^M\int_{r_1}^R\left[\frac{B_r^2}{8\pi\rho c^2}\left(\frac{L^2c^2}{r^2\omega^2}\right)+\frac{B_\theta^2}{8\pi\rho c^2}\left(1-\frac{L^2c^2}{r^2\omega^2}\frac{M^2-\mu^2}{1-\mu^2}\right)+\right.$$

$$\left.+\frac{B_\phi^2}{8\pi\rho c^2}\left(1-\frac{L^2c^2}{r^2\omega^2}\frac{1-M^2}{1-\mu^2}\right)\right]\frac{d\mu(dr/c)}{\sqrt{M^2-\mu^2}\sqrt{1-L^2c^2/\omega^2r^2}}$$

There is no simple separation of the radial and angular variables in terms of the Legendre polynomial and a-coefficients.
However, the magnetic frequency splitting can be calculated for solar-cycle dynamo models and compared with helioseismic observations.

By the order of magnitude, the magnetic frequency splitting:

$$\frac{\Delta\omega_{nlm}}{\omega}\sim\frac{B^2}{8\pi\rho c^2}\sim\frac{B^2}{8\pi\gamma P}\sim\frac{1}{2\gamma}\frac{B^2/4\pi}{P}\sim\frac{1}{2\gamma\beta}$$

where $\beta=\frac{4\pi P}{B^2}$ is the plasma parameter β - ratio of the gas pressure to the magnetic pressure.

Lecture 15
Effects of solar asphericity, rotation and magnetic field
The a-coefficients

(Stix, Chapter 5.3.1; Kosovichev, p.34-41, 44-48; Christensen-Dalsgaard, Chapters 5.5)

Solar oscillation spectrum obtained from the HMI instrument on Solar Dynamics Observatory.

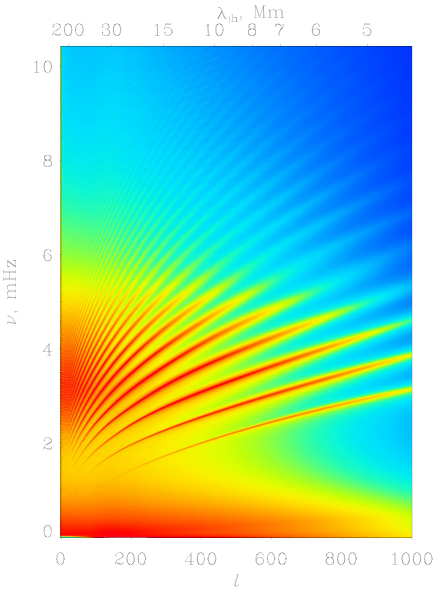

Spectrum of normal modes calculated for a standard solar model. Note the 'avoided crossing effect' for f and g-modes.

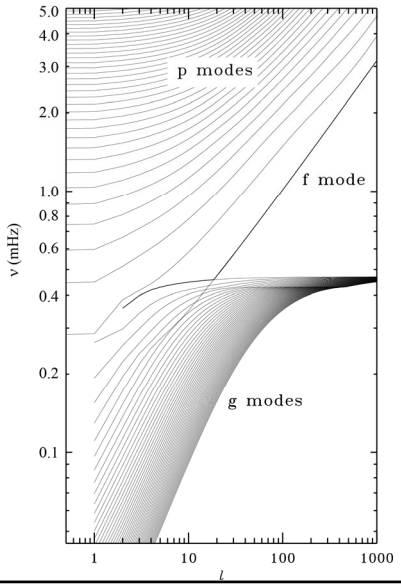

Acoustic travel time

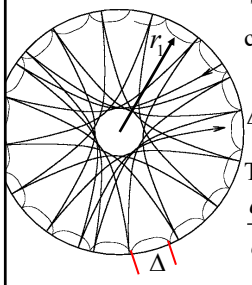

The distance, Δ, between the surface points for one skip can be calculated as the integral:

$$\Delta = 2\int_{r_1}^{R} d\theta = 2\int_{r_1}^{R} \frac{L/r}{\sqrt{\omega^2/c^2 - L^2/r^2}}\,dr \equiv 2\int_{r_1}^{R} \frac{c/r}{\sqrt{\omega^2/L^2 - c^2/r^2}}\,dr.$$

The corresponding travel time is calculated by integrating equation:

$$\frac{dr}{dt} = \frac{\partial\omega}{\partial k_r}: \qquad dt = \frac{dr}{c\left(1 - k_h^2 c^2/\omega^2\right)^{1/2}}.$$

$$\tau = 2\int_{r_1}^{R} dt = 2\int_{r_1}^{R} \frac{dr}{c\left(1 - k_h^2 c^2/\omega^2\right)^{1/2}} \equiv 2\int_{r_1}^{R} \frac{dr}{c\left(1 - L^2 c^2/r^2\omega^2\right)^{1/2}}$$

These equations give a *time-distance* relation, $\tau - \Delta$, for acoustic waves traveling between two surface points through the solar interior. The ray representation of the solar modes and the time-distance relation provided a motivation for developing *time-distance helioseismology*

Duvall's law (asymptotic p-mode relation)

Consider the p-mode dispersion relation:

$$\int_{r_1}^{R} k_r\,dr = \pi(n+\alpha)$$

$$\int_{r_1}^{R} \left(\frac{\omega^2}{c^2} - \frac{L^2}{r^2}\right)^{1/2} dr = \pi(n+\alpha)$$

Dividing left and right-hand sides by ω we get:

$$\int_{r_1}^{R} \left(\frac{r^2}{c^2} - \frac{L^2}{\omega^2}\right)^{1/2} \frac{dr}{r} = \frac{\pi(n+\alpha)}{\omega}$$

Radius r_1 (or r_t) of the lower turning point depends only on ratio L/ω. Hence, the left-hand side is a function of L/ω:

$$F\left(\frac{L}{\omega}\right) = \frac{\pi(n+\alpha)}{\omega}$$

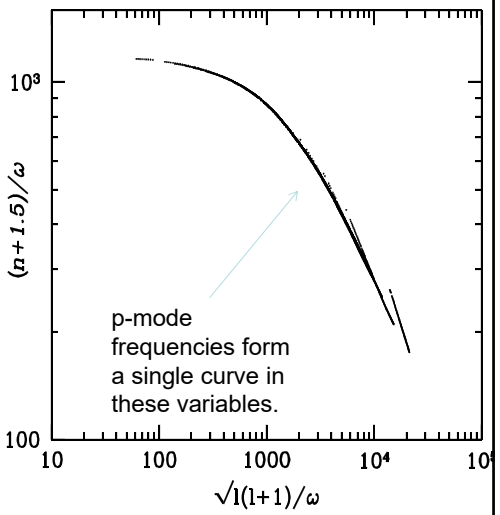

where $L = \sqrt{l(l+1)}$ $\qquad \alpha \approx 1.5$

Differential asymptotic sound-speed inversion. 1

To find corrections to the standard solar model we consider small perturbations to the sound speed profile and oscillation frequencies, and linearize the dispersion relation by using the first-order Taylor expansion:

$$\int_{r_1}^{R}\left[\frac{(\omega+\Delta\omega)^2}{(c+\Delta c)^2}-\frac{L^2}{r^2}\right]^{1/2} dr=\pi(n+\alpha+\Delta\alpha).$$

$$\int_{r_1}^{R}\frac{\omega^2}{c^2}\frac{\left(\frac{\Delta\omega}{\omega}-\frac{\Delta c}{c}\right)dr}{\left(\frac{\omega^2}{c^2}-\frac{L^2}{r^2}\right)^{1/2}}=\pi\Delta\alpha$$

$$\frac{\Delta\omega}{\omega}\int_{r_1}^{R}\frac{dr}{c\left(1-\frac{L^2c^2}{r^2\omega^2}\right)^{1/2}}=\int_{r_1}^{R}\frac{\Delta c}{c}\frac{dr}{c\left(1-\frac{L^2c^2}{r^2\omega^2}\right)^{1/2}}+\frac{\pi\Delta\alpha}{\omega}.$$

$T(L/\omega)$ $\quad$ $\Phi(L/\omega)$ $\quad$ $\beta(\omega)$

r_1 is a function of L/ω.

Differential asymptotic sound-speed inversion. 2

The p-mode travel time is calculated by using the ray-path theory.
It corresponds to the half-skip time: T=τ/2, and is a function of L/ω.
Therefore, the observed frequency difference can be represented in the form:

$$\frac{\Delta\omega}{\omega}T=\Phi\left(\frac{L}{\omega}\right)+\beta(\omega)$$

$$\Phi\left(\frac{L}{\omega}\right)=\int_{r_1}^{R}\frac{\Delta c}{c}\frac{dr}{c\left(1-\frac{L^2c^2}{r^2\omega^2}\right)^{1/2}}$$

Once the function Φ(L/ω) is determined from the observed frequency difference we can find Δc/c as a function of radius by solving the integral equation. This equation is reduced to the Abel integral equation, and has an analytical solution.

Functions Φ(L/w) and β(ω) are determined by fitting (Δω/ω)T which depends on both L/ω and ω.

Effects solar asphericity

For a spherically symmetrical solar structure, when the sound speed is a function of radius, $c = c(r)$, the p-mode frequencies are determined from the Bohr quantization rule:

$$\int_{r_1}^{R} k_r dr = \pi(n+\alpha)$$

where $k_r = \sqrt{\frac{\omega^2}{c^2} - \frac{L^2}{r^2}}$, and $L^2 = l(l+1)$. The RHS of this equation can be considered as averaging of the radial wave vector, k_r, within the wave propagation region, $[r_1, R]$.

If the sound-speed variations are not spherically symmetric, e.g. due internal flows and magnetic fields, $c = c(r,\theta,\phi)$, then we have to use the EBK quantization rule, and average the wave vector over the 3D wavepath great circle:

$$\frac{1}{2\pi}\int_0^{2\pi}\int_{r_1}^{R} k_r dr d\phi' = \pi(n+\alpha)$$

where ϕ' is the polar angle along the great circle.

3D propagation region

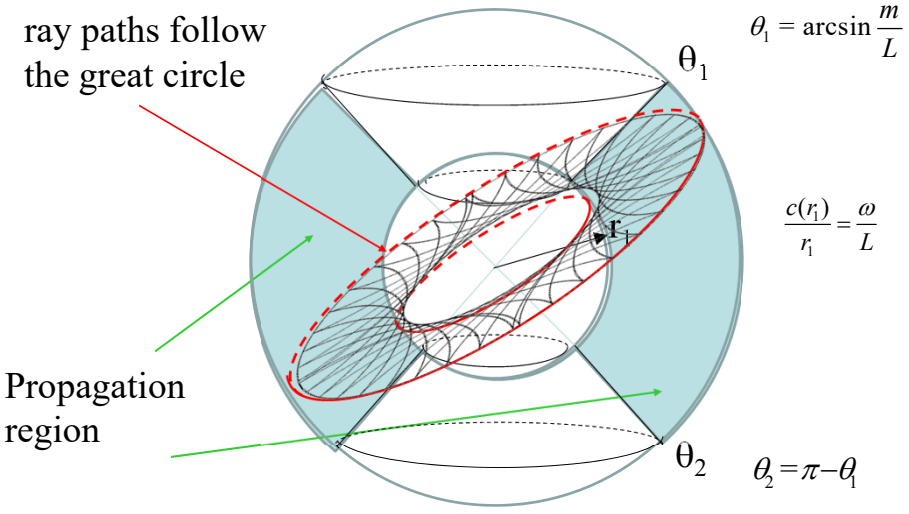

Differentiating this equation, we find $d\phi'$ as a function of colatitude θ: $\sin\phi' d\phi' = -\frac{\sin\theta}{\cos\theta_1} d\theta$.

$$d\phi' = -\frac{\sin\theta}{\cos\theta_1}\frac{1}{\sqrt{1-\cos^2\theta/\cos^2\theta_1}}d\theta = -\frac{\sin\theta d\theta}{\sqrt{\cos^2\theta_1-\cos^2\theta}} = \frac{d\mu}{\sqrt{M^2-\mu^2}},$$

where $\mu = \cos\theta$, and $M^2 = \cos^2\theta_1 = 1-\sin^2\theta_1 = 1-\frac{m^2}{L^2}$.

Substituting in the 3D quantization equation:

$$\frac{1}{\pi}\int_0^{\pi} d\phi' \int_{r_1}^{R} k_r dr = \frac{1}{\pi}\int_{-M}^{M} \frac{d\mu}{\sqrt{M^2-\mu^2}} \int_{r_1}^{R} k_r dr = \pi(n+\alpha)$$

or

$$\frac{2}{\pi}\int_0^{M} \frac{d\mu}{\sqrt{M^2-\mu^2}} \int_{r_1}^{R} \sqrt{\frac{\omega_{nml}^2}{c^2(r,\mu)} - \frac{L^2}{r^2}}\, dr = \pi(n+\alpha)$$

In this case, the oscillation frequencies depend on all three quantum numbers: radial order n, angular degree l, and angular degree m.

Because all the ray paths sample the sound speed over the whole range of longitude ϕ, only the azimuthally averaged 2D sound-speed component $c(r,\theta)$ or $c(r,\mu)$ can be determined from the oscillation frequencies. However, this is valid only when the deviations from the sphericity are small.

Effects of the sound-speed aspericity

Repeating the linearization procedure for the case of small deviations $\Delta c(r,\mu)$ from a spherically symmetrical solar model, we obtain the equation for the 2D differential asymptotic inversion:

$$\frac{\Delta\omega_{nlm}}{\omega_{0,nl}} = \frac{2}{\pi T}\int_0^{M} d\mu \int_{r_1}^{R} \frac{\frac{\Delta c}{c}(r,\mu)}{\sqrt{M^2-\mu^2}\sqrt{1-L^2c^2/\omega_{0,nl}^2 r^2}} \frac{dr}{c}$$

where $\Delta\omega_{nlm} = \omega_{nlm} - \omega_{0,nl}$ is the difference between the observed frequencies ω_{nlm} and model frequencies $\omega_{0,nl}$.

The model frequencies are calculated for a spherically symmetric solar model and do not depend on m. The latitudinal dependence of the sound speed (solar asphericity) lifts the frequency degeneracy with respect to m.

This equation represents a 2D Abel integral equation, and can be solved similarly to the 1D equation.

Effects of rotation

Solar rotation and other plasma flows inside the Sun cause Doppler shift of the wave frequencies. The dispersion relation for the acoustic waves becomes:

$$(\omega - \vec{k}\vec{v})^2 = \omega_c^2 + k^2 c^2$$

where $\vec{k}$ is the wave vector, and $\vec{v}$ is the plasma velocity.

Because of the acoustic ray paths travel in the great circles, they sample the radial and latitudinal components of velocity twice in the opposite directions. Thus, the contribution of these components to the quantization integral is canceled in the first approximation, and the mode frequencies depend only on the azimuthal component, v_ϕ:

$$(\omega - k_\phi v_\phi)^2 = \omega_c^2 + k^2 c^2$$

where $k_\phi = \dfrac{m}{r\sin\theta}$. Representing v_ϕ in terms of the angular velocity, $\Omega(r,\theta)$:

$$v_\phi = r\sin\theta\,\Omega(r,\theta),$$

we get:

$$(\omega - m\Omega)^2 = \omega_c^2 + k^2 c^2$$

The EBK quantization equation takes form:

$$\frac{2}{\pi}\int_0^M \frac{d\mu}{\sqrt{M^2-\mu^2}}\int_{r_1}^R \sqrt{\frac{(\omega_{nlm}-m\Omega)^2}{c^2} - \frac{L^2}{r^2}}\,dr = \pi(n+\alpha)$$

Assuming that $m\Omega/\omega_{nlm} \ll 1$ and that the background solar structure is spherically symmetric, we represent ω_{nlm} in terms of the frequency deviations from the model frequencies: $\Delta\omega_{nlm} = \omega_{nlm} - \omega_{0,nl}$.

$$\frac{2}{\pi}\int_0^M \frac{d\mu}{\sqrt{M^2-\mu^2}}\int_{r_1}^R \sqrt{\frac{(\omega_{0,nl}+\Delta\omega_{nlm}-m\Omega)^2}{c^2} - \frac{L^2}{r^2}}\,dr = \pi(n+\alpha)$$

Performing the first-order Taylor expansion and subtracting the quantization rule for the background state, we get:

$$\frac{2}{\pi}\int_0^M \frac{d\mu}{\sqrt{M^2-\mu^2}}\int_{r_1}^R \frac{\omega^2}{c^2}\frac{\left[\dfrac{\Delta\omega_{nlm}}{\omega} - \dfrac{m\Omega}{\omega}\right]}{\sqrt{\dfrac{\omega^2}{c^2} - \dfrac{L^2}{r^2}}}\,dr = 0$$

where for simplicity we drop subscript for the model frequencies: $\omega = \omega_{0,nl}$.

Thus, we obtain:

$$\Delta\omega_{nlm} = \frac{2}{\pi T}\int_0^M \int_{r_1}^R \frac{m\Omega(r,\mu)dr d\mu}{c\sqrt{M^2-\mu^2}\sqrt{1-L^2c^2/r^2\omega^2}}$$

where $T = \int_{r_1}^R \frac{dr}{c\sqrt{1-L^2c^2/r^2\omega^2}}$ is the "half-skip" travel time of acoustic waves.

The solar rotation causes 'rotational frequency splitting' proportional to the mode angular degree m.

The physical interpretation is that the modes with positive m travel in the same direction as the solar rotation and thus have higher frequencies then the modes with negative m traveling in the opposite direction.

Recall that that the oscillation modes are represented in terms of the spherical harmonics: $\xi_r(r,\theta,\phi,t) \propto P_l^m(\theta)\exp(im\phi - i\omega t)$, and thus, in the form of azimuthal traveling waves

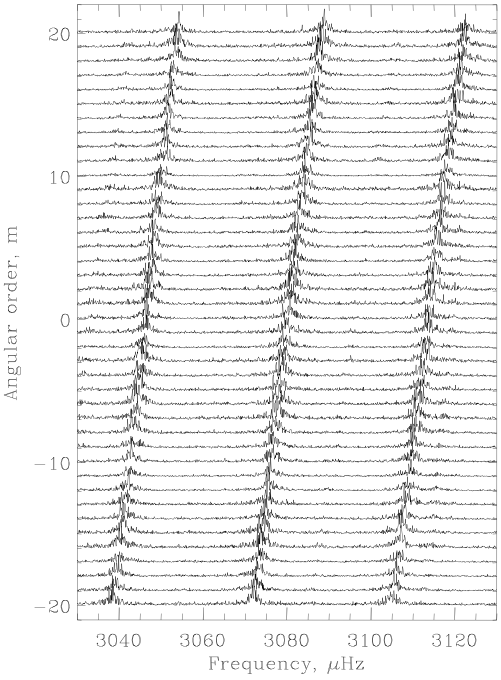

Illustration of the frequency shift due to the solar rotation

Typical power spectra of solar oscillation data from the MDI instrument on SOHO. Each horizontal curve shows three lines of the power spectrum for different azimuthal order m with radial order $n = 15$ and angular degree $l = 19, 20$, and 21 (from left to right). The slope of the modal lines is due to the rotational frequency shift: prograde modes with positive m have higher frequencies than retrograde modes with negative m.

Frequency splitting, l=150

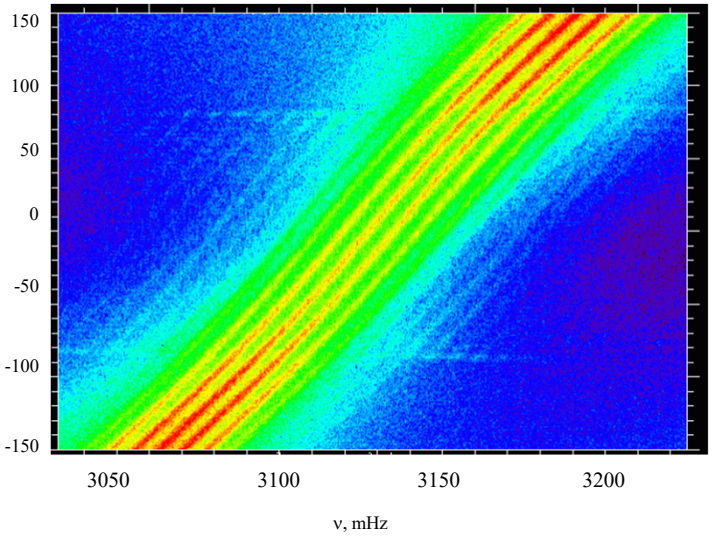

(F. Hill)

By comparing the effect of the sound-speed asphericity and rotation:

$$\frac{\Delta\omega_{nlm}}{\omega} = \frac{2}{\pi T}\int_0^M \int_{r_1}^R \frac{\left[\Delta c(r,\mu)/c\right] dr d\mu}{c\sqrt{M^2-\mu^2}\sqrt{1-L^2c^2/\omega^2 r^2}}$$

$$\Delta\omega_{nlm} = \frac{2}{\pi T}\int_0^M \int_{r_1}^R \frac{m\Omega(r,\mu) dr d\mu}{c\sqrt{M^2-\mu^2}\sqrt{1-L^2c^2/r^2\omega^2}}$$

where $M = \sqrt{1-m^2/L^2}$

We notice that the frequency splitting due to the sound-speed asphericity is an even function of m and an odd function of m due the rotation.

This difference allows us to separate effects of the solar asphericity and rotation in the observational data.

The a-coefficients

The observational data are often represented as an expansion in terms of the Legendre polynomials:

$$\Delta\nu_{nlm} = \Delta\omega_{nlm} / 2\pi = L\sum_{k=1}^{N} a_k^{nl} P_k\left(-\frac{m}{L}\right)$$

For a more accurate (non-asymptotic) representation, the expansion is performed in terms of Clebsch-Gordon coefficients, which will be considered later.

In this representation, the 'even' a-coefficients represent effects of the solar asphericity, and the 'odd' a-coefficients represent the internal solar rotation and its variations with latitude (zonal flows). In addition, the representations in the form of the a-coefficients allows us to replace the 2D inversions of $\Delta\omega_{nlm}$ with a series of 1D inversions of the a-coefficients.

Specifically, representing the sound-speed perturbation in terms of the Legendre polynomials:

$$\frac{\Delta c}{c}(r,\mu) = \sum_{j=1}^{J} A_{2j}(r) P_{2j}(\mu)$$

where $\mu = \cos\theta$.

Substituting this representation of $\frac{\Delta c}{c}(r,\mu)$ in the equation for $\Delta\omega_{nlm} / \omega$, we obtain:

$$\frac{\Delta\omega_{nlm}}{\omega} = \sum_{j=1}^{J} \frac{1}{T}\int_{r_1}^{R} \frac{A_{2j}(r)dr}{\sqrt{1 - L^2c^2 / r^2\omega^2}} \left(\frac{2}{\pi}\int_0^M \frac{P_{2j}(\mu)}{\sqrt{M^2 - \mu^2}} d\mu\right)$$

The second integral is calculated analytically:

$$\frac{2}{\pi}\int_0^M \frac{P_{2j}(\mu)}{\sqrt{M^2 - \mu^2}} d\mu = (-1)^j P_{2j}(0) P_{2j}(m / L)$$

Thus, both the observational data and the angular integral of the sound-speed asphericity are represented in terms of the series of Legendre polynomial $P_{2j}(m / L)$.

We obtain a series of the Abel integral equations for the radial functions of the asphericity, $A_{2j}(r)$:

$$\frac{1}{T}\int_{r_1}^{R} \frac{A_{2j}(r)dr}{\sqrt{1 - L^2c^2 / \omega^2 r^2}} = (-1)^j \frac{La_{2j}^{ln}}{P_{2j}(0)}.$$

These equations establish a relationship between the even a-coefficients and the solar asphericity expressed in terms of the Legendre polynomials.

A similar type of solution can be obtained for the angular velocity $\Omega(r,\mu)$. In this case, it is convenient to use the expansion in terms of associate Legendre functions:

$$\Omega(r,\mu) = \sum_{j=0}^{J} \Omega_{2j+1}(r) \frac{P_{2j+1}^{1}(\cos\theta)}{\sin\theta}$$

Substituting in:

$$\Delta\omega_{nlm} = \frac{2}{\pi T} \int_0^M \int_{r_1}^R \frac{m\Omega(r,\mu) dr d\mu}{c\sqrt{M^2-\mu^2}\sqrt{1-L^2c^2/r^2\omega^2}}$$

we obtain:

$$\Delta\omega_{nlm} = \sum_{j=0}^{J} \frac{1}{T} \int_{r_1}^R \frac{\Omega_{2j+1}(r) dr}{c\sqrt{1-L^2c^2/r^2\omega^2}} \left(\frac{2m}{\pi} \int_0^M \frac{P_{2j+1}^{1} d\mu}{\sqrt{1-\mu^2}\sqrt{M^2-\mu^2}} \right)$$

The second integral is calculated analytically:

$$\int_0^M \frac{P_{2j+1}^{1} d\mu}{\sqrt{1-\mu^2}\sqrt{M^2-\mu^2}} = -\frac{\pi}{2}(2j+1) P_{2j}(0) \frac{L}{m} P_{2j+1}\left(\frac{m}{L}\right)$$

Both the observational data and the angular integral of the solar rotation are expressed in terms of the odd Legendre polynomial of m/L.

Thus, we obtain a series of the 1D Abel integral equations for the radial functions of the solar rotation expansion:

$$\frac{1}{T} \int_{r_1}^R \frac{(\Omega_{2j+1}(r)/2\pi) dr/c}{\sqrt{1-\frac{L^2r^2}{c^2\omega_{0,nl}^2}}} = \frac{a_{2j+1}^{nl}}{(2j+1)P_{2j}(0)}$$

In the asymptotic JWKB/EBK approximation, the a-coefficients are the functions of the ratio L/ω or the lower turning point radius, r_1. This helps to identify 'outliers' in the observational data.

$\Omega/2\pi$ is the rotation rate. It is measured in nHz as well as the a-coeffients.

$$\Delta\nu_{nlm} = \Delta\omega_{nlm}/2\pi = L\sum_{k=1}^{N} a_k^{nl} P_k\left(-\frac{m}{L}\right)$$

The minus sign was instroduces to get the a-coefficients of the same sign as the corresponding rotation law terms.

Solar rotation law

Consider a special case of a three-term solar differential rotation law:

$$\Omega / 2\pi = a + b\cos^2\theta + c\cos^4\theta$$

where a, b, and c are measured in nHz. The corresponding representation in terms of the associated Legendre polynomials: Consider the intergrals for the $A_{2j+1}(r)$ as averaging over the propagation regions, $[r_1, R]$.

$$\overline{A}_1 = \frac{1}{T}\int_{r_1}^{R} \frac{A_1(r)}{\sqrt{1-r^2/r_1^2}}\frac{dr}{c} \qquad T = \int_{r_1}^{R} \frac{1}{\sqrt{1-r^2/r_1^2}}\frac{dr}{c}$$

- a 'half-skip' travel time, $r_1 = c(r_1)\omega_{nl}/L$ is the turning point radius.

Then, we write the integral equations in terms of the averaged A coefficients:

$$\overline{A}_1 = a_1^{nl} / P_0(0) = a_1^{nl} \qquad \overline{A}_3 = a_3^{nl} / 3P_2(0) = -\frac{2}{3}a_3^{nl} \qquad \overline{A}_5 = a_5^{nl} / 5P_3(0) = \frac{8}{15}a_5^{nl}$$

Substituting $P_1^1(\cos\theta) = -\sin\theta$ $P_3^1(\cos\theta) = -\frac{3}{2}\sin\theta(5\cos^2\theta - 1)$

$$P_5^1(\cos\theta) = -\frac{15}{8}\sin\theta(21\cos^4\theta - 14\cos^2\theta + 1)$$

we get: $\overline{\Omega}/2\pi = (a_1 + a_3 + a_5) - (5a_3 + 14a_5)\cos^2\theta + 21a_5\cos^4\theta$

where I dropped the mode indexes n, l, m.

Effects of magnetic field

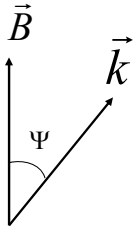

In the presence of magnetic field, acoustic waves become fast-magnetoacoustic waves with the dispersion relation:

$$\omega^2 = k^2c^2 + k^2V_A^2\sin^2\Psi$$

where $V_A = B/\sqrt{4\pi\rho}$ is the Alfven speed, Ψ is the angle between the wave vector, $\vec{k}$ and magnetic field $\vec{B}$.

Assuming $V_A \ll c$ and applying the same procedure as for the sound-speed perturbations, we obtain:

$$\frac{\Delta\omega_{nlm}}{\omega} = \frac{2}{\pi T}\int_0^M d\mu \int_{r_1}^{R} \frac{\left(V_A^2/2c^2\right)\sin^2\Psi}{\sqrt{M^2-\mu^2}\sqrt{1-L^2c^2/\omega^2r^2}}\frac{dr}{c}$$

$$\frac{V_A^2}{2c^2}\sin^2\Psi = \frac{V_1^2}{2c^2}(1-\cos^2\Psi) = \left[1 - \frac{(\vec{k}\cdot\vec{B})}{(k^2B^2)}\right] = \frac{1}{8\pi\rho c^2k^2}\left[k^2B^2 - (\vec{k}\cdot\vec{B})\right] =$$

$$= \frac{1}{8\pi c^2k^2}[B_r^2(k^2-k_r^2) + B_\theta^2(k^2-k_\theta^2) + B_\phi^2(k^2-k_\phi^2)] \equiv \frac{1}{8\pi c^2k^2}\left[b_r + b_\theta + b_\phi\right]$$

Substituteing the wave vector $k^2 = \frac{\omega^2}{c^2}$ and its components:

$$k_r^2 = \frac{\omega^2}{c^2} - \frac{L^2}{c^2}, \quad k_\theta^2 = \frac{L^2}{c^2} - \frac{m^2}{r^2 \sin^2\theta}, \quad k_\phi^2 = \frac{m^2}{r^2 \sin^2\theta}$$

and using the definitions: $\mu = \cos\theta$ and $M^2 = 1 - \frac{m^2}{L^2}$,

we calculate:

$$b_r = B_r^2 \left(k^2 - \frac{\omega^2}{c^2} + \frac{L^2}{r^2} \right) = B_r^2 k^2 \frac{L^2 c^2}{r^2 c^2}$$

$$b_\theta = B_\theta^2 \left(\frac{\omega^2}{c^2} - \frac{L^2}{r^2} + \frac{m^2}{r^2 \sin^2\theta} \right) = B_\theta^2 k^2 \left[1 - \frac{L^2 c^2}{\omega^2 r^2} \left(\frac{M^2 - \mu^2}{1 - \mu^2} \right) \right]$$

$$b_\phi = B_\phi^2 k^2 \left(1 - \frac{c^2}{\omega^2} \frac{m^2}{r^2 \sin^2\theta} \right) = B_\phi^2 k^2 \left[1 - \frac{L^2 c^2}{r^2 \omega^2} \left(\frac{1 - M^2}{1 - \mu^2} \right) \right]$$

Putting it all together:

$$\frac{\Delta\omega_{nlm}}{\omega} = \frac{2}{\pi T} \int_0^M \int_{r_1}^R \left[\frac{B_r^2}{8\pi\rho c^2} \left(\frac{L^2 c^2}{r^2 \omega^2} \right) + \frac{B_\theta^2}{8\pi\rho c^2} \left(1 - \frac{L^2 c^2}{r^2 \omega^2} \frac{M^2 - \mu^2}{1 - \mu^2} \right) + \right.$$

$$\left. + \frac{B_\phi^2}{8\pi\rho c^2} \left(1 - \frac{L^2 c^2}{r^2 \omega^2} \frac{1 - M^2}{1 - \mu^2} \right) \right] \frac{d\mu (dr/c)}{\sqrt{M^2 - \mu^2} \sqrt{1 - L^2 c^2 / \omega^2 r^2}}$$

There is no simple separation of the radial and angular variables in terms of the Legendre polynomial and a-coefficients.
However, the magnetic frequency splitting can be calculated for solar-cycle dynamo models and compared with helioseismic observations.

By the order of magnitude, the magnetic frequency splitting:

$$\frac{\Delta\omega_{nlm}}{\omega} \sim \frac{B^2}{8\pi\rho c^2} \sim \frac{B^2}{8\pi\gamma P} \sim \frac{1}{2\gamma} \frac{B^2 / 4\pi}{P} \sim \frac{1}{2\gamma\beta}$$

where $\beta = \frac{4\pi P}{B^2}$ is the plasma parameter β - ratio of the gas pressure to the magnetic pressure.

Observational data

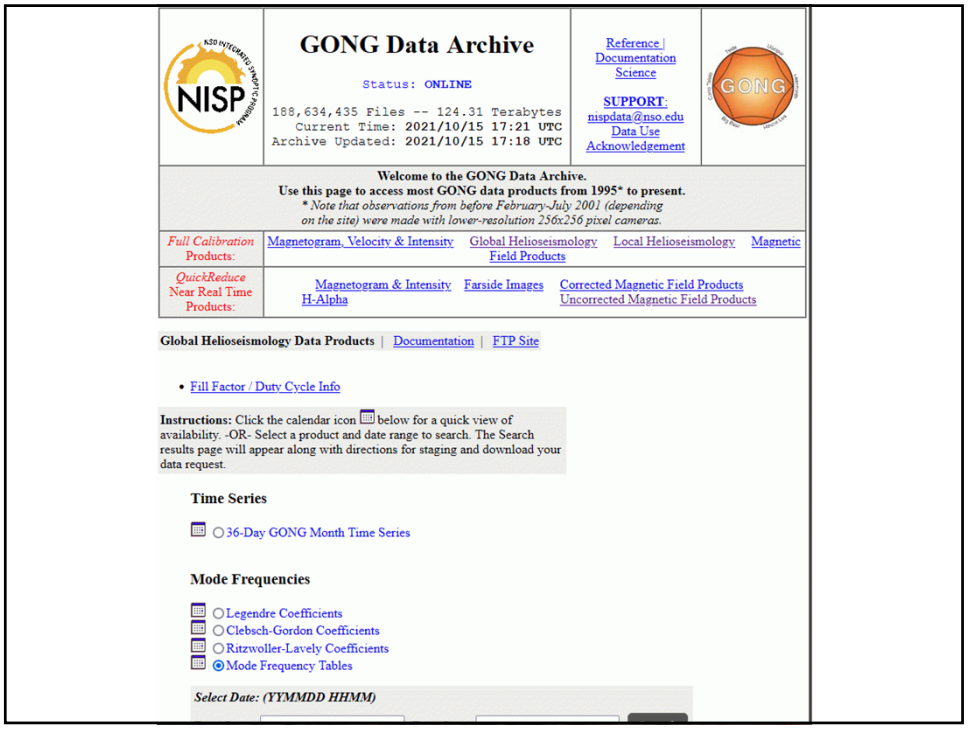

GONG Data Archive

Status: ONLINE

188,634,435 Files -- 124.31 Terabytes
Current Time: 2021/10/15 17:21 UTC
Archive Updated: 2021/10/15 17:18 UTC

Reference | Documentation
Science

SUPPORT:
nispdata@nso.edu
Data Use Acknowledgement

Welcome to the GONG Data Archive.
Use this page to access most GONG data products from 1995* to present.
** Note that observations from before February-July 2001 (depending on the site) were made with lower-resolution 256x256 pixel cameras.*

Full Calibration Products:	Magnetogram, Velocity & Intensity · Global Helioseismology · Local Helioseismology · Magnetic Field Products
QuickReduce Near Real Time Products:	Magnetogram & Intensity · Farside Images · Corrected Magnetic Field Products · Uncorrected Magnetic Field Products · H-Alpha

Global Helioseismology Data Products | Documentation | FTP Site

- Fill Factor / Duty Cycle Info

Instructions: Click the calendar icon below for a quick view of availability. -OR- Select a product and date range to search. The Search results page will appear along with directions for staging and download your data request.

Time Series

- 36-Day GONG Month Time Series

Mode Frequencies

- Legendre Coefficients
- Clebsch-Gordon Coefficients
- Ritzwoller-Lavely Coefficients
- Mode Frequency Tables

Select Date: (YYMMDD HHMM)

```
#Id: leg.readme,v 1.2 2018/11/29 19:30:25 dsdsops Exp
#  Frequency and splitting coeffcients table for GONG 3-month data
#
#  Frequencies and splitting coefficients have been obtained by
#  fitting Legendre polynomials to the frequencies for
#  individual modes, i.e.
#
#  \nu_{n,l,m}=\nu_{n,l}+L\sum_i a_{i,n,l}P_i(m/L)
#
#  where L=\sqrt{l(l+1)} and a_{i,n,l} are the splitting coefficients
#  which are tabulated in these tables.
#
#  The error estimates given in these tables are those estimated from
#  the errors in individual modes and do not include any other systematic  errors, that may be present.
#
#  For those (n,l) values where the number of modes is not sufficient
#  to determine all the five splitting coefficients, some of the higher
#  ones are not determined and in those cases the corresponding errors#  are set to zero.
#  Table Legendrefh.tab  Thu 15:14:40 22-Jul-2021

#    n    l       nu      dnu       a1       da1       a2       da2       a3       da3       a4       da4       a5       da5       a6
da6       a7       da7       a8       da8       a9       da9
#              microHz  microHz    nanoHz    nanoHz    nanoHz    nanoHz    nanoHz    nanoHz    nanoHz    nanoHz    nanoHz
nanoHz    nanoHz    nanoHz    nanoHz    nanoHz    nanoHz    nanoHz    nanoHz    nanoHz    nanoHz    nanoHz
 13    0 1957.3079   0.0976    0.0000    0.0000    0.0000    0.0000    0.0000    0.0000    0.0000    0.0000
0.0000    0.0000    0.0000    0.0000    0.0000    0.0000    0.0000    0.0000    0.0000    0.0000    14    0
2093.3416   0.1845    0.0000    0.0000    0.0000    0.0000    0.0000    0.0000    0.0000    0.0000    0.0000
0.0000    0.0000    0.0000    0.0000    0.0000    0.0000    0.0000    0.0000    0.0000    0.0000
```

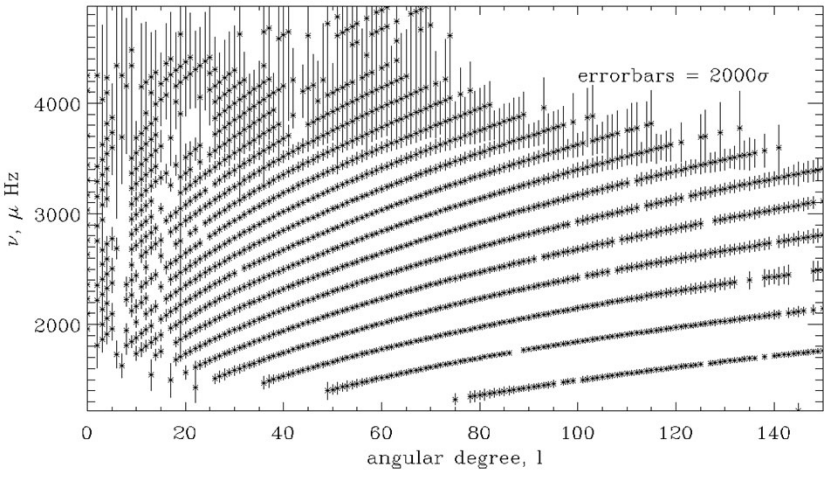

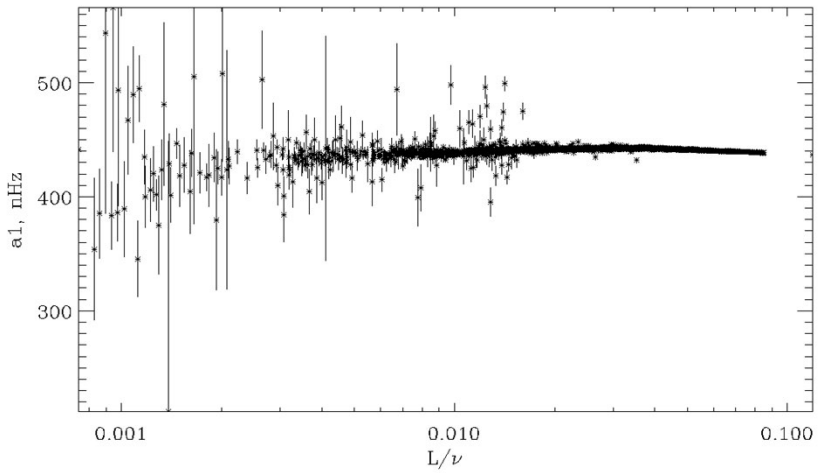
500
400
300
a1, nHz
0.001
0.010
0.100
L/ν

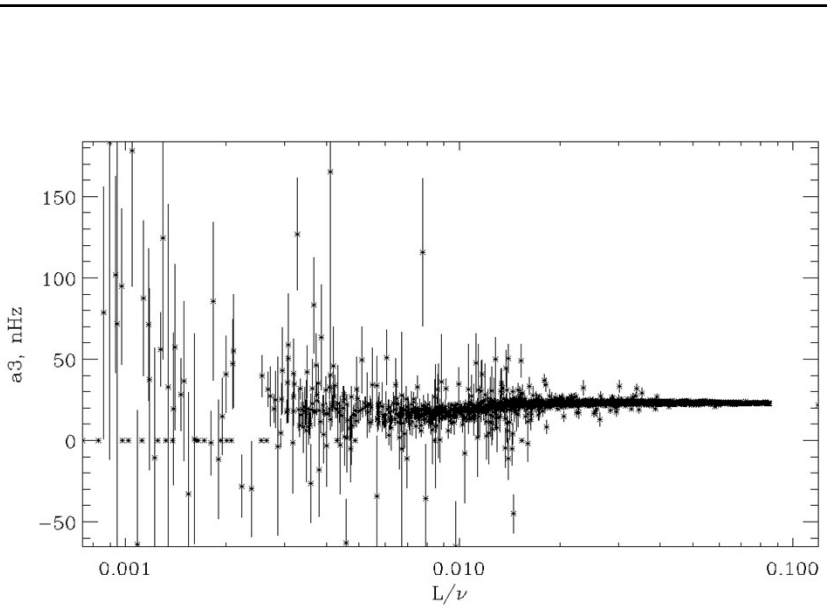
150
100
50
0
−50
a3, nHz
0.001
0.010
0.100
L/ν

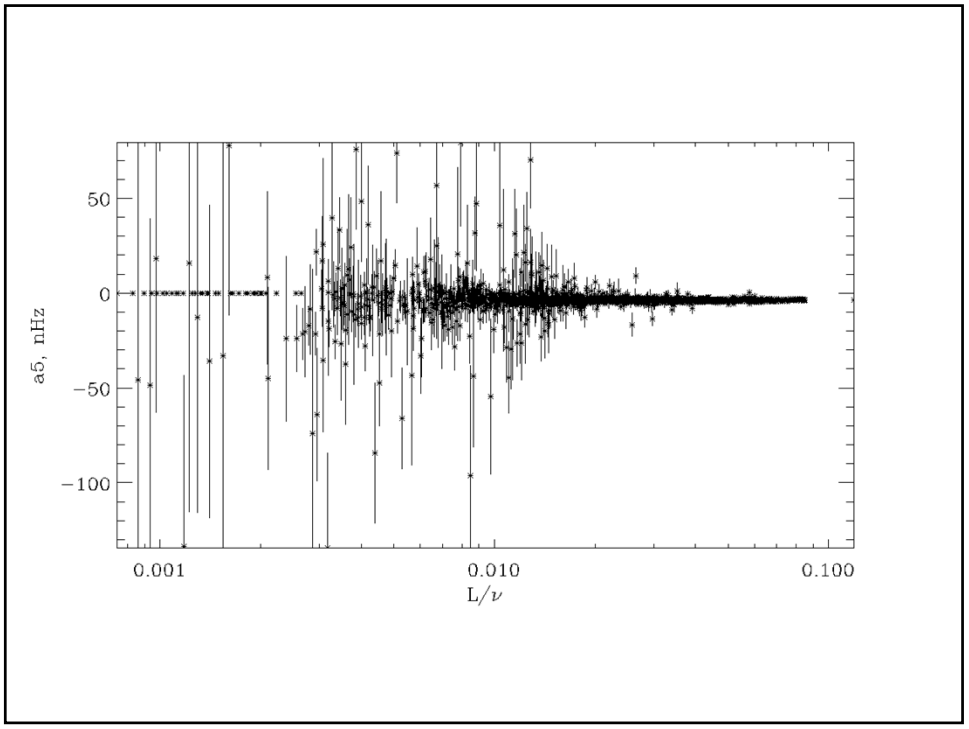
50
0
−50
−100
a5, nHz
0.001
0.010
0.100
L/ν

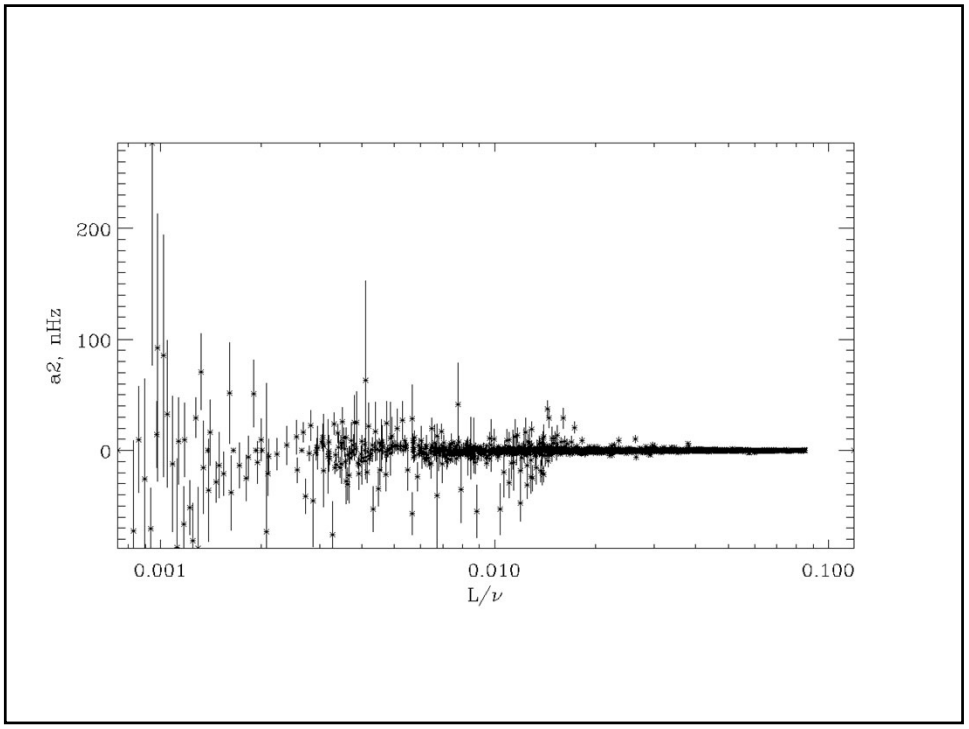
200
100
0
a2, nHz
0.001
0.010
0.100
L/ν

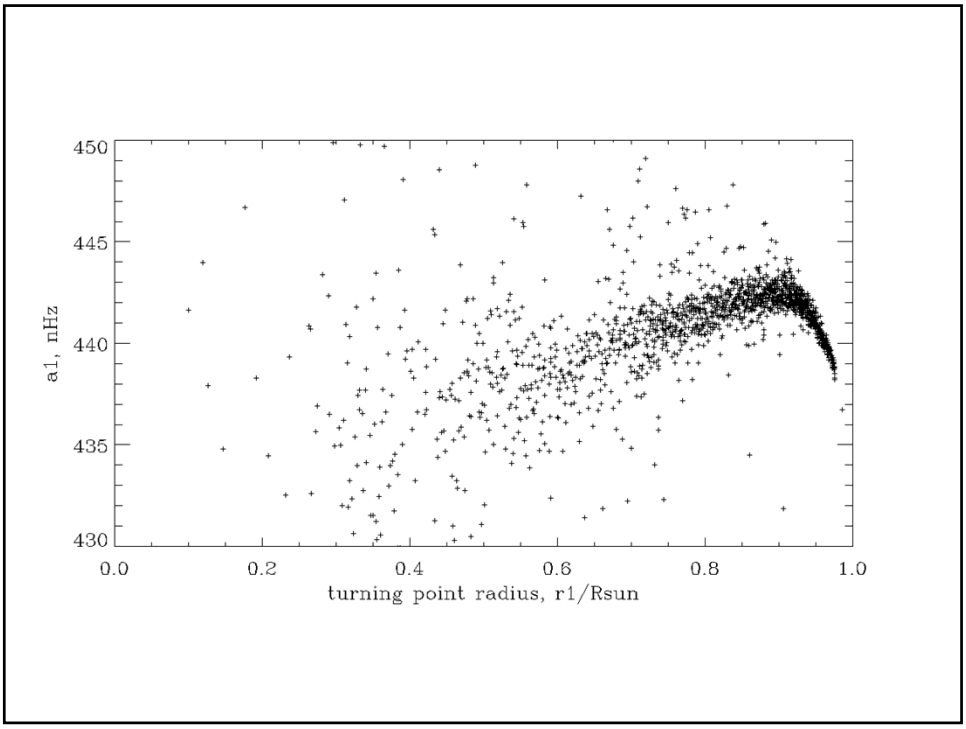
450
445
440
435
430
a1, nHz
0.0
0.2
0.4
0.6
0.8
1.0
turning point radius, r1/Rsun

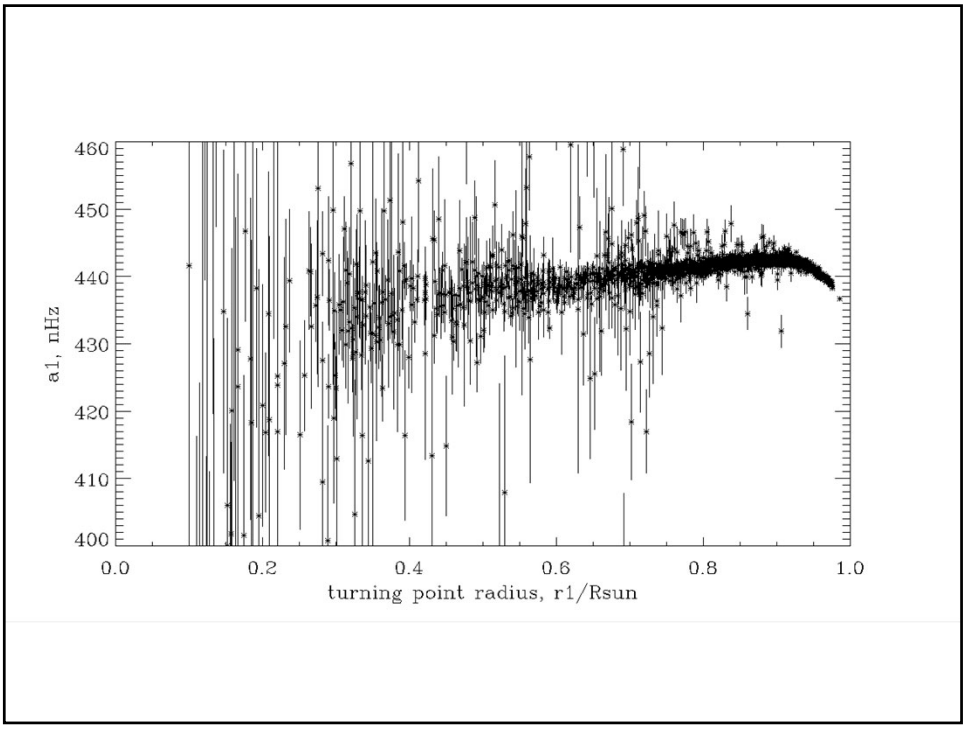
460
450
440
430
420
410
400
a1, nHz
0.0
0.2
0.4
0.6
0.8
1.0
turning point radius, r1/Rsun

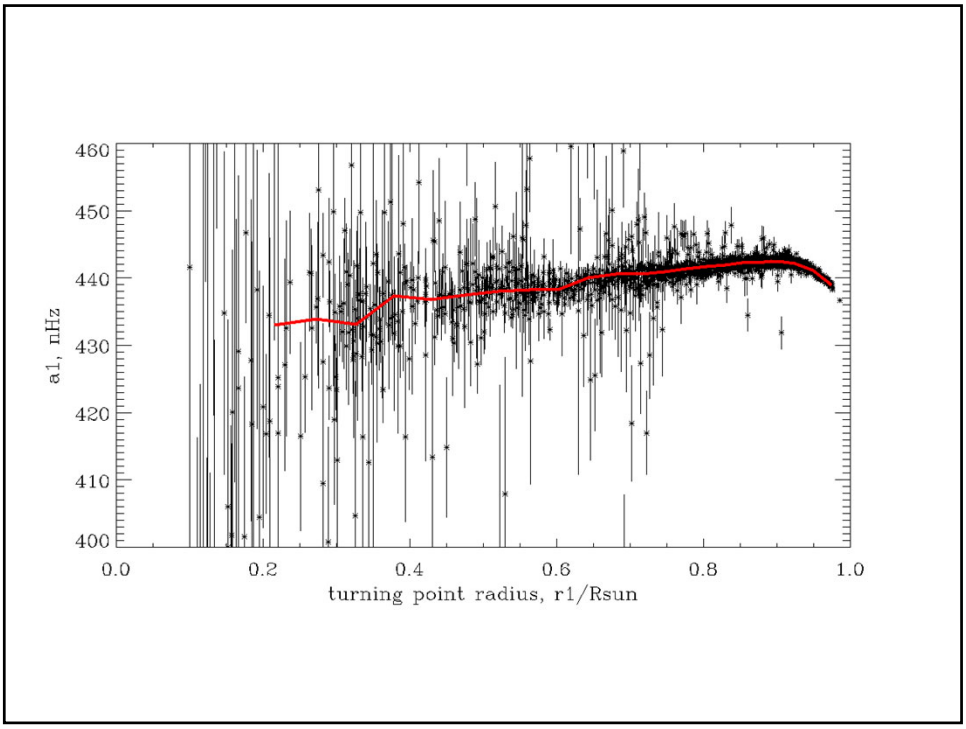
460
450
440
430
420
410
400
a1, nHz
0.0
0.2
0.4
0.6
0.8
1.0
turning point radius, r1/Rsun

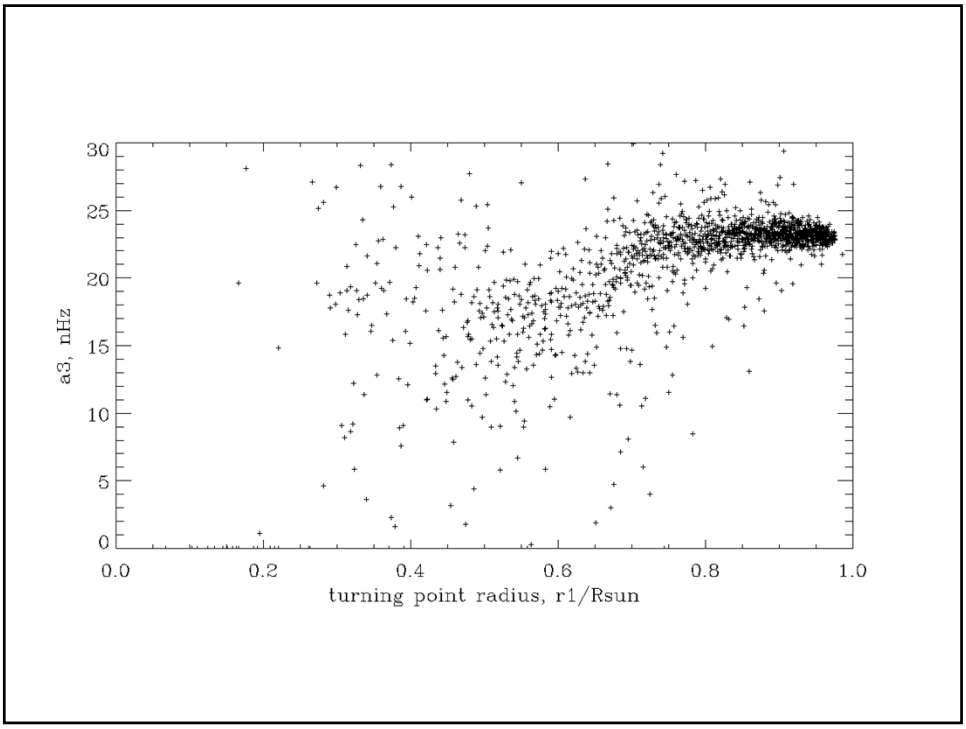
30
25
20
15
10
5
0
a3, nHz
0.0
0.2
0.4
0.6
0.8
1.0
turning point radius, r1/Rsun

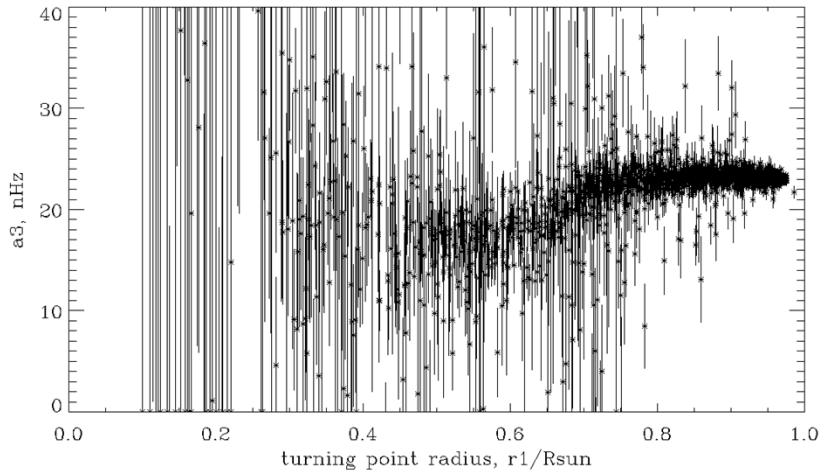
40
30
20
10
0
a3, nHz
0.0
0.2
0.4
0.6
0.8
1.0
turning point radius, r1/Rsun

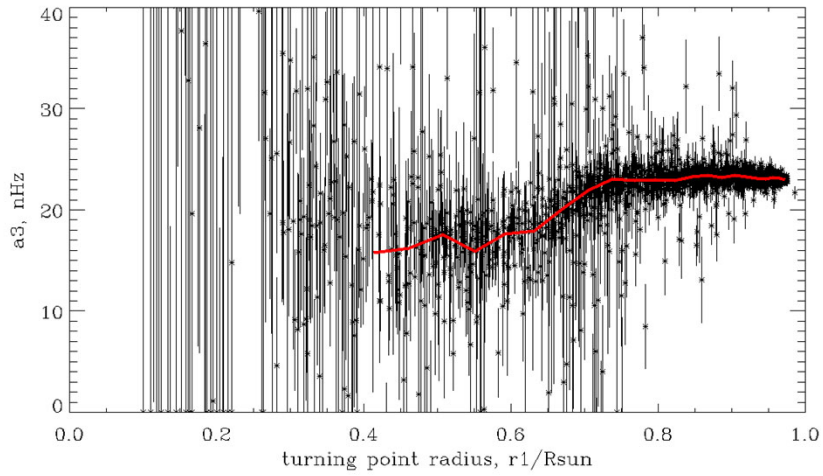
40
30
20
10
0
a3, nHz
0.0
0.2
0.4
0.6
0.8
1.0
turning point radius, r1/Rsun

Lecture 16
Stellar structure.
General helioseismic inverse problem.

(Stix, Chapter 5.3.1; Kosovichev, p.34-41, 44-48;
Christensen-Dalsgaard, Chapters 5.5)

The Main Sequence

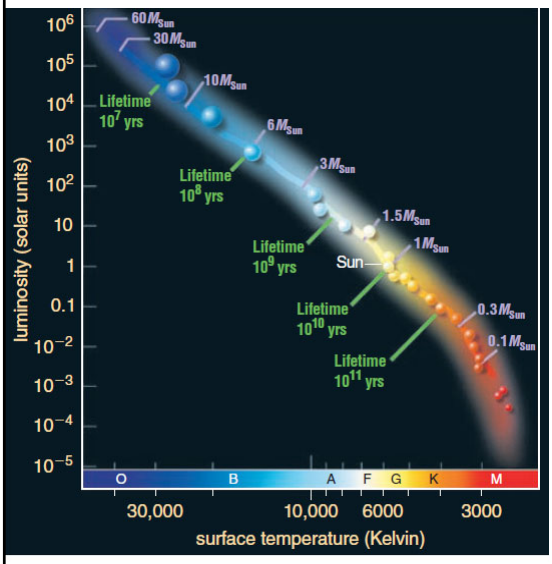

FIGURE 8.18

The main sequence shows how masses and lifetimes vary along it. Notice that more massive hydrogen-fusing stars are brighter and hotter than less massive ones, but have shorter lifetimes. (Stellar masses are given in units of solar masses: 1 M_{Sun} = 2 * 10^{30} kg.)

At the upper end of the main sequence are the hot, luminous O stars, with masses as high as 150 times that of the Sun.

On the lower end of the main sequence are the cool, dim M stars, with as little as 0.08 times the mass of the Sun.

Sun's Evolution on HR Diagram

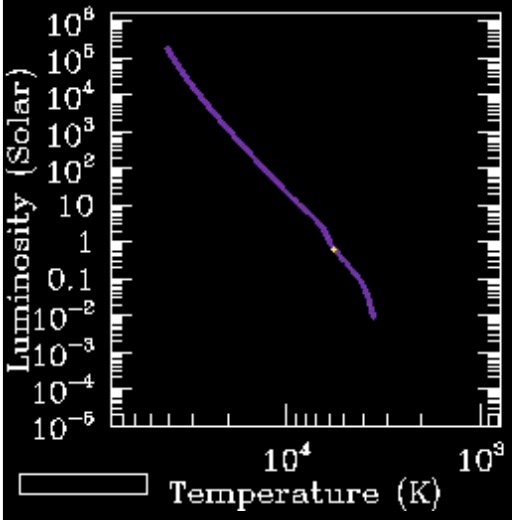

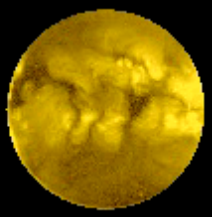

Equations of Stellar Structure

1. Hydrostatic Equations

Basic assumptions:

1. hydrostatic equilibrium: gravity force = pressure gradient;
2. thermal balance: energy generation rate = luminosity.

Consider a thin spherical shell of radius r, thickness δr, mass δm, and density ρ. The mass conservation equation is:

$$dm = 4\pi\rho r^2 dr$$

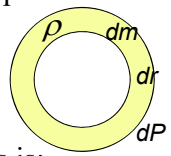

or

$$\frac{dm}{dr} = 4\pi\rho r^2.$$

The balance between the pressure and gravity forces is:

$$4\pi r^2 dP = -\frac{Gmdm}{r^2} = -Gm\frac{4\pi\rho r^2 dr}{r^2},$$

or

$$\frac{dP}{dr} = -\frac{Gm\rho}{r^2}.$$

Energy transfer and balance equations

The total energy flux, $L = 4\pi r^2 F$, integrated over a sphere of radius r:

$$L = -\frac{16\pi acT^3}{3\kappa\rho}\frac{dT}{dr}.$$

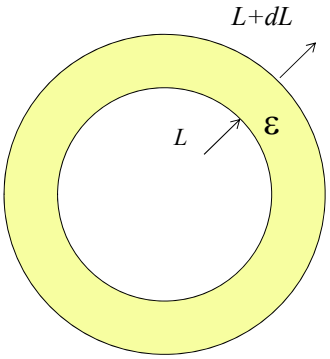

If ε is the energy release per unit mass then the energy flux change in a shell *dr* is:

$$dL = \varepsilon\rho 4\pi r^2 dr$$

$$\frac{dL}{dr} = 4\pi\rho r^2\varepsilon$$

This is the equation for conservation of energy (energy balance).

Equations of the stellar structure

$$\frac{dm}{dr} = 4\pi\rho r^2 \quad (1)$$

$$\frac{dP}{dr} = -\frac{Gm\rho}{r^2} \quad (2)$$

$$\frac{dL}{dr} = 4\pi\rho r^2\varepsilon \quad (3)$$

$$\frac{dT}{dr} = -\frac{\kappa\rho}{16\pi r^2 acT^3}L \equiv -F \quad (4)$$

$$P = \frac{\Re\rho T}{\mu} \quad (5)$$

$$\mu = \frac{1}{2X + \frac{3}{4}Y + \frac{1}{2}Z} \quad (6)$$

$$\varepsilon = \varepsilon_0 X^2 \rho T^4 \quad (7)$$

$$\kappa = \kappa_0 (X+1) Z \rho T^{-3.5} \quad (8)$$

Kramer's opacity law

These equations describe the structure of stellar radiative zones. In the convection zone Eq.(4) is replaced by an equation of convective energy transport, e.g. mixing length theory.

A numerical code for solving these equations is available in the book: C.J. Hansen, S.D. Kawaler, *Stellar Interiors. Physical Principles, Structure and Evolution,* Springer, 1995.

Scaling Laws

Simple estimates can be obtained without solving the equations for solar structure numerically.
Temperature inside the Sun can be roughly estimated from the equation of hydrostatic balance and the equation of state.

Using Eq.(1-2) and (4) we obtain the following relations:

$$\left.\begin{aligned} \frac{dm}{dr} &= 4\pi\rho r^2 \\ \frac{dP}{dr} &= -\frac{Gm\rho}{r^2} \\ P &= \frac{\Re\rho T}{\mu} \end{aligned}\right\} \qquad \begin{aligned} \rho &\sim \frac{M}{R^3} \\ \frac{P}{R} &\sim \frac{GM^2}{R^5} \\ P &\sim \frac{\Re\rho T}{\mu_0}. \end{aligned}$$

The molecular weight for $X \sim 0.7$, $Y \sim 0.28$, and $Z \sim 0.02$ is: $\mu_0 \sim 0.6$.

Then, $T \sim \frac{GM\mu_0}{R\Re} \sim \frac{6.67\times10^{-8}\cdot 2\times10^{33}\cdot 0.6}{8.31\times10^{7}\cdot 7\times10^{10}} \sim 1.4\times10^{7}\,\mathrm{K}.$ (9)

Low-degree p-modes (*l*=0,1,2, and 3)

For $l << n$, $r_1 \approx 0$, and we get: $\omega \approx \frac{\pi(n + L/2 + \alpha)}{\int_0^R \frac{dr}{c}}$.

That is the spectrum of low-degree p-modes is approximately equidistant with frequency spacing: $\Delta\nu = \left(4\int_0^R \frac{dr}{c}\right)^{-1}$. $\nu_{nl} \approx \Delta\nu(2n + l + \frac{1}{2} + 2\alpha) \approx \Delta\nu(2n + l + \frac{3}{2})$

Large frequency separation: Δν=68 μHz

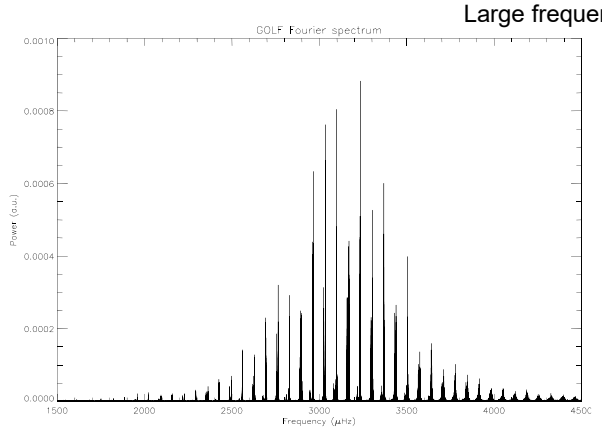

$$\delta\nu_{nl} = \nu_{nl} - \nu_{n-1,l+2} \approx$$

$$\approx -(4l+6)\frac{\Delta_{nl}}{2\pi^2\nu_{nl}}\int_0^{R_\odot}\frac{dc}{dr}\frac{dr}{r}$$

Small frequency separation : δν=9μHz

Solar -modes from 1979 days of the GOLF experiment, B. Gelly - M. Lazrek- G. Grec - A. Ayad - F. X. Schmider- C. Renaud - D. Salabert - E. Fossat· A&A 394, 285-297 (2002)

Asteroseismology Scaling Law

Using the scaling laws:

$$\rho \sim \frac{M}{R^3}, \qquad \frac{P}{R} \sim \frac{GM^2}{R^5}$$

we obtain the scaling law for the speed of sound:

$$c \sim \sqrt{\frac{\gamma P}{\rho}} \sim \sqrt{\frac{M}{R}}.$$

Then, the scaling law for the oscillation frequencies is:

$$\nu \sim \frac{c}{R} \sim \sqrt{\frac{M}{R^3}}$$

Since for the Sun the large frequency separation: $\Delta\nu$=68 μHz we can estimate $\Delta\nu$ for other stars:

$$\Delta\nu \approx 68\left(\frac{M}{M_\odot}\right)^{1/2}\left(\frac{R}{R_\odot}\right)^{-3/2} \quad (\mu Hz)$$

Using the Scaling Law to estimate stellar radius and mass

If we measure the stellar mass and radius in the solar units: $M_\odot = 1,\ R_\odot = 1,$ then:

$$\Delta\nu = \Delta\nu_\odot M^{1/2} R^{-3/2}$$

Spectroscopic observations provide estimates of the gravity acceleration, for which the scaling law is:

$$g = g_\odot M R^{-2}$$

Therefore, from the observed $\Delta\nu$ and R we can estimate the stellar radius and mass:

$$R = \frac{g}{g_\odot}\left(\frac{\Delta\nu_\odot}{\Delta\nu}\right)^2, \qquad M = \frac{g}{g_\odot}R^2$$

Standard solar model

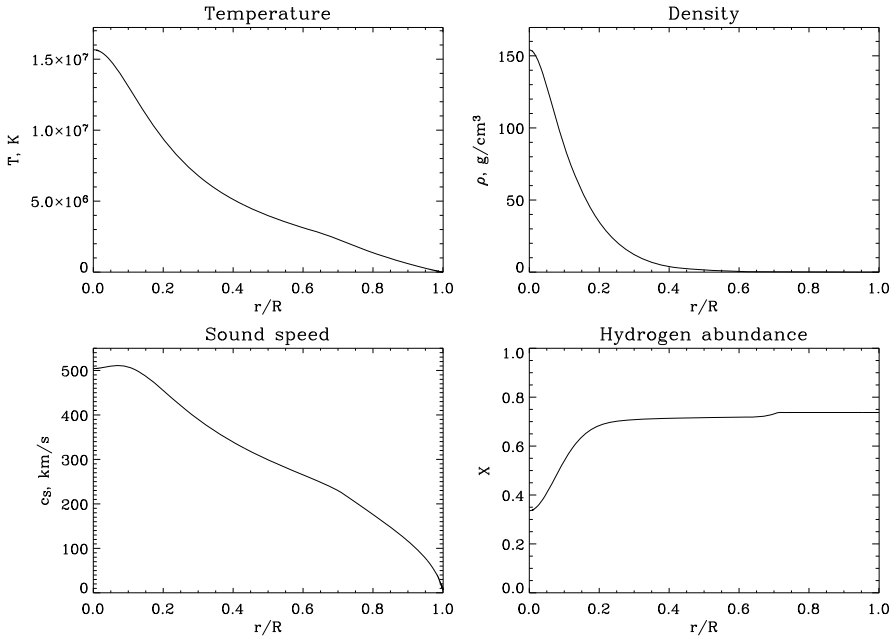

Solar oscillation spectrum obtained from the HMI instrument on Solar Dynamics Observatory.

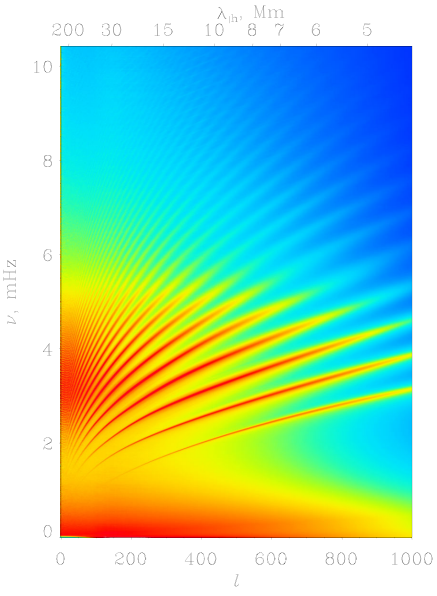

Spectrum of normal modes calculated for a standard solar model. Note the 'avoided crossing effect' for f and g-modes.

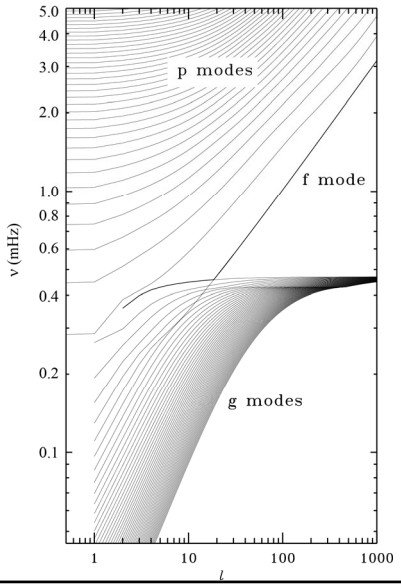

Basic Equations

Basic assumptions:

1. linearity: $\vec{v}/c_s << 1$
2. adiabaticity: $dS/dt = 0$
3. spherical symmetry of the background
4. magnetic forces and Reynolds stresses are negligible

The basic equations are conservations of mass, momentum, energy and Newton's gravity law.

1. Conservation of mass (continuity equation):

The rate of mass change in a fluid element of volume V is equal to the mass flux through the surface of this element (of area A):

$$\frac{\partial}{\partial t}\int_V \rho dV = -\int_A \rho\vec{v}d\vec{a} = -\int_V \nabla(\rho\vec{v})dV.$$

divergence

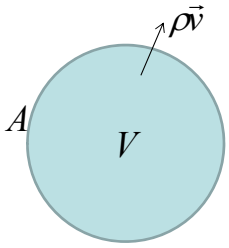

Then,

$$\frac{\partial\rho}{\partial t} + \nabla(\rho\vec{v}) = 0,$$

or

$$\frac{d\rho}{dt} + \rho\nabla\vec{v} = 0.$$

where $\frac{d\rho}{dt} = \frac{\partial\rho}{\partial t} + (\vec{v}\cdot\nabla)\rho$ is the 'material' derivative

2. Momentum equation (conservation of momentum of a fluid element): $\rho\frac{d\vec{v}}{dt} = -\nabla P + \rho\vec{g},$

where P is pressure, $\vec{g}$ is the gravity acceleration, which can be expressed in terms of gravitational potential Φ: $\vec{g} = \nabla\Phi.$

Also, $\frac{d\vec{v}}{dt} = \frac{\partial\vec{v}}{\partial t} + (\vec{v}\cdot\nabla)\vec{v}$. This is the 'material' derivative.

e.g. $v_x\frac{\partial v_x}{\partial x} + v_y\frac{\partial v_x}{\partial y} + v_z\frac{\partial v_x}{\partial z}$ for v_x component

3. Adiabaticity equation (conservation of energy) for a fluid element:

$$\frac{d}{dt}\left(\frac{P}{\rho^\gamma}\right) = 0, \quad \text{or} \quad \frac{dP}{dt} = c^2\frac{d\rho}{dt},$$

where $c^2 = \gamma P/\rho$ is the adiabatic sound speed.

4. Poisson equation: $\nabla^2\Phi = 4\pi G\rho.$

Then, the linearized equations are:

$$\rho' + \nabla(\rho_0 \vec{\xi}) = 0, \quad \text{the continuity (mass conservation) equation}$$

$$\rho_0 \frac{\partial^2 \vec{\xi}}{\partial t^2} = -\nabla P' - g_0 \vec{e}_r \rho' + \rho_0 \nabla \Phi', \text{ the momentum equation}$$

$$P' + \xi_r \frac{dP_0}{dr} = c_0^2 (\rho' + \xi_r \frac{d\rho_0}{dr}), \text{ the adibaticity (energy) equation, or}$$

$$\delta P = c_0^2 \delta \rho \text{ for the Largangian perturbations of pressure and density.}$$

$$\nabla^2 \Phi' = 4\pi G \rho'. \text{ the equation for the gravitational potential}$$

2. Cowling approximation: $\Phi' = 0.$

5. Consider the separation of radial and angular variables in the form:

$$\rho'(r,\theta,\phi) = \rho'(r) \cdot f(\theta,\phi),$$
$$P'(r,\theta,\phi) = P'(r) \cdot f(\theta,\phi),$$
$$\xi_r(r,\theta,\phi) = \xi_r(r) \cdot f(\theta,\phi),$$
$$\vec{\xi}_h(r,\theta,\phi) = \xi_h(r) \nabla_h f(\theta,\phi).$$

Then, the continuity equation is:

$$\left[\rho' + \frac{1}{r^2} \frac{\partial}{\partial r} (r^2 \rho \xi_r) \right] f(\theta,\phi) + \frac{\rho}{r} \xi_h \nabla_h^2 f = 0.$$

The variables are separated if

$$\nabla_h^2 f = \alpha f,$$

where α is a constant.
This equation has non-zero solutions regular at the poles, $\theta = 0, \pi$ only when

$$\alpha = -l(l+1),$$

where l is an integer.

6. The non-zero solution of equation $\nabla_h^2 f + l(l+1) f = 0$ represents the spherical harmonics:

$$f(\theta,\phi) = Y_l^m(\theta,\phi) = C P_l^m(\theta) e^{im\phi},$$

where $P_l^m(\theta)$ is the Legendre function.

General helioseismic inverse problem

1) Variational principle
2) Perturbation theory
3) Kernel transformation
4) Solution of inverse problem
   A. Optimally Localized Averages Method
   B. Regularized Least-Squares Method
5) Inversion results for the solar structure
6) Inversions for solar rotation

Generalized Helioseismic Inverse Problem

In the asymptotic (high-frequency of short wavelength) approximation the oscillation frequencies depend only on the sound-speed profile. This dependence is expressed in terms of the Abel integral equation that can be solved analytically.

In the general case, the relation between the frequencies and internal properties is non-linear, and there is no analytical solution. Generally, the frequencies determined from the oscillation equation depend on the density, $\rho(r)$, the pressure, $P(r)$, and the adiabatic exponent, $\gamma(r)$. However, ρ and P are not independent, and related to each other through the hydrostatic equation:

$$\frac{dP}{dr} = -g\rho,$$

where

$$g = \frac{Gm}{r^2}, \quad m = 4\pi\int_0^r \rho r'^2 dr'.$$

Therefore, only two thermodynamic (hydrostatic) properties of the Sun are independent, e.g. (ρ,γ), (P,γ), or their combinations: $(P/\rho,\gamma)$, (c^2,γ), (c^2,ρ) etc.

The general inverse problem in helioseismology is formulated in terms of small corrections to the standard solar model because the differences between the Sun and the standard model are typically 1% or less. When necessary the corrections can be applied repeatedly, using an iterative procedure.

Variational Principle: Rayleigh's Quotient

Consider the oscillation equations as a formal operator equation in terms of the vector displacement, $\vec{\xi}$:

$$\omega^2\vec{\xi} = L(\vec{\xi}),$$

where L in the general case is an integro-differential operator. If we multiply this by $\vec{\xi}^*$ and integrate over the mass of the Sun we get:

$$\omega^2\int_V \rho\vec{\xi}^*\cdot\vec{\xi}dV = \int_V \vec{\xi}^*\cdot L\vec{\xi}\rho dV,$$

where ρ_0 is the model density, V is the solar volume.
Then, the oscillation frequencies are:

$$\omega^2 = \frac{\int_V \vec{\xi}^*\cdot L\vec{\xi}\rho dV}{\int_V \rho\vec{\xi}^*\cdot\vec{\xi}dV}.$$

The frequencies are expressed in terms of **eigenfunctions** $\vec{\xi}$ and the solar properties represented by coefficients of operator L.

Sometimes, this equation is called **Rayleigh's Quotient** (the original formulation: for an oscillatory system the averaged over period kinetic energy is equal the averaged potential energy).

Rayleigh

THE

THEORY OF SOUND

BY

JOHN WILLIAM STRUTT, BARON RAYLEIGH, Sc.D., F.R.S.

HONORARY FELLOW OF TRINITY COLLEGE, CAMBRIDGE

1877

88. The interpretation of the equations of motion leads to a theorem of considerable importance, which may be thus stated[1]. The period of a conservative system vibrating in a constrained type about a position of stable equilibrium is stationary in value when the type is normal. .We might prove this from the original equations of vibration, but it will be more convenient to employ the normal co-ordinates. The constraint, which may be supposed

Orthogonality of the eigenfunctions

Consider the general oscillation equations in the operator form:

$$\omega^2 \vec{\xi} = L[\vec{\xi}]$$

where $\vec{\xi} = (\xi_r, \xi_h)$ is the displacement vector (which we expressed in terms of the radial and horizontal components, ξ_r and ξ_h).

Non-zero solution, $\xi \neq 0$, exists only for a discrete number of eigenfrequencies ω_{nl} and eigenfunctions $\vec{\xi}_{nl}$.

It can be shown that for the 'zero' boundary conditions: $\vec{\xi} = 0$ at $r = 0$ and $\delta P = 0$ at $r = R$, operator L is Hermitian, that is for two eigenfunctions ξ_1 and ξ_2 the integral over the stellar volume:

$$\int_V \vec{\xi}_1 \cdot L\vec{\xi}_2 \rho dV = \int_V \vec{\xi}_2 \cdot L\vec{\xi}_1 \rho dV$$

Using this property, we can show the oscillation eigenfunctions for different oscillation modes are orthogonal:

$$\int_V \vec{\xi}^*_{nl} \vec{\xi}_{n'l'} \rho dV = 0$$

if $l \neq l'$ and $n \neq n'$.

Proof

Multiplying equation: $\omega_1^2 \vec{\xi}_1 = L\vec{\xi}_1$

by $\vec{\xi}_2$, integrating the product over the stellar mass and using $\omega_2^2 \vec{\xi}_2 = L\vec{\xi}_2$,

we get:

$$\omega_1^2 \int_V \vec{\xi}^*_2 \cdot \vec{\xi}_1 \rho dV = \int_V \vec{\xi}^*_2 \cdot L\vec{\xi}_1 \rho dV = \int_V \vec{\xi}_1 \cdot L\vec{\xi}^*_2 \rho dV = \omega_2^2 \int_V \vec{\xi}_1 \cdot \vec{\xi}^*_2 \rho dV$$

Thus,

$$(\omega_1^2 - \omega_2^2) \int_V \vec{\xi}_1 \cdot \vec{\xi}^*_2 \rho dV = 0$$

If $\omega_1 \neq \omega_2$ then $\int_V \vec{\xi}_1 \cdot \vec{\xi}^*_2 \rho dV = 0$

Variational Principle

Consider small variations of the squared frequency and eigenfunction in the Rayleigh equations:

$$(\omega^2+\Delta\omega^2)\int_V(\vec{\xi}+\Delta\vec{\xi})^*\cdot(\vec{\xi}+\Delta\vec{\xi})\rho dV=\int_V(\vec{\xi}+\Delta\vec{\xi})^*\cdot L(\vec{\xi}+\Delta\vec{\xi})\rho dV$$

Because L is a linear operator: $L(\vec{\xi}+\Delta\vec{\xi})=L(\vec{\xi})+L(\Delta\vec{\xi})$.

Keeping the first-order terms:

$$\omega^2\int_V\vec{\xi}^*\vec{\xi}\rho dV+\omega^2\int_V(\vec{\xi}^*\cdot\Delta\vec{\xi}+\Delta\vec{\xi}^*\cdot\vec{\xi})\rho dV+\Delta\omega^2\int_V\vec{\xi}^*\vec{\xi}\rho dV=$$

$$=\int_V\vec{\xi}^*L\vec{\xi}\rho dV+\int_V\Delta\vec{\xi}^*L\vec{\xi}\rho dV+\int_V\vec{\xi}^*(L\Delta\vec{\xi})\rho dV$$

After the cancellation of the terms satisfying the oscillation equation and using the Hermitian property of L, we obtain:

$$\Delta\omega^2\int_V\vec{\xi}^*\vec{\xi}\rho dV=\int_V\Delta\vec{\xi}^*(-\omega^2\vec{\xi}+L\vec{\xi})\rho dV+\int_V\Delta\vec{\xi}(-\omega^2\vec{\xi}^*+L\vec{\xi})\rho dV=0$$

Thus, variations of the oscillation frequencies, $\Delta\omega^2$, do not depend on the variations of the eigenfunctions, Δ, to the first order.

In other words, ω^2 is stationary with respect to perturbations of $\vec{\xi}$.

Variational Principle

For small perturbations of the solar parameters the frequency change will depend on these perturbations and the corresponding perturbations of the eigenfunctions, e.g.

$$\delta\omega^2=\Psi[\delta\rho,\delta\gamma,\delta\vec{\xi}].$$

The variational principle states that the perturbation of the eigenfunctions $\delta\vec{\xi}$ constitutes second-order corrections, that are in the first-order approximation:

$$\delta\omega^2\approx\Psi[\delta\rho,\delta\gamma].$$

This allows us to neglect the perturbation of the eigenfunctions in the first-order perturbation theory.

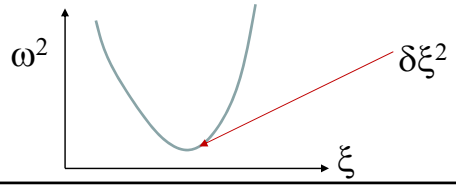

Derivation of the variational principle for solar oscillations

Consider the linearized hydrodynamic equations for oscillations with frequency ω:

conservation of mass: $\rho' = -\mathrm{div}\rho\vec{\xi}$

momentum equation: $-\omega^2\rho\vec{\xi} = -\nabla p' + \frac{\rho'}{\rho^2}\nabla P + \rho\nabla\Phi'$

conservation of entropy: $p' = -\vec{\xi}\nabla P - \gamma P\mathrm{div}\vec{\xi}$

equation for gravitational potential: $\nabla^2\Phi' = 4\pi G\rho'$

where ρ and P are unperturbed distributions of density and pressure inside a star.

An integral equation for the frequency can be obtained by multiplying the momentum equation by $\vec{\eta} = \vec{\xi}^*$, eliminating perturbations of density, ρ' and pressure p' and integrating over the volume.

$$\omega^2\int_V \vec{\eta}\cdot\vec{\xi}\rho dV = \int_V\left(\vec{\eta}\cdot\nabla p' - \frac{\rho'}{\rho^2}\vec{\eta}\cdot\nabla P - \rho\vec{\eta}\cdot\nabla\Phi'\right)dV$$

Transform the first integral in the RHS by integrating by parts:

$$\int_V \vec{\eta}\cdot\nabla p' dV = -\int_V p'\mathrm{div}\vec{\eta}dV + \int_S \vec{\eta}p'd\vec{S} = \int_V\left[\vec{\xi}\cdot\nabla P\mathrm{div}\vec{\eta} + \gamma P\mathrm{div}\vec{\eta}\mathrm{div}\vec{\xi}\right]dV$$

Here we assume that the pressure perturbation on the stellar surface, $p' = 0$.

Eliminating ρ' in the second integral, we write:

$$\int\frac{\rho'}{\rho^2}(\vec{\eta}\cdot\nabla P)dV = -\int_V\frac{1}{\rho}(\vec{\xi}\cdot\nabla\rho)(\vec{\eta}\cdot\nabla P)dV - \int_V\mathrm{div}\vec{\xi}(\vec{\eta}\cdot\nabla P)dV$$

Integrating by parts the third term and using the solution for the Poisson equations: $\Phi'(\vec{r}) = G\int_{V'}\frac{\rho'(\vec{r}')}{|\vec{r}-\vec{r}'|}dV' = -G\int_{V'}\frac{\mathrm{div}\rho\vec{\xi}}{|\vec{r}-\vec{r}'|}dV'$ we obtain:

$$\int_V\rho\vec{\eta}\cdot\Phi' dV = -\int_V\Phi'\mathrm{div}\rho\vec{\eta} + \int_S\Phi'\rho\vec{\eta}d\vec{S}$$

We assume that the density on the stellar surface is zero, so that the surface integral is zero.

Getting all terms together: $\omega^2 = \frac{W(\vec{\xi},\vec{\eta})}{I(\vec{\xi},\vec{\eta})}$, where: $I(\vec{\xi},\vec{\eta}) = \int_V \rho\vec{\xi}\cdot\vec{\eta}dV$,

$$W(\vec{\xi},\vec{\eta}) = \int_V \left[\gamma P \mathrm{div}\vec{\xi}\,\mathrm{div}\vec{\eta} + \vec{\xi}\cdot\nabla P \mathrm{div}\vec{\eta} + \vec{\eta}\cdot\nabla P \mathrm{div}\vec{\xi} + \frac{1}{\rho}(\vec{\xi}\cdot\nabla\rho)(\vec{\eta}\cdot\nabla P)\right]dV -$$

$$-G\iint \frac{\mathrm{div}[\rho\vec{\xi}]\mathrm{div}'[\rho\vec{\eta}]}{|\vec{r}-\vec{r}'|}dVdV'$$

Substituting $\vec{\eta} = \vec{\xi}^*$, we get:

$$W = \int_V [\gamma P(\mathrm{div}\vec{\xi})^2 + 2(\vec{\xi}\cdot\nabla P)\mathrm{div}\vec{\xi} + \frac{1}{\rho}(\vec{\xi}\cdot\nabla\rho)(\vec{\xi}\cdot\nabla P)]dV - G\int_V\int_{V'} \frac{div(\rho\vec{\xi}\,\mathrm{div}'(\rho\vec{\xi})}{|\vec{r}-\vec{r}'|}dVdV'$$

is a quantity proportional to the potential energy of the mode averaged over the period of the oscillation.

$$I = \int_V \rho\,|\vec{\xi}\,|^2\,dV$$

is the mode inertia, $\omega^2 I$ is the averaged over the period kinetic energy.

Perturbation theory

Perturbations of the solar structure properties, $\delta\rho$ and $\delta\gamma$ can be considered as a perturbation of the operator, L: $L\vec{\xi} = L_0\vec{\xi} + L_1\vec{\xi}$, where L_0 describes oscillations of a solar model: $\omega_0^2\vec{\xi}_0 = L_0\vec{\xi}_0$, and ω_0 and $\vec{\xi}_0$ are unperturbed eigenfrequency and eigenfunction.

The corresponding frequency perturbation can be determined from the Rayleigh's quotient, in which we neglect the perturbation of the eigenfunction:

$$(\omega_0 + \delta\omega)^2 = \frac{\int_V \vec{\xi}^*(L_0\vec{\xi}_0 + L_1\vec{\xi}_0)\rho dV}{\int_V \vec{\xi}_0^*\vec{\xi}\rho dV}$$

$$2\omega_0\delta\omega = \frac{\int_V \vec{\xi}^*(L_1\vec{\xi}_0)\rho dV}{\int_V \vec{\xi}_0^*\vec{\xi}\rho dV}$$

$$\frac{\delta\omega}{\omega_0} = \frac{1}{2I\omega_0^2}\int_V \vec{\xi}^* L_1\vec{\xi}\rho dV$$

where $I = \int_V \vec{\xi}_0^*\vec{\xi}_0\rho dV$ is called the 'mode inertia' or 'mode mass'.

The quantity $E = I\omega_0^2$ is the oscillation mode energy.

Calculation of the mode inertia

We express the mode inertia in terms of the radial and horizontal components of the displacement: $\vec{\xi} = \left[\xi_r(r) Y_l^m(\theta,\phi), \xi_h(r) \nabla_h Y_l^m(\theta,\phi) \right]$

In the spherical coordinates: $dV = \sin\theta d\theta d\pi$.

$$I = \int_V \vec{\xi}^* \cdot \vec{\xi} \rho dV = I_r + I_h$$

$$I_r = \int_V \xi_r^* \xi_r (Y_l^{m*} Y_l^m \sin\theta d\theta d\phi) r^2 dr = \int_0^R |\xi_r|^2 \rho r^2 dr$$

where we used the normalization condition for the spherical harmonics: $\int_0^{2\pi} \int_0^{\pi} Y_l^{m*} Y_l^m \sin\theta d\theta d\phi = 1$.

Similarly,

$$I_h = \int_V \xi_h^* \xi_h (\vec{\nabla}_h Y_l^m)^* \cdot (\vec{\nabla}_h Y_l^m) \sin\theta d\theta d\phi \rho r^2 dr = l(l+1) \int_0^R |\xi_h(r)|^2 \rho r^2 dr$$

where to calculate the angular integrals we used the integration by parts and the equation for spherical harmonics: $\nabla^2 Y_l^m = l(l+1) Y_l^m$.

Finally, $I = \int_0^R \left[\xi_r^2 + l(l+1) \xi_h^2 \right] \rho r^2 dr$.

Perturbation theory

We consider a small perturbation of the operator L caused by variations of the solar structure properties:

$$L(\vec{\xi}) = L_0(\vec{\xi}) + L_1(\vec{\xi}).$$

Then, the corresponding frequency perturbations are determined from the following equation:

$$\left(\omega_0 + \delta\omega\right)^2 = \frac{\int_V \vec{\xi}^* \cdot (L_0 \vec{\xi} + L_1 \vec{\xi}) \rho dV}{\int_V \rho \vec{\xi}^* \cdot \vec{\xi} dV},$$

or

$$\frac{\delta\omega}{\omega} = \frac{1}{2\omega_0 I} \int_V \vec{\xi}^* \cdot L_1 \vec{\xi} \rho dV,$$

where

$$I = \int_V \rho \vec{\xi}^* \cdot \vec{\xi} dV$$

is so-called *mode inertia* or *mode mass*.

The *mode energy* is $E = I\omega_0^2 a^2$, where a is the amplitude of the surface displacement. The mode eigenfunctions are usually normalized such that $\xi_r(R) = 1$.

Rayleigh's Quotient for normal modes

For a normal mode, i, the variational principle gives an integral relation for the eigenfrequency, ω_i:

$$\omega_i^2 = W_i / I_i,$$

where

$$W_i = \int_V [\gamma p (\mathrm{div}\vec{\xi}_i)^2 + 2(\vec{\xi}_i \cdot \nabla p)\mathrm{div}\vec{\xi}_i + \rho^{-1}(\vec{\xi}_i \cdot \nabla \rho)(\vec{\xi}_i \cdot \nabla p)]dV -$$

$$- G\int_V \int_V |\vec{r}_i - \vec{r}_i|^{-1} \mathrm{div}[\rho\vec{\xi}_i]\mathrm{div}[\rho'\vec{\xi}_i]dVdV'$$

is a quantity proportional to the potential energy of the mode averaged over the period of the oscillation, and

$$I_i = \int_V \rho \vec{\xi}_i^2 dV$$

Sensitivity kernels

Using explicit formulations for operator L_1 the variational principle can be reduced to a system of integral equations for a chosen pair of independent variables, e.g. for (ρ, γ)

$$\frac{\delta\omega^{(n,l)}}{\omega^{(n,l)}} = \int_0^R K_{\rho,\gamma}^{(n,l)} \frac{\delta\rho}{\rho} dr + \int_0^R K_{\gamma,\rho}^{(n,l)} \frac{\delta\gamma}{\gamma} dr,$$

where $K_{\rho,\gamma}^{(n,l)}(r)$ and $K_{\gamma,\rho}^{(n,l)}(r)$ are sensitivity (or 'seismic') kernels. These are calculated using the initial solar model parameters, ρ_0, P_0, γ, and the oscillation eigenfunctions for these model, $\vec{\xi}$.

Explicit form of sensitivity kernels in terms of oscillation eigenfunctions for mode i=(n,l)

$$K_i^{(\rho,\gamma)}(r)=\frac{\rho r^2}{E_i}\left\{\begin{array}{l}-\omega_i^2\left[\xi_i^2+l(l+1)\eta_i^2\right]+2\xi_i\left(g'_i+4\pi G\rho\xi_i-F_i g\right)+\\ \qquad+\dfrac{2l(l+1)}{r}\eta_i\Phi'_i-C_{1,i}g+4\pi G\left(S_i-S_{1,i}\right)\end{array}\right\}$$

where ξ is the vertical displacement, and η is the horizontal displacement.

$$E_i=\omega_i^2\int_0^R\left[\xi_i^2+l(l+1)\eta_i^2\right]\rho r^2dr$$

is proportional to the energy of mode i;

$$F_i=\frac{1}{r}\left[2\xi_i-l(l+1)\eta_i\right];\qquad C_{1,i}=-\frac{1}{r^2}\int_0^r\gamma K_i r'^2dr'$$

$$S_{1,i}=\int_r^R\rho C_{1,i}dr';\qquad S_i=-2\int_r^R\rho\xi_i F_i dr'$$

$$K_i=\left(\frac{d\xi_i}{dr}+F_i\right)^2\equiv(\mathrm{div}\vec{\xi}_i)^2$$

$$K_i^{(\gamma,\rho)}(r)=\frac{r^2}{E_i}\gamma pK_i$$

Examples of the sensitivity kernels

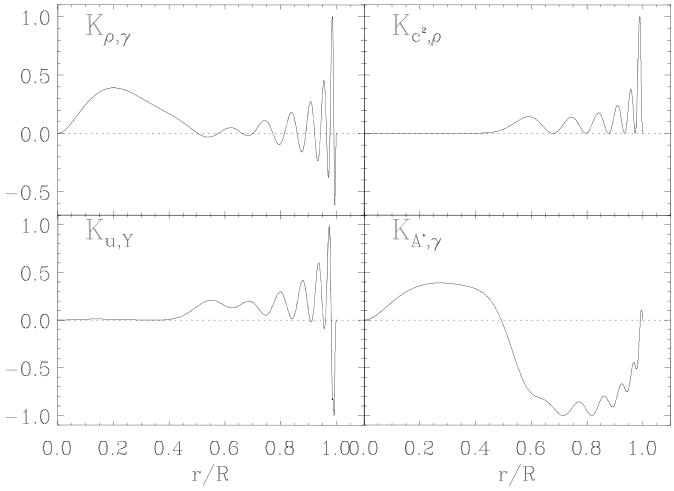

Equation for the sensitivity kernels

If we define:

$$\vec{z}_1 = \left(\frac{\delta\rho}{\rho}, \frac{\delta\gamma}{\gamma} \right)$$

$$\vec{K}_i^{(1)} = \left(K_i^{(\rho,\gamma)}, K_i^{(\gamma,\rho)} \right)$$

then the perturbation equation can be written in the form:

$$\frac{\delta\omega_i^2}{\omega_i^2} = \left\langle \vec{K}_i^{(1)} \cdot \vec{z}_1 \right\rangle,$$

where $\left\langle u \cdot v \right\rangle = \int_0^R uv\, dr$.

Kernel Transformations. 1

The sensitivity for various pairs of solar parameters can be obtained by using the relations among these parameters, which follows from the equations of solar structure ('stellar evolution theory').

A general procedure for calculating the sensitivity kernels can be illustrated in an operator form. Consider two pairs of solar variables, $\vec{X}$ and $\vec{Y}$, e.g.

$$\vec{X} = \left(\frac{\delta\rho}{\rho}, \frac{\delta\gamma}{\gamma} \right); \ \vec{X} = \left(\frac{\delta u}{u}, \frac{\delta Y}{Y} \right),$$

where $u = P/\rho$, Y is the helium abundance.

The linearized structure equations (the hydrostatic equilibrium equation and the equation of state) that relate these variables can be written symbolically:

$$A\vec{X} = \vec{Y}.$$

Kernel Transformations. 2

Let $\vec{K}_X$ and $\vec{K}_Y$ be the sensitivity kernels for X and Y, then the frequency perturbation is:

$$\frac{\delta\omega}{\omega} = \int_0^R \vec{K}_X \cdot \vec{X} dr \equiv \left\langle \vec{K}_X \cdot \vec{X} \right\rangle,$$

where $< \cdot >$ denotes the inner product. Similarly,

$$\frac{\delta\omega}{\omega} = \left\langle \vec{K}_Y \cdot \vec{Y} \right\rangle.$$

Then from the stellar structure equation $A\vec{X} = \vec{Y}$:

$$\left\langle \vec{K}_Y \cdot \vec{Y} \right\rangle = \left\langle \vec{K}_Y \cdot A\vec{X} \right\rangle = \left\langle A^* \vec{K}_Y \cdot \vec{X} \right\rangle,$$

where A^* is an adjoint operator.

Thus: $\left\langle A^* \vec{K}_Y \cdot \vec{X} \right\rangle = \left\langle \vec{K}_X \cdot \vec{X} \right\rangle.$

This is valid for any $\vec{X}$ if $\boxed{A^* \vec{K}_Y = \vec{K}_X.}$

That means that the equation for the sensitivity kernels is adjoint to the stellar structure equations.

Examples of the sensitivity kernels

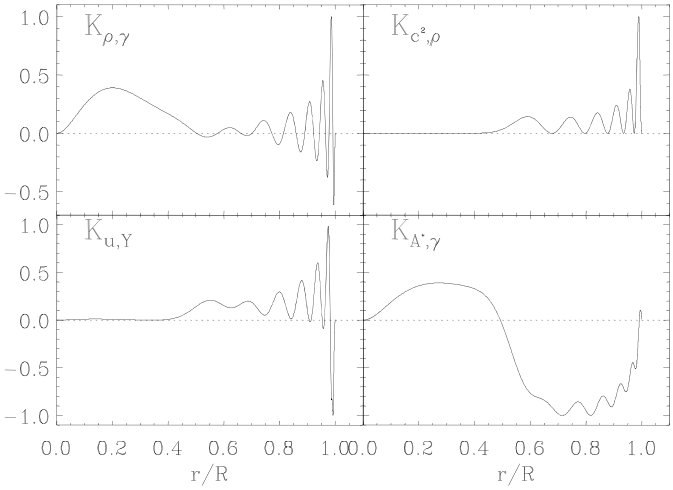

Lecture 17
General helioseismic inverse problem. Perturbation theory. Kernel transformations

(Stix, Chapter 5.3.1; Kosovichev, p.34-41, 44-48;
Christensen-Dalsgaard, Chapters 5.5)

General helioseismic inverse problem

1) Variational principle
2) Perturbation theory
3) Kernel transformation
4) Solution of inverse problem
   A. Optimally Localized Averages Method
   B. Regularized Least-Squares Method
5) Inversion results for the solar structure
6) Inversions for solar rotation

Generalized Helioseismic Inverse Problem

In the asymptotic (high-frequency of short wavelength) approximation the oscillation frequencies depend only on the sound-speed profile. This dependence is expressed in terms of the Abel integral equation that can be solved analytically.
In the general case, the relation between the frequencies and internal properties is non-linear, and there is no analytical solution. Generally, the frequencies determined from the oscillation equation depend on the density, $\rho(r)$, the pressure, $P(r)$, and the adiabatic exponent, $\gamma(r)$. However, ρ and P are not independent, and related to each other through the hydrostatic equation:

$$\frac{dP}{dr} = -g\rho,$$

where

$$g = \frac{Gm}{r^2},\ m = 4\pi\int_0^r \rho r'^2 dr'.$$

Therefore, only two thermodynamic (hydrostatic) properties of the Sun are independent, e.g. (ρ,γ), (P,γ), or their combinations: $(P/\rho,\gamma)$, (c^2,γ), (c^2,ρ) etc.
The general inverse problem in helioseismology is formulated in terms of small corrections to the standard solar model because the differences between the Sun and the standard model are typically 1% or less. When necessary, the corrections can be applied repeatedly, using an iterative procedure.

Variational Principle: Rayleigh's Quotient

Consider the oscillation equations as a formal operator equation in terms of the vector displacement, $\vec{\xi}$:

$$\omega^2\vec{\xi} = \mathcal{L}(\vec{\xi}),$$

where $\mathcal{L}$ in the general case is an integro-differential operator. If we multiply this by $\vec{\xi}^*$ and integrate over the mass of the Sun we get:

$$\omega^2\int_V \rho\vec{\xi}^*\cdot\vec{\xi}\,dV = \int_V \vec{\xi}^*\cdot\mathcal{L}\vec{\xi}\rho dV,$$

where ρ_0 is the model density, V is the solar volume.
Then, the oscillation frequencies are:

$$\omega^2 = \frac{\int_V \vec{\xi}^*\cdot\mathcal{L}\vec{\xi}\rho dV}{\int_V \rho\vec{\xi}^*\cdot\vec{\xi}\,dV}.$$

The frequencies are expressed in terms of **eigenfunctions** $\vec{\xi}$ and the solar properties represented by coefficients of operator $\mathcal{L}$.

Sometimes, this equation is called **Rayleigh's Quotient** (the original formulation: for an oscillatory system the averaged over period kinetic energy is equal the averaged potential energy).

Variational Principle

For small perturbations of the solar parameters the frequency change will depend on these perturbations and the corresponding perturbations of the eigenfunctions, e.g.

$$\delta\omega^2 = \Psi[\delta\rho, \delta\gamma, \delta\vec{\xi}].$$

The variational principle states that the perturbation of the eigenfunctions $\delta\vec{\xi}$ constitutes second-order corrections, that are in the first-order approximation:

$$\delta\omega^2 \approx \Psi[\delta\rho, \delta\gamma].$$

This allows us to neglect the perturbation of the eigenfunctions in the first-order perturbation theory.

Perturbation theory

We consider a small perturbation of the operator $\mathcal{L}$ caused by variations of the solar structure properties:

$$\mathcal{L}(\vec{\xi}) = \mathcal{L}_0(\vec{\xi}) + \mathcal{L}_1(\vec{\xi}).$$

Then, the corresponding frequency perturbations are determined from the following equation:

$$(\omega_0 + \delta\omega)^2 = \frac{\int_V \vec{\xi}^* \cdot (\mathcal{L}_0\vec{\xi} + \mathcal{L}_1\vec{\xi})\rho dV}{\int_V \rho\vec{\xi}^* \cdot \vec{\xi} dV},$$

or

$$\frac{\delta\omega}{\omega} = \frac{1}{2\omega_0 I}\int_V \vec{\xi}^* \cdot \mathcal{L}_1\vec{\xi}\rho dV,$$

where

$$I = \int_V \rho\vec{\xi}^* \cdot \vec{\xi} dV$$

is so-called *mode inertia* or *mode mass*.

The *mode energy* is $E = I\omega_0^2 a^2$, where a is the amplitude of the surface displacement. The mode eigenfunctions are usually normalized such that $\xi_r(R) = 1$.

Sensitivity kernels

Using explicit formulations for operator $\mathcal{L}_1$ the variational principle can be reduced to a system of integral equations for a chosen pair of independent variables, e.g. for (ρ,γ)

$$\frac{\delta\omega^{(n,l)}}{\omega^{(n,l)}} = \int_0^R K^{(n,l)}_{\rho,\gamma}\frac{\delta\rho}{\rho}dr + \int_0^R K^{(n,l)}_{\gamma,\rho}\frac{\delta\gamma}{\gamma}dr,$$

where $K^{(n,l)}_{\rho,\gamma}(r)$ and $K^{(n,l)}_{\gamma,\rho}(r)$ are sensitivity (or 'seismic') kernels. These are calculated using the initial solar model parameters, ρ_0, P_0, γ, and the oscillation eigenfunctions for these model, $\vec{\xi}$.

Inversions for the solar structure

Variational principle for oscillation frequencies

The motions in a star in the simplest case with no heat sources and no heat exchange and extra forces (such as magnetic and Reynolds stress forces) are described by the hydrodynamic equations of conservation of mass, momentum, energy and by Poisson's equation:

$$\frac{\partial\rho}{\partial t} + \mathrm{d}iv(\rho\mathbf{v}) = 0$$

$$\rho\left(\frac{\partial\mathbf{v}}{\partial t} + \mathbf{v}\cdot\nabla\mathbf{v}\right) = -\nabla p - \rho\nabla\Phi$$

$$\frac{\partial S}{\partial t} + \mathbf{v}\cdot\nabla S = 0$$

$$\nabla^2\Phi = 4\pi G\rho.$$

Here ρ, $\mathbf{v}$, p, Φ, T and S are the density, fluid velocity, pressure, gravitational potential, temperature and specific entropy, respectively, and G is the gravitational constant. These equations are complemented by the equation of state: $S = S(p,\rho)$, and boundary conditions of regularity at the star center.

Since the amplitude of solar oscillations is small they can be described in terms of small perturbations to a stationary equilibrium state which in the first approximation is a function of only radius r. The perturbation equations are

$$\frac{\partial \rho'}{\partial t} + \mathrm{d}iv(\rho \mathbf{v}') = 0$$

$$\rho \frac{\partial \mathbf{v}'}{\partial t} = -\nabla p' - \rho \nabla \Phi' - \rho' \nabla \Phi$$

$$\frac{\partial p'}{\partial t} + \mathbf{v}' \cdot \nabla p - \left(\frac{\partial p}{\partial \rho} \right)_S \left(\frac{\partial \rho'}{\partial t} + \mathbf{v}' \cdot \nabla \rho \right) = 0$$

$$\nabla^2 \Phi' = 4\pi G \rho',$$

where the variables without subscript denote properties of the equilibrium state, and the prime sign refers to small perturbations of the properties due to oscillations; $(\partial p / \partial \rho)_S \equiv c^2$ is the adiabatic sound speed, which is also represented in terms of the adiabatic exponent, $\gamma \equiv (\partial \log P / \partial \log \rho)_S$: $c^2 = \gamma P / \rho$. This system of equations is complemented by boundary conditions describing regularity of the solution at the star center, $r = 0$, and the absence of external forces ($\delta p = 0$)on the surface $r = R$.

The oscillatory solution of this system has time dependence $\exp(i\omega t)$, and can be expressed it terms of Fourier components of the fluid displacement, $\boldsymbol{\xi}$,

$$\mathbf{v}' = \partial \boldsymbol{\xi} / \partial t = i\omega \boldsymbol{\xi},$$

where ω in the oscillation frequency.

As a result, we obtain an eigenvalue problem for a fourth-order system of ordinary linear differential equations.

In this formulation, the eigenvalue problem is non-linear in terms of the squared eigenfrequency, ω^2, and typically solved by iterations for a given initial equilibrium state.

The inverse problem of helioseismology is to estimate the properties of the equilibrium state from a set of observed eigenfrequencies. The standard approach to this problem is to find corrections to models of the equilibrium state which are sufficiently close to the real Sun, so that a perturbation theory can be employed.

The oscillation equations together with the boundary conditions can also be represented in a linear operator form:

$$L\boldsymbol{\xi} + \omega^2 \boldsymbol{\xi} = 0,$$

where L is a self-adjoint (Hermitian) integro-differential operator. Therefore, the eigenfunctions $\boldsymbol{\xi}$ are orthogonal. Eigenvalues ω^2 are real and obey a variational principle.

For a normal mode, i, the variational principle gives an integral relation for the eigenfrequency, ω_i (Rayleigh's Quotient):

$$\omega_i^2 = W_i / I_i,$$

where

$$W_i = \int_V [\gamma p (\mathrm{d}iv\boldsymbol{\xi}_i)^2 + 2(\boldsymbol{\xi}_i \cdot \nabla p)\mathrm{d}iv\boldsymbol{\xi}_i + \rho^{-1}(\boldsymbol{\xi}_i \cdot \nabla\rho)(\boldsymbol{\xi}_i \cdot \nabla p)]dV$$
$$-G\int_V\int_V |\mathbf{r}_i - \mathbf{r}_{i'}|^{-1}\, \mathrm{d}iv[\rho\boldsymbol{\xi}_i]\mathrm{d}iv[\rho'\boldsymbol{\xi}_i']dVdV'$$

is a quantity proportional to the potential energy of the mode averaged over the period of the oscillation, and

$$I_i = \int_V \rho\boldsymbol{\xi}_i^2 dV$$

can be regarded as mode inertia. Physically this equation represents the balance between the potential and kinetic energies averaged over the period of the oscillation modes.

In a spherically-symmetric star, the displacement eigenfunctions, $\boldsymbol{\xi}_i$, can be expressed in terms of spherical harmonics $Y_{lm}(\theta,\phi)$:

$$\boldsymbol{\xi}_i(r,\theta,\phi) = \mathbf{e}_r \xi_{r,i}(r) Y_{lm}(\theta,\phi) + \xi_{h,i}(r)\nabla_\perp Y_{lm}(\theta,\phi),$$

where $\xi_{r,i}(r)$ and $\xi_{h,i}(r)$ represent the radial dependence of the radial and horizontal components of the displacement vector, $\nabla_\perp = \mathbf{e}_\theta \dfrac{\partial}{\partial\theta} + \mathbf{e}_\phi \dfrac{1}{\sin\theta}\dfrac{\partial}{\partial\phi}$ is the angular part of the gradient in spherical coordinates, (r,θ,ϕ), and $\mathbf{e}_r, \mathbf{e}_\theta, \mathbf{e}_\phi$ are units vectors in the directions of r,θ,ϕ.

Thus, the equations and the variational principle for a oscillation mode with frequency, ω_i, can be written in term of $\xi_{r,i}$ and $\xi_{r,i}$, and perturbation of the gravitational potential Φ':

$$W_i = 4\pi\int_0^R \gamma p\left(\frac{d\xi_{r,i}}{dr} + \frac{2\xi_{r,i}}{r} - \frac{l(l+1)\xi_{h,i}}{r}\right)^2 r^2 dr +$$
$$+4\pi\int_0^R \rho r^2\left[-\frac{4}{r}g\xi_{r,i}^2 + \xi_{r,i}\left(g_i' + 4\pi G\rho\xi_{r,i}\right) + l(l+1)\frac{\xi_{h,i}}{r}\left(\Phi_i' + 2g\xi_{r,i}\right)\right]dr,$$

$$I_i = 4\pi\int_0^R \rho r^2\left[\xi_{r,i}^2 + l(l+1)\xi_{h,i}^2\right]dr,$$

where

$$g' = \frac{\partial\Phi'}{\partial r}; \quad \nabla^2\Phi' = 4\pi G\rho'; \quad g = \frac{Gm}{r^2} \equiv \frac{4\pi G}{r^2}\int_0^r \rho r'^2 dr';$$

R is radius of the Sun, and m is the mass within a sphere of radius r.

The variational principle asserts that the eigenfrequencies are stationary with respect to variations in $\boldsymbol{\xi}_i$, i.e., if a perturbation in an eigenfunction is $O(\epsilon)$, then the perturbation in the corresponding eigenfrequency, ω_i is $O(\epsilon^2)$.

Consequently, one can calculate small corrections to the frequencies due to changes in the physical conditions inside the Sun by linearizing the Rayleigh Quotient in terms perturbations of the structure properties, e.g. density ρ, pressure p, and the adiabatic exponent, γ, and using the unperturbed eigenfunctions.

From the variational principle one can obtain:

$$\frac{\delta\omega_i^2}{\omega_i^2} = \int_0^R K_i^{(\rho,\gamma)} \frac{\delta\rho}{\rho} dr + \int_0^R K_i^{(\gamma,\rho)} \frac{\delta\gamma}{\gamma} dr,$$

where $K_i^{(\rho,\gamma)}$ defines the sensitivity of the mode frequency to perturbations of the density, ρ, at constant γ, and $K_i^{(\gamma,\rho)}$ is the sensitivity ('kernel') function for variations of γ at constant ρ.

$$K_i^{(\rho,\gamma)}(r) = \frac{\rho r^2}{E_i}\left\{-\omega_i^2\left[\xi_{r,i}^2 + l(l+1)\xi_{h,i}^2\right] + 2\xi_{r,i}\left(g_i' + 4\pi G\rho\xi_{r,i} - F_i g\right) + \right.$$

$$\left. \frac{2l(l+1)}{r}\xi_{h,i}\Phi_i' - C_{1,i}g + 4\pi G\left(S_i - S_{1,i}\right)\right\}$$

and $E_i = \omega_i^2 \int_0^R \left[\xi_{r,i}^2 + l(l+1)\xi_{h,i}^2\right]\rho r^2 dr$ is proportional to the energy of mode i;

$$F_i = \frac{1}{r}\left[2\xi_{r,i} - l(l+1)\xi_{h,i}\right]; \quad C_{1,i} = -\frac{1}{r^2}\int_0^r \gamma K_{i'} r'^2 dr'; \quad S_{1,i} = \int_r^R \rho C_{1,i} dr';$$

$$S_i = -2\int_r^R \rho\xi_{r,i}F_i dr'; \quad K_{i'} = \left(\frac{d\xi_{r,i}}{dr} + F_i\right)^2 \equiv (\mathrm{div}\boldsymbol{\xi}_i)^2; \quad K_i^{(\gamma,\rho)}(r) = \frac{r^2}{E_i}\gamma p K_{i'}.$$

Examples of the sensitivity kernels for ρ and γ

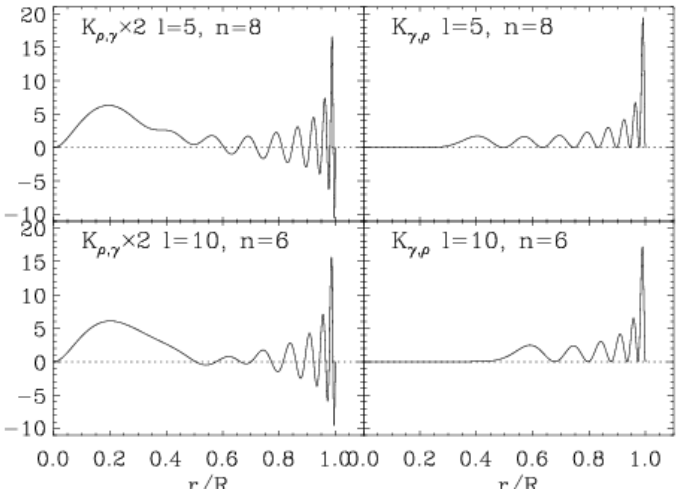

If we define vector functions: $\mathbf{z}_1 = \left(\frac{\delta\rho}{\rho}, \frac{\delta\gamma}{\gamma}\right)$, $\mathbf{K}_i^{(1)} = \left(K_i^{(\rho,\gamma)}, K_i^{(\gamma,\rho)}\right)$,

then equation $\frac{\delta\omega_i^2}{\omega_i^2} = \int_0^R K_i^{(\rho,\gamma)} \frac{\delta\rho}{\rho} dr + \int_0^R K_i^{(\gamma,\rho)} \frac{\delta\gamma}{\gamma} dr,$

can be written in the form: $\frac{\delta\omega_i^2}{\omega_i^2} = \left\langle \mathbf{K}_i^{(1)} \cdot \mathbf{z}_1 \right\rangle$, where $\langle \mathbf{uv} \rangle = \int_0^R \mathbf{u} \cdot \mathbf{v} dr$.

These equations provide integral constraints on unknown functions $\delta\rho/\rho$ and $\delta\gamma/\gamma$ with kernels $K_i^{(\rho,\gamma)}$ and $K_i^{(\gamma,\rho)}$. These kernels determine the sensitivity of the oscillation frequencies to density variations at constant adiabatic exponent γ and to variations of γ at constant ρ respectively. The similar integral equations can be obtained for some other parameters of solar structure. These equations are used for inferring the structure parameters from the relative differences between the observed frequencies and frequencies of a reference solar model. For a given reference model eigenfrequencies ω_i and kernels $K_i^{(\gamma,\rho)}$ and $K_i^{(\rho,\gamma)}$ can be computed numerically with standard methods.

Kernel transformation. Method of adjoint equations.

The hydrostatic structure of the Sun is uniquely determined by the two 'primary' properties: density $\rho(r)$ and the adiabatic exponent $\gamma(r)$. Other, 'secondary' properties of the solar structure, such as the squared sound speed $c^2 = \gamma p / \rho$, the parameter of convective stability

$A^* = \frac{1}{\gamma}\frac{d\log p}{d\log r} - \frac{d\log \rho}{d\log r}$, temperature T or abundances of helium, Y, and heavier elements, Z, can be determined from ρ and γ using the equations of stellar structure.

These equations describe the hydrostatic and thermal equilibria and the thermodynamic state of the solar plasma. Some of the 'secondary' properties (e.g. c^2 and A^*) can be determined using only the hydrostatic equations, while others (e.g. T and Y) require both the hydrostatic and thermodynamic equations.

In the helioseismic applications, it is often of interest to obtain direct estimates of these ('secondary') properties from the oscillation frequencies. Such a situation arises, for instance, when the available frequency information allows the determination of solar properties only in some particular regions of the solar interior. The integral equations which relates the variations of the 'secondary' properties to the frequency difference can be obtained by the method of adjoint functions.

In mathematics, an ajoint operator $\mathcal{A}^*$ (or Hermitian conjugate operator) is defined according to the rule: $\langle \mathcal{A}\mathbf{x}, \mathbf{y}\rangle = \langle \mathbf{x}, \mathcal{A}^*\mathbf{y}\rangle$.

For matrix A: $\langle A\mathbf{x}, \mathbf{y}\rangle = \langle \mathbf{x}, A^T\mathbf{y}\rangle$ where A^T is matrix transposed to A

The idea of this method is very simple. The relation between the 'primary', $\mathbf{z}_1$, and 'secondary', $\mathbf{z}_2$, properties that follows from the linearized stellar structure equations can be written in the following symbolic form:

$$\mathcal{A}\mathbf{z}_1 = \mathbf{z}_2,$$

where $\mathcal{A}$ is a linear operator. If $\mathbf{K}^{(2)}$ is the integral kernel for $\mathbf{z}_2$ then the relative frequency differences can be expressed in terms of both $\mathbf{z}_1$ and $\mathbf{z}_2$:

$$\delta\omega^2 / \omega^2 = \langle \mathbf{K}^{(1)}\mathbf{z}_1\rangle = \langle \mathbf{K}^{(2)}\mathbf{z}_2\rangle.$$

Then, substituting $\mathbf{z}_2$ from the structure equations, we obtain:

$$\langle \mathbf{K}^{(1)}\mathbf{z}_1\rangle = \langle \mathbf{K}^{(2)}\mathbf{z}_2\rangle = \langle \mathbf{K}^{(2)}, \mathcal{A}\mathbf{z}_1\rangle = \langle \mathcal{A}^*\mathbf{K}^{(2)}, \mathbf{z}_1\rangle.$$

where operator $\mathcal{A}^*$ is adjoint to operator $\mathcal{A}$. Comparing the first and last terms we obtain the equation for the 'secondary' kernels, $\mathbf{K}^{(2)}$:

$$\mathcal{A}^*\mathbf{K}^{(2)} = \mathbf{K}^{(1)},$$

which is adjoint to the structure equation.

The sensitivity kernels can be interpreted as a `response' of the oscillation frequencies to point perturbations. If an *i*-component of the structure variables $\mathbf{z}_{1,i} = \delta(r - r_0)$ then $\delta\omega^2 / \omega^2 = \langle \mathbf{K}^{(1)}\mathbf{z}_1\rangle = \mathbf{K}_i^{(1)}(r_0)$.

Generally, the relation between the 'primary' and 'secondary' properties of the solar structure is obtained from the equations of hydrostatic and thermal balance and constitutes a system of linear differential and algebraic equations:

$$\frac{d\mathbf{y}}{dx} = A\mathbf{y} + B\mathbf{z}_2$$
$$\mathbf{z}_1 = C\mathbf{y} + D\mathbf{z}_2,$$

where $x = \log(r)$ and $\mathbf{y}(x)$ is a vector-function of some properties of the stellar structure different from $\mathbf{z}_1$ and $\mathbf{z}_2$ (e.g. gas pressure and fractional mass). The equations are complemented by the boundary conditions of regularity at the stellar center and surface.

These equations represent an explicit form the operator equation:

$$\mathcal{A}\mathbf{z}_1 = \mathbf{z}_2$$

. If the function $\mathbf{z}_2$ is known then $\mathbf{z}_1$ can be determined by solving these equations. Our task is to find the explicit form of the adjoint operator A^*, such as

$$\mathcal{A}^*\mathbf{K}^{(2)} = \mathbf{K}^{(1)}$$

where $\mathbf{K}^{(1)}$ and $\mathbf{K}^{(2)}$ satisfy the equation: $\langle \mathbf{K}^{(1)}\mathbf{z}_1 \rangle = \langle \mathbf{K}^{(2)}\mathbf{z}_2 \rangle$

To find a kernel function $\mathbf{K}^{(2)}$ for $\mathbf{z}_2$ we introduce a new vector-function $\mathbf{w} = (w_1, w_2)$ and calculate the inner product of $\mathbf{w}$ with the first equation:

$$\frac{d\mathbf{y}}{dx} = A\mathbf{y} + B\mathbf{z}_2$$

$$\left\langle \mathbf{w} \cdot \frac{d\mathbf{y}}{dx} \right\rangle = \left\langle \mathbf{w} \cdot A\mathbf{y} \right\rangle + \left\langle \mathbf{w} \cdot B\mathbf{z}_2 \right\rangle.$$

Using integration by parts and assuming that

$$\mathbf{w} \cdot \mathbf{y} = 0 \quad at \quad both \quad r = 0 \quad and \quad r = R$$

we find

$$-\left\langle \mathbf{y} \cdot \frac{d\mathbf{w}}{dx} \right\rangle = \left\langle \mathbf{y} \cdot A^T\mathbf{w} \right\rangle + \left\langle \mathbf{w} \cdot B\mathbf{z}_2 \right\rangle,$$

where A^T is transposition of matrix A.

Then, we calculate the inner product of $\mathbf{K}^{(1)}$ with the second eqution:

$$\mathbf{z}_1 = C\mathbf{y} + D\mathbf{z}_2,$$

and use the equation $\langle \mathbf{K}^{(1)} \cdot \mathbf{z}_1 \rangle = \langle \mathbf{K}^{(2)} \cdot \mathbf{z}_2 \rangle$

$$\left\langle \mathbf{K}^{(2)} \cdot \mathbf{z}_2 \right\rangle = \left\langle \mathbf{K}^{(1)} \cdot C\mathbf{y} \right\rangle + \left\langle \mathbf{K}^{(1)} \cdot D\mathbf{z}_2 \right\rangle.$$

If $\mathbf{w}$ is such that

$$\left\langle \mathbf{K}^{(1)} \cdot C\mathbf{y} \right\rangle = \left\langle \mathbf{w} \cdot B\mathbf{z}_2 \right\rangle,$$

then the inner product equation

$$-\left\langle \mathbf{y} \cdot \frac{d\mathbf{w}}{dx} \right\rangle = \left\langle \mathbf{y} \cdot A^T\mathbf{w} \right\rangle + \left\langle \mathbf{w} \cdot B\mathbf{z}_2 \right\rangle,$$

can be written as:

$$-\left\langle \mathbf{y} \cdot \frac{d\mathbf{w}}{dx} \right\rangle = \left\langle \mathbf{y} \cdot A^T\mathbf{w} \right\rangle + \left\langle \mathbf{y} \cdot C^T\mathbf{K}^{(1)} \right\rangle, \qquad \frac{d\mathbf{w}}{dx} = -A^T\mathbf{w} - C^T\mathbf{K}^{(1)},$$

$$\left\langle \mathbf{z}_2 \cdot \mathbf{K}^{(2)} \right\rangle - \left\langle \mathbf{z}_2 \cdot D^T\mathbf{K}^{(1)} \right\rangle = \left\langle \mathbf{z}_2 \cdot B^T\mathbf{w} \right\rangle, \qquad \mathbf{K}^{(2)} = D^T\mathbf{K}^{(1)} + B^T\mathbf{w}.$$

These equations are valid for arbitrary structure variables $\mathbf{z}_2$ and $\mathbf{y}$, if

$$\frac{d\mathbf{w}}{dx} = -A^T\mathbf{w} - C^T\mathbf{K}^{(1)},$$

$$\mathbf{K}^{(2)} = D^T\mathbf{K}^{(1)} + B^T\mathbf{w}.$$

These two relations together with the boundary conditions for $\mathbf{w}$:

$$\mathbf{w} \cdot \mathbf{y} = 0 \quad \text{at} \quad r = 0 \quad \text{and} \quad r = R$$

determine kernels $\mathbf{K}^{(2)}$ for the 'secondary' structure variable $\mathbf{z}_2$.

Thus, to find the kernels $\mathbf{K}^{(2)}$ one has to solve the differential equations for $\mathbf{w}$ with the boundary conditions, and then use of the second equation.

Compare these adjoint equations with the equations for the structure variables:

$$\frac{d\mathbf{y}}{dx} = A\mathbf{y} + B\mathbf{z}_2$$

$$\mathbf{z}_1 = C\mathbf{y} + D\mathbf{z}_2,$$

Examples of the kernel transformation

Kernels for isothermal sound speed and helium abundance.

As an example, we derive kernels $\mathbf{K}^{(2)}$ for function $\mathbf{z}_2 = (\delta \ln u, \delta Y)$, where $u \equiv p/\rho$, the ratio of the gas pressure to density, which is approximately proportional to the ratio of the temperature to the molecular weight, and Y is the abundance of helium. These 'secondary' properties are related to the 'primary' properties, ρ and γ, through the hydrostatic equations:

$$\frac{dp}{dr} = -\frac{Gm\rho}{r^2}, \quad \frac{dm}{dr} = 4\pi\rho r^2,$$

and the equation of state $\gamma = \gamma(p, \rho, Y)$.

The corresponding linearized equations are:

$$\frac{d}{dx}\left(\frac{\delta p}{p}\right) = -V\left(\frac{\delta m}{m} - \frac{\delta p}{p} + \frac{\delta\rho}{\rho}\right),$$

$$\frac{d}{dx}\left(\frac{\delta m}{m}\right) = U\left(-\frac{\delta m}{m} + \frac{\delta\rho}{\rho}\right), \quad \frac{\delta u}{u} = \frac{\delta p}{p} - \frac{\delta\rho}{\rho},$$

$$\frac{\delta\gamma}{\gamma} = \left(\frac{\partial \ln\gamma}{\partial \ln p}\right)_{\rho,Y}\frac{\delta p}{p} + \left(\frac{\partial \ln\gamma}{\partial \ln\rho}\right)_{p,Y}\frac{\delta\rho}{\rho} + \left(\frac{\partial \ln\gamma}{\partial Y}\right)_{p,\rho}\delta Y,$$

where $x = \ln r$, $V = -\frac{d\ln p}{d\ln r} = \frac{Gm\rho}{rp}$, and $U = \frac{d\ln m}{d\ln r} = \frac{4\pi\rho r^3}{m}$.

Boundary conditions are the regularity conditions at $r = 0$, and $\delta m/m = 0$ at $r = R$.

These equations can be written in the matrix form:

$$\frac{d\mathbf{y}}{dx} = A_1\mathbf{y} + B_1\mathbf{z}_1 + B_2\mathbf{z}_2,$$

$$D_1\mathbf{z}_1 = C_1\mathbf{y} + D_2\mathbf{z}_2,$$

where $\mathbf{y} = (\delta p/p, \delta m/m)$, $\mathbf{z}_1 = (\delta\rho/\rho, \delta\gamma/\gamma)$, $\mathbf{z}_2 = (\delta u/u, \delta Y)$, A_1, B_1, B_2, C_1, D_1 and D_2 are (2×2)-matrices:

$$A_1 = \begin{pmatrix} V & -V \\ 0 & -U \end{pmatrix}, \quad B_1 = \begin{pmatrix} -V & 0 \\ U & 0 \end{pmatrix}, \quad B_2 = \begin{pmatrix} 0 & 0 \\ 0 & 0 \end{pmatrix},$$

$$D_1 = \begin{pmatrix} 1 & 0 \\ -\left(\frac{\partial \ln\gamma}{\partial \ln\rho}\right)_{p,Y} & 1 \end{pmatrix}, \quad C_1 = \begin{pmatrix} 1 & 0 \\ \left(\frac{\partial \ln\gamma}{\partial \ln p}\right)_{\rho,Y} & 0 \end{pmatrix},$$

$$D_2 = \begin{pmatrix} -1 & 0 \\ 0 & \left(\frac{\partial \ln\gamma}{\partial Y}\right)_{p,\rho} \end{pmatrix}.$$

Since $\det(D_1) \neq 0$ we can reduce the equations to the standard form:

$$\frac{d\mathbf{y}}{dx} = A\mathbf{y} + B\mathbf{z}_2,$$

$$\mathbf{z}_1 = C\mathbf{y} + D\mathbf{z}_2,$$

where

$$A = A_1 + B_1 D_1^{-1} C_1, \quad B = B_1 D_1^{-1} D_2 + B_2,$$
$$C = D_1^{-1} C_1, \quad D = D_1^{-1} D_2.$$

Thus, the kernel functions $\mathbf{K}^{(2)} = \left(K^{(u,Y)}, K^{(Y,u)}\right)$ can be found by solving the corresponding equations with the matrices, A, B, C and D:

$$\frac{d\mathbf{w}}{dx} = -A^T\mathbf{w} - C^T\mathbf{K}^{(1)},$$

$$\mathbf{K}^{(2)} = D^T\mathbf{K}^{(1)} + B^T\mathbf{w}.$$

Examples of the sensitivity kernels for $u=p/\rho$ and Y

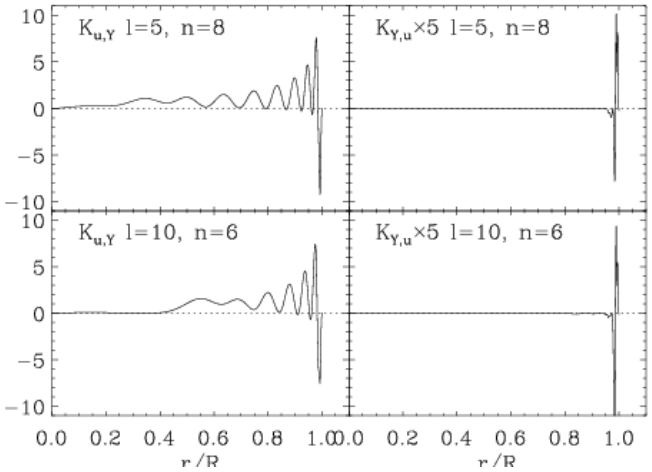

Kernels for the parameter of convective stability.

The parameter of convective stability $A^* = \frac{1}{\gamma}\frac{d\log p}{d\log r} - \frac{d\log \rho}{d\log r}$ plays an important role for the internal structure of the Sun. When this parameter is positive the solar structure is stable against convection, and when it is negative the structure is unstable. In the bulk of the convection zone A^* is negative and close to zero, in the upper convection zone this parameter experiences a sharp minimum near the surface where highly unstable convective motions (granulation) are developed.

In this case, we add to the previous hydrostatic solar structure equations the linearized equation for A^*:

$$\frac{d}{dx}\left(\frac{\delta\rho}{\rho}\right) = V_g\left(\frac{\delta p}{p} - \frac{\delta m}{m} - \frac{\delta\rho}{\rho} + \frac{\delta\gamma}{\gamma}\right) - \delta A^*,$$

where $V_g = V/\gamma$. Defining $\mathbf{y} = (\delta p/p, \delta m/m, \delta\rho/\rho)$, $\mathbf{z}_1 = (\delta\rho/\rho, \delta\gamma/\gamma)$, $\mathbf{z}_2 = (\delta A^*, \delta\gamma/\gamma)$, we obtain the adjoint equations the kernel function $\mathbf{K}^{(2)} = \left(K^{(A^*,\gamma)}, K^{(\gamma,A^*)}\right)$ in the standard form with the following matrices:

$$A = \begin{pmatrix} V & -V & -V \\ 0 & -U & -U \\ V_g & -V_g & -V_g \end{pmatrix}, \quad B = \begin{pmatrix} 0 & 0 \\ 0 & 0 \\ -1 & V_g \end{pmatrix}, \quad C = \begin{pmatrix} 0 & 0 & 1 \\ 0 & 0 & 0 \end{pmatrix}, \quad D = \begin{pmatrix} 0 & 0 \\ 0 & 1 \end{pmatrix}.$$

Examples of the sensitivity kernels for parameter of convective stability A^* and γ

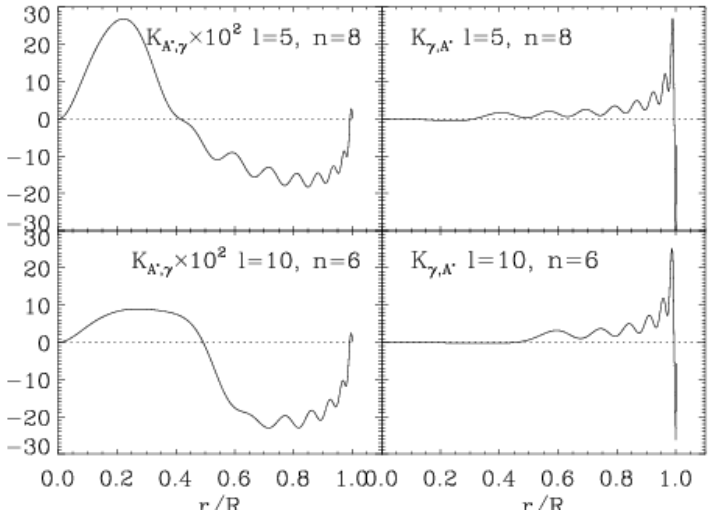

Similar transformations of integral kernels can be derived for other appropriate pairs of unknown functions of solar structure.

It is important to note that the integral kernels for temperature and element abundances in the solar radiative core, which are important in astrophysical applications (e.g. the solar neutrino problem), can be determined by including the equations of thermal equilibrium in addition to the hydrostatic equations.

Equations of the stellar structure

$$\frac{dm}{dr} = 4\pi\rho r^2 \quad (1)$$

$$\frac{dP}{dr} = -\frac{Gm\rho}{r^2} \quad (2)$$

$$\frac{dL}{dr} = 4\pi\rho r^2 \varepsilon \quad (3)$$

$$\frac{dT}{dr} = -\frac{\kappa\rho}{16\pi r^2 acT^3} L \equiv -F \quad (4)$$

$$P = \frac{\Re\rho T}{\mu} \quad (5)$$

$$\mu = \frac{1}{2X + \frac{3}{4}Y + \frac{1}{2}Z} \quad (6)$$

$$\varepsilon = \varepsilon_0 X^2 \rho T^4 \quad (7)$$

$$\kappa = \kappa_0 (X+1) Z \rho T^{-3.5} \quad (8)$$

Kramer's opacity law

These equations describe the structure of stellar radiative zones. In the convection zone Eq.(4) is replaced by an equation of convective energy transport, e.g. mixing length theory.

A numerical code for solving these equations is available in the book: C.J. Hansen, S.D. Kawaler, *Stellar Interiors. Physical Principles, Structure and Evolution,* Springer, 1995.

Examples of the sensitivity kernels

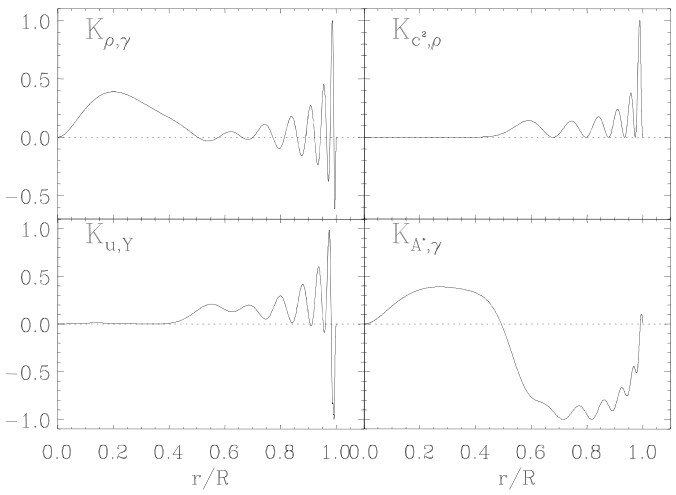

Lecture 18
Solution of the helioseismic inverse problem. Optimally localized averaging method.

(Stix, Chapter 5.3.1; Kosovichev, p.34-41, 44-48; Christensen-Dalsgaard, Chapters 5.5)

General helioseismic inverse problem

1) Variational principle
2) Perturbation theory
3) Kernel transformation
4) Solution of inverse problem
   A. Optimally Localized Averages Method
   B. Regularized Least-Squares Method
5) Inversion results for the solar structure
6) Inversions for solar rotation

Variational Principle: Rayleigh's Quotient

Consider the oscillation equations as a formal operator equation in terms of the vector displacement, $\vec{\xi}$:

$$\omega^2\vec{\xi} = L(\vec{\xi}),$$

where L in the general case is an integro-differential operator. If we multiply this by $\vec{\xi}^*$ and integrate over the mass of the Sun we get:

$$\omega^2\int_V \rho\vec{\xi}^*\cdot\vec{\xi}dV = \int_V \vec{\xi}^*\cdot L\vec{\xi}\rho dV,$$

where ρ_0 is the model density, V is the solar volume.
Then, the oscillation frequencies are:

$$\omega^2 = \frac{\int_V \vec{\xi}^*\cdot L\vec{\xi}\rho dV}{\int_V \rho\vec{\xi}^*\cdot\vec{\xi}dV}.$$

The frequencies are expressed in terms of **eigenfunctions** $\vec{\xi}$ and the solar properties represented by coefficients of operator L.

Sometimes, this equation is called **Rayleigh's Quotient** (the original formulation: for an oscillatory system the averaged over period kinetic energy is equal the averaged potential energy).

Variational Principle

For small perturbations of the solar parameters the frequency change will depend on these perturbations and the corresponding perturbations of the eigenfunctions, e.g.

$$\delta\omega^2 = \Psi[\delta\rho, \delta\gamma, \delta\vec{\xi}].$$

The variational principle states that the perturbation of the eigenfunctions $\delta\vec{\xi}$ constitutes second-order corrections, that are in the first-order approximation:

$$\delta\omega^2 \approx \Psi[\delta\rho, \delta\gamma].$$

This allows us to neglect the perturbation of the eigenfunctions in the first-order perturbation theory.

Perturbation theory

We consider a small perturbation of the operator L caused by variations of the solar structure properties:

$$L(\vec{\xi}) = L_0(\vec{\xi}) + L_1(\vec{\xi}).$$

Then, the corresponding frequency perturbations are determined from the following equation:

$$\left(\omega_0 + \delta\omega\right)^2 = \frac{\int_V \vec{\xi}^* \cdot (L_0\vec{\xi} + L_1\vec{\xi})\rho dV}{\int_V \rho\vec{\xi}^* \cdot \vec{\xi} dV},$$

or

$$\frac{\delta\omega}{\omega} = \frac{1}{2\omega_0 I}\int_V \vec{\xi}^* \cdot L_1\vec{\xi}\rho dV,$$

where

$$I = \int_V \rho\vec{\xi}^* \cdot \vec{\xi} dV$$

is so-called *mode inertia* or *mode mass*.

The *mode energy* is $E = I\omega_0^2 a^2$, where a is the amplitude of the surface displacement. The mode eigenfunctions are usually normalized such that $\xi_r(R) = 1$.

Sensitivity kernels

Using explicit formulations for operator L_1 the variational principle can be reduced to a system of integral equations for a chosen pair of independent variables, e.g. for (ρ, γ)

$$\frac{\delta\omega^{(n,l)}}{\omega^{(n,l)}} = \int_0^R K_{\rho,\gamma}^{(n,l)} \frac{\delta\rho}{\rho} dr + \int_0^R K_{\gamma,\rho}^{(n,l)} \frac{\delta\gamma}{\gamma} dr,$$

where $K_{\rho,\gamma}^{(n,l)}(r)$ and $K_{\gamma,\rho}^{(n,l)}(r)$ are sensitivity (or 'seismic') kernels. These are calculated using the initial solar model parameters, ρ_0, P_0, γ, and the oscillation eigenfunctions for these model, $\vec{\xi}$.

Operator form of the linearized stellar structure equations

The sensitivity for various pairs of solar parameters can be obtained by using the relations among these parameters, which follows from the equations of solar structure ('stellar evolution theory').

A general procedure for calculating the sensitivity kernels can be illustrated in an operator form. Consider two pairs of solar variables, $\vec{X}$ and $\vec{Y}$, e.g.

$$\vec{z}_1 = \left(\frac{\delta\rho}{\rho}, \frac{\delta\gamma}{\gamma} \right); \; \vec{z}_2 = \left(\frac{\delta u}{u}, \frac{\delta Y}{Y} \right),$$

where $u = P/\rho$, Y is the helium abundance.

The linearized structure equations (the hydrostatic equilibrium equation and the equation of state) that relate these variables can be written symbolically:

$$A\vec{z}_1 = \vec{z}_2 .$$

Equation for the sensitivity kernels in the operator form

If we define:

$$\vec{z}_1 = \left(\frac{\delta\rho}{\rho}, \frac{\delta\gamma}{\gamma} \right)$$

$$\vec{K}_i^{(1)} = \left(K_i^{(\rho,\gamma)}, K_i^{(\gamma,\rho)} \right)$$

then the perturbation equation can be written in the form:

$$\frac{\delta\omega_i^2}{\omega_i^2} = \left\langle \vec{K}_i^{(1)} \cdot \vec{z}_1 \right\rangle,$$

where operator $\left\langle \vec{u} \cdot \vec{v} \right\rangle = \int_0^R \vec{u} \cdot \vec{v} \, dr$.

Kernel Transformations. Method of Adjoint Functions.

The idea of this method is very simple. The relation between the 'primary', z_1, and 'secondary', z_2, properties that follows from the linearized stellar structure equations can be written in the following symbolic form:

$$Az_1 = z_2, \qquad (1)$$

where A is a linear operator. If $K^{(2)}$ is the integral kernel for z_2 then the relative frequency differences can be expressed in terms of both z_1 and z_2:

$$\delta\omega^2 / \omega^2 = \left\langle K^{(1)} \cdot z_1 \right\rangle = \left\langle K^{(2)} \cdot z_2 \right\rangle.$$

Then using the structure equation (1) and operator A^* adjoint to A we obtain:

$$\left\langle K^{(1)} \cdot z_1 \right\rangle = \left\langle K^{(2)} \cdot z_2 \right\rangle = \left\langle K_2 \cdot Az_1 \right\rangle = \left\langle A^* K^{(2)} \cdot z_1 \right\rangle.$$

Comparing the first and last terms we obtain the equation for the 'secondary' kernels, $K^{(2)}$:

$$A^* K^{(2)} = K^{(1)},$$

which is adjoint to the structure equation (1). This means that the equation for the sensitivity kernels is adjoint to the stellar structure equations.

Examples of the sensitivity kernels

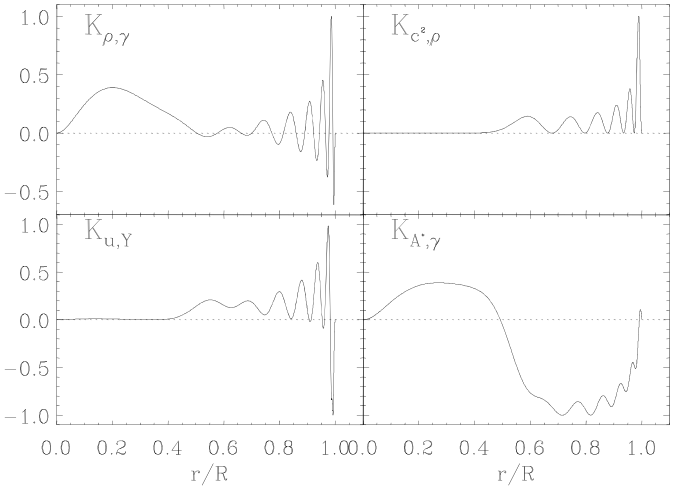

Inversion methods

The variational principle and the method of adjoint functions allow us to determine linear integral relations between the observed quantities, relative frequency differences between the Sun and a reference solar model, and the deviations of solar properties, $f(r)$ and $g(r)$, (such as density, pressure, sound speed, γ, etc.)from this model.

$$\frac{\delta\omega_i^2}{\omega_i^2} = \int_0^R K_i^{(f,g)} \frac{\delta f}{f} dr + \int_0^R K_i^{(g,f)} \frac{\delta g}{g} dr,$$

These relations constitute a linear inverse problem of determining the solar structure.

Mathematically, it belongs to the class of ill-posed problems because it does not have a unique solution. Rapidly oscillating with radius functions can be added to the solution without changing the integral values.

This problem can be solved by regularization methods, such as the method of optimally localized averages or the regularized least-squares method. A specific feature of this inverse problem is that it contains two unknown functions.

Idea of Optimally Localized Averages (OLA)

The idea of the OLA method is to find a linear combination of data such as the corresponding linear combination of the sensitivity kernels for one unknown will have an isolated peak at a given radial point, r_0, (resemble a δ-function), and the combination for the other unknown will be close to zero. Then this linear combination provides an estimate for the first unknown at r_0.

$$\sum a^{(n,l)} \frac{\delta\omega^{(n,l)}}{\omega^{(n,l)}} = \int_0^R \sum a^{(n,l)} K_{\rho,\gamma}^{(n,l)} \frac{\delta\rho}{\rho} dr + \int_0^R \sum a^{(n,l)} K_{\gamma,\rho}^{(n,l)} \frac{\delta\gamma}{\gamma} dr.$$

If the coefficients are such that $\sum a^{(n,l)} K_{\rho,\gamma}^{(n,l)}(r) \sim \delta(r - r_0),$

and $\sum a^{(n,l)} K_{\gamma,\rho}^{(n,l)}(r) \sim 0,$

then the linear combination gives an estimate of the density perturbation at $r = r_0$:

$$\overline{\left(\frac{\delta\rho}{\rho}\right)}_{r_0} = \sum a^{(n,l)} \frac{\delta\omega^{(n,l)}}{\omega^{(n,l)}},$$

The coefficients, $a^{(n,l)}$, are different for different target radii r_0.

Method of optimally localized averages

From a finite number of measured frequencies with errors, the unknown functions can be determined only with a finite spatial resolution; in other words, only certain average values of these functions can be determined.

The idea of the Backus-Gilbert inversion method is to determine the optimally localized averages of the solar parameters at a target location along the radius.

If $f(r)$ and $g(r)$ are two independent properties of the solar structure, which are related to the variations of eigenfrequencies via the integral relations:

$$\frac{\delta\omega_i^2}{\omega_i^2} = \int_0^R K_i^{(f,g)} \frac{\delta f}{f} dr + \int_0^R K_i^{(g,f)} \frac{\delta g}{g} dr,$$

where $K_i^{(f,g)}$ and $K_i^{(g,f)}$ are the corresponding seismic kernels, then the localized averages of the variations of these properties at $r = r_0$ are estimated as linear combinations of the frequency variations:

$$\left(\frac{\overline{\delta f}}{f}\right)_{r_0} \approx \sum_{i=1}^{N} a_i^{(f,g)}(r_0) \frac{\delta\omega_i^2}{\omega_i^2},$$

$$\left(\frac{\overline{\delta g}}{g}\right)_{r_0} \approx \sum_{i=1}^{N} a_i^{(g,f)}(r_0) \frac{\delta\omega_i^2}{\omega_i^2},$$

where $a_i^{(f,g)}(r_0)$ and $a_i^{(g,f)}(r_0)$ are the averaging coefficients.

The localization of the averaged properties around the target positions $r = r_0$ can be expressed in terms of the averaging kernels: $A^{(f,g)}(r_0, r)$ and $A^{(g,f)}(r_0, r)$:

$$\left(\frac{\overline{\delta f}}{f}\right)_{r_0} = \int_0^R A^{(f,g)}(r_0, r) \frac{\delta f}{f} dr$$

$$\left(\frac{\overline{\delta g}}{g}\right)_{r_0} = \int_0^R A^{(g,f)}(r_0, r) \frac{\delta g}{g} dr$$

The averaging kernels are represented by the corresponding linear combinations of the sensitivity kernels:

$$A^{(f,g)}(r_0, r) = \sum_{i=1}^{N} a_i^{(f,g)}(r_0) K_i^{(f,g)}(r),$$

$$A^{(g,f)}(r_0, r) = \sum_{i=1}^{N} a_i^{(g,f)}(r_0) K_i^{(g,f)}(r).$$

By applying the averaging procedure to the equation:

$$\frac{\delta\omega_i^2}{\omega_i^2} = \int_0^R K_i^{(f,g)} \frac{\delta f}{f} dr + \int_0^R K_i^{(g,f)} \frac{\delta g}{g} dr,$$

and changing the order of summation and integration, we find that the linear combination of the frequency perturbations depends on both structural properties, f and g:

$$\sum_{i=1}^{N} a_i^{(f,g)}(r_0) \frac{\delta\omega_i^2}{\omega_i^2} = \int_0^R \sum_{i=1}^{N} a_i^{(f,g)}(r_0) K_i^{(f,g)} \frac{\delta f}{f} dr + \int_0^R \sum_{i=1}^{N} a_i^{(f,g)}(r_0) K_i^{(g,f)} \frac{\delta g}{g} dr$$

$$\sum_{i=1}^{N} a_i^{(f,g)}(r_0) \frac{\delta\omega_i^2}{\omega_i^2} = \int_0^R A^{(f,g)}(r_0, r) \frac{\delta f}{f} dr + \int_0^R B^{(f,g)}(r_0, r) \frac{\delta g}{g} dr$$

$$\sum_{i=1}^{N} a_i^{(f,g)}(r_0) \frac{\delta\omega_i^2}{\omega_i^2} = \left(\overline{\frac{\delta f}{f}} \right)_{r_0} + \int_0^R B^{(f,g)}(r_0, r) \frac{\delta g}{g} dr$$

where kernel $B^{(f,g)}(r_0, r) = \sum_{i=1}^{N} a_i^{(f,g)}(r_0) K_i^{(g,f)}(r)$ defines the contribution of the property g in the localized average estimates of f.

Our goal is to find such coefficients $a_i^{(f,g)}(r_0)$ that they provide localization of the averaging kernel $A^{(f,g)}(r_0, r)$ around $r = r_0$ while minimizing the kernel $B^{(f,g)}(r_0, r)$ everywhere along the radius.

Such coefficients are obtained by making the averaging kernel close to a delta-function by applying a 'δ-ness constraint' for the averaging kernels for one of the variables while minimizing the contribution of the other variable.

Thus, for estimating $\delta f / f$, the δ-ness criterion for $A^{(f,g)}(r_0, r)$ is complemented by the minimization of the averaging function of the other variable, $\delta g / g$:

$$B^{(f,g)}(r_0, r) = \sum_{i=1}^{N} a_i^{(f,g)}(r_0) K_i^{(g,f)}(r).$$

Formulation of the δ-ness measure by Backus and Gilbert

There are different measures of δ-ness of the averaging kernels. Following the Optimally Localized Averaging (OLA) method of Backus and Gilbert (1970) we consider the 'spread' of function $A(r)$ around a target point r_0:

$$s(r_0, A) = 12\int_0^R (r - r_0)^2 A(r)^2 dr$$

The averaging are normalized, like a δ-function, to unity:

$$\int_0^R A(r)dr = 1$$

The motivation is that if $A(r)$ is a step-like function with a width l:

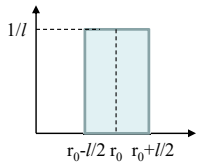

$$A(r) = \begin{cases} l^{-1} & \text{if } |r - r_0| \le l/2 \\ 0 & \text{otherwise} \end{cases}$$

For this function: $s(r_0, A) = 12l^{-2}\int_{r_0 - l/2}^{r_0 + l/2} (r - r_0)^2 dr = l$.

Thus the 'spread' of this function is equal to the function width, and the center of this function coincides with the target position r_0.

For any fixed A, $s(r_0, A) = 12\int_0^R (r - r_0)^2 A(r)^2 dr$ is a quadratic function of r_0 with a minimum at r_c, which we find by differentiating $s(r_0, A)$ with respect to r_0 and finding the minimum:

$$\frac{ds(r_0, A)}{dr_0} = 24\int_0^R (r - r_0) A^2(r) dr = 0\big|_{r = r_c}$$

thus

$$r_c = \int_0^R rA^2(r)dr \Big/ \int_0^R A^2(r)dr$$

is the 'center' of the function $A(r)$.

We define the 'width' of A as the value of the spread at the center: $w = s(r_c, A)$.

$$w = 12\int_0^R (r - r_c)^2 A^2 dr$$

The function spread at the target position r_0 can be calculated in terms of w and r_c by adding and subtracting r_c in the definition of $s(r_0, A)$ and opening the rearranging the terms:

$$s(r_0, A) = 12\int_0^R (r - r_0)^2 A^2 dr = \int_0^R (r - r_c + r_c - r_0)^2 A^2 dr =$$

$$= w + 12(r_c - r_0)^2 \int_0^R A^2 dr$$

Thus, the spread calculated at the target point measures both the function width and the deviation of the center from the target.

The OLA method

A set of such optimal coefficients $a_i^{(f,g)}$ can be determined by minimizing the following quadratic function:

$$M(r_0, A, \alpha, \beta) = \int_0^R J(r_0, r)\left[A^{(f,g)}(r_0, r)\right]^2 dr + \beta \int_0^R \left[B^{(f,g)}(r_0, r)\right]^2 dr + \alpha \sum_{i,j} E_{ij} a_i^{(f,g)} a_j^{(f,g)},$$

where $J(r_0, r) = 12(r - r_0)^2$, E_{ij} is a covariance matrix of observational errors, α and β are the regularization parameters.

The first integral represents the Backus-Gilbert criterion of δ-ness for $A^{(f,g)}(r_0, r)$; the second term minimizes the contribution of $B^{(f,g)}(r_0, r)$, thus, effectively eliminating the second unknown function, $\delta g / g$; and the last term minimizes the errors.

The numerical procedure to compute $a_i^{(f,g)}(r_0)$ for given α and β is to substitute the equations for $A^{(f,g)}(r_0, r)$ and $B^{(f,g)}(r_0, r)$ and minimize M as a positively defined quadratic function of $a_i^{(f,g)}$ subject to the normalization constraint (corresponding to the δ-ness of $A^{(f,g)}(r_0, r)$):

$$\int_0^R A^{(f,g)}(r_0, r) dr \equiv \sum_{i=1}^N a_i^{(f,g)}(r_0) \int_0^R K^{(f,g)}(r_0, r) dr = 1.$$

The minimization of the constrained quadratic function by the method of Lagrange multipliers leads to a system of linear equations:

$$\sum_{j=1,N} W_{ij} a_j^{(f,g)} + \lambda v_i = 0, \quad \sum_{j=1,N} v_j a_j^{(f,g)} = 1$$

where λ is a Lagrange multiplier, $v_i = \int_0^R K_i^{(f,g)}(r) dr$

$$W_{ij} = S_{ij}^{(f,g)} + \beta S_{ij}^{(g,f)} + \alpha E_{ij},$$

$$S_{ij}^{(f,g)} = r_0^2 S_{0,ij}^{(f,g)} - 2 r_0 S_{1,ij}^{(f,g)} + S_{2,ij}^{(f,g)}, \quad S_{ij}^{(g,f)} = 12 \int_0^R K_i^{(g,f)}(r) K_j^{(g,f)}(r) dr$$

$$S_{p,ij}^{(f,g)} = 12 \int_0^R r^p K_i^{(f,g)}(r) K_j^{(f,g)}(r) dr,$$

These equations can be written in the matrix form:

$$W\mathbf{a} + \lambda \mathbf{v} = 0$$
$$\mathbf{v} \cdot \mathbf{a} = 1,$$

where $\mathbf{a} = \left(a_1^{(f,g)}, ..., a_N^{(f,g)}\right)$, $\mathbf{v} = (v_1, ..., v_N)$, and λ is a Lagrange multiplier.

Substituting $\mathbf{a} = -\lambda W^{-1}\mathbf{v} \equiv -\lambda \mathbf{y}$, where $\mathbf{y} = W^{-1}\mathbf{v}$, in the second equation, we obtain: $\lambda = -\dfrac{1}{\mathbf{y} \cdot \mathbf{v}}$.

Then, substituting the value of λ in the first equation, we find the coefficients $\mathbf{a}$:

$$\mathbf{a} = \frac{\mathbf{y}}{(\mathbf{y} \cdot W\mathbf{y})}$$

Using these coefficients, we estimate the localized averages of $\delta f / f$:

$$\left(\frac{\overline{\delta f}}{f}\right)_{r_0} = \sum_{i=1}^{N} a_i^{(f,g)}(r_0)\frac{\delta \omega_i^2}{\omega_i^2} = \int_0^R A^{(f,g)}(r_0, r)\frac{\delta f}{f}dr + \left(\frac{\overline{\delta g}}{g}\right),$$

where $\left(\dfrac{\overline{\delta g}}{g}\right) = \int_0^R B^{(f,g)}(r_0, r)\dfrac{\delta g}{g}dr$ is the contribution of the second, 'eliminated', variable. This contribution causes errors in the estimated localized averages of the first function, and, therefore, has to be made sufficiently small, e.g.

$$\left(\frac{\overline{\delta g}}{g}\right)_{max} \le \epsilon$$

where $\epsilon = \left(\sum_{i,j} a_i^{(f,g)} a_j^{(f,g)} E_{ij}\right)^{1/2}$ is an estimate of random errors in the inversion results. If we assume that $|\delta g / g| < C$, then we obtain the following criterion for choosing the regularization parameter β:

$$\int_0^R B^{(f,g)}(r_0, r)dr \le C^{-1}\epsilon.$$

The regularization parameter α is determined as a trade-off between the spatial resolution and error magnification.

The resolution of inversions is characterized by the spread of the averaging kernels

$$s_0 = \sum_{i,j} a_i^{(f,g)} a_j^{(f,g)} S_{ij}^{(f,g)}$$

and their width

$$w = \sum_{i,j} a_i^{(f,g)} a_j^{(f,g)} S_{2,ij}^{(f,g)} - \frac{\left[\sum_{i,j} a_i^{(f,g)} a_j^{(f,g)} S_{1,ij}^{(f,g)}\right]^2}{\sum_{i,j} a_i^{(f,g)} a_j^{(f,g)} S_{0,ij}^{(f,g)}}.$$

The central location of the averaging kernels can be estimated from

$$r_c(r_0) = \frac{\sum_{i,j} a_i^{(f,g)}(r_0) a_j^{(f,g)}(r_0) S_{1,ij}^{(f,g)}}{\sum_{i,j} a_i^{(f,g)}(r_0) a_j^{(f,g)}(r_0) S_{0,ij}^{(f,g)}}.$$

L-curve method for choosing the regularization parameter

Regularization parameter α is chosen from the trade-off between the resolution and error magnification: smaller α leads to higher resolution but larger errors.

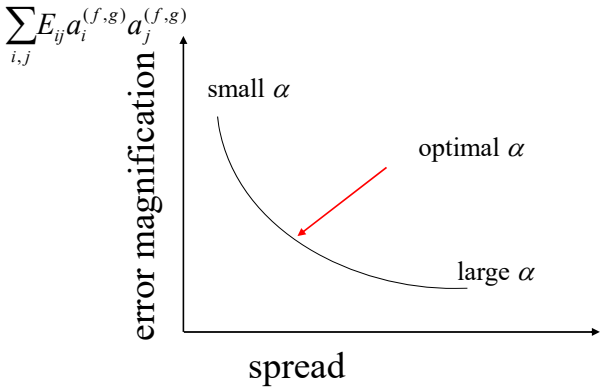

$$M(r_0, A, \alpha, \beta) = \int_0^R (r - r_0)^2 \left[A^{(f,g)}(r_0, r)\right]^2 dr + \beta \int_0^R \left[B^{(f,g)}(r_0, r)\right]^2 dr + \alpha \sum_{i,j} E_{ij} a_i^{(f,g)} a_j^{(f,g)},$$

spread — error magnification

Nonadiabatic (surface) effects

Nonadiabatic effects near the solar surface cause systematic frequency shifts which may affect the inversion results. If the observed frequencies are

$$\omega_{obs,i} = \omega_{ad,i} + \delta\omega_{nonad,i},$$

then the localized averages of $\delta f / f$ are

$$\left(\frac{\overline{\delta f}}{f}\right)_{obs} = \left(\frac{\overline{\delta f}}{f}\right)_{ad} + \sum_{i=1}^{N} a_i^{(f,g)} \frac{\delta\omega_{nonad,i}^2}{\omega_i^2},$$

where $\omega_i \equiv \omega_{ad,i}$.

Therefore, the nonadiabatic effects cause systematic errors in the localized averages estimated by using the adiabatic variational principle. In the Sun, most non-adiabatic effects occur near the solar surface. In this case, the non-adiabatic frequency shift can be approximated by a smooth function of frequency, $F(\omega)$ scaled with the factor, $Q \equiv I(\omega)/I_0(\omega)$, where $I(\omega)$ is the mode inertia, and $I_0(\omega)$ is the mode inertia of radial modes ($l = 0$), calculated at frequency ω, that is:

$$\frac{\delta\omega_{nonad,i}^2}{\omega_i^2} = F(\omega_i)/Q(\omega_i).$$

Function $F(\omega)$ can be approximated by a polynomial function of degree K:

$$F(\omega_i) = \sum_{k=0}^{K} c_k \omega_i^k,$$

then the influence of the nonadiabatic effects can be reduced by applying $K+1$ additional constraints for a_i:

$$\sum_{i=1}^{N} a_i \omega_i^k Q(\omega_i) = 0, \quad k = 0, ..., K.$$

The function $F(\omega)$ can be also represented in terms of Legendre polynomials:

$$F(\omega) = \sum_k c_k P_k\left(\frac{2\omega - \omega_{max} - \omega_{min}}{\omega_{max} - \omega_{min}}\right),$$

where ω_{min} and ω_{max} are the boundaries of the observed frequency range.

These equations are considered as additional constraints in the minimization procedure of $M(r_0, A, \alpha, \beta)$. If we represent these $K+1$ constraints together with the constraint previously derived from the kernel normalization equation ($\int_0^R A dr = 1$) in the matrix form: $B\mathbf{a} = \mathbf{c}$,

then the minimization procedure leads to the equation:

$$W\mathbf{a} + \boldsymbol{\lambda} B = 0,$$

where $\boldsymbol{\lambda} = (\lambda_1, ..., \lambda_{K+2})$ are Lagrange multipliers.

Solving these equations we obtain the coefficients of the optimally localized averages:

$$\mathbf{a} = \left(W^{-1}B^T\right)\left(BW^{-1}B^T\right)^{-1}\mathbf{c},$$

where B^T is a matrix transposed to B.

The SOLA (Subtracting Optimally Localized Averages) method

The OLA methods at each target location r_0 involves inversion of (N+1)x(N+1) matrices, where N is the number of observed frequencies, which can be very large. A modification of this method with a different δ-ness criterion leads to a less computationally expensive procedure, where the matrices do not depend on the target location. In this method, we minimize the squred difference between the averaging kernel and a target δ-like function, e.g. a localized Gaussian.

A set of such optimal coefficients $a_i^{(f,g)}$ can be determined by minimizing the following quadratic function:

$$M(r_0, A, \alpha, \beta) = \int_0^R \left[A^{(f,g)}(r_0, r) - T(r_0, r)\right]^2 dr + \beta \int_0^R \left[B^{(f,g)}(r_0, r)\right]^2 dr + \alpha \sum_{i,j} E_{ij} a_i^{(f,g)} a_j^{(f,g)},$$

where $T(r_0, r) = \frac{1}{\Delta}\exp[-(r - r_0)^2 / \Delta^2]$ is the target δ-like function, E_{ij} is a covariance matrix of observational errors, α and β are the regularization parameters.

The first integral minimizes the deviation of the averaging kernel from the target function; the second term minimizes the contribution of $B^{(f,g)}(r_0, r)$, thus, effectively eliminating the second unknown function, $\delta g / g$; and the last term minimizes the errors.

Regularized Least-Squares Techniques

The Regularized Least-Squares (RLS) method is based on minimization of the quantity

$$E \equiv \sum_i \frac{1}{\sigma_i^2}\left[\frac{\delta\omega_i^2}{\omega_i^2} - \int_0^R \left(K_i^{(f,g)}\frac{\delta f}{f} + K_i^{(g,f)}\frac{\delta g}{g}\right) dr - \frac{F(\omega_i)}{Q}\right]^2 +$$

$$+\int_0^R \left[\alpha_1\left(L_1\frac{\delta f}{f}\right)^2 + \alpha_2\left(L_2\frac{\delta g}{g}\right)^2\right] dr,$$

in which the unknown structure correction functions, $\frac{\delta f}{f}$ and $\frac{\delta g}{g}$, are both represented by piece-wise linear functions or by cubic splines, and the coefficients in these expansions are determined together with coefficients c_k in the presentation of the surface effects F.

The second integral specifies smoothness constraints for the unknown functions, in which L_1 and L_2 are linear differential operators, e.g. $L_{1,2} = \frac{d^2}{d^2 r}$; σ_i are error estimates of the relative frequency differences.

In this inversion method, the estimates of the structure corrections are, once again, linear combinations of the frequency differences obtained from observations, and corresponding averaging kernels exist too.

However, unlike the OLA kernels $A(r_0;r)$, the RLS averaging kernels may have negative sidelobes and significant peaks near the surface, thus making interpretation of the inversion results to some extent ambiguous.

If the variations of the structural properties are represented in a parametric form then the unknown parameters can be evaluated from the helioseismic equations by using a least-squares technique. This approach was applied this parametric inversion technique for determining the depth of the convection zone and the helium abundance.

Finally, 'super-resolution' techniques can be developed by applying, for instance, nonlinear constraints in order to study some particular features of the interior structure, like overshooting and other sharp variations of the interior properties. In addition to the inversions, model calibrations are used to estimate the parameters of the solar structure.

Results

As an example, I present the results of inversion of the recent data obtained from the SOI-MDI instrument onboard the SOHO space observatory. The data represent 2176 frequencies of solar oscillations of the angular degree, l, from 0 to 250. These frequencies were obtained by fitting peaks in the oscillation power spectra from a 360-day observing run, between May 1, 1996 and April 25, 1997.

Two different methods have been used to estimate the frequencies of the solar normal modes from the oscillation power spectra. In the first so-called "mean-multiplet" method, the power spectral peaks are assumed to have a symmetric Lorentzian shape, and a maximum likelihood method is employed to determine the parameters of Lorentzian profiles.

The peaks are fit simultaneously in all of the $2l+1$ individual power spectra for each rotationally split multiplet so that the effects of overlapping peaks can be included in the fits. These $2l+1$ frequencies are effectively averaged to yield a single mean frequency, ω_{nl}, for that multiplet. The second frequency estimation technique employs the m-averaged power spectra rather than the $2l+1$ individual power spectra.

The reference solar model

The reference standard solar model chosen for this inversion used the OPAL equation of state and opacity tables. Nuclear reaction parameters were obtained from the work of Bahcall (1992). Helium and heavy-element gravitational settling was included, using the Michaud and Proffitt coefficients. The present value of the ratio of the heavy element abundance to the hydrogen abundance on the solar surface is 0.0245, while the age of the present Sun was assumed to be 4.6 Gyr.

The relative frequency difference between the Sun and the model

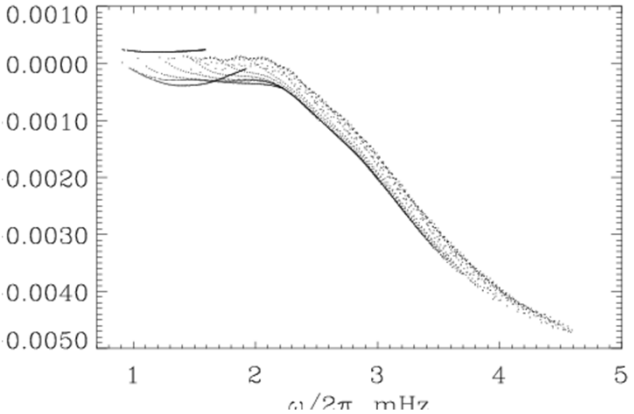

The figure shows the relative frequency difference scaled with the factor Q , which varies between 0.28 and 1. This difference depends mainly on frequency alone meaning that most of the difference between the Sun and the reference solar model is in the near-surface layers. However, there is also a significant scatter along with the general frequency trend. This spread is due to the variations of the structure in the deep interior, and it is the primary task of the inversion methods to uncover the variations.

Optimally localized averaging kernels

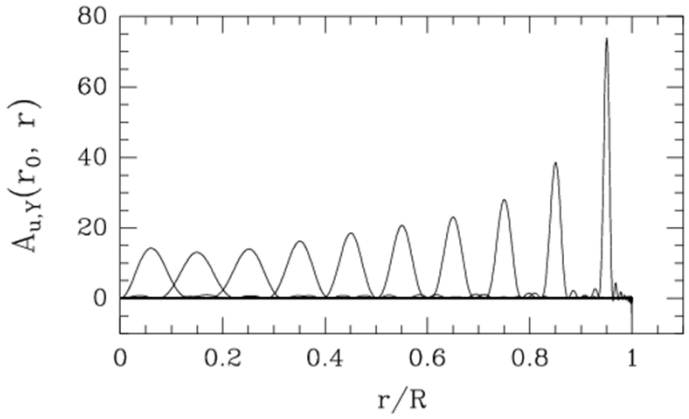

A sample of the optimally localized averaging kernels for the structure function, $u = P / \rho$, the ratio of pressure, p , to density, ρ .

Test inversion

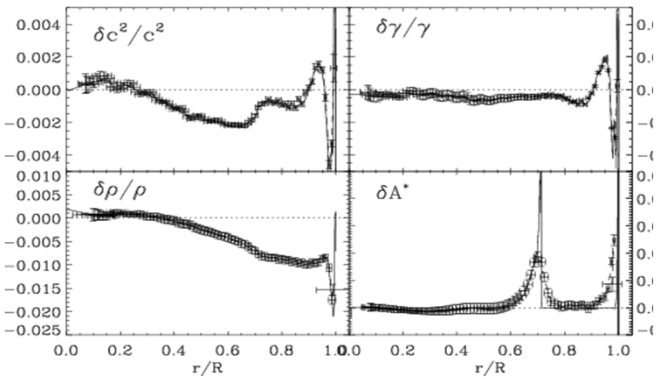

The results of test inversions (points with the error bars, connected with dashed curves) of frequency differences between two solar models for the squared sound speed, c^2, the adiabatic exponent, γ, the density, ρ, and the parameter of convective stability, A^*. The solid curves show the actual differences between the two models. Random Gaussian noise was added to the frequencies of a test solar model. The vertical bars show the formal error estimates, the horizontal bars show the characteristic width of the localized averaging kernels. The central points of the averages are plotted at the centers of gravity of the averaging kernels.

Inversion of the solar data

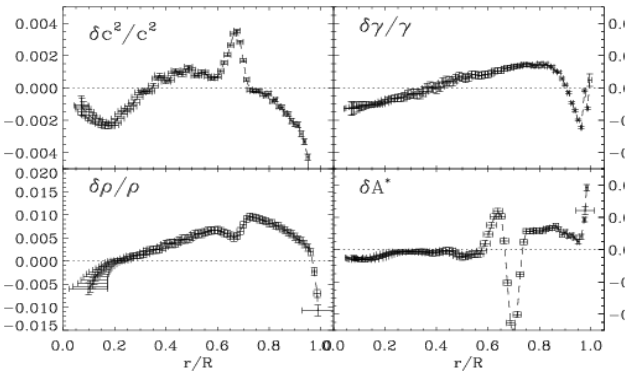

The relative differences between the Sun and the standard solar model in the squared sound speed, c^2, the adiabatic exponent, γ, the density, ρ, and the parameter of convective stability, A^*, inferred from the solar frequencies determined from the 360-day series of SOHO MDI data.

Interpretation of the inversion results: 3D modeling

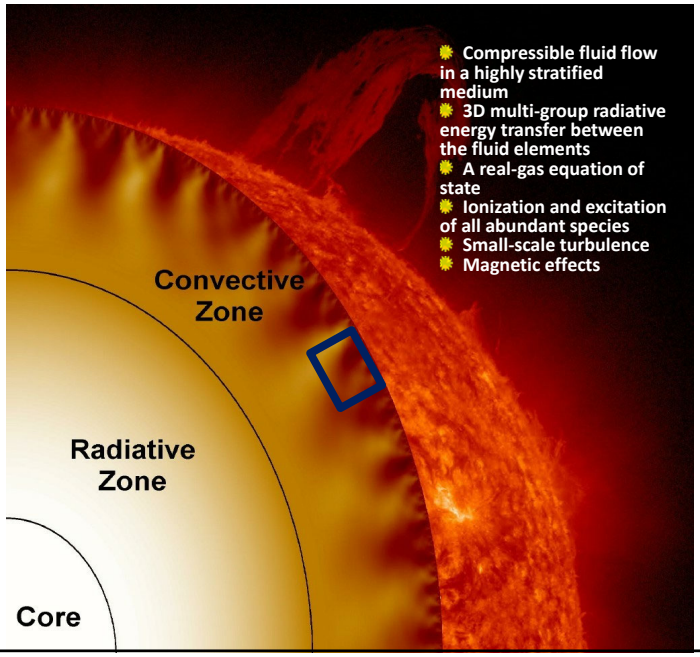

KIC9962653, M=1.47M_{SUN}

Vertical slice through the computational domain shows:
a) vertical velocity, b) density, c) temperature and d) sound speed perturbations from the stellar photosphere to the radiative zone.
Large-scale density fluctuations in the radiative zone are caused by internal gravity waves (g-modes) excited by convective overshooting.

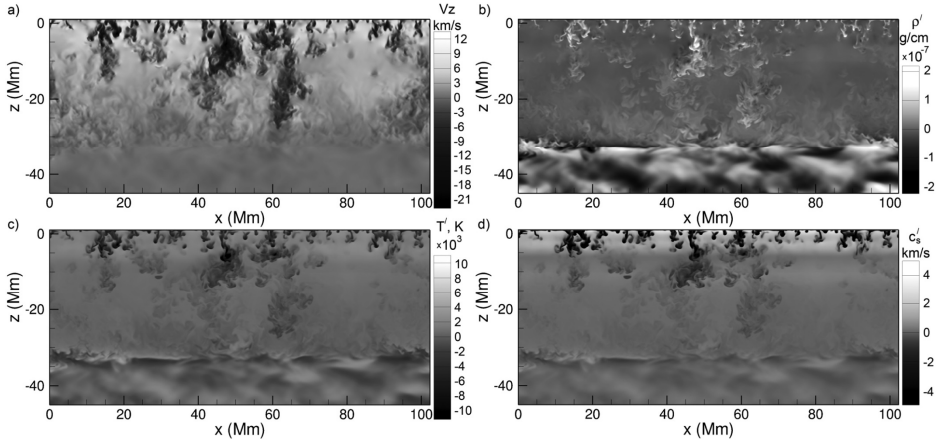

KIC9962653, M=1.47M_{SUN}

For this star we model the whole 30 Mm deep outer convection zone, including the overshoot region. Left panels show variations of the convection structure at different depths of the convection zone and in the overshooting region.

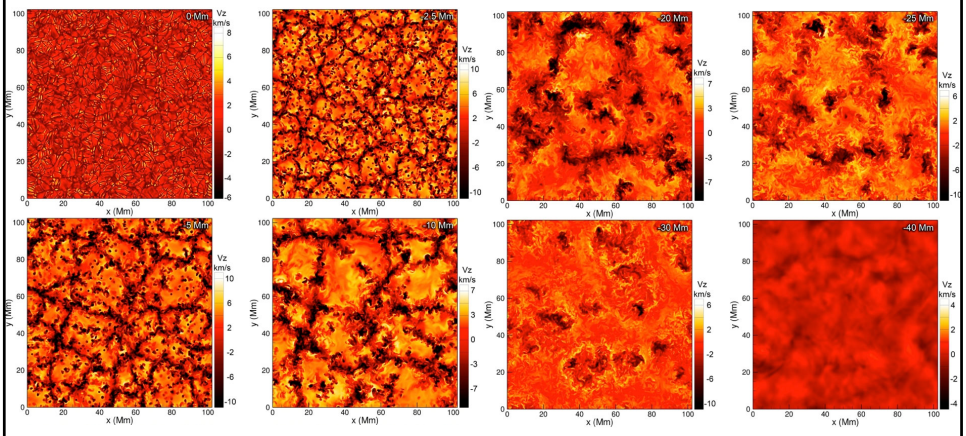

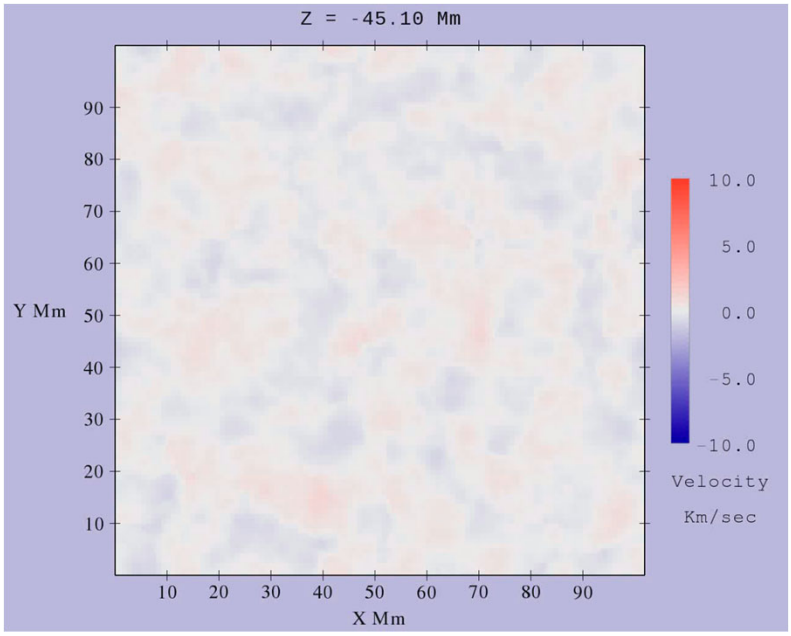

KIC9962653, M=1.47M_{SUN}

Vertical slice through the computational domain shows:
a) vertical velocity, b) density, c) temperature and d) sound speed perturbations from the stellar photosphere to the radiative zone.
Large-scale density fluctuations in the radiative zone are caused by internal gravity waves (g-modes) excited by convective overshooting.

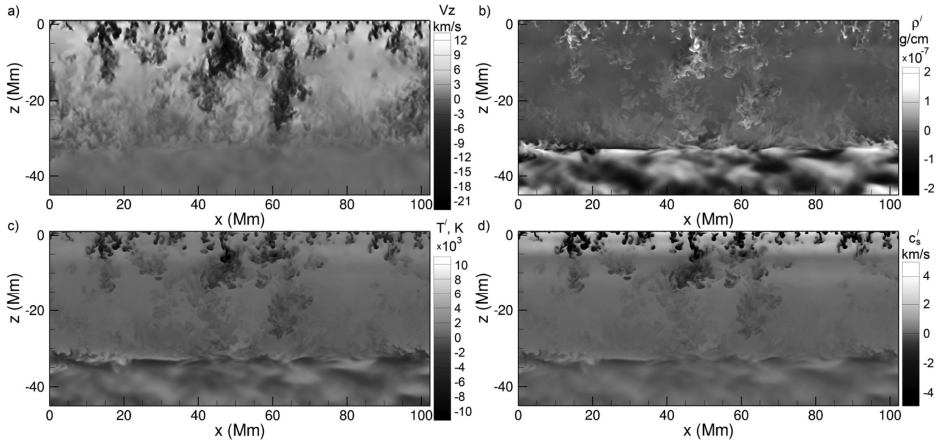

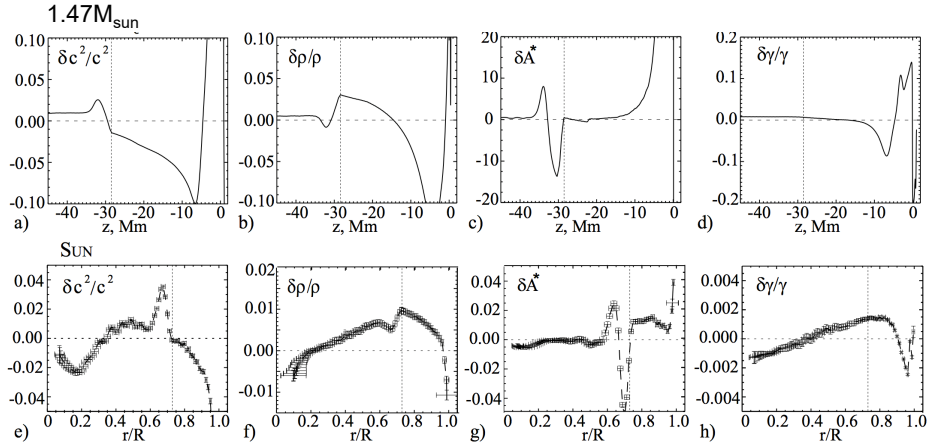

The deviations between the 3D simulation and 1D model of a star with mass M=1.47 M_{sun} as a function of depth, z=r-R, for: a) the squared sound speed, $\delta c^2/c^2$; b) density, $\delta\rho/\rho$; c) the Ledoux parameter of convective stability, A*; and d) the adiabatic exponent, γ. Panels e-h) show the corresponding deviations of the solar properties obtained by helioseismology inversion (Kosovichev 1999, 2011) from the 1D standard solar model (Christensen-Dalsgaard et al. 1996). Vertical dotted lines show the location of the bottom boundary of the convection zone.

Kitiashvili et al., 2016

Theoretical adiabatic exponent (Rogers F.J., & Iglesias C.A. 1992)

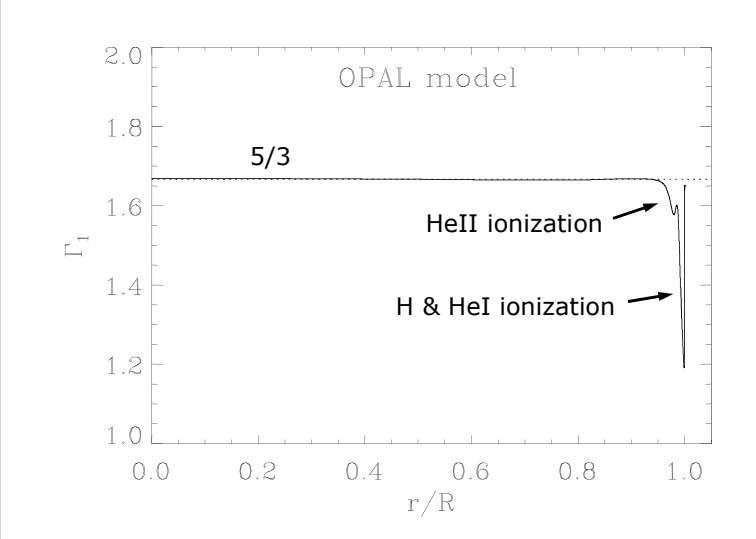

Two models of the equation of state:

1. "MHD" - Mihalas D., Däppen W., & Hummer D.G. (1988)
   - *The chemical picture* assumes a factorizable canonical partition function, allowing the total free energy to be written as the sum of the internal free energy, the translational free energy, and the free energy of the interactions between the electrons and nuclei; the ionization state of the plasma is found by minimizing the total free energy with respect to the occupation numbers of the different possible ionization levels.
2. "OPAL" - Rogers F.J., & Iglesias C.A. (1992)
   - *The physical picture* describes the plasma in terms of its fundamental constituents, electrons and nuclei, without dealing explicitly with atoms or molecules – the latter are embodied in the many-body interactions included between electrons and nuclei.

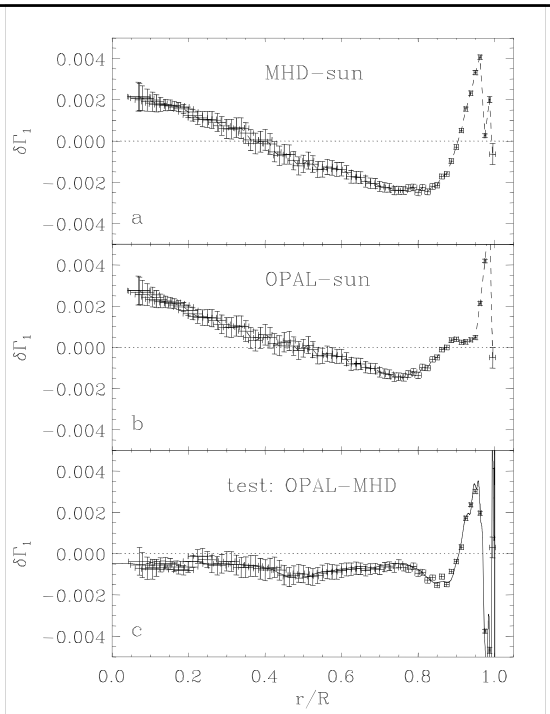

Relativistic effect on Γ_1

The number density of ionization electrons, n_e, can be written:

$$n_e = \frac{8\pi}{\lambda_c^3}\int_0^\infty \frac{p^2 dp}{e^{\varepsilon/T-\psi}+1},$$

where p and ε are the electron momentum and energy in units of mc and mc^2 respectively, T is the temperature in units of mc^2/k, ψ is the degeneracy parameter, and λ_c is the Compton wavelength h/mc of the electron. In the non-relativistic case,

$$2\varepsilon = p^2,$$

$$n_e = \frac{8\pi}{\lambda_c^3}\int_0^\infty \frac{\sqrt{2\varepsilon}\,d\varepsilon}{e^{\varepsilon/T-\psi}+1}.$$

In the relativistic case, the relation between energy and momentum becomes:

$$2\varepsilon + \varepsilon^2 = p^2,$$

and the corresponding equation for the electron density is:

$$n_e = \frac{8\pi}{\lambda_c^3}\int_0^\infty \frac{\sqrt{2\varepsilon}(1+\varepsilon/4)(1+\varepsilon)d\varepsilon}{e^{\varepsilon/T-\psi}+1}.$$

$$\frac{\delta\Gamma_1}{\Gamma_1} \approx -\frac{2+2X}{3+5X}T$$

X – hydrogen abundance

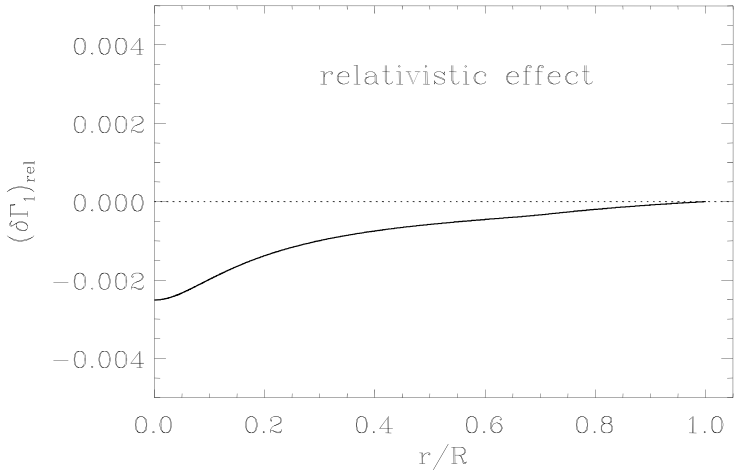

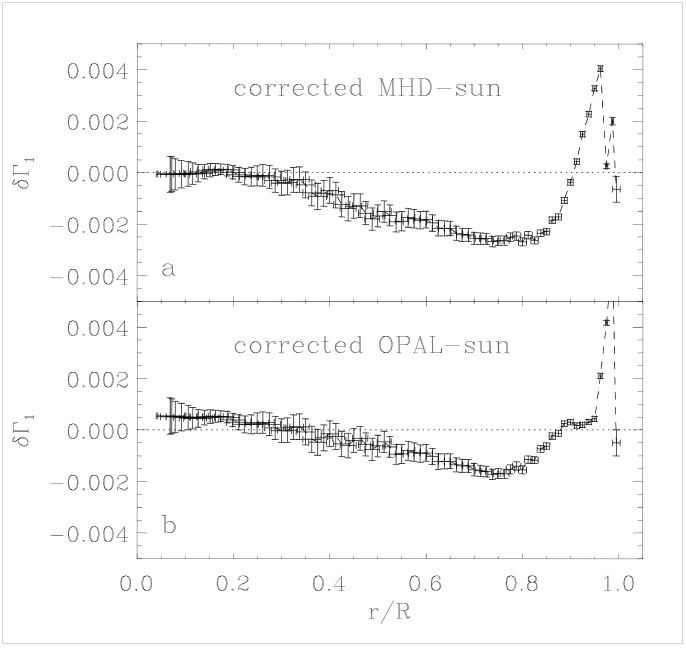

(Elliott and Kosovichev, 1998)

The relativistic corrections and the age of the Sun (Bonanno, Schlattl, Patterno, 2002)

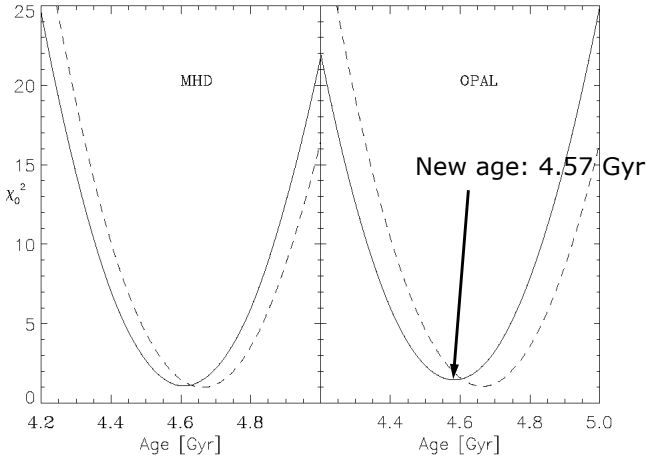

Helioseismic calibration of the Sun's age: reduction by 0.05-0.08 Gyr in agreement with the meteoritic estimates of the solar age.

Revision of solar surface abundances

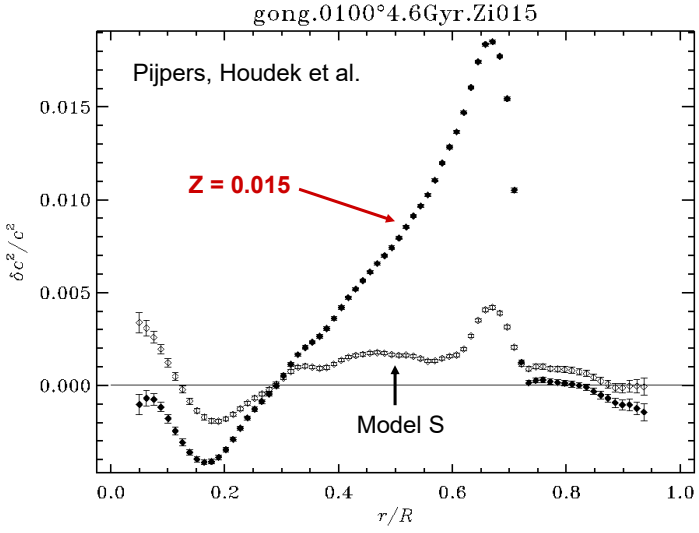

Lecture 19
Inversion for solar rotation. Regularized least-squares method.

(Stix, Chapter 5.3.8; Kosovichev, p.53-57;
Christensen-Dalsgaard, Chapter 8)

Please, upload in Canvas your HW1files and presentations by tomorrow

- 1.1 (a) Bryce
- 1.1 (b-d) Youra
- 1.2 (a) John
- 1.2 (b) Sadaf
- 1.3 (a-c) Yunpeng
- 1.3 (d-f) Sheldon
- 1.4 Ying
- 1.5 Ivan

Please, upload in Canvas HW2 files by tomorrow
HW2 presentations (Monday Nov.22+ Quiz 3)

- 2.1 (a) Ying
- 2.1 (b) Sheldon
- 2.2 Sadaf
- 2.3 Bhairavi
- 2.4 Yunpeng

General helioseismic inverse problem

1) Variational principle
2) Perturbation theory
3) Kernel transformation
4) Solution of inverse problem
   A. Optimally Localized Averages Method
   B. Regularized Least-Squares Method
5) Inversion results for the solar structure
6) Inversions for solar rotation

Solution to the Inverse Problem

We have a system integral equations

$$\frac{\delta\omega^{(n,l)}}{\omega^{(n,l)}} = \int_0^R K_{\rho,\gamma}^{(n,l)} \frac{\delta\rho}{\rho} dr + \int_0^R K_{\gamma,\rho}^{(n,l)} \frac{\delta\gamma}{\gamma} dr,$$

for a set of observed mode frequencies. If the number of observed frequencies is N (typically 2000), then we have a problem of determining two functions from this finite set. In general, it is impossible to determine these functions precisely. We can always find some rapidly oscillating functions, $f(r)$, that being added to the unknowns, $\delta\rho/\rho$ and $\delta\gamma/\gamma$, do not change the values of the integrals, e.g.

$$\int_0^R K_{\rho,\gamma}^{(n,l)}(r) f(r) dr = 0.$$

Such problems without an unique solution are called "ill-posed". The general approach is to find a smooth solution that satisfies the integral equations by applying some smoothness constraints to the unknown functions. This is called a "regularization procedure".

There are two basic methods for the helioseismic inverse problem:

1. Optimally Localized Averages (OLA) method - (Backus-Gilbert method)
2. Regularized Least-Squares (RLS) method - (Tikhonov method)

Optimally Localized Averages Method

The idea of the OLA method is to find a linear combination of data such as the corresponding linear combination of the sensitivity kernels for one unknown will have an isolated peak at a given radial point, r_0, (resemble a δ-function), and the combination for the other unknown will be close to zero. Then this linear combination provides an estimate for the first unknown at r_0.

$$\sum a^{(n,l)} \frac{\delta\omega^{(n,l)}}{\omega^{(n,l)}} =$$

$$= \int_0^R \sum a^{(n,l)} K_{\rho,\gamma}^{(n,l)} \frac{\delta\rho}{\rho} dr + \int_0^R \sum a^{(n,l)} K_{\gamma,\rho}^{(n,l)} \frac{\delta\gamma}{\gamma} dr.$$

If $$\sum a^{(n,l)} K_{\rho,\gamma}^{(n,l)}(r) \sim \delta(r - r_0),$$

and

$$\sum a^{(n,l)} K_{\gamma,\rho}^{(n,l)}(r) \sim 0,$$

then

$$\overline{\left(\frac{\delta\rho}{\rho}\right)}_{r_0} = \sum a^{(n,l)} \frac{\delta\omega^{(n,l)}}{\omega^{(n,l)}},$$

is an estimate of the density perturbation at $r = r_0$.

The coefficients, $a^{(n,l)}$, are different for different target radii r_0.

Averaging Kernels

The functions,

$$\sum a^{(n,l)} K^{(n,l)}_{\rho,\gamma}(r) \equiv A(r_0, r),$$

$$\sum a^{(n,l)} K^{(n,l)}_{\gamma,\rho}(r) \equiv B(r_0, r),$$

are called "averaging kernels".

The coefficients, a^i, are determined my minimizing a quadratic form (here, we use index i instead of double index (n,l)):

$$M(r_0, A, \alpha, \beta) = \int_0^R J(r_0, r)\left[A(r_0, r)\right]^2 dr +$$
$$+\beta \int_0^R \left[B(r_0, r)\right]^2 dr + \alpha \sum_{i,j} E_{ij} a^i a^j,$$

where $J(r_0, r) = 12(r - r_0)^2$, E_{ij} is a covariance matrix of observational errors, α and β are the regularization parameters. The first integral in this equation represents the Backus-Gilbert criterion of δ-ness for $A(r_0, r)$; the second term minimizes the contribution from $B(r_0, r)$, thus, effectively eliminating the second unknown function, ($\delta\gamma/\gamma$ in this case); and the last term minimizes the errors.

Optimally localized averaging kernels

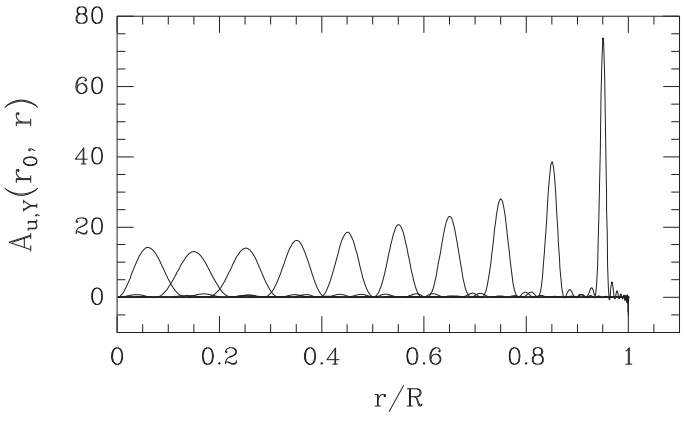

Inversion results for the observed solar frequencies

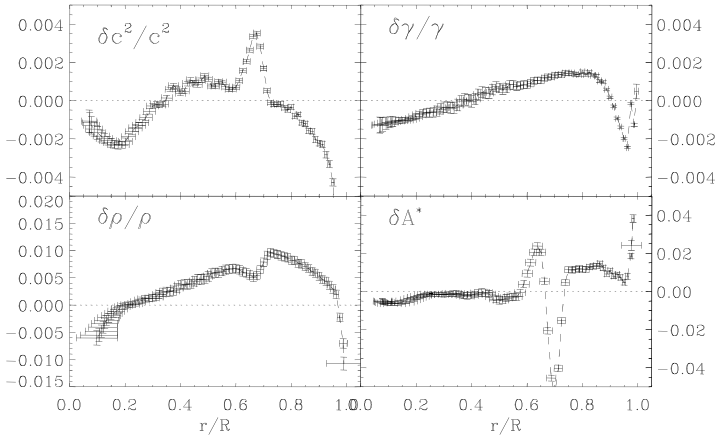

Inversions for solar rotation

- Measurements of
  - Solar differential rotation
  - Tachocline
  - Torsional oscillations

Inversions for solar rotation

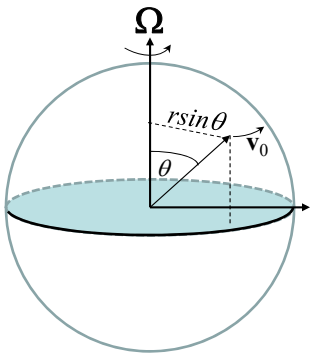

In the absence of rotation, the oscillation frequencies are degenerate with respect to the azimuthal order m. Rotation removes the degeneracy and leads to 'rotational frequency splitting'.

The angular velocity of the Sun is not uniform. It varies with the radius and latitude, $\Omega(r,\theta)$, where θ is colatitude. The corresponding flow velocity in the spherical coordinates has only the azimuthal component:

$$\mathbf{v}_0 = (0, 0, r\sin\theta\Omega)$$

. We substitute it in the linearized momentum equation:

$$\rho_0 \frac{d\mathbf{v}'}{dt} = \nabla p' + \mathbf{g}\rho' + \rho_0 \nabla \Phi'$$

Because of this background flow, in the LHS, we have to consider the full material derivative:

$$\frac{d\mathbf{v}'}{dt} = \frac{\partial \mathbf{v}'}{\partial t} + (\mathbf{v}_0 \nabla)\mathbf{v}'$$

In terms of the displacement $\boldsymbol{\xi}$:

$$\mathbf{v}' = \frac{d\boldsymbol{\xi}}{dt} = \frac{\partial \boldsymbol{\xi}}{\partial t} + (\mathbf{v}_0 \nabla)\boldsymbol{\xi}$$

$$\rho_0 \left(\frac{\partial}{\partial t} + \mathbf{v}_0 \nabla \right)^2 \boldsymbol{\xi} = -\nabla p' + \mathbf{g}\rho' + \rho_0 \nabla \Phi'$$

Perturbations p', ρ' and Φ' can be determined in terms $\boldsymbol{\xi}$ from the continuity and energy equations and the equation for gravitational potential. We define the RHS as operator $L(\boldsymbol{\xi})$:

$$\rho_0 \left(\frac{\partial}{\partial t} + \mathbf{v}_0 \nabla \right)^2 \boldsymbol{\xi} = L(\boldsymbol{\xi})$$

We seek periodic solutions $\boldsymbol{\xi} \propto e^{-i\omega t}$, and assume that the rotational velocity causes only small corrections to $\omega = \omega_0 + \Delta\omega$. Then, to the first order:

$$\rho_0(-\omega + \mathbf{v}\nabla)^2 \approx \rho_0(\omega^2 - 2i\omega\mathbf{v}_0\nabla)\boldsymbol{\xi}$$

Substituting ω, we get:

$$\rho_0[-\omega_0^2 - 2\omega_0\Delta\omega - 2i\omega_0(\mathbf{v}_0\nabla)]\boldsymbol{\xi} = L(\boldsymbol{\xi})$$

We cancel the first term in the LHS and the RHS because they satisfy to the unperturbed equation: $-\rho_0\omega_0^2\boldsymbol{\xi} = L(\boldsymbol{\xi})$.

Multiplying by complex conjugate $\boldsymbol{\xi}$ and integrating over the volume, we obtain:

$$2\omega_0\Delta\omega\int_V \rho_0\boldsymbol{\xi}^*\boldsymbol{\xi}dV = -2i\omega_0\int_V \boldsymbol{\xi}^*(\mathbf{v}_0\nabla)\boldsymbol{\xi}dV$$

$$\Delta\omega = -\frac{i\int_V \rho_0\boldsymbol{\xi}^*(\mathbf{v}_0\nabla)\boldsymbol{\xi}dV}{\int_V \rho_0\boldsymbol{\xi}^*\boldsymbol{\xi}dV}$$

In this derivation, we apply the variational principle and neglect the variations eigenfunctions caused by rotation.

Expressing the rotational flow velocity $vecv_0$ in terms of the angular velocity $\boldsymbol{\Omega} = \mathbf{v}\times\mathbf{r}$, where $vecr$ is the radius-vector:

$$(\mathbf{v}_0\nabla)\boldsymbol{\xi} = \Omega\frac{\partial\boldsymbol{\xi}}{\partial\phi} + \boldsymbol{\Omega}\times\boldsymbol{\xi}$$

Because the unperturbed eigenfunctions are expressed in terms of the spherical harmonics: $\boldsymbol{\xi} \propto Y_l^m(\theta)e^{im\phi}$, $\frac{\partial\boldsymbol{\xi}}{\partial\phi} = im\boldsymbol{\xi}$. Thus,

$$\Delta\omega_{nlm} = \frac{m\int_V \Omega\boldsymbol{\xi}_{nl}^*\boldsymbol{\xi}_{nl}\rho dV - i\int_v \boldsymbol{\xi}_{nl}^*(\boldsymbol{\Omega}\times\boldsymbol{\xi}_{nl})\rho dV}{I_{nl}}$$

where $I_{nl} = \int_V \boldsymbol{\xi}_{nl}^*\boldsymbol{\xi}_{nl}\rho dV$ is the mode inertia. If $\Omega = const$ then the first term: $\Delta\Omega = m\Omega$ can be interpreted as a result of wave advection by flows (in analogy to the Doppler effect).

Indeed $\boldsymbol{\xi} \propto \exp(-i\omega_0 t + im\phi)$ because of rotation the wave phase changes as $\phi = \Omega t$. Thus, $\boldsymbol{\xi} \propto \exp[-i(\omega_0 - m\Omega)t] \propto \exp(-i\omega t)$, where $\omega = \omega_0 + m\Omega$.

The second term in $\Delta\omega_{nlm}$ describe the effect of the Coriolis forcs and is relatively small.

If the angular velocity depends only on the radius, r, $\Omega = \Omega(r)$, then

$$\Delta\omega_{nlm} = \frac{m}{I_{nl}} \int_0^R \Omega(r) \left[\xi_r^2 + l(l+1)\xi_h^2 - 2\xi_r \xi_h - \xi_h^2 \right] \rho r^2 dr$$

where $\xi_r(r)$ and $\xi_h(r)$ are the radial and horizontal components of the displacement.

$$I_{nl} = \int_0^R \left[\xi_r^2 + l(l+1)\xi_h^2 \right] \rho r^2 dr$$

The rotational frequency splitting can be written as

$$\Delta\omega_{nlm} = m \int_0^R K_\Omega^{nl} \Omega(r) dr$$

or $\Delta\omega_{nlm} = m\overline{\Omega}$, where $\overline{\Omega}$ is a weighted average of the angular velocity, and $K_\Omega^{nl}(r)$ is the averaging kernel.

In the general case, $\Omega = \Omega(r\theta)$:

$$\Delta\omega_{nlm} = m \int_0^R \int_0^\pi K_\omega^{nl}(r,\theta) \Omega(r,\theta) dr d\theta$$

Effects of rotation (asymptotic JWKB approximation, Lec.15)

Solar rotation and other plasma flows inside the Sun cause Doppler shift of the wave frequencies. The dispersion relation for the acoustic waves becomes:

$$(\omega - \vec{k}\vec{v})^2 = \omega_c^2 + k^2 c^2$$

where $\vec{k}$ is the wave vector, and $\vec{v}$ is the plasma velocity.

Because of the acoustic ray paths travel in the great circles, they sample the radial and latitudinal components of velocity twice in the opposite directions. Thus, the contribution of these components to the quantization integral is canceled in the first approximation, and the mode frequencies depend only on the azimuthal component, v_ϕ:

$$(\omega - k_\phi v_\phi)^2 = \omega_c^2 + k^2 c^2$$

where $k_\phi = \frac{m}{r \sin\theta}$. Representing v_ϕ in terms of the angular velocity, $\Omega(r,\theta)$:

$$v_\phi = r \sin\theta \, \Omega(r,\theta),$$

we get:

$$(\omega - m\Omega)^2 = \omega_c^2 + k^2 c^2$$

The EBK quantization equation takes form:

$$\frac{2}{\pi}\int_0^M \frac{d\mu}{\sqrt{M^2-\mu^2}}\int_{r_1}^R \sqrt{\frac{(\omega_{nlm}-m\Omega)^2}{c^2}-\frac{L^2}{r^2}}dr=\pi(n+\alpha)$$

Assuming that $m\Omega/\omega_{nlm}\ll 1$ and that the background solar structure is spherically symmetric, we represent ω_{nlm} in terms of the frequency deviations from the model frequencies: $\Delta\omega_{nlm}=\omega_{nlm}-\omega_{0,nl}$.

$$\frac{2}{\pi}\int_0^M \frac{d\mu}{\sqrt{M^2-\mu^2}}\int_{r_1}^R \sqrt{\frac{(\omega_{0,nl}+\Delta\omega_{nlm}-m\Omega)^2}{c^2}-\frac{L^2}{r^2}}dr=\pi(n+\alpha)$$

Performing the first-order Taylor expansion and subtracting the quantization rule for the background state, we get:

$$\frac{2}{\pi}\int_0^M \frac{d\mu}{\sqrt{M^2-\mu^2}}\int_{r_1}^R \frac{\omega^2}{c^2}\frac{\left[\frac{\Delta\omega_{nlm}}{\omega}-\frac{m\Omega}{\omega}\right]}{\sqrt{\frac{\omega^2}{c^2}-\frac{L^2}{r^2}}}dr=0$$

where for simplicity we drop subscript for the model frequencies: $\omega=\omega_{0,nl}$.

Thus, we obtain:

$$\Delta\omega_{nlm}=\frac{2}{\pi T}\int_0^M\int_{r_1}^R \frac{m\Omega(r,\mu)drd\mu}{c\sqrt{M^2-\mu^2}\sqrt{1-L^2c^2/r^2\omega^2}}$$

where $T=\int_{r_1}^R \frac{dr}{c\sqrt{1-L^2c^2/r^2\omega^2}}$ is the "half-skip" travel time of acoustic waves.

The solar rotation causes ‘rotational frequency splitting’ proportional to the mode angular degree m.

The physical interpretation is that the modes with positive m travel in the same direction as the solar rotation and thus have higher frequencies then the modes with negative m traveling in the opposite direction.

Recall that that the oscillation modes are represented in terms of the spherical harmonics: $\xi_r(r,\theta,\phi,t)\propto P_l^m(\theta)\exp(im\phi-i\omega t)$, and thus, in the form of azimuthal traveling waves

By comparing the effect of the sound-speed asphericity and rotation:

$$\frac{\Delta\omega_{nlm}}{\omega} = \frac{2}{\pi T}\int_0^M \int_{r_1}^R \frac{\left[\Delta c(r,\mu)/c\right] dr d\mu}{c\sqrt{M^2-\mu^2}\sqrt{1-L^2c^2/\omega^2 r^2}}$$

$$\Delta\omega_{nlm} = \frac{2}{\pi T}\int_0^M \int_{r_1}^R \frac{m\Omega(r,\mu) dr d\mu}{c\sqrt{M^2-\mu^2}\sqrt{1-L^2c^2/r^2\omega^2}}$$

where $M = \sqrt{1-m^2/L^2}$

We notice that the frequency splitting due to the sound-speed asphericity is an even function of m and an odd function of m due the rotation.

This difference allows us to separate effects of the solar asphericity and rotation in the observational data.

The a-coefficients

The observational data are often represented as an expansion in terms of the Legendre polynomials:

$$\Delta\omega_{nlm} = L\sum_{k=1}^{N} a_k^{nl} P_k\left(\frac{m}{L}\right)$$

For a more accurate (non-asymptotic) representation, the expansion is performed in terms of Clebsch-Gordon coefficients, which will be considered later.

In this representation, the 'even' a-coefficients represent effects of the solar asphericity, and the 'odd' a-coefficients represent the internal solar rotation and its variations with latitude (zonal flows). In addition, the representations in the form of the a-coefficients allows us to replace the 2D inversions of $\Delta\omega_{nlm}$ with a series of 1D inversions of the a-coefficients.

Specifically, representing the sound-speed perturbation in terms of the Legendre polynomials:

$$\frac{\Delta c}{c}(r,\mu) = \sum_{j=1}^{J} A_{2j}(r) P_{2j}(\mu)$$

where $\mu = \cos\theta$.

Substituting this representation of $\frac{\Delta c}{c}(r,\mu)$ in the equation for $\Delta\omega_{nlm}/\omega$, we obtain:

$$\frac{\Delta\omega_{nlm}}{\omega}=\sum_{j=1}^{J}\frac{1}{T}\int_{r_1}^{R}\frac{A_{2j}(r)dr}{\sqrt{1-L^2c^2/r^2\omega^2}}\left(\frac{2}{\pi}\int_0^M\frac{P_{2j}(\mu)}{\sqrt{M^2-\mu^2}}d\mu\right)$$

The second integral is calculated analytically:

$$\frac{2}{\pi}\int_0^M\frac{P_{2j}(\mu)}{\sqrt{M^2-\mu^2}}d\mu=(-1)^j P_{2j}(0)P_{2j}(m/L)$$

Thus, both the observational data and the angular integral of the sound-speed asphericity are represented in terms of the series of Legendre polynomial $P_{2j}(m/L)$.

We obtain a series of the Abel integral equations for the radial functions of the asphericity, $A_{2j}(r)$:

$$\frac{1}{T}\int_{r_1}^{R}\frac{A_{2j}(r)dr}{\sqrt{1-L^2c^2/\omega^2r^2}}=(-1)^j\frac{La_{2j}^{ln}}{P_{2j}(0)}.$$

These equations establish a relationship between the even a-coefficients and the solar asphericity expressed in terms of the Legendre polynomials.

A similar type of solution can be obtained for the angular velocity $\Omega(r,\mu)$. In this case, it is convenient to use the expansion in terms of associate Legendre functions:

$$\Omega(r,\mu)=\sum_{j=0}^{J}\Omega_{2j+1}(r)\frac{P_{2j+!}^1(\cos\theta)}{\sin\theta}$$

Substituting in:

$$\Delta\omega_{nlm}=\frac{2}{\pi T}\int_0^M\int_{r_1}^{R}\frac{m\Omega(r,\mu)drd\mu}{c\sqrt{M^2-\mu^2}\sqrt{1-L^2c^2/r^2\omega^2}}$$

we obtain:

$$\Delta\omega_{nlm}=\sum_{j=0}^{J}\frac{1}{T}\int_{r_1}^{R}\frac{\Omega_{2j+1}(r)dr}{c\sqrt{1-L^2c^2/r^2\omega^2}}\left(\frac{2m}{\pi}\int_0^M\frac{P_{2j+1}^1d\mu}{\sqrt{1-\mu^2}\sqrt{M^2-\mu^2}}\right)$$

The second integral is calculated analytically:

$$\frac{2m}{\pi}\int_0^M \frac{P_{2j+1}^1 d\mu}{\sqrt{1-\mu^2}\sqrt{M^2-\mu^2}} = -\frac{\pi}{2}(2j+1)P_{2j}(0)\frac{L}{m}P_{2j+1}\left(\frac{m}{L}\right)$$

Both the observational data and the angular integral of the solar rotation are expressed in terms of the odd Legendre polynomial of m/L.

Thus, we obtain a series of the 1D Abel integral equations for the radial functions of the solar rotation expansion:

$$\frac{1}{T}\int_{r_1}^R \frac{\Omega_{2j+1}(r)dr/c}{\sqrt{1-\frac{L^2r^2}{r^2\omega_{0,nl}^2}}} = -\frac{a_{2j+1}^{nl}}{(2j+1)P_{2j}(0)}$$

In the asymptotic JWKB/EBK approximation, the a-coefficients are the functions of the ratio L/ω or the lower turning point radius, r_1. This helps to identify 'outliers' in the observational data.

The second integral is calculated analytically:

$$\int_0^M \frac{P_{2j+1}^1 d\mu}{\sqrt{1-\mu^2}\sqrt{M^2-\mu^2}} = -\frac{\pi}{2}(2j+1)P_{2j}(0)\frac{L}{m}P_{2j+1}\left(\frac{m}{L}\right)$$

Both the observational data and the angular integral of the solar rotation are expressed in terms of the odd Legendre polynomial of m/L.

Thus, we obtain a series of the 1D Abel integral equations for the radial functions of the solar rotation expansion:

$$\frac{1}{T}\int_{r_1}^R \frac{(\Omega_{2j+1}(r)/2\pi)dr/c}{\sqrt{1-\frac{L^2r^2}{c^2\omega_{0,nl}^2}}} = \frac{a_{2j+1}^{nl}}{(2j+1)P_{2j}(0)}$$

In the asymptotic JWKB/EBK approximation, the a-coefficients are the functions of the ratio L/ω or the lower turning point radius, r_1. This helps to identify 'outliers' in the observational data.

$\Omega/2\pi$ is the rotation rate. It is measured in nHz as well as the a-coeffients.

$$\Delta\nu_{nlm} = \Delta\omega_{nlm}/2\pi = L\sum_{k=1}^N a_k^{nl}P_k\left(-\frac{m}{L}\right)$$

The minus sign was instroduces to get the a-coefficients of the same sign as the corresponding rotation law terms.

Solar rotation law (asymptotic JWKB approximation – ray theory)

Consider a special case of a three-term solar differential rotation law:

$$\Omega / 2\pi = a + b\cos^2\theta + c\cos^4\theta$$

where a, b, and c are measured in nHz. The corresponding representation in terms of the associated Legendre polynomials: Consider the intergrals for the $A_{2j+1}(r)$ as averaging over the propagation regions for each mode, $[r_1, R]$.

$$\overline{A}_{2j+1} = \frac{1}{T}\int_{r_1}^{R} \frac{A_{2j+1}(r)}{\sqrt{1-r^2/r_1^2}}\frac{dr}{c} \rightarrow \qquad T = \int_{r_1}^{R} \frac{1}{\sqrt{1-r^2/r_1^2}}\frac{dr}{c}$$

- a 'half-skip' travel time, $r_1 = c(r_1)\omega_{nl}/L$ is the turning point radius.

Then, we write the integral equations in terms of the averaged A coefficients:

$$\overline{A}_1 = a_1^{nl}/P_0(0) = a_1^{nl} \qquad \overline{A}_3 = a_3^{nl}/3P_2(0) = -\frac{2}{3}a_3^{nl} \qquad \overline{A}_5 = a_5^{nl}/5P_3(0) = \frac{8}{15}a_5^{nl}$$

Substituting $P_1^1(\cos\theta) = -\sin\theta$ $\quad P_3^1(\cos\theta) = -\frac{3}{2}\sin\theta(5\cos^2\theta - 1)$

$$P_5^1(\cos\theta) = -\frac{15}{8}\sin\theta(21\cos^4\theta - 14\cos^2\theta + 1)$$

we get: $\quad \overline{\Omega}/2\pi = (a_1 + a_3 + a_5) - (5a_3 + 14a_5)\cos^2\theta + 21a_5\cos^4\theta$

where I dropped the mode indexes n,l.

Solar rotation law (variational principle – wave theory)

Consider a special case of a three-term solar differential rotation law:

$$\Omega / 2\pi = a + b\cos^2\theta + c\cos^4\theta$$

where a, b, and c are measured in nHz. The corresponding representation in terms of the associated Legendre polynomials: Consider the intergrals for the $A_{2j+1}(r)$ as averaging over the voliume:

$$\overline{A}_{2j+1} = \frac{1}{I^{(n,l)}}\int_0^R K_{2j+1}^{(n,l)}(r)\rho r^2 dr \qquad I^{(n,l)} = \int_0^R [(\xi_r^{(n,l)})^2 + l(l+1)(\xi_h^{(n,l)})^2]\rho r^2 dr$$

- the mode inertia, l is the mode angular degree, n is the radial order. $\xi_r^{(n,l)}$ and $\xi_h^{(n,l)}$ are the radial and horizontal components of displacement.

Then, we write the integral equations in terms of the averaged A coefficients:

$$\overline{A}_1 = a_1^{nl}/P_0(0) = a_1^{nl} \qquad \overline{A}_3 = a_3^{nl}/3P_2(0) = -\frac{2}{3}a_3^{nl} \qquad \overline{A}_5 = a_5^{nl}/5P_3(0) = \frac{8}{15}a_5^{nl}$$

Substituting $P_1^1(\cos\theta) = -\sin\theta$ $\quad P_3^1(\cos\theta) = -\frac{3}{2}\sin\theta(5\cos^2\theta - 1)$

$$P_5^1(\cos\theta) = -\frac{15}{8}\sin\theta(21\cos^4\theta - 14\cos^2\theta + 1)$$

we get: $\quad \overline{\Omega}/2\pi = (a_1 + a_3 + a_5) - (5a_3 + 14a_5)\cos^2\theta + 21a_5\cos^4\theta$

where I dropped the mode indexes n,l,m.

Theory of Rotational Frequency Splitting. I

The eigenfrequencies of a spherically-symmetrical static star are degenerate with respect to the azimuthal number m. Rotation breaks the symmetry and splits each mode of radial order, n, and angular degree, l, into $(2l+1)$ components of $m=-l,...,l$ ('mode multiplets'). The rotational frequency splitting can be computed using the variational principle. From this variational principle, one can obtain mode frequencies ω_{nlm} relative to the degenerate frequency ω_{nl} of the non-rotating star:

$$\Delta\omega_{nlm} \equiv \omega_{nlm} - \omega_{nl} = \frac{1}{I_{nl}} \int_V \left[m\, \vec{\xi} \cdot \vec{\xi}^{\,*} + i e_\Omega (\vec{\xi} \times \vec{\xi}^{\,*}) \right] \Omega \rho dV,$$

where e_Ω is the unit vector defining the rotation axis, and $\Omega = \Omega(r,\theta)$ is the angular velocity which is a function of radius r and co-latitude θ, and I_{nl} is the mode inertia.

Using the eigenfunctions in terms of the radial and horizontal displacements, $\vec{\xi} = \vec{e}_r \xi_r + \vec{e}_h \xi_h$, this equation can be rewritten as a two-dimensional integral equation for $\Omega(r,\theta)$:

$$\Delta\omega_{nlm} = \int_0^R \int_0^\pi K_{nlm}^{(\Omega)}(r,\theta) \Omega(r,\theta) d\theta dr.$$

where $K_{nlm}^{(\Omega)}(r,\theta)$, the rotational splitting kernels:

$$K_{nlm}^{(\Omega)}(r,\theta) = \frac{m}{I_{nl}} 4\pi\rho r^2 \left\{ (\xi_{r,nl}^{\,2} - 2\xi_{r,nl}\xi_{h,nl})(P_l^m)^2 + \xi_{h,nl}^{\,2} \left[\left(\frac{dP_l^m}{d\theta} \right)^2 - 2P_l^m \frac{dP_l^m}{d\theta} \frac{\cos\theta}{\sin\theta} + \frac{m^2}{\sin^2\theta} (P_l^m)^2 \right] \right\} \sin\theta.$$

Theory of Rotational Frequency Splitting. II

Here $\xi_{r,nl}$ and $\xi_{h,nl}$ are the radial and horizontal components of eigenfunctions of the mean spherically symmetric structure of the Sun, $P_l^m(\theta)$ is an associated normalized Legendre function ($\int_0^\pi (P_l^m)^2 \sin\theta d\theta = 1$).

The kernels are symmetric relative to the equator, $\theta = \pi/2$.

Therefore, the frequency splittings are sensitive only to the symmetric component of rotation in the first approximation. The non-symmetric component can, in principle, be determined from the second-order correction to the frequency splitting, or from local helioseismic techniques, such as time-distance seismology and ring-diagram analysis.

For a given set of observed frequency splittings the equation for $\Delta\omega_{nlm}$ constitutes a two-dimensional linear inverse problem for the angular velocity, $\Omega(r,\theta)$.

Optimally Localized Averaging Methods

Similarly to the 1-D solar structute inversions these methods explicitly form linear combinations of the data and corresponding kernels such that the resulting averaging kernels are, to the extent possible, localized near the target positions, r_0, θ_0, through appropriate choice of the coefficients $a_i^{(\Omega)}(r_0, \theta_0)$:

$$\overline{\Omega}(r_0, \theta_0) = \sum_{i=1}^{M} a_i^{(\Omega)}(r_0, \theta_0) d_i = \int_0^R \int_0^\pi K(r_0, \theta_0, r, \theta) \Omega(r, \theta) d\theta dr,$$

where d_i is the observed property, frequency splitting $\Delta\omega_{nlm}$, or splitting coefficients $a_j(n,l)$ (83), $K(r_0, \theta_0, r, \theta)$ is the averaging kernel given by

$$K(r_0, \theta_0, r, \theta) = \sum_{i=1}^{M} a_i^{(\Omega)}(r_0, \theta_0) K_i^{(\Omega)}(r, \theta),$$

and M is the total number of data points. However, the application of the Backus-Gilbert δ-ness criterion leads to $M \times M$ linear equations at each of the target positions.

A modification called 'Subtractive Optimally Localized Averaging' (2dSOLA) allows to keep the same matrix for all target points, and, thus, is computationally more efficient. In this formulation, sometimes the goal is to approximate K to a prescribed target $T(r_0, \theta_0, r, \theta)$, by minimizing

$$\int_0^R \int_0^\pi \left[T(r_0, \theta_0, r, \theta) - K(r_0, \theta_0, r, \theta) \right]^2 \mathrm{d}\theta \mathrm{d}r + \lambda \sum_{i=1}^{M} \left[\sigma_i a_i^{(\Omega)}(r_0, \theta_0) \right]^2$$

subject to K being unimodular.

Here the first term ensures that the averaging kernel is close to the target form, while the second controls the error in the inferred solution, the trade-off between the two being controlled by the parameter λ.

The results of this method depend on the choice of the target function, $T(r_0, \theta_0, r, \theta)$, and, currently, there is no general recipe for choosing this function. One of approaches is to employ Gaussian targets symmetrized around the equator, with the radial width chosen proportional to the local sound speed and constant width in latitude.

Regularized Least-Squares Method

The goal of this method is to obtain a smooth solution that fits the data rather than to construct well localized averaging kernels. This solution is obtained by minimizing the following functional:

$$\sum_{i=1}^{M}\frac{1}{\sigma_i^2}\left[\int_0^R\int_0^\pi K_i\Omega(r,\theta)\mathrm{d}\theta\mathrm{d}r - d_i\right]^2 + \alpha_r\int_0^R\int_0^\pi f_r(r,\theta)\left(\frac{\partial^2\Omega}{\partial r^2}\right)^2\mathrm{d}\theta\mathrm{d}r +$$

$$\alpha_\theta\int_0^R\int_0^\pi f_\theta(r,\theta)\left(\frac{\partial^2\Omega}{\partial\theta^2}\right)^2\mathrm{d}\theta\mathrm{d}r,$$

where d_i are the observed frequency splittings or splitting coefficients, K_i are the corresponding seismic kernels, σ_i are the error estimates of the data, and α_r and α_θ are the regularization parameters, and f_r and f_θ are some weight functions which can be used to regulate the degree of smoothing in different regions. The last two terms provide smoothing using the second-derivative constraints, which provided good results for artificial and real data .

For the numerical solution function $\Omega(r,\theta)$ is represented in the form of a discretized piece-wise linear functions with unknown coefficients or local splines. The coefficients are calculated using the standard methods of linear algebra.

Rotational frequency splitting

The modes with $m \neq 0$ represent azimuthally propagating waves. The modes with $m > 0$ propagate in the direction of solar rotation and, thus, have higher frequencies in the inertial frame than the modes $m < 0$ which propagate in opposite direction. As a result the modes with fixed n and l are split in frequency: $\Delta\nu_{nlm} = \nu_{nlm} - \nu_{nl0}$. Thus, the internal rotation is inferred from splitting of normal mode frequencies with respect to the azimuthal order, m .

$$\vec{\xi} \propto e^{-i\omega t}Y_l^m(\theta,\phi) = CP_l^m(\theta)e^{im\phi - i\omega t}$$

- displacement of the solar surface in solar modes

$\nu = \omega / 2\pi$

- ν is cyclic frequency, measured in Hz
- The oscillation period is 1/ν (in sec, min, etc).

ω is the angular frequency, measured in rad/s

Observations of the Sun as a star

rotational frequency splitting is observed only for 'even modes', for which $l+m$ is even because the rotation axis is almost perpendicular to the ecliptic. The 'odd modes' are antisymmetric relative to the equator, and their signal is canceled.

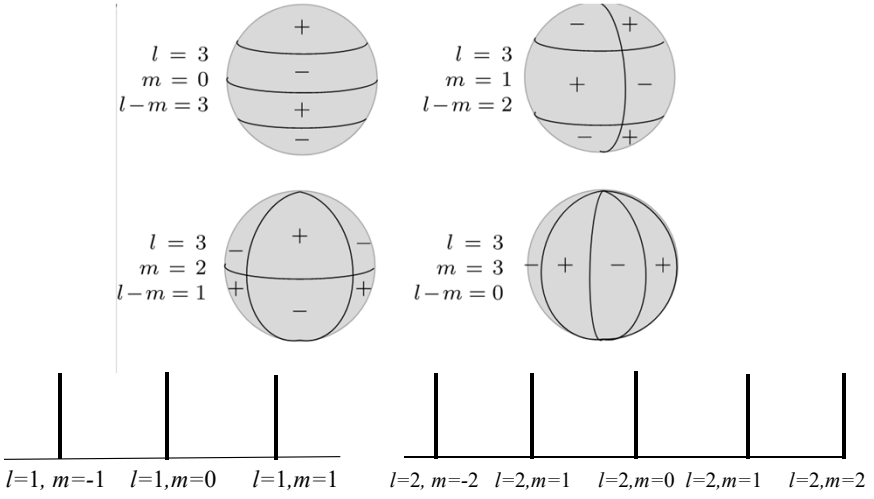

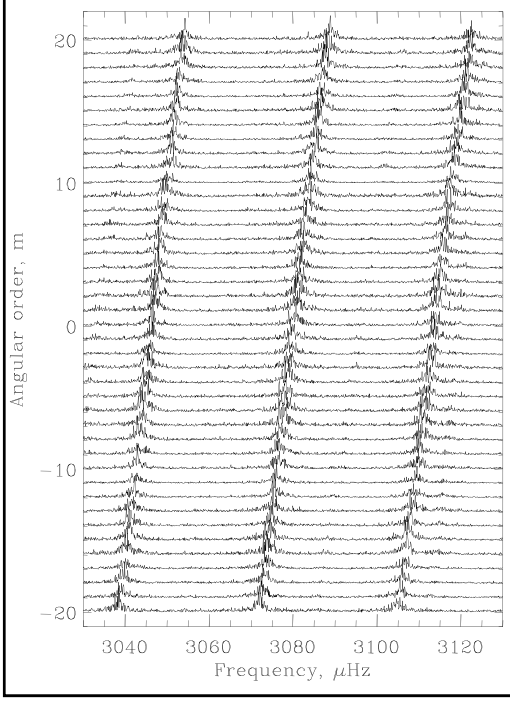

Illustration of the frequency shift due to the solar rotation

Typical power spectra of solar oscillation data from the MDI instrument on SOHO. Each horizontal curve shows three lines of the power spectrum for different azimuthal order m with radial order $n = 15$ and angular degree $l = 19, 20$, and 21 (from left to right). The slope of the modal lines is due to the rotational frequency shift: prograde modes with positive m have higher frequencies than retrograde modes with negative m.

Frequency splitting, *l*=150

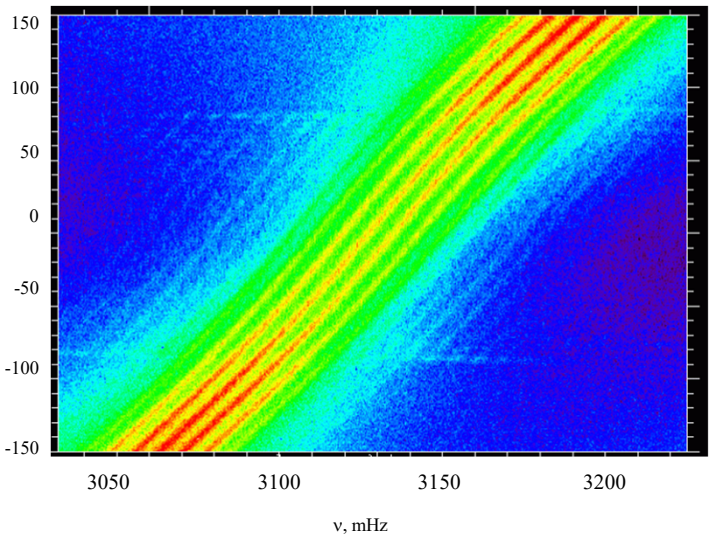

(F. Hill)

Comparison of the sensitivity kernels for rotation (A-C), and examples of the averaging kernels (D)

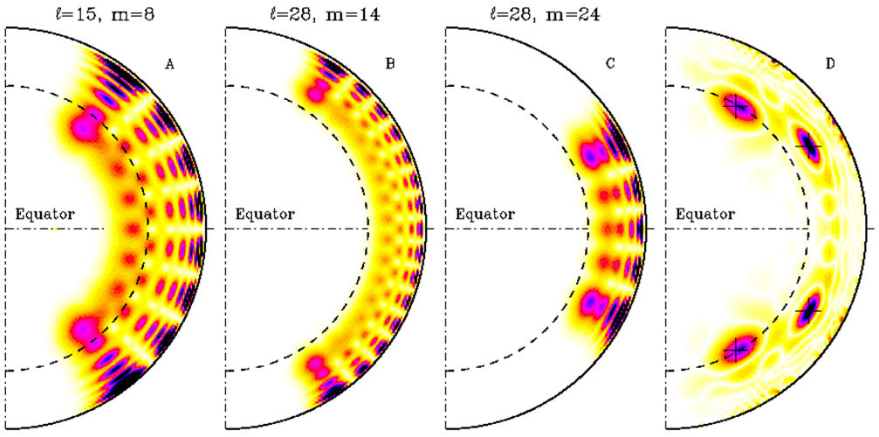

JWKB solution for the angular equation. 3

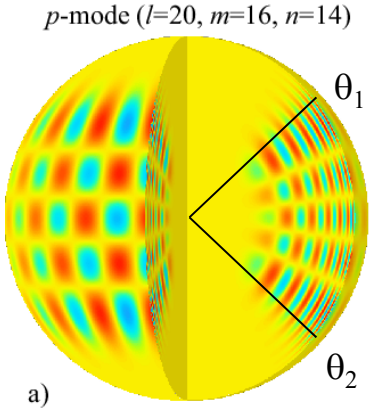

The propagation region $k_\theta^2 > 0$ is where $L^2 > \frac{m^2}{\sin^2\theta}$ or $|\sin\theta| > \frac{m}{L}$.

Therefore, the ratio $\frac{m}{L}$ determines the latitudinal turning points θ_1 and θ_2 for the acoustic modes: $|\sin\theta_{1,2}| = \frac{m}{L}$.

If $m = 0$ then the mode propagation region is extended from the pole to pole.

If $m = l$ then the modes are confined in a narrow equatorial strip.

Comparison of solar modes

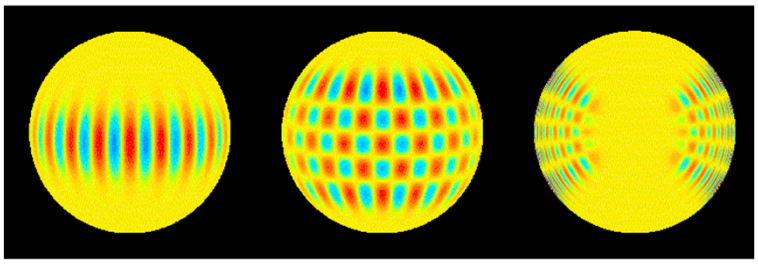

l=19, m=19 l=19, m=15 l=19, m=15,n=11

Inversion of MDI data by two different techniques

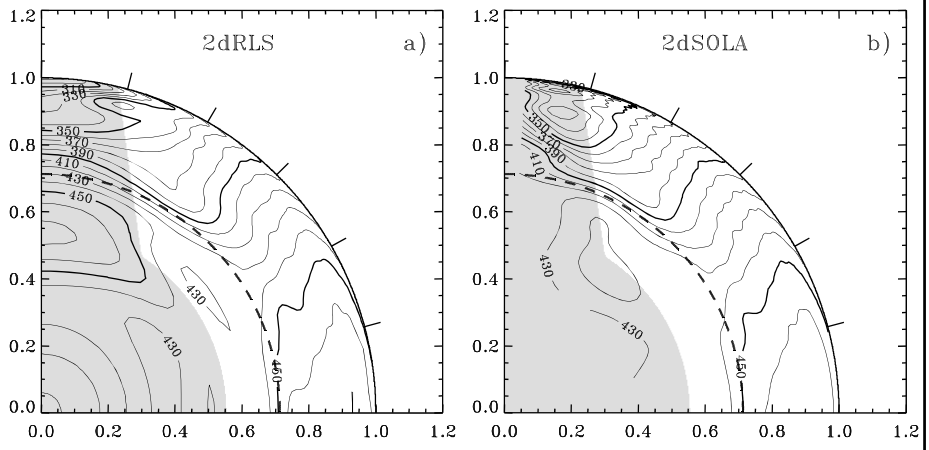

Averaging kernels for the solar rotation rate

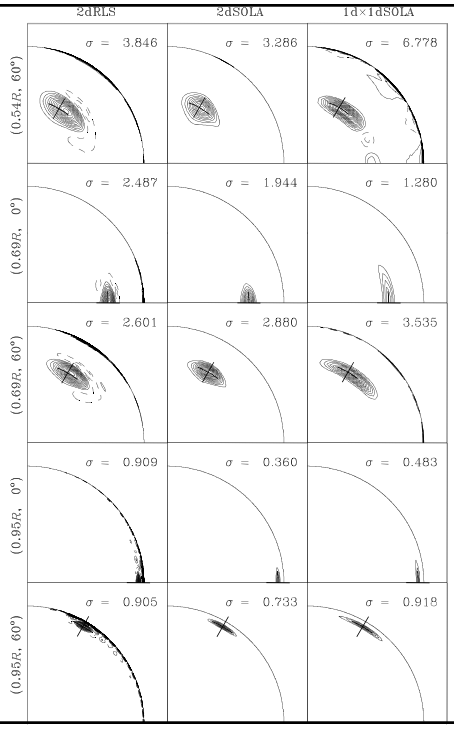

Solar tachocline

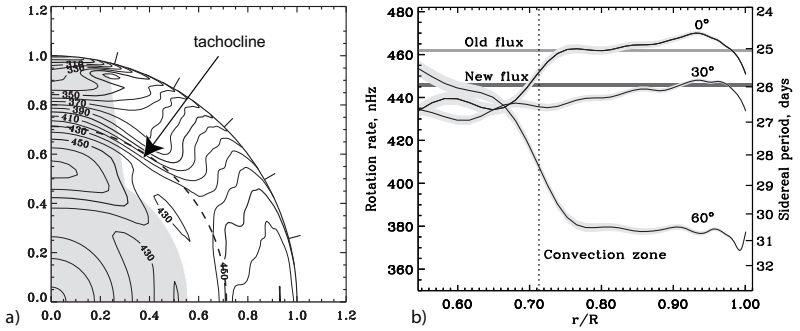

Torsional oscillations

Torsional oscillations (Howard & LaBonte 1980)

Evolution of surface velocity field (upper panel) and surface magnetic field (lower panel)

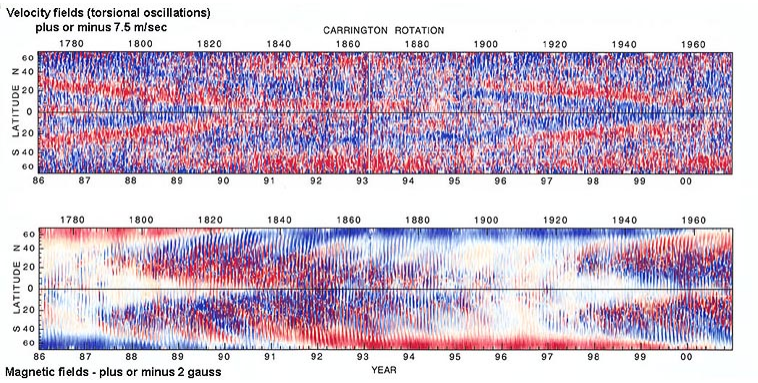

1986 **2000**

Ulrich 2001

Variations of the differential rotation ("torsional oscillations") provide insight in the dynamo mechanism

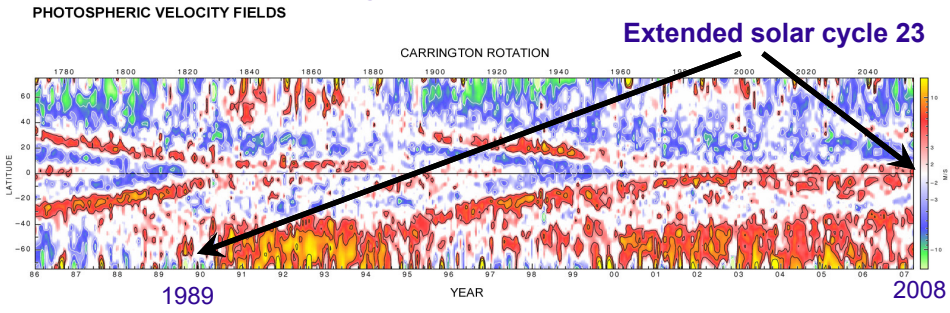

Courtesy of Roger Ulrich (http://obs.astro.ucla.edu/torsional.html)

Torsional Oscillations were discovered by Carnegie astronomers Robert Howard and Barry LaBonte using 150-Foot solar telescope data in 1980.

SOLAR MAGNETIC CYCLES

It was found that the strength of polar magnetic field measured at a solar minimum predicts the next solar maximum.

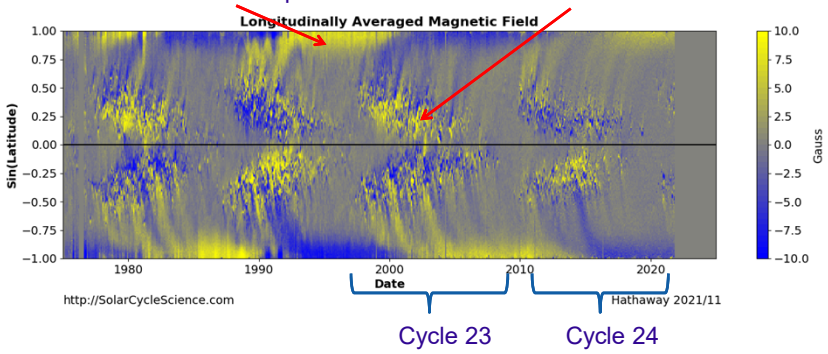

Variations of the depth of the meridional flows with the solar activity cycle

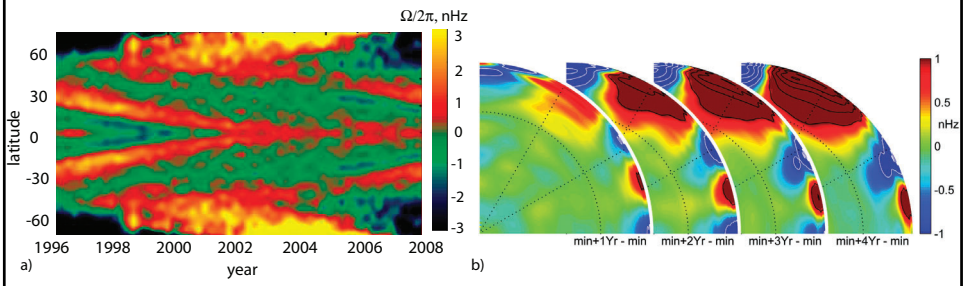

Vorontsov et al. 2002

Two paradigms in solar dynamo

Flux-transport theory (Babcock-Leighton)

- The dynamo process is controlled by meridional circulation.
- Toroidal magnetic field is generated and stored in the tachocline region. Meridional flow in the tachocline produces the butterfly diagram.

Dynamo-wave theory (Parker)

- The butterfly diagram is produced by dynamo waves.
- Theoretical argument: "Dynamo waves propagate along isorotation surfaces" (Parker, 1955; Yoshimura, 1975).

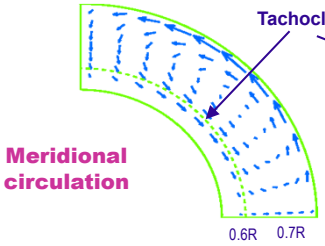

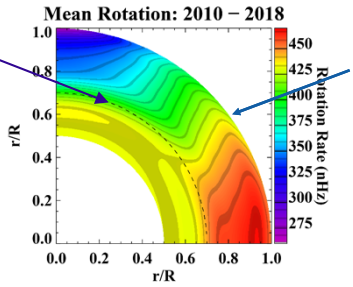

Because of the subsurface shear layer the dynamo wave can propagate towards the equator (Brandenburg 2005; Pipin & Kosovichev, 2011; Paradkar, Chitre, & Krishan, 2019).

Torsional oscillations at different depth are measured by global helioseismology for two solar cycles

- Comparison of the magnetic butterfly diagram with the corresponding maps of the zonal flows (torsional oscillations) at five different depth in the convection zone during Cycles 23 and 24.
- Inclined dashed lines illustrate an apparent migration of the flow pattern with radius. They are drawn through the points where the accelerated equatorial branch crosses the equator (around the solar maxima).

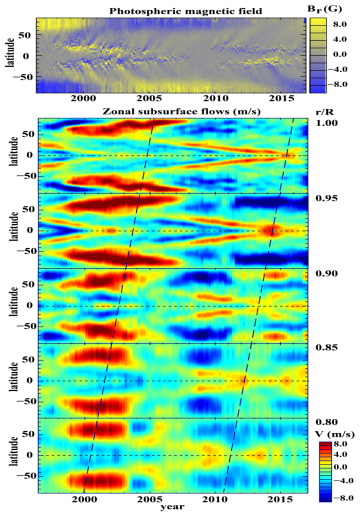

Analysis of zonal flow acceleration

- The zonal flow acceleration calculated after applying Gaussian spatial and temporal filters to smooth noise and small-scale variations and reveal large-scale patterns
- Overlay of the zonal acceleration (color image) and the radial magnetic field (gray-scale) reveals that the regions of magnetic field emergence at mid and low latitudes coincide with the zones of flow deceleration.

(Kosovichev & Pipin, 2019)

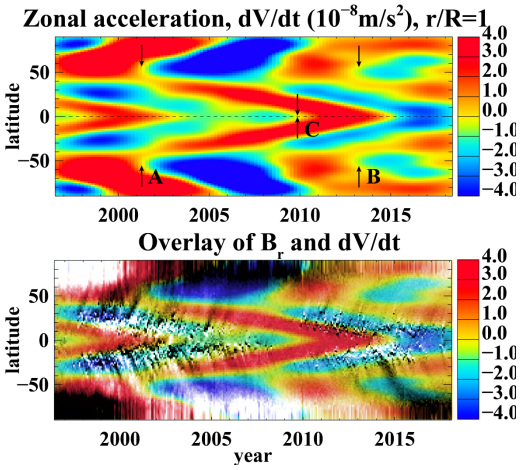

ZONAL ACCELERATION REVEALS PATTERNS OF DYNAMO WAVES

Measurements of the zonal acceleration revealed zones of deceleration, caused by internal magnetic fields (blue areas in the movie).

The flow deceleration originates at the base of the solar convection zone, 200 Mm beneath the solar surface, at about 60 degrees latitude.

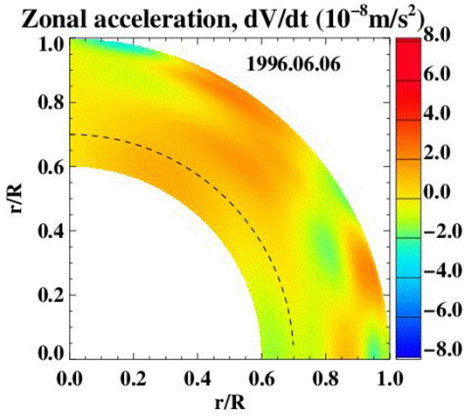

Principal component analysis (PCA)

PCA converts observational data into a set of linearly uncorrelated orthogonal components called principal components, which are ordered so that the first few **retain most of the variation present in the original data**

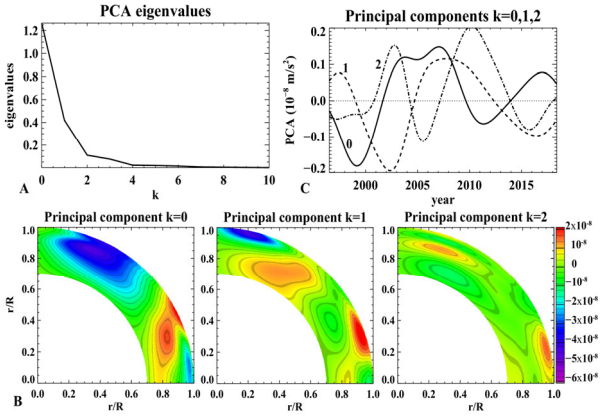

MIGRATION OF DYNAMO WAVES

The dynamo waves originate at the base of the convection zone (in the "solar tachocline") and migrate towards the poles and the equator with a speed of 1-2 m/s.

It reaches the surface near the poles in 1-2 years, but it takes about 10 years to reach the surface at low latitudes where it forms sunspots.

This explains why the polar magnetic field predicts the next sunspot maximum.

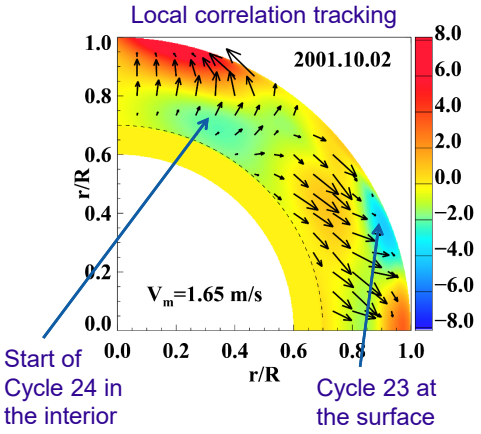

Tracking the zonal acceleration through the convection zone

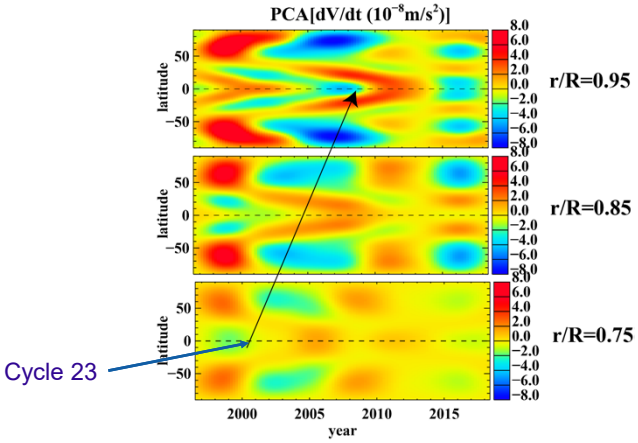

HELIOSEISMOLOGY CAN DETECT THE NEXT SOLAR CYCLE IN THE INTERIOR

- In the solar interior we already see the signal associated with the next sunspot cycle (Cycle 25).
- It appears that it will be even weaker than the current cycle, indicating on continuing long-term decrease of solar activity.

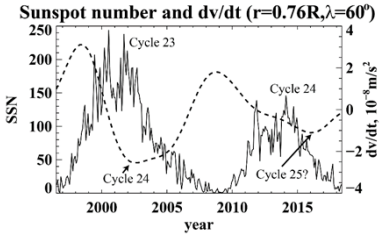

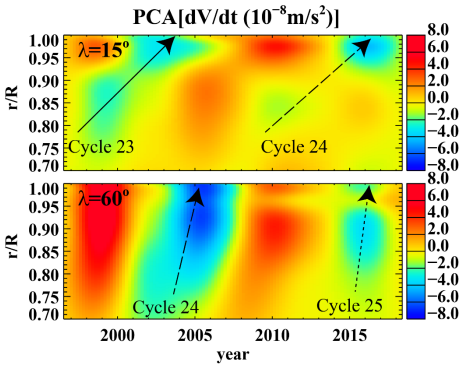

Solar Phys
DOI 10.1007/s11207-016-1008-9

CrossMark

Comparative Analyses of Brookhaven National Laboratory Nuclear Decay Measurements and Super-Kamiokande Solar Neutrino Measurements: Neutrinos and Neutrino-Induced Beta-Decays as Probes of the Deep Solar Interior

P.A. Sturrock[1] · E. Fischbach[2] · J.D. Scargle[3]

Received: 23 March 2016 / Accepted: 20 October 2016

Abstract An experiment carried out at the Brookhaven National Laboratory over a period of almost 8 years acquired 364 measurements of the beta-decay rates of a sample of ^{32}Si and, for comparison, of a sample of ^{36}Cl. The experimenters reported finding "*small periodic annual deviations of the data points from an exponential decay… of uncertain origin*". We find that power-spectrum and spectrogram analyses of these datasets show evidence not only of the annual oscillations, but also of transient oscillations with frequencies near 11 year^{-1} and 12.5 year^{-1}. Similar analyses of 358 measurements of the solar neutrino flux acquired by the Super-Kamiokande neutrino observatory over a period of about 5 years yield evidence of an oscillation near 12.5 year^{-1} and another near 9.5 year^{-1}. An oscillation near 12.5 year^{-1} is compatible with the influence of rotation of the radiative zone. We suggest that an oscillation near 9.5 year^{-1} may be indicative of rotation of the solar core, and that an oscillation near 11 year^{-1} may have its origin in a tachocline between the core and the radiative zone. Modulation of the solar neutrino flux may be attributed to an influence of the Sun's internal magnetic field by the Resonant Spin Flavor Precession (RSFP) mechanism, suggesting that neutrinos and neutrino-induced beta decays can provide information about the deep solar interior.

Inner tachocline?

P.A. Sturrock *et al.*

Figure 15 Equatorial cut of the conjectured internal rotation of the Sun.

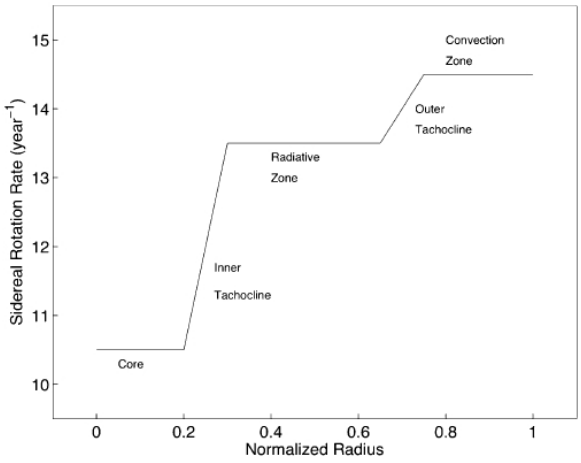

Lecture 20
Overview of local helioseismology

(Stix, Chapter 5.3.8-5.3.9; Kosovichev, p.53-64;
Christensen-Dalsgaard, Chapter 8)

Class plan

- Nov.22 – HW2+Quiz3. Lec. 21. Local Helioseismology I.
- Nov. 23 – Lec. 22 Local Helioseismology II.
- Nov. 29 – Work on the final projects in class
- Nov. 30 – Lec. 23 Solar interior modeling (Prof. Guerrero)
- Dec. 6-7 - Presenation of the final projects

Overview of local helioseismology

Two principal approaches

- Global Helioseismology – measure global oscillation modes from the oscillation power spectra obtained by applying the spherical harmonic transform to the full-disk oscillation data
- Local Helioseismology - measure variations of oscillation frequencies in local areas by applying the Fourier transform to the oscillations in these area, or by measuring the travel times of phase shifts in local areas.

Methods of local-area helioseismology:

Method	Observable	Inferences
Ring-diagram analysis (Gough, Hill, November, Toomre, 1981)	Local variations of oscillation frequencies	Large-scale sound speed perturbations and horizontal flows
Time-distance helioseismology (Duvall et al. 1993)	Phase and group travel times of acoustic and surface gravity waves	3D sound speed, density and flows
Acoustic Imaging (Chou, LaBonte, et al. 1990)	Phase and amplitude variations	3D sound speed and flows
Acoustic Holography (Lindsey & Braun, 1990)	Phase and amplitude variations	Phase variations and amplitude maps

Input Data

Dopplergrams-

observational requirements:

- long duration (>4 hours)
- high-resolution (0.5 arcsec per pixel)
- high-cadence (45-sec cadence)
- stability

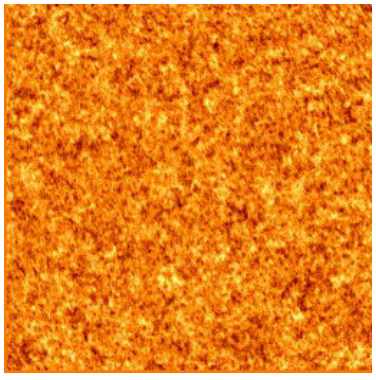

SDO high-resolution Dopplergrams

3D Power Spectrum

Velocity of oscillations $v(x, y, t)$ can be represented in terms of its Fourier components:

$$a(k_x, k_y, \omega) = \iiint v(x, y, t) e^{i(k_x x + k_y y + \omega t)} dx dy dt,$$

where k_x and k_y are components of the wave vector, ω is the frequency.

The power spectrum is:

$P(k_x, k_y, \omega) = a^* a,$

where a^* is complex conjugate.

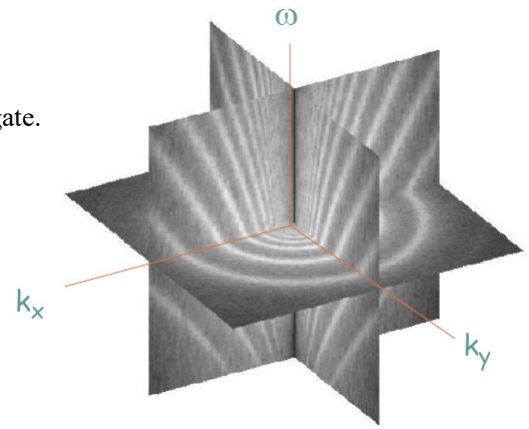

Compare with the global oscillation power spectrum

Spectrum of global oscillations of the sphere

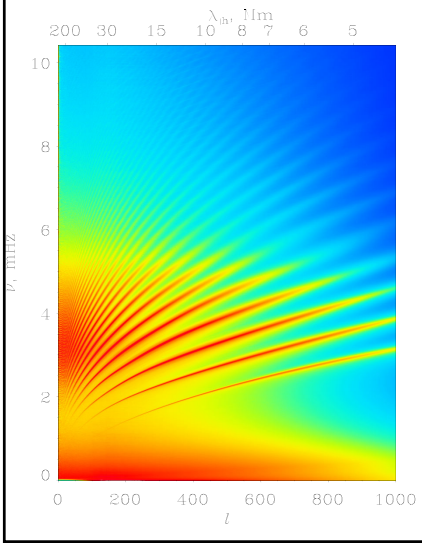

Spectrum of oscillations in a local area

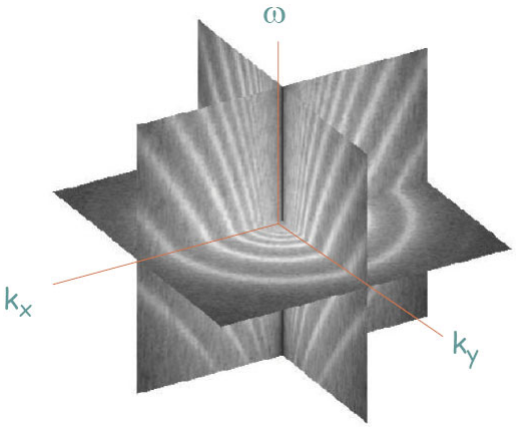

Cuts of the local power spectra at constant frequencies produce rings

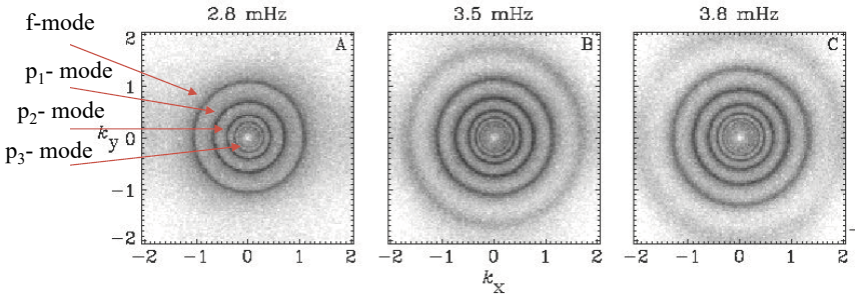

Flows cause displacement of rings (Doppler shift of solar waves)

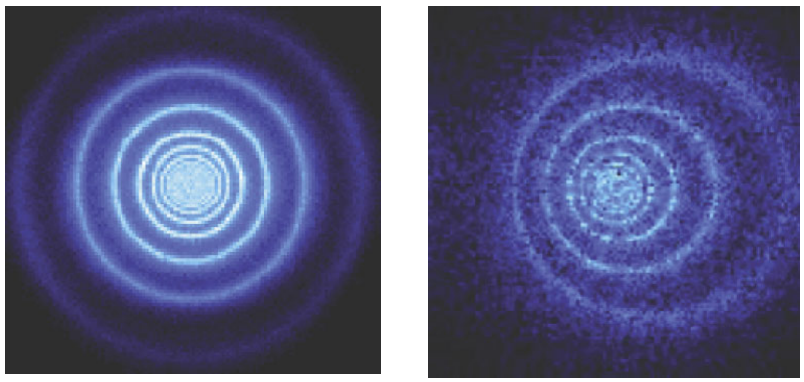

$$(\omega - k_x U)^2 = \omega_c^2 + c^2 k^2$$

Frequency shift caused by flow with velocity U along x-axis. By measuring the shift for various modes one can determine the depth dependence of U.

Ring-Diagram Analysis

The ring-diagram method is based on inversion of the local dispersion relation (3D power spectrum) for acoustic waves.

Perturbation to the local variation in frequency of the component of the wave pattern whose local horizontal wave number is k is given by

$$\frac{\Delta\omega}{\omega} = \frac{\vec{k}}{\omega}\int B\vec{U}dz + \int F\frac{\delta c^2}{c^2}dz + \int G\frac{\delta\gamma}{\gamma}dz$$

$\vec{U}$ is the horizontal component of flow velocity, $\delta c^2/c^2$ and $\delta\gamma/\gamma$ are perturbations to the local sound speed and adiabatic exponent; B(z), F(z), and G(z) are the sensitivity functions that are similar to the global helioseismology Using this equation one can infer the horizontal flow velocity and sound-speed perturbations averaged over some areas (15^ox15^o) as a function of depth.

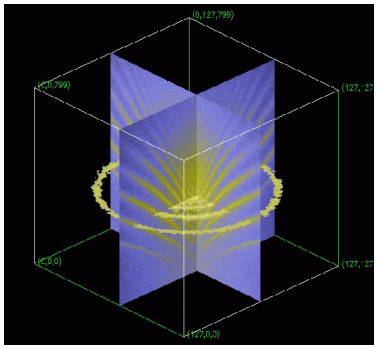

Local 3D power spectrum of acoustic waves as a function of horizontal wave numbers k_x, k_y (horizontal axes) and frequency ω (vertical axis).

Time-distance helioseismology

Measures travel times of acoustic or surface gravity waves propagating between different surface points through the interior. The travel times τ depend on conditions, flow velocity U and sound speed variations c along the ray path Γ.

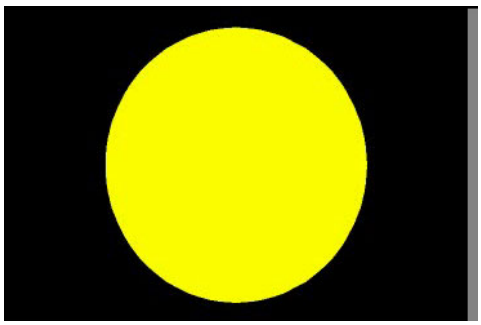

In practice, travel-time variations are measured:

$$\delta\tau = -\int_\Gamma \frac{k}{\omega}\frac{\delta c}{c}ds - \int_\Gamma \frac{\left(\vec{n}\cdot\vec{U}\right)}{c^2}ds$$

ω/k is the wave phase speed

$\vec{n}$ is a unit vector along the ray path.

Time-distance diagnostics

- Using the time-distance diagram one can measure the travel time of acoustic waves for various distances, and then infer the sound speed along the wave paths.
- Can we measure the travel times by using the stochastic wave field continuously generated by the turbulent convection?

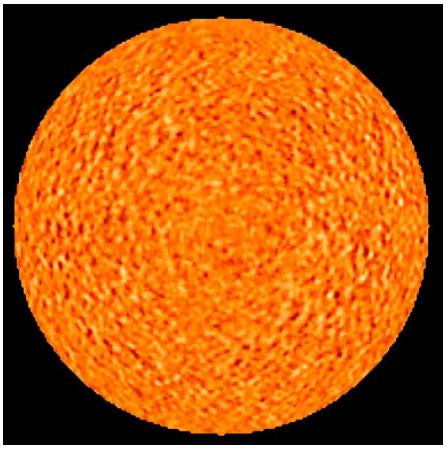

Time-distance helioseismology

A remarkable discovery was made by Tom Duvall in 1993 that the travel times of the solar waves can be measured by using a cross-covariance function of the stochastic wave field:

$$\psi(\tau,\Delta)=\int_0^T f(t,r)\,f^*(t+\tau,r+\Delta)\,dt$$

Integration time

or C(¿; ¢)

Time

Distance

Oscillation signal (Doppler velocity, intensity etc) at two points on the Sun's surface

Time-distance measurements

Travel times are determined from the cross-covariance function:

$$\psi(\tau,\Delta)=\int_0^T f(t,r)f^*(t+\tau,r+\Delta)dt$$

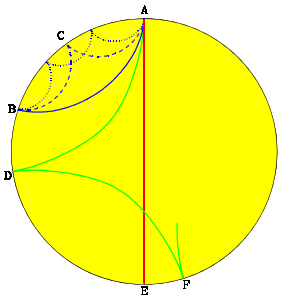

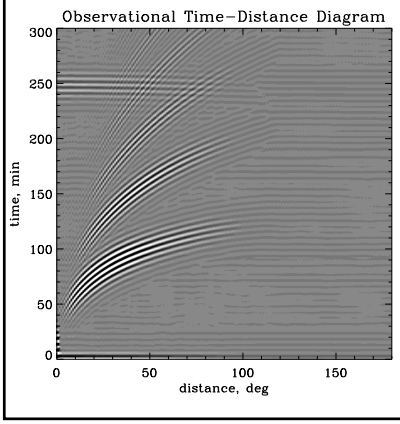

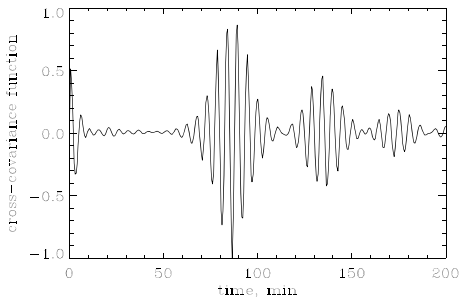

Cross-covariance function for a particular distance (30 degrees in this case) represents a series of wave packets.

Simple interpretation of time-distance measurements

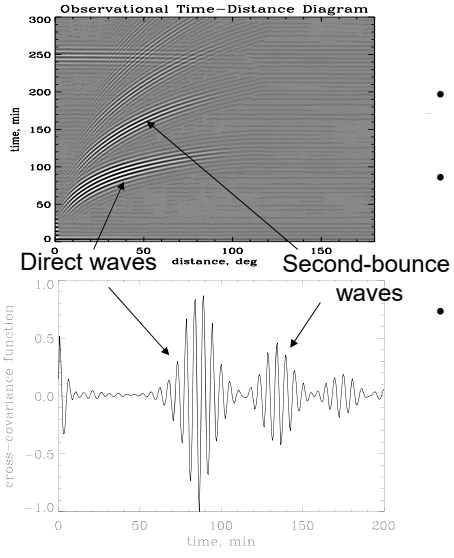

- The cross-covariance function collects coherent signals for solar waves excited at a given point and traveling to another point
- The cross-covariance signal corresponds to a strong point source (similar to the flare signal) – Claerbout's conjecture
- The cross-covariance signal corresponds to a wave packet of waves in a finite frequency range. The solar oscillations have periods around 5 min. Thus, we see the 5-min periodicity in the wave packet.
- The cross-covariance function can be used for measuring group and phase travel times.

We measure the group and phase travel times from these diagrams.

Two levels of time-distance helioseismology

- Minimalist approach (the next 3 slides)
- Lots and lots of math
  - relationship between oscillation frequencies and travel times (ray-mode duality)
  - calculations of the ray paths
  - Fermat's principle
  - magnetic field effects and diagnostics
  - finite wavelength effects (Born approximation, banana-doughnut kernels)
  - phase-speed filtering
  - inversion methods (multi-channel deconvolution, LSQR), etc
  - Ref. http://soi.stanford.edu/papers/dissertations/
    - Peter Giles, Thesis, 1999
    - Aaron Birch, Thesis, 2002
    - Laurent Gizon, Thesis, 2003
    - Junwei Zhao, Thesis, 2004

Time-distance inferences of the sound speed and flow velocity

Measures travel times of acoustic or surface gravity waves propagating between different surface points through the interior. The travel times depend on conditions, flow velocity and sound speed along the ray path:

$$\delta\tau = -\int_\Gamma \frac{k}{\omega}\frac{\delta c}{c}\,ds - \int_\Gamma \frac{\left(\vec{n}\cdot\vec{U}\right)}{c^2}\,ds$$

The sound speed and flow velocity signals are separated by measuring the travel times for waves propagating in the opposite directions along the same ray paths and calculating the mean travel times and the differences:

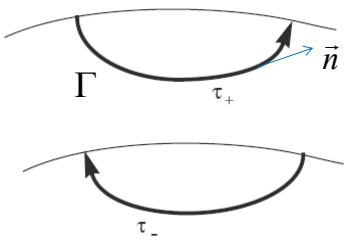

$$\delta\tau_{\text{mean}} = \frac{1}{2}(\tau_+ + \tau_-) = -\int_\Gamma \frac{k}{\omega}\frac{\delta c}{c}\,ds$$

$$\delta\tau_{\text{diff}} = \tau_+ - \tau_- = -\int_\Gamma \frac{\left(\vec{n}\cdot\vec{U}\right)}{c^2}\,ds$$

Vector velocity measurement scheme

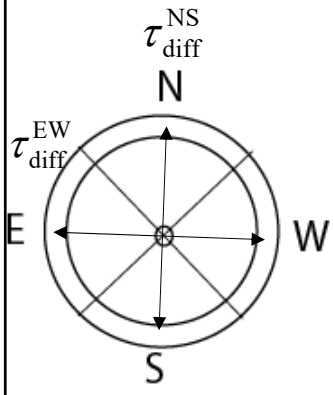

τ^{oi}_{diff} is a travel time difference averaged over the full annulus.

Typically, we measure times for acoustic waves to travel between points on the solar surface and surrounding quadrants symmetrical relative to the North, South, East and West directions. In each quadrant, the travel times are averaged over narrow ranges of travel distance Δ.

Then, the times for northward-directed waves are subtracted from the times for south-directed waves to yield the time, τ^{NS}_{diff}, which predominantly measures north-south motions. Similarly, the time differences, τ^{EW}_{diff}, between westward- and eastward directed waves yields a measure of east-ward motion. The time, τ^{oi}_{diff}, between outward- and inward-directed waves, averaged over the full annuli, is mainly sensitive to vertical motion and the horizontal divergence.

This provides a qualitative picture of the motions, and is useful for a preliminary analysis. However, in numerical inversions, all three components of the flow velocity are properly taken into account. The averaging procedure is essential for reducing noise in the data.

Tomographic Inversion

We assume that the convective structures and flows do not change during the observations and represent them by a discrete model. In the model, the 3D region of wave propagation is divided into rectangular blocks. The perturbations of the sound speed and the three of the flow velocity are approximated by linear functions of coordinates within each block, e.g.

$$\delta c(x,y,z) = \sum c_{ijk}\left[1-\frac{|x-x_i|}{x_{i+1}-x_i}\right]\left[1-\frac{|y-y_j|}{y_{j+1}-y_j}\right]\left[1-\frac{|z-z_k|}{z_{k+1}-z_k}\right]$$

According to the averaging procedure of the cross-covariance function, the travel time measured at a point on the surface is the result of the cumulative effects of the perturbations in each of the traversed rays of the 3D ray systems (see Figure below). Therefore, we average the equations for $\delta\tau$ over the ray systems corresponding to the different radial distance intervals of the data, using approximately the same number of ray paths as in the observational procedure. As a result, we obtain two systems of linear equations that relate the data to the sound speed variation and to the flow velocity, e.g. for the sound speed

$$\delta\tau_{\lambda\mu\nu} = \sum_{ijk} A^{ijk}_{\lambda\mu\nu}\ \delta c_{ijk}$$

where matrix A maps the structure properties into the observed travel time variations, λ and μ define the location of the central point of a ray system on the surface, and ν labels surrounding annuli. The equation is solved by a regularized least-squares technique.

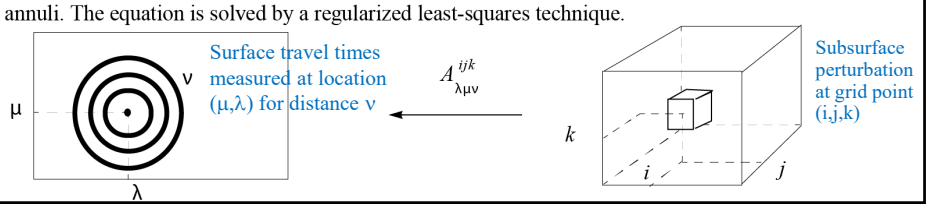

Deep- and surface-focusing observing schemes

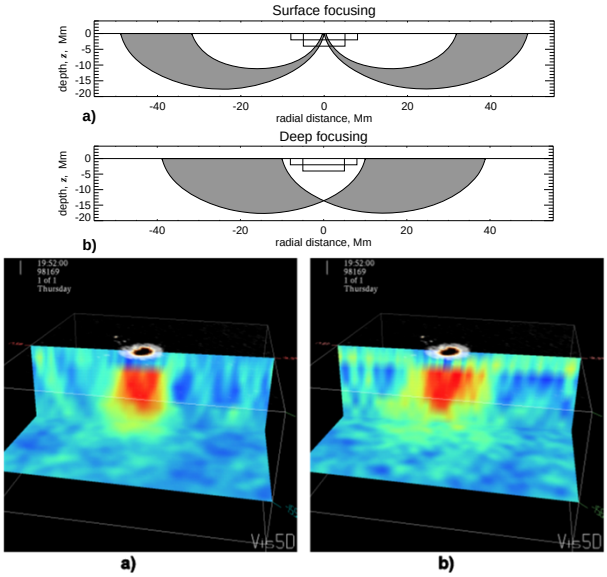

Helioseismic holography

The idea of helioseismic holography is to reconstruct the acoustic wave field at particular locations beneath the surface by using measurements on the surface and a theoretical Green's functions for the wave propagation from point sources.

The ingression and egression estimate of the wave field at some point in the solar interior assuming that the observed wave field resulted entirely from waves diverging from that point (for the egression) or waves converging towards that point (for the ingression). Egression propagates signals back in time.

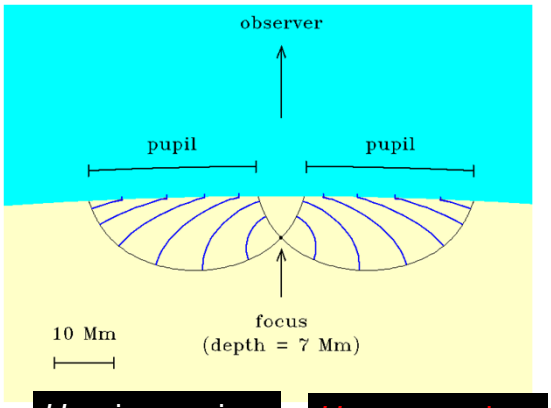

H_- = ingression H_+ = egression

$$H_{\pm}(\mathbf{r},z,t) = \int_P d^2\mathbf{r}'\ G_{\pm}(\mathbf{r},\mathbf{r}',z,t)\,\psi(\mathbf{r}',t)$$

(z = depth, **r** = horizontal position, ψ= surface amplitude, $G_{\pm}$= Greens' functions)

(Lindsey & Braun, 1990)

The ingression and egression power is sensitive to sources, sinks at focus.

Far-side imaging with helioseismic holography

Helioseismic holography is used to obtain images of solar active region on the far-side of the Sun by placing the focal point on the far-side surface.

The analysis on calculations of the phase shift (or equivalent travel time) between the ingression and egression signals.

1. egression, ingression:

$$H_{\pm}(\mathbf{r},z,\nu)=\int_P d^2\mathbf{r}'\;\; G_{\pm}(\mathbf{r},\mathbf{r}',z,\nu)\,\psi(\mathbf{r}',\nu)$$

2. correlation:

$$C(\mathbf{r},z,\nu)\equiv H_{+}(\mathbf{r},z,\nu)\;H_{-}^{*}(\mathbf{r},z,\nu)$$

3. correlation phase:

$$\varphi(\mathbf{r},z)=\arg\left(\left\langle C(\mathbf{r},z,\nu)\right\rangle_{\Delta\nu}\right)$$

4. travel-time perturbation:

$$\delta t(\mathbf{r},z)=\varphi(\mathbf{r},z)/2\pi\nu_{\circ}$$

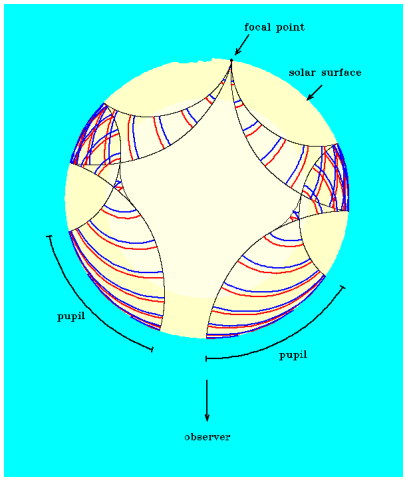

Lindsey & Braun 2000, *Science* **287**, 1799

Daily far-side imaging data are used for space-weather forecasts because most solar storms are produced by active regions

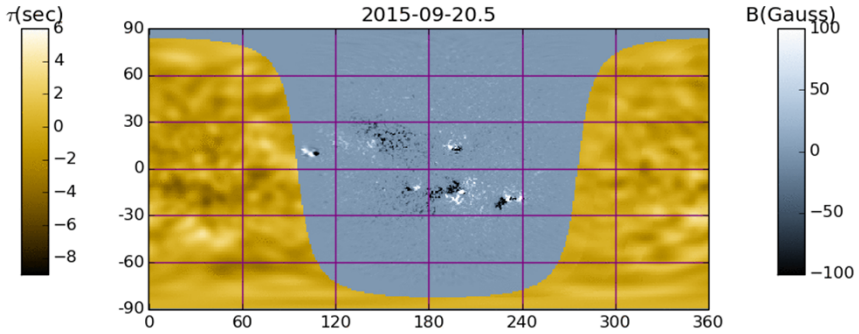

Composite Map of Far and Near Solar Hemispheres. Line-of-sight magnetic field in the Sun's near hemisphere is rendered in blue-gray, in Gauss. Seismic map of the Sun's far hemisphere is rendered in yellow. The far-side seismic image maps a phase shift between solar acoustic noise with periods of about five minutes embarking into the solar interior from the Sun's near hemisphere and its echos from respective locations in the far hemisphere. This phase shift is expressed here as a travel-time perturbation in seconds.

http://jsoc.stanford.edu/data/farside/

http://gong.nso.edu/data/farside

Diagnostics of sunspots and emerging active regions

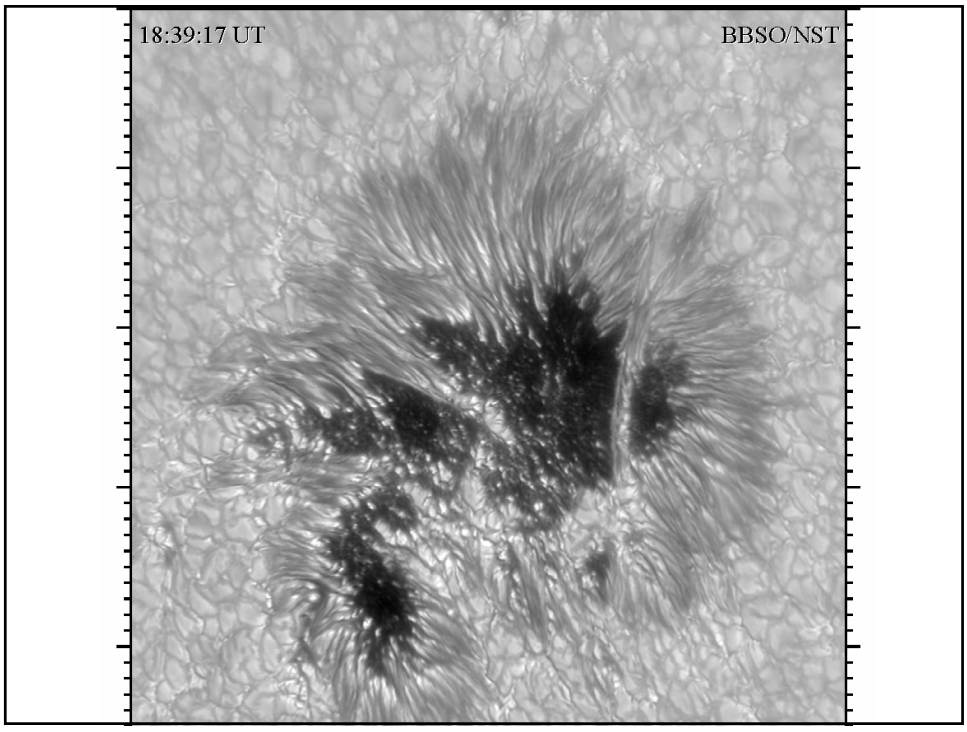

Flow patterns under the sunspot

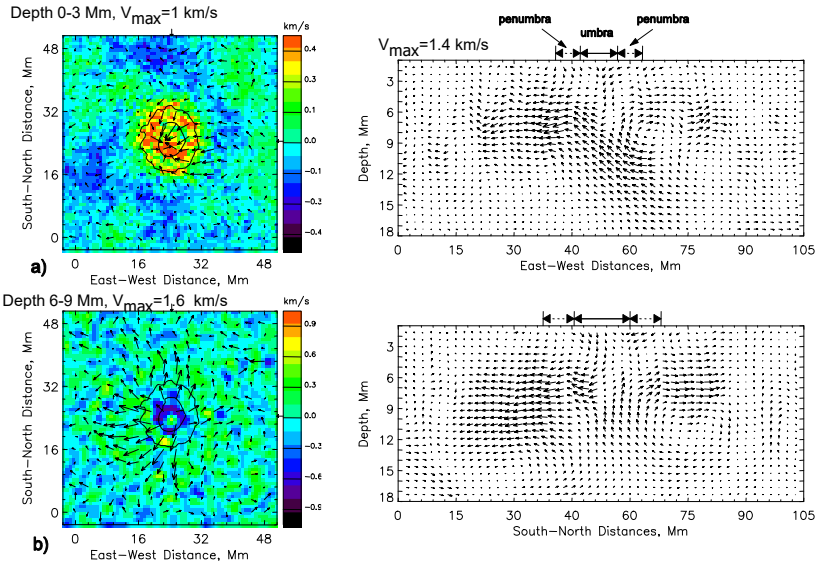

Observations of emerging active region by time-distance helioseismology

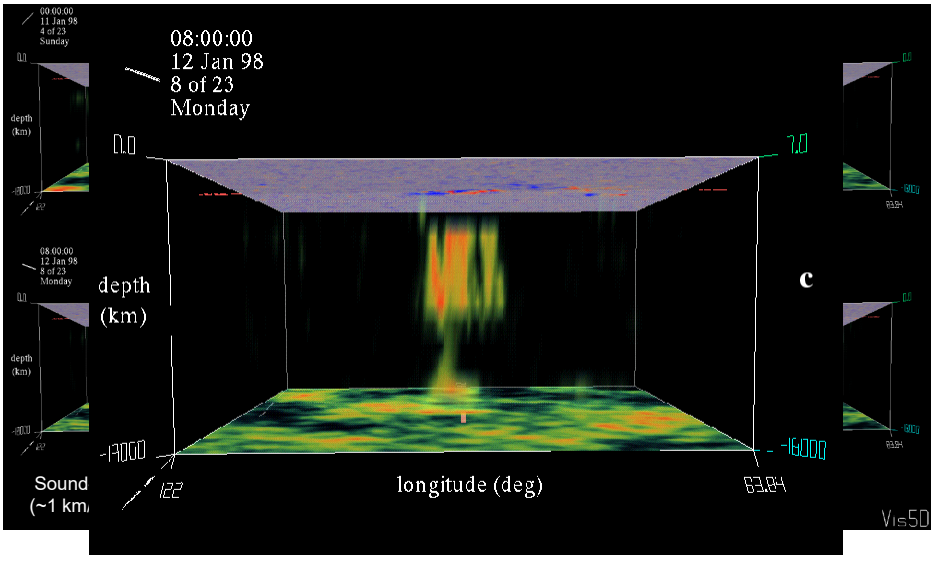

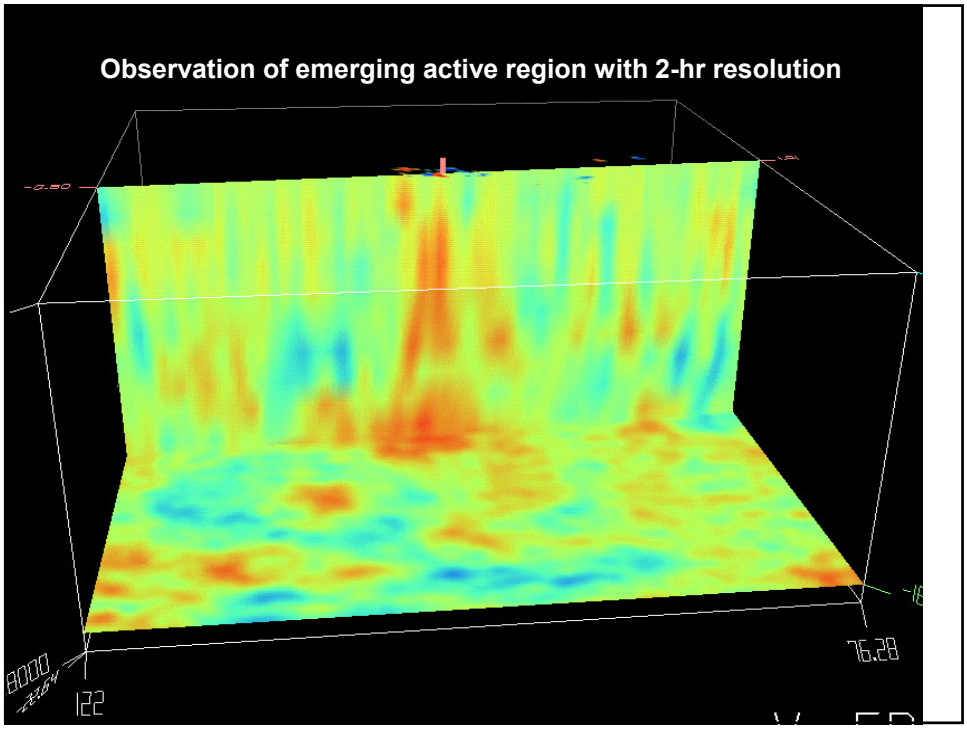

Subphotospheric imaging of active regions

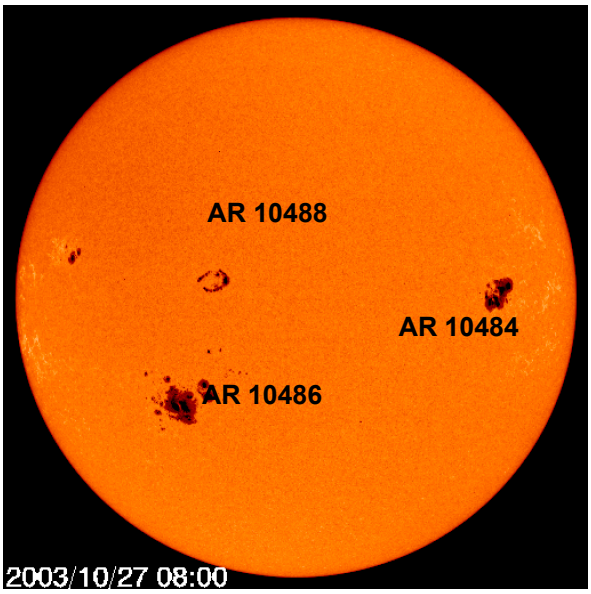

Evolution of AR 10486-488: October 24 – November 2, 2003

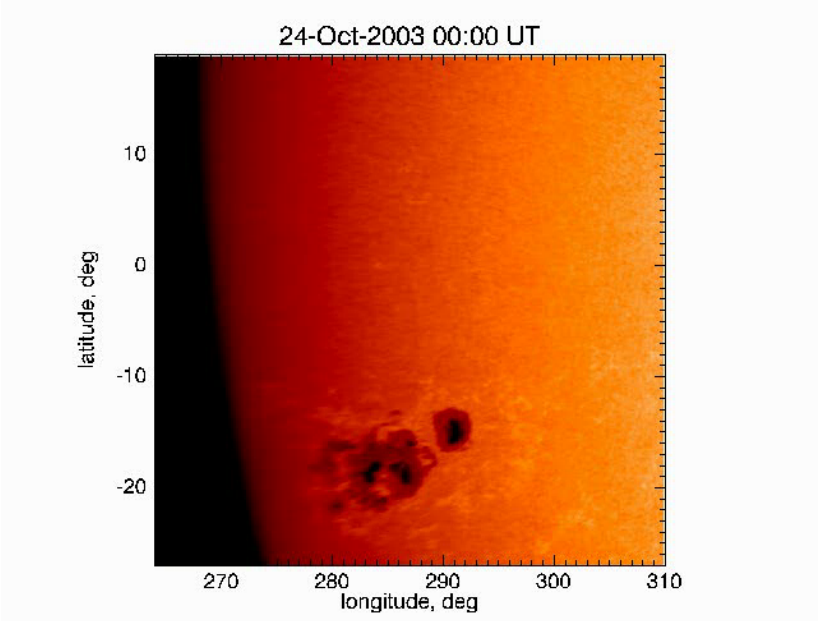

Sound-speed map and magnetogram of AR 10486 on October 25, 2003, 4:00 UT
(depth of the lower panel: 45 Mm)

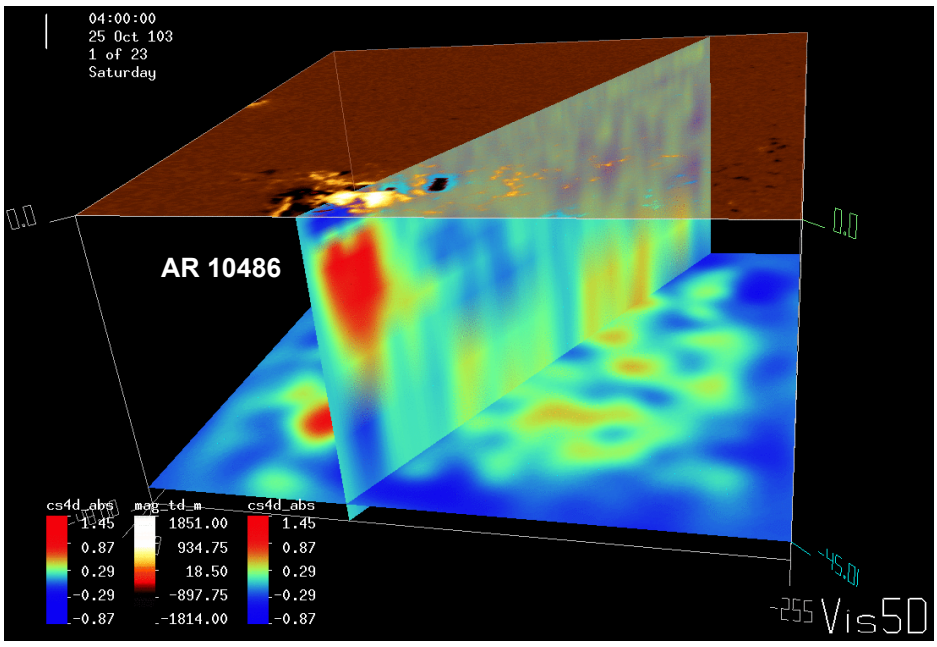

Sound-speed map and magnetogram of AR 10486 on October 26, 2003, 12:00 UT
AR 10488 is emerging

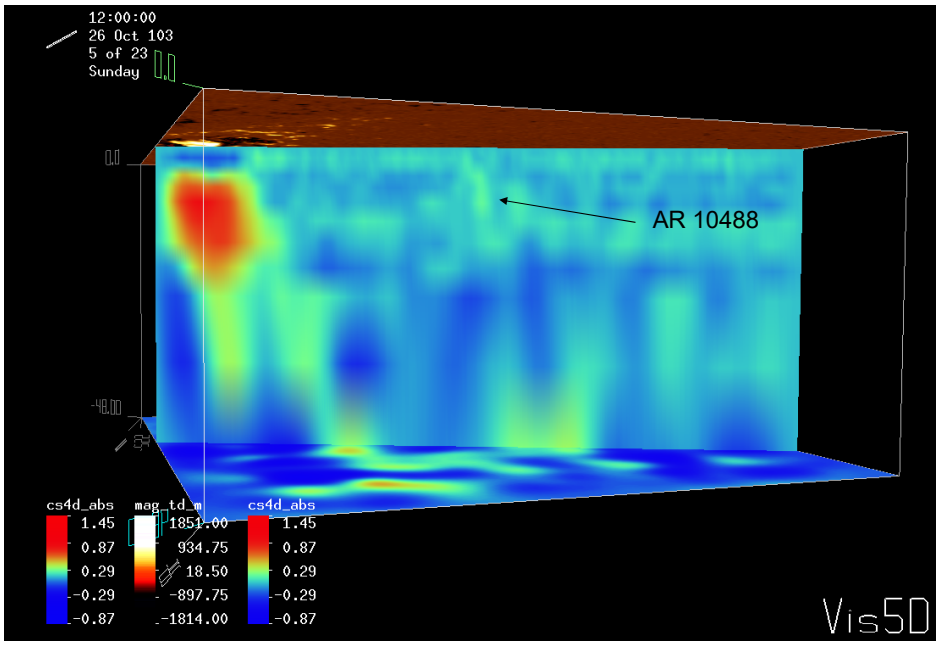

Emergence of AR 10488, October 26, 2003, 20:00 UT

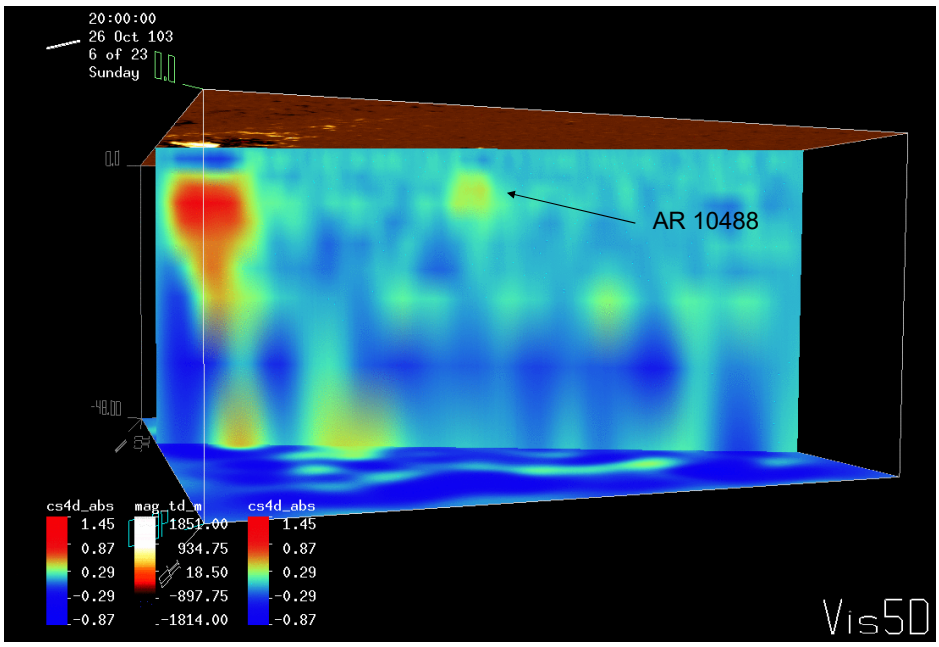

Emergence of AR 10488, October 26, 2003, 20:00 UT

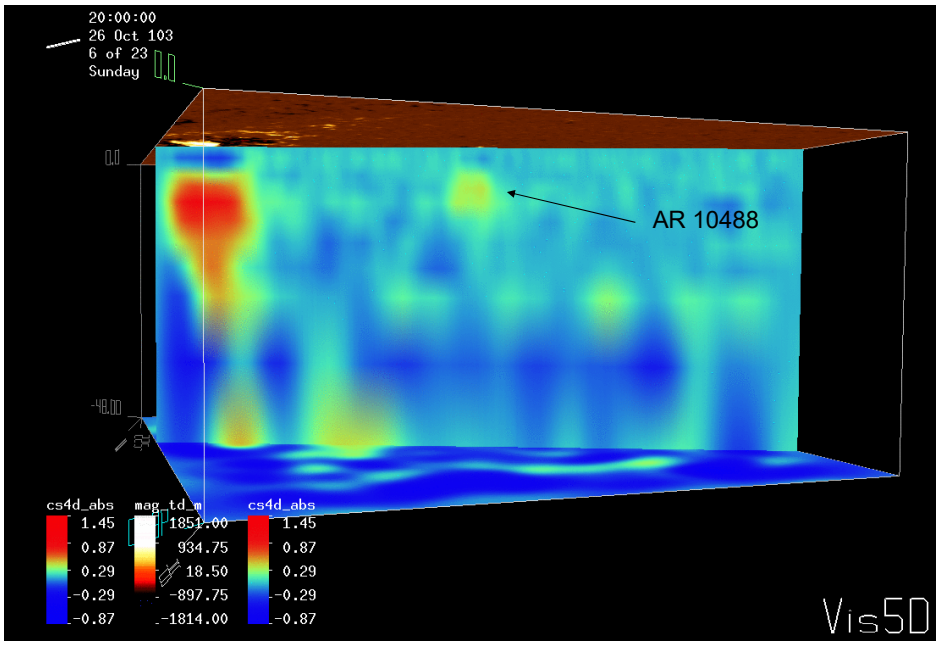

Emergence of AR 10488, October 27, 2003, 4:00 UT

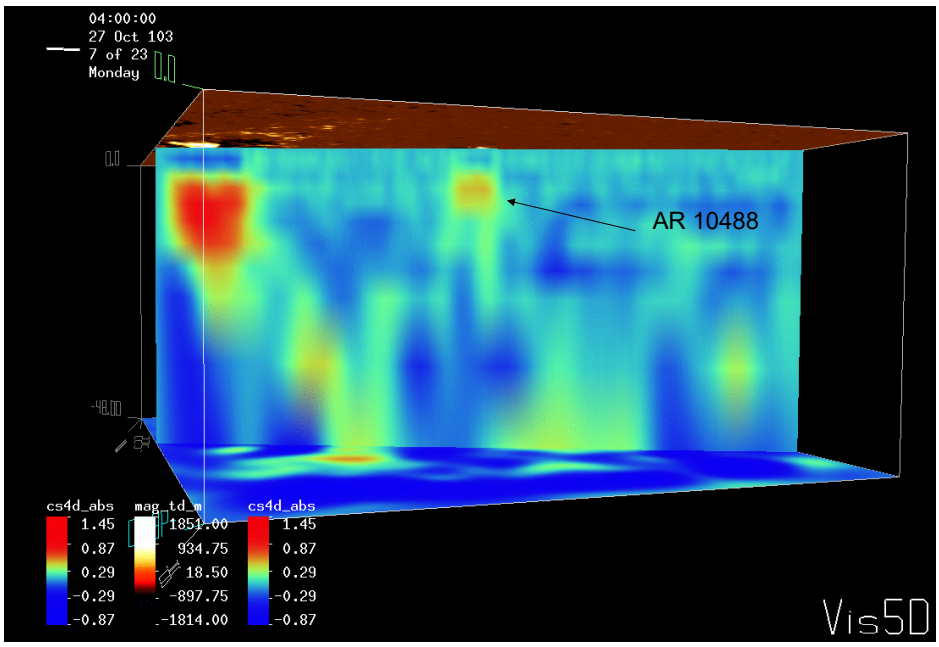

Growth and formation of sunspots of AR 10488, October 29, 2003, 4:00 UT

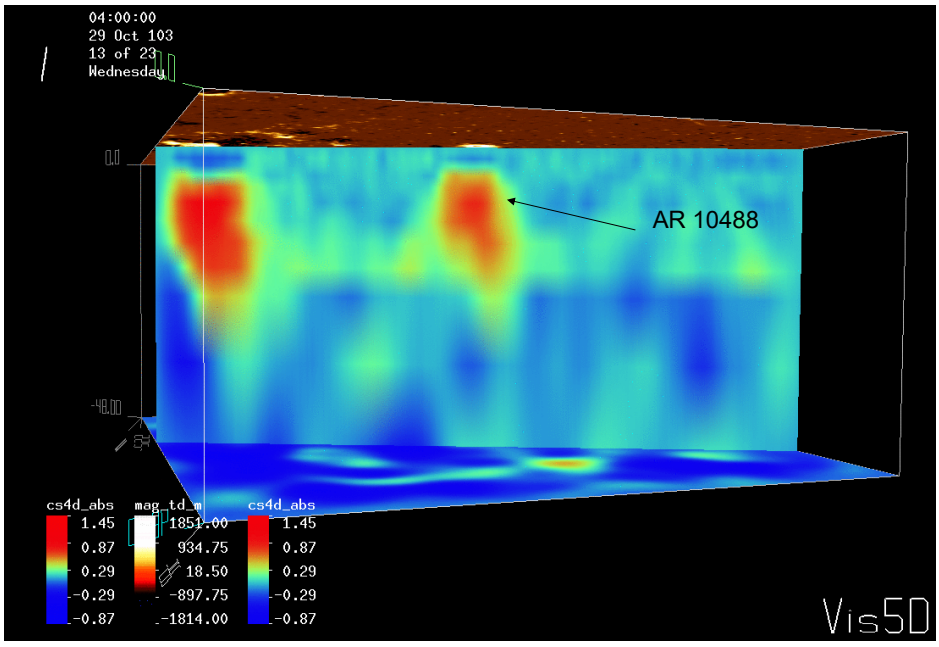

Growth and formation of sunspots of AR 10488, October 31, 2003, 12:00 UT

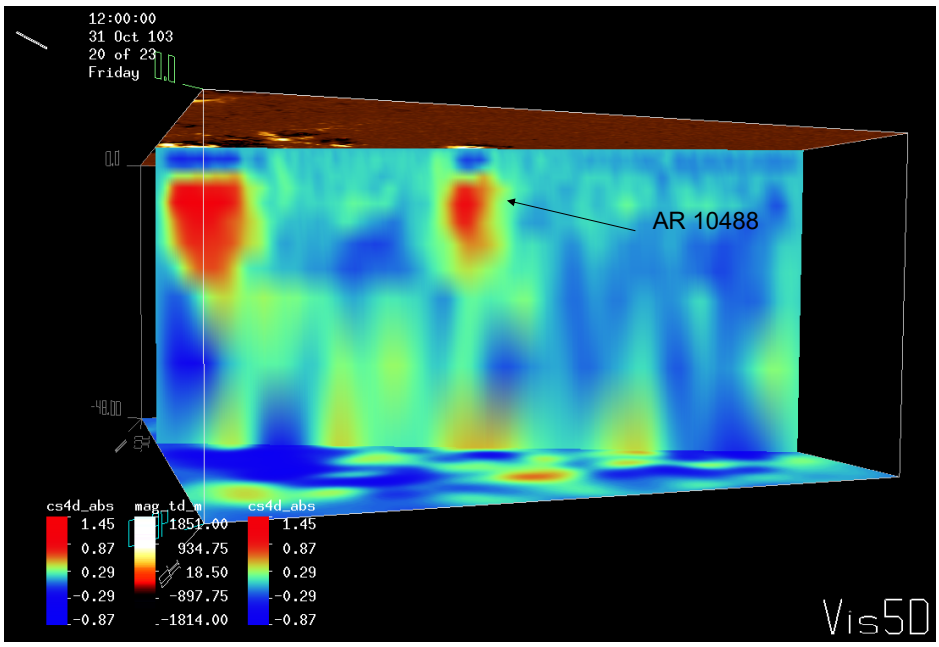

Cut in East-West direction through both magnetic polarities, showing a loop-like structure beneath AR 10488, October 30, 2003, 20:00 UT

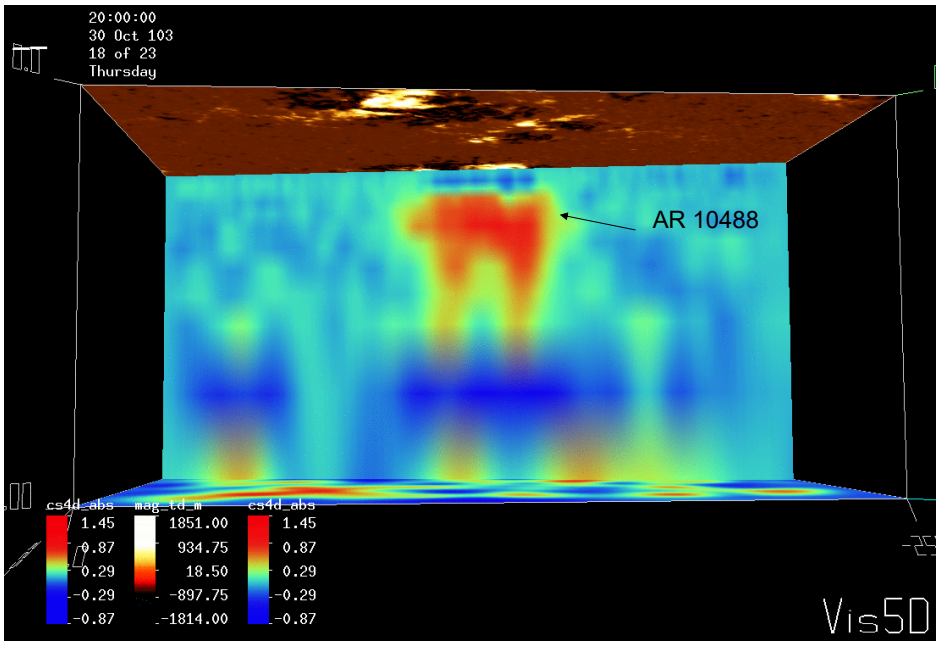

New helioseismology method of detection of emerging magnetic flux inside the Sun

Deep-focus Time-Distance Helioseismology: solar oscillation signal is filtered to select acoustic waves traveling to depth 40-70 Mm (right), averaged over arcs (left), and cross-correlated for opposite arcs. Travel-time perturbations are measured by fitting Gabor wavelet. This method has been tested with 3 different instruments (MDI, HMI, GONG) for many quiet and emerging flux regions.

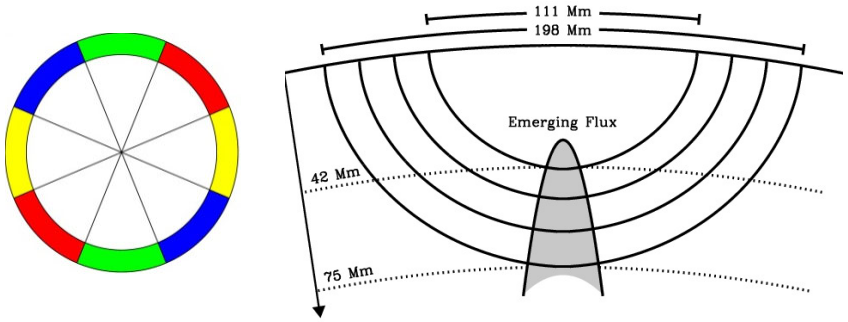

Ilonidis, et al., 2011; Stefan, 2020

Results of ARs 10488, 8164, 8171, 7978

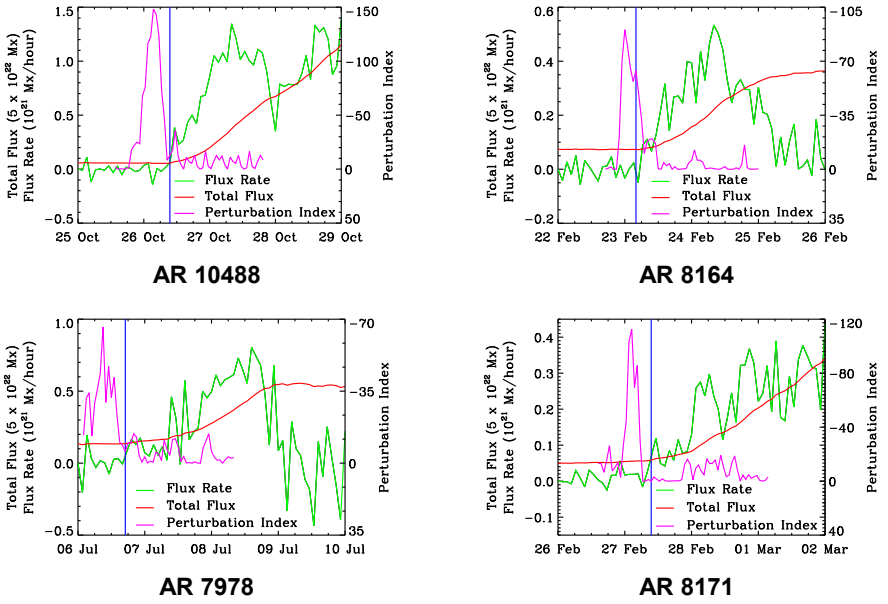

Active region NOAA 1158, February 2011

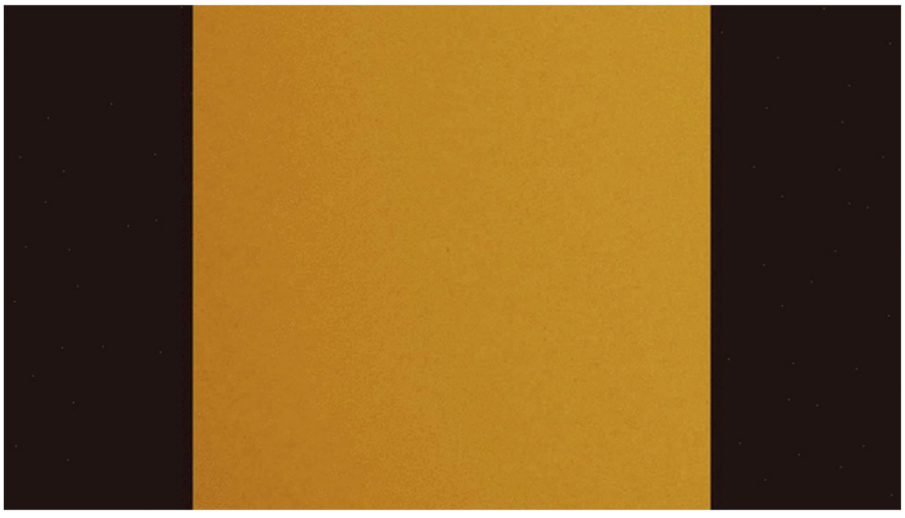

Solar Subsurface Weather

Synoptic maps of subsurface flows (0-20 Mm)

Depth 2 Mm

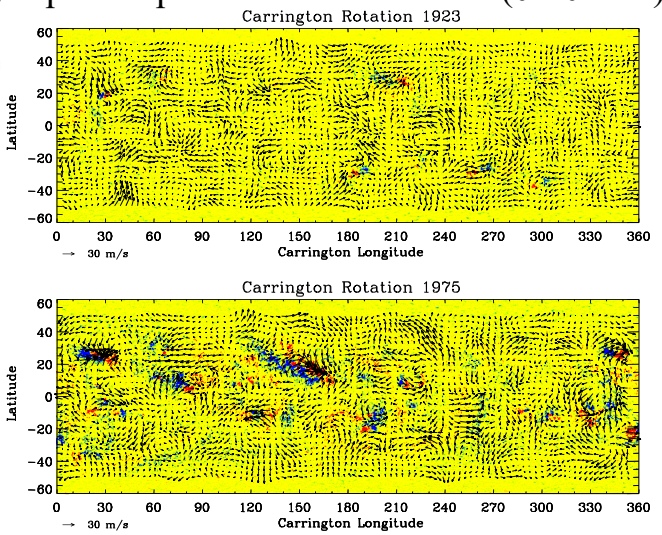

Similar maps are obtained from the ring analysis (Haber et al 2002)

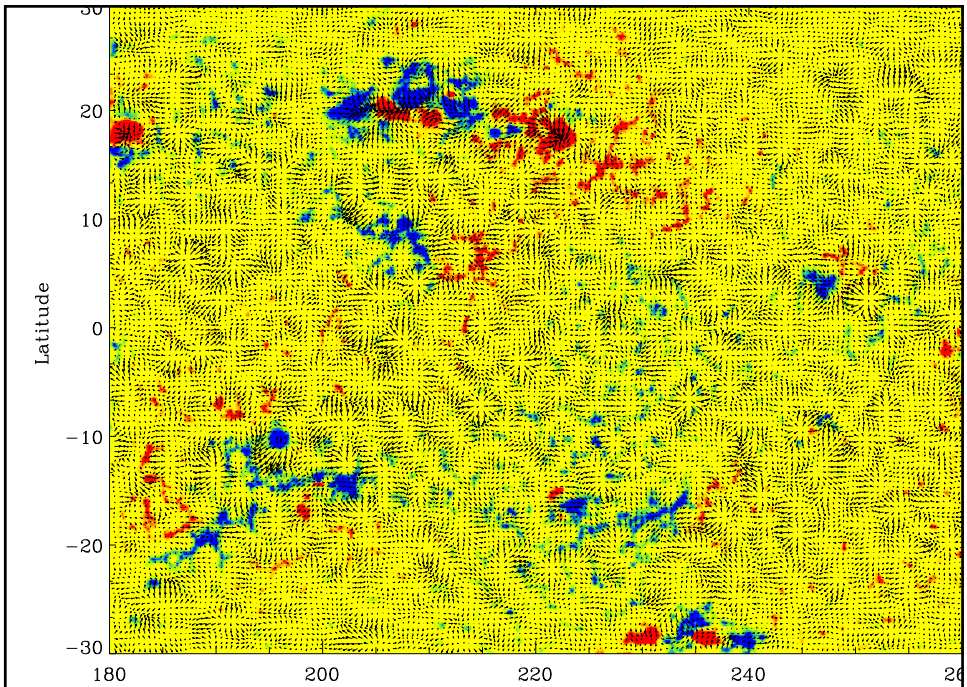

A small sample of a synoptic map of subsurface flows

Global characteristics of the synoptic flows for CR 1923

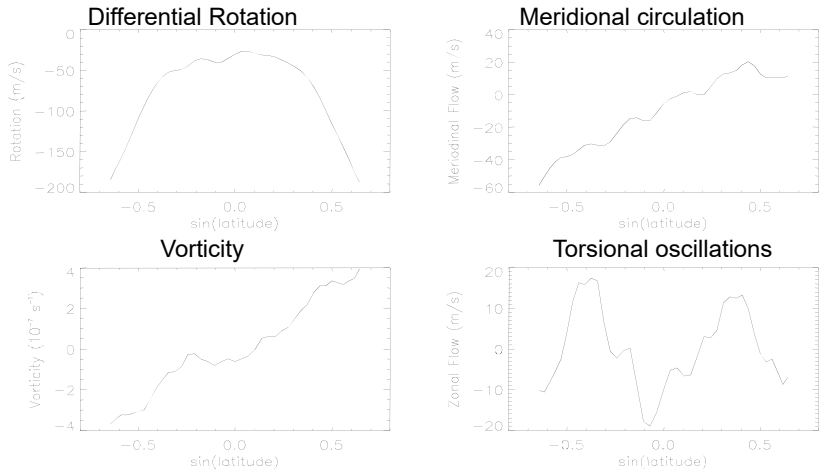

Large-scale flows around active regions:

(example AR9433, April 2001)

- converging 40 m/s flow toward the neutral line in the upper layers
- diverging flow below 9 Mm

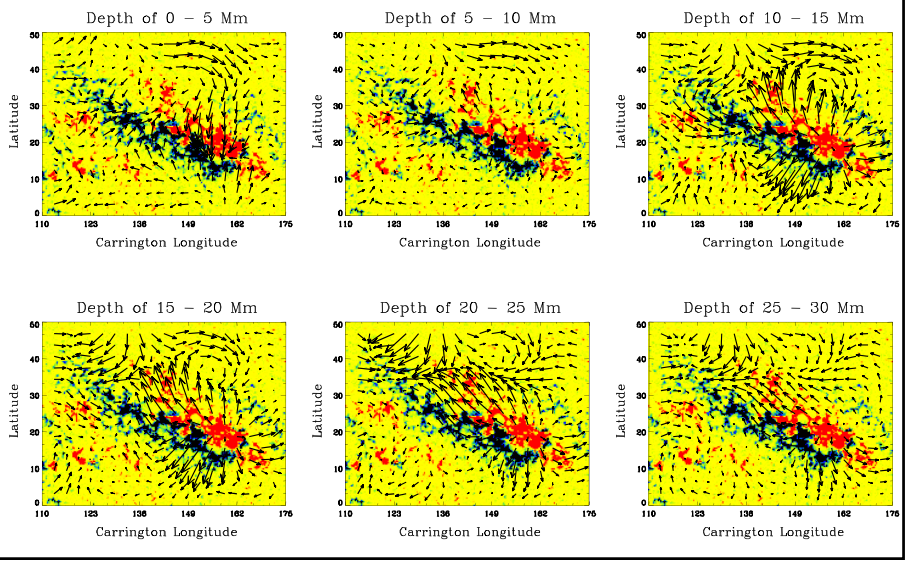

Lecture 21
Time-distance helioseismology

Quiz 3 in Canvas 1:05-1:20pm

Please, upload in Canvas HW2 files by tomorrow
HW2 presentations (Monday Nov.22+ Quiz 3)

- 2.1 (a) Ying
- 2.1 (b) Sheldon
- 2.2 Sadaf
- 2.3 Bhairavi
- 2.4 Yunpeng

Class plan

- Nov.22 – Quiz3+HW3. Lec. 21. Local Helioseismology I.
- Nov. 23 – Lec. 22 Local Helioseismology II.
- Nov. 29 – Work on the final projects in class
- Nov. 30 – Lec. 23 Solar interior modeling (Prof. Guerrero)
- Dec. 6-7 - Presenation of the final projects

Overview of local helioseismology

Two principal approaches

- Global Helioseismology – measure global oscillation modes from the oscillation power spectra obtained by applying the spherical harmonic transform to the full-disk oscillation data
- Local Helioseismology - measure variations of oscillation frequencies in local areas by applying the Fourier transform to the oscillations in these area, or by measuring the travel times of phase shifts in local areas.

Methods of local-area helioseismology:

Method	Observable	Inferences
Ring-diagram analysis (Gough, Hill, November, Toomre, 1981)	Local variations of oscillation frequencies	Large-scale sound speed perturbations and horizontal flows
Time-distance helioseismology (Duvall et al. 1993)	Phase and group travel times of acoustic and surface gravity waves	3D sound speed, density and flows
Acoustic Imaging (Chou, LaBonte, et al. 1990)	Phase and amplitude variations	3D sound speed and flows
Acoustic Holography (Lindsey & Braun, 1990)	Phase and amplitude variations	Phase variations and amplitude maps

3D Power Spectrum

Velocity of oscillations $v(x, y, t)$ can be represented in terms of its Fourier components:

$$a(k_x, k_y, \omega) = \iiint v(x, y, t) e^{i(k_x x + k_y y + \omega t)} dx dy dt,$$

where k_x and k_y are components of the wave vector, ω is the frequency.

The power spectrum is:

$P(k_x, k_y, \omega) = a^* a,$

where a^* is complex conjugate.

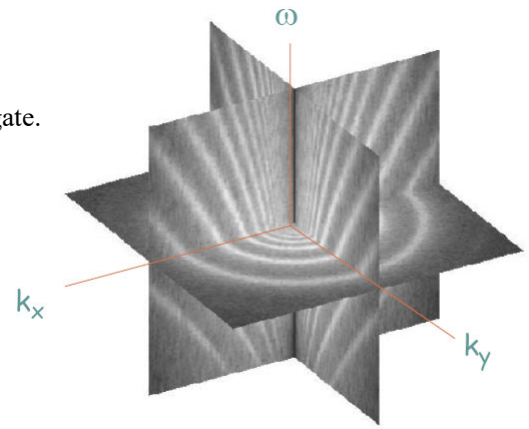

Compare with the global oscillation power spectrum

Spectrum of global oscillations of the sphere

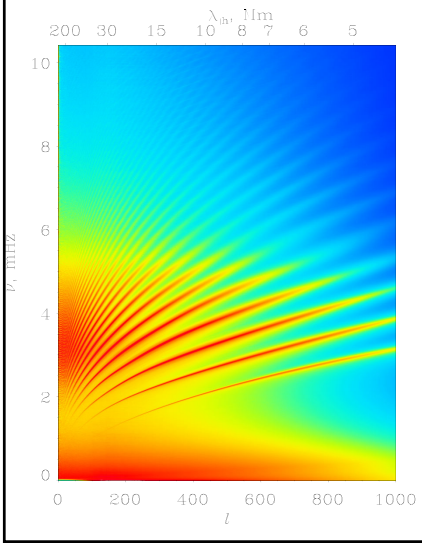

Spectrum of oscillations in a local area

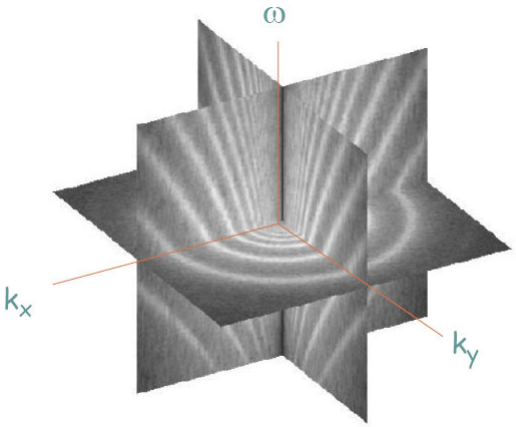

Cuts of the local power spectra at constant frequencies produce rings

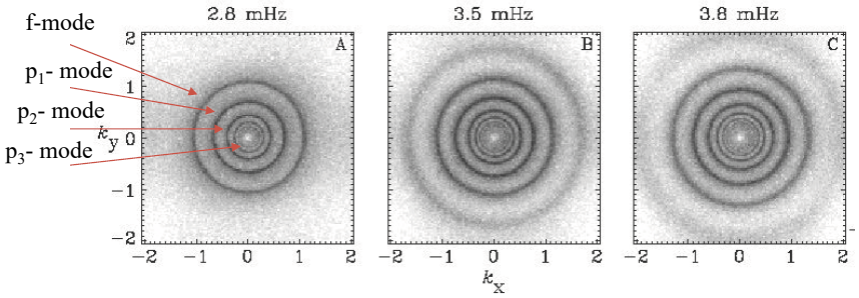

Flows cause displacement of rings (Doppler shift of solar waves)

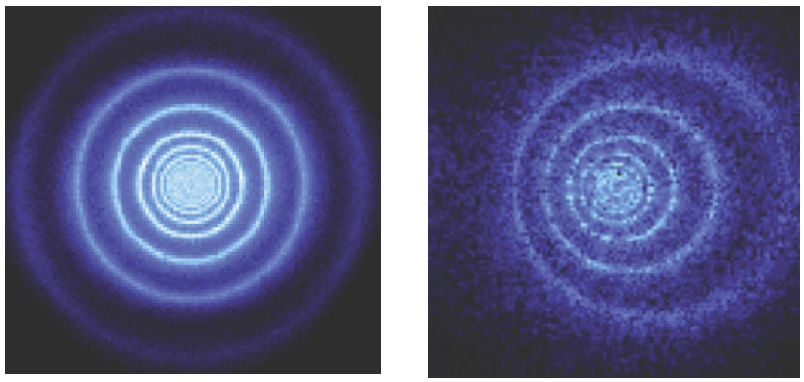

$$(\omega - k_x U)^2 = \omega_c^2 + c^2 k^2$$

Frequency shift caused by flow with velocity U along x-axis. By measuring the shift for various modes one can determine the depth dependence of U.

Ring-Diagram Analysis

The ring-diagram method is based on inversion of the local dispersion relation (3D power spectrum) for acoustic waves.

Perturbation to the local variation in frequency of the component of the wave pattern whose local horizontal wave number is k is given by

$$\frac{\Delta\omega}{\omega} = \frac{\vec{k}}{\omega}\int B\vec{U}dz + \int F\frac{\delta c^2}{c^2}dz + \int G\frac{\delta\gamma}{\gamma}dz$$

$\vec{U}$ is the horizontal component of flow velocity, $\delta c^2/c^2$ and $\delta\gamma/\gamma$ are perturbations to the local sound speed and adiabatic exponent; B(z), F(z), and G(z) are the sensitivity functions that are similar to the global helioseismology Using this equation one can infer the horizontal flow velocity and sound-speed perturbations averaged over some areas (15°x15°) as a function of depth.

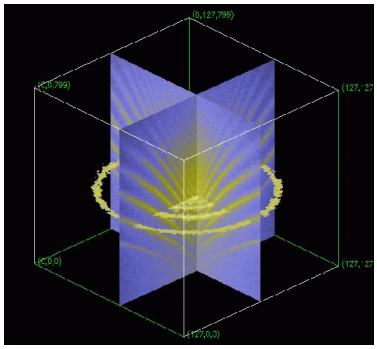

Local 3D power spectrum of acoustic waves as a function of horizontal wave numbers k_x, k_y (horizontal axes) and frequency ω (vertical axis).

Time-distance helioseismology

Measures travel times of acoustic or surface gravity waves propagating between different surface points through the interior. The travel times τ depend on conditions, flow velocity U and sound speed variations c along the ray path Γ.

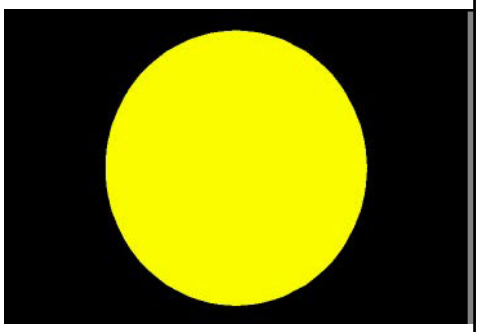

In practice, travel-time variations are measured:

$$\delta\tau = -\int_\Gamma \frac{k}{\omega}\frac{\delta c}{c}ds - \int_\Gamma \frac{\left(\vec{n}\cdot\vec{U}\right)}{c^2}ds$$

ω/k is the wave phase speed

$\vec{n}$ is a unit vector along the ray path.

Time-distance diagnostics

- Using the time-distance diagram one can measure the travel time of acoustic waves for various distances, and then infer the sound speed along the wave paths.
- Can we measure the travel times by using the stochastic wave field continuously generated by the turbulent convection?

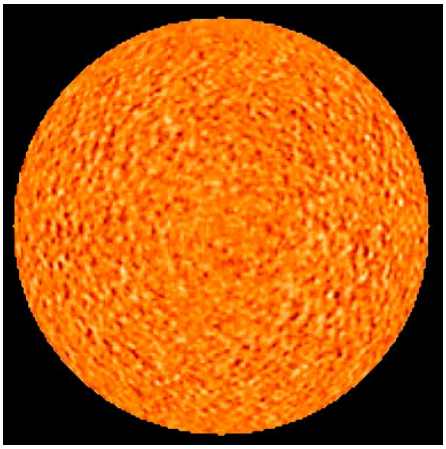

Time-distance helioseismology

A remarkable discovery was made by Tom Duvall in 1993 that the travel times of the solar waves can be measured by using a cross-covariance function of the stochastic wave field:

$$\psi(\tau,\Delta)=\int_0^T f(t,r)\,f^*(t+\tau,r+\Delta)\,dt$$

Integration time

or C(¿; ¢)

Time

Distance

Oscillation signal (Doppler velocity, intensity etc) at two points on the Sun's surface

Time-distance measurements

Travel times are determined from the cross-covariance function:

$$\psi(\tau,\Delta)=\int_0^T f(t,r)f^*(t+\tau,r+\Delta)dt$$

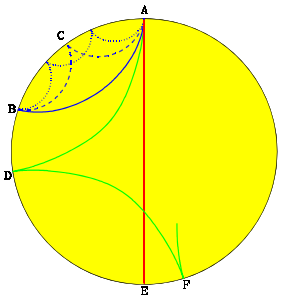

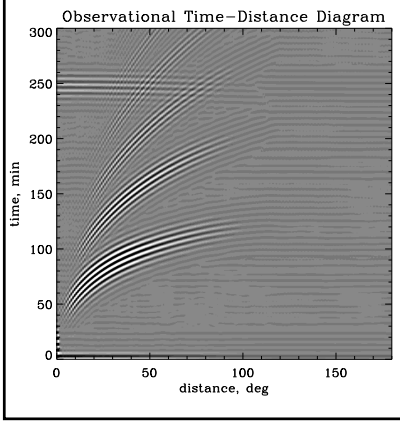

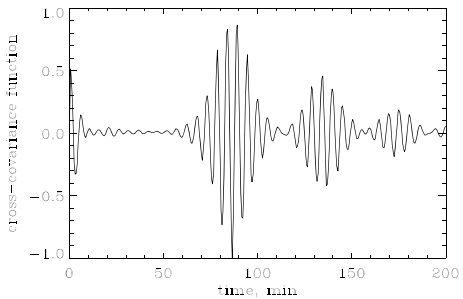

Cross-covariance function for a particular distance (30 degrees in this case) represents a series of wave packets.

Simple interpretation of time-distance measurements

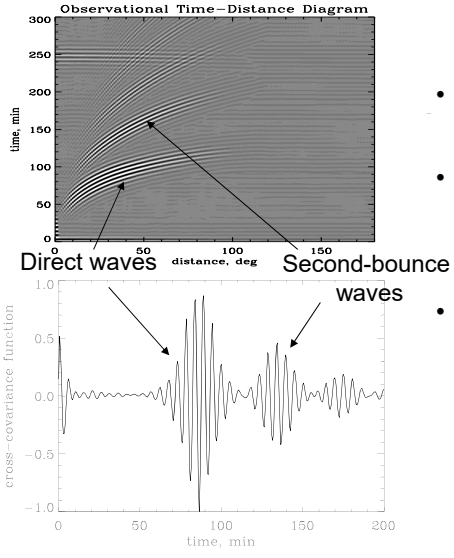

- The cross-covariance function collects coherent signals for solar waves excited at a given point and traveling to another point
- The cross-covariance signal corresponds to a strong point source (similar to the flare signal) – Claerbout's conjecture
- The cross-covariance signal corresponds to a wave packet of waves in a finite frequency range. The solar oscillations have periods around 5 min. Thus, we see the 5-min periodicity in the wave packet.
- The cross-covariance function can be used for measuring group and phase travel times.

We measure the group and phase travel times from these diagrams.

Time-distance inferences of the sound speed and flow velocity

Measures travel times of acoustic or surface gravity waves propagating between different surface points through the interior. The travel times depend on conditions, flow velocity and sound speed along the ray path:

$$\delta\tau = -\int_\Gamma \frac{k}{\omega}\frac{\delta c}{c}\,ds - \int_\Gamma \frac{\left(\vec{n}\cdot\vec{U}\right)}{c^2}ds$$

The sound speed and flow velocity signals are separated by measuring the travel times for waves propagating in the opposite directions along the same ray paths and calculating the mean travel times and the differences:

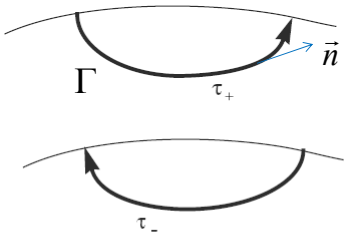

$$\delta\tau_{\text{mean}} = \frac{1}{2}(\tau_+ + \tau_-) = -\int_\Gamma \frac{k}{\omega}\frac{\delta c}{c}\,ds$$

$$\delta\tau_{\text{diff}} = \tau_+ - \tau_- = -\int_\Gamma \frac{\left(\vec{n}\cdot\vec{U}\right)}{c^2}ds$$

Vector velocity measurement scheme

$\tau^{\text{NS}}_{\text{diff}}$

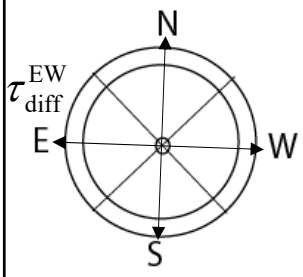

$\tau^{\text{EW}}_{\text{diff}}$

$\tau^{\text{oi}}_{\text{diff}}$

is a travel time difference averaged over the full annulus.

Typically, we measure times for acoustic waves to travel between points on the solar surface and surrounding quadrants symmetrical relative to the North, South, East and West directions. In each quadrant, the travel times are averaged over narrow ranges of travel distance Δ.

Then, the times for northward-directed waves are subtracted from the times for south-directed waves to yield the time, $\tau^{\text{NS}}_{\text{diff}}$, which predominantly measures north-south motions. Similarly, the time differences, $\tau^{\text{EW}}_{\text{diff}}$, between westward- and eastward directed waves yields a measure of east-ward motion. The time, $\tau^{\text{oi}}_{\text{diff}}$, between outward- and inward-directed waves, averaged over the full annuli, is mainly sensitive to vertical motion and the horizontal divergence.

This provides a qualitative picture of the motions, and is useful for a preliminary analysis. However, in numerical inversions, all three components of the flow velocity are properly taken into account. The averaging procedure is essential for reducing noise in the data.

Tomographic Inversion

We assume that the convective structures and flows do not change during the observations and represent them by a discrete model. In the model, the 3D region of wave propagation is divided into rectangular blocks. The perturbations of the sound speed and the three of the flow velocity are approximated by linear functions of coordinates within each block, e.g.

$$\delta c(x,y,z) = \sum c_{ijk}\left[1-\frac{|x-x_i|}{x_{i+1}-x_i}\right]\left[1-\frac{|y-y_j|}{y_{j+1}-y_j}\right]\left[1-\frac{|z-z_k|}{z_{k+1}-z_k}\right]$$

According to the averaging procedure of the cross-covariance function, the travel time measured at a point on the surface is the result of the cumulative effects of the perturbations in each of the traversed rays of the 3D ray systems (see Figure below). Therefore, we average the equations for $\delta\tau$ over the ray systems corresponding to the different radial distance intervals of the data, using approximately the same number of ray paths as in the observational procedure. As a result, we obtain two systems of linear equations that relate the data to the sound speed variation and to the flow velocity, e.g. for the sound speed

$$\delta\tau_{\lambda\mu\nu} = \sum_{ijk} A^{ijk}_{\lambda\mu\nu}\ \delta c_{ijk}$$

where matrix A maps the structure properties into the observed travel time variations, λ and μ define the location of the central point of a ray system on the surface, and ν labels surrounding annuli. The equation is solved by a regularized least-squares technique.

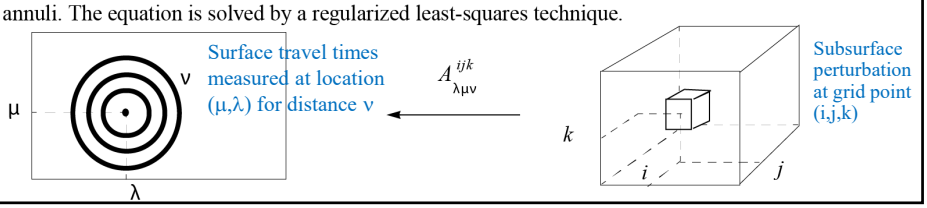

Deep- and surface-focusing observing schemes

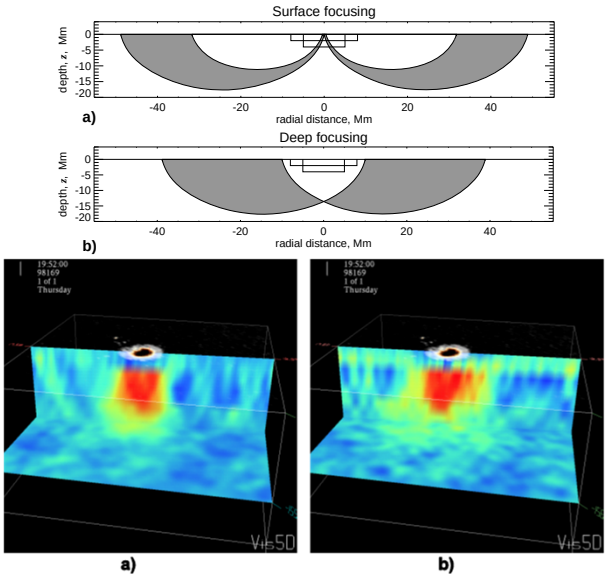

Definition of normal modes

One way to represent the oscillations is as a sum of standing waves or normal modes, where the signal observed at a point (r,θ,ϕ) at time t is given by

$$f(r,\theta,\phi,t) = \sum_{nlm} a_{nlm}\xi_{nlm}(r,\theta,\phi)\exp(i[\omega_{nlm}t + \alpha_{nlm}]). \quad (1)$$

In this equation, the three integers n, l, and m identify each mode and are commonly called the *radial order*, *angular degree*, and *azimuthal order* respectively. For each mode, a_{nlm} is the mode amplitude, ω_{nlm} is the eigenfrequency, and α_{nlm} is the phase.

The spatial eigenfunction for each mode is denoted by ξ_{nlm}. For an axisymmetrical Sun, the eigenfunctions can be separated into radial and angular components:

$$\xi_{nlm}(r,\theta,\phi) = \xi_{nl}(r)Y_{lm}(\theta,\phi), \quad (2)$$

where Y_{lm} is the spherical harmonic and the radial eigenfunction is denoted now by $\xi_{nl}(r)$.

Cross-covariance function in terms of normal modes

The *cross covariance* function of the oscillation signals f for two points at coordinates $\mathbf{r}_1$ and $\mathbf{r}_2$ on the solar surface is defined as the integral

$$\psi(\tau,\Delta) = \int_0^T f(\mathbf{r}_1,t+\tau)f^*(\mathbf{r}_2,t)\,dt. \quad (3)$$

Here Δ is used to denote the angular distance between the two points and T is the total length of the observations. The time delay τ measures the amount that one signal is shifted relative to the other. In practice, it is quite time-consuming to compute the cross correlation with the integral in equation 3. Fortunately, the convolution theorem allows us to change the integral into a product in the Fourier domain,

$$\Psi(\omega,\tau,\Delta) = F(\mathbf{r}_1,\omega)F^*(\mathbf{r}_2,\omega). \quad (4)$$

Here Ψ is used to represent the temporal (τ) Fourier transform of ψ, and F represents the temporal Fourier transform of f. The length T of the observations is assumed to be long compared to any time lag τ of interest. Since Fourier transforms can be computed very efficiently, equation 4 provides a relatively fast way to compute cross correlations.

Calculation of the cross-covariance function

Convolution theorem: the Fourier transform of a convolution of two functions is the product of their Fourier transforms.

Using the convolution notation, we write:

$$\Psi(\tau,\Delta)=\int_0^T f(\mathbf{r}+\Delta,\tau)f(\mathbf{r},t)dt$$

as $\Psi(\tau,\Delta)=f_1*f_2$.

If F is the Fourier transform in time, then the according to the convolution theorem:

$$F[\Psi(\tau,\Delta)]=F[f_1*f_2]=F[f_1]\cdot F[f_2^*]$$

The cross-covariance of two functions is calculated using the inverse Fourier transform of the product of the Fourier transforms of these functions:

$$\Psi(\tau,\Delta)=F^{-1}[F[f_1]\cdot F[f_2^*]]$$

The oscillation signals f_1 and f_2 can be represented in terms of the superposition of the normal modes with random phases α_{nlm}. The phases are random because of the stochastic excitation of solar oscillations.

$$f(r,\theta,\phi,t)=\sum_{nlm}a_{nlm}\xi_{nlm}(r)Y_{lm}(\theta,\phi)e^{-i\omega_{nl}t+i\alpha_{nlm}}$$

The eigenfunctions are normalized as $\xi_{nl}(R)=1$.

Thus, at the surface ($r=R$):

$$F[f]=\sum_{nlm}a_{nlm}Y_{nlm}(\theta,\phi)e^{i\alpha_{nlm}}\delta(\omega-\omega_{nlm})$$

Here we used

$$\frac{1}{2\pi}\int_{-\infty}^{\infty}e^{-i(\omega-\omega_{nlm})t}dt=\delta(\omega_{nlm}-\omega)$$

Because the solar oscillation spectrun has a shape close to a Gaussian with the central frequency ω_0 (the corresponding cyclic frequency is about 3 mHz), we approximate the mode amplitudes as:

$$a_{nlm}=A\exp\left[-\frac{(\omega-\omega_0)^2}{2\delta\omega^2}\right]$$

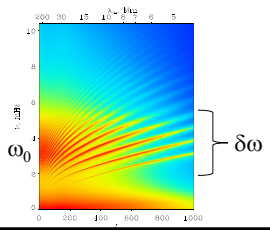

Then,

$$F[f] = A\sum_{nlm} \exp\left[-\frac{(\omega-\omega_0)^2}{2\delta\omega^2}\right]\delta(\omega-\omega_{nlm})e^{i\alpha_{nlm}}Y_{nl}(\theta,\phi)$$

Defining $G_{nl}(\omega) = \exp\left[-\frac{(\omega-\omega_0)^2}{2\delta\omega^2}\right]\delta(\omega-\omega_{nlm})$, we get:

$$F[f_1]\cdot F[f_2^*] = A^2\left[\sum_{nlm} G_{nl}(\omega)e^{i\alpha_{nlm}}Y_{lm}(\theta_1,\phi_1)\right]\left[\sum_{n'l'm'} G_{n'l'}(\omega)e^{-i\alpha_{n'l'm'}}Y_{l'm'}(\theta_2,\phi_2)\right]$$

Because the mode frequencies ω_{nl} are different for different n,l, and α_{nlm} is a random function, all terms except $n'=n, l'=l, m'=m$ are canceled.

Thus,

$$F[f_1]\cdot F[f_2^*] = A^2\sum_{nl} \exp\left[-\frac{(\omega-\omega_0)^2}{2\delta\omega^2}\right]\delta(\omega-\omega_{nlm})\sum_{m=-l}^{l} Y_{lm}(\theta_1,\phi_1)Y_{lm}^*(\theta_2,\phi_2)$$

Using the addition theorem (Jackson, Classical Electrodynamics):

$$\sum_{m=-l}^{l} Y_{lm}(\theta_1,\phi_1)Y_{lm}^*(\theta_2,\phi_2) = \frac{2l+1}{4\pi}P_l(\cos\theta)$$

where Δ is the great circle distance between the points:

$$\cos\Delta = \cos\theta_1\cos\theta_2 - \sin\theta_1\sin\theta_2\cos(\phi_1-\phi_2)$$

and performing the inverse Fourier transform, we obtain:

$$\Psi(\tau,\Delta) = A^2\sum_{nl}\left[\int_{-\infty}^{\infty} e^{-i\omega\tau}\exp\left(-\frac{(\omega-\omega_0)^2}{2\delta\omega^2}\right)\delta(\omega-\omega_{nlm})d\omega\right]\frac{2l+1}{4\pi}P_l(\cos\Delta)$$

the real part of the Fourier transform:

$$\Psi(\tau,\Delta) = A^2\sum_{nl}\cos(\omega_{nl}\tau)\exp\left(-\frac{(\omega_{nl}-\omega_0)^2}{2\delta\omega^2}\right)\frac{2l+1}{4\pi}P_l(\cos\Delta)$$

Following Jackson, for $\Delta l \gg 1$ we approximate:

$$P_l(\cos\theta) \approx J_0\left[(2l+1)\sin\frac{\Delta}{2}\right] \approx \sqrt{\frac{2}{\pi L\Delta}}\cos(L\Delta - \pi/4)$$

where J_0 is the Bessel function, and $L = l + 1/2 \approx \sqrt{l(l+1)}$.
Then,

$$\Psi(\tau,\Delta) \approx A^2 \sum_{nl} \sqrt{\frac{2}{\pi\Delta L}} \frac{L}{2\pi} \exp\left(-\frac{(\omega_{nl}-\omega_0)^2}{2\delta\omega^2}\right)\cos(\omega_{nl}\tau)\cos(L\Delta)$$

$$\Psi(\tau,\Delta) \approx A_1 \sum_{nl} L^{1/2} \exp\left(-\frac{(\omega_{nl}-\omega_0)^2}{2\delta\omega^2}\right)\cos(\omega_{nl}\tau)\cos(L\Delta)$$

Now the double sum can be reduced to a convenient sum of integrals if we regroup the modes so that the outer sum is over the ratio $v \equiv \omega / L$ and the inner sum is over ω.

We have learned that the radius of the lower turning point is determined by the ratio $v \equiv \omega / L$. Thus, the travel distance Δ of an acoustic wave is also determined by this ratio v; Δ is otherwise independent of ω.

In this case, given the band-limited nature of the function G, only values of L which are close to $L_0 \equiv \omega_0/v$ will contribute to the sum, and we can expand L near the central frequency ω_0:

$$L\Delta \approx \Delta\left[L(\omega_0) + \frac{\partial L}{\partial\omega}(\omega-\omega_0)\right] = \Delta\left[\frac{\omega_0}{v} + \frac{\omega-\omega_0}{u}\right],$$

where $u \equiv \partial\omega/\partial L$.

Furthermore, the product of cosines can be changed into a sum; one term is

$$\cos\left[\left(\tau - \frac{\Delta}{u}\right)\omega + \left(\frac{1}{u} - \frac{1}{v}\right)\Delta\omega_0\right],$$

and the other term is identical except that τ has been replaced with $-\tau$ (*i.e.* the time lag is negative). The result is that the double sum becomes

$$\psi(\tau,\Delta) = \sum_v \frac{2}{\sqrt{\pi\Delta}} \sum_\omega \exp\left(-\frac{(\omega-\omega_0)^2}{\delta\omega^2}\right)\cos\left(\left[\pm\tau - \frac{\Delta}{u}\right]\omega + \left[\frac{1}{u} - \frac{1}{v}\right]\Delta\omega_0\right).$$

The inner sum can be approximated by an integral over ω:

$$\int_{-\infty}^{\infty} d\omega \exp\left(-\frac{(\omega-\omega_0)^2}{\delta\omega^2}\right)\cos\left(\left[\tau-\frac{\Delta}{u}\right]\omega-\left[\frac{1}{u}-\frac{1}{v}\right]\Delta\omega_0\right)=$$

$$=\sqrt{\pi\,\delta\omega^2}\exp\left(-\frac{\delta\omega^2}{4}\left[\tau-\frac{\Delta}{u}\right]^2\right)\cos\left(\omega_0\left(\tau-\frac{\Delta}{v}\right)\right).$$

The limits $(-\infty,\infty)$ pose no particular problem since the amplitude function G^2 is essentially zero for very large and very small frequencies.

Finally, then, the cross correlation can be expressed as

$$\psi(\tau,\Delta)\propto\sum_{v}\exp\left(-\frac{\delta\omega^2}{4}\left[\tau\pm\frac{\Delta}{u}\right]^2\right)\cos\left(\omega_0\left[\tau\pm\frac{\Delta}{v}\right]\right)$$

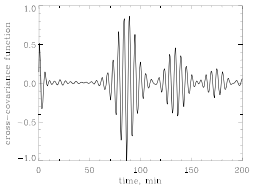

where $v\equiv\omega/L$ and $u\equiv\partial\omega/\partial L$.

The cross correlation function at any particular distance is thus described by two characteristic times; the *group time*, defined as $\tau_g\equiv\Delta/u$, and the *phase time*, defined as $\tau_p\equiv\Delta/v$. Furthermore, the cross correlation will have two peaks; one near $+\tau_g$, and the other near $-\tau_g$. These two peaks correspond to the two directions of propagation.

Two representations of the covariance function

$$\psi(\tau,\Delta)\propto\sum_{nl}\exp\left(-\frac{(\omega_{nl}-\omega_0)^2}{\delta\omega^2}\right)\cos(\omega_{nl}\tau)\cos(L\Delta).$$

-in terms of the normal mode frequencies. (Once you know changes in mode frequencies you can find the corresponding changes in the cross-covariance function and travel times.)

$$\psi(\tau,\Delta)\propto\sum_{v}\exp\left(-\frac{\delta\omega^2}{4}\left[\tau\pm\frac{\Delta}{u}\right]^2\right)\cos\left(\omega_0\left[\tau\pm\frac{\Delta}{v}\right]\right)$$

- in terms of the phase and group velocities or travel times.

The key difference between "global" helioseismology and time-distance helioseismology is the mode coupling in the cross-covariance function. Thus, we can apply time-distance helioseismology to the non-axisymmetrical Sun.

Summary

$$\Psi(\tau,\Delta)=\int_0^T f(t,r_1)f^*(t+\tau,r_2)dt, \qquad G(\omega)=\exp\left[-\left(\frac{\omega-\omega_0}{\delta\omega}\right)^2\right],$$

- frequency filter

$$f(t,r,\theta,\phi)=\sum_{nlm} a_{nlm}\xi_{nlm}(r,\theta,\phi)\exp(i\omega_{nlm}t+i\phi_{nlm}), \qquad \xi_{nlm}(r,\theta,\phi)=\xi_{nl}(r)Y_{lm}(\theta,\phi),$$

$$\Psi(\tau,\Delta)=\int_{-\infty}^{\infty} F(\omega,r_1)F^*(\omega,r_2)\exp(i\omega\tau)d\omega,$$

$$F(\omega,r,\theta,\phi)\approx\sum_{nlm} a_{nl}\xi_{nl}(r)Y_{lm}(\theta,\phi)\delta(\omega-\omega_{nl})\exp\left[-\left(\frac{\omega-\omega_0}{\delta\omega}\right)^2\right],$$

$$\Psi(\tau,r_1,r_2)=\sum_{nl}\sigma_{nl}\exp\left[-\left(\frac{\omega-\omega_0}{\delta\omega}\right)^2+i\omega_{nl}\tau\right]\sum_{m=-l}^{l} Y_{lm}(\theta_1,\phi_1)Y_{lm}^*(\theta_2,\phi_2).$$

$$\sum_{m=-l}^{l} Y_{lm}(\theta_1,\phi_1)Y_{lm}^*(\theta_2,\phi_2)=\alpha_l P_l(\cos\Delta), \qquad \cos\Delta=\cos\theta_1\cos\theta_2+\sin\theta_1\sin\theta_2\cos(\phi_2-\phi_1)$$

$$\alpha_l=(2l+1)/4\pi$$

$$\Psi(\tau,\Delta)\approx\sum_{nl} a_{nl}\alpha_l P_l(\cos\Delta)\exp\left[-\left(\frac{\omega_{nl}-\omega_0}{\delta\omega}\right)^2+i\omega_{nl}\tau\right].$$

$$\Psi(\tau,\Delta)\propto\sum_{\delta\nu} a_{\delta\nu}\cos\left[\omega_0\left(\tau-\frac{\Delta}{v}\right)\right]\exp\left[-\frac{\delta\omega^2}{4}\left(\tau-\frac{\Delta}{u}\right)^2\right],$$

Phase speed:

$v=\omega_{nl}/L \qquad L=l+1/2$

u - group velocity

Ray approximation

- Originally, time-distance helioseismology was intuitively derived from the picture of acoustic ray paths.
- In fact, the acoustic waves observed on the Sun can be considered high-frequency acoustic waves. In most of the region in which these waves are confined, their wavelengths are short compared to the local temperature and density scale heights. In this wavelength regime, the wave propagation can be approximated with ray theory.

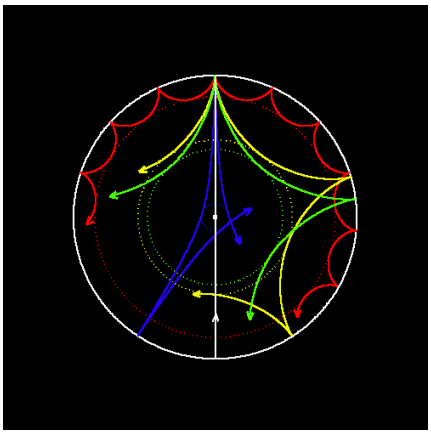

Time-distance diagnostics

Fermat's Principle

A powerful property of ray paths is that they obey Fermat's Principle, which states that the travel time along the ray is stationary with respect to small changes in the path. This implies that if a small perturbation is made to the background state, the ray path is unchanged.

The perturbation to the travel time can then be expressed as

$$\tau - \tau_0 = \frac{1}{\omega}\int_{\Gamma_0} \delta k \, ds.$$

Here δk is the perturbation to the wavevector due to inhomogeneities in the background state, and Fermat's principle allows us to make the integral along the unperturbed ray path Γ_0.

In the solar convection zone, the Brunt-Väisälä frequency N is small compared to the acoustic cutoff frequency and the typical frequencies of solar oscillations. Neglecting this frequency, the dispersion relation can be written as

$$k_r^2 = \frac{1}{c^2}\left(\omega^2 - \omega_C^2\right) - k_h^2,$$
$$k_h^2 = \frac{l(l+1)}{r^2}.$$

If we allow small perturbations (relative to the background state) in ω, c^2, and ω_C^2, then the integrand in Fermat's equation can be written to first order as

$$\frac{\delta k \, ds}{\omega} = \left[\frac{\delta\omega}{c^2 k} - \left(\frac{\delta c}{c}\right)\frac{k}{\omega} - \left(\frac{\delta\omega_C}{\omega_C}\right)\left(\frac{\omega_C^2}{c^2\omega^2}\right)\frac{\omega}{k}\right] ds,$$

where I have neglected terms which are second-order in $\delta c/c$ and $|u|/c$.

Effect of velocity field

One possible perturbation to the spherically symmetric background state is a velocity field. If the flow field is described by $\mathbf{u}$ then the observed frequency will be Doppler shifted by the advection of the oscillations,

$$\delta\omega = -k\hat{\mathbf{n}}\cdot\mathbf{u},$$

so that the Fermat's equation becomes

$$\tau^{\pm} - \tau_0 = -\int_{\Gamma_0}\left[\frac{\mathbf{u}\cdot(\pm\hat{\mathbf{n}})}{c^2} + \left(\frac{\delta c}{c}\right)\frac{k}{\omega} + \left(\frac{\delta\omega_C}{\omega_C}\right)\left(\frac{\omega_C^2}{c^2\omega^2}\right)\frac{\omega}{k}\right]ds,$$

where $\hat{\mathbf{n}}$ is a unit vector tangent to the ray path. Here I have defined the quantity τ^+ as the perturbed travel time in one direction along the ray path (unit vector $+\hat{\mathbf{n}}$) and τ^- as the perturbed travel time in the opposite (reciprocal) direction (unit vector $-\hat{\mathbf{n}}$).

Separation of the velocity field signal from the other perturbations

To separate the effects of the velocity field from the other perturbations, we thus define

$$\delta\tau_{\text{diff}} \equiv \tau^+ - \tau^- = -2\int_{\Gamma_0}\frac{\mathbf{u}\cdot\hat{\mathbf{n}}}{c^2}ds$$

$$\delta\tau_{\text{mean}} \equiv \frac{(\tau^+ + \tau^-)}{2} = \tau_0 - \int_{\Gamma_0}\left[\left(\frac{\delta c}{c}\right)\frac{k}{\omega} + \left(\frac{\delta\omega_C}{\omega_C}\right)\left(\frac{\omega_C^2}{c^2\omega^2}\right)\frac{\omega}{k}\right]ds.$$

This equation thus provides the link between the measured travel time differences and the flow field along the ray path. This simple equation is in the heart of the time-distance helioseismology.

Magnetic field effects

- Magnetic field in sunspots, particularly, in the sunspot umbra may significantly affect the time-distance diagnostics for 3 main reasons:
  - The standard Doppler shift measurements may not provide accurate estimate of the actual line-of-sight velocity
  - Magnetic field inhibits convection (reducing excitation) and presumably absorbs waves causing inhomogeneous distribution of the acoustic power on the solar surface, resulting systematic shifts in the standard travel times (Woodard's effect)
  - Magnetic field causes changes in the dispersion properties of acoustic waves resulting in anisotropy in the travel times
- Magnetic effects are particularly strong when plasma parameter is of the order of unity or smaller: $\beta=4\pi p/B^2$.
- For most sunspot models this happens above the photosphere. This regime is poorly understood, and avoid this we mostly work with low-frequency waves that are reflected below the photosphere.
- At high frequencies, magnetic effects ("shower-glass effect", "inclined field effect") become strong, particularly, in acoustic holography (Doug Braun's talk tomorrow). Our tests show that for time-distance measurements these are much less significant.

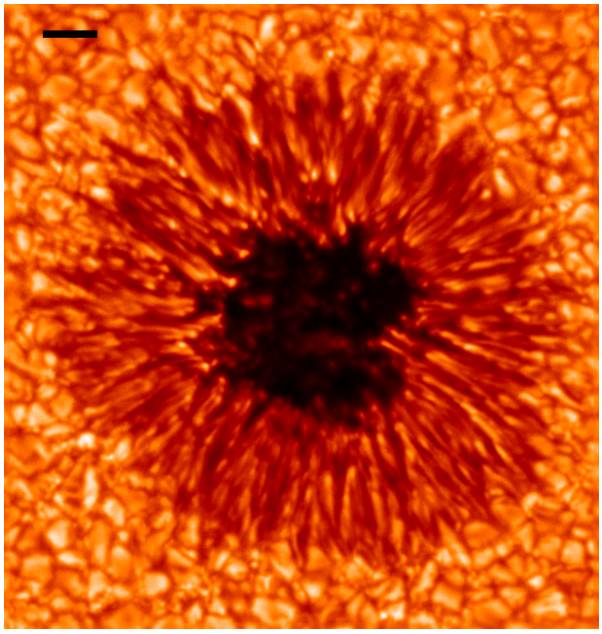

Sensitivity kernels for travel-time measurements in the Born approximation

- Properties of the solar interior are related to the measured travel times through sensitivity kernels (e.g. for sound speed):

$$\delta\tau(\Delta) = \int_V K_T(\vec{r},\Delta)\frac{\delta c}{c}dV$$

where integration is over the whole volume of the Sun.

- These kernel are calculated in the Born approximation as in terms as a combination of normal mode eigenfunctions.
- The sound-speed variations, flow velocity and other solar properties are determined from this equation by inversion.

"Banana-doughnut kernel"

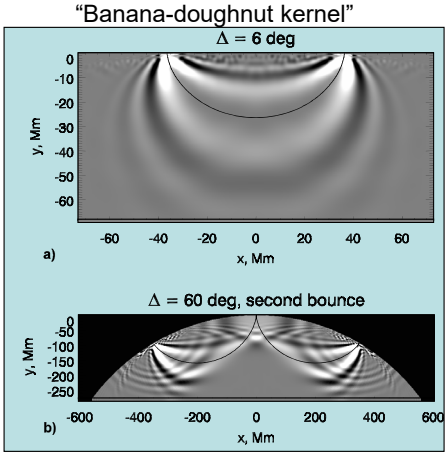

Examples of travel-time sensitivity kernels for the first and second bounces calculated in the Born approximation. The black curves show the corresponding ray paths.

Testing the ray and Born approximations for a simple spherical sound-speed perturbation

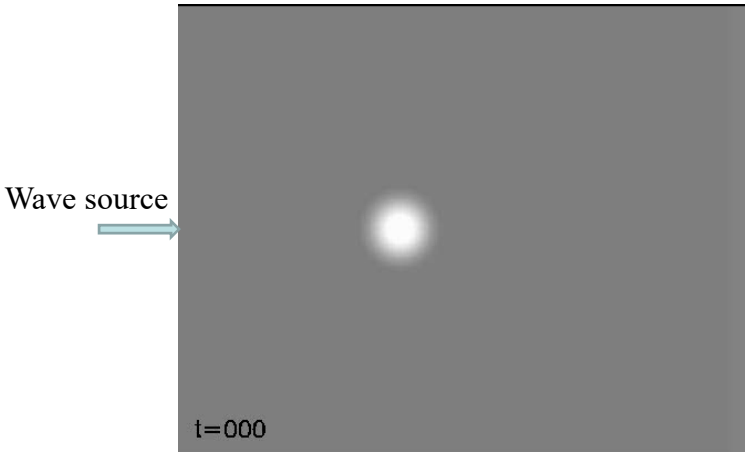

Banana-doughnut structure of the travel-time sensitivity kernels is caused by the wave-healing effect

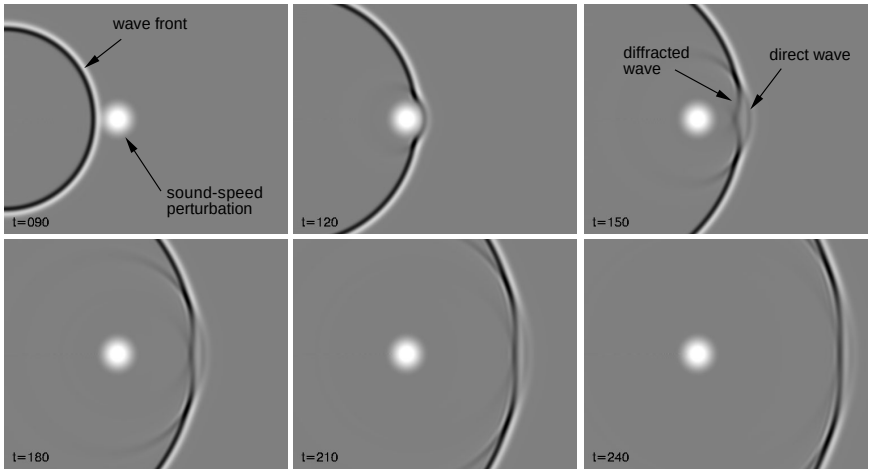

Comparison of the ray and Born approximations with numerical simulations

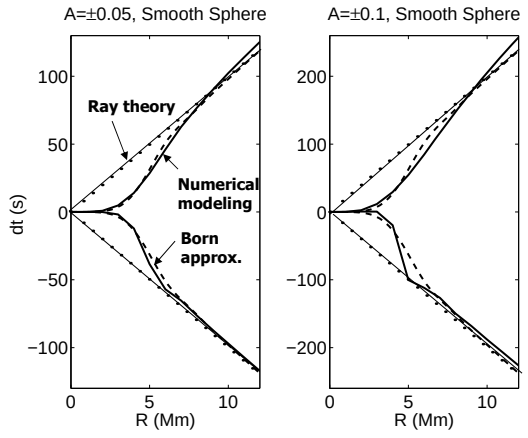

Ray approximation overestimates travel times for small structures. This means that such structures are underestimated in the inversion results.

Born approximation is sufficiently adequate when diffraction effects are not significant.

Sound-speed structure beneath a sunspot (Couvidat et al 2005)

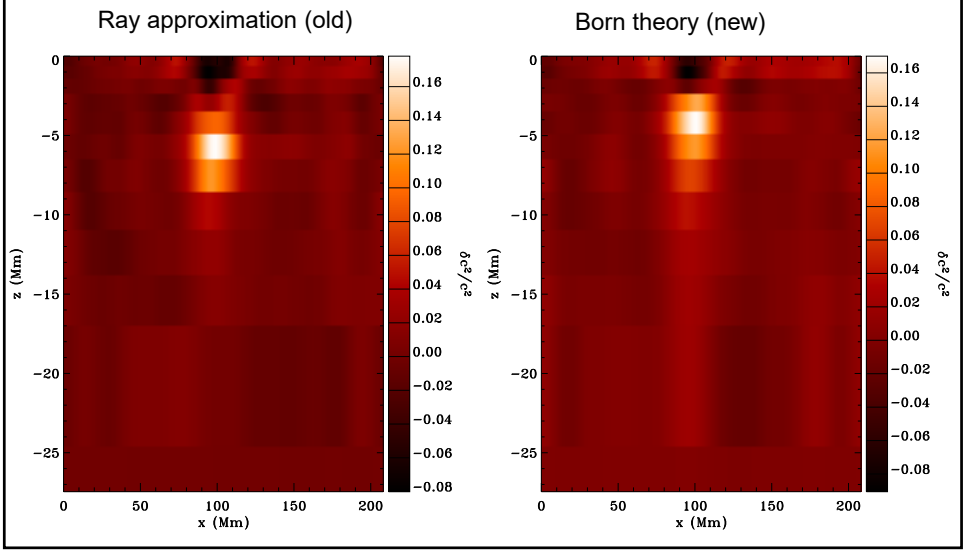

Lecture 22
Time-distance helioseismology II

Time-distance measurements

Travel times are determined from the cross-covariance function:

$$\psi(\tau,\Delta)=\int_0^T f(t,r)f^*(t+\tau,r+\Delta)dt$$

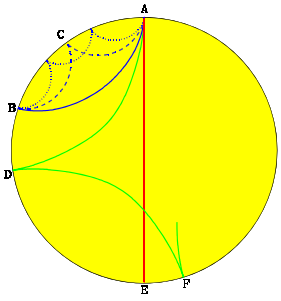

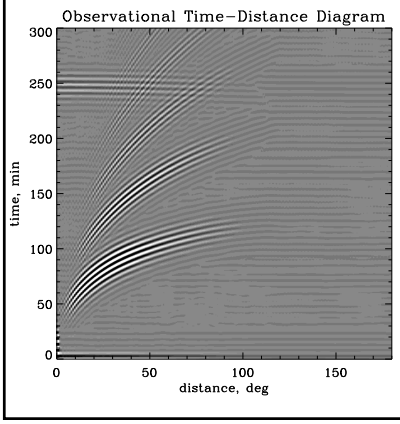

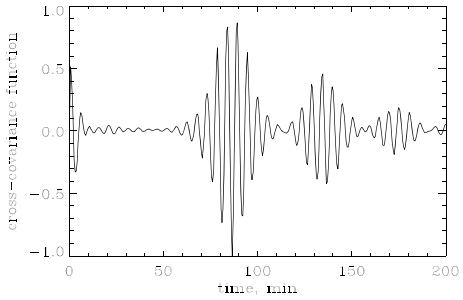

Cross-covariance function for a particular distance (30 degrees in this case) represents a series of wave packets.

Simple interpretation of time-distance measurements

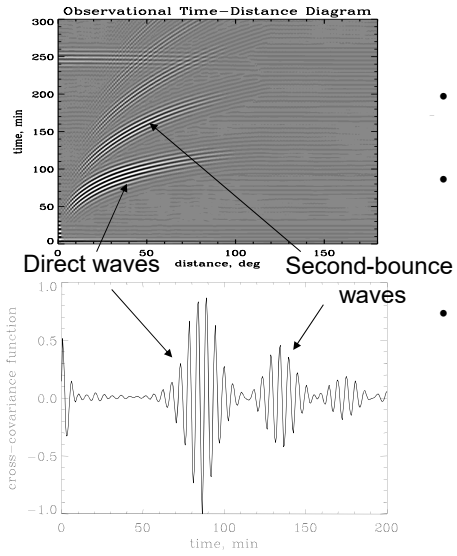

- The cross-covariance function collects coherent signals for solar waves excited at a given point and traveling to another point
- The cross-covariance signal corresponds to a strong point source (similar to the flare signal) – Claerbout's conjecture
- The cross-covariance signal corresponds to a wave packet of waves in a finite frequency range. The solar oscillations have periods around 5 min. Thus, we see the 5-min periodicity in the wave packet.
- The cross-covariance function can be used for measuring group and phase travel times.

We measure the group and phase travel times from these diagrams.

Definition of normal modes

One way to represent the oscillations is as a sum of standing waves or normal modes, where the signal observed at a point (r,θ,ϕ) at time t is given by

$$f(r,\theta,\phi,t) = \sum_{nlm} a_{nlm}\xi_{nlm}(r,\theta,\phi)\exp(i[\omega_{nlm}t + \alpha_{nlm}]). \quad (1)$$

In this equation, the three integers n, l, and m identify each mode and are commonly called the *radial order*, *angular degree*, and *azimuthal order* respectively. For each mode, a_{nlm} is the mode amplitude, ω_{nlm} is the eigenfrequency, and α_{nlm} is the phase.

The spatial eigenfunction for each mode is denoted by ξ_{nlm}. For an axisymmetrical Sun, the eigenfunctions can be separated into radial and angular components:

$$\xi_{nlm}(r,\theta,\phi) = \xi_{nl}(r)Y_{lm}(\theta,\phi), \quad (2)$$

where Y_{lm} is the spherical harmonic and the radial eigenfunction is denoted now by $\xi_{nl}(r)$.

Cross-covariance function in terms of normal modes

The *cross covariance* function of the oscillation signals f for two points at coordinates $\mathbf{r}_1$ and $\mathbf{r}_2$ on the solar surface is defined as the integral

$$\psi(\tau,\Delta) = \int_0^T f(\mathbf{r}_1, t+\tau) f^*(\mathbf{r}_2, t)\, dt. \qquad (3)$$

Here Δ is used to denote the angular distance between the two points and T is the total length of the observations. The time delay τ measures the amount that one signal is shifted relative to the other. In practice, it is quite time-consuming to compute the cross correlation with the integral in equation 3. Fortunately, the convolution theorem allows us to change the integral into a product in the Fourier domain,

$$\Psi(\omega,\tau,\Delta) = F(\mathbf{r}_1,\omega) F^*(\mathbf{r}_2,\omega). \qquad (4)$$

Here Ψ is used to represent the temporal (τ) Fourier transform of ψ, and F represents the temporal Fourier transform of f. The length T of the observations is assumed to be long compared to any time lag τ of interest. Since Fourier transforms can be computed very efficiently, equation 4 provides a relatively fast way to compute cross correlations.

Calculation of the cross-covariance function

Convolution theorem: the Fourier transform of a convolution of two functions is the product of their Fourier transforms.

Using the convolution notation, we write:

$$\Psi(\tau,\Delta) = \int_0^T f(\mathbf{r}+\Delta,\tau) f(\mathbf{r},t) dt$$

as $\Psi(\tau,\Delta) = f_1 * f_2$.

If F is the Fourier transform in time, then the according to the convolution theorem:

$$F[\Psi(\tau,\Delta)] = F[f_1 * f_2] = F[f_1] \cdot F[f_2^*]$$

The cross-covariance of two functions is calculated using the inverse Fourier transform of the product of the Fourier transforms of these functions:

$$\Psi(\tau,\Delta) = F^{-1}[F[f_1] \cdot F[f_2^*]]$$

The oscillation signals f_1 and f_2 can be represented in terms of the superposition of the normal modes with random phases α_{nlm}. The phases are random because of the stochastic excitation of solar oscillations.

$$f(r,\theta,\phi,t)=\sum_{nlm} a_{nlm}\xi_{nlm}(r)Y_{lm}(\theta,\phi)e^{-i\omega_{nl}t+i\alpha_{nlm}}$$

The eigenfunctions are normalized as $\xi_{nl}(R)=1$.

Thus, at the surface ($r = R$):

$$F[f]=\sum_{nlm} a_{nlm}Y_{lm}(\theta,\phi)e^{i\alpha_{nlm}}\delta(\omega-\omega_{nl})$$

Here we used

$$\frac{1}{2\pi}\int_{-\infty}^{\infty} e^{-i(\omega-\omega_{nl})t}dt=\delta(\omega_{nl}-\omega)$$

Because the solar oscillation spectrun has a shape close to a Gaussian with the central frequency ω_0 (the corresponding cyclic frequency is about 3 mHz), we approximate the mode amplitudes as:

$$a_{nlm}=A\exp\left[-\frac{(\omega-\omega_0)^2}{2\delta\omega^2}\right]$$

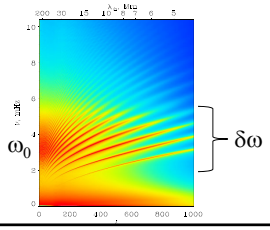

Then,

$$F[f]=A\sum_{nlm}\exp\left[-\frac{(\omega-\omega_0)^2}{2\delta\omega^2}\right]\delta(\omega-\omega_{nl})e^{i\alpha_{nlm}}Y_{lm}(\theta,\phi)$$

Defining $G_{nl}(\omega)=\exp\left[-\frac{(\omega-\omega_0)^2}{2\delta\omega^2}\right]\delta(\omega-\omega_{nl})$, we get:

$$F[f_1]\cdot F[f_2^*]=A^2\left[\sum_{nlm}G_{nl}(\omega)e^{i\alpha_{nlm}}Y_{lm}(\theta_1,\phi_1)\right]\left[\sum_{n'l'm'}G_{n'l'}(\omega)e^{-i\alpha_{n'l'm'}}Y_{l'm'}(\theta_2,\phi_2)\right]$$

Because the mode frequencies ω_{nl} are different for different n,l, and α_{nlm} is a random function, all terms except $n'=n, l'=l, m'=m$ are canceled.

Thus,

$$F[f_1]\cdot F[f_2^*]=A^2\sum_{nl}\exp\left[-\frac{(\omega-\omega_0)^2}{2\delta\omega^2}\right]\delta(\omega-\omega_{nl})\sum_{m=-l}^{l}Y_{lm}(\theta_1,\phi_1)Y_{lm}^*(\theta_2,\phi_2)$$

Using the addition theorem (Jackson, Classical Electrodynamics):

$$\sum_{m=-l}^{l} Y_{lm}(\theta_1,\phi_1)Y_{lm}^*(\theta_2,\phi_2) = \frac{2l+1}{4\pi} P_l(\cos\Delta)$$

where Δ is the great circle distance between the two points:

$$\cos\Delta = \cos\theta_1\cos\theta_2 - \sin\theta_1\sin\theta_2\cos(\phi_1-\phi_2)$$

and performing the inverse Fourier transform, we obtain:

$$\Psi(\tau,\Delta) = A^2\sum_{nl}\left[\int_{-\infty}^{\infty} e^{-i\omega\tau}\exp\left(-\frac{(\omega-\omega_0)^2}{2\delta\omega^2}\right)\delta(\omega-\omega_{nlm})d\omega\right]\frac{2l+1}{4\pi}P_l(\cos\Delta)$$

the real part of the Fourier transform:

$$\Psi(\tau,\Delta) = A^2\sum_{nl}\cos(\omega_{nl}\tau)\exp\left(-\frac{(\omega_{nl}-\omega_0)^2}{2\delta\omega^2}\right)\frac{2l+1}{4\pi}P_l(\cos\Delta)$$

Following Jackson, for $\Delta l \gg 1$ we approximate:

$$P_l(\cos\Delta) \approx J_0\left[(2l+1)\sin\frac{\Delta}{2}\right] \approx \sqrt{\frac{2}{\pi L\Delta}}\cos(L\Delta-\pi/4)$$

where J_0 is the Bessel function, and $L = l+1/2 \approx \sqrt{l(l+1)}$.
Then,

$$\Psi(\tau,\Delta) \approx A^2\sum_{nl}\sqrt{\frac{2}{\pi\Delta L}}\frac{L}{2\pi}\exp\left(-\frac{(\omega_{nl}-\omega_0)^2}{2\delta\omega^2}\right)\cos(\omega_{nl}\tau)\cos(L\Delta)$$

$$\Psi(\tau,\Delta) \approx A_1\sum_{nl}L^{1/2}\exp\left(-\frac{(\omega_{nl}-\omega_0)^2}{2\delta\omega^2}\right)\cos(\omega_{nl}\tau)\cos(L\Delta)$$

Now the double sum can be reduced to a convenient sum of integrals if we regroup the modes so that the outer sum is over the ratio $v \equiv \omega/L$ and the inner sum is over ω.

We have learned that the radius of the inner turning point is determined by the ratio $v \equiv \omega / L$. Thus, the travel distance Δ of an acoustic wave is also determined by this ratio v; Δ is otherwise independent of ω.

In this case, given the band-limited nature of the function G, only values of L which are close to $L_0 \equiv \omega_0/v$ will contribute to the sum, and we can expand L near the central frequency ω_0:

$$L\Delta \approx \Delta\left[L(\omega_0) + \frac{\partial L}{\partial \omega}(\omega - \omega_0) \right] = \Delta\left[\frac{\omega_0}{v} + \frac{\omega - \omega_0}{u} \right],$$

where $u \equiv \partial\omega/\partial L$ is the group angular velocity (recall $k_h = L/r$).

Furthermore, the product of cosines can be changed into a sum; one term is

$$\cos\left[\left(\tau - \frac{\Delta}{u} \right)\omega + \left(\frac{1}{u} - \frac{1}{v} \right)\Delta\omega_0 \right],$$

and the other term is identical except that τ has been replaced with $-\tau$ (*i.e.* the time lag is negative). The result is that the double sum becomes

$$\psi(\tau, \Delta) = \sum_v \frac{2}{\sqrt{\pi\Delta}} \sum_\omega \exp\left(-\frac{(\omega - \omega_0)^2}{\delta\omega^2} \right) \cos\left(\left[\pm\tau - \frac{\Delta}{u} \right]\omega + \left[\frac{1}{u} - \frac{1}{v} \right]\Delta\omega_0 \right).$$

The inner sum can be approximated by an integral over ω:

$$\int_{-\infty}^{\infty} d\omega \exp\left(-\frac{(\omega - \omega_0)^2}{\delta\omega^2} \right) \cos\left(\left[\tau - \frac{\Delta}{u} \right]\omega - \left[\frac{1}{u} - \frac{1}{v} \right]\Delta\omega_0 \right) =$$

$$= \sqrt{\pi\,\delta\omega^2} \exp\left(-\frac{\delta\omega^2}{4}\left[\tau - \frac{\Delta}{u} \right]^2 \right) \cos\left(\omega_0 \left(\tau - \frac{\Delta}{v} \right) \right).$$

The limits $(-\infty, \infty)$ pose no particular problem since the amplitude function G^2 is essentially zero for very large and very small frequencies.

Finally, then, the cross correlation can be expressed as

$$\psi(\tau, \Delta) \propto \sum_v \exp\left(-\frac{\delta\omega^2}{4}\left[\tau \pm \frac{\Delta}{u} \right]^2 \right) \cos\left(\omega_0 \left[\tau \pm \frac{\Delta}{v} \right] \right)$$

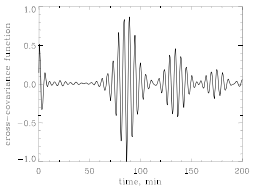

where $v \equiv \omega / L$ and $u \equiv \partial\omega/\partial L$.

The cross correlation function at any particular distance is thus described by two characteristic times; the *group time*, defined as $\tau_g \equiv \Delta/u$, and the *phase time*, defined as $\tau_p \equiv \Delta/v$. Furthermore, the cross correlation will have two peaks; one near $+\tau_g$, and the other near $-\tau_g$. These two peaks correspond to the two directions of propagation.

Two representations of the covariance function

$$\psi(\tau,\Delta) \propto \sum_{nl} \exp\left(-\frac{(\omega_{nl}-\omega_0)^2}{\delta\omega^2}\right)\cos(\omega_{nl}\tau)\cos(L\Delta).$$

-in terms of the normal mode frequencies. (Once you know changes in mode frequencies you can find the corresponding changes in the cross-covariance function and travel times.)

$$\psi(\tau,\Delta) \propto \sum_{v} \exp\left(-\frac{\delta\omega^2}{4}\left[\tau \pm \frac{\Delta}{u}\right]^2\right)\cos\left(\omega_0\left[\tau \pm \frac{\Delta}{v}\right]\right)$$

- in terms of the phase and group velocities or travel times.

The key difference between "global" helioseismology and time-distance helioseismology is the mode coupling in the cross-covariance function. Thus, we can apply time-distance helioseismology to the non-axisymmetrical Sun.

Ray approximation

- Originally, time-distance helioseismology was intuitively derived from the picture of acoustic ray paths.
- In fact, the acoustic waves observed on the Sun can be considered high-frequency acoustic waves. In most of the region in which these waves are confined, their wavelengths are short compared to the local temperature and density scale heights. In this wavelength regime, the wave propagation can be approximated with ray theory.

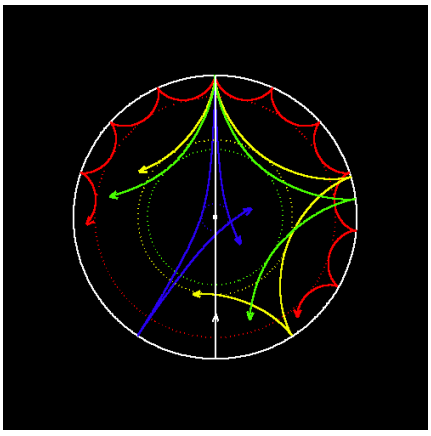

Time-distance diagnostics

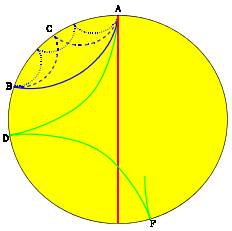

Fermat's PrincipleA powerful property of ray paths is that they obey Fermat's Principle, which states that the travel time along the ray is stationary with respect to small changes in the path. This implies that if a small perturbation is made to the background state, the ray path is unchanged.

The perturbation to the travel time can then be expressed as

$$\tau - \tau_0 = \frac{1}{\omega}\int_{\Gamma_0} \delta k \, ds.$$

Here δk is the perturbation to the wavevector due to inhomogeneities in the background state, and Fermat's principle allows us to make the integral along the unperturbed ray path Γ_0.

In the solar convection zone, the Brunt-Väisälä frequency N is small compared to the acoustic cutoff frequency and the typical frequencies of solar oscillations. Neglecting this frequency, the dispersion relation can be written as

$$k_r^2 = \frac{1}{c^2}\left(\omega^2 - \omega_C^2\right) - k_h^2,$$
$$k_h^2 = \frac{l(l+1)}{r^2}.$$

If we allow small perturbations (relative to the background state) in ω, c^2, and ω_C^2, then the integrand in Fermat's equation can be written to first order as

$$\frac{\delta k \, ds}{\omega} = \left[\frac{\delta\omega}{c^2 k} - \left(\frac{\delta c}{c}\right)\frac{k}{\omega} - \left(\frac{\delta\omega_C}{\omega_C}\right)\left(\frac{\omega_C^2}{c^2\omega^2}\right)\frac{\omega}{k}\right] ds,$$

where I have neglected terms which are second-order in $\delta c/c$ and $|u|/c$.

Effect of velocity field

One possible perturbation to the spherically symmetric background state is a velocity field. If the flow field is described by $\mathbf{u}$ then the observed frequency will be Doppler shifted by the advection of the oscillations,

$$\delta\omega = -k\hat{\mathbf{n}}\cdot\mathbf{u},$$

so that the Fermat's equation becomes

$$\tau^{\pm} - \tau_0 = -\int_{\Gamma_0}\left[\frac{\mathbf{u}\cdot(\pm\hat{\mathbf{n}})}{c^2} + \left(\frac{\delta c}{c}\right)\frac{k}{\omega} + \left(\frac{\delta\omega_C}{\omega_C}\right)\left(\frac{\omega_C^2}{c^2\omega^2}\right)\frac{\omega}{k}\right]ds,$$

where $\hat{\mathbf{n}}$ is a unit vector tangent to the ray path. Here I have defined the quantity τ^+ as the perturbed travel time in one direction along the ray path (unit vector $+\hat{\mathbf{n}}$) and τ^- as the perturbed travel time in the opposite (reciprocal) direction (unit vector $-\hat{\mathbf{n}}$).

Separation of the velocity field signal from the other perturbations

To separate the effects of the velocity field from the other perturbations, we thus define

$$\delta\tau_{\text{diff}} \equiv \tau^+ - \tau^- = -2\int_{\Gamma_0}\frac{\mathbf{u}\cdot\hat{\mathbf{n}}}{c^2}ds$$

$$\delta\tau_{\text{mean}} \equiv \frac{(\tau^+ + \tau^-)}{2} = \tau_0 - \int_{\Gamma_0}\left[\left(\frac{\delta c}{c}\right)\frac{k}{\omega} + \left(\frac{\delta\omega_C}{\omega_C}\right)\left(\frac{\omega_C^2}{c^2\omega^2}\right)\frac{\omega}{k}\right]ds.$$

This equation thus provides the link between the measured travel time differences and the flow field along the ray path. This simple equation is in the heart of the time-distance helioseismology.

Magnetic field effects

- Magnetic field in sunspots, particularly, in the sunspot umbra may significantly affect the time-distance diagnostics for 3 main reasons:
  - The standard Doppler shift measurements may not provide accurate estimate of the actual line-of-sight velocity
  - Magnetic field inhibits convection (reducing excitation) and presumably absorbs waves causing inhomogeneous distribution of the acoustic power on the solar surface, resulting systematic shifts in the standard travel times (Woodard's effect)
  - Magnetic field causes changes in the dispersion properties of acoustic waves resulting in anisotropy in the travel times
- Magnetic effects are particularly strong when plasma parameter is of the order of unity or smaller: $\beta=4\pi p/B^2$.
- For most sunspot models this happens above the photosphere. This regime is poorly understood, and avoid this we mostly work with low-frequency waves that are reflected below the photosphere.
- At high frequencies, magnetic effects ("shower-glass effect", "inclined field effect") become strong, particularly, in acoustic holography (Doug Braun's talk tomorrow). Our tests show that for time-distance measurements these are much less significant.

Sensitivity kernels for travel-time measurements in the Born approximation

- Properties of the solar interior are related to the measured travel times through sensitivity kernels (e.g. for sound speed):

$$\delta\tau(\Delta) = \int_V K_T(\vec{r},\Delta)\frac{\delta c}{c}dV$$

where integration is over the whole volume of the Sun.

- These kernel are calculated in the Born approximation as in terms as a combination of normal mode eigenfunctions.
- The sound-speed variations, flow velocity and other solar properties are determined from this equation by inversion.

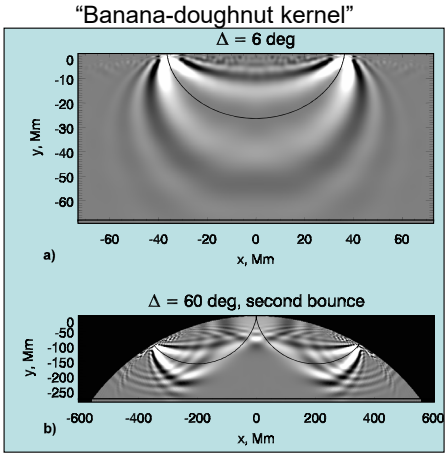

Examples of travel-time sensitivity kernels for the first and second bounces calculated in the Born approximation. The black curves show the corresponding ray paths.

Testing the ray and Born approximations for a simple spherical sound-speed perturbation

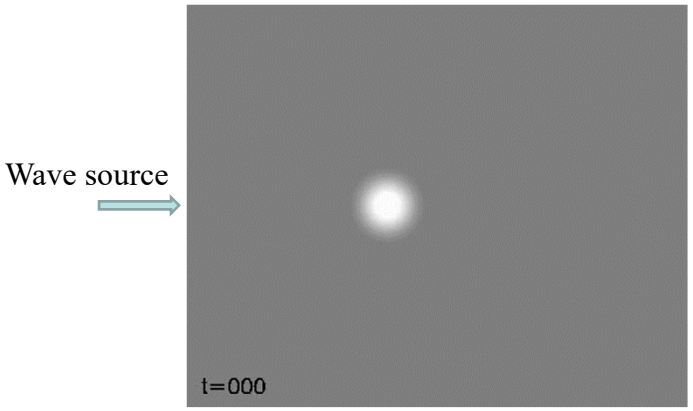

Banana-doughnut structure of the travel-time sensitivity kernels is caused by the wave-healing effect

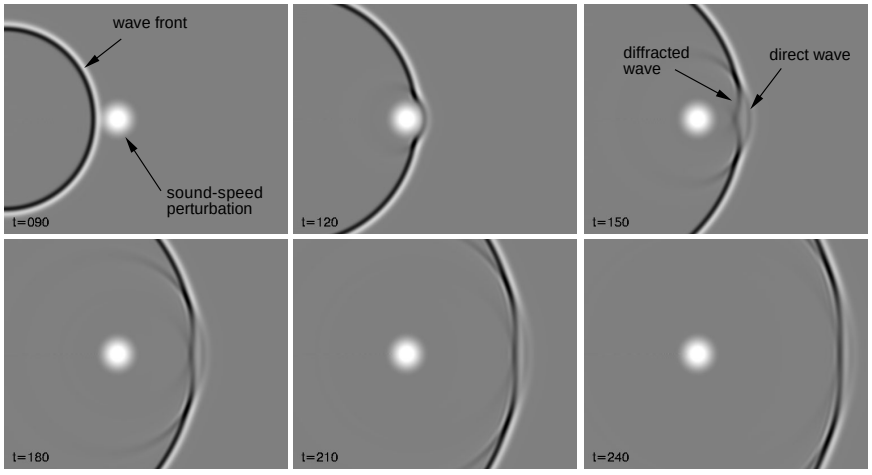

Comparison of the ray and Born approximations with numerical simulations

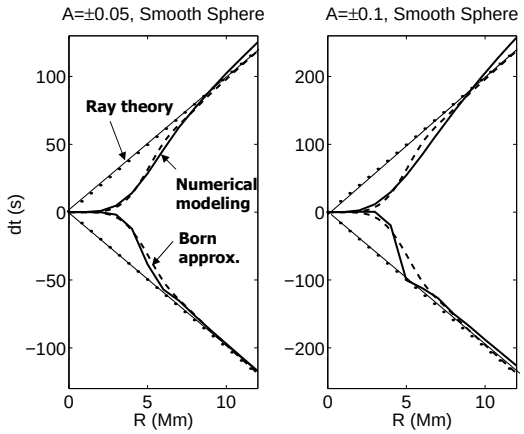

Ray approximation overestimates travel times for small structures. This means that such structures are underestimated in the inversion results.

Born approximation is sufficiently adequate when diffraction effects are not significant.

Sound-speed structure beneath a sunspot (Couvidat et al 2005)

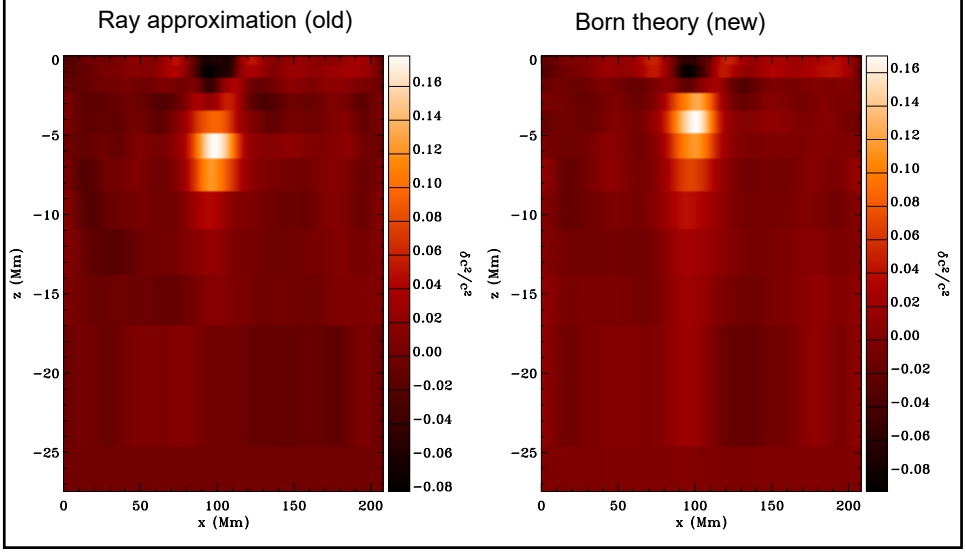

Detailed maps of subsurface flows

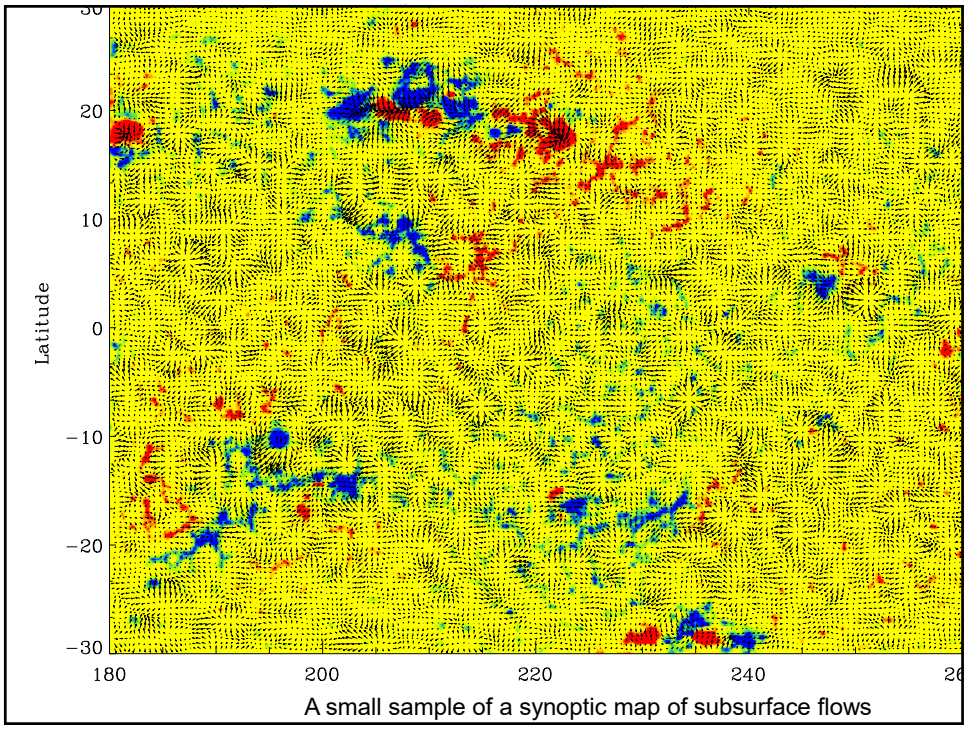

A small sample of a synoptic map of subsurface flows

Solar Subsurface Weather

Synoptic maps of subsurface flows (0-20 Mm)

Depth 2 Mm

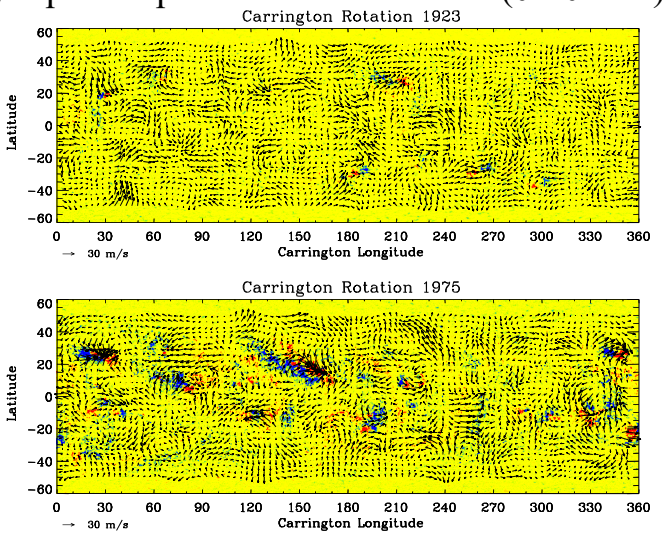

Similar maps are obtained from the ring analysis (Haber et al 2002)

Large-scale flows around active regions:

(example AR9433, April 2001)

- converging 40 m/s flow toward the neutral line in the upper layers
- diverging flow below 9 Mm

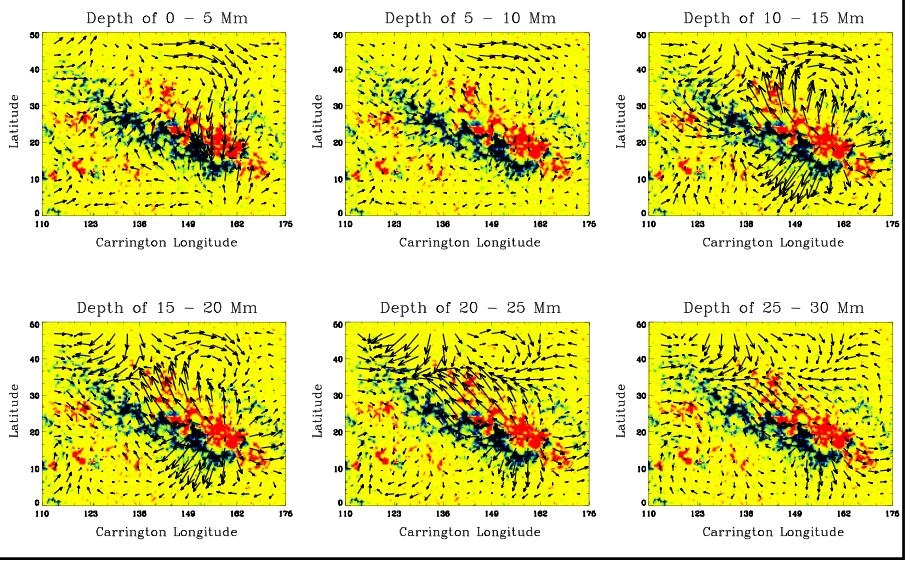

Sunspot structure and dynamics

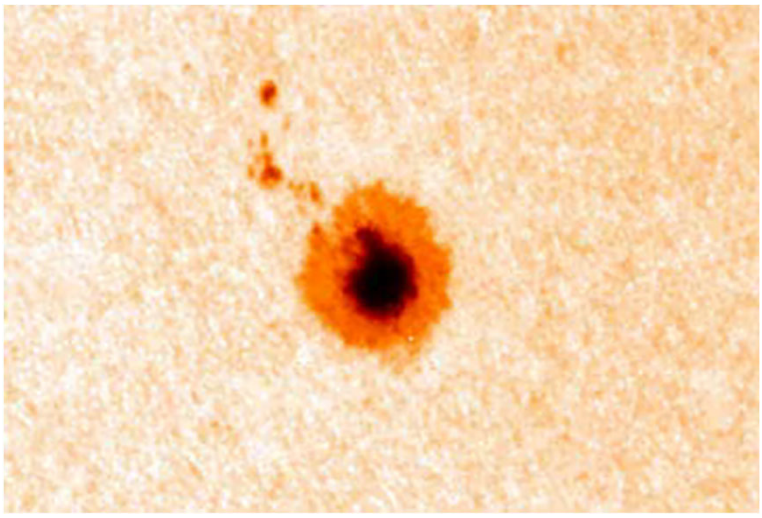

Parker's model

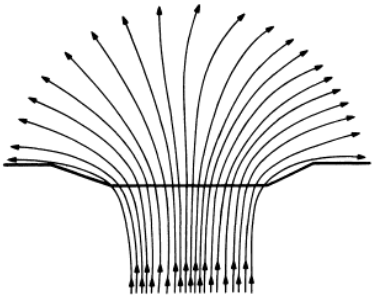

FIG. 1.—A sketch of the conventional idea of the magnetic field configuration of a sunspot. The heavy line represents the visible surface of the Sun.

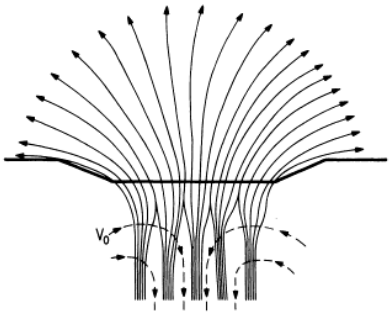

FIG. 2.—A sketch of the proposed magnetic field configuration, in which the field divides into individual flux tubes some distance below the visible surface. The dashed arrows represent the presumed convective downdraft which helps to hold the separate flux tubes together in the tight cluster that constitutes the sunspot.

Monolithic model

Cluster Model

Helioseismology provides strong evidence for the cluster model.

Observations of emerging active region by time-distance helioseismology

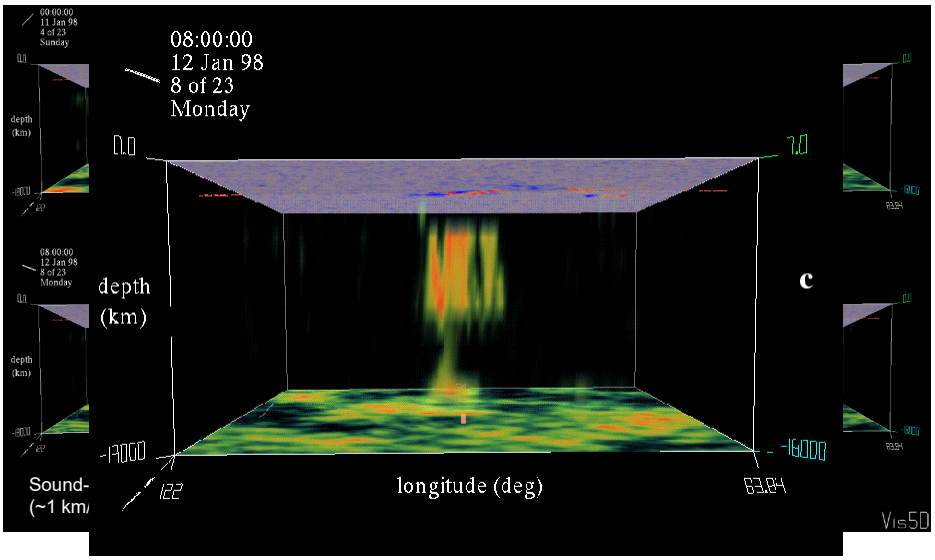

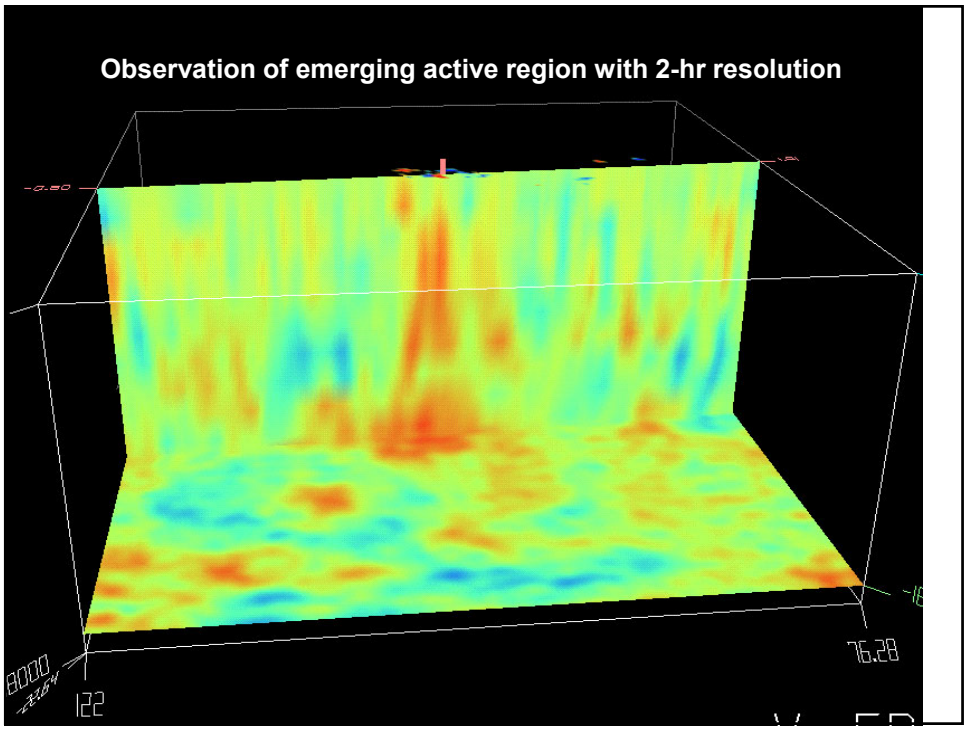

Evolution of AR 10486-488: October 24 – November 2, 2003

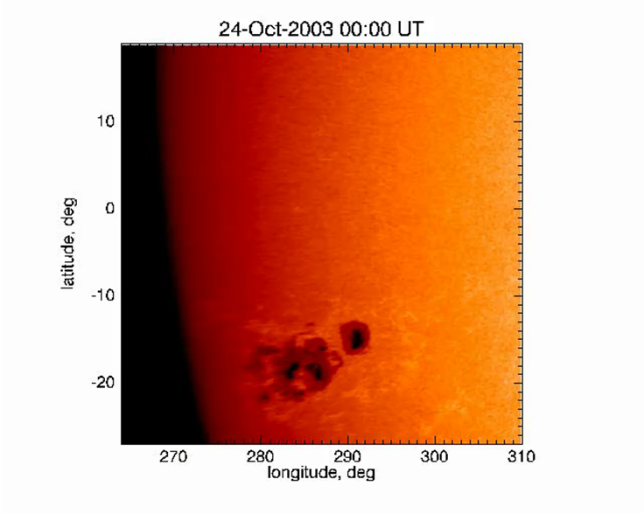

Sound-speed map and magnetogram of AR 10486 on October 25, 2003, 4:00 UT (depth of the lower panel: 45 Mm)

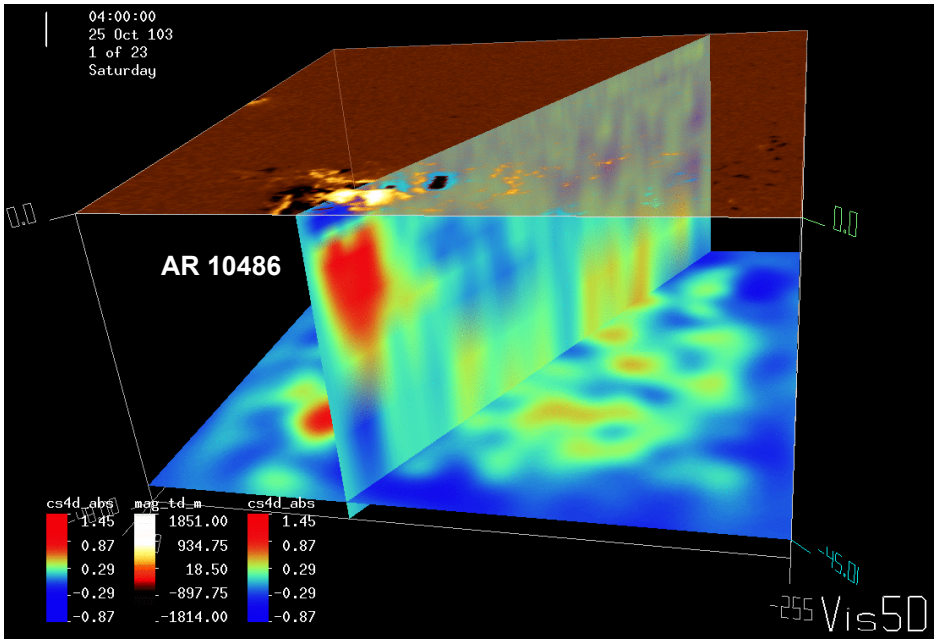

Sound-speed map and magnetogram of AR 10486 on October 26, 2003, 12:00 UT
AR 10488 is emerging

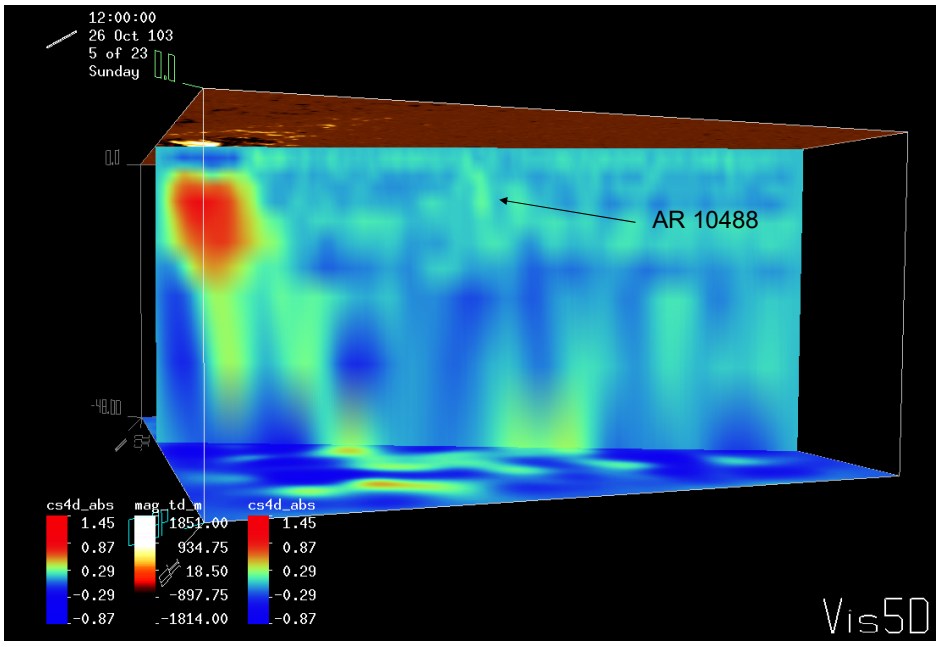

Emergence of AR 10488, October 26, 2003, 20:00 UT

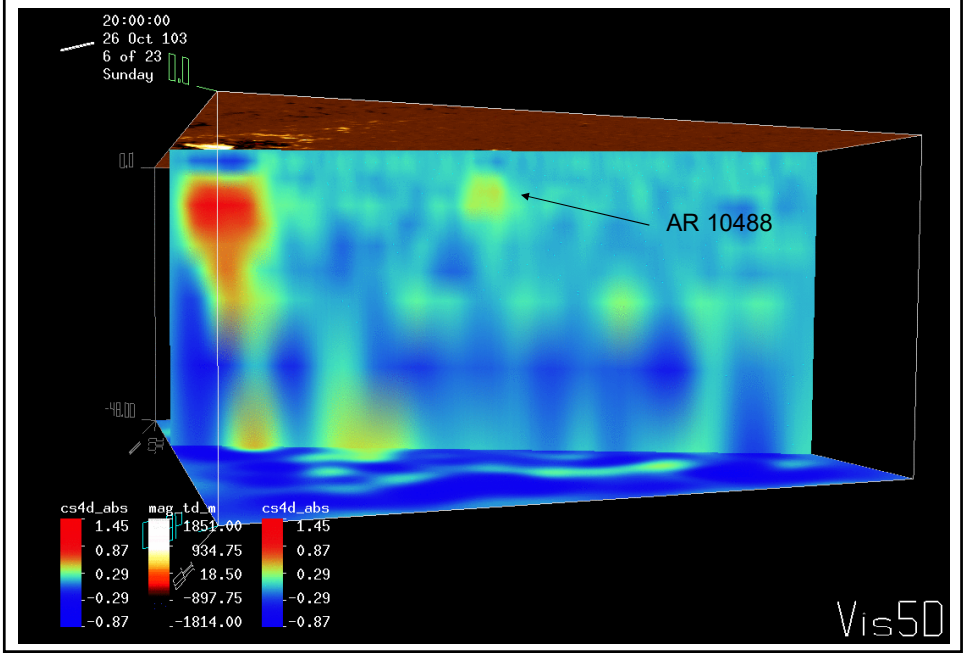

Emergence of AR 10488, October 27, 2003, 4:00 UT

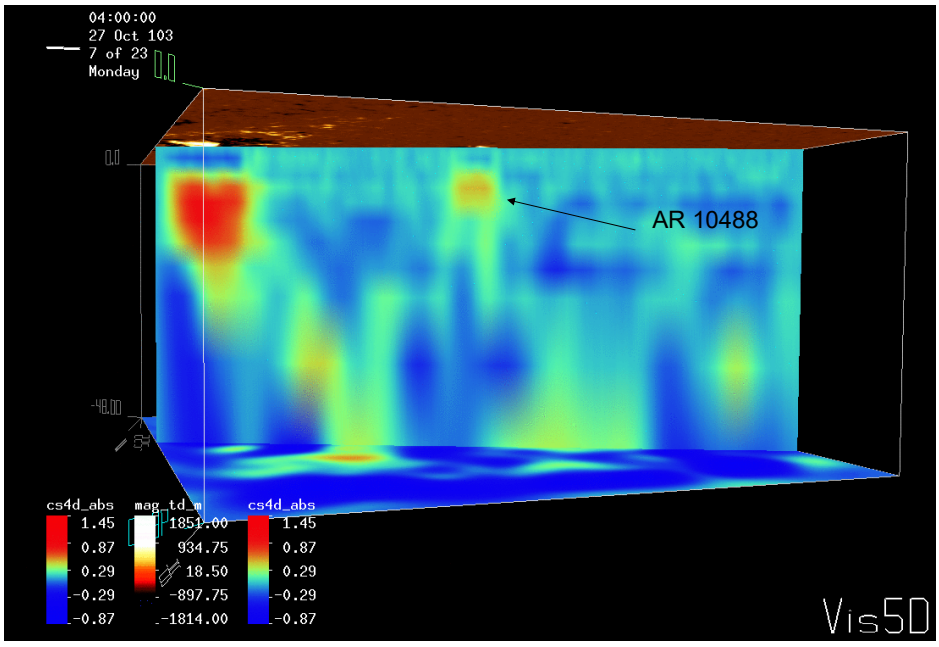

Growth and formation of sunspots of AR 10488, October 29, 2003, 4:00 UT

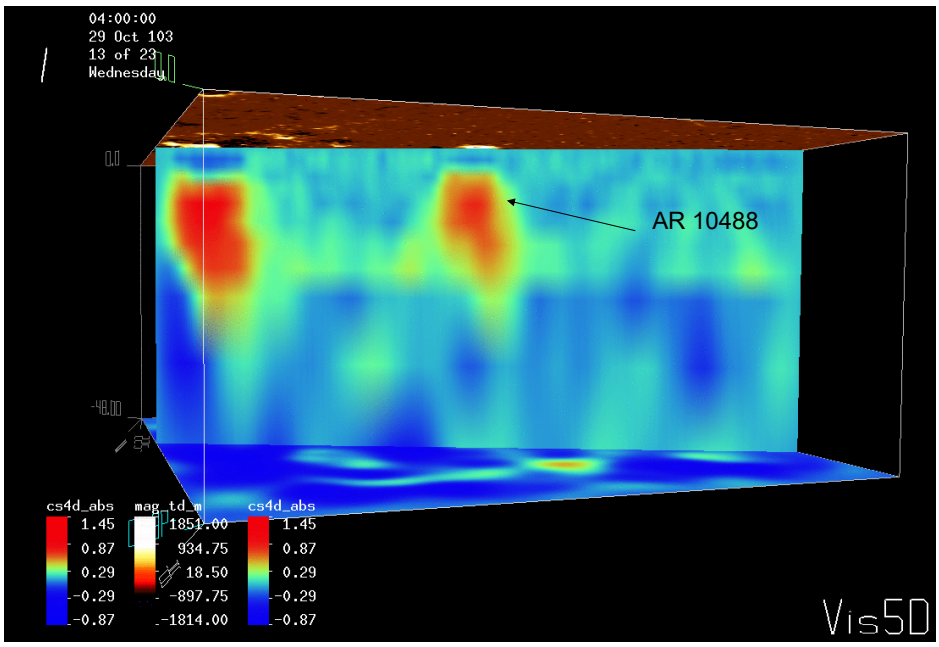

Growth and formation of sunspots of AR 10488, October 31, 2003, 12:00 UT

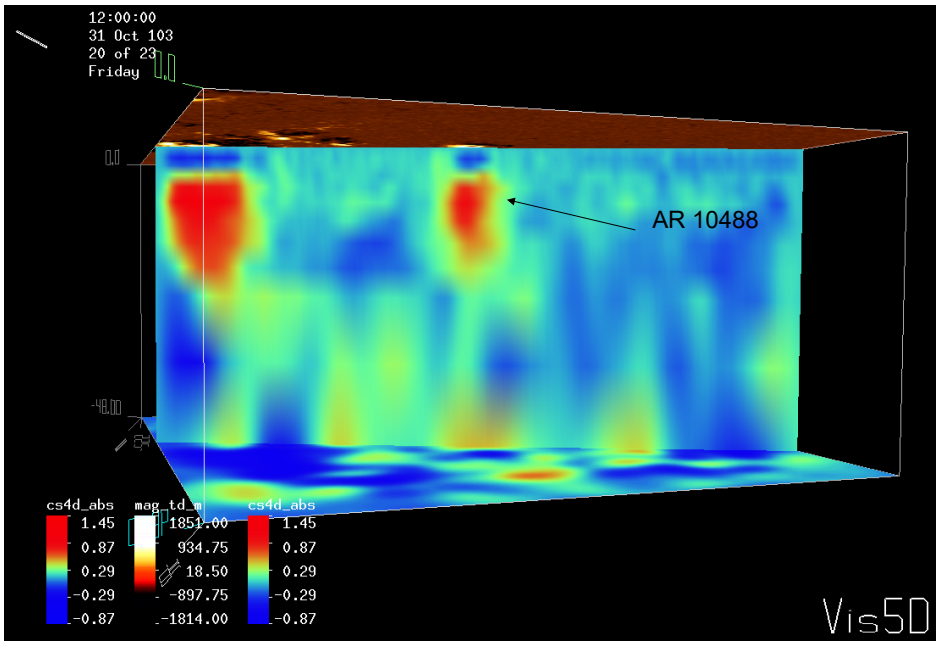

Cut in East-West direction through both magnetic polarities, showing a loop-like structure beneath AR 10488, October 30, 2003, 20:00 UT

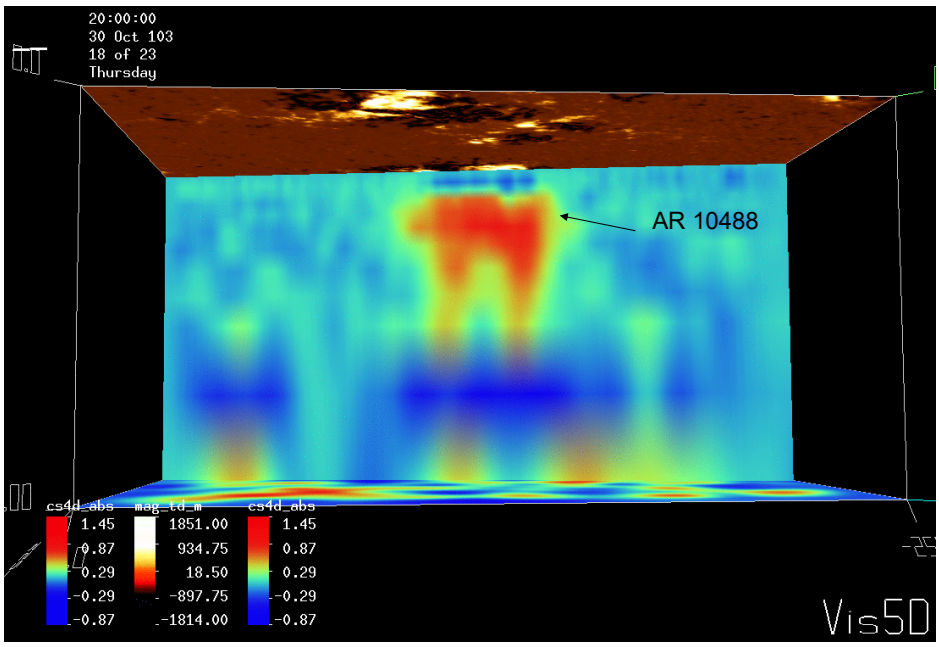

Detection of Emerging Active Regions in the Deep Interior

New methodology of detection of emerging flux

Deep-focus Time-Distance Helioseismology: solar oscillation signal is filtered to select acoustic waves traveling to depth 40-70 Mm (right), averaged over arcs (left), and cross-correlated for opposite arcs. Travel-time perturbations are measured by fitting Gabor wavelet. This method has been tested with 3 different instruments (MDI, HMI, GONG) for many quiet and emerging flux regions

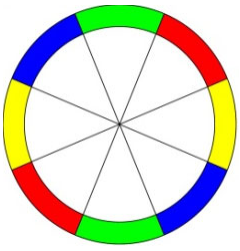

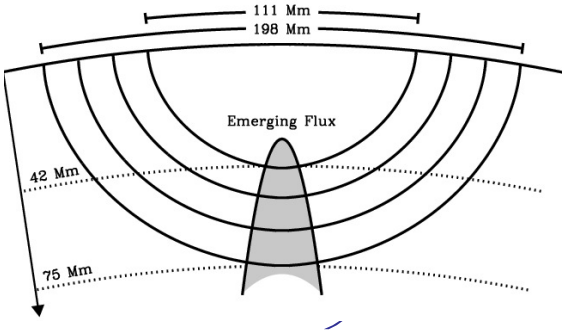

Ilonidis et al (2011)

Example: Emergence of AR 10488: Oct 24 – Nov 2, 2003

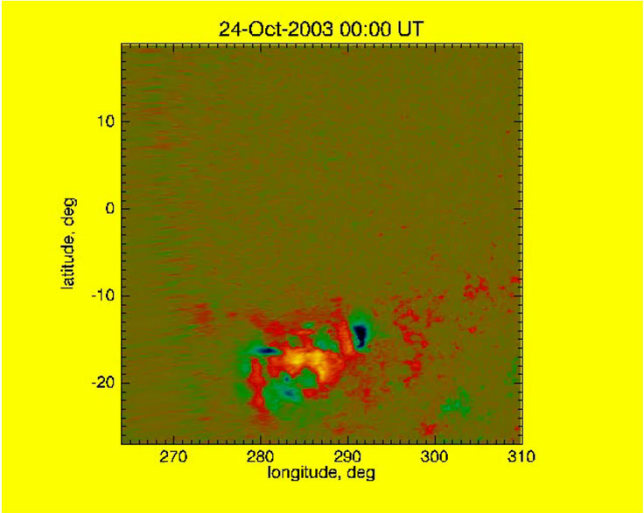

Results for AR 10488

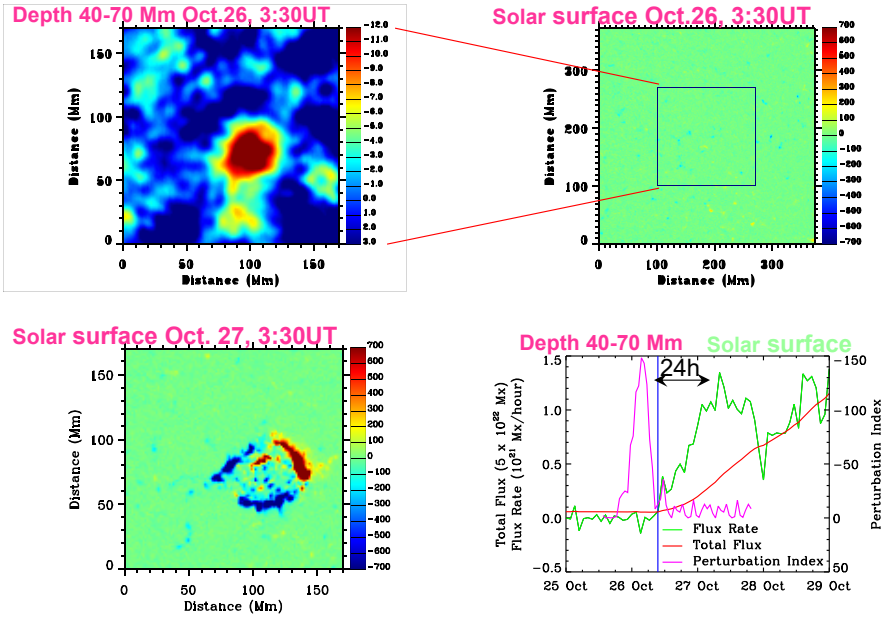

Travel-time maps of AR 10488

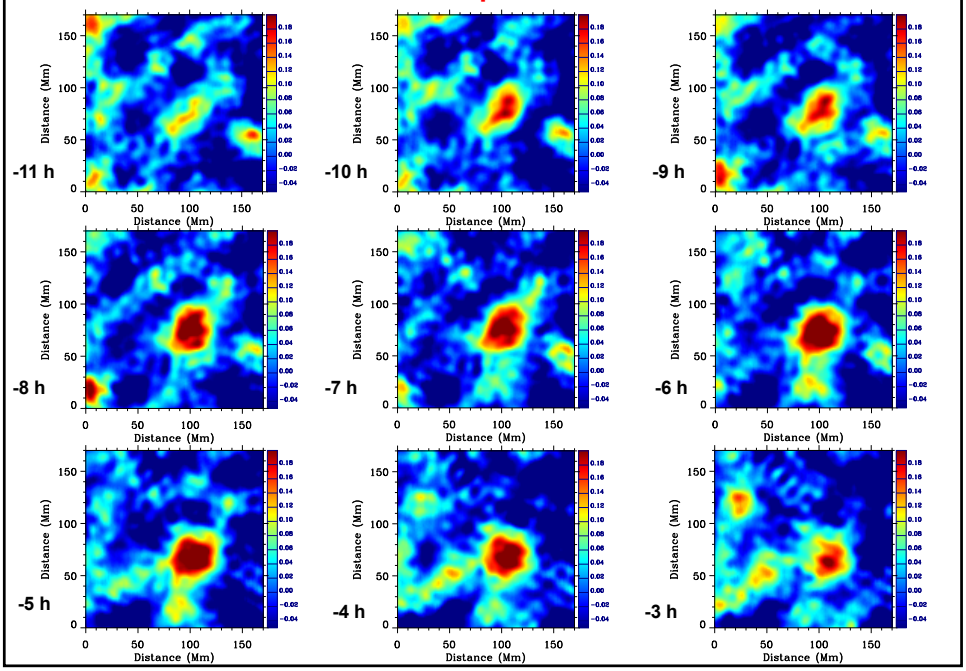

Active region NOAA 11158, February 2011

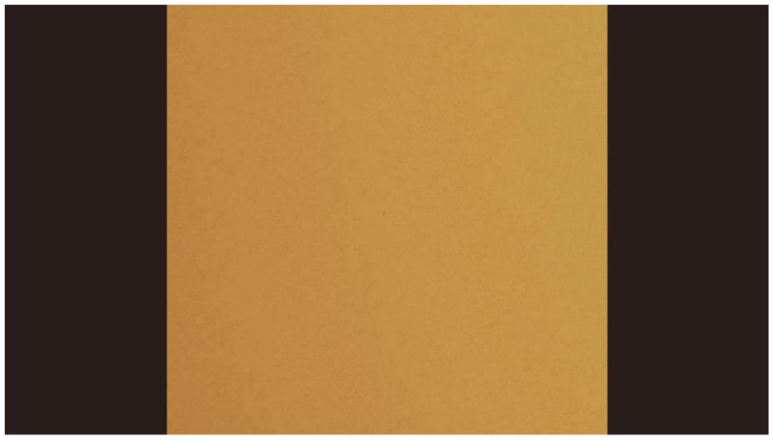

Example of analysis of subsurface flows in flaring AR 11158

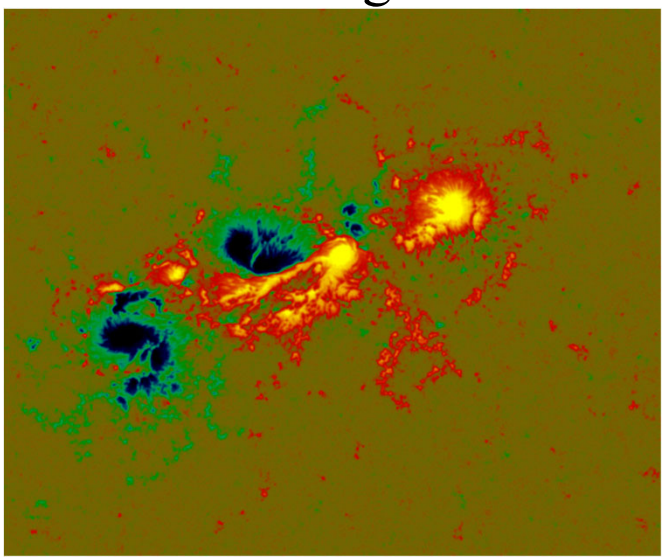

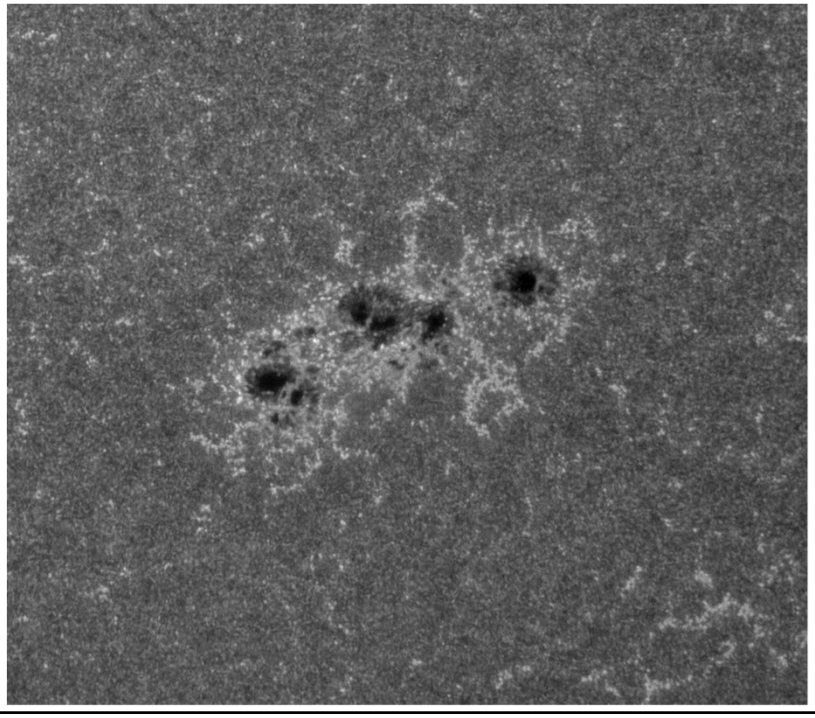

Photospheric magnetic field and subsurface flows at depth 0-1 Mm in AR 11158, February 10-18, 2011

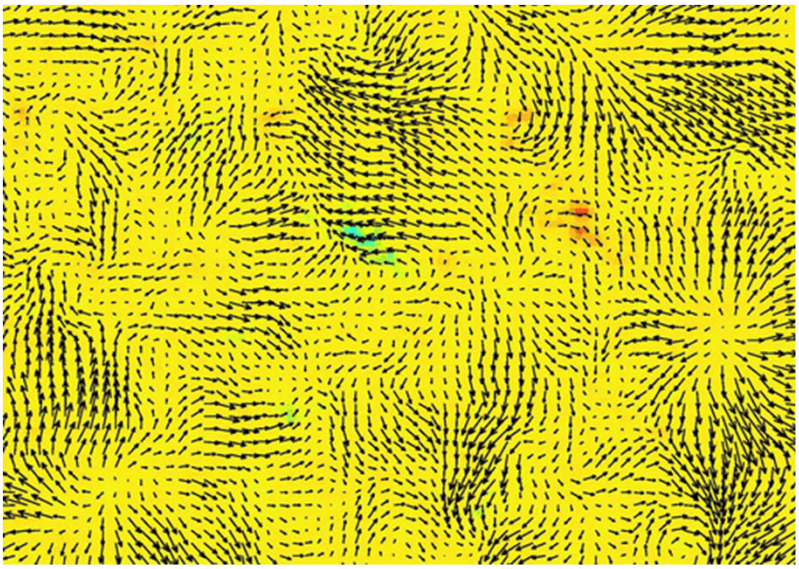

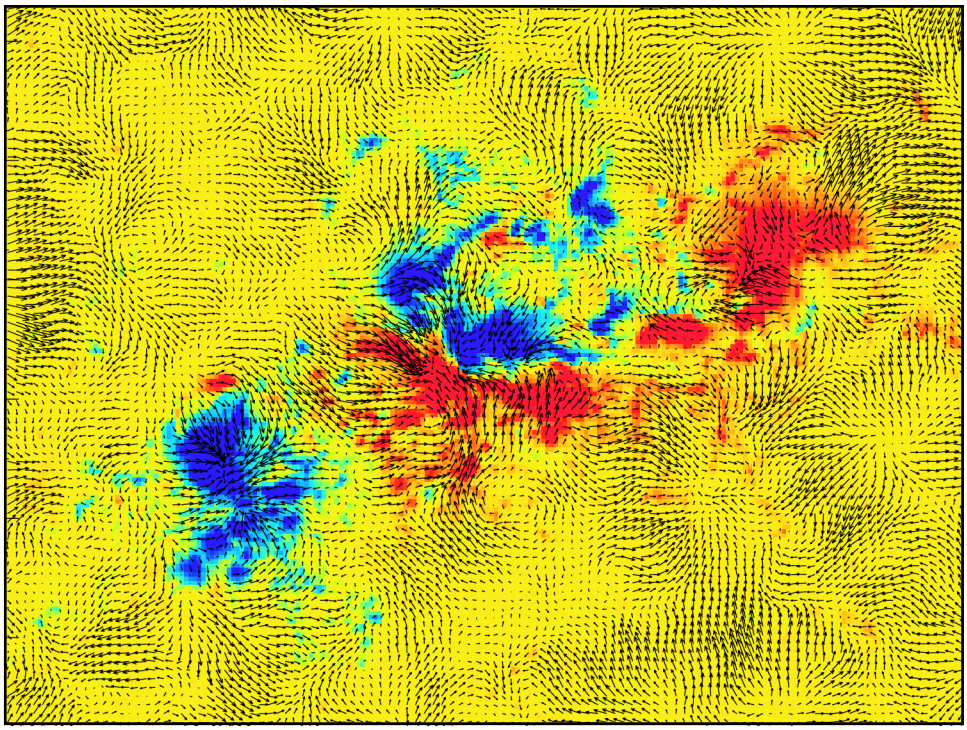

Subsurface converging flows and X2.2 flare

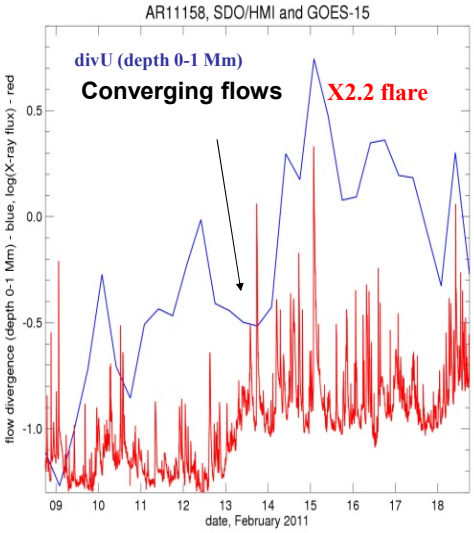

- **Approximately one day before the X-class flare strong shearing flows are developed 0-3 Mm below the surface. This is reflected in a sharp increase of the flow convergence.**
- **Potentially new method of forecasting flaring and CME activity of active regions based on helioseismology analysis and MHD modeling of subsurface flows.**

Lecture 23
Time-distance helioseismology: Fermat principle Inversion results

(Stix, Chapter 5.3.8-5.3.9; Kosovichev, p.53-64; Christensen-Dalsgaard, Chapter 8)

Solar oscillation spectrum obtained from the HMI instrument on Solar Dynamics Observatory.

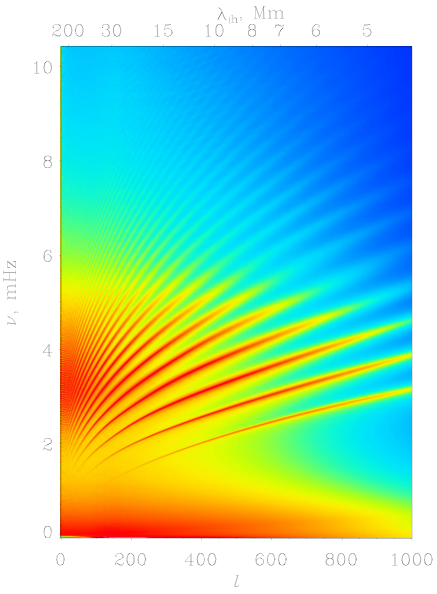

Spectrum of normal modes calculated for a standard solar model. Note the 'avoided crossing effect' for f and g-modes.

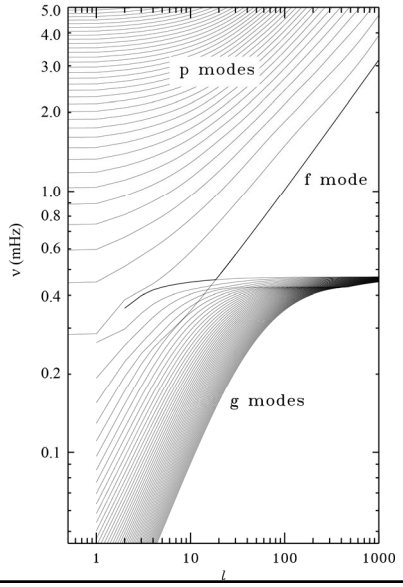

Low-degree p-modes (l=0,1,2, and 3)

For $l \ll n$, $r_1 \approx 0$, and we get: $\omega \approx \frac{\pi(n + L/2 + \alpha)}{\int_0^R \frac{dr}{c}}$.

That is the spectrum of low-degree p-modes is approximately equidistant with frequency spacing: $\Delta\nu = \left(4\int_0^R \frac{dr}{c}\right)^{-1}$. $\nu_{nl} \approx \Delta\nu(2n + l + \frac{1}{2} + 2\alpha) \approx \Delta\nu(2n + l + \frac{3}{2})$

Large frequency separation: Δν=68 μHz

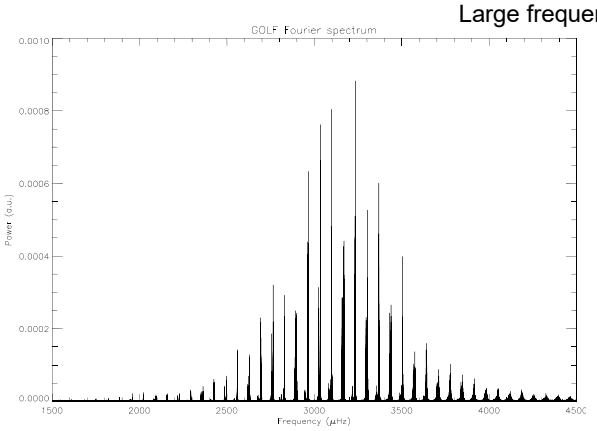

$$\delta\nu_{nl} = \nu_{nl} - \nu_{n-1,l+2} \approx$$

$$\approx -(4l + 6)\frac{\Delta_{nl}}{2\pi^2\nu_{nl}}\int_0^{R_\odot} \frac{dc}{dr}\frac{dr}{r}$$

Small frequency separation : δν=9μHz

Solar -modes from 1979 days of the GOLF experiment, B. Gelly - M. Lazrek- G. Grec - A. Ayad - F. X. Schmider- C. Renaud - D. Salabert - E. Fossat· A&A 394, 285-297 (2002)

Asteroseismology Scaling Law

Using the scaling laws:

$$\rho \sim \frac{M}{R^3}, \qquad \frac{P}{R} \sim \frac{GM^2}{R^5}$$

we obtain the scaling law for the speed of sound:

$$c \sim \sqrt{\frac{\gamma P}{\rho}} \sim \sqrt{\frac{M}{R}}.$$

Then, the scaling law for the oscillation frequencies is:

$$\nu \sim \frac{c}{R} \sim \sqrt{\frac{M}{R^3}}$$

Since for the Sun the large frequency separation: Δν=68 μHz we can estimate Δν for other stars:

$$\Delta\nu \approx 68\left(\frac{M}{M_\odot}\right)^{1/2}\left(\frac{R}{R_\odot}\right)^{-3/2} \quad (\mu Hz)$$

Solution to the Inverse Problem

We have a system integral equations

$$\frac{\delta\omega^{(n,l)}}{\omega^{(n,l)}} = \int_0^R K_{\rho,\gamma}^{(n,l)} \frac{\delta\rho}{\rho} dr + \int_0^R K_{\gamma,\rho}^{(n,l)} \frac{\delta\gamma}{\gamma} dr,$$

for a set of observed mode frequencies. If the number of observed frequencies is N (typically 2000), then we have a problem of determining two functions from this finite set. In general, it is impossible to determine these functions precisely. We can always find some rapidly oscillating functions, $f(r)$, that being added to the unknowns, $\delta\rho/\rho$ and $\delta\gamma/\gamma$, do not change the values of the integrals, e.g.

$$\int_0^R K_{\rho,\gamma}^{(n,l)}(r) f(r) dr = 0.$$

Such problems without an unique solution are called "ill-posed". The general approach is to find a smooth solution that satisfies the integral equations by applying some smoothness constraints to the unknown functions. This is called a "regularization procedure".

There are two basic methods for the helioseismic inverse problem:

1. Optimally Localized Averages (OLA) method - (Backus-Gilbert method)
2. Regularized Least-Squares (RLS) method - (Tikhonov method)

Examples of the sensitivity kernels

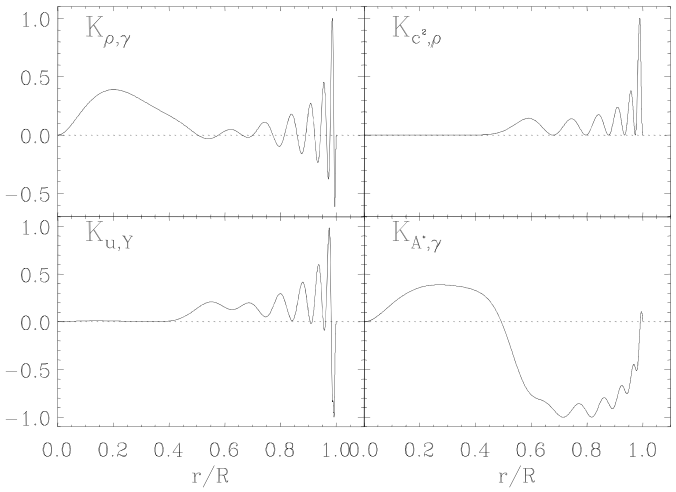

Optimally Localized Averages Method

The idea of the OLA method is to find a linear combination of data such as the corresponding linear combination of the sensitivity kernels for one unknown will have an isolated peak at a given radial point, r_0, (resemble a δ-function), and the combination for the other unknown will be close to zero. Then this linear combination provides an estimate for the first unknown at r_0:

$$\sum a^{(n,l)} \frac{\delta\omega^{(n,l)}}{\omega^{(n,l)}} = \int_0^R \sum a^{(n,l)} K_{\rho,\gamma}^{(n,l)} \frac{\delta\rho}{\rho} dr + \int_0^R \sum a^{(n,l)} K_{\gamma,\rho}^{(n,l)} \frac{\delta\gamma}{\gamma} dr.$$

If $\sum a^{(n,l)} K_{\rho,\gamma}^{(n,l)}(r) \sim \delta(r - r_0),$ and $\sum a^{(n,l)} K_{\gamma,\rho}^{(n,l)}(r) \sim 0,$

then

$$\overline{\left(\frac{\delta\rho}{\rho}\right)}_{r_0} = \sum a^{(n,l)} \frac{\delta\omega^{(n,l)}}{\omega^{(n,l)}},$$

is an estimate of the density perturbation at $r = r_0$.

The coefficients, $a^{(n,l)}$, are different for different target radii r_0.

Averaging Kernels

The functions,

$$\sum a^{(n,l)} K_{\rho,\gamma}^{(n,l)}(r) \equiv A(r_0, r),$$

$$\sum a^{(n,l)} K_{\gamma,\rho}^{(n,l)}(r) \equiv B(r_0, r),$$

are called "averaging kernels".

The coefficients, a^i, are determined my minimizing a quadratic form (here, we use index i instead of double index (n,l)):

$$M(r_0, A, \alpha, \beta) = \int_0^R J(r_0, r)\left[A(r_0, r)\right]^2 dr +$$
$$+\beta \int_0^R \left[B(r_0, r)\right]^2 dr + \alpha \sum_{i,j} E_{ij} a^i a^j,$$

where $J(r_0, r) = 12(r - r_0)^2$, E_{ij} is a covariance matrix of observational errors, α and β are the regularization parameters. The first integral in this equation represents the Backus-Gilbert criterion of δ-ness for $A(r_0, r)$; the second term minimizes the contribution from $B(r_0, r)$, thus, effectively eliminating the second unknown function, ($\delta\gamma/\gamma$ in this case); and the last term minimizes the errors.

Optimally localized averaging kernels

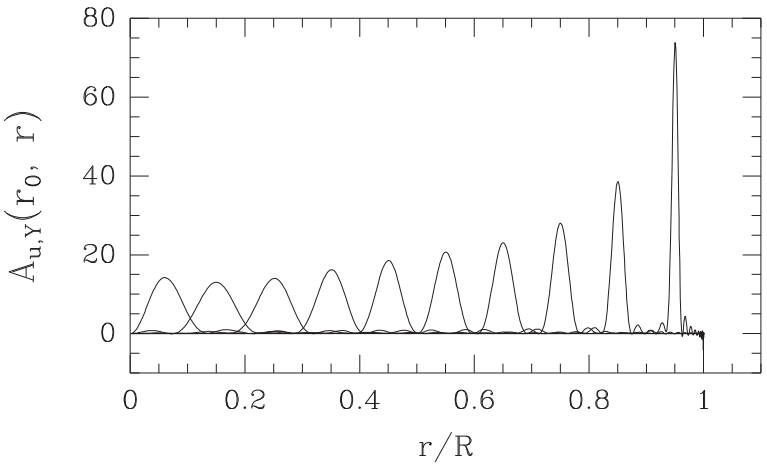

Inversion results for the observed solar frequencies

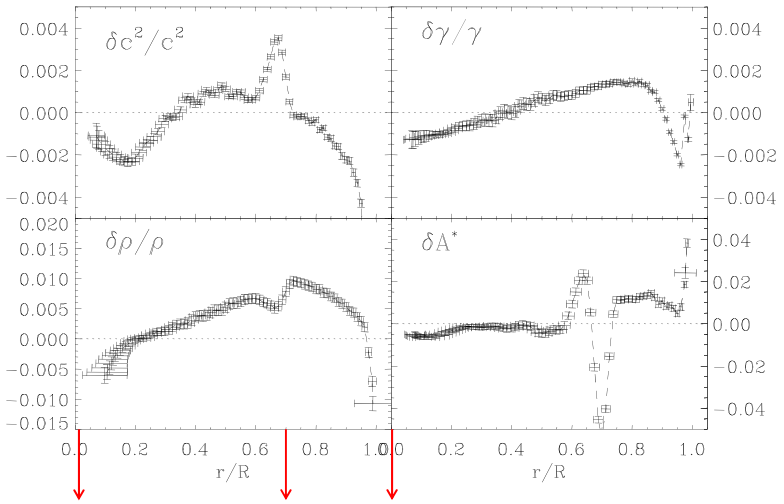

Solar radius R=696 Mm

Theory of Rotational Frequency Splitting. I

The eigenfrequencies of a spherically-symmetrical static star are degenerate with respect to the azimuthal number m. Rotation breaks the symmetry and splits each mode of radial order, n, and angular degree, l, into $(2l+1)$ components of $m = -l,...,l$ ('mode multiplets'). The rotational frequency splitting can be computed using the variational principle. From this variational principle, one can obtain mode frequencies ω_{nlm} relative to the degenerate frequency ω_{nl} of the non-rotating star:

$$\Delta\omega_{nlm} \equiv \omega_{nlm} - \omega_{nl} = \frac{1}{I_{nl}} \int_V \left[m\, \vec{\xi} \cdot \vec{\xi}^{\,*} + i e_\Omega (\vec{\xi} \times \vec{\xi}^{\,*}) \right] \Omega \rho dV ,$$

where e_Ω is the unit vector defining the rotation axis, and $\Omega = \Omega(r,\theta)$ is the angular velocity which is a function of radius r and co-latitude θ, and I_{nl} is the mode inertia.

The first term is due to the wave advection by rotation; the second term represents the Coriolis effect.

$\Delta\omega_{nlm} = m\bar{\Omega}$, where $\bar{\Omega}$ is a mean angular velocity.

For the rotational frequency splitting measured in Hz:

$\Delta\nu_{nlm} = m\bar{\Omega}/2\pi$. For the Sun: $\bar{\Omega}/2\pi \approx 460$ nHz

The corresponding mean period of rotation: $P = 2\pi/\bar{\Omega}$

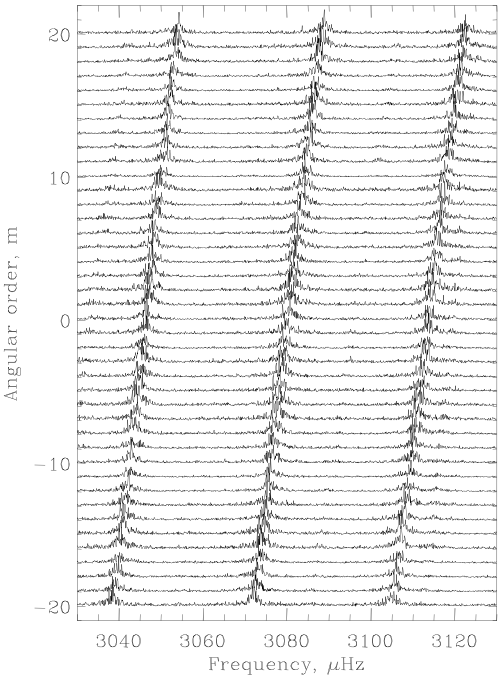

Illustration of the frequency shift due to the solar rotation

Typical power spectra of solar oscillation data from the MDI instrument on SOHO. Each horizontal curve shows three lines of the power spectrum for different azimuthal order m with radial order $n = 15$ and angular degree $l = 19, 20$, and 21 (from left to right). The slope of the modal lines is due to the rotational frequency shift: prograde modes with positive m have higher frequencies than retrograde modes with negative m.

Inversion results for solar rotation

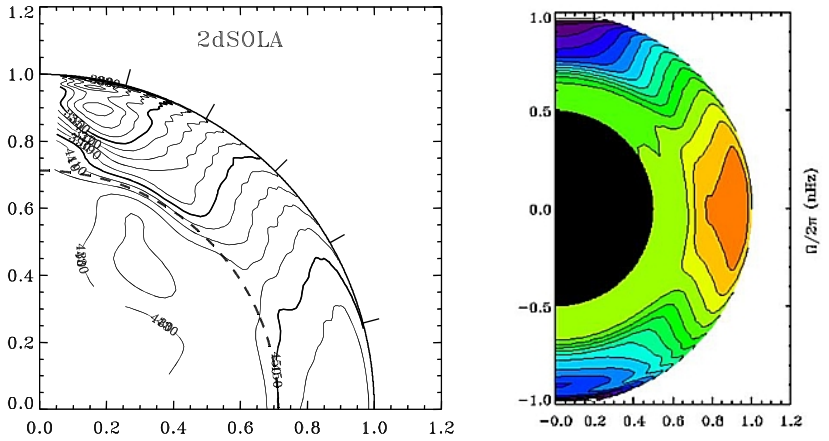

The radial profile of solar rotation

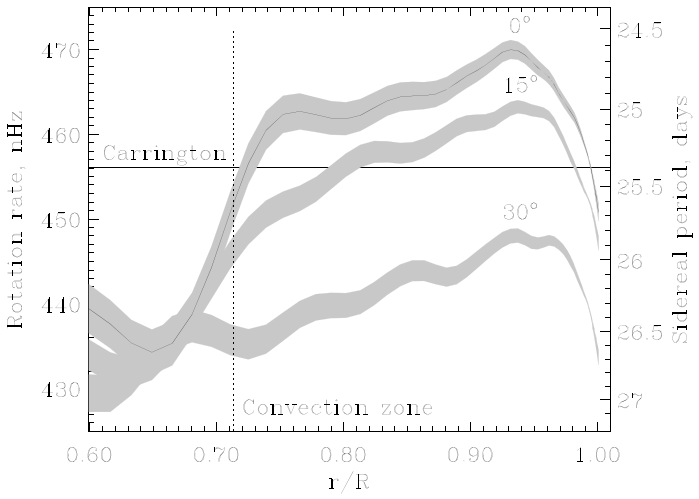

Quiz

Two principal approaches

- Global Helioseismology – measure global oscillation modes from the oscillation power spectra obtained by applying the spherical harmonic transform to the full-disk oscillation data
- Local Helioseismology - measure variations of oscillation frequencies in local areas by applying the Fourier transform to the oscillations in these area, or by measuring the travel times of phase shifts in local areas.

Time-distance helioseismology

A remarkable discovery was made by Tom Duvall in 1993 that the travel times of the solar waves can be measured by using a cross-covariance function of the stochastic wave field:

Integration time

$$\psi(\tau,\Delta) = \int_0^T f(t,r) f^*(t+\tau, r+\Delta) dt$$

or C(¿; ¢)

Time

Distance

Oscillation signal (Doppler velocity, intensity etc) at two points on the Sun's surface

Definition of normal modes

One way to represent the oscillations is as a sum of standing waves or normal modes, where the signal observed at a point (r,θ,ϕ) at time t is given by

$$f(r,\theta,\phi,t) = \sum_{nlm} a_{nlm} \xi_{nlm}(r,\theta,\phi) \exp(i[\omega_{nlm} t + \alpha_{nlm}]). \quad (1)$$

In this equation, the three integers n, l, and m identify each mode and are commonly called the *radial order*, *angular degree*, and *azimuthal order* respectively. For each mode, a_{nlm} is the mode amplitude, ω_{nlm} is the eigenfrequency, and α_{nlm} is the phase.

The spatial eigenfunction for each mode is denoted by ξ_{nlm}. For an axisymmetrical Sun, the eigenfunctions can be separated into radial and angular components:

$$\xi_{nlm}(r,\theta,\phi) = \xi_{nl}(r) Y_{lm}(\theta,\phi), \quad (2)$$

where Y_{lm} is the spherical harmonic and the radial eigenfunction is denoted now by $\xi_{nl}(r)$.

Is the Sun axisymmetrical?

What happens to the normal modes if the structure is not axisymmetrical?

Cross-covariance function in terms of normal modes

The *cross covariance* function of the oscillation signals f for two points at coordinates $\mathbf{r}_1$ and $\mathbf{r}_2$ on the solar surface is defined as the integral

$$\psi(\tau,\Delta)=\int_0^T f(\mathbf{r}_1,t+\tau)f^*(\mathbf{r}_2,t)\,dt. \qquad (3)$$

Here Δ is used to denote the angular distance between the two points and T is the total length of the observations. The time delay τ measures the amount that one signal is shifted relative to the other. In practice, it is quite time-consuming to compute the cross correlation with the integral in equation 3. Fortunately, the convolution theorem allows us to change the integral into a product in the Fourier domain,

$$\Psi(\omega,\tau,\Delta)=F(\mathbf{r}_1,\omega)\,F^*(\mathbf{r}_2,\omega). \qquad (4)$$

Here Ψ is used to represent the temporal (τ) Fourier transform of ψ, and F represents the temporal Fourier transform of f. The length T of the observations is assumed to be long compared to any time lag τ of interest. Since Fourier transforms can be computed very efficiently, equation 4 provides a relatively fast way to compute cross correlations.

Assuming that the oscillation signal f can be written in the form of equation 1, the Fourier transform F of the observed oscillation signal is given by

$$F(\omega,R,\theta,\phi)=\sum_{nlm} a_{nlm}\xi_{nl}(R)Y_{lm}(\theta,\phi)e^{-i\alpha_{nlm}}\delta(\omega-\omega_{nlm}). \qquad (5)$$

Here the solar surface is denoted by $r=R$. The power spectrum of solar oscillations is band-limited. For convenience, let us assume that the amplitudes depend on n and l in the following way:

$$\sum_{nlm} a_{nlm}\xi_{nl}(R)Y_{lm}(\theta,\phi)e^{-i\alpha_{nlm}}\delta(\omega-\omega_{nlm})=\sum_{nlm} G_l(\omega_{nl})Y_{lm}(\theta,\phi)e^{-i\alpha_{nlm}}\delta(\omega-\omega_{nlm}), \quad (6)$$

where $$G_l^2(\omega)=\sqrt{2l+1}\exp\left(-\frac{(\omega-\omega_0)^2}{\delta\omega^2}\right). \qquad (7)$$

If I then compute the product in equation 4 and perform the inverse Fourier integral, the result is

$$\psi(\tau,\Delta)=\sum_{nl} G_l^2(\omega_{nl})\exp(i\omega_{nl}\tau)\sum_m\sum_{m'} Y_{lm}(\theta_1,\phi_1)e^{i\alpha_{nlm}}Y_{lm'}^*(\theta_2,\phi_2)e^{-i\alpha_{nlm'}}. \qquad (8)$$

Since the phases are random, we assume that on average the terms $e^{i(\alpha_{nlm}-\alpha_{nlm'})}$ will tend to cancel, except of course when $m=m'$. In this case, equation 8 becomes

$$\psi(\tau,\Delta)=\sum_{nl} G_l^2(\omega_{nl})\exp(i\omega_{nl}\tau)\sum_m Y_{lm}(\theta_1,\phi_1)Y_{lm}^*(\theta_2,\phi_2). \qquad (9)$$

The addition theorem for spherical harmonics

$$\sum_{m=-l}^{l} Y_{lm}(\theta_1,\phi_1)Y_{lm}^*(\theta_2,\phi_2) = \alpha_l P_l(\cos\Delta),$$

(see, for example, Jackson, Classical Electrodynamics) allows the simplification

$$\psi(\tau,\Delta) = \sum_{nl} G_l^2(\omega_{nl})\exp(i\omega_{nl}\tau)\left(\frac{2l+1}{4\pi}\right)P_l(\cos\Delta), \qquad (10)$$

where Δ is the distance between the two points (θ_1,ϕ_1) and (θ_2,ϕ_2):

$$\cos\Delta = \cos\theta_1\cos\theta_2 + \sin\theta_1\sin\theta_2\cos(\phi_1-\phi_2), \qquad (11)$$

and P_l is the Legendre polynomial of order l.

Again following Jackson we can approximate

$$P_l(\cos\Delta) \approx J_0\left(\left[2l+1\right]\sin\frac{\Delta}{2}\right) \approx \sqrt{\frac{2}{\pi L\Delta}}\cos\left(L\Delta - \frac{\pi}{4}\right), \qquad (12)$$

where J_0 is the Bessel function of the first kind. We have introduced the new symbol $L \equiv l+1/2$; these approximations are valid where Δ is small, but $L\Delta$ is large.

Then we have

$$\psi(\tau,\Delta) = \sum_{nl}\frac{2}{\sqrt{\pi\Delta}}\exp\left(-\frac{(\omega_{nl}-\omega_0)^2}{\delta\omega^2}\right)\cos(\omega_{nl}\tau)\cos(L\Delta). \qquad (13)$$

Now the double sum can be reduced to a convenient sum of integrals if we regroup the modes so that the outer sum is over the ratio $v \equiv \omega/L$ and the inner sum is over ω.

You have learned that the radius of the lower turning point is determined by the ratio $v \equiv \omega/L$. Thus, the travel distance Δ of an acoustic wave is also determined by this ratio v; Δ is otherwise independent of ω.

In this case, given the band-limited nature of the function G, only values of L which are close to $L_0 \equiv \omega_0/v$ will contribute to the sum, and we can expand L near the central frequency ω_0:

$$L\Delta \approx \Delta\left[L(\omega_0) + \frac{\partial L}{\partial\omega}(\omega-\omega_0)\right] = \Delta\left[\frac{\omega_0}{v} + \frac{\omega-\omega_0}{u}\right], \qquad (14)$$

where $u \equiv \partial\omega/\partial L$.

Furthermore, the product of cosines in equation 13 can be changed into a sum; one term is

$$\cos\left[\left(\tau - \frac{\Delta}{u}\right)\omega + \left(\frac{1}{u} - \frac{1}{v}\right)\Delta\omega_0\right], \qquad (15)$$

and the other term is identical except that τ has been replaced with $-\tau$ (*i.e.* the time lag is negative). The result is that the double sum in equation 13 becomes

$$\psi(\tau,\Delta) = \sum_{v}\frac{2}{\sqrt{\pi\Delta}}\sum_{\omega}\exp\left(-\frac{(\omega-\omega_0)^2}{\delta\omega^2}\right)\cos\left(\left[\pm\tau - \frac{\Delta}{u}\right]\omega + \left[\frac{1}{u} - \frac{1}{v}\right]\Delta\omega_0\right). \qquad (16)$$

The inner sum can be approximated by an integral over ω; it can be shown that

$$\int_{-\infty}^{\infty} d\omega \exp\left(-\frac{(\omega-\omega_0)^2}{\delta\omega^2}\right)\cos\left(\left[\tau-\frac{\Delta}{u}\right]\omega-\left[\frac{1}{u}-\frac{1}{v}\right]\Delta\omega_0\right)=$$

$$\sqrt{\pi\,\delta\omega^2}\exp\left(-\frac{\delta\omega^2}{4}\left[\tau-\frac{\Delta}{u}\right]^2\right)\cos\left(\omega_0\left(\tau-\frac{\Delta}{v}\right)\right). \qquad (17)$$

The limits $(-\infty,\infty)$ pose no particular problem since the amplitude function G^2 is essentially zero for very large and very small frequencies.

Finally, then, the cross correlation can be expressed as

$$\psi(\tau,\Delta)\propto\sum_{v}\exp\left(-\frac{\delta\omega^2}{4}\left[\tau\pm\frac{\Delta}{u}\right]^2\right)\cos\left(\omega_0\left[\tau\pm\frac{\Delta}{v}\right]\right) \qquad (18)$$

The cross correlation function at any particular distance is thus described by two characteristic times; the *group time*, defined as $\tau_g\equiv\Delta/u$, and the *phase time*, defined as $\tau_p\equiv\Delta/v$. Furthermore, the cross correlation will have two peaks; one near $+\tau_g$, and the other near $-\tau_g$. These two peaks correspond to the two directions of propagation.

Two representations of the covariance function

$$\psi(\tau,\Delta)=\sum_{nl}\frac{2}{\sqrt{\pi\Delta}}\exp\left(-\frac{(\omega_{nl}-\omega_0)^2}{\delta\omega^2}\right)\cos(\omega_{nl}\tau)\cos(L\Delta).$$

-in terms of the normal mode frequencies. (Once you know changes in mode frequencies you can find the corresponding changes in the cross-covariance function and travel times.)

$$\psi(\tau,\Delta)\propto\sum_{v}\exp\left(-\frac{\delta\omega^2}{4}\left[\tau\pm\frac{\Delta}{u}\right]^2\right)\cos\left(\omega_0\left[\tau\pm\frac{\Delta}{v}\right]\right)$$

- in terms of the phase and group velocities or travel times.

The key difference between "global" helioseismology and time-distance helioseismology is the mode coupling in the cross-covariance function. Thus, we can apply time-distance helioseismology to the non-axisymmetrical Sun.

Time-distance measurements

Travel times are determined from the cross-covariance function:

$$\psi(\tau,\Delta)=\int_0^T f(t,r)f^*(t+\tau,r+\Delta)dt$$

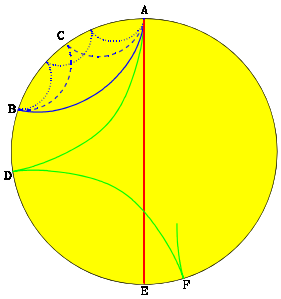

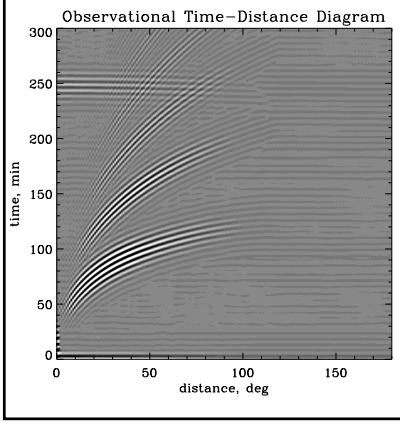

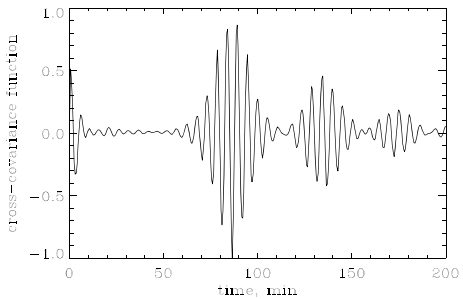

Cross-covariance function for a particular distance (30 degrees in this case) represents a series of wave packets.

Simple interpretation of time-distance measurements

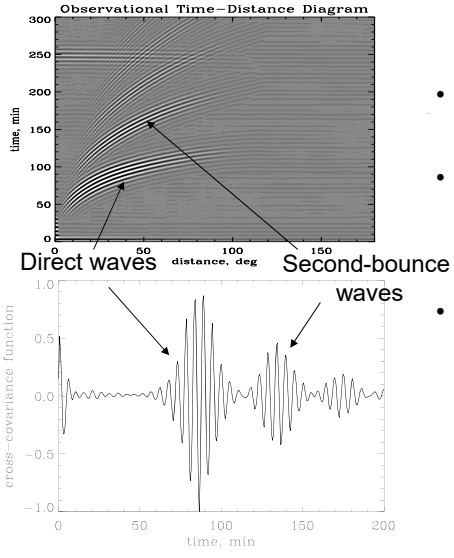

- The cross-covariance function collects coherent signals for solar waves excited at a given point and traveling to another point
- The cross-covariance signal corresponds to a strong point source (similar to the flare signal) – Claerbout's conjecture
- The cross-covariance signal corresponds to a wave packet of waves in a finite frequency range. The solar oscillations have periods around 5 min. Thus, we see the 5-min periodicity in the wave packet.
- The cross-covariance function can be used for measuring group and phase travel times.

We measure the group and phase travel times from these diagrams.

Book: Passive Imaging With Ambient Noise

J. Garnier, G. Papanicolaou, 2016

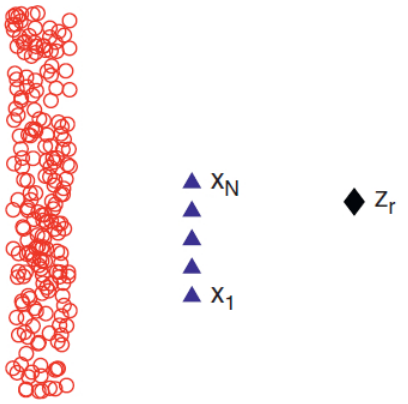

Correlation-based imaging with an array of passive sensors(triangles). Data acquisition, in which the reflector to be imaged (diamond) is located at Zr, and is illuminated by noise source (circles).

Time-distance diagnostics

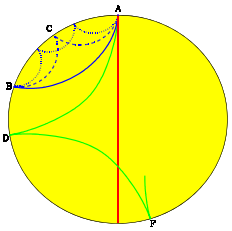

Fermat's PrincipleA powerful property of ray paths is that they obey Fermat's Principle, which states that the travel time along the ray is stationary with respect to small changes in the path. This implies that if a small perturbation is made to the background state, the ray path is unchanged.

The perturbation to the travel time can then be expressed as

$$\tau - \tau_0 = \frac{1}{\omega}\int_{\Gamma_0} \delta k \, ds.$$

Here δk is the perturbation to the wavevector due to inhomogeneities in the background state, and Fermat's principle allows us to make the integral along the unperturbed ray path Γ_0.

Travel time of acoustic waves

In the solar convection zone, the Brunt-Väisälä frequency N is small compared to the acoustic cutoff frequency and the typical frequencies of solar oscillations. Neglecting this frequency, the dispersion relation can be written as

$$k_r^2 = \frac{1}{c^2}\left(\omega^2 - \omega_C^2\right) - k_h^2,$$
$$k_h^2 = \frac{l(l+1)}{r^2}.$$

If we allow small perturbations (relative to the background state) in ω, c^2, and ω_C^2, then the integrand in Fermat's equation can be written to first order as

$$\frac{\delta k\, ds}{\omega} = \left[-\left(\frac{\delta c}{c}\right)\frac{k}{\omega} - \left(\frac{\delta\omega_C}{\omega_C}\right)\left(\frac{\omega_C^2}{c^2\omega^2}\right)\frac{\omega}{k}\right] ds,$$

where I have neglected terms which are second-order in $\delta c/c$ and $|u|/c$.

Effect of velocity field

One possible perturbation to the spherically symmetric background state is a velocity field. If the flow field is described by $\mathbf{u}$ then the observed frequency will be Doppler shifted by the advection of the oscillations,

$$\delta\omega = -k\hat{\mathbf{n}}\cdot\mathbf{u},$$

so that the Fermat's equation becomes

$$\tau^{\pm} - \tau_0 = -\int_{\Gamma_0}\left[\frac{\mathbf{u}\cdot(\pm\hat{\mathbf{n}})}{c^2} + \left(\frac{\delta c}{c}\right)\frac{k}{\omega} + \left(\frac{\delta\omega_C}{\omega_C}\right)\left(\frac{\omega_C^2}{c^2\omega^2}\right)\frac{\omega}{k}\right] ds,$$

where $\hat{\mathbf{n}}$ is a unit vector tangent to the ray path. Here I have defined the quantity τ^+ as the perturbed travel time in one direction along the ray path (unit vector $+\hat{\mathbf{n}}$) and τ^- as the perturbed travel time in the opposite (reciprocal) direction (unit vector $-\hat{\mathbf{n}}$).

Separation of the velocity field signal from the other perturbations

To separate the effects of the velocity field from the other perturbations, we thus define

$$\delta\tau_{\text{diff}} \equiv \tau^{+} - \tau^{-} = -2\int_{\Gamma_0} \frac{\mathbf{u}\cdot\hat{\mathbf{n}}}{c^2} ds$$

$$\delta\tau_{\text{mean}} \equiv \frac{(\tau^{+} + \tau^{-})}{2} = \tau_0 - \int_{\Gamma_0} \left[\left(\frac{\delta c}{c}\right)\frac{k}{\omega} + \left(\frac{\delta\omega_C}{\omega_C}\right)\left(\frac{\omega_C^2}{c^2\omega^2}\right)\frac{\omega}{k} \right] ds.$$

This equation thus provides the link between the measured travel time differences and the flow field along the ray path. This simple equation is in the heart of the time-distance helioseismology.

For simplicity, we will neglect variations of $\delta\omega_c$.
This is not valid in sunspot regions.

Time-distance inferences of the sound speed and flow velocity

Measures travel times of acoustic or surface gravity waves propagating between different surface points through the interior. The travel times depend on conditions, flow velocity and sound speed along the ray path:

$$\delta\tau = -\int_{\Gamma} \frac{k}{\omega}\frac{\delta c}{c} ds - \int_{\Gamma} \frac{\left(\vec{n}\cdot\vec{U}\right)}{c^2} ds$$

The sound speed and flow velocity signals are separated by measuring the travel times for waves propagating in the opposite directions along the same ray paths and calculating the mean travel times and the differences:

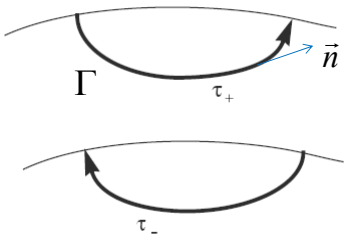

$$\delta\tau_{\text{mean}} = \frac{1}{2}(\tau_+ + \tau_-) = -\int_{\Gamma} \frac{k}{\omega}\frac{\delta c}{c} ds$$

$$\delta\tau_{\text{diff}} = \tau_+ - \tau_- = -\int_{\Gamma} \frac{\left(\vec{n}\cdot\vec{U}\right)}{c^2} ds$$

Vector velocity measurement scheme

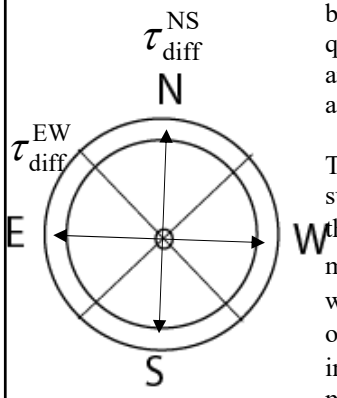

τ^{oi}_{diff} is a travel time difference averaged over the full annulus.

Typically, we measure times for acoustic waves to travel between points on the solar surface and surrounding quadrants symmetrical relative to the North, South, East and West directions. In each quadrant, the travel times are averaged over narrow ranges of travel distance Δ.

Then, the times for northward-directed waves are subtracted from the times for south-directed waves to yield the time, τ^{NS}_{diff}, which predominantly measures north-south motions. Similarly, the time differences, τ^{EW}_{diff}, between westward- and eastward directed waves yields a measure of east-ward motion. The time, τ^{oi}_{diff}, between outward- and inward-directed waves, averaged over the full annuli, is mainly sensitive to vertical motion and the horizontal divergence.

This provides a qualitative picture of the motions, and is useful for a preliminary analysis. However, in numerical inversions, all three components of the flow velocity are properly taken into account. The averaging procedure is essential for reducing noise in the data.

Tomographic Inversion

We assume that the convective structures and flows do not change during the observations and represent them by a discrete model. In the model, the 3D region of wave propagation is divided into rectangular blocks. The perturbations of the sound speed and the three of the flow velocity are approximated by linear functions of coordinates within each block, e.g.

$$\delta c(x,y,z) = \sum c_{ijk}\left[1-\frac{|x-x_i|}{x_{i+1}-x_i}\right]\left[1-\frac{|y-y_j|}{y_{j+1}-y_j}\right]\left[1-\frac{|z-z_k|}{z_{k+1}-z_k}\right]$$

According to the averaging procedure of the cross-covariance function, the travel time measured at a point on the surface is the result of the cumulative effects of the perturbations in each of the traversed rays of the 3D ray systems (see Figure below). Therefore, we average the equations for $\delta\tau$ over the ray systems corresponding to the different radial distance intervals of the data, using approximately the same number of ray paths as in the observational procedure. As a result, we obtain two systems of linear equations that relate the data to the sound speed variation and to the flow velocity, e.g. for the sound speed

$$\delta\tau_{\lambda\mu\nu} = \sum_{ijk} A^{ijk}_{\lambda\mu\nu}\ \delta c_{ijk}$$

where matrix A maps the structure properties into the observed travel time variations, λ and μ define the location of the central point of a ray system on the surface, and ν labels surrounding annuli. The equation is solved by a regularized least-squares technique.

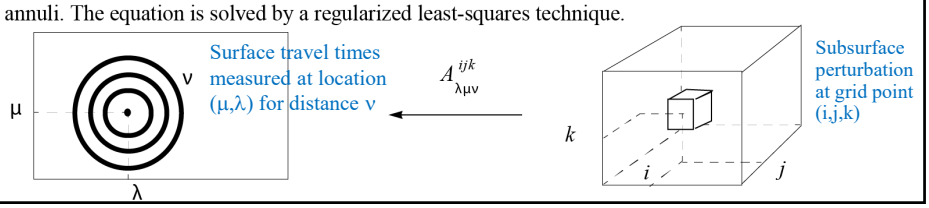

Deep- and surface-focusing observing schemes

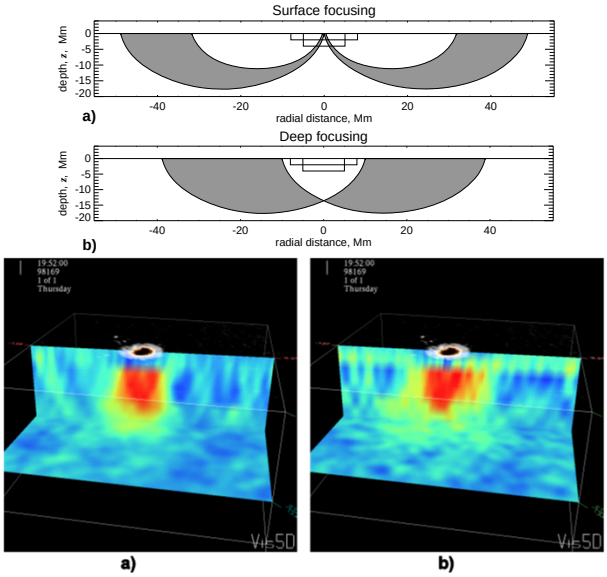

Ray approximation

- Originally, time-distance helioseismology was intuitively derived from the picture of acoustic ray paths.
- In fact, the acoustic waves observed on the Sun can be considered high-frequency acoustic waves. In most of the region in which these waves are confined, their wavelengths are short compared to the local temperature and density scale heights. In this wavelength regime, the wave propagation can be approximated with ray theory.

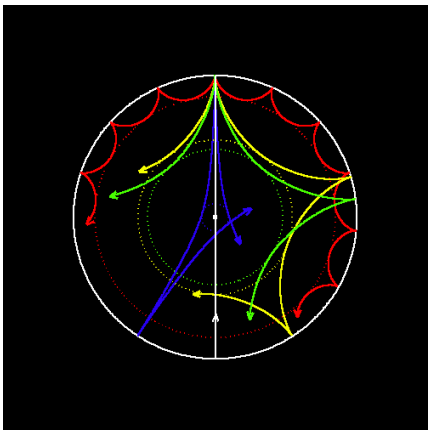

Sensitivity kernels for travel-time measurements in the Born approximation

- Properties of the solar interior are related to the measured travel times through sensitivity kernels (e.g. for sound speed):

$$\delta\tau(\Delta) = \int_V K_T(\vec{r},\Delta)\frac{\delta c}{c}dV$$

where integration is over the whole volume of the Sun.

- These kernel are calculated in the Born approximation as in terms as a combination of normal mode eigenfunctions.
- The sound-speed variations, flow velocity and other solar properties are determined from this equation by inversion.

"Banana-doughnut kernel"

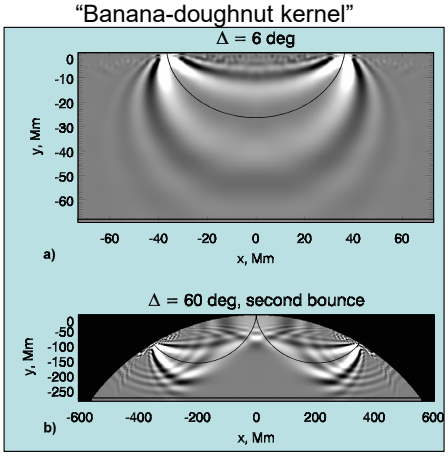

Examples of travel-time sensitivity kernels for the first and second bounces calculated in the Born approximation. The black curves show the corresponding ray paths.

Sound-speed structure beneath a sunspot (Couvidat et al 2005)

Ray approximation (old) | Born theory (new)

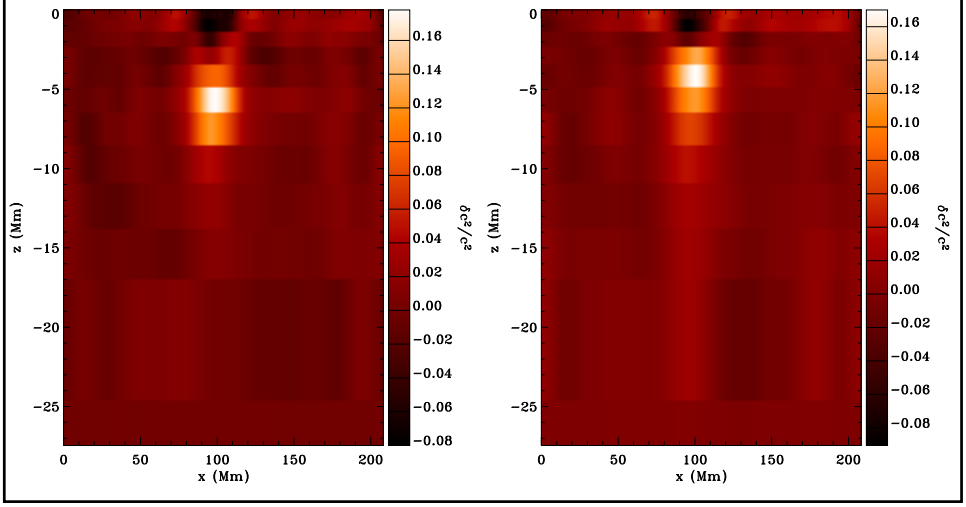

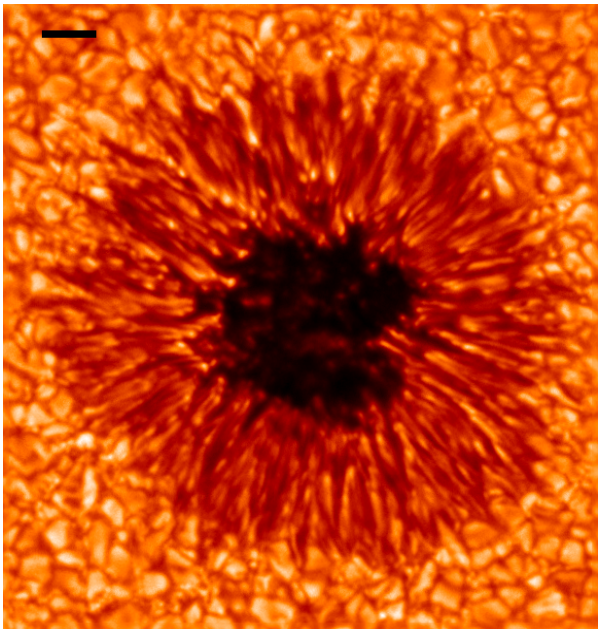

Magnetic field effects

- Magnetic field in sunspots, particularly, in the sunspot umbra may significantly affect the time-distance diagnostics for 3 main reasons:
  - The standard Doppler shift measurements may not provide accurate estimate of the actual line-of-sight velocity
  - Magnetic field inhibits convection (reducing excitation) and presumably absorbs waves causing inhomogeneous distribution of the acoustic power on the solar surface, resulting systematic shifts in the standard travel times (Woodard's effect)
  - Magnetic field causes changes in the dispersion properties of acoustic waves resulting in anisotropy in the travel times
- Magnetic effects are particularly strong when plasma parameter is of the order of unity or smaller: $\beta = 4\pi P / B^2 \sim 1$
- For most sunspot models this happens above the photosphere. This regime is poorly understood, and avoid this we mostly work with low-frequency waves that are reflected below the photosphere.
- At high frequencies, magnetic effects ("shower-glass effect", "inclined field effect") become strong, particularly, in acoustic holography (Doug Braun's talk tomorrow). Our tests show that for time-distance measurements these are much less significant.

Detailed maps of subsurface flows

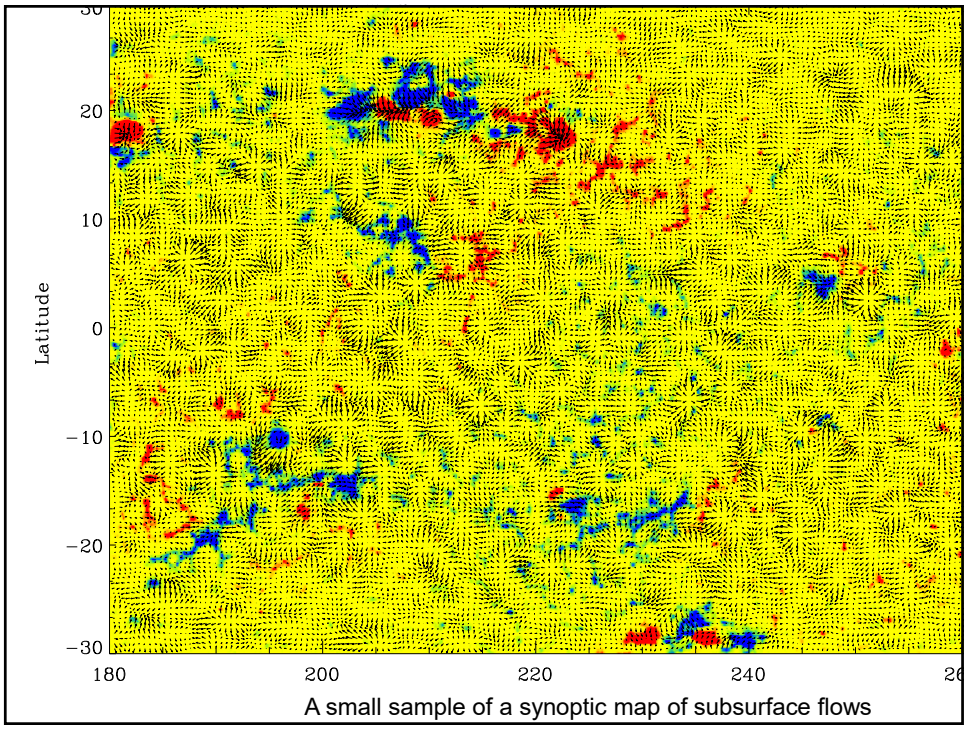

A small sample of a synoptic map of subsurface flows

Solar Subsurface Weather

Synoptic maps of subsurface flows (0-20 Mm)

Depth 2 Mm

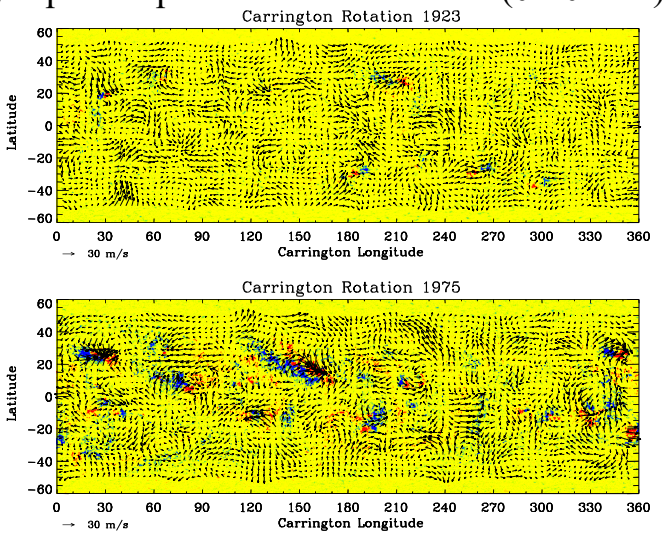

Similar maps are obtained from the ring analysis (Haber et al 2002)

Large-scale flows around active regions:

(example AR9433, April 2001)

- converging 40 m/s flow toward the neutral line in the upper layers
- diverging flow below 9 Mm

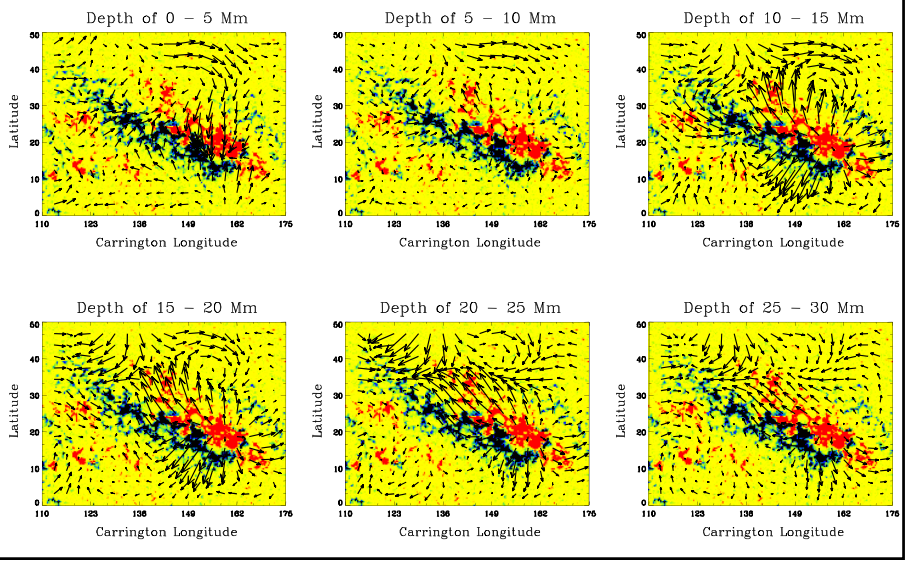

Sunspot structure and dynamics

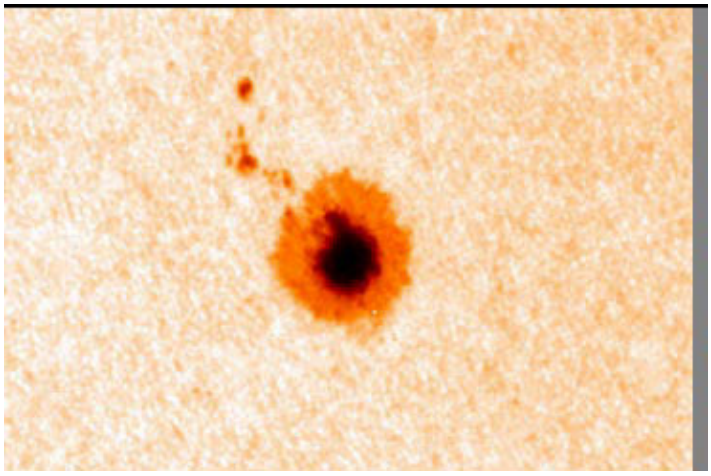

Parker's model

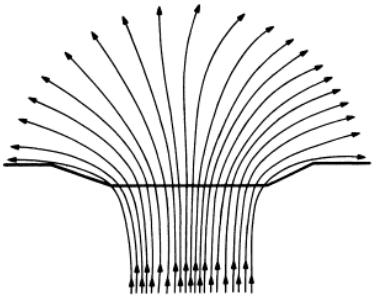

FIG. 1.—A sketch of the conventional idea of the magnetic field configuration of a sunspot. The heavy line represents the visible surface of the Sun.

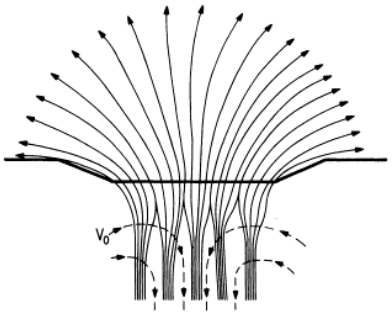

FIG. 2.—A sketch of the proposed magnetic field configuration, in which the field divides into individual flux tubes some distance below the visible surface. The dashed arrows represent the presumed convective downdraft which helps to hold the separate flux tubes together in the tight cluster that constitutes the sunspot.

Monolithic model

Cluster Model

Helioseismology provides strong evidence for the cluster model.

Observations of emerging active region by time-distance helioseismology

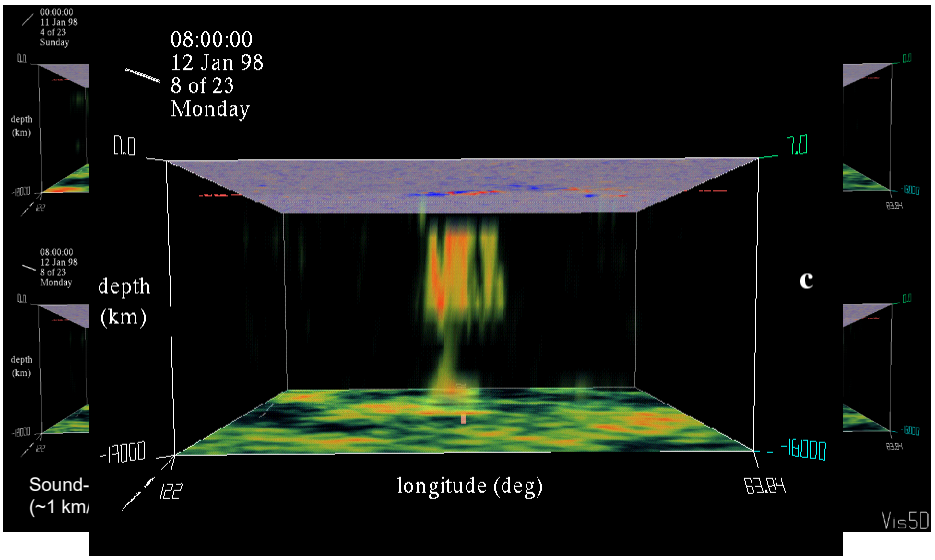

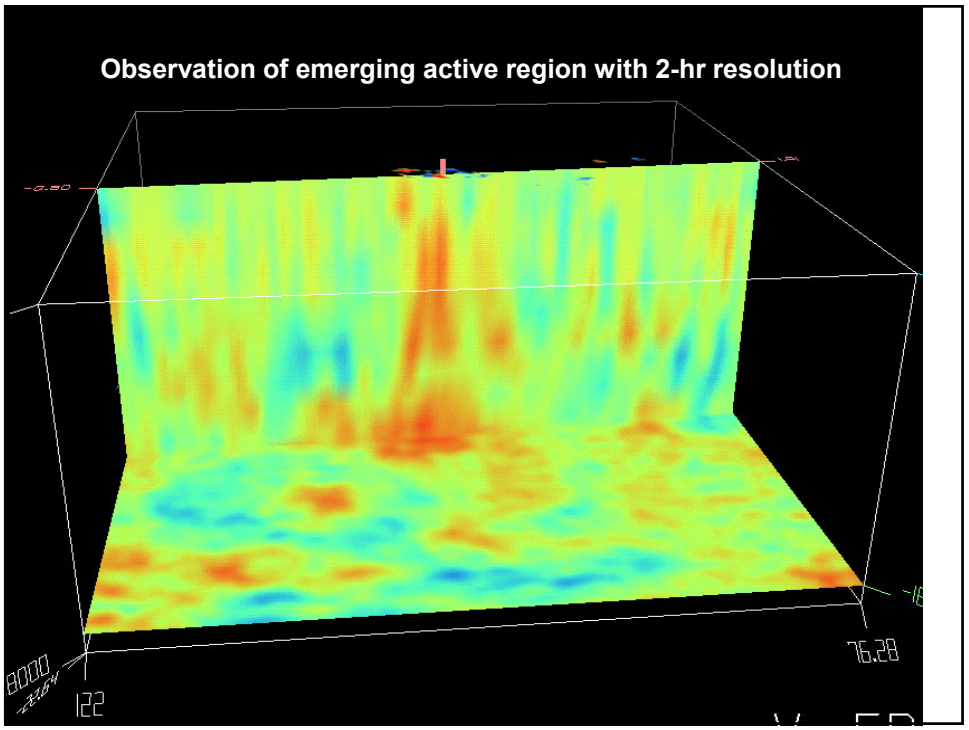

Evolution of AR 10486-488: October 24 – November 2, 2003

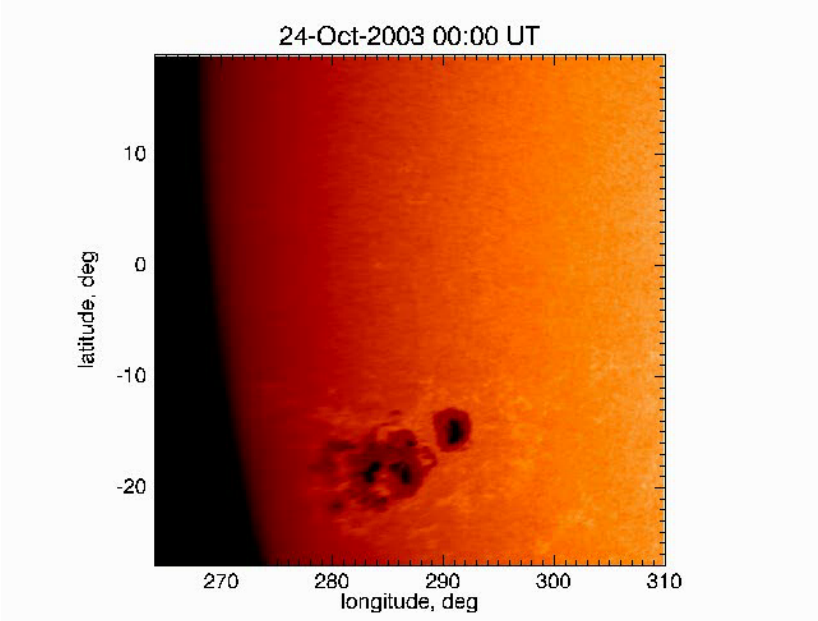

Sound-speed map and magnetogram of AR 10486 on October 25, 2003, 4:00 UT
(depth of the lower panel: 45 Mm)

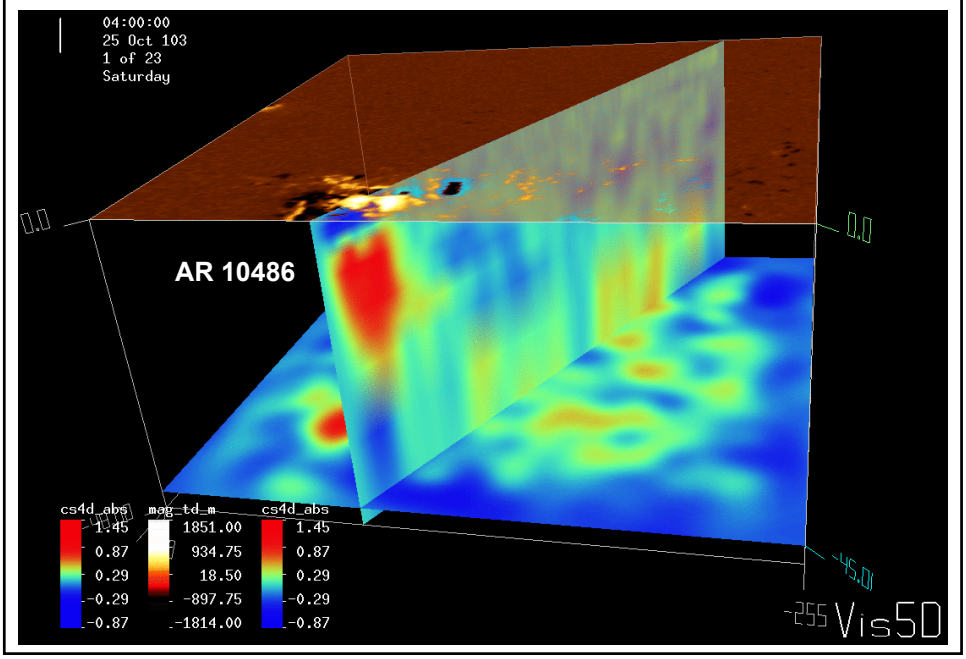

Sound-speed map and magnetogram of AR 10486 on October 26, 2003, 12:00 UT
AR 10488 is emerging

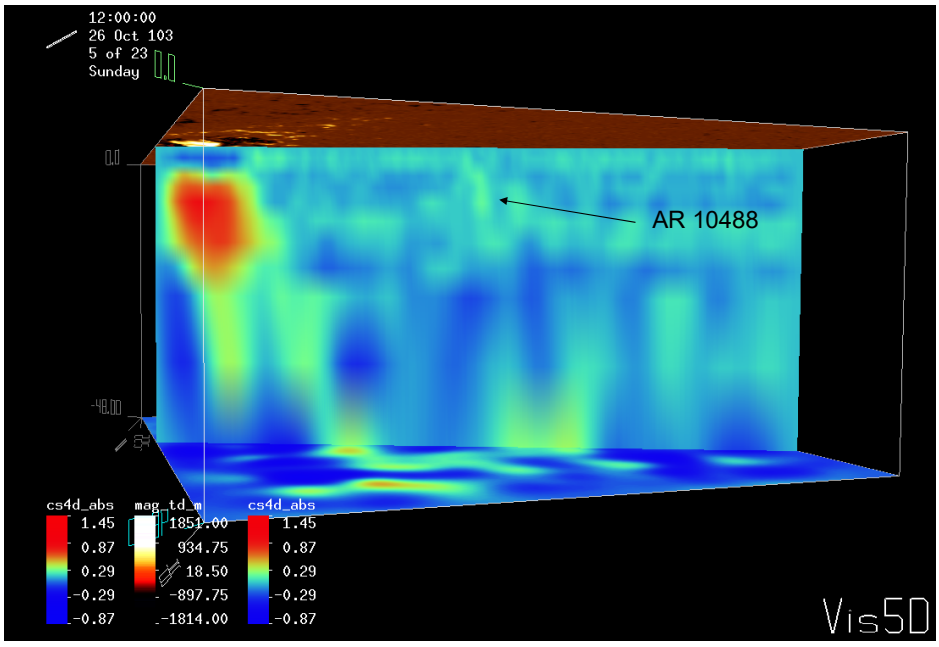

Emergence of AR 10488, October 26, 2003, 20:00 UT

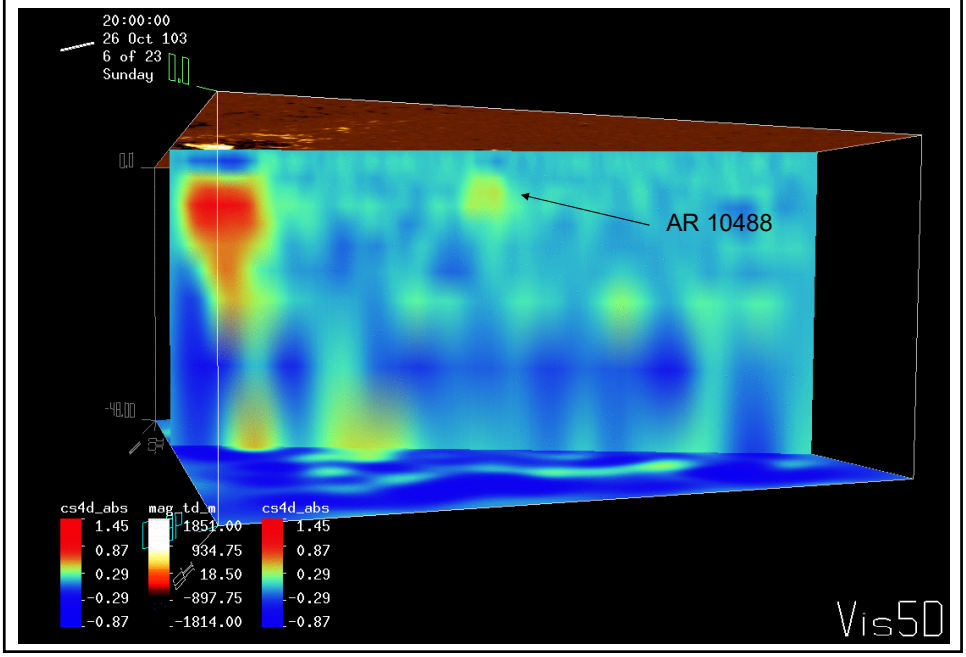

Emergence of AR 10488, October 27, 2003, 4:00 UT

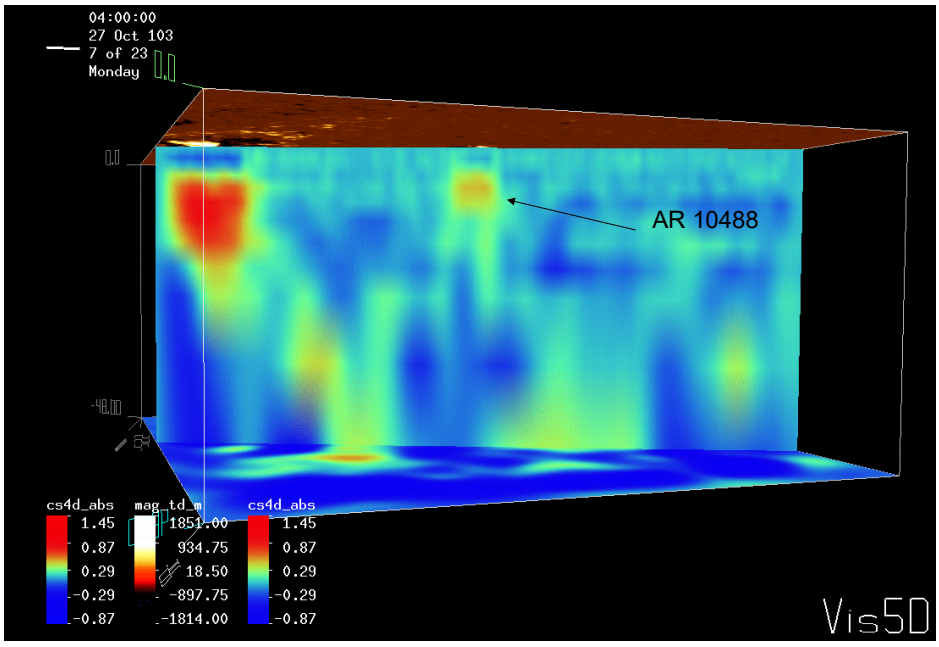

Growth and formation of sunspots of AR 10488, October 29, 2003, 4:00 UT

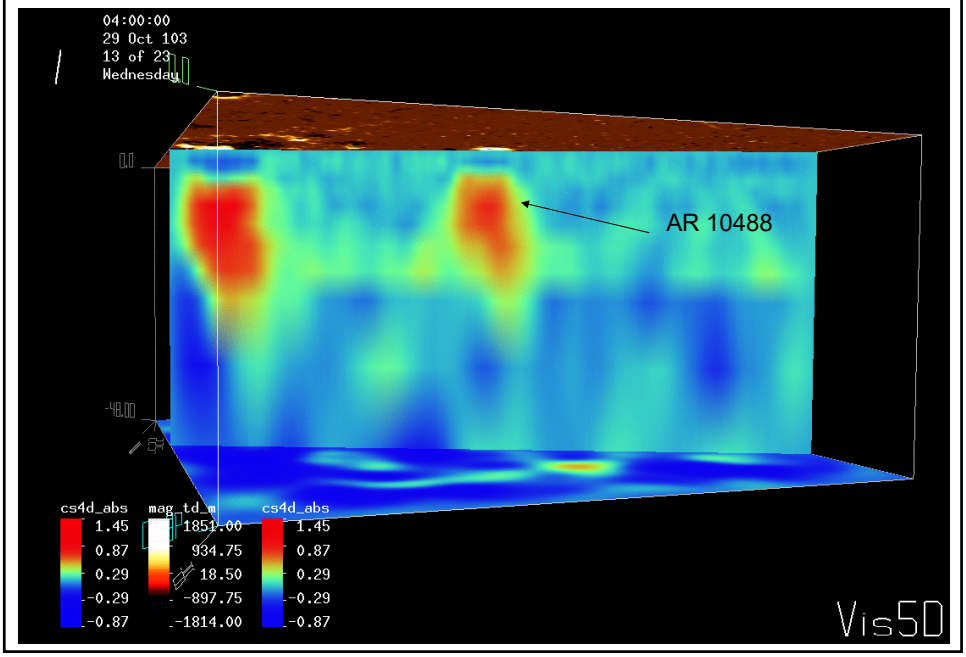

Growth and formation of sunspots of AR 10488, October 31, 2003, 12:00 UT

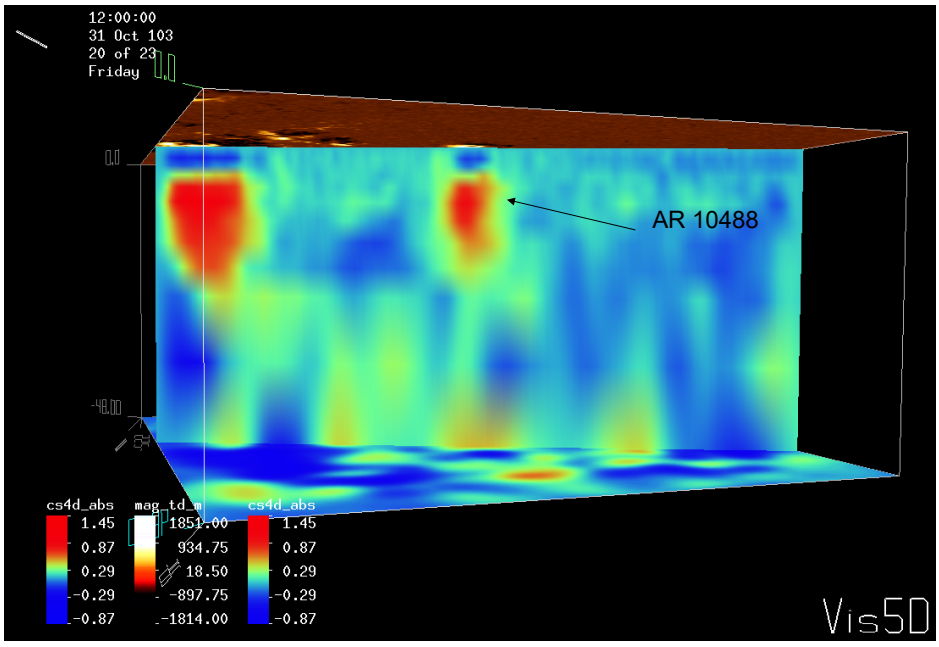

Cut in East-West direction through both magnetic polarities, showing a loop-like structure beneath AR 10488, October 30, 2003, 20:00 UT

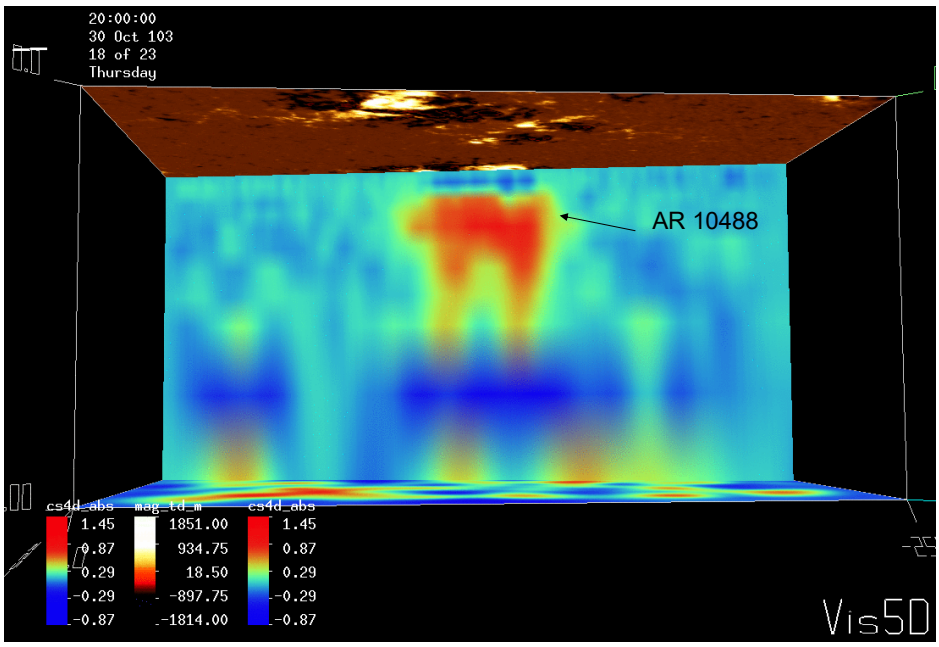

Detection of Emerging Active Regions in the Deep Interior

New methodology of detection of emerging flux

Deep-focus Time-Distance Helioseismology: solar oscillation signal is filtered to select acoustic waves traveling to depth 40-70 Mm (right), averaged over arcs (left), and cross-correlated for opposite arcs. Travel-time perturbations are measured by fitting Gabor wavelet. This method has been tested with 3 different instruments (MDI, HMI, GONG) for many quiet and emerging flux regions

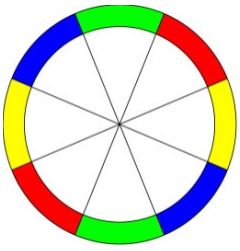

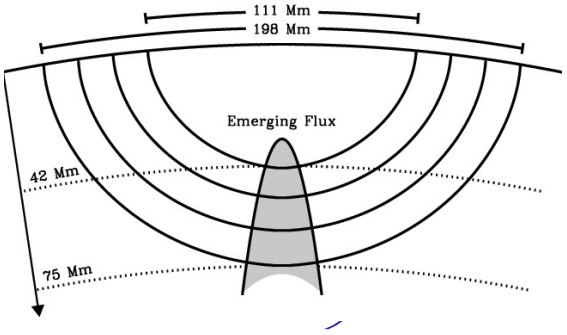

Ilonidis et al (2011)

Results for AR 10488

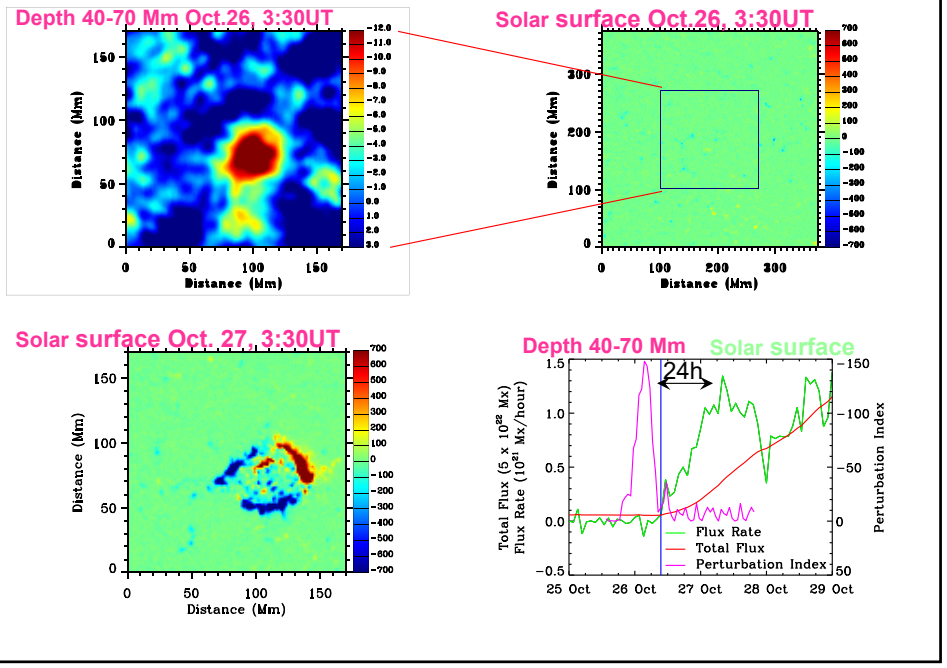

Travel-time maps of AR 10488

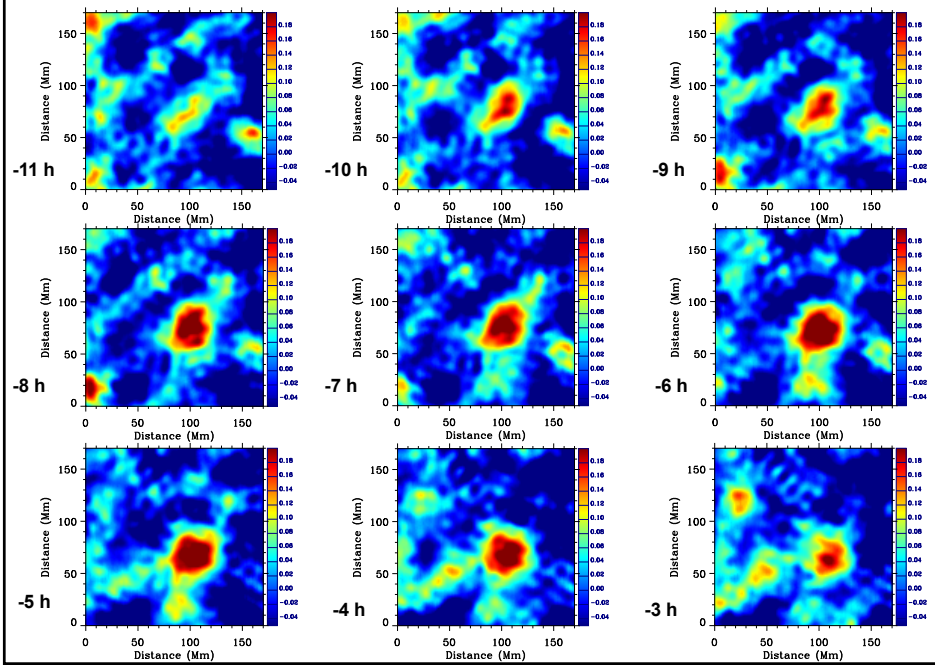

Example: Emergence of AR 10488: Oct 24 – Nov 2, 2003

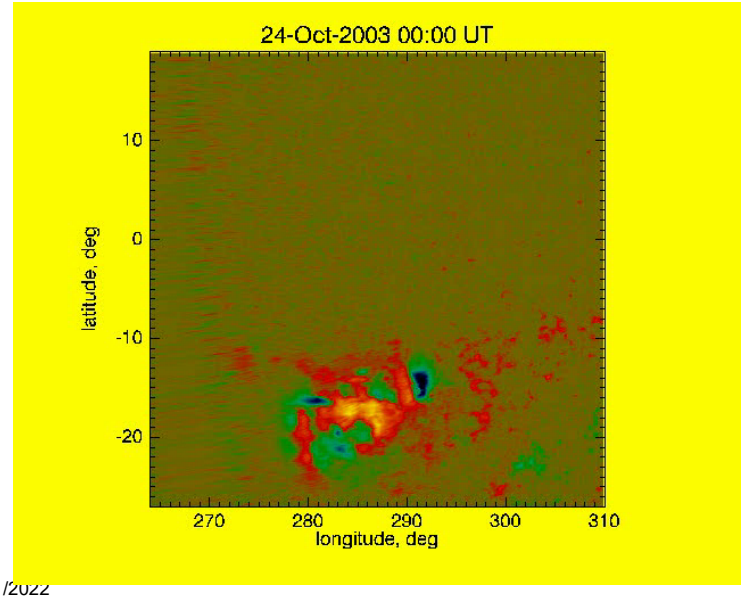

Active region NOAA 11158, February 2011

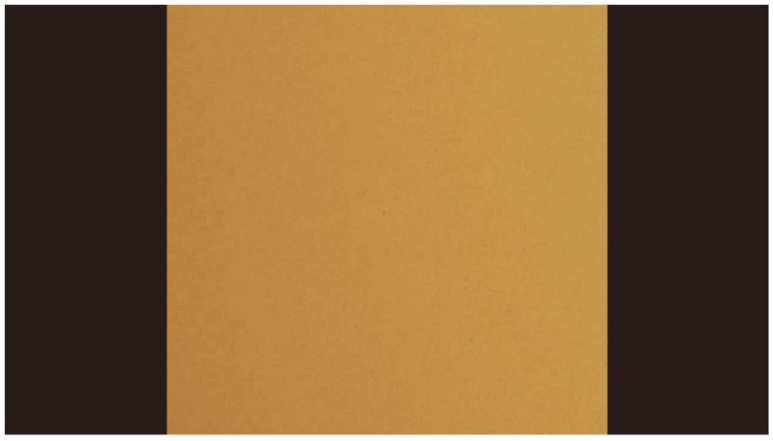

Example of analysis of subsurface flows in flaring AR 11158

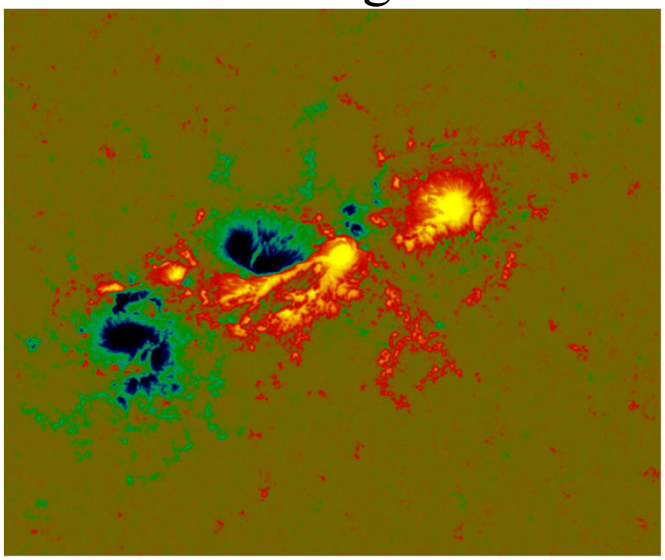

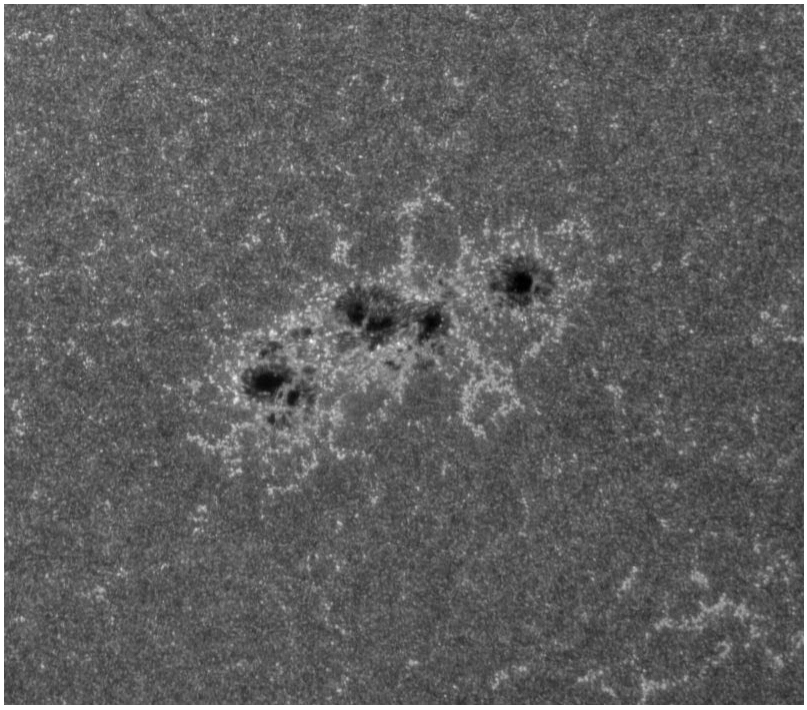

Photospheric magnetic field and subsurface flows at depth 0-1 Mm in AR 11158, February 10-18, 2011

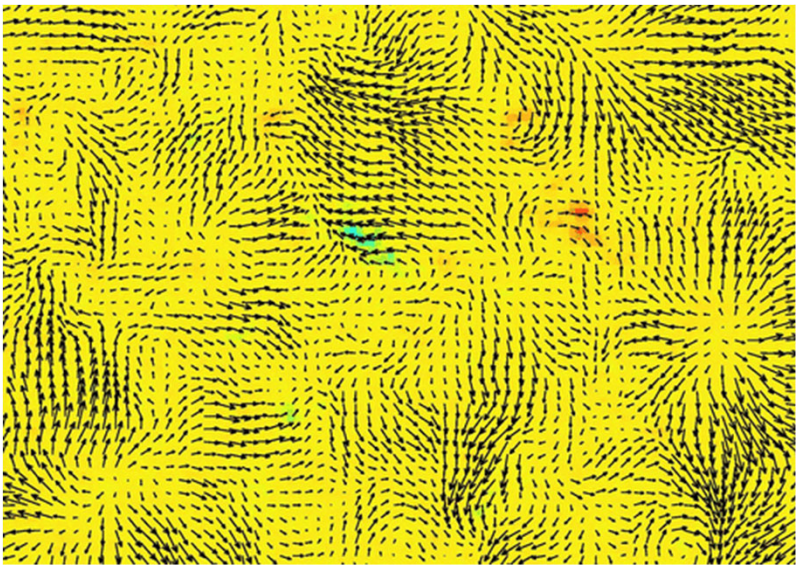

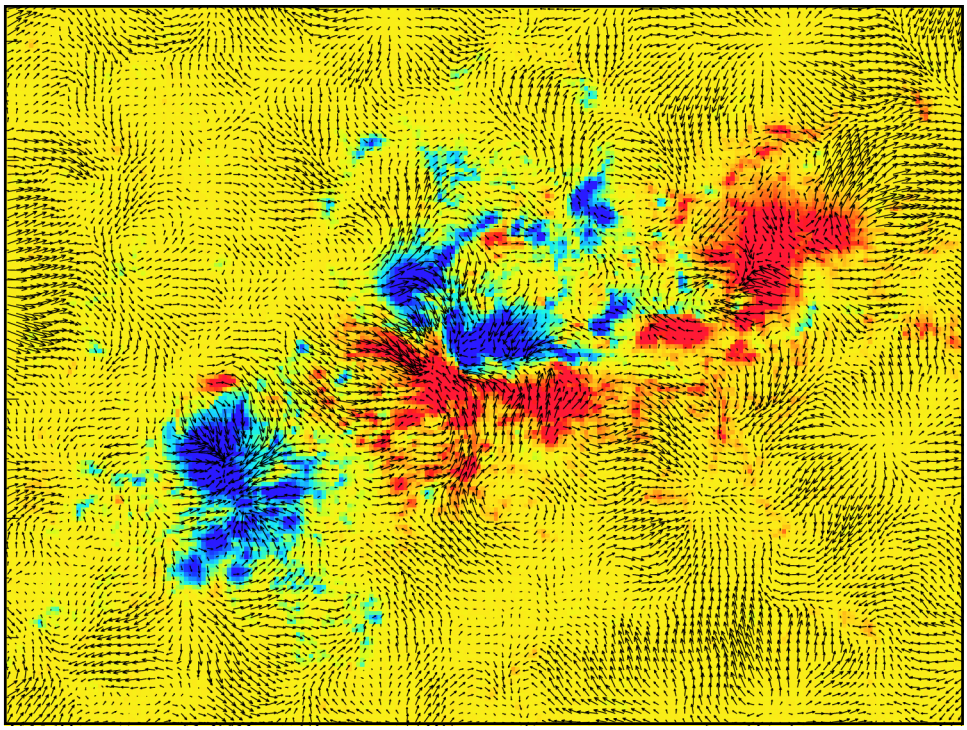

Subsurface converging flows and X2.2 flare

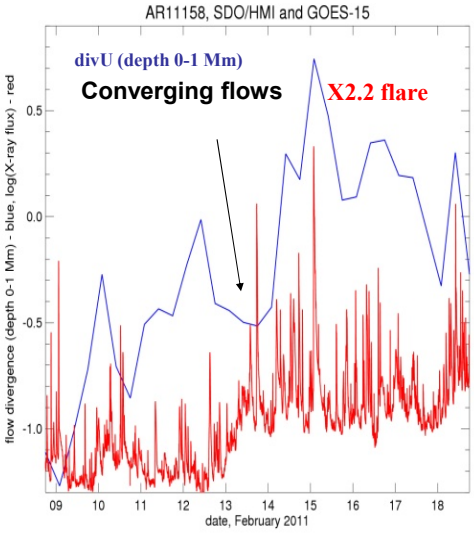

- **Approximately one day before the X-class flare strong shearing flows are developed 0-3 Mm below the surface. This is reflected in a sharp increase of the flow convergence.**
- **Potentially new method of forecasting flaring and CME activity of active regions based on helioseismology analysis and MHD modeling of subsurface flows.**